ELSEVIER

Fundamentals of THERMOPHOTOVOLTAIC ENERGY CONVERSION

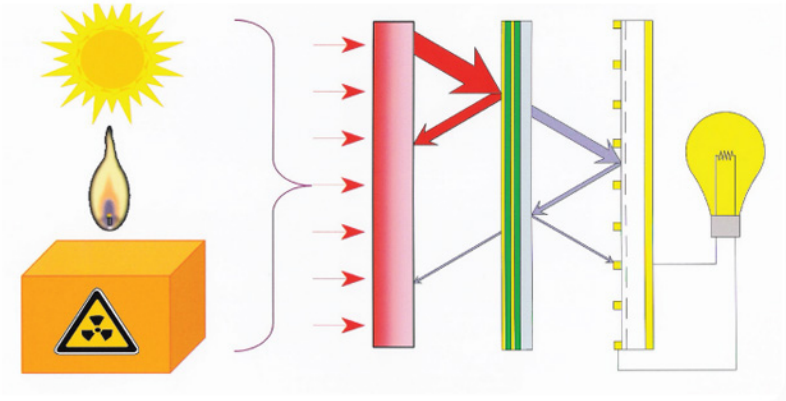

Donald L. Chubb

Fundamentals of

THERMOPHOTOVOLTAIC ENERGY CONVERSION

This page intentionally left blank

Fundamentals of
THERMOPHOTOVOLTAIC ENERGY CONVERSION

Donald L. Chubb
NASA Glenn Research Center
21000 Brookpark Road, MS 302-1
Cleveland, OH 44135
USA

ELSEVIER

Amsterdam • Boston • Heidelberg • London • New York • Oxford
Paris • San Diego • San Francisco • Singapore • Sydney • Tokyo

Elsevier
Radarweg 29, PO Box 211, 1000 AE Amsterdam, The Netherlands
Linacre House, Jordan Hill, Oxford OX2 8DP, UK

First edition 2007

Published by Elsevier B.V. 2007

Library of Congress Cataloging-in-Publication Data
A catalog record for this book is available from the Library of Congress

British Library Cataloguing in Publication Data
A catalogue record for this book is available from the British Library

ISBN: 978-0-444-52721-9
ISBN: 978-0-444-53111-7 (insert CD ROM only)

For information on all Elsevier publications
visit our website at books.elsevier.com

Printed and bound in The Netherlands

07 08 09 10 11 10 9 8 7 6 5 4 3 2 1

Acknowledgements

I began writing this text in 1996 while on a sabbatical leave at the Space Power Institute at Auburn University. M. Frank Rose was director of the Space Power Institute at that time. I thank him for giving me the opportunity to begin writing the text during my stay at Auburn.

I owe special thanks to two people: Barbara Madej for the very tedious job of typing the text. And my wife, Nancy, for proofreading the text and correcting my grammatical errors.

This page intentionally left blank

Preface

Although energy conversion is a technology that is vital for modern life, few textbooks have been written on the fundamentals of the various energy conversion systems. Thermophotovoltaics (TPV) is a simple energy conversion concept well suited for description in a fundamental text. TPV is a static conversion system with no moving parts and only three major parts: an emitter heated by a thermal energy source, and optical cavity for spectral control, and a photovoltaic (PV) array for converting the emitted radiation to electricity.

The book has been written as a text rather than as a review of current TPV research. However, there is some mention of that research.

Most of the material is introduced at the level where physics becomes engineering. For example, radiation transfer theory, which can be considered an engineering discipline, is used throughout the book. The theory is based upon the radiation transfer equation, which originates from basic physics. All the theoretical developments are as self-contained as possible.

The text begins with a chapter that introduces several topics from electromagnetic wave propagation and radiation transfer theory. This is the background material necessary to describe the emitter and optical cavity of a TPV system. Chapter 2 uses a simplified model of a TPV system to illustrate several important properties of the TPV energy conversion concept. In the next three chapters, the theory necessary to describe the performance of emitters, optical filters used for spectral control, and photovoltaic arrays is presented. The final three chapters deal with the performance of the whole TPV system.

Five appendices are included. They provide background material for the main text. Also, Mathematica computer programs for calculating the optical properties of interference filters and for calculating the performance of a planar TPV system are included on a CD-ROM disk. Problem sets are included at the end of each chapter.

This page intentionally left blank

Table of Contents

This page intentionally left blank

Chapter 1
Introduction

The opening chapter defines the thermophotovoltaic (TPV) energy conversion process, presents a short history of TPV research with possible TPV applications and introduces several concepts from electromagnetic wave propagation and radiation transfer theory. These concepts will be used throughout the text.

1.1 Symbols

A	surface area, m^2
a	absorption coefficient, cm^{-1}
B	magnetic induction, Weber/m^2
c	speed of light in material other than a vacuum, m/sec
c_o	speed of light in a vacuum (2.9979×10^8 m/sec)
D	electric displacement, Coul/m^2
E	photon energy, J or electric field, V/m
e	spectral emissive power, W/m^2/μm
e_T	total emissive power, W/m^2
$F_{o-\lambda T}$	fraction of total blackbody intensity or emissive power lying in region $0 - \lambda T$
H	magnetic field, Amp/m
h	Plank's constant (6.6262×10^{-34} J.sec)
I	time average of the Poynting vector for plane waves, W/m^2
i	radiation intensity, W/m^2/μm/steradian
j	$\sqrt{-1}$
K	extinction coefficient, cm^{-1}
k	Boltzmann constant (1.3806×10^{-23} J/K)
$\vec{k}$	wave vector, m^{-1}
n	index of refraction
Q	radiant energy per unit time per unit wavelength, W/μm
$\overline{Q}$	radiant energy per unit time, W
q	radiant energy per unit time per unit wavelength per unit area, W/μm/m^2
$\overline{q}$	radiant energy per unit time per unit area, W/m^2
R	reflectivity at an interface
r	Fresnel reflection coefficient
S	source function, W/m^2/μm, steradian
T	transmissivity at an interface or temperature, K

α	absorptance
Ω	scattering albedo
ε	emittance or electric permittivity, Farad/m (ε_o = vacuum permittivity = 8.855×10^{-12} $Amp^2sec^4/kg\ m^3$)
$\overline{\varepsilon}$	complex dielectric constant
ρ	reflectance or charge density, $coul/m^3$
σ	conductivity, $\Omega^{-1}m^{-1}$
σ_s	scattering coefficient, cm^{-1}
τ	transmittance or Fresnel transmission coefficient
μ	magnetic permeability, Henry/m (μ_o = vacuum permeability = 1.2556×10^{-6} mkg/sec^2Amp^2)
λ	Wavelength, nm
σ_{sb}	Stefan Boltzmann constant (5.67×10^{-8} $W/m^2/K^4$)

Subscripts

b	blackbody
g	corresponding to PV cell bandgap energy
R	real number
I	imaginary number
i	incident radiation
o	outgoing radiation

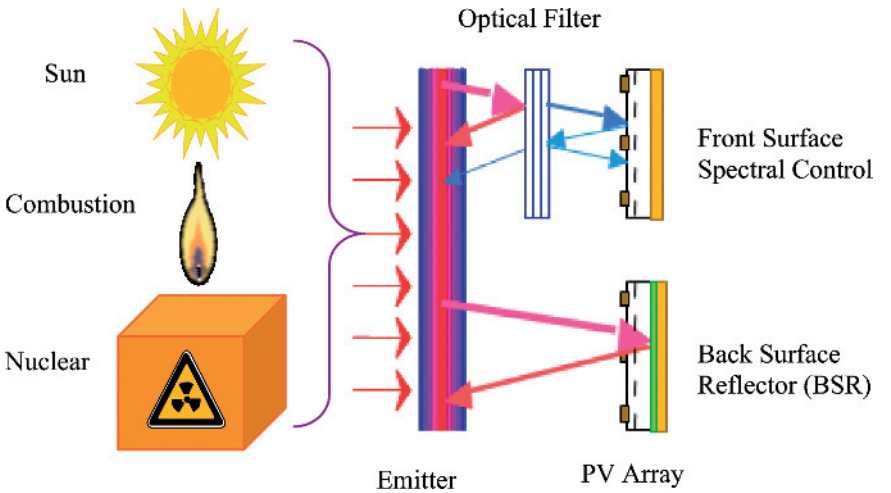

Figure 1.1 Thermophotovoltaic (TPV) energy conversion concept.

1.2 Thermphotovoltaic (TPV) Energy Conversion Concept

Similar to all energy conversion concepts, TPV energy conversion is a method for converting thermal energy to electrical energy. The concept is illustrated in Figure 1.1. Thermal energy from any of the thermal sources shown in Figure 1.1 is supplied to an emitter. Radiation from the emitter is directed to photovoltaic (PV) cells where the radiation is converted to electrical energy. In order to make the process efficient, the energy of the photons reaching the PV array must be greater than the bandgap energy of the PV cells. Shaping of the radiation or *spectral control* is accomplished in the following ways. One method is to use a selective emitter that has large emittance for photon energies above the bandgap energy of the PV cells and small emittance for photon energies less than the bandgap energy. Similar results can be accomplished by using a gray body emitter (constant emittance) and a band pass filter. The bandpass filter should have large transmittance for photon energies above the PV cells bandgap energy and large reflectance for photon energies below the PV cells bandgap energy. A back surface reflector on the PV array can also be used to reflect the low energy photons back to the emitter. It is also possible to combine all three of these methods.

1.3 A Short History of TPV Energy Conversion

Robert E. Nelson, who has done significant early research on rare earth selective emitters for TPV and is familiar with early TPV work, related the following story about the invention of TPV energy conversion. In the mid-1950's, Henry H. Kolm at

Massachusetts Institute of Technology's (MIT) Lincoln Laboratory, received a phone call from someone in the defense department who informed Kolm that Russians had developed a method for generating electricity from a lantern flame. He then asked Kolm if he could do the same thing. Kolm's solution was to place a silicon solar cell, which was in the earliest stage of development at Bell Laboratories, next to the mantel of a Coleman Lantern. He measured the electrical power output and published the result in a Lincoln Laboratory progress report [1] in May 1956. The irony is that the Russian method was thermoelectric, not TPV.

During a technical meeting in Europe in 1960, Kolm informed Pierre Aigrain of France of his experiment. Aigrain, who was a science advisor to Charles de Gaulle, immediately began to work on the concept. Aigrain is generally considered to be the first to have presented the concept in a series of lectures he gave at MIT in 1960. Early papers by D.C. White, B.D. Wedlock and J. Blair [2] and B.D. Wedlock [3] and [4] present the earliest theoretical and experimental TPV research results. The first term used to describe the concept was thermal-photo-voltaic, which then became thermo-photo-voltaic, and finally, thermophotovoltaic. General Motors (GM) also had an early interest in TPV.

At GM, TPV work was also begun in 1960 [5] through [7]. In 1963 Werth [6] demonstrated TPV conversion using a propane-heated emitter and a germanium (Ge) PV cell. The emitter temperature was approximately 1700 K. Shockley and Queisser [8] had shown that for a blackbody radiation source, the efficiency of a PV cell was strongly dependent upon the ratio of the cell bandgap energy, E_g, to the radiation source temperature, T_E. In fact, $E_g/kT_E \approx 2.0$ to obtain maximum efficiency for a blackbody source. In order to obtain maximum efficiency using silicon (Si), which was the most efficient PV cell available, the emitter temperature would have to be approximately 6000 K.

No workable materials exist at these temperatures. Therefore, for efficient TPV energy conversion at reasonable temperatures, a blackbody source cannot be used. As a result, TPV research has been directed at tailoring the emitter radiation to the PV cell bandgap energy. In other words, by producing radiation within a narrow energy band that lies just above the bandgap energy of the PV cell (where PV cell is most efficient), it is possible to have an efficient system. In addition, just as for the blackbody emitter, there will be an optimum value for E_g/kT_E. For reasonable emitter temperatures ($T_E \leq 2000$ K) achieving this optimum condition requires that $E_g \leq 1.0$ eV. Therefore, low bandgap energy PV cells are required for high efficiency in addition to radiation matched to the PV cell bandgap energy.

The early TPV research of the 1960's and 1970's was confined to using either silicon (E_g = 1.12 eV) or germanium (E_g = 0.66 eV) PV cells. However, silicon requires a large emitter temperature ($T_E \approx 2000$ K) for an efficient TPV system, and Ge cells were of low efficiency, although having reasonable bandgap energy for TPV

conversion. Thus, lack of suitable PV cells plus unsuccessful attempts at obtaining radiation matched to the PV cell bandgap energy resulted in a loss of interest in TPV energy conversion. However, in the 1980's new efficient PV cell materials such as gallium antimonide (GaSb, E_g = 0.72 eV) and indium gallium arsenide ($In_xGa_{1-x}As$, where $0.36 \leq E_g \leq 1.42$ eV depending on value of x), became available. In addition, new selective emitters and filters that can produce the bandgap matched radiation were being developed. As a result, beginning in the late 1980's, a resurgence of interest in TPV energy conversion occurred.

An extensive bibliography of all TPV research papers has been complied by Lars Browman [9]. Other excellent references for TPV research results are the proceedings of the National Renewable Energy Laboratory (NREL) Conferences on Thermophotovoltaic Generation of Electricity.

1.4 TPV Applications

Besides the development of new PV cell and emitter technology, the many applications for TPV energy conversion are also a driving force in the resurgence of TPV interest. The simplicity and potential high efficiency of TPV conversion are the two attractive features that lead to many potential applications. Since TPV is a direct energy conversion process, the only moving parts in the system are fans or pumps that may be used for cooling the PV cells. The components of the system are the thermal source, the emitter (and possibly a filter), the PV cells, and the waste heat rejection system. Each of these components is in the solid state with only the PV cells and possibly the filter being a somewhat complex solid state device. In addition to simplicity and potential high conversion efficiency, TPV can be easily coupled to any thermal source.

Applications for TPV exist where the thermal source may be solar, nuclear, or combustion. At first it would appear that a solar TPV (STPV) system would have no advantage over a conventional solar PV system. What can be gained by adding an emitter and possibly a filter to the conventional solar PV system? By adding a selective emitter or thermal emitter plus filter, the solar spectrum, which corresponds approximately to a 6000 K gray body emitter, can be shifted to match the bandgap energy of the PV cells. As a result, the STPV system will yield higher efficiency than the conventional solar PV systems. Besides efficiency, an even more important reason for interest in STPV energy conversion is the ability to use thermal energy storage and combustion energy input so that the system can operate when the sun is not available. With the capability of 24-hour-a-day operation, STPV is viable for electric utility use.

A TPV system powered by radioisotope decay (RTPV) is a potential power system for deep space missions where the solar radiation energy density is too low for a conventional PV power system to be used. The first radioisotope decay power systems

used thermoelectric energy converters (RTG). However, TPV has the potential for higher efficiency than thermoelectrics; therefore it is being considered as a replacement.

Combustion driven TPV has many potential commercial applications. For natural gas-fired appliances such as furnaces and hot water tanks, TPV can be added for the cogeneration of electricity. In such applications, attaining high TPV efficiency is not essential since the waste heat for the TPV conversion process is completely utilized. Portable power supplies for both commercial and military use is another important combustion TPV application. An important TPV advantage over existing internal combustion-driven applications is quiet operation. This is especially true in military missions that require the mission to be undetected. Another combustion-driven TPV application with commercial potential is the power supply for hybrid electric vehicles. In such an application the TPV system is sized to provide enough power for operation at cruise speed and battery charging. For acceleration power the batteries are utilized.

One important advantage of all TPV applications is that they are environmentally benign. The TPV system is nearly silent and emits no pollutants. This is obvious in the case of a solar driven system. For a nuclear powered system there are no combustion products; however, care must be taken to insure that no radioactive material is released. Atmospheric pressure burning occurs in the combustion-driven TPV systems. Therefore, the combustion temperature can be well controlled so that the production of toxic nitrous oxides (NOX) is small.

Although there appears to be unlimited potential TPV applications, whether or not they are feasible, will depend upon their cost. At this stage of development, it is impossible to say which applications will be cost effective.

1.5 Propagation of Electromagnetic Waves

Energy transfer between the components of a TPV system is mainly by radiation that consists of propagating electromagnetic waves. The derivation of the equation describing radiation transfer does not require electromagnetic wave propagation theory. However, electromagnetic wave theory is required to obtain equations for the optical properties reflectivity and transmissivity at an interface. Values for these properties are required in analyzing a TPV system. Also, wave propagation must be considered in analyzing the various optical filters that can be used in a TPV system.

1.5.1 Plane Wave Solution to Maxwell's Equations

Much of the material to be covered in this section can be found in the classic optics text by Born and Wolf [10]. As is well known, Maxwell's equations describe the propagation of all electromagnetic waves. For TPV applications the electromagnetic waves of interest are mostly in the infrared region ($\lambda > 800$ nm) of the spectrum. In the International System of Units (SI), Maxwell's Equations for the electric field, $\vec{E}$, and magnetic field, $\vec{H}$, are the following [11],

$$\nabla \times \vec{H} = \vec{J} + \frac{\partial \vec{D}}{\partial t} \qquad \text{Ampere's Law} \qquad (1.1)$$

$$\nabla \times \vec{E} = -\frac{\partial \vec{B}}{\partial t} \qquad \text{Faraday's Law} \qquad (1.2)$$

$$\nabla \bullet \vec{D} = \rho \qquad \text{Coulomb's Law} \qquad (1.3)$$

$$\nabla \bullet \vec{B} = 0 \qquad \text{Absence of free magnetic poles} \qquad (1.4)$$

where $\vec{J}$ is the conduction current, $\vec{D}$ is the electric displacement, $\vec{B}$ the magnetic induction and ρ is the electric charge density. In addition to Maxwell's Equations so-called *constitutive relations* for the media are required.

$$\vec{D} = \varepsilon_o \vec{E} + \vec{P} = (\varepsilon_o + \chi)\vec{E} = \varepsilon \vec{E} \qquad (1.5)$$

$$\vec{B} = \mu_o (\vec{H} + \vec{M}) = \mu_o (1 + \chi_m)\vec{H} = \mu \vec{H} \qquad (1.6)$$

$$\vec{J} = \sigma \vec{E} \qquad (1.7)$$

Appearing in equation (1.5) is the electric dipole moment per unit volume, $\vec{P}$, which for most media depends linearly upon $\vec{E}$. Therefore, the second two forms for $\vec{D}$ result, where ε_o is the vacuum permittivity, χ is the *electric susceptibility* and $\varepsilon = \varepsilon_o + \chi$ is the *electric permittivity*. Similar to $\vec{D}$, the magnetic field, $\vec{B}$, has two parts: $\vec{H}$ and the magnetic dipole moment per unit volume, $\vec{M}$. For most media $\vec{M}$ is a linear function of $\vec{H}$, which results in the second two forms for $\vec{B}$ in equation (1.6). Here μ_o is the vacuum permeability, χ_m is the *magnetic susceptibility*, and $\mu = \mu_o (1 + \chi_m)$ is the *magnetic permeability*. The properties of the medium (ε, μ, and σ) appearing in equations (1.5) to (1.7) are scalar quantities and therefore independent of direction. Thus the media is called *isotropic*. Also, $\vec{D}$, $\vec{B}$, and $\vec{J}$ are linear functions of $\vec{E}$ and $\vec{H}$ so the media is called a *linear isotropic media*. In general, the properties may depend upon direction (anisotropic) so that they are tensor quantities. And $\vec{E}$ and $\vec{H}$ can appear as higher order terms in the constitutive relations so that the

media may be nonlinear. Finally, for plane electromagnetic waves the properties must be independent of time (*stationary media*) and space (*homogeneous media*).

The quantum mechanical theory necessary to determine the medium properties (ε, μ, σ) is beyond the scope of this text. However, the discussion of optical filters in Chapter 4 uses a macroscopic model called the Drude model to calculate ε.

The wave equation for $\vec{E}$ is obtained by first taking the curl (∇×) of equation (1.2) and making use of the vector identity $\nabla \times (\nabla \times \vec{A}) = \nabla(\nabla \bullet \vec{A}) - \nabla^2 \vec{A}$, where $\nabla^2 = \nabla \bullet \nabla$. Then using equations (1.1), (1.3), and the constitutive relations, equations (1.5) to (1.7), the following result is obtained.

$$\nabla^2 \vec{E} - \frac{\partial}{\partial t}\left(\mu \frac{\partial \varepsilon \vec{E}}{\partial t}\right) - \frac{\partial}{\partial t}\left(\mu\sigma\vec{E}\right) = \nabla\left(\nabla \bullet \vec{E}\right) + \frac{\partial}{\partial t}\left(\nabla\mu \times \vec{H}\right) \quad \text{linear isotropic media} \tag{1.8}$$

So far, the only approximation that has been made is that the media is linear and isotropic. Now assume the media is stationary so that properties are independent of time, t, and that μ = constant. Therefore, equation (1.8) becomes the following.

$$\nabla^2 \vec{E} - \mu\varepsilon \frac{\partial^2 \vec{E}}{\partial t^2} - \mu\sigma \frac{\partial \vec{E}}{\partial t} = \nabla(\nabla \bullet \vec{E}) \quad \text{linear, stationary, isotropic media } \mu\text{=constant} \tag{1.9}$$

Solution of equation (1.9) depends upon the properties (μ,ε,σ) and the boundary conditions. There is no indication that wave solutions follow naturally from this equation. No wave vector, $\vec{k}$, or frequency, ω, appears in equation (1.9). Experimentally it has been shown that light has wave-like behavior. Therefore, a wave solution should satisfy equation (1.9) if Maxwell's equations apply to electromagnetic waves of all frequencies including light. The simplest wave solution is the so-called *harmonic plane wave*,

$$\vec{E}' = \vec{E}'_o \cos\left(\omega t - \vec{k} \bullet \vec{x}\right) \tag{1.10a}$$

or using complex notation,

$$\vec{E} = \vec{E}_o \exp\left[\, j\left(\omega t - \vec{k} \bullet \vec{x}\right)\right] \tag{1.10b}$$

$$\vec{E}' = \mathrm{Re}\left[\vec{E}\right] \tag{1.10c}$$

where $\vec{E}_o$ is a constant and can be complex and equation (1.10a) is the real part of equation (1.10b). Note that $j\left(\vec{k}\cdot\vec{x}-\omega t\right)$ in the exponential of equation (1.10b) yields the same result for equation (1.10a) as $j\left(\omega t-\vec{k}\cdot\vec{x}\right)$. The spatial and time variations all enter in the exponential term. And $\vec{k}$, the wave vector that points in the direction of wave propagation, can be complex but must be independent of $\vec{x}$ and t. The frequency, ω, is a real number and also must be independent of $\vec{x}$ and t. In using complex notation, equation (1.10b), care must be exercised when considering products, since Re[A]Re[B] ≠ Re[AB].

If $\vec{k}$ is real, then $\vec{E}$ will remain a constant in a plane where the *phase of the wave*, $\omega t-\vec{k}\cdot\vec{x}$, remains a constant. Thus, equation (1.10) is called a *plane wave*. The velocity of this plane is in the direction of the wave propagation ($\vec{k}$ direction) and has the magnitude, v_ϕ, which can be derived as follows.

For constant $\vec{E}$,

$$\vec{k}\bullet\vec{x}-\omega t=\text{ constant} \tag{1.11a}$$

$$\vec{k}\bullet\frac{d\vec{x}}{dt}-\omega=0 \tag{1.11b}$$

and since the *phase velocity* is in the direction of $\vec{k}$,

$$v_\phi=\left|\frac{d\vec{x}}{dt}\right|=\frac{\omega}{k} \tag{1.12}$$

the *index of refraction*, n, is defined as follows,

$$n\equiv\frac{c_o}{v_\phi}=\frac{c_o}{\omega}k=\frac{\lambda}{2\pi}k \tag{1.13}$$

where c_o is the speed of light in vacuum (3×10^8 m/sec) and $\lambda = 2\pi c_o/\omega$ is the wavelength in vacuum. As will be shown shortly,

$$c_o=\frac{1}{\sqrt{\mu_o\varepsilon_o}} \tag{1.14}$$

where ε_o is the vacuum permittivity and μ_o is the vacuum permeability. Obviously, if k is complex, n will also be complex. It should be noted that if k and n are complex, then the phase velocity, which is always real, is no longer related to n and k by equation (1.13).

Now consider how k and ω are related to the media properties for plane waves. This relation, called the dispersion relation, is obtained by substituting equation (1.10b) in equation (1.9). Using the operators $\nabla = -j\vec{k}$ and $\partial/\partial t = j\omega$ that apply for plane waves (problem 1.1) the following result is obtained.

$$\left[k^2 - \mu\varepsilon\omega^2 + j\mu\sigma\omega\right]\vec{E}_o = \left(\vec{k}\cdot\vec{E}_o\right)\vec{k} \tag{1.15}$$

For the vector equation (1.15) to be satisfied $\vec{E}_o$ and $\vec{k}$ must be either in the same direction or perpendicular to each other. If they are in the same direction, then the physically impossible result $\varepsilon = j\,\sigma/\omega$ is obtained. Therefore, $\vec{k}$ and $\vec{E}$ must be perpendicular. This same result for plane waves can be obtained using equations (1.1), (1.5) and (1.7) (problem 1.2). In that case equation (1.15) becomes the following.

$$k^2 - \mu\varepsilon\omega^2 + j\mu\sigma\omega = 0 \qquad \text{linear, homogeneaous, stationary, isotropic medium} \tag{1.16}$$

Several important conclusions can be drawn from equation (1.16). First, since k and ω are constants for plane waves, the medium properties must also be constants for the plane wave solution to apply. Therefore, for a linear isotropic medium, plane waves only apply when the medium is also homogeneous and stationary as stated earlier. However, if the medium is linear, stationary, homogeneous but anisotropic it is still possible to have plane wave solutions [12]. The second conclusion drawn from equation (1.16) is that k must be complex for a *conductive* ($\sigma \neq 0$) medium. However, if $\sigma = 0$ (*dielectric*), it is still possible for a component of $k\left(= k_x\hat{i} + k_y\hat{j} + k_z\hat{k}\right)$ to be purely imaginary and equation (1.16) to still be satisfied since $k^2 = k_x^2 + k_y^2 + k_z^2$. In fact, that is the situation for total internal reflection at a boundary between two dielectrics. Finally, for the plane wave solution, equation (1.10) to apply $\nabla\cdot\vec{E} = 0$ and the charge density, ρ, must vanish (problem 1.3). If k has an imaginary part, then equation (1.10b) shows that $\left|\vec{E}\right| \sim e^{\vec{k}_I\cdot\vec{x}}$. Obviously, $\vec{k}_I\cdot\vec{x}$ must be negative to insure that $\left|\vec{E}\right|$ decays rather than grows exponentially.

If $\nabla \cdot \vec{E} = 0$, equation (1.9) becomes the following

$$\nabla^2 \vec{E} - \mu\varepsilon \frac{\partial^2 E}{\partial t^2} - \mu\sigma \frac{\partial E}{\partial t} = 0 \quad \begin{array}{c}\text{linear, homogeneous, stationary, isotropic,} \\ \text{medium with no space change}\end{array} \tag{1.17}$$

This equation applies when the medium is linear, homogeneous and isotropic, and when no space charge exists. Under the same conditions a similar equation can be obtained for $\vec{H}$ (problem 1.4). Therefore, plane wave solutions apply for both $\vec{E}$ and $\vec{H}$ under the medium conditions just described. However, the condition $\rho = 0$ is not required to obtain the $\vec{H}$ wave equation.

If a complex wave vector and index of refraction is defined as follows,

$$\left(k_R - jk_I\right)\hat{s} = \frac{\omega}{c_o}\left(n_R - jn_I\right)\hat{s} \tag{1.18}$$

where $\hat{s}$ is a real unit vector pointing in the direction of wave propagation, then the dispersion relation, equation (1.16), can be solved for the real, k_R, and imaginary, k_I, parts of k. A negative sign appears before the imaginary parts of k and n to ensure $\left|\vec{E}\right|$ and $\left|\vec{H}\right|$ decay with distance. Substituting equation (1.18) in equation (1.16) and equating real and imaginary parts yields the following.

$$k_R^2 - k_I^2 = \mu\varepsilon\omega^2 \tag{1.19}$$

$$2k_R k_I = \mu\sigma\omega \tag{1.20}$$

Therefore,

$$k_R = \frac{\omega}{c_o} n_R = \omega\left(\frac{\mu}{2}\right)^{1/2} \left\{\sqrt{\varepsilon^2 + \left(\frac{\sigma}{\omega}\right)^2} + \varepsilon\right\}^{1/2} \tag{1.21}$$

$$k_I = \frac{\omega}{c_o} n_I = \omega\left(\frac{\mu}{2}\right)^{1/2} \left\{\sqrt{\varepsilon^2 + \left(\frac{\sigma}{\omega}\right)^2} - \varepsilon\right\}^{1/2} \tag{1.22}$$

Obviously, for a dielectric ($\sigma = 0$), $k_I = 0$ and

$$k = k_R = \omega\sqrt{\mu\varepsilon} = \frac{\omega}{c_o}\sqrt{\mu_r\varepsilon_r} = \frac{\omega}{c_o}n_R \quad \text{for } \sigma = 0 \tag{1.23}$$

and,

$$v_\phi = \frac{\omega}{k_R} = \frac{1}{\sqrt{\mu\varepsilon}} \tag{1.24}$$

$$n_R = \frac{c_o}{v_\phi} = \frac{1}{\sqrt{\mu_r\varepsilon_r}} \tag{1.25}$$

where $\varepsilon_r = \varepsilon/\varepsilon_o$ is the *dielectric constant* and $\mu_r = \mu/\mu_o$ is the *relative permeability*. For a vacuum, $v_\phi = c_o = 1/\sqrt{\mu_o\varepsilon_o}$. The fact that k has no imaginary part if $\sigma = 0$ seems to contradict the discussion proceeding equation (1.17). It was stated that $\vec{k}$ could have a component that is purely imaginary for a dielectric ($\sigma = 0$). In that case however, the definition for $\vec{k}$ given by equation (1.18) does not apply. Equation (1.18) defines the magnitude of $\vec{k}$ as being complex and the unit vector, $\hat{s}$, as being real. However for the case of a dielectric ($\sigma = 0$), the magnitude of $\vec{k}$ is real but the unit vector, $\hat{s}$, can be complex. As already stated, this is the case for total internal reflection at a boundary between two dielectrics. This will be discussed in detail in Section 1.5.4.

The wave number, k, and therefore the index of refraction, n, are given in terms of the real properties, μ, ε, and σ by equations (1.21) and (1.22). However, referring to the dispersion relation, equation (1.16), it yields,

$$k^2 = \mu_r\frac{\omega^2}{c_o^2}\bar{\varepsilon} = \frac{\omega^2}{c_o^2}n^2 \tag{1.26a}$$

$$k = \frac{\omega}{c_o}n = \frac{\omega}{c_o}\sqrt{\mu_r\bar{\varepsilon}} \tag{1.26b}$$

if a *complex dielectric constant* is defined as follows,

$$\bar{\varepsilon} = \bar{\varepsilon}_R - j\bar{\varepsilon}_I \tag{1.27}$$

where the real part of $\bar{\varepsilon}$,

$$\bar{\varepsilon}_R = \frac{\varepsilon}{\varepsilon_o} \tag{1.28a}$$

is proportional to the displacement current $\left(\frac{\partial \varepsilon \vec{E}}{\partial t}\right)$ and the imaginary part,

$$\bar{\varepsilon}_I = \frac{\sigma}{\omega \varepsilon_o} \tag{1.28b}$$

is proportional to the conduction current $\left(\sigma \vec{E}\right)$. Thus for a plane wave in a *nonmagnetic material* ($\mu_r = 1$), the electrical properties of the media can be combined in a single parameter; the complex dielectric constant, $\bar{\varepsilon}$. This is convenient since the theoretical models for the electrical properties in time-varying fields, such as the Drude model ([13], pg. 225-226), lead to a complex dielectric constant that conforms to equation (1.27).

By defining a complex dielectric constant the governing equation for $\vec{E}$ or $\vec{H}$, equation (1.17), reduces to the standard wave equation.

$$\nabla^2 \vec{E} - \mu \varepsilon_o \bar{\varepsilon} \frac{\partial^2 \vec{E}}{\partial t^2} = 0 \tag{1.29}$$

Using equation (1.28a) and equation (1.28b) in equations (1.21) and (1.22) results in the following relations between k, n, and $\bar{\varepsilon}$.

$$k_R = \frac{2\pi}{\lambda} n_R = \frac{2\pi}{\lambda}\left(\frac{\mu_r}{2}\right)^{1/2} \left\{\sqrt{\bar{\varepsilon}_R^2 + \bar{\varepsilon}_I^2} + \bar{\varepsilon}_R\right\}^{1/2} \tag{1.30a}$$

$$k_I = \frac{2\pi}{\lambda} n_I = \frac{2\pi}{\lambda}\left(\frac{\mu_r}{2}\right)^{1/2} \left\{\sqrt{\bar{\varepsilon}_R^2 + \bar{\varepsilon}_I^2} - \bar{\varepsilon}_R\right\}^{1/2} \tag{1.30b}$$

For a nonmagnetic ($\mu_r = 1$), dielectric $\left(\bar{\varepsilon}_I = 0\right)$ material, equations (1.30) become

$$n_R = \frac{\lambda}{2\pi} k_R = \sqrt{\bar{\varepsilon}_R}, \qquad n_I = k_I = 0, \qquad \text{for } \bar{\varepsilon}_I = 0,\ \mu_r = 1 \tag{1.31}$$

Notice that if $\bar{\varepsilon}_R < 0$, which is the case for many metals at high frequency, $k_R\left(\bar{\varepsilon}_R > 0\right) \to k_I\left(\bar{\varepsilon}_R < 0\right)$ and $k_I\left(\bar{\varepsilon}_R > 0\right) \to k_R\left(\bar{\varepsilon}_R < 0\right)$.

When k has an imaginary part then the plane wave will be attenuated in the direction of k_I. This can be seen by considering the exponential term in equation (1.10b) (problem 1.5).

So far only the dispersion relation for plane waves and resulting relationships between the wave vector, $\bar{k}$, index of refraction, n, and dielectric constant $\bar{\varepsilon}_r$ have been discussed. There are several other plane wave properties that will be used in later chapters.

1.5.2 Energy Flux for Plane Electromagnetic Waves

As already shown in obtaining the disperison relation, $\vec{k}$ and $\vec{E}$ are perpendicular. Also, since $\vec{H}$ satisfies the same wave equation as $\vec{E}$, equation (1.17), it is also given by a plane wave solution.

$$\vec{H} = \vec{H}_o \exp\left[j\left(\omega t - \vec{k}\cdot\vec{x}\right)\right] \tag{1.32}$$

Therefore, from equations (1.4) and (1.6) for plane waves in a homogeneous media,

$$\vec{k}\bullet\vec{H} = 0 \tag{1.33}$$

so that $\vec{k}$ and $\vec{H}$ are perpendicular. Also, from equation (1.2)

$$\vec{k}\times\vec{E} = \omega\mu\vec{H} \tag{1.34}$$

and since $\vec{k}\perp\vec{E}$,

$$Y \equiv \frac{H}{E} = \frac{\left|\vec{H}\right|}{\left|\vec{E}\right|} = \frac{k}{\omega\mu} = \frac{n}{c_o\mu} \tag{1.35}$$

The quantity, Y, is called the *optical admittance* of the medium. The three vectors, $\vec{k}$, $\vec{E}$, and $\vec{H}$ form an orthogonal system, where $\vec{E}\times\vec{H}$ is in the direction of $\vec{k}$ (problem 1.6) as shown in Figure 1.2. The magnitude of the electric and magnetic fields varies in the $\vec{k}$ direction. However, their directions are perpendicular to $\vec{k}$. Such a wave is called *transverse*. If the directions are parallel to $\vec{k}$, the wave is called *longitudinal*.

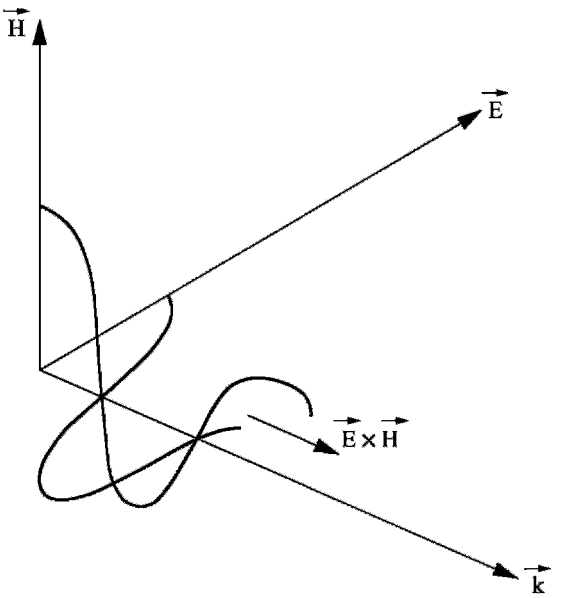

Figure 1.2.—Mutually orthogonal system for plane electromagnetic wave.

The energy flux associated with plane waves is given by the *Poynting vector*, $\vec{S}$.

$$\vec{S} = \vec{E} \times \vec{H} \tag{1.36}$$

As already mentioned, $\vec{k}$ is in the direction of $\vec{E} \times \vec{H}$ so that it will also point in the direction of energy flow. Since $\vec{S}$ is a product, the complex representation of $\vec{E}$ and $\vec{H}$ cannot be used but Re[$\vec{E}$] and Re[$\vec{H}$] must be used in equation (1.36) to calculate Re[$\vec{S}$]. It is the time average of $|\vec{S}|$, which is defined as the intensity, that is used in calculating the optical properties. It should be pointed out that the intensity, $\vec{I}$, defined below is not the same as the radiation intensity, i, that will be used later in radiation transfer theory. The magnitude of $\vec{I}$ (=I) is the energy flux (W/m^2) of the electromagnetic (or radiation) field at a particular frequency, ω (or wavelength, λ). In radiation transfer theory the intensity, i, is the energy flux (W/m^2) per solid angle, Ω, per frequency, ω, (or wavelength, λ)

$$\vec{I} = \frac{\omega}{2\pi} \int_0^{2\pi/\omega} \mathrm{Re}\left[\vec{E}\right] \times \mathrm{Re}\left[\vec{H}\right] dt \qquad W/m^2 \tag{1.37}$$

For a plane wave $\vec{E}$ and $\vec{H}$ are perpendicular and their magnitudes are related by equations (1.34) and (1.35). Therefore, if $\hat{s}$ is the unit vector in the $\hat{k}$ direction equation (1.37) becomes the following.

$$\vec{I} = \frac{\omega}{2\pi}\hat{s}\int_0^{2\pi/\omega} \mathrm{Re}[E]\mathrm{Re}[YE]dt \tag{1.38}$$

It can be shown (problem 1.7) that equation (1.37) becomes the following,

$$\vec{I} = \frac{1}{2}\mathrm{Re}\left[\vec{E}\times\vec{H}^*\right] = \frac{1}{2}\mathrm{Re}\left[EY^*E^*\right]\hat{s} = \frac{1}{2}\frac{n_R}{c_o\mu}EE^*\hat{s} \tag{1.39}$$

where * denotes the complex conjugate and n_R is the real part of n. The last two expressions in equation (1.39) for $\vec{I}$ apply for a single plane wave. However, the first expression applies in general, where $\vec{E}$ and $\vec{H}$ are the total electric and magnetic fields. Thus, if more than a single plane wave exists at some position then $\vec{I}$ must be calculated using the sum of $\vec{E}$ and $\vec{H}$ for the plane waves at that position. Now consider the magnitude of $\vec{I}$ for the case of a plane wave where $\vec{k}$ has real and imaginary parts and is given by equations (1.18), (1.21), and (1.22).

$$\left|\vec{I}\right| = I = \frac{1}{2}\frac{n_R}{c_o\mu}E_oE_o^*\exp\left[-2k_I\hat{s}\cdot\vec{x}\right] \tag{1.40}$$

The quantity $\hat{s}\cdot\vec{x}$ is just the distance along the direction of propagation. Therefore, $(2k_I)^{-1}$ is the distance along the propagation direction for the intensity to be reduced 1/e of its initial value. The quantity $2k_I$ is called the *absorption coefficient,* a. Using equation (1.13), a, can be expressed in terms of the imaginary part of the index of refraction, n_I.

$$a = 2k_I = \frac{2\omega}{c_o}n_I = \frac{4\pi}{\lambda}n_I \qquad \mathrm{cm}^{-1} \tag{1.41}$$

In optics the imaginary part of the index of refraction, which is dimensionless, is called the *extinction coefficient.* However, in radiation transfer theory, the extinction coefficient is the sum of the absorption and scattering coefficients ([13], pg. 454). In this text the radiation transfer definition for the extinction coefficient, which has the dimension cm^{-1} is used.

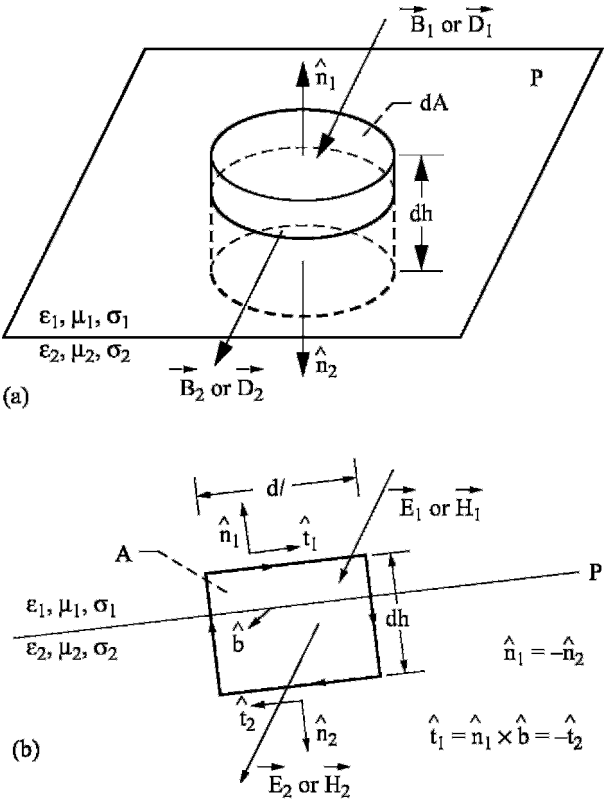

Figure 1.3.—Boundary conditions for Maxwell's equations. (a) Boundary conditions for the normal components of $\vec{B}$ and $\vec{D}$. (b) Boundary conditions for tangential components of $\vec{E}$ and $\vec{H}$.

1.5.3 Boundary Conditions at an Interface

In the solution of Maxwell's equations proper boundary conditions must be applied. Consider an interface, P between the two media, 1 and 2, shown in Figure 1.3(a). At this interface the two Maxwell's equations, $\nabla \cdot \vec{B} = 0$ and $\nabla \cdot \vec{D} = \rho$, must be satisfied. Apply Gauss' theorem to $\nabla \cdot \vec{D} = \rho$ for the cylindrical volume dh dA. Since dA is small $\vec{D}_1$ and $\vec{D}_2$ are constant over the area dA. Also, at the interface dh $\rightarrow 0$.

Therefore, Gauss' theorem yields the following result.

$$\int_V \nabla \cdot \vec{D} dV = \int_S \vec{D} \cdot \hat{n} dS = \left(D_1 \cdot \hat{n}_1 + D_2 \cdot \hat{n}_2\right) dA = \lim_{dh \to 0} \int_V \rho dV \qquad (1.42a)$$

Define a surface charge density, ρ_A (charge/area), as follows.

$$\lim_{dh\to 0}\int_V \rho dV = \rho_A dA \tag{1.42b}$$

Since dA can be made very small and also $\hat{n}_1 = -\hat{n}_2$ equations (1.42) become the following.

$$\left(\vec{D}_1 - \vec{D}_2\right)\bullet n_1 = \rho_A \tag{1.43}$$

Therefore, *at an interface with a surface charge density, ρ_A, the normal component of the electric displacement $\vec{D}\cdot\hat{n}$, changes abruptly by the amount ρ_A.* In the same manner the following result is obtained for the magnetic induction, $\vec{B}$.

$$\left(\vec{B}_1 - \vec{B}_2\right)\bullet\hat{n}_1 = 0 \tag{1.44}$$

Thus *at an interface the normal component, $\vec{B}\cdot\hat{n}$, of the magnetic induction is continuous.*

The two divergence equations, $\nabla\bullet\vec{B} = 0$ and $\nabla\bullet\vec{D} = \rho$, yield boundary conditions for the normal components of $\vec{B}$ and $\vec{D}$. The two curl equations, $\nabla\times\vec{E} = -\dfrac{\partial\vec{B}}{\partial t}$ and $\nabla\times\vec{H} = \vec{J} + \dfrac{\partial\vec{D}}{\partial t}$ will now be shown to yield boundary conditions on the tangential components of $\vec{E}$ and $\vec{H}$. Consider the interface P between media 1 and 2 as shown in Figure 1.3(b). Apply Stokes theorem to $\nabla\times\vec{H} = \vec{J} + \dfrac{\partial\vec{D}}{\partial t}$ for a rectangular area, A, that has sides parallel and perpendicular to the interface and the unit vector $\hat{b}$ perpendicular to dA.

$$\int_A \left(\nabla\times\vec{H}\right)\bullet\hat{b}\,dA = \oint_\ell \vec{H}\bullet d\vec{\ell} = \int_A \left[\vec{J} + \frac{\partial\vec{D}}{\partial t}\right]\bullet\hat{b}\,dA \tag{1.45}$$

Apply equation (1.45) to an infinitesimal dA such that $\vec{H}_1$ and $\vec{H}_2$ are constants over the length $d\ell$ and width dh. Note that $\hat{t}_1 = -\hat{t}_2 = \hat{n}_1\times\hat{b}$.

$$\vec{H}_1 \bullet \hat{t}_1 d\ell - \vec{H}_1 \bullet \hat{n}_1 dh/2 + \vec{H}_2 \bullet \hat{n}_2 dh/2 + \vec{H}_2 \bullet \hat{t}_2 d\ell - \vec{H}_2 \bullet \hat{n}_2 dh/2 + \vec{H}_1 \bullet \hat{n}_1 dh/2 = \hat{b} \bullet \int_A \left[\vec{J} + \frac{\partial \vec{D}}{\partial t} \right] dA$$

$$\left(\vec{H}_1 - \vec{H}_2 \right) \bullet \left(\hat{n}_1 \times \hat{b} \right) d\ell = \hat{b} \bullet \int_A \left[\vec{J} + \frac{\partial \vec{D}}{\partial t} \right] dA$$

$$\hat{b} \bullet \hat{n}_1 \times \left(\vec{H}_1 - \vec{H}_2 \right) d\ell = \hat{b} \bullet \int_A \left[\vec{J} + \frac{\partial \vec{D}}{\partial t} \right] dA \tag{1.46}$$

Now define a surface current density, $\vec{J}_A$, similar to the surface charge density, ρ_A.

$$\lim_{dh \to 0} \int_A \vec{J} \, dA = \vec{J}_A \, d\ell \tag{1.47}$$

Also assuming that $\frac{\partial \vec{D}}{\partial t}$ remains finite as $dh \to 0$, equation (1.46) yields the following results.

$$\hat{n}_1 \times \left(\vec{H}_1 - \vec{H}_2 \right) = \vec{J}_A \tag{1.48}$$

Thus *at an interface where a surface current density, $\vec{J}_A$, exists, the tangential magnetic field, $\vec{n} \times \vec{H}$, changes abruptly by the amount* $\vec{J}_A$. Similarly, from $\nabla \times \vec{E} = -\frac{\partial \vec{B}}{dt}$ the following boundary condition on the tangential electric field is obtained.

$$\hat{n}_1 \times \left(\vec{E}_1 - \vec{E}_2 \right) = 0 \tag{1.49}$$

Therefore, *at an interface the tangential electric field, $\hat{n} \times \vec{E}$, is continuous.*

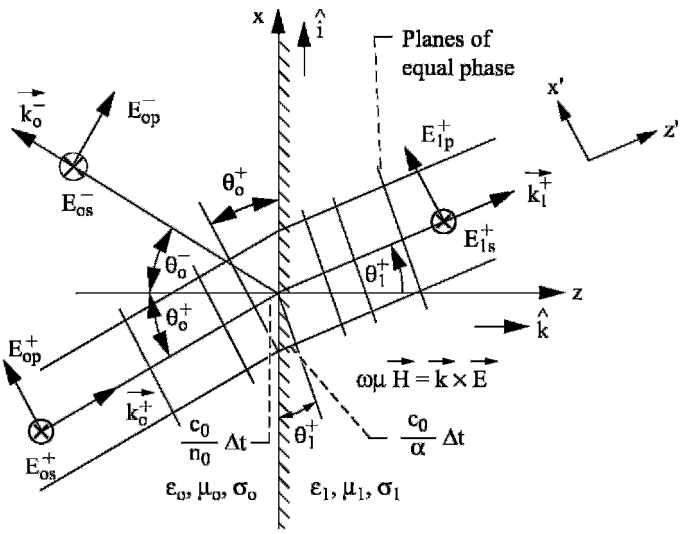

Figure 1.4.—Reflection and refraction of a plane wave at the interface between two media of different optical constants, ε_o, μ_o, σ_o and ε_1, μ_1, σ_1. The symbol ⊗ denotes a vector pointing out of the page which is the + y direction designated by the unit vector, $\hat{j}$.

1.5.4 The Law of Reflection and Snell's Law of Refraction

Using the boundary conditions just discussed, consider what happens when a plane wave falls on the interface between two media of different optical constants, ε, μ, and σ. When a plane wave in media o with wave vector, $\vec{k}_o^+$, is incident on an interface, it is split into two waves: a transmitted wave in media 1 with wave vector, $\vec{k}_1^+$, and reflected wave in media o with wave vector, $\vec{k}_o^-$. This is illustrated in Figure 1.4. The interface is located in the xy plane at z = 0. For a plane wave the spatial and time variation depends only upon the phase factor, $\omega t - \vec{r} \bullet \vec{k}$. Therefore, to satisfy any of the boundary conditions on $\vec{E}$ or $\vec{H}$ at z = 0, the phase factors for the incident, reflected and transmitted waves must be equal.

$$\omega t - \vec{r} \bullet \vec{k}_o^+ = \omega t - \vec{r} \bullet \vec{k}_o^- = \omega t - \vec{r} \bullet \vec{k}_1^+ \tag{1.50}$$

Therefore, at the boundary $\vec{r}$ = (x,y,0) the following is obtained.

$$x k_{ox}^+ + y k_{oy}^+ = x k_{ox}^- + y k_{oy}^- = x k_{1x}^+ + y k_{1y}^+ \tag{1.51}$$

The only way this can be satisfied for all x and y is the following.

$$k_{ox}^{+} = k_{ox}^{-} = k_{1x}^{+}, \quad k_{oy}^{+} = k_{oy}^{-} = k_{1y}^{+} \tag{1.52}$$

Now choose the normal to the interface to be in the -z direction so that the normal unit vector is $-\hat{k}$. Therefore, because equation (1.52) applies,

$$\hat{k} \times \vec{k}_o^{+} = \hat{k} \times \vec{k}_o^{-} = \hat{k} \times \vec{k}_1^{+} \tag{1.53}$$

Therefore, *all three wave vectors and the normal to the interface lie in the same plane, which is called the plane of incidence.* As shown in Figure 1.4, the xz plane is the plane of incidence. Therefore, using the first expression in equation (1.52), the following is obtained.

$$k_{ox}^{+} = k_o^{+} \sin\theta_o^{+} = k_o^{-} \sin\theta_o^{-} = k_1^{+} \sin\theta_1^{+} \tag{1.54}$$

Since $\vec{k}_o^{-}$ and $\vec{k}_o^{+}$ are both in medium o, their magnitudes are the same, $k_o^{+} = k_o^{-} = k_o$ so that equation (1.54) yields the following result,

$$\theta_o^{+} = \theta_o^{-} \tag{1.55}$$

which is *the law of reflection*, where θ_o^{-} is *the angle of reflection*. Also, since $k = \frac{\omega}{c_o} n$, equation (1.13), the following is also obtained from equation (1.54).

$$n_o \sin\theta_o^{+} = n_1 \sin\theta_1^{+} \tag{1.56}$$

This is *Snell's Law for refraction*, where θ_1^{+} is the *refraction angle*. If $n_o \le n_1$, (medium o is *optically less dense* than medium 1), then Snell's Law is satisfied for all possible incident angles ($0 \le \theta_o^{+} \le \pi/2$). However, if medium o is optically more dense than medium 1 ($n_o > n_1$), then the largest real value of θ_o^{+} occurs when $\theta_1^{+} = \pi/2$. This angle of incidence is called *the critical angle*,

$$\sin\theta_{ocr}^{+} = n_1/n_o \qquad\qquad n_o > n_1 \tag{1.57}$$

For $\theta_o^+ > \theta_{ocr}^+$ total reflection occurs at the interface and there is no refracted wave. The angle of refraction, θ_1^+, becomes an imaginary number in this case.

For two pure dielectric media ($\sigma = 0$), the magnitude of the wave vector, k, must be real in both media. However, as stated earlier in Section 1.5.1, the wave vector can have an imaginary unit vector, $\hat{s}$, where $\vec{k} = k\hat{s}$. Consider the wave vector, $\vec{k}_1^+$, in medium 1. From Figure 1.4 the following applies.

$$\vec{k}_1^+ = k_1\hat{s}_1 = k_1\left[\sin\theta_1^+\hat{i} + \cos\theta_1^+\hat{k}\right] \tag{1.58}$$

Using Snell's law, equation (1.56), equation (1.13), and the identity $\cos\theta_1^+ = \pm\sqrt{1-\sin^2\theta_1^+}$ when $\theta_o^+ > \theta_{ocr}^+$, $\left(\frac{n_1}{n_o} < 1\right)$, in equation (1.58) yields the following result.

$$\vec{k}_1^+ = \frac{\omega}{c_o}n_o\left[\sin\theta_o^+\hat{i} \pm j\sqrt{\sin\theta_o^+ - \left(\frac{n_1}{n_o}\right)^2}\,\hat{k}\right] = \frac{\omega}{c_o}n_o\hat{s}_1 \qquad \text{for } \theta_o^+ > \theta_{ocr}^+ \tag{1.59}$$

The unit vector, $\hat{s}_1$, has a purely imaginary z component. As a result, the phase factor in medium 1 is the following.

$$j\left[\omega t - \vec{k}_1 \bullet \vec{r}\right] = j\omega\left[t - \frac{n_o}{c_o}x\sin\theta_o^+\right] \mp \frac{\omega}{c_o}n_o z\sqrt{\sin^2\theta_o^+ - \left(\frac{n_1}{n_o}\right)^2} \tag{1.60}$$

Thus, equation (1.60) says that in the refracted medium 1 for $\theta_o^+ > \theta_{ocr}^+$, the electric and magnetic fields are described by a plane wave that propagates along the interface at z = 0 and either decays or grows in the z direction. Obviously, since there are no sources (current or charge) at z = 0 for $\vec{E}$ and $\vec{H}$, the negative sign must apply for the z dependence and $\vec{E}$ and $\vec{H}$ decay in the z direction. For $\theta_+^o > \theta_{+cr}^o$ ($n_o > n_1$) the incident wave is totally reflected. There is no energy transfer into the refracted medium for this case.

Now consider the case where media 1 in Figure 1.4 has finite conductivity ($\sigma, \neq 0$) so that absorption occurs and the index of refraction, n, has an imaginary part. Therefore, in order to satisfy Snell's law, equation (1.56), $\sin\theta_1^+$ must be complex and the refraction angle can no longer be obtained from Snell's law. Referring to Figure

1.4, the wave propagating from media o into media 1 is refracted with angle θ_1^+ to the z' direction and decays in the z direction. After refraction, the planes of equal phase are still normal to the direction of propagation and they propagate with a phase velocity, $\frac{c_o}{\alpha}$. This phase velocity will be related to the real and imaginary parts of the index of refraction, $n_1=n_{1R}-jn_{1I}$. The attenuation of the wave is in the z direction so that the planes of equal amplitude are perpendicular to the z axis. By analogy with equation (1.10b), where $k=\frac{\omega}{c_o}n$ has an imaginary part, the electric field of a p-polarized wave in media 1 is the following,

$$E_{x'}=E_{ox'}\exp\left[j\left(\omega t-\frac{\omega}{c_o}\alpha z'\right)\right]\exp\left(-\frac{\omega}{c_o}\beta z\right) \tag{1.61}$$

where β is analogous to $2n_I$ in the absorption coefficient given by equation (1.41) and will be related to n_1. The electric field, $E_{x'}$, must satisfy the wave equation (1.17).

$$\frac{\partial^2 E_{x'}}{\partial x'}+\frac{\partial^2 E_{x'}}{\partial z'}-\mu_1\varepsilon_1\frac{\partial^2 E_{x'}}{\partial t^2}-\mu_1\sigma_1\frac{\partial E_{x'}}{\partial t}=0 \tag{1.62}$$

Referring to Figure 1.4, $z=z'\cos\theta_1^+$ so that equation (1.61) becomes the following.

$$E_{x'}=E_{ox'}\exp(j\omega t)\exp\left[-z'\left(\frac{j\omega\alpha}{c_\infty}+\frac{\omega\beta\cos\theta_1^+}{c_\infty}\right)\right]\exp\left(x'\frac{\omega\beta\cos\theta_1^+}{c_\infty}\right) \tag{1.63}$$

Substituting equation (1.63) into (1.62) yields the following.

$$\left(\frac{\omega\beta\cos\theta_1^+}{c_\infty}\right)^2+\left(\frac{j\omega\alpha}{c_\infty}+\frac{\omega\beta\cos\theta_1^+}{c_\infty}\right)^2=-\mu_1\varepsilon_1\omega^2+\mu_1\sigma_1 j\omega \tag{1.64}$$

From equations (1.19) to (1.22), the following is obtained.

$$\mu_1\varepsilon_1\omega^2=k_{1R}^2-k_{1I}^2=\frac{\omega^2}{c_o^2}\left(n_{1R}^2-n_{1I}^2\right) \tag{1.65}$$

$$\mu_1\sigma_1\omega^2 = 2k_{1R}k_{1I} = \frac{\omega^2}{c_o^2}n_{1R} - n_{1I} \tag{1.66}$$

Therefore, equating real and imaginary parts in equation (1.64) and using equations (1.65) and (1.66) yield the following results.

$$\alpha^2 - \beta^2 = n_{1R}^2 - n_{1I}^2 \tag{1.67}$$

$$\alpha\beta\cos\theta_1^+ = n_{1R}n_{1I} \tag{1.68}$$

There are now two equations for the three unknown quantities α, β, and θ_1^+. A third equation is obtained from the phase velocity. For the time interval, Δt, the wave front in media o travels a distance $\frac{c_o}{n_o}\Delta t$ while the wave front in media 1 travels a distance $\frac{c_o}{\alpha}\Delta t$. Therefore, referring to Figure 1.4 the following is obtained.

$$\frac{\frac{c_o}{n_o}\Delta t}{\sin\theta_o^+} = \frac{\frac{c_o}{\alpha}\Delta t}{\sin\theta_1^+}$$

So that

$$\sin\theta_1^+ = \frac{n_o}{\alpha}\sin\theta_o^+ \tag{1.69}$$

Equations (1.67) to (1.69) can now be solved for α, β, θ_1^+ in terms of n_{1R}, n_{1I}, and θ_o^+.

Notice that if $\alpha > n_o$, there is a *critical refraction angle*, θ_{1cr}^+, which occurs when $\theta_o^+ = \frac{\pi}{2}$.

$$\sin\theta_{1cr}^+ = \frac{n_o}{\alpha_{cr}} \qquad \theta_o^+ = \frac{\pi}{2}, \alpha_{cr} > n_o \tag{1.70}$$

Combining equations (1.67) to (1.69) leads to the following solution for α^2 and β^2.

$$\alpha^2 = \frac{1}{2}\left[n_o^2 \sin^2\theta_o^+ + n_{1R}^2 - n_{1I}^2 + \sqrt{\left(n_{1R}^2 + n_{1I}^2\right)^2 + n_o^2 \sin^2\theta_o^+ \left[n_o^2 \sin^2\theta_o^+ - 2\left(n_{1R}^2 - n_{1I}^2\right)\right]}\right] \quad (1.71)$$

$$\beta^2 = \frac{1}{2}\left[n_o^2 \sin^2\theta_o^+ - n_{1R}^2 + n_{1I}^2 + \sqrt{\left(n_{1R}^2 + n_{1I}^2\right)^2 + n_o^2 \sin^2\theta_o^+ \left[n_o^2 \sin^2\theta_o^+ - 2\left(n_{1R}^2 - n_{1I}^2\right)\right]}\right] \quad (1.72)$$

Thus for normal incidence $\theta_o^+ = 0$, $\alpha = n_{1R}$ and $\beta = n_{1I}$ and the wave phase velocity, $\frac{c_o}{\alpha}$ are the same as that of a pure dielectric. However, for $\theta_o^+ \neq 0$ the phase velocity depends upon θ_o^+, as well as n_{1R} and n_{1I}.

At wavelengths beyond the visible, $n_{1R}^2 \gg n_o^2$ for metals. In that case, the radical term in equations (1.71) and (1.72) can be expanded to obtain the results: $\alpha \approx n_{1R}$ and $\beta \approx n_{1I}$. Therefore, the wave propagates with the phase velocity $\frac{c_o}{n_{1R}}$ and is attenuated in the z direction with an absorption coefficient $\frac{2\omega}{c_o} n_{1I} = \frac{4\pi}{\lambda_o} n_{1I}$. Also, for $n_{1R} \gg n_o$ equation (1.69) yields $\sin\theta_1^+ \approx 0$ so that the angle of refraction, $\theta_1^+ \approx 0$. Therefore, the angle of incidence for emitted radiation from a metal is limited to nearly normal incidence.

1.5.5 Reflectivity and Transmissivity at an Interface

Now consider the relations between the electric and magnetic fields of the incident, reflected and transmitted waves at an interface. Referring to Figure 1.4, split the electric fields, $\vec{E}$, into a component parallel to the plane of incidence, E_p, and component perpendicular to the plane of incidence, E_s. If $\vec{E}$ has only a E_p component, then $\vec{E}$ is said to have *p-polarization or parallel polarization*, E_{op}^+. If $\vec{E}$ has only a E_s component, then $\vec{E}$ is said to have *s-polarization or perpendicular polarization*, E_{os}^+ The subscripts denote the medium and the polarization while the superscript denotes whether the wave is propagating in the +z direction or the –z direction. Once $\vec{E}$ is known, $\vec{H}$ is obtained using equation (1.34). Referring to Figure 1.4, the components of the electric and magnetic fields for the incident wave are the following,

$$E_{ox}^+ = E_{op}^+ \cos\theta_o^+ e^{-j\tau_o^+}, \quad E_{oy}^+ = E_{os}^+ e^{-j\tau_o^+}, \quad E_{oz}^+ = -E_{op}^+ \sin\theta_o^+ e^{-j\tau_o^+} \quad (1.73)$$

$$\omega\mu_o H_{ox}^+ = -k_o E_{os}^+ \cos\theta_o^+ e^{-j\tau_o^+}, \quad \omega\mu_o H_{oy}^+ = k_o E_{op}^+ e^{-j\tau_o^+}, \quad \omega\mu_o H_{oz}^+ = k_o E_{os}^+ \sin\theta_o^+ e^{-j\tau_o^+} \quad (1.74)$$

where the phase factor for the incident wave is the following.

$$\tau_o^+ = \omega t - \vec{k}_o^+ \bullet \vec{r} = \omega t - k_o \left(x \sin\theta_o^+ + z \cos\theta_o^+ \right) \tag{1.75}$$

For the reflected wave the following is obtained, remembering that $\theta_o^- = \theta_o^+$.

$$E_{ox}^- = E_{op}^- \cos\theta_o^+ e^{-j\tau_o^-}, \quad E_{oy}^- = E_{os}^- e^{-j\tau_o^-}, \quad E_{oz}^- = E_{op}^- \sin\theta_o^+ e^{-j\tau_o^-} \tag{1.76}$$

$$\omega\mu_o H_{ox}^- = k_o E_{os}^- \cos\theta_o^+ e^{-j\tau_o^-}, \quad \omega\mu_o H_{oy}^- = -k_o E_{op}^- e^{-j\tau_o^-}, \quad \omega\mu_o H_{oz}^- = k_o E_{os}^- \sin\theta_o^+ e^{-j\tau_o^-} \tag{1.77}$$

The phase factor for the reflected wave is the following.

$$\tau_o^- = \omega t - \vec{k}_o^- \bullet \vec{r} = \omega t - k_o \left(x \sin\theta_o^+ - z \cos\theta_o^+ \right) \tag{1.78}$$

Finally, for the refracted wave the following is obtained.

$$E_{1x}^+ = E_{1p}^+ \cos\theta_1^+ e^{-j\tau_1^+}, \quad E_{1y}^+ = E_{1s}^+ e^{-j\tau_1^+}, \quad E_{1z} = -E_{1p}^+ \sin\theta_1^+ e^{-j\tau_1^+} \tag{1.79}$$

$$\omega\mu_1 H_{1x}^+ = -k_1 E_{1s}^+ \cos\theta_1^+ e^{-j\tau_1^+}, \quad \omega\mu_1 H_{1y}^+ = k_1 E_{1p}^+ e^{-j\tau_1^+}, \quad \omega\mu_1 H_{1z}^+ = k_1 E_{1s}^+ \sin\theta_1^+ e^{-j\tau_1^+} \tag{1.80}$$

$$\tau_1^+ = \omega t - \vec{k}_1 \bullet \vec{r} = \omega t - k_1 \left(x \sin\theta_1^+ + z \cos\theta_1^+ \right) \tag{1.81}$$

Now apply the boundary conditions for $\vec{E}$ and $\vec{H}$ at z = 0. These will yield relations between the incident, reflected and refracted $\vec{E}$ and $\vec{H}$. If no surface current exists, $\vec{J}_A = 0$, the boundary conditions, equations (1.48) and (1.49), demand that the tangential components of $\vec{E}$ and $\vec{H}$ be continuous. Since the law of reflectance and Snell's law require that $\tau_o^-(x, y, 0) = \tau_o^+(x, y, 0) = \tau_1^+(x, y, 0)$, and $\theta_o^+ = \theta_o^-$, the following results are obtained.

$$\left(E_{op}^{+}+E_{op}^{-}\right)\cos\theta_{o}^{+}=E_{1p}^{+}\cos\theta_{1}^{+}$$

$$E_{os}^{+}+E_{os}^{-}=E_{1s}^{+}$$

$$\frac{n_o}{\mu_o}\left(E_{os}^{+}-E_{os}^{-}\right)\cos\theta_{o}^{+}=\frac{n_1}{\mu_1}E_{1s}^{+}\cos\theta_{1}^{+} \qquad (1.82)$$

$$\frac{n_o}{\mu_o}\left(E_{op}^{+}-E_{op}^{-}\right)=\frac{n_1}{\mu_1}E_{1p}^{+}$$

In equations (1.82), $k=\frac{\omega}{c_o}n$ has been used to replace k.

Notice that equations (1.82) fall into two groups: one that contains only the p or parallel components and the other containing only the s or perpendicular components. Thus, the two kinds of waves, one that we say is *p-polarized* and the other being *s-polarized*, are independent of each other. Solving equations (1.82) for the reflected and refracted fields in terms of the incident field, result in the following relations.

$$\left.\begin{aligned} t_p &\equiv \frac{E_{1p}^{+}}{E_{op}^{+}}=\frac{2\left(\frac{n_o}{\mu_o}\right)\cos\theta_{o}^{+}}{\left(\frac{n_o}{\mu_o}\right)\cos\theta_{1}^{+}+\left(\frac{n_1}{\mu_1}\right)\cos\theta_{o}^{+}} \\ r_p &\equiv \frac{E_{op}^{-}}{E_{op}^{+}}=\frac{\left(\frac{n_o}{\mu_o}\right)\cos\theta_{1}^{+}-\left(\frac{n_1}{\mu_1}\right)\cos\theta_{o}^{+}}{\left(\frac{n_o}{\mu_o}\right)\cos\theta_{1}^{+}+\left(\frac{n_1}{\mu_1}\right)\cos\theta_{o}^{+}} \end{aligned}\right\} \qquad (1.83)$$

$$\left.\begin{aligned} t_s &\equiv \frac{E_{1s}^{+}}{E_{os}^{+}}=\frac{2\left(\frac{n_o}{\mu_o}\right)\cos\theta_{o}^{+}}{\left(\frac{n_o}{\mu_o}\right)\cos\theta_{o}^{+}+\left(\frac{n_1}{\mu_1}\right)\cos\theta_{1}^{+}} \\ r_s &\equiv \frac{E_{os}^{-}}{E_{os}^{+}}=\frac{\left(\frac{n_o}{\mu_o}\right)\cos\theta_{o}^{+}-\left(\frac{n_1}{\mu_1}\right)\cos\theta_{1}^{+}}{\left(\frac{n_o}{\mu_o}\right)\cos\theta_{o}^{+}+\left(\frac{n_1}{\mu_1}\right)\cos\theta_{1}^{+}} \end{aligned}\right\} \qquad (1.84)$$

Equations (1.83) and (1.84) are called *Fresnel formulae*, having first been derived by Fresnel [14] in 1823. The reflection coefficient r_p given in equation (1.83) differs in sign from that given in some texts (for example [10] and [15]). In the case of [10] the sign difference results because in [10] the angle of reflection, θ_o^-, is measured from the +z axis rather than the –z axis as in Figure 1.4. In reference 15 the direction chosen for E_{op}^- is opposite to that in Figure 1.4, thus resulting in the sign difference. Since the definition of θ_o^- and the direction of E_{op}^- is arbitrary, this result is not surprising. However, when reflectivity and transmissivity are calculated with either definition of θ_o^- and E_{op}^-, the results will agree, as they must if all definitions are allowable.

Using Snell's law, the *reflection coefficients* r_s and r_p and the *transmission coefficients* t_s and t_p can be rewritten in terms of θ_o^+ and θ_1^+ (problem 1.9). In that case it is easy to see that for dielectric materials ($\sigma = 0$, $n_I = 0$, $\mu_o = \mu_1$) where $n_o < n_1$ that $r_s < 0$. In other words, $\vec{E}_{os}^-$ and $\vec{E}_{os}^+$ point in opposite directions and their phases differ by π.

For normal incidence $\left(\theta_o^+ = \theta_1^+ = 0\right)$ the transmission coefficients, t_s and t_p are equal as are the reflection coefficients, r_s and r_p.

$$\left.\begin{aligned} t_s = t_p &= \frac{2\dfrac{n_o}{\mu_o}}{\dfrac{n_o}{\mu_o}+\dfrac{n_1}{\mu_1}} \\ r_s = r_p &= -\frac{\dfrac{n_1}{\mu_1}-\dfrac{n_o}{\mu_o}}{\dfrac{n_o}{\mu_o}+\dfrac{n_1}{\mu_1}} \end{aligned}\right\} \theta_o^+ = \theta_1^+ = 0 \qquad (1.85)$$

For nonmagnetic materials ($\mu_o = \mu_1$) the μ factors in equations (1.83) to (1.85) disappear.

The Fresnel formulae relate the refracted and reflected fields to the incident field. However, reflectivity and transmissivity refer to reflected and transmitted energy. To calculate reflectivity and transmissivity at an interface the energy flux (time average of the Poynting vector), $\vec{I}$, as given by equation (1.39) must be used.

$$\vec{I} = \frac{1}{2}\mathrm{Re}\left[\vec{E}\times\vec{H}^*\right] \qquad (1.86)$$

The electric field in equation (1.86) is the total electric field. In other words, on the incident side of the interface, it is the sum of the incident wave and reflected wave electric fields. On the transmitted side of the interface, it is the transmitted wave electric field only. If there is no surface current or surface charge, then the incident intensity, I_o, must equal the transmitted intensity, I_1. The incident intensity is the z component of $\vec{I}$, which consists of the x and y components of $\vec{E}$ and $\vec{H}^*$,

$$I_o = \frac{1}{2}\mathrm{Re}\left[E_{xin}H^*_{yin} - E_{yin}H^*_{xin}\right] \quad \text{at} \quad z = 0 \tag{1.87}$$

where the x and y components of $\vec{E}_{in}$ and $\vec{H}_{in}$ are the sum of the x and y components of the incident and reflected electric and magnetic fields given by equations (1.73), (1.74), (1.76), and (1.77). Therefore, equation (1.87) becomes the following.

$$I_o = \frac{1}{2}\frac{n_{oR}}{c_o\mu_o}\left[E^+_{op}E^{+*}_{op}\left(1 - r_p r^*_p + \frac{2n_{oI}}{n_{oR}}\mathrm{Im}\left[r_p\right]\right) + E^+_{os}E^{+*}_{os}\left(1 - r_s r^*_s + \frac{2n_{oI}}{n_{oR}}\mathrm{Im}\left[r_s\right]\right)\right]\cos\theta^+_o \tag{1.88}$$

If equation (1.86) is applied to the incident and reflected waves at z = 0 separately the following results are obtained.

$$I^+_o = \frac{1}{2}\mathrm{Re}\left[E^+_{ox}H^{+*}_{oy} - E^+_{oy}H^{+*}_{ox}\right] = \frac{1}{2}\frac{n_{oR}}{c_o\mu_o}\left[E^+_{op}E^{+*}_{op} + E^+_{os}E^{+*}_{os}\right]\cos\theta^+_o \tag{1.89}$$

$$I^-_o = \frac{1}{2}\mathrm{Re}\left[E^-_{ox}H^{-*}_{oy} - E^-_{oy}H^{-*}_{ox}\right] = \frac{1}{2}\frac{n_{oR}}{c_o\mu_o}\left[r_p r^*_p E^+_{op}E^{+*}_{op} + r_s r^*_s E^-_{os}E^{-*}_{os}\right]\cos\theta^+_o \tag{1.90}$$

Intuitively, it would seem that $I_o = I^+_o - I^-_o$. That is, the intensity at z = 0 should be the difference between the intensity associated with the incident wave and the reflected wave. However, from equations (1.88) to (1.90) the following is obtained.

$$I^+_o - I^-_o = I_o - \frac{n_{oI}}{c_o\mu_o}\cos\theta^+_o\left[E^+_{op}E^{+*}_{op}\,\mathrm{Im}\left[r_p\right] + E^+_{os}E^{+*}_{os}\,\mathrm{Im}\left[r_s\right]\right] \tag{1.91}$$

Thus, only when the incident and reflected waves are in a non-absorptive, dielectric medium ($n_{oI} = 0$) does $I_o = I^+_o - I^-_o$. For the general case it is incorrect to split the intensity into incident and reflected parts. A coupling between the incident and

reflected waves occurs when the incident medium is absorptive ($n_{oI} \neq 0$) that produces the term proportional to n_{oI} in equations (1.88) and (1.91).

Since only a single transmitted wave exists, the transmitted intensity is given by the following equation.

$$I_1 = \frac{1}{2}\mathrm{Re}\left[E_{1x}^{+}H_{1y}^{+*} - E_{1y}^{+}H_{1x}^{+*}\right] \quad \text{at} \quad z = 0 \tag{1.92}$$

Using equations (1.79), (1.80), (1.83), and (1.84) this becomes the following:

$$I_1 = \frac{1}{2}\frac{n_{1R}}{c_o\mu_1}\left[E_{op}^{+}E_{op}^{+*}t_p t_p^{*} + E_{os}^{+}E_{os}^{+*}t_s t_s^{*}\right] \quad \cos\theta_1^{+} \tag{1.93}$$

And since $I_o = I_1$, equation (1.91) yields the following.

$$I_o^{+} - I_o^{-} + \frac{n_{oI}}{c_o\mu_o}\left[E_{op}^{+}E_{op}^{+*}\,\mathrm{Im}\left[r_p\right] + E_{os}^{+}E_{os}^{+*}\,\mathrm{Im}\left[r_s\right]\right] \quad \cos\theta_o^{+} = I_1 \tag{1.94}$$

The *reflectivity*, R, and *transmissivity*, T, are defined as follows.

$$R \equiv \frac{I_o^{-}}{I_o^{+}} = \frac{E_{op}^{+}E_{op}^{+*}r_p r_p^{*} + E_{os}^{+}E_{os}^{+}r_s r_s^{*}}{E_{op}^{+}E_{op}^{+*} + E_{os}^{+}E_{os}^{+}} \tag{1.95}$$

$$T \equiv \frac{I_1}{I_o^{+}} = \frac{\mu_o n_{1R}\cos\theta_1^{+}}{\mu_1 n_{oR}\cos\theta} \frac{E_{op}^{+}E_{op}^{+*}t_p t_p^{*} + E_{os}^{+}E_{os}^{+}t_s t_s^{*}}{E_{op}^{+}E_{op}^{+*} + E_{os}^{+}E_{os}^{+}} \tag{1.96}$$

Where equations (1.89), (1.90), and (1.93) have been used for I_o^{+}, I_o^{-} and I_1. If only p polarized waves exist, then

$$R_p = r_p r_p^{*}, \quad T_p = \frac{\mu_o n_{1R}}{\mu_1 n_{oR}}\frac{\cos\theta_1^{+}}{\cos\theta_o^{+}} t_p t_p^{*} \tag{1.97}$$

Similarly, if only s polarized waves exist, the following results.

$$R_s = r_s r_s^{*}, \quad T_s = \frac{\mu_o n_{1R}}{\mu_1 n_{oR}}\frac{\cos\theta_1^{+}}{\cos\theta_o^{+}} t_s t_s^{*} \tag{1.98}$$

Using equations (1.96) and (1.97) in (1.94) yields the following.

$$R + T = 1 + \frac{n_{oI}}{c_o \mu_o}\left[E_{op}^{+} E_{op}^{+*}\, \mathrm{Im}\left[r_p \right] + E_{os}^{+} E_{os}^{+*}\, \mathrm{Im}\left[r_s \right] \right] \quad \cos\theta_o^{+} \tag{1.99}$$

This result is an expression for the conservation of energy $I_o = I_1$, at an interface. Intuitively, it is expected that R + T = 1 to express energy conservation at an interface. However, only if $n_{oI} = 0$ does R + T = 1 apply.

Now let α_o be the angle that the electric field, $\vec{E}_o^{+}$, of the incident wave makes with the plane of incidence. Therefore,

$$E_{op}^{+} = E_o^{+} \cos\alpha_o, \quad E_{os}^{+} = E_o^{+} \sin\alpha_o \tag{1.100}$$

Substituting equation (1.100) in (1.95) and (1.96) yields the following results for reflectivity and transmissivity.

$$R = r_p r_p^{*} \cos^2\alpha_o + r_s r_s^{*} \sin^2\alpha_o = R_p \cos\alpha_o^2 + R_s \sin^2\alpha_o \tag{1.101}$$

$$T = \frac{n_{1R}}{n_{oR}} \frac{\mu_o}{\mu_1}\left[t_p t_p^{*} \cos^2\alpha_o + t_s t_s^{*} \sin^2\alpha_o \right] \frac{\cos\theta_1^{+}}{\cos\theta_o^{+}} = T_p \cos^2\alpha_o + T_s \sin^2\alpha_o \tag{1.102}$$

Thus R and T are functions of the optical properties, as well as the incident angle and the angle α_o. In the case of a TPV system, the radiation originates from hot surfaces. For this so-called natural light [10], the direction of $\vec{E}$ is random. Therefore, the reflectivity and transmissivity that describe this situation are obtained by averaging R and T over all possible α_o ($0 \le \alpha_o \le \pi$). Since $\frac{1}{\pi}\int_o^{\pi} \sin^2\alpha_o d\alpha_o = \frac{1}{\pi}\int_o^{\pi} \cos^2\alpha_o d\alpha_o = \frac{1}{2}$, the following result is obtained for reflectivity, $\overline{R}$, and transmissivity, $\overline{T}$.

$$\overline{R} = \frac{1}{2}\left(r_p r_p^{*} + r_s r_s^{*} \right) = \frac{1}{2}\left(R_p + R_s \right) \tag{1.103}$$

$$\overline{T} = \frac{1}{2}\frac{n_{1R}}{n_{oR}}\frac{\mu_o}{\mu_1}\left[t_p t_p^{*} + t_s t_s^{*} \right] = \frac{1}{2}\left(T_p + T_s \right) \tag{1.104}$$

The reflectivity and transmissivity are just the average values of the p and s polarized reflectivities and transmissivities.

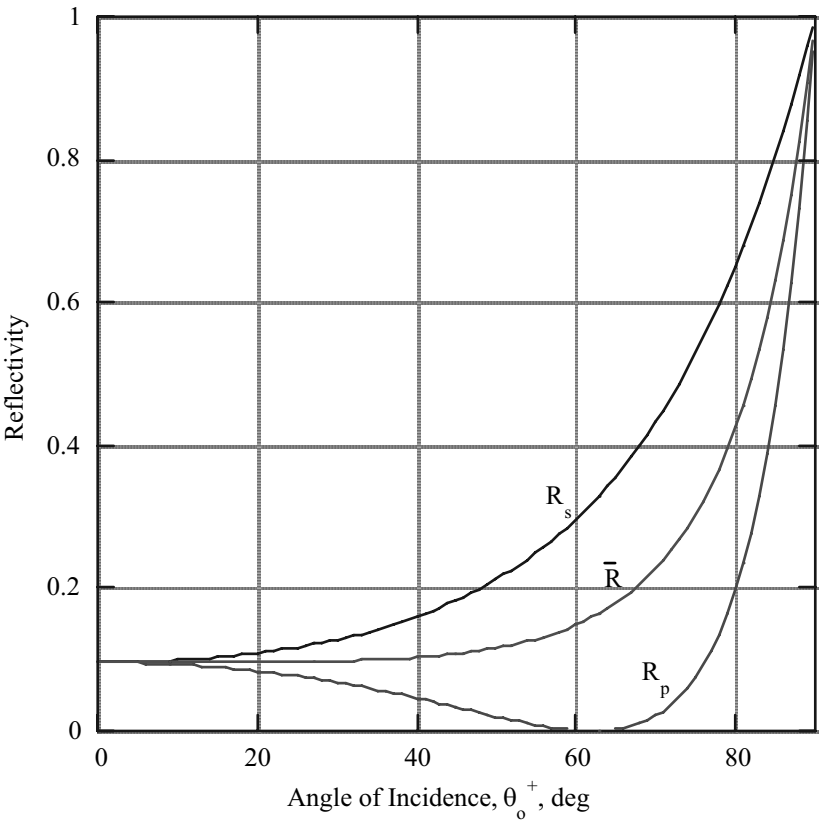

Figure 1.5 - Reflectivities at the interface between vacuum(n_o=1.) and a dielectric with index of refraction, n_1=1.9. R_p is reflectivity for p polarization, R_s is refectivity for s polarization and $\overline{R}$ is average reflectivity.

In Figure 1.5 the reflectivities, R_p, R_s, and $\overline{R}$ are shown as a function of the angle of incidence, θ_o^+, for the interface between a vacuum ($n_o = n_{oR} = 1$) and a pure dielectric ($n_{1I} = 0$) with $n_1 = n_{1R} = 1.9$. Some of the selective emitter materials discussed in Chapter 3 can be characterized by an index of refraction of approximately 1.9. As Figure 1.5 shows, the reflectivity, $\overline{R}$, is nearly constant for $\theta_o^+ \le 60^\circ$. Only for large angles of incidence does $\overline{R}$ change rapidly. Therefore, it is a reasonable approximation to assume $\overline{R}$ is independent of θ_o^+ and has the value for normal incidence ($\theta_o^+ = 0$). This approximation is used in later chapters. Notice also in Figure

1.5 that p-polarization reflectivity, R_p, vanishes at $\theta_o^+ = 62^\circ$. This angle of incidence is called the *Brewster angle* and is given by the following expression (problem 1.9).

$$\tan\theta_o^+ = \frac{n_1}{n_o}\frac{\mu_o}{\mu_1} \tag{1.105}$$

At normal incidence the reflectivity and transmissivity are the following.

$$R_p = R_s = \overline{R} = \left[\frac{\frac{n_o}{\mu_o} - \frac{n_1}{\mu_1}}{\frac{n_o}{\mu_o} + \frac{n_1}{\mu_1}}\right]\left[\frac{\frac{n_o}{\mu_o} - \frac{n_1}{\mu_1}}{\frac{n_o}{\mu_o} + \frac{n_1}{\mu_1}}\right]^* \tag{1.106}$$

$$\theta_o^+ = \theta_1^+ = 0$$

$$T_s = T_p = \overline{T} = \frac{\mu_1}{\mu_o}\frac{n_{1R}}{n_{oR}}\left[\frac{\frac{n_o}{\mu_o}}{\frac{n_o}{\mu_o} + \frac{n_1}{\mu_1}}\right]\left[\frac{\frac{n_o}{\mu_o}}{\frac{n_o}{\mu_o} + \frac{n_1}{\mu_1}}\right]^* \tag{1.107}$$

Nonmagnetic materials ($\mu_o = \mu_1$) are used in TPV systems so that the μ terms disappear. In that case equations (1.85), (1.106), and (1.107) become the following.

$$r_s = r_p = \frac{n_o - n_1}{n_o + n_1} = \frac{(n_{oR} - n_{1R}) + i(n_{oI} - n_{1I})}{(n_{oR} + n_{1R}) + i(n_{oI} + n_{1I})} \tag{1.108}$$

$$t_s = t_p = \frac{2n_o}{n_o + n_1} = \frac{2(n_{oR} + i\,n_{oI})}{(n_{oR} + n_{1R}) + i(n_{oI} + n_{1I})} \tag{1.109}$$

$\theta_o^+ = \theta_1^+ = 0$

$\mu_o = \mu_1$

$$R_p = R_s = \overline{R} = \frac{(n_{oR} - n_{1R})^2 + (n_{oI} - n_{1I})^2}{(n_{oR} + n_{1R})^2 + (n_{oI} + n_{1I})^2} \tag{1.110}$$

$$T_p = T_s = \overline{T} = \frac{4n_{1R}(n_{oR}^2 + n_{oI}^2)}{n_{oR}\left[(n_{oR} + n_{1R})^2 + (n_{oI} + n_{1I})^2\right]} \tag{1.111}$$

Equations (1.108) to (1.111) apply only at the interface (z = 0 in Figure 1.4). However, if both media are non-absorptive ($n_{oI} = n_{1I} = 0$) then the reflectivity is the

fraction of incident intensity, I_o^+, that is reflected back into media o and is the same at all points in media o. Similarly, the transmissivity is the fraction of the incident intensity that appears at all points in media 1. As discussed earlier, if media o is absorptive ($n_{oI} \neq 0$), then the intensity cannot be split into incident and reflected parts. Therefore, the definition used for R does not yield the reflected intensity in terms of the incident intensity and $R + T \neq 1$. But as long as media o is non-absorptive ($n_{oI} = 0$), then equation (1.110) yields the fraction of incident intensity that is reflected even if media 1 is absorptive.

1.5.6 Connections between Electromagnetic Theory and Radiation Transfer Theory

Up to now radiation has been treated as propagating electromagnetic waves. The electromagnetic theory relates the optical properties such as reflectivity and transmissivity at an interface between two media to the indices of refraction, n, of the media. An imaginary part to the index of refraction accounts for absorption of radiation. However, in a medium that is emitting, scattering, and absorbing radiation, the electromagnetic theory of plane wave propagation does not apply. In this case, sources for emission, scattering, and absorption must be included. Radiation transfer theory accounts for these sources in a macroscopic manner through the introduction of absorption and scattering coefficients. These properties depend upon the atomic structure of the medium. To determine these properties a quantum mechanical model must be employed. However, in the analysis to follow, the absorption coefficient, a, and the scattering coefficient, σ_s, are treated as given properties. As discussed in Section 1.5.2 the absorption coefficient in the electromagnetic theory is related to the imaginary part of the index of refraction, equation (1.41).

In the electromagnetic theory calculation of reflectivity and transmissivity it is assumed that the interface is perfectly flat. Therefore, for uneven surfaces, which are most probable, these results do not necessarily apply. However, an uneven surface can be approximated as a series of flat surfaces. And since reflectivity is nearly constant for most angles of incidence, as already discussed in Section 1.5.5, it is a reasonable approximation to use the zero angle of incidence reflectivity calculated by electromagnetic theory even for rough surfaces. In Chapter 3 the spectral emittance of an emitting medium will be calculated using radiation transfer theory. In that calculation the electromagnetic theory reflectivity, which is defined in terms of the energy flux, I, is used to determine the reflected intensity, i, at an interface. Thus the emittance calculation combines both electromagnetic and radiation transfer theory.

1.6 Introduction to Radiation Transfer

Radiation transfer is a major part of TPV energy conversion. Emission of radiation from the emitter and transport of radiation to the PV cells are two important parts of the energy conversion process. These topics are covered in detail in later chapters. At this point it is appropriate to introduce some radiation transfer concepts that are used throughout the book. An excellent textbook on radiation transfer was written by Siegel and Howell [16].

1.6.1 Radiation Intensity

Spectral radiation intensity, i, is defined as the radiation energy passing through an area per unit time, per unit of projected area, per unit solid angle, and per unit wavelength interval. This definition applies to radiation leaving a surface or to radiation in some medium.

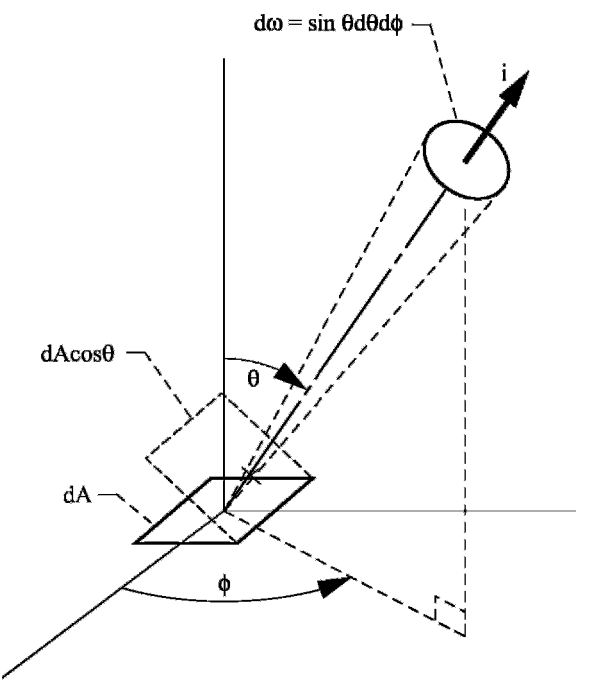

Figure 1.6.—Radiation intensity definition.

One important point is that i is based on the projected area; that is the area perpendicular to the direction of i. Referring to Figure 1.6 and based upon the definition of i, the radiation energy per unit time passing through or leaving an area dA is the following.

$$dqdAd\lambda = i(\theta,\phi,\lambda)\cos\ \theta\ d\omega\ dA\ d\lambda \tag{1.112}$$

$$dqdAd\lambda = i(\theta,\phi,\lambda)\cos\ \theta \sin\theta\ d\theta\ d\phi\ dA\ d\lambda \tag{1.113}$$

Where θ is the angle between i and the normal to dA and $d\omega$ is the solid angle and dq is the infinitesimal radiation energy per unit time per unit area per unit wavelength.

If dA is the source of i then equations (1.112) and (1.113) give the radiation energy per unit of time leaving dA within the solid angle $d\omega$. If i is *isotropic (independent of θ and ϕ)* then the θ and ϕ integrations can be performed.

$$qdAd\lambda = i(\lambda)\ dA\ d\lambda \int_{\phi=0}^{2\pi} d\phi \int_{\theta=0}^{\pi/2} \cos\theta \sin\theta\, d\theta$$
$$q = \pi i(\lambda) \qquad \text{for isotropic i} \tag{1.114}$$

When considering an emitting surface, it is more useful to define a quantity, e, that gives the energy emitted in terms of the surface area rather than the projected area as in equation (1.112). In that case

$$dqdAd\lambda = e(\theta,\phi,\lambda)\, d\omega\, dA\, d\lambda \tag{1.115}$$

the quantity $e(\theta,\phi,\lambda)$ is called the *directional spectral emissive power for the surface*. Comparing equations (1.112) and (1.115), the following applies.

$$e(\theta,\phi,\lambda) = i(\theta,\phi,\lambda)\cos\theta \tag{1.116}$$

If i is isotropic then

$$e(\theta,\lambda) = i(\lambda)\cos\theta \tag{1.117}$$

Equation (1.117) is known as *Lambert's Cosine Law*. Surfaces where i is isotropic and the emissive power is given by equation (1.117) are called *diffuse surfaces*. For a diffuse surface it can be shown (problem 1.10) that,

$$e(\lambda) \equiv q = \pi\, i(\lambda) \tag{1.118}$$

where e(λ) is the *spectral emissive power of the surface* and has the units energy per sec, per unit area, and per unit wavelength.

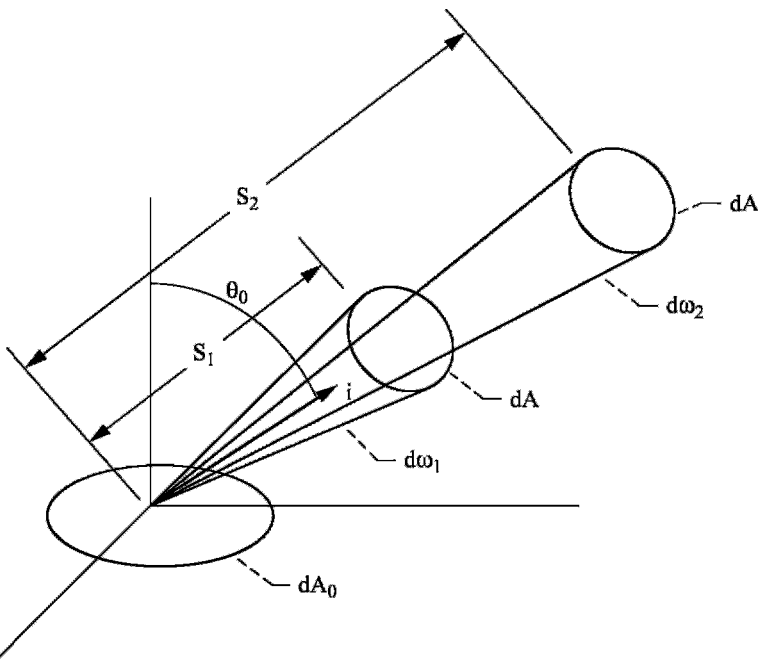

Power measured by detector of area dA at $S_1 = dq_1 dA d\lambda = i\cos\theta_0 dA_0 d\omega_1 d\lambda$
Power measured by detector of area dA at $S_2 = dq_2 dA d\lambda = i\cos\theta_0 dA_0 d\omega_2 d\lambda$

$$\frac{dq_1 dA d\lambda}{d\omega_1} = \frac{dq_2 dA d\lambda}{d\omega_2}$$

Figure 1.7.—Radiant energy in a medium without absorption or emission.

In a medium that is neither absorbing nor emitting and does not scatter radiation, the spectral intensity, i, will be spatially constant. Consider a surface that is emitting into a vacuum as shown in Figure 1.7. If i is measured at any point along a straight line emanating from the surface, i is the same everywhere along that line. Often i is confused with the radiant power that would be measured by a radiation detector of area dA placed anywhere along the line. This quantity is not a constant along that line. The radiant power that is constant along the line is $dqdA d\lambda/d\omega$ which is the power per solid angle. This is illustrated in Figure 1.7.

Only in a medium that does not emit, absorb, or scatter radiation will the intensity, i, be a constant. For all other media, the intensity will be a function of position. The

spatial dependence of intensity is governed by a differential equation known as the equation of transfer or radiation transfer equation. In Section 1.6.5 the radiation transfer equation is introduced.

1.6.2 Blackbody

An important part of radiation transfer theory is the concept of a blackbody. A blackbody is defined as a body that absorbs all incident radiation. This is true for all wavelengths and for all angles of incidence. Thus, a blackbody neither reflects nor transmits radiation. In addition to being a perfect absorber, a blackbody is a perfect emitter. This can be seen by considering a blackbody at uniform temperature placed in a vacuum within a perfectly insulated enclosure of arbitrary shape whose walls are also composed of blackbodies at a different uniform temperature. Eventually, the blackbody and the surrounding blackbody must come to the same equilibrium temperature. At this equilibrium the blackbody must radiate exactly as much energy as it absorbs. If it does not, then a net amount of heat transfer occurs between the blackbodies both at the same temperature. This is a violation of the second law of thermodynamics. Therefore, it follows that since the blackbody is by definition absorbing the maximum possible radiation from the enclosure at all wavelengths and from all incident angles, then it must also be emitting the maximum possible radiation at all wavelengths and all directions. Thus, a blackbody is a perfect emitter (emits the maximum possible radiation), as well as a perfect absorber.

No materials behave exactly like a blackbody. However, certain materials such as carbon black, platinum black, gold black, and silicon carbide (SiC) approach a blackbody. The name blackbody derives from the observation that good absorbers of incident visible light appear black to the eye. However, the human eye responds to only a narrow ($400 < \lambda < 800$ nm) wavelength range so that a surface that appears black in the visible may be a poor absorber in other regions of the spectrum. Thus, the human eye is not a good instrument for determining the absorptance of a surface for the entire spectrum.

In measuring optical properties, it is necessary to have a calibration standard for intensity measurements. This standard is usually a blackbody. The method for obtaining a blackbody is to construct a cavity with a small opening. Therefore, any radiation that enters through the small hole will be reflected and absorbed by a wall of the cavity. The part that is reflected will strike another wall of the cavity and again will be absorbed and reflected. Thus, if the opening is small, very little of the entering radiation will escape back out the hole, and the cavity behaves like a blackbody. By heating the cavity, a source of blackbody radiation is obtained. To maintain the internal radiation in thermal equilibrium, care must be taken to achieve a uniform temperature throughout the cavity. It is not necessary for the internal walls of the cavity to be perfect emitters. When the blackbody radiation within the cavity strikes a wall, part

will be absorbed and the remainder will be reflected. If the walls are well insulated to prevent heat conduction and convection, then the absorbed energy must be re-emitted on the inside. Thus, the sum of the emitted and reflected radiation from the wall must equal the incident blackbody radiation.

1.6.3 Blackbody Spectral Emissive Power

All the blackbody properties discussed to this point can be demonstrated by thermodynamic arguments. However, to determine the dependence of the emitted intensity on wavelength and temperature, the quantum theory developed by Max Planck must be used [17]. As already stated, blackbody intensity, i_b, is isotropic so that equation (1.118) applies. Therefore, the blackbody spectral emissive power, e_b, is given as follows.

$$e_b(\lambda, T) = \pi i_b(\lambda, T) \tag{1.119}$$

From the Planck theory the blackbody spectral emissive power in a vacuum as a function of absolute temperature, T, and wavelength, λ, is the following [17].

$$e_b(\lambda, T)\, d\lambda = \pi i_b(\lambda, T)\, d\lambda = \frac{2\pi\, hc_o^2\, d\lambda}{\lambda^5\left(e^{hc_o/\lambda kT} - 1\right)} \qquad \frac{W}{m^2} \tag{1.120}$$

Appearing in this equation are Planck's constant, $h = 6.6262 \times 10^{-34}$ J sec, the Boltzmann constant, $k = 1.38 \times 10^{-23}$K, and the vacuum speed of light, $c_o = 2.9979 \times 10^8$ m/sec. The blackbody emissive power can also be written in terms of the photon energy, E, or frequency, ν.

$$E = h\nu \qquad J \tag{1.121}$$

$$\nu = \frac{c_o}{\lambda} \qquad \sec^{-1} \tag{1.122}$$

Therefore,

$$\frac{d\lambda}{\lambda^2} = -\frac{d\nu}{c_o} = -\frac{dE}{hc_o} \tag{1.123}$$

Using equations (1.121) to (1.123) in equation (1.120) yields the following results.

$$e_b(E,T)\,dE = \pi i_b(E,T)\,dE = \frac{2\pi E^3\,dE}{h^3 c_o^2\left(e^{E/kT}-1\right)} \qquad \frac{W}{m^2} \qquad (1.124)$$

$$e_b(\nu,T)\,d\nu = \pi i_b(\nu,T)\,d\nu = \frac{2\pi\, h\nu^3\,d\nu}{c_o^2\left(e^{h\nu/kT}-1\right)} \qquad \frac{W}{m^2} \qquad (1.125)$$

The blackbody emissive power given by equations (1.120), (1.124), and (1.125) applies for emission in a vacuum. If the emission is in a medium where the speed of light, c, is different from c_o then c_o must be replaced by c, and λ must be replaced by the wavelength in the medium, $\lambda_m = c/\nu$. Both ν and E remain the same in both the medium and a vacuum. Therefore, in terms of the medium's index of refraction,

$$n \equiv \frac{c_o}{c} \qquad (1.126)$$

equations (1.120), (1.124), and (1.125) become the following.

$$e_b(\lambda,T)\,d\lambda = \pi n^2 i_b(\lambda,T)\,d\lambda = n^2\,\frac{2\pi\, hc_o^2\,d\lambda}{\lambda^5\left(e^{hc_o/\lambda kT}-1\right)} \qquad (1.127)$$

$$e_b(E,T)\,dE = \pi n^2 i_b(E,T)\,dE = n^2\,\frac{2\pi E^3\,dE}{h^3 c_o^2\left(e^{E/kT}-1\right)} \qquad (1.128)$$

$$e_b(\nu,T)\,d\nu = \pi n^2 i_b(\nu,T)\,d\nu = n^2\,\frac{2\pi\, h\nu^3\,d\nu}{c_o^2\left(e^{h\nu/kT}-1\right)} \qquad (1.129)$$

Notice that equation (1.127) is written in terms of the vacuum wavelength, λ rather than the medium wavelength, λ_m.

$$\lambda_m = \frac{c}{\nu} = \frac{c_o}{n\nu} = \frac{\lambda}{n} \qquad (1.130)$$

If n varies spatially or with time, equation (1.127) should be written in terms of λ_m. However, if n has no spatial or time variation, then equation (1.127) is a more convenient form that will be used later in the text. Previously, the definition allowed

the index of refraction to be complex. In this case n is defined to always be a real number.

Referring to equation (1.120) or (1.127) the blackbody spectral emissive power is a function of both wavelength and absolute temperature. However, the quantity e_b/T^5 is a function of the single variable λT.

$$\frac{e_b(\lambda, T)}{T^5} = \frac{2\pi\, hc_o^2}{(\lambda T)^5 \left(e^{hc_o/k\lambda T} - 1\right)} \tag{1.131}$$

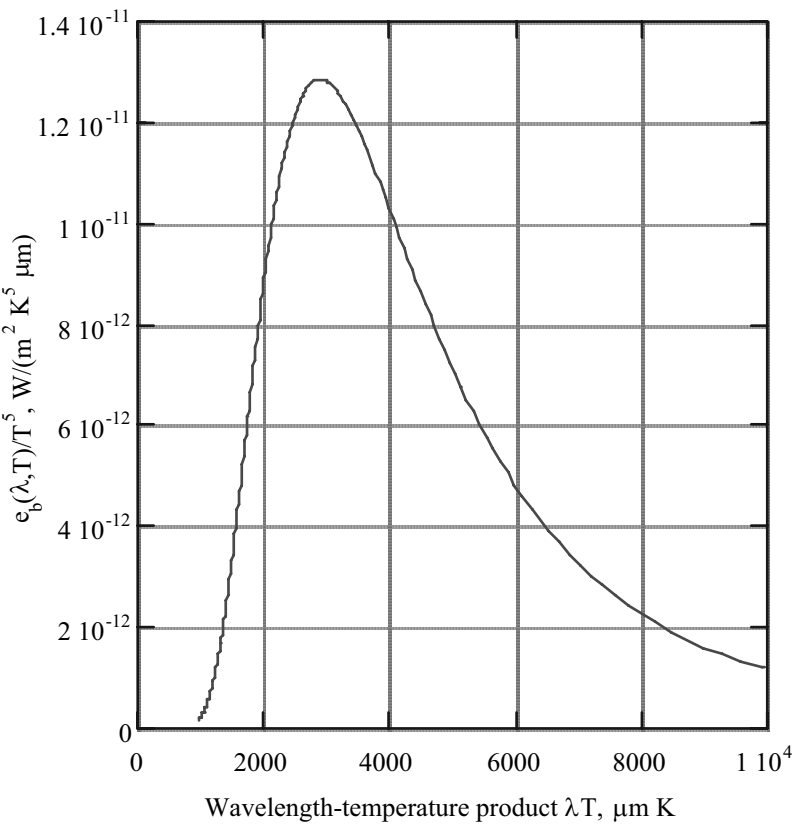

Figure 1.8 - Spectral distribution of blackbody emissive power.

Thus, the functional behavior of e_b can be displayed as a function of the single variable, λT. In Figure 1.8, e_b/T^5 is shown as a function of λT. Note that the maximum value for e_b/T^5 occurs at $\lambda T = 2898 K\ \mu m$. Thus, for a given temperature the wavelength for maximum blackbody emissive power is given by the following expression (problem 1.11).

$$\lambda_{max} T = 2898\ \ K \bullet \mu m \tag{1.132}$$

Since PV cells are most efficient for photons with energy $\approx E_g$, it is desirable to match the wavelength for maximum emissive power, λ_{max}, to the bandgap energy, E_g, of the PV cells. For $E_g = hc_o/\lambda_{max}$ equation (1.132) yields the following,

$$E_g = \frac{hc_o}{\lambda_{max}} = 4.28 \times 10^{-4} T \quad eV \tag{1.133}$$

where T is in degrees Kelvin and E_g is in electron-volts. Thus, if the blackbody emitter, is operating at T = 1700 K, then $E_g = 0.73$ eV in order for the maximum emissive power to occur at the photon energy E_g. The most widely used PV cells are silicon ($E_g = 1.12$ eV) and gallium arsenide (GaAs, $E_g = 1.42$ eV) which obviously do not meet the requirement, $E_g = 0.73$ eV. As pointed out earlier, the development of new low bandgap energy PV cells, such as gallium antimonide (GaSb, $E_g = 0.72$ eV), has made efficient TPV energy conversion possible.

1.6.4 Blackbody Total Emissive Power

Equation (1.133) gives the condition for matching E_g to the wavelength for maximum blackbody emissive power. However, at that condition only 25% of the total blackbody emissive power will have photon energies greater than E_g and thus be convertible to electrical energy by the PV cells. This can be shown as follows.

First define the *total blackbody emissive power, e_{bT}, into a vacuum* as follows.

$$e_{bT}(T) \equiv \int_o^\infty e_b(\lambda, T)d\lambda = \int_o^\infty e_b(E, T)dE = \int_o^\infty e_b(\nu, T)d\nu \tag{1.134}$$

Using equation (1.120) in equation (1.134) yields the following result (problem 1.12).

$$\boxed{e_{bT}(T) \equiv \sigma_{sb} T^4} \qquad \frac{W}{m^2} \tag{1.135}$$

Where σ_{sb} is the *Stefan-Boltzmann constant*.

$$\sigma_{sb} = \frac{2\pi^5}{15}\frac{k^4}{h^3 c_o^2} = 5.6696\times10^{-8}\,W/m^2/K^4 \qquad (1.136)$$

The T^4 dependence of the total blackbody emissive power, e_{bT}, is an important property of radiation transfer. Thus the performance of a TPV energy converter will be strongly dependent upon the temperature of the emitter, which is the source of the radiation.

The fraction of e_{bT} that lies in the wavelength range between 0 and λ is given by the following expression.

$$F_{0-\lambda T} = \int_0^{\lambda}\frac{e_b(\lambda,T)\,d\lambda}{\sigma_{sb}T^4} = \frac{1}{\sigma_{sb}}\int_0^{\lambda T}\frac{e_b(\lambda,T)\,d(\lambda T)}{T^5} = \frac{15}{\pi^4}\int_{\frac{hc_o}{k\lambda T}}^{\infty}\frac{u^3}{e^u-1}du \qquad (1.137)$$

From equation (1.131) we know that e_b/T^5 is a function of λT only. The last integral in equation (1.137) is obtained by using equation (1.124) for e_b (problem 1.13). For most TPV applications $hc_o/k\lambda T = E/kT > 1$. In that case $F_{0-\lambda T}$ is given by an approximate algebraic expression (problem 1.14). The quantity, $F_{0-\lambda T}$, is shown in Figure 1.9 as a function of λT. Notice that at the condition for maximum blackbody spectral emissive power, equation (1.132), $F_{o\text{-}\lambda_{max}T} = 0.25$. Thus, as stated earlier, even if E_g for the PV cells is matched to the maximum spectral emissive power of a blackbody emitter, only 25% of the total radiation will be convertible to electricity by the PV cells. To achieve high efficiency in a TPV energy conversion system that uses a blackbody emitter requires that the 75% of the total radiation not convertible to electricity be returned to the emitter where it can be absorbed. As mentioned in Section 1.2, one method for doing this is to use a bandpass filter.

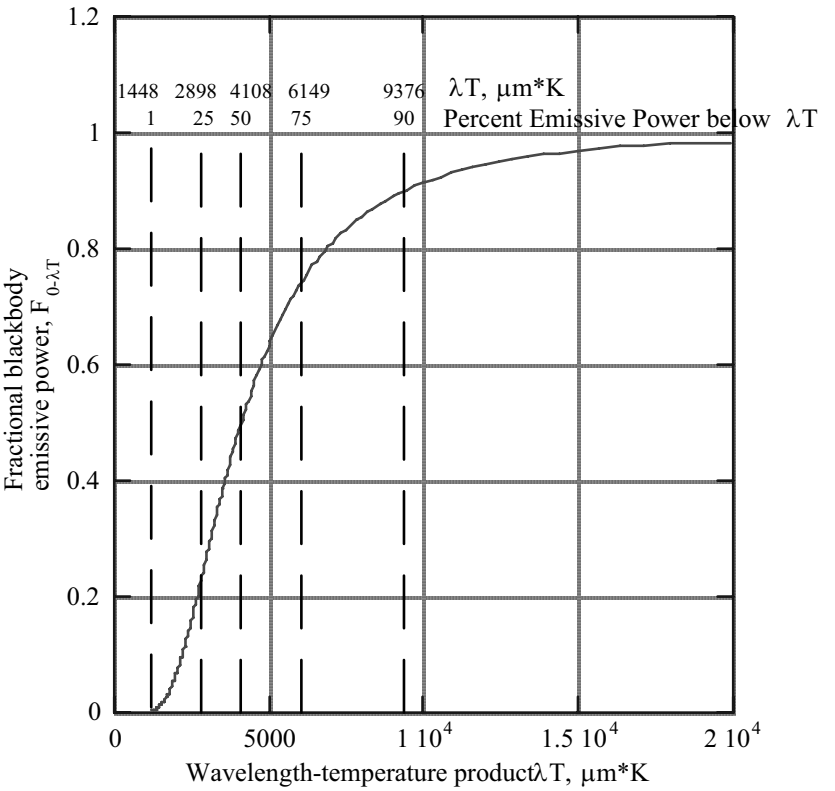

Figure 1.9 - Fractional blackbody emissive power in range 0 to λT

1.6.5 Equations for Radiation Energy Transfer

The radiation transfer equation applies to a medium where the excited state densities are in Boltzmann equilibrum. In that case, the relation between the density of state i, n_i, and density of state, j, n_j, depends upon the temperature and is given by the following expression.

$$\frac{n_i}{n_j} = \frac{g_i}{g_j} \exp\left[-\frac{E_i - E_j}{kT}\right], \quad E_i > E_j \tag{1.138}$$

Appearing in equation (1.138) are the energies E_i and E_j and degeneracies g_i and g_j of the states i and j. Thus, the radiative transfer equation goes not apply to a nonequilibrium situation such as a laser where excited state densities do not obey Boltzmann equilibrium. However, for TPV emitters at constant temperature,

Boltzmann equilibrium does exist. As a result, the radiative transfer equation governs the behavior of the intensity, i.

Derivations of the equation of transfer are given in several texts [16], [18]. The result is the following equation.

$$\hat{s}\cdot\nabla i\left(\hat{r},\hat{s},\lambda\right)=\underbrace{-a(\lambda)i\left(\vec{r},\hat{s},\lambda\right)}_{\substack{\text{loss by}\\ \text{absorption}}}+\underbrace{a(\lambda)n^2 i_b\left(\lambda,T\right)}_{\substack{\text{gain by}\\ \text{emission}}}-\underbrace{\sigma_s(\lambda)i\left(\vec{r},\hat{s},\lambda\right)}_{\substack{\text{loss by}\\ \text{scattering}}}+\underbrace{\frac{\sigma_s(\lambda)}{4\pi}\int_{\omega=4\pi} i\left(\vec{r},\hat{s},\lambda\right)d\omega}_{\substack{\text{gain by}\\ \text{scattering into}\\ \hat{s}\text{ direction}}} \tag{1.139}$$

Equation (1.139) gives the change in the intensity at position, $\vec{r}$, and wavelength, λ in the direction of the unit vector $\hat{s}$ as a result of absorption, emission and scattering. The absorption coefficient, a (cm^{-1}), and the scattering coefficient, σ_s(cm^{-1}), are functions of the wavelength. Notice the emission term contains the blackbody intensity, i_b. This result occurs because thermodynamic equilibrium is assumed. It is also assumed that the scattering is the same in all directions (*isotropic scattering*). As equation (1.139) indicates the intensity depends on a, σ_s and index of refraction, n. Combining the terms that represent losses by absorption and scattering, equation (1.139) becomes the following,

$$\hat{s}\cdot\nabla i=-K\left[i-n^2\left(1-\Omega\right)i_b-\frac{\Omega}{4\pi}\int_{\omega=4\pi} i\,d\omega\right] \tag{1.140}$$

where,

$$K\left(\lambda\right)\equiv a(\lambda)+\sigma_s\left(\lambda\right) \tag{1.141}$$

is the *extinction coefficient* and

$$\Omega(\lambda)\equiv\frac{\sigma_s(\lambda)}{a(\lambda)+\sigma_s(\lambda)}=\frac{\sigma_s(\lambda)}{K(\lambda)} \tag{1.142}$$

is the *scattering albedo*.

In the case where emission and scattering can be neglected, the equation of transfer becomes the following,

$$\hat{s}\cdot\nabla i=\frac{di}{ds}=-Ki \tag{1.143}$$

where $\hat{s}\cdot\nabla i$ has been replaced by the directional derivative, $\frac{di}{ds}$, in the direction of $\hat{s}$. Equation (1.143) can be integrated to yield the following result,

$$\boxed{i(s) = i(0)e^{-\kappa(s)}} \tag{1.144}$$

where $\kappa(s)$ is called the *optical depth*.

$$\boxed{\kappa(s) \equiv \int_0^s K(s^*)ds^*} \tag{1.145}$$

Equation (1.144) is known as Bouguer's Law. It is also sometimes called Lambert's Law, the Bouguer-Lambert Law, or Beer's Law ([16], pg. 425).

If the left hand side of equation (1.140) is replaced by the directional derivative, di/ds, and the change of variable from s to the optical depth, κ, is made, then the following is obtained,

$$\frac{di}{d\kappa} + i(\kappa) = S(\kappa) \tag{1.146}$$

where *$S(\kappa)$ is called the source function* for isotropic scattering.

$$S(\kappa) = n^2(1-\Omega)i_b(\kappa) + \frac{\Omega}{4\pi}\int_{\omega=4\pi} i(\kappa,\omega)d\omega \tag{1.147}$$

Multiply equation (1.146) by the integrating factor e^{κ}. Therefore, equation (1.146) can be integrated from $\kappa = 0$ to $\kappa(s)$ to yield the following.

$$\boxed{i(\kappa) = i(0)e^{-\kappa} + \int_0^{\kappa(s)} S(\kappa^*)\exp\left[-(\kappa-\kappa^*)\right]d\kappa^*} \tag{1.148}$$

Thus a solution for i in terms of the boundary condition i(0) and the source function, S, is obtained. If equation (1.148) is substituted for i in equation (1.147) an integral equation for S is obtained.

$$S(\kappa) = n^2(1-\Omega)i_b(\kappa) + \frac{\Omega}{4\pi}\left[\int_{\omega=4\pi} i(0,\omega)e^{-\kappa}d\omega + \int_{\omega=4\pi} d\omega \int_0^{\kappa} S(\kappa^*)\exp\left[-\kappa-\kappa^*\right]d\kappa^*\right] \quad (1.149)$$

Once the source function equation is solved, the result can be used in equation (1.148) to calculate i(κ).

Equations (1.148) and (1.149) give i and S in terms of the optical depth, κ, and the boundary condition i(0) for isotropic scattering. The optical depth, equation (1.145), depends upon the path length s, which, in turn, is a function of the geometry or coordinate system being used. Thus, before equations (1.148) and (1.149) can be solved for i and S they must be adapted to a particular coordinate system. In Chapter 3 they are written for one dimensional, planar, and cylindrical coordinate systems.

1.6.6 Energy Conservation Including Radiation

The intensity and source function depend upon the temperature of the medium through the blackbody intensity term in equations (1.148) and (1.149). Therefore only if the medium temperature is a constant, can the intensity and source function be calculated from equations (1.148) and (1.149). In general, the radiation must be included in the equation for the conservation of energy. Therefore, a coupled system of equations for radiation energy flux and temperature will result.

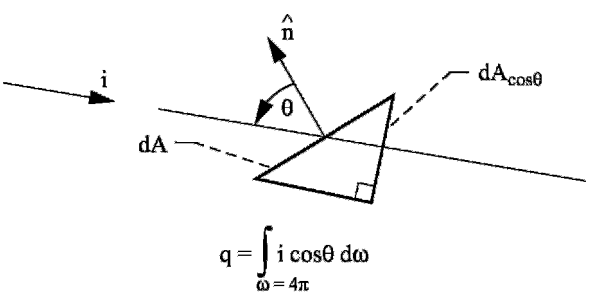

Figure 1.10.—Radiation energy flux.

Now consider how the radiation energy flux is related to the intensity. Referring to Figure 1.10, the intensity is the energy per second per unit solid angle crossing dA per unit area normal to i. Thus, the energy per second crossing dA as a result of radiation intensity i is idAcosθ dω. The radiation energy flux, q, crossing dA as a result of intensities incident from all directions is,

$$q = \int_{\omega=4\pi} i \cos\theta d\omega \qquad \frac{W}{m^2 nm} \tag{1.150}$$

where θ is the angle from the normal of dA, $\hat{n}$, to the direction of i. Since θ is in the integral, q depends upon the direction of $\hat{n}$ and is thus a vector quantity. Thus, if $\hat{n}$ is the unit vector in the x-direction, the radiation energy flux in the direction, q_x, is the following,

$$q_x = \int_{\omega=4\pi} i \cos\theta_x d\omega \tag{1.151a}$$

where θ_x is the angle from the x-axis to i. Similarly, for the y and z directions,

$$q_y = \int_{\omega=4\pi} i \cos\theta_y d\omega \tag{1.151b}$$

$$q_z = \int_{\omega=4\pi} i \cos\theta_z d\omega \tag{1.151c}$$

and the *radiation energy flux vector* is the following.

$$\vec{q} = q_x \hat{i} + q_y \hat{j} + q_z \hat{k} \tag{1.152}$$

Remember, $\vec{q}$ is the radiation energy flux per unit wavelength. For the equation of conservation of energy it is the total radiation flux $\vec{\bar{q}}$ that must be considered,

$$\vec{\bar{q}} = \bar{q}_x \hat{i} + \bar{q}_y \hat{j} + \bar{q}_z \hat{k} \tag{1.153}$$

where

$$\bar{q}_x = \int_0^\infty q_x d\lambda, \quad \bar{q}_y = \int_0^\infty q_y d\lambda, \quad \bar{q}_z = \int_0^\infty q_z d\lambda \tag{1.154}$$

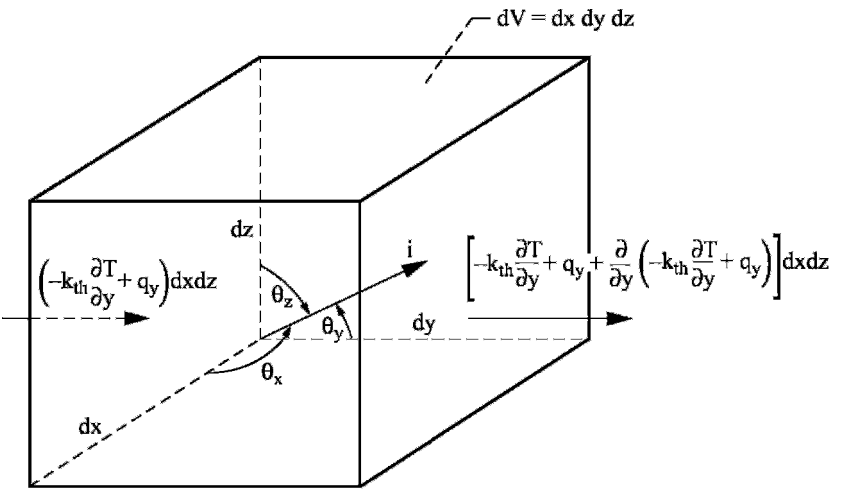

Figure 1.11.—Thermal conduction and radiation energy fluxes through volume, dV, in y direction.

Now consider the conservation of energy for a non-deforming media at rest. Referring to Figure 1.11, apply the conservation of energy to the volume element, dV. Since the media is non-deforming and at rest, there will be no convective energy flow through the volume or work done on the surroundings by the volume. Thus, all energy entering and leaving the volume will be by thermal conduction and radiation. Therefore, the conservation of energy for the volume, dV, is the following,

$$\begin{pmatrix}\text{rate of energy accumulation}\\ \text{within dV}\end{pmatrix} = \begin{pmatrix}\text{rate of addition of energy to dV by thermal}\\ \text{conduction and radiation + heat source within dV}\end{pmatrix} \tag{1.155}$$

$$\text{rate of energy accumulation in dV} = \frac{\partial}{\partial I}\left(\rho c_v T\right) dx\ dy\ dz \tag{1.156}$$

where ρ is the density and c_v is the specific heat. Referring to Figure 1.11, the rate of energy addition to the volume entering in the y direction is the following,

$$\begin{pmatrix}\text{rate of energy addition to dV by thermal}\\ \text{conduction and radiation in the y direction}\end{pmatrix} = -\frac{\partial}{\partial y}\left[\bar{q}_y - k_{th}\frac{\partial T}{\partial y}\right] dx\ dy\ dz \tag{1.157}$$

where $-k_{th}\,\partial T/\partial y$ is the thermal conduction in the y-direction and $\bar{q}_y$ is the radiation flux in the y-direction.

For the x and z directions expressions are similar to equation (1.157) so that the conservation of energy equation becomes the following,

$$\frac{\partial\left(\rho c_v T\right)}{\partial t} = \frac{\partial}{\partial x}\left[k_{th}\frac{\partial T}{\partial x} - \overline{q}_x\right] + \frac{\partial}{\partial y}\left[k_{th}\frac{\partial T}{\partial y} - \overline{q}_y\right] + \frac{\partial}{\partial z}\left[k_{th}\frac{\partial T}{\partial z} - \overline{q}_z\right] + q' \qquad (1.158)$$

where q' is the local heat source per unit volume (W/m^3). Equation (1.158) can be written in vector form as follows.

$$\boxed{\frac{\partial\left(\rho c_v T\right)}{\partial t} = \nabla\bullet\left[k_{th}\nabla T - \vec{\overline{q}}\right] + q'} \qquad (1.159)$$

For steady state conditions and no heat sources, the energy equation is the following

$$\boxed{\nabla\bullet\left[k_{th}\nabla T - \vec{\overline{q}}\right] = 0} \qquad (1.160)$$

The energy equation, the intensity equation (1.148), and the source function equation (1.149) make up the set of equations that apply for a non-deforming media at rest. A solution to these coupled equations will yield the source function, the intensity (and thus $\vec{\overline{q}}$) and the temperature. In Chapter 3 they are applied to calculate the spectral emittance of planar and cylindrical emitters.

1.7 Optical Properties

In Section 1.5.5, reflectivity and transmissivity at an interface between two media are calculated as functions of the indices of refraction of the media. Other optical properties required for the understanding of TPV energy conversion are emittance, reflectance, transmittance, and absorptance (the inverse of emittance). Notice that a distinction is made between reflectivity and reflectance and transmissivity and transmittance. The suffix -ity is used to define a so-called *intensive property*. An intensive property is independent of the dimensions of the material. A so-called *extensive property*, denoted by the suffix -ance, depends upon the dimensions of the material. Thus, the term emissivity should be used to define an emission process that is independent of the material dimensions. However, radiation from any material comes from depths below the surface, as well as from the surface. These depths are generally very small (< 1 μm), especially for metals. In the case of selective emitters used in TPV applications, the depths from which emitted radiation originates is in the order of 100 μm and the emitted intensity or emissive power is strongly dependent upon the thickness of the emitter. In that case, the emission process is an extensive property;

therefore it uses the suffix -ance. Since the emission process really does depend upon dimensions, only the term emittance is used in this text.

Reflectivity and transmissivity are used to describe the reflection and transmission process that occurs at an interface and is thus independent of dimensions. When the terms reflectance, transmittance, and absorptance are used; the process depends upon dimensions.

1.7.1 Emittance and Absorptance

As already stated, for a given temperature in a medium with index of refraction, n_o, the blackbody spectral intensity, $n_o^2 i_b(\lambda,T)$, and spectral emissive power, $n_o^2 e_b(\lambda,T)$, are the maximum possible spectral intensity and emissive power that can be achieved. At the same temperature, all other surfaces emitting into the medium will produce a lower intensity and emissive power. Therefore, it is useful to define the emitted spectral intensity, i_E, and spectral emissive power, e_E, in terms of the blackbody intensity and emissive power. In the case of i_E define the *directional spectral emittance*, ε', as follows.

$$\varepsilon'(\theta,\phi,\lambda,T_E,d) \equiv \frac{dq_E(\theta,\phi,\lambda,T_E,d)}{n_o^2 i_b(\lambda,T_E)\cos\theta d\omega} \le 1 \tag{1.161}$$

Usually the n_o^2 term in the denominator of equation (1.161) is omitted since emission is generally assumed to be into a vacuum ($n_o = 1$). However, if emission were into a medium where $n_o > 1$, then omission of the n_o^2 term could result in $\varepsilon' > 1$ since in that case it is possible for $dq_E > i_b \cos\theta d\omega$. The emitted power, dq_E, per unit area and wavelength within the solid angle $d\omega$ is given by equation (1.112). Notice that the length parameter, d, appears in the argument of ε' and dq_E. It is included to show that emittance can be a function of the emitter dimensions.

$$dq_E = i_E(\theta,\phi,\lambda,T_E,d)\cos\theta d\omega \tag{1.162}$$

Therefore,

$$\varepsilon'(\theta,\phi,\lambda,T_E,d) = \frac{i_E(\theta,\phi,\lambda,T_E,d)}{n_o^2 i_b(\lambda,T_E)} = \frac{\pi i_E(\theta,\phi,\lambda,T_E,d)}{n_o^2 e_b(\lambda,T_E)} \le 1 \tag{1.163}$$

Similar to ε' we define a *directional spectral absorptance*, α', as follows,

$$\alpha'(\theta,\phi,\lambda,T_A,d) \equiv \frac{dq_A}{dq_i} \le 1 \tag{1.164}$$

where dq_A is the power absorbed per unit area and wavelength at temperature T_A within the solid angle $d\omega$ and dq_i is the incident power per unit area and wavelength within the solid angle $d\omega$.

$$dq_i = i_i(\theta,\phi,\lambda)\cos\theta d\omega \tag{1.165}$$

Using equation (1.161), the power emitted by dA within the solid angle $d\omega$ and wavelength range $d\lambda$ is the following.

$$dq_E dA d\lambda = n_o^2 \varepsilon'(\theta,\phi,\lambda,T_E,d) i_b(\lambda,T_E)\cos\theta d\omega dA d\lambda \tag{1.166}$$

If the element dA at temperature T_E is placed in a blackbody enclosure at temperature, T_E, where the intensity is $n_o^2 i_b(\lambda,T_E)$, which is isotropic (independent of θ and ϕ), then equations (1.164) and (1.165) yield the following for the power absorbed by dA within the solid angle $d\omega$ and wavelength range $d\lambda$.

$$dq_A dA d\lambda = n_o^2 \alpha'(\theta,\phi,\lambda,T_E,d) i_b(\lambda,T_E)\cos\theta d\omega dA d\lambda \tag{1.167}$$

To maintain isotropy of radiation in the blackbody enclosure, the emitted power and absorbed power must be equal. As a result, $dq_A = dq_E$ so that by equating equations (1.166) and (1.167) the following equivalence is obtained.

$$\varepsilon'(\theta,\phi,\lambda,T_E,d) = \alpha'(\theta,\phi,\lambda,T_E,d) \tag{1.168}$$

This relation is called *Kirchhoff's Law*. It was derived for a blackbody radiation field for which the s and p components, see Section 1.5.5, of the field are the same. As a result, to be strictly accurate it applies only for a radiation field with equal s and p components. Also, Kirchhoff's Law was derived assuming thermodynamic equilibrium so that a constant temperature must exist and there can be no net heat transfer to or from the surface. However, experimentally it has been found that α' and ε' are not greatly affected by the surrounding radiation field. Thus it appears that most materials are able to maintain themselves in thermodynamic equilibrium. Thus, the excited states that account for emission and absorption are at Boltzmann equilibrium [equation

(1.138)]. And Kirchhoff's Law can be applied when there is net heat transfer to or from the surface.

Now consider the emittance defined in terms of the power emitted in all directions from the surface dA at temperature T_E. This emittance is called the *hemispherical spectral emittance*, $\varepsilon(\lambda,T_E,d)$, and is the emittance that is used in determining the optical performance of a TPV system emitter,

$$\varepsilon\left(\lambda,T_E,d\right)\equiv\frac{q_E}{n_o^2 e_b\left(\lambda,T_E\right)}\le 1 \tag{1.169}$$

where $n_o^2 e_b(\lambda,T_E)$ is the blackbody spectral emissive power in a medium of index of refraction, n_o, and q_E is the power emitted per unit area per unit wavelength by dA at temperature T_E

$$q_E=\int_{\Omega} i_E\left(\theta,\phi,\lambda,T_E,d\right)\cos\theta\,d\omega=\int_{\phi=0}^{2\pi}d\phi\int_{\theta=0}^{\pi/2} i_E\cos\theta\sin\theta\,d\theta \tag{1.170}$$

where $\int_{\Omega} d\omega$ denotes integration over the hemispherical solid angle. Using equation (1.163) for i_E in equation (1.170) yields the following result for the hemispherical spectral emittance.

$$\varepsilon\left(\lambda,T_E,d\right)=\frac{1}{\pi}\int_{\Omega}\varepsilon'\left(\theta,\phi,\lambda,T_E,d\right)\cos\theta\,d\omega \tag{1.171}$$

Thus, if the emitting surface is *diffuse* (i_E and ε' independent of θ and ϕ), then the hemispherical and directional emittances are equal.

$$\varepsilon\left(\lambda,T_E,d\right)=\varepsilon'\left(\lambda,T_E,d\right)\quad\text{for diffuse surface} \tag{1.172}$$

The corresponding *hemispherical spectral absorptance* is defined as follows,

$$\alpha\left(\lambda,T,d\right)\equiv\frac{q_a}{q_i}\le 1 \tag{1.173}$$

where q_A is the radiation power absorbed per unit area per unit wavelength by dA at temperature T_A over the hemisphere.

$$q_A = \int_{\Omega} \alpha'(\theta,\phi,\lambda,T_A,d)\, i_i(\theta,\phi,\lambda)\cos\theta d\omega \tag{1.174}$$

And q_i is the radiation power per unit area and wavelength incident on dA from all directions within the hemisphere.

$$q_i = \int_{e} i_i(\theta,\phi,\lambda)\cos\theta d\omega \tag{1.175}$$

Thus, using equations (1.174) and (1.175) in equation (1.173) yields the hemispherical spectral absorptance.

$$\alpha(\lambda,T,d) = \frac{\int_{\Omega} \alpha'(\theta,\phi,\lambda,T_A,d) i_i(\theta,\phi,\lambda)\cos\theta d\omega}{\int_{\Omega} i_i(\theta,\phi,\lambda,T_A,d)\cos\theta d\omega} \le 1 \tag{1.176}$$

Using Kirchhoff's Law, α' can be replaced by ε'.

$$\alpha(\lambda,T,d) = \frac{\int_{\Omega} \varepsilon'(\theta,\phi,\lambda,T_A,d) i_i(\theta,\phi,\lambda)\cos\theta d\omega}{\int_{\Omega} i_i(\theta,\phi,\lambda)\cos\theta d\omega} \le 1 \tag{1.177}$$

Thus there are two conditions that result in the equivalence of $\varepsilon(\lambda,T,d)$ and $\alpha(\lambda,T,d)$. First of all, if the surface is diffuse so that ε' is independent of θ and ϕ. Secondly, if the incident intensity, i_i, is istropic so that i_i can be cancelled in equation (1.177), the denominator reduces to π and equation (1.171) shows $\alpha(\lambda,T,d) = \varepsilon(\lambda, T,d)$.

$$\alpha(\lambda,T,d) = \varepsilon(\lambda,T,d) \quad \begin{matrix}\text{for diffuse surface or} \\ \text{istropic incident intensity}\end{matrix} \tag{1.178}$$

In the analyses of TPV systems presented in the following chapters it is usually assumed that surfaces are diffuse. Therefore, the hemispherical spectral emittance $\varepsilon(\lambda,T,d)$ and hemispherical spectral absorptance, $\alpha(\lambda,T)$ are equivalent in that case.

The *hemispherical total emittance*, $e_T(T,d)$, is defined as follows,

$$\varepsilon_T\left(T_E,d\right)\equiv\frac{\int_o^\infty q_E d\lambda}{n_o^2\sigma_{sb}T_E^4}=\frac{\int_o^\infty \varepsilon\left(\lambda,T_E,d\right)e_b\left(\lambda,T_E\right)d\lambda}{\sigma_{sb}T_E^4}\le 1 \tag{1.179}$$

where the denominator includes the total blackbody emissive power, $e_{bT}\left(T_E\right)=\sigma_{sb}T_E^{\,4}$ (equation (1.135) and equation (1.169) were used to determine q_E). *If $\varepsilon(\lambda,T_E,d)$ is independent of λ, the emitting surface is said to be gray.* In that case we obtain the result.

$$\varepsilon_T\left(T_E,d\right)=\varepsilon\left(T_E,d\right)\qquad\text{for gray surface} \tag{1.180}$$

Now define the *hemispherical total absorptance* as follows,

$$\alpha_T\left(T,d\right)\equiv\frac{\int_o^\infty q_A d\lambda}{\int_o^\infty q_i d\lambda}=\frac{\int_o^\infty \alpha\left(\lambda,T,d\right)q_i d\lambda}{\int_o^\infty q_i d\lambda} \tag{1.181}$$

where equation (1.173) has been used for $q_A d\lambda dA$. If the surface is diffuse, $\varepsilon(\lambda,T,d)=\alpha(\lambda,T,d)$. In addition, if the surface is gray, $\varepsilon_T(T,d)=\varepsilon(T,d)$. Therefore, for a *diffuse-gray surface* the following applies.

$$\varepsilon'\left(T,d\right)=\varepsilon\left(T,d\right)=\varepsilon_T\left(T,d\right)=\alpha'\left(T,d\right)=\alpha\left(T,d\right)=\alpha_T\left(T,d\right)\quad\text{for diffuse-gray surface} \tag{1.182}$$

The only case where equation (1.182) is exact is for a blackbody where $\varepsilon'=\varepsilon=\varepsilon_T=\alpha'=\alpha=\alpha_T=1$. However, in order to simplify a radiation transfer problem, the diffuse-gray approximation is often used.

1.7.2 Hemispherical Spectral and Hemispherical Total Reflectivity

In Section 1.5.5 expressions for the reflectivity, $\overline{R}$ (equation (1.103)), and transmissivity, $\overline{T}$ [equation (1.104)], at an interface between two materials were derived. These quantities apply to an interface that obeys the law of reflection (angle of incidence = angle of reflection). *An interface that obeys the law of reflection is called a specular surface*. They also apply to so-called natural light where the direction of the incident wave electric field is random, as is the case for radiation originating from hot surfaces such as the emitter in a TPV system. Reflectivity and transmissivity depend upon the indices of refraction, which are functions of wavelength and the angle of

incidence. Since $\overline{R}$ and $\overline{T}$ apply to specular surfaces and depend upon direction, as well as wavelength, they should be called *the specular directional spectral reflectivity,* $\overline{R}$, and *specular directional spectral transmissivity,* $\overline{T}$. However, $\overline{R}$ and $\overline{T}$ do not depend upon the dimensions of the reflecting and transmitting materials.

Reflectivity, $\overline{R}$, determines the reflected power at a reflection angle, θ_r, where $\theta_r = \theta_i$ (angle of incidence) for a specular surface. However, as discussed in Sections 1.5.5 and 1.5.6, $\overline{R}$ is nearly a constant for $0 \le \theta_i \le 60°$. Also, an uneven surface can be approximated as a series of flat specular surfaces. Therefore, it is a reasonable approximation to assume $\overline{R}$ is independent of direction and use the zero angle of incidence ($\theta_i = 0$) reflectivity given by equation (1.110) for reflectivity of all surface conditions. We have used the term *diffuse* to describe a material that has emittance and absorptance that is independent of direction. The term diffuse is generally used to describe a material where all the optical properties are independent of angle. Thus the term diffuse means that reflectivity, reflectance, tranmissivity, transmittance, as well as, emittance and absorptance are independent of angle.

Define a *hemispherical spectral reflectivity, for an interface* as follows,

$$R_{\frown}(\lambda) \equiv \frac{q_r}{q_i} \tag{1.183}$$

where q_i is the incident power per unit area and wavelength from all angles in the hemisphere and is given by equation (1.175). The reflected power into the hemisphere is given in terms of the directional spectral reflectivity, $R'(\theta,\phi,\lambda)$.

$$q_r(\lambda) = \int_o R'(\theta,\phi,\lambda) i_i(\theta,\phi,\lambda) \cos\theta d\omega \tag{1.184}$$

If the interface is diffuse so that R' is independent of angle, then the following is true.

$$R_{\frown}(\lambda) = R'(\lambda) \qquad \text{for diffuse interface} \tag{1.185}$$

For a specular interface ($\theta_i = \theta_r$, $\phi_r = \phi + \pi$) so that the following result occurs.

$$R'(\theta_i = \theta_r, \phi_i = \phi_r + \pi, \lambda), = \overline{R}(\theta_i = \theta_r, \lambda) \qquad \text{for specular interface} \tag{1.186}$$

And $\overline{R}$ is the specular directional spectral reflectivity given by equation (1.103). As already mentioned, $\overline{R}(\theta_i = \pi/2, \lambda)$ is a good approximation for $\overline{R}$ for all incident angles, θ_I, and for a diffuse interface, as well as a specular interface.

The final reflectivity to be defined is the *hemispherical total reflectivity*, R_T.

$$R_T \equiv \frac{\int_o^\infty q_r d\lambda}{\int_o^\infty q_i d\lambda} \tag{1.187}$$

Using equation (1.183) for q_r yields the following.

$$R_T = \frac{\int_o^\infty R_{\sphericalangle}(\lambda)\ \ q_i d\lambda}{\int_o^\infty q_i d\lambda} \tag{1.188}$$

Thus, if $R_{\sphericalangle}(\lambda)$ is independent of λ,

$$R_T = R_{\sphericalangle} \qquad \text{for } R_{\sphericalangle}(\lambda) \text{ independent of } \lambda \tag{1.189}$$

and if the interface is also diffuse, the following is obtained.

$$R_T = R_{\sphericalangle} = R' \qquad \text{for diffuse interface and } R_{\sphericalangle}(\lambda) \text{ independent of } \theta \tag{1.190}$$

1.7.3 Independence of Emitted (Absorbed), Reflected, and Transmitted Radiation

The radiation transfer equations (1.148) and (1.149) govern the behavior of the radiation intensity, i, in a material where the scattering is isotropic and Boltzmann equilibrium exists. In considering the components of a TPV system it is desirable to separate the reflected, transmitted, and emitted (or absorbed) intensities. This is possible because of the nature of the radiative transfer equations.

Consider the one-dimensional model, where i depends only upon the x coordinate, shown in Figure 1.12. The one-dimensional model applies when the thickness, d, is much less than the y and z dimensions of the body. The body is characterized by its index of refraction n, extinction coefficient K, and scattering albedo, Ω. It is surrounded by a medium with index of refraction, n_o. We also assume $d > \lambda$ so that interference effects can be neglected.

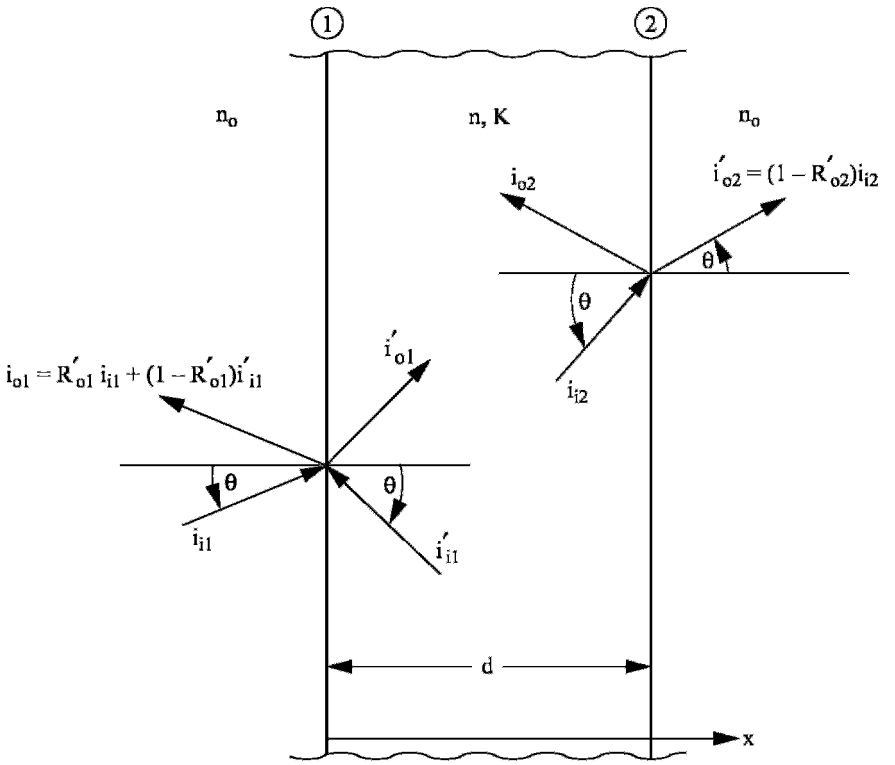

Figure 1.12.—One dimensional radiation model for an emitting, absorbing and transmitting medium.

There is an incident intensity from the surroundings, i_{i1}, at interface 1. Leaving interface 1 in the –x direction is intensity, i_{o1}, and in the +x direction, i'_{o1}. There is also an incident intensity from within the body at interface 1, i'_{i1}. There are similar intensities at interface 2, except there is no incident intensity from the surroundings.

The form of the radiation transfer, equation (1.148), allows the portion of the intensities i_{o1} and i'_{o2} that results from incident intensity i_{i1} to be separated from the portions that result from emission. Equation (1.148) can be written as follows,

$$i(\kappa) = i(0)e^{-\kappa} + f(s) \tag{1.191}$$

where the first term accounts for absorption and the second term, f(s), accounts for emission and scattering, and depends upon the source function. The optical depth, κ, in the one-dimensional model is the following.

$$\kappa = \int_0^s K ds^* = \int_0^x K(x^*)\frac{dx^*}{\cos\theta} = \frac{1}{\cos\theta}\int_0^x K(x^*)dx^* = \frac{\kappa_x}{\cos\theta} \tag{1.192}$$

If scattering is negligible ($\Omega \ll 1$), then the source function, equation (1.149), will be independent of the boundary intensity i(0). Thus the intensity within the body can be separated into a portion dependent upon the boundary value [first term in equation (1.191)], and a portion dependent on the emitted value [second term in equation (1.191)]. Therefore, the incident intensities within the body can be written as follows,

$$\left.\begin{aligned} i'_{i1} &= i_{o2}t + F(s) \\ i_{i2} &= i'_{o1}t + F(s) \end{aligned}\right\} \text{ for } \Omega \ll 1 \tag{1.193, 1.194}$$

where t is the internal transmittance,

$$t = \exp\left[\frac{-\kappa_d}{\cos\theta}\right] \tag{1.195}$$

and

$$\kappa_d = \int_0^d K(x)dx \tag{1.196}$$

The emission is symmetrical so that the emission term F(s) is the same for i'_{i1} and i_{i2}. The intensity leaving interface 1 within the body, i'_{o1}, is the sum of the reflected intensity and the transmitted intensity at the interface,

$$i'_{o1} = R'_{o1}i'_{i1} + \left(1 - R'_{o1}\right)i_{i1} \tag{1.197}$$

where R'_{o1} is the directional spectral reflectivity at interface 1, and since we assume n_o is a real number, $(1 - R'_{o1})$ is the transmissivity at interface 1. Similarly, the intensity, i_{o2} is the following,

$$i_{o2} = R'_{o2}i_{i2} \tag{1.198}$$

where R'_{o2} is the directional spectral reflectivity at interface 2. The intensities leaving the two interfaces are the following.

$$i_{o1} = R'_{o1} i_{i1} + \left(1 - R'_{o1}\right) i'_{i1} \tag{1.199}$$

$$i'_{o2} = \left(1 - R'_{o2}\right) i_{i2} \tag{1.200}$$

Equations (1.193), (1.194), and (1.197) to (1.190) can be solved for i_{o1} and i'_{o2} in terms of i_{i1} and F(s) to obtain the following result (problem 1.16),

$$i_{o1} = \rho'_1 i_{i1} + \frac{\left(1 - R'_{o1}\right)\left(1 + R'_{o2} t\right)}{1 - R_{o1} R_{o2} t^2} F(s) \tag{1.201}$$

$$i'_{o2} = \tau' i_{i1} + \frac{\left(1 - R'_{o1}\right)\left(1 + R'_{o1} t\right)}{1 - R_{o1} R_{o2} t^2} F(s) \tag{1.202}$$

where ρ'_1 is the *directional spectral reflectance* at interface 1,

$$\rho'_1\left(\theta, \phi, \lambda, d, T\right) \equiv \frac{i_{r1}}{i_{i1}} = \frac{R'_{o1} + R'_{o2} t^2 \left(1 - 2R'_{o1}\right)}{1 - R'_{o1} R'_{o2} t^2} \tag{1.203}$$

and i_{r1} is the portion of i_{o1} that results from reflection of i_{i1}. Also, τ' is the *directional spectral transmittance*, which is the same for both interfaces,

$$\tau'\left(\theta, \phi, \lambda, d, T\right) \equiv \frac{i_{t2}}{i_{i1}} = \frac{t\left(1 - R'_{o1}\right)\left(1 - R'_{o2}\right)}{1 - R'_{o1} R'_{o2} t^2} \tag{1.204}$$

where i_{t2} is the transmitted portion of i_{i1}. The second term in equations (1.201) and (1.202) is the emitted part of i_{01} and i'_{o2}. Thus, equations (1.201) and (1.202) demonstrate that the intensity leaving a surface can be split into reflected, transmitted and emitted parts if scattering can be neglected. The emitted portion, using the definition of emittance, equation (1.163), is $\varepsilon'\left(\theta, \phi, \lambda, T, d\right) n_o^2 i_b\left(\lambda, T\right)$. In general, when scattering can be neglected, the intensity leaving a surface of the one-dimensional model can be written as follows,

$$\boxed{i_o = \rho' i_i + \tau' i'_i + n_o^2 \varepsilon' i_b\left(\lambda, T\right)} \qquad \Omega \ll 1 \tag{1.205}$$

where i_o is the intensity leaving the surface, i_i is the intensity incident on the surface, i_i' is the intensity incident on the opposite side and i_b is the blackbody intensity. Remember it has been assumed that i is independent of y and z so that the intensity is uniform over the surface. Also, scattering must be negligible ($\Omega << 1$) in order to separate the intensity into reflected, transmitted and emitted parts.

Now integrate equation (1.205) over the hemispherical solid angle at any point on the surface to determine the radiation flux, q_o, leaving the surface.

$$q_o = \int_{\Omega} i_o \cos\theta \, d\omega = \int_{\Omega} \rho' i_i \cos\theta \, d\omega + \int_{\Omega} \tau' i_i' \cos\theta \, d\omega + \int_{\Omega} n_o^2 \varepsilon' i_b \cos\theta \, d\omega \quad (1.206)$$

The *hemispherical spectral reflectance*, ρ, and *hemispherical spectral transmittance*, τ, are now defined as follows,

$$\rho(\lambda, d, T) \equiv \frac{q_r}{q_i} = \frac{\int_{\Omega} \rho' i_i \cos\theta \, d\omega}{\int_{\Omega} i_i \cos\theta \, d\omega} \quad (1.207)$$

$$\tau(\lambda, d, T) \equiv \frac{q_t}{q_i'} = \frac{\int_{\Omega} \tau' i_i' \cos\theta \, d\omega}{\int_{\Omega} i_i' \cos\theta \, d\omega} \quad (1.208)$$

where q_r is the reflected portion of the radiation flux, q_o, leaving the surface, and q_t is the transmitted portion of q_o. Using equations (1.171), (1.207), and (1.208) in equation (1.206) results in the following,

$$\boxed{q_o = \rho q_i + \tau q_i' + n_o^2 \varepsilon e_b(\lambda, T)} \qquad \Omega \ll 1 \quad (1.209)$$

where $e_b(\lambda,T) = \pi i_b(\lambda,T)$ is the blackbody emissive power.

Now integrate equation (1.209) over all wavelengths.

$$\overline{q}_o = \int_0^{\infty} q_o d\lambda = \int_0^{\infty} \rho q_i d\lambda + \int_0^{\infty} \tau q_i' d\lambda + n_o^2 \int_0^{\infty} \varepsilon e_b(\lambda, T) d\lambda \quad (1.210)$$

Define the *total hemispherical reflectance*, ρ_T, and *total hemispherical transmittance*, τ_T, as follows.

$$\rho_T(d,T) \equiv \frac{\overline{q}_r}{\overline{q}_i} = \frac{\int_0^\infty \rho q_i d\lambda}{\int_0^\infty q_i d\lambda} \tag{1.211}$$

$$\tau_T(d,T) \equiv \frac{\overline{q}_t}{\overline{q}_i'} = \frac{\int_0^\infty \tau q_i' d\lambda}{\int_0^\infty q_i' d\lambda} \tag{1.212}$$

Therefore, using equations (1.179), (1.211), and (1.212) in equation (1.210) yields the following result.

$$\boxed{\overline{q}_o = \rho_T \overline{q}_i + \tau_T \overline{q}_i' + n_o^2 \varepsilon_T \sigma_{sb} T^4} \qquad \Omega \ll 1 \tag{1.213}$$

Equations (1.205), (1.209), and (1.213) are the relations for the radiation intensity, i_o, radiation flux, q_o, and total radiation flux, $\overline{q}_o$, leaving the surface of a one dimensional body in terms of the optical properties. If the material is diffuse so that the optical properties are independent of angle, then the following relations apply.

$$\left.\begin{aligned} \rho' &= \rho \\ \tau' &= \tau \\ \varepsilon' &= \alpha' = \varepsilon = \alpha \end{aligned}\right\} \text{diffuse material} \tag{1.214, 1.215, 1.216}$$

In an addition, if the material is diffuse and gray (properties independent of wavelength), the following applies.

$$\left.\begin{aligned} \rho' &= \rho = \rho_T \\ \tau' &= \tau = \tau_T \\ \varepsilon' &= \varepsilon = \varepsilon_T = \alpha' = \alpha = \alpha_T \end{aligned}\right\} \text{diffuse} - \text{gray material} \tag{1.217, 1.218, 1.219}$$

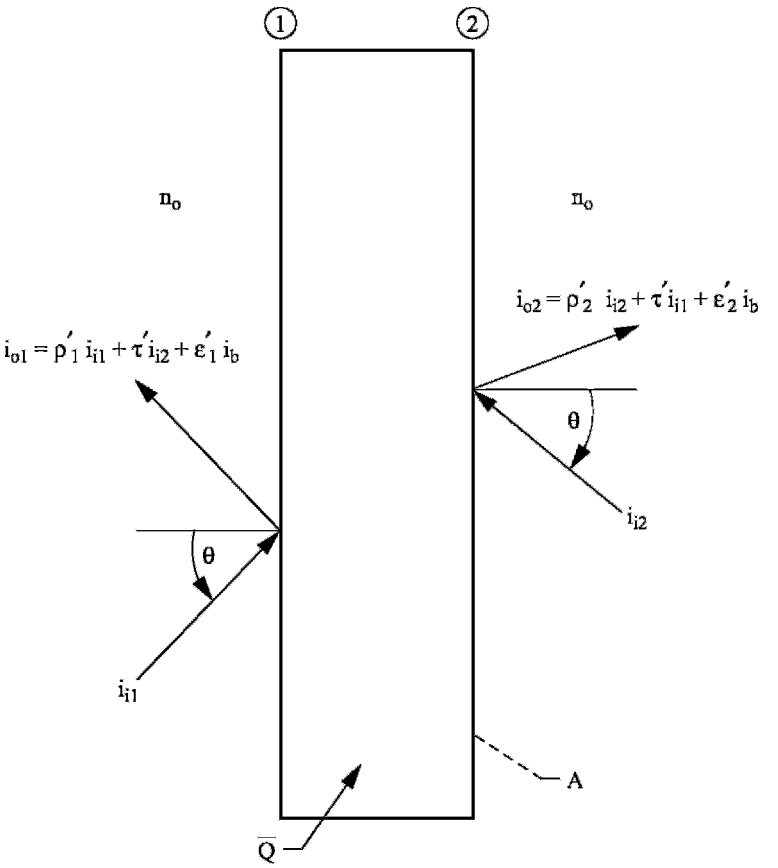

Figure 1.13.—Conservation of energy for one dimensional model.

1.8 Radiation Energy Balance for One Dimensional Model

Now consider the conservation of energy for the one-dimensional model shown in Figure 1.13, where there are incident intensities i_{i1} and i_{i2}. In order to maintain a steady state, energy must be either added or taken away when the material is emitting or absorbing. Therefore, using equation (1.205) for the intensities i_{01} and i_{02} the steady state conservation of energy is the following,

power in = power out

$$\overline{Q} + \int_o^\infty d\lambda \int_A dA \int_\Omega \left[i_{i1} + i_{i2} \right] \cos\theta d\omega = \tag{1.220}$$

$$\int_o^\infty d\lambda \int_A dA \int_\Omega \left[\left(\rho_1' + \tau' \right) i_{i1} + \left(\rho_2' + \tau' \right) i_{i2} + n_o^2 \left(\varepsilon_1' + \varepsilon_2' \right) i_b \left(\lambda, T \right) \right] \cos\theta d\omega$$

where A is the surface area and $\overline{Q}$ is the power supplied or removed. If power is being supplied $\overline{Q} > 0$ and if power is being taken away, $\overline{Q} < 0$. Rearranging equation (1.220) yields the following result.

$$\overline{Q} = \int_0^\infty d\lambda \int_A dA \int_\Omega \left[n_o^2 \left(\varepsilon_1' + \varepsilon_2' \right) i_b \left(\lambda, T \right) - \left(1 - \rho_1' - \tau' \right) i_{i1} - \left(1 - \rho_2' - \tau' \right) i_{i2} \right] \cos\theta d\omega \tag{1.221}$$

The conservation of energy can also be expressed by using the hemispherical directional spectral absorptance, α'. In that case,

$$\overline{Q} = \int_0^\infty d\lambda \int_A dA \int_\Omega n_o^2 \left[\varepsilon_1' + \varepsilon_2' \right] i_b \left(\lambda, T \right) \cos\theta d\omega - \int_0^\infty d\lambda \int_A dA \int_\Omega \left[\alpha_1' i_{i1} + \alpha_2' i_{i2} \right] \cos\theta d\omega \tag{1.222}$$

Subtracting equation (1.221) from (1.222) we see that the following must be true.

$$\int_o^\infty d\lambda \int_A dA \int_o \left[\left(1 - \rho_1' - \tau' - \alpha_1' \right) i_{i1} + \left(1 - \rho_2' - \tau' - \alpha_2' \right) i_{i2} \right] \cos\theta d\omega = 0 \tag{1.223}$$

The only way for equation (1.223) to be satisfied for all possible incident intensities is for the following to be true.

$$\rho_1' + \tau' + \alpha_1' = \rho_2' + \tau' + \alpha_2' = 1 \tag{1.224}$$

In general, for the one-dimensional model when scattering is negligible, the sum of the reflectance, transmittance, and absorptance is 1.

$$\boxed{\rho' + \tau' + \alpha' = 1} \qquad \Omega << 1 \tag{1.225}$$

And since $\varepsilon' = \alpha'$ the following also applies.

$$\boxed{\rho' + \tau' + \varepsilon' = 1} \qquad \Omega \ll 1 \tag{1.226}$$

If the hemispherical solid angle integration is carried out using equations (1.176), (1.207), and (1.208), then equation (1.223) becomes the following,

$$\int_0^\infty d\lambda \int_A \left[\left(1 - \rho_1 - \tau - \alpha_1\right) q_{i1} + \left(1 - \rho_2 - \tau - \alpha_2\right) q_{i2} \right] dA = 0 \tag{1.227}$$

where ρ, τ, and α are the hemispherical spectral reflectance, transmittance, and absorptance. For equation (1.227) to be valid for all q_{i1} and q_{i2} the following must be satisfied.

$$\boxed{\rho + \tau + \alpha = 1} \qquad \Omega \ll 1 \tag{1.228}$$

And if the material is diffuse or the incident intensity is isotropic then $\alpha = \varepsilon$ and the following applies.

$$\boxed{\rho + \tau + \varepsilon = 1} \qquad \Omega \ll 1 \text{ and material is diffuse or incident intensity is isotropic} \tag{1.229}$$

Finally, if the λ integration in equation (1.227) is carried out using equations (1.181) and (1.211) and (1.212), then the following is obtained.

$$\int_A \left[\left(1 - \rho_{T1} - \tau_T - \alpha_T\right) \bar{q}_{i1} + \left(1 - \rho_{T2} - \tau_T - \alpha_{T2}\right) \bar{q}_{i2} \right] dA = 0 \tag{1.230}$$

Thus to satisfy this result for all values of $\bar{q}_{i1}$ and $\bar{q}_{i2}$ the following must apply.

$$\boxed{\rho_T + \tau_T + \alpha_T = 1} \qquad \Omega \ll 1 \tag{1.231}$$

If the material is diffuse-gray, then $\alpha_T = \varepsilon_T$ and thus the following is time.

$$\boxed{\rho_T + \tau_T + \varepsilon_T = 1} \qquad \Omega \ll 1 \text{ and material is diffuse-gray} \tag{1.232}$$

Since the sum of reflectance, absorptance, and transmittance equals one, knowing two of these properties allows the third to be calculated.

Now return to the conservation of energy equation (1.222). In the one-dimensional model it is assumed that the intensities are uniform over the surface area, A. Therefore, if the ω and A integrations are carried out, the following is obtained.

$$\frac{\overline{Q}}{A} = \int_0^\infty \left[n_o^2 \left(\varepsilon_1 + \varepsilon_2 \right) e_b(\lambda, T) - \alpha_1 q_{i1} - \alpha_2 q_{i2} \right] d\lambda \tag{1.233}$$

For most TPV applications assume diffuse behavior so that $\alpha = \varepsilon$.

$$\frac{\overline{Q}}{A} = \int_0^\lambda \left[\varepsilon_1 \left(n_o^2 e_b - q_{i1} \right) + \varepsilon_2 \left(n_o^2 e_b - q_{i2} \right) \right] d\lambda \tag{1.234}$$

In addition, most TPV components are symmetrical so that $\varepsilon = \varepsilon_1 = \varepsilon_2$. Therefore, the energy balance equation that will be used to describe most TPV components is the following.

$$\boxed{\frac{\overline{Q}}{A} = \int_0^\lambda \varepsilon \left(2 n_o^2 e_b - q_{i1} - q_{i2} \right) d\lambda} \quad \text{for diffuse, symmetrical, one-dimensional material} \tag{1.235}$$

And if the material is diffuse-gray as well, $\varepsilon' = \varepsilon = \varepsilon_T = \alpha' = \alpha' = \alpha_T$ and equation (1.235) is the following.

$$\boxed{\frac{\overline{Q}}{A} = \varepsilon_T \left[2 n_o^2 \sigma_{sb} T^4 - \overline{q}_{i1} - \overline{q}_{i2} \right]} \quad \text{for diffuse-gray, symmetrical, one-dimensional material} \tag{1.236}$$

Thus the power input per unit surface area, $\overline{Q} / A$, is the difference between the power per unit area emitted by a blackbody minus the incident power per unit area multiplied by the total emittance, ε_T. For a one-dimensional material that emits on only one side, the factor of 2 in equations (1.235) and (1.236) must be removed.

1.9 Emittance of a Metal into a Dielectric

For most all metals, the extinction coefficient, K(λ), is large. As a result, the optical depth, $\kappa_d(\lambda)$ (equation (1.196)) is also large and the internal transmittance, t(λ) (equation (1.195)) is small. Therefore, if $t \approx 0$ the one-dimensional model (equations (1.203) and (1.204)) yields $\rho' = R'$ and $\tau' = 0$ where ρ' and τ' are the directional spectral

reflectance and transmittance and R′ is directional spectral reflectivity at the dielectric-metal interface. Thus the one-dimensional model (equation (1.226)) for negligible scattering ($\Omega \ll 1$) yields the following result for the directional spectral emittance.

$$\varepsilon' = 1 - \rho' = 1 - R' \qquad \text{for } \kappa_d \gg 1 \tag{1.237}$$

For a specular interface, $R' = \bar{R}$ (equation (1.103)) where $\bar{R}$ is the specular directional spectral reflectivity. In Section 1.5.4 it was pointed out that for wavelengths beyond the visible region, the real and imaginary parts of the index of refraction for a metal are large compared to the vacuum index of refraction (n_o = 1). As a result, Snell's Law says that the angle of refraction, θ_1^+, for radiation leaving a vacuum and entering a metal is $\theta_1^+ \approx 0$. For $\theta_1^+ \approx 0$, $\bar{R}$ (equation (1.103)) is the following,

$$\bar{R} = \frac{1}{2}\left(R_p + R_s\right) \tag{1.103}$$

where,

$$R_p = \frac{\left(n_{1R}\cos\theta_o^+ - n_o\right)^2 + n_{1I}^2\cos^2\theta_o^+}{\left(n_{1R}\cos\theta_o^+ + n_o\right)^2 + n_{1I}^2\cos^2\theta_o^+} \Bigg\} n_{1R}^2, n_{1I}^2, >> n_o^2 \tag{1.238}$$

$$R_s = \frac{\left(n_{1R} - n_o\cos\theta_o^+\right)^2 + n_{1I}^2}{\left(n_{1R} + n_o\cos\theta_o^+\right)^2 + n_{1I}^2} \Bigg\} \tag{1.239}$$

and θ_o^+ is the angle of incidence for radiation passing from the dielectric with index of refraction, n_o, into the metal with real and imaginary parts n_{1R} and n_{1I} of its complex index of refraction, $n_1 = n_{1R} - jn_{1I}$.

Using equation (1.103) for R′ in equation (1.237) yields the following result for the directional spectral emittance of a metal into a dielectric.

$$\varepsilon' = \frac{1}{2}\left(\varepsilon_p' + \varepsilon_s'\right) = 1 - \bar{R} \tag{1.240}$$

Where, $\bar{R}$ is given by equation (1.103) and ε_p' and ε_s' are the following.

$$\left.\begin{aligned}\varepsilon'_p &= 1-R_p = \frac{4n_o n_{1R}\cos\theta_o^+}{\left(n_o+n_{1R}\cos\theta_o^+\right)^2+n_{1I}^2\cos\theta_o^+} \\ \varepsilon'_s &= 1-R_s = \frac{4n_o n_{1R}\cos\theta_o^+}{\left(n_o\cos\theta_o^++n_{1R}\right)^2+n_{1I}^2}\end{aligned}\right\} n_{1R}^2, n_{1I}^2 >> n_o^2 \qquad (1.241),(1.242)$$

To obtain the hemispherical spectral emittance, ε, equation (1.240) must be substituted into equation (1.171) and the integration carried out.

$$\begin{aligned}\varepsilon(\lambda) &= \frac{1}{\pi}\int_{\theta=0}^{\pi/2}\int_{\phi=0}^{2\pi}\varepsilon'\left(\theta_o^+,\lambda\right)\cos\theta_o^+\sin\theta_o^+ d\phi d\theta_o^+ \\ &= 2\int_o^1 \varepsilon'(\mu,\lambda)\mu d\mu, \qquad \mu=\cos\theta_o^+ \\ &= \int_o^1\left[\varepsilon'_p(\mu,\lambda)+\varepsilon'_s(\mu,\lambda)\right]\mu d\mu\end{aligned} \qquad (1.243)$$

Integration of equation (1.243) yields the following result for the hemispherical spectral emittance of a metal into a dielectric when $n_{1R}^2, n_{1I}^2 >> n_o^2$.

$$\varepsilon(\lambda)=\frac{4n_{1R}}{n_o}\left\{1-\frac{n_{1R}}{n_o}\ln\left(\frac{n_m^2+2n_o n_{1R}+n_o^2}{n_m^2}\right)+\frac{n_o^2}{n_m^2}\left[1-\frac{n_o n_{1R}}{n_m^2}\ln\left(\frac{n_m^2+2n_o n_{1R}+n_o^2}{n_o^2}\right)\right]\right.$$
$$\left.+\frac{n_o^3\left(n_{1I}^2-n_{1R}^2\right)}{n_{1I}}\left[\frac{n_m^4+n_o^4}{n_o^4 n_m^4}\tan^{-1}\left(\frac{n_{1R}}{n_{1I}}\right)-\frac{1}{n_m^4}\tan^{-1}\left(\frac{n_m^2+n_o n_{1R}}{n_o n_{1I}}\right)-\frac{1}{n_o^4}\tan^{-1}\left(\frac{n_o+n_{1R}}{n_{1I}}\right)\right]\right\} \qquad (1.244)$$

Appearing in equation (1.244) is the quantity n_m defined as follows.

$$n_m^2 = n_{1R}^2+n_{1I}^2 \qquad (1.245)$$

The normal spectral emittance, $\varepsilon_n(\lambda)$, which is obtained by using equation (1.110) for $\bar{R}_n$ where $n_{oI} = 0$, is the following.

$$\varepsilon_n(\lambda)=1-\bar{R}_n=\frac{4n_o n_{1R}}{\left(n_o+n_{1R}\right)^2+n_{1I}^2} \qquad (1.246)$$

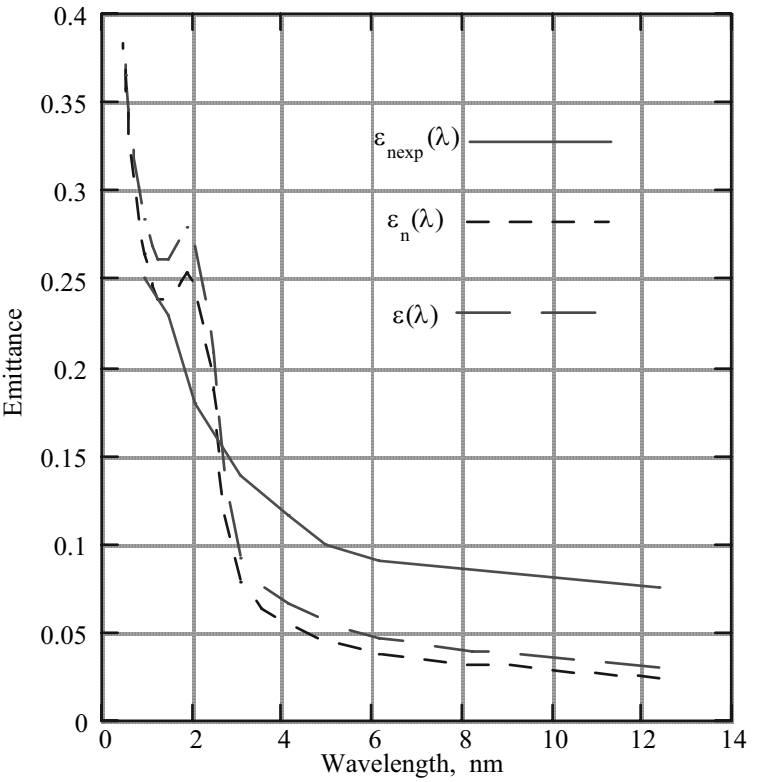

Figure 1.14 - Comparison of calculated hemispherical, $\varepsilon(\lambda)$, and normal, $\varepsilon_n(\lambda)$, spectral emittances with experimental normal spectral emittance, $\varepsilon_{nexp}(\lambda)$, into a vacuum for platinum. Experimental $\varepsilon_{nexp}(\lambda)$ taken from reference [19].□

In Figure 1.14, $\varepsilon(\lambda)$ and $\varepsilon_n(\lambda)$ for platinum (Pt) calculated using equations (1.244) and (1.246) are compared with the measured normal emittance, ε_{nexp}, taken from [19]. The calculated emittances used index of refraction data, n_{1R} and n_{1I}, for Pt taken from [20]. As the Figure shows, the calculated $\varepsilon_n(\lambda)$ and $\varepsilon(\lambda)$ are nearly the same. Also, they approximate the experimental ε_{nexp} fairly well. At large λ, $\varepsilon_n(\lambda)$ is smaller than ε_{nexp}, but for $\lambda < 3\mu m$, ε_n is larger than ε_{nexp}. Some of the difference at large λ results from experimental error (see [19]) in measuring small values of emittance like those that exist at large λ. For $\lambda < 1\mu m$ the indices of refraction, n_{1R} and n_{1I}, no longer satisfy $n_{1R}^2, n_{1I}^2 \gg n_o^2$. Therefore, the calculated results for $\varepsilon(\lambda)$ in Figure 1.14 for $\lambda < 1\mu m$ are

questionable. However, the calculated value for $\varepsilon_n(\lambda)$ given by equation (1.246) is applicable for all λ since the assumption $n_{1R}^2, n_{1I}^2 > n_o^2$ is not used.

The emittances, $\varepsilon(\lambda)$ and $\varepsilon_n(\lambda)$ given by equations (1.244) and (1.246) apply for a metal with a flat specular surface. However, just as discussed in Section 1.5.6, an uneven surface can be approximated as a series of flat surfaces. And since $\varepsilon' = 1 - R' \approx 1 - \overline{R}$, equations (1.244) and (1.246) should be good approximations for an uneven metal surface.

1.10 Summary

The TPV energy conversion concept was introduced, and the importance of matching the emitted radiation to the PV cells bandgap energy was pointed out. After a discussion of the history and applications for TPV energy conversion, electromagnetic wave propagation and radiation transfer have been introduced. Familiarity with these subjects is required in order to understand the optical properties such as emittance, reflectance and transmittance, which are necessary in calculating the performance of a TPV system.

Several of the important results from electromagnetic wave propagation and radiation transfer are the following.

1) Electromagnetic wave propagation (radiation) is described by Maxwell's equations. For a homogeneous, stationary medium, the electric and magnetic fields are determined by the so-called harmonic plane wave solution to Maxwell's equations.
2) A conductive medium ($\sigma \neq 0$) is described by an index of refraction, n, which has both real and imaginary parts. The imaginary part, which determines the dissipation, is related to the medium absorption coefficient, a.
3) Application of the proper boundary conditions at an interface between two media with indices of refraction n_1 and n_2 leads to the law of reflection for a specular interface and Snell's Law $n_1 \sin\theta_i = n_2 \sin\theta_r$ where θ_i is the angle of incidence and θ_r is angle of refraction.
4) Reflectivity, R, and transmittivity, T, at a specular interface have been calculated for so-called natural light (direction of electric field is random), which is appropriate for TPV applications.
5) Radiation transfer theory is required to analyze a medium that is emitting, absorbing, and scattering. The radiation intensity, i, has been defined and the radiation transfer equations and the energy equation appropriate for TPV applications have been presented.
6) Application of radiation transfer theory to a one-dimensional medium with negligible scattering produced results for the radiation flux, q_o, leaving a

surface and the reflectance, ρ, and transmittance, τ. Conservation of energy for the one-dimensional medium leads to the relation $\rho + \tau + \alpha = 1$, where α is the absorptance.

7) A blackbody absorbs and emits the maximum possible radiation at any wavelength and direction for a given temperature.
8) Blackbody spectral emissive power into a vacuum, $e_b(\lambda,T)$ is given by Plank's distribution (equation (1.120)) and total emissive power, $e_{bT} = \sigma_{sb}T^4$.
9) The quantity, $F_{0-\lambda T}$, which is the fraction of the total blackbody emissive power, e_{bT}, that lies in the wavelength range 0 to λ, has been derived. $F_{o-\lambda T}$ is important for determining the performance of an emitter in a TPV system.
10) Since the total emissive power, $q_E = n_o^2 \varepsilon_T \sigma_{sb} T_E^4$, is very sensitive to T_E the performance of a TPV energy converter strongly depends upon the emitter temperature, T_E.

References

[1] H.H. Kolm, Quarterly Progress Report, Solid State Research, Group 35, MIT-Lincoln Laboratory, Lexington, MA, May 1, 1956, 13.
[2] D.C. White, B.D. Wedlock, and J. Blair, Proc. 15th Power Sources Conf., (1961) 125.
[3] B.D. Wedlock, Proc. 3rd PV Specialists Conf., Vol. III, (1963) A-4-1.
[4] B.D. Wedlock, Proc. IEEE 51, (1963) 694.
[5] J. Werth, Proc. 17th Power Source Conf., (1963) 23.
[6] J. Werth, Proc. 3rd PV Specialists Conf. Vol. II, (1963) A-6-1.
[7] R. E. Henderson, Proc. 3rd PV Specialists Conf., Vol. II, (1963) A-5-1.
[8] W. Shockley, H. J. Queisser, J. Appl. Physics, 32, (1961) 136.
[9] L. Broman, Process in Photovoltaics: Research and Applications, 3, (1995) 65, also NREL/TP 412–6845, (1994).
[10] M. Born, E. Wolf, Principles of Optics, Electromagnetic Theory of Propagation Interference and Diffraction of Light, Pergamon Press, Fourth edition 1970, Chapter 1.
[11] A. M. Portis, Electromagnetic Fields, Sources and Media, John Wiley & Sons, 1978, Chapter 12.
[12] J. A. Kong, Electromagnetic Wave Theory, John Wiley and Sons, 1986.
[13] J. D. Jackson, Classical Electrodynamics, second edition, John Wiley and Sons, 1975.
[14] A. Fresnel, Mén.de ℓ'Acad., 11 (1832), 393; Ownes, 1, 767.
[15] L. Ward, The Optical Constants of Bulk Materials and Films, Adam Hilger, 1988.

[16] R. Siegel and J. R. Howell, Thermal Radiation Heat Transfer, 2nd ed., Hemisphere Publishing Corp., New York, 1981.
[17] R. Eisberg and R. Resnick, Quantum Physics of Atoms, Molecules, Solids, Nuclei and Particles, 2nd ed., John Wiley and Sons, New York, 1985, 13.
[18] S. Chandrasekhar, Radiative Transfer, Dover Publications, 1960.
[19] T. S. Touloukian and D. P. DeWitt, Thermophysical Properties of Matter, vol. 7", Plenum Press, 1970.
[20] Handbook of Chemistry and Physics, 71st ed., edited by D. R. Lide, 1990-1991, 12-95.

Problems

1.1 For a plane wave,

$$A = A_o \exp\left[j\left(\omega t - \vec{k}\cdot\vec{x}\right)\right]$$

where A_o, $\vec{k}$, and ω are constants show that

$$\frac{\partial A}{\partial t} = j\omega A \qquad \left(\frac{\partial}{\partial t} = j\omega\right)$$

and

$$\nabla A = -j\vec{k}A \qquad \left(\nabla = -j\vec{k}\right)$$

1.2 Show that for the plane wave solutions, $\vec{E} = \vec{E}_o \exp\left[j\left(\omega t - \vec{k}\cdot\vec{x}\right)\right]$ and $\vec{H} = \vec{H}_o \exp\left[j\left(\omega t - \vec{k}\cdot\vec{x}\right)\right]$ to be valid solutions of Maxwell's equations for an isotropic, stationary medium, $\vec{k}\cdot\vec{E} = \vec{k}\cdot\vec{H} = 0$.

1.3 For a plane wave, $\vec{E} = \vec{E}_o \exp\left[j\left(\omega t - \vec{k}\cdot\vec{x}\right)\right]$, the wave vector, $\vec{k}$, must be perpendicular to the electric field, $\vec{E}$, and the medium must be homogenous and stationary. Show that this requires $\nabla\cdot\vec{E} = 0$ and no charge density can exist ($\rho = 0$).

1.4 For a linear, isotropic, stationary medium, derive the following wave equation for $\vec{H}$ from Maxwell's equations.

$$\nabla^2\vec{H} - \sigma\mu\frac{\partial\vec{H}}{\partial t} - \varepsilon\mu\frac{\partial^2\vec{H}}{\partial t^2} = 0$$

Notice it is not necessary to assume that the charge density must vanish ($\rho = 0$) to obtain this result.

Hint: $\nabla\times\nabla\times\vec{A} = \nabla\left(\nabla\cdot\vec{A}\right) - \left(\nabla\cdot\nabla\right)\vec{A}, \quad \nabla\cdot\nabla \equiv \nabla^2$

1.5 Show that an imaginary part of $\vec{k} = \left(k_R - jk_I\right)\hat{s}$ leads to attenuation of a plane wave in the direction of propagation, $\hat{s}$.

1.6 Show that $\vec{E}\times\vec{H}$ points in the direction of $\vec{k}$ for plane electromagnetic waves.

1.7 Show that the time average over a period, $2\pi/\omega$, of the product of the real parts of two sinusoidal varying quantities, $A = A_o \exp[i(\omega t - a)]$ and $B = B_o \exp[i(\omega t - b)]$ is the following.

$$\frac{\omega}{2\pi}\int_o^{\frac{2\pi}{\omega}} \mathrm{Re}\left[A\right]\mathrm{Re}\left[B\right]dt = \frac{1}{2}\mathrm{Re}\left[AB^*\right]$$

Where A_o, a, B_o, b are complex constants and ω and t are real. (* denotes complex conjugate)

1.8 The magnitude of the complex wave vector, $k = k_R - jk_I$, and index of refraction, $n = n_R - jn_I$, are given in terms of the complex dielectric constant $\bar{\varepsilon}_r = \varepsilon_R - i\varepsilon_I$ by equations (1.26b) and (1.30a) and (1.30b). Obtain expressions for ε_R and ε_I in terms of n_R and n_I.

1.9 Using Snell's Law, rewrite the reflection and transmission coefficients given by equations (1.83) and (1.84) in terms of θ_o^+ and θ_1^+ only. Show that $r_s < 0$ if $n_o < n_1$ for dielectric materials, ($\sigma = n_I = 0$, $\mu = \mu_o$). Also, for dielectrics determine the angle of incidence, θ_o^+, in terms of the indices of refraction for which $r_p = 0$. This is called the Brewster Angle.

1.10 Consider a diffuse ($e(\theta,\lambda) = i(\lambda)\cos\theta$) emitting surface. Calculate q the energy radiated per unit area per unit of wavelength from an elemental area, dA, of the surface to obtain the spectral emissive power.

$$e(\lambda) \equiv \frac{qdAd\lambda}{dA\, d\lambda} = \pi i(\lambda)$$

1.11 For the case $\frac{hc_o}{k\lambda T} > 1$, the approximation $\exp\left[\frac{hc_o}{k\lambda T}\right] \gg 1$ can be used in the blackbody spectral emissive power expression given by equation (1.120). This results in Wien's formula.

$$\frac{e_b(\lambda, T)}{T^5} = \frac{2\pi hc_o^2}{(\lambda T)^5} e^{-hc_o/k\lambda T}$$

Use this approximation to obtain the following result for the value of λT that yields maximum $e_b(\lambda,T)$.

$$\lambda_{max} T = \frac{hc_o}{5k} = 2878\ \mu m\ K$$

1.12 Using equations (1.120) and (1.134) and also

$$\int_0^\infty \frac{u^3}{e^u - 1} du = \frac{\pi^4}{15}$$

show that equation (1.135) is obtained for e_{bT}, the total blackbody emissive power into a vacuum.

1.13 Show that the fraction of the blackbody total emissive power that lies in the wavelength range between 0 and λ, as given by equation (1.137) can be written as follows.

$$F_{o-\lambda T} = \frac{15}{\pi^4} \int_u^\infty \frac{x^3}{e^x - 1} dx$$

Where

$$u = \frac{hc_o}{k\lambda T} = \frac{E}{kT} = \frac{h\nu}{kT}$$

1.14 In most TPV applications $u = \frac{hc_o}{k\lambda T} = \frac{E}{kT} = \frac{h\nu}{kT} > 1$ Therefore, the approximation $e^u \gg 1$ can be made. For $e_u \gg 1$ show that,

$$F_{o-\lambda T} = \frac{15}{\pi^4} e^{-u}\left[u^3 + 3u^2 + 6u + 6\right], \quad u = \frac{hc_o}{k\lambda T} = \frac{E}{kT}$$

1.15 A selective emitter efficiency can be defined as follows.

$$\eta_E \equiv \frac{\text{Emitted radiation that is convertible to electrical energy by PV cell}}{\text{Total emitted radiation}}$$

$$\eta_E = \frac{\int_o^{\lambda g} \varepsilon_E e_b(\lambda, T_E)\, d\lambda}{\int_o^{\infty} \varepsilon_E e_b(\lambda, T_E)\, d\lambda}$$

Where, ε_E is the emitter spectral emittance, e_b is the blackbody spectral emissive power, $\lambda_g = \frac{hc_o}{E_g}$ is the wavelength corresponding to the PV cells bandgap energy, E_g, and T_E is the emitter temperature.

a) Show that,

$$\eta_E = \frac{1}{1 + \frac{\varepsilon_\ell}{\varepsilon_b}\left[\frac{1}{F_{o-\lambda_g T_E}} - 1\right]}$$

where

$$\varepsilon_b = \frac{\int_o^{\lambda g} \varepsilon_E e_b(\lambda, T_E)\, d\lambda}{\int_o^{\lambda g} e_b(\lambda, T_E)\, d\lambda} \qquad \varepsilon_\ell = \frac{\int_{\lambda g}^{\infty} \varepsilon_E e_b(\lambda, T_E)\, d\lambda}{\int_{\lambda g}^{\infty} e_b(\lambda, T_E)\, d\lambda}$$

b) Assuming $\varepsilon_\ell/\varepsilon_b$ is independent of T_E show that η_E is a monotonically increasing function of $\lambda_g T_E$ with $\eta_E = 0$ for $\lambda_g T_E = 0$ and $\eta_E = 1$ for $\lambda_g T_E \to \infty$.

c) For $\varepsilon_b = 0.7$, $\varepsilon_\ell = 0.15$, $T_E = 1700$K and $\lambda_g = 1.5$ μm calculate η_E using $F_{0-\lambda_g T_E}$ given in problem 1.14.

1.16 Solve equations (1.193) and (1.194), and (1.197) to (1.200) for the radiation intensities i_{o1} and $i_{o2'}$ leaving the one-dimensional radiation model shown in Figure 1.12.

1.17 Consider a one-dimensional, diffuse-gray body in a vacuum, so that no heat is conducted in or out of the body. What is its temperature if illuminated on one side by the sun at Earth orbit? (solar radiation flux at Earth orbit ≈ 0.14 W/cm2).

1.18 Consider two infinite parallel, opaque (no transmittance, $\tau = 0$) plates in a vacuum that can be approximated as diffuse-gray bodies. Solve for the net radiation energy exchange, $\bar{q}$, between the plates in terms of their temperatures T_1 and T_2 ($T_1 > T_2$) and their total hemispherical emittances εT_1 and εT_2. (Hint: all radiation leaving one plate is incident on the other plate, $\bar{q}_{01} = \bar{q}_{i2}$ and $\bar{q}_{02} = \bar{q}_{i1}$. What is $\bar{q}$, if $T_1 = 1700$ K, $T_1 = 300$ K, $\varepsilon T_1 = 0.8$, and $\varepsilon T_2 = 0.2$?

1.19 1.19 Consider two concentric, opaque cylinders that can be approximated as diffuse-gray bodies of radii r_1 and r_2 ($r_1 < r_2$) and length, ℓ, in a vacuum. Assume $\ell \gg r_1, r_2$ so that all radiation leaving each cylinder is incident on the other cylinder. Calculate the radiation energy exchange per unit length, $\frac{\bar{Q}}{\ell}$, between the cylinders in terms of their temperatures T_1 and T_2 ($T_1 > T_2$), total hemispherical emittances, εT_1 and εT_2, and their radii r_1 and r_2. $\left(\text{Hint: } \bar{Q} = 2\pi r_1 \ell \left(q_{01} - q_{i1}\right) = 2\pi r_2 \ell \left(q_{i2} - q_{02}\right)\right)$. What is $\frac{\bar{Q}}{2\pi r_1 \ell}$ and $\frac{\bar{Q}}{2\pi r_2 \ell}$ if $T_1 = 1700$ K, $T_2 = 300$ K, $\varepsilon T_1 = 0.8$, $\varepsilon T_2 = 0.2$, $r_1 = 5$cm and $r_2 = 5.2$cm?

1.20 Show that for $T_1^4 \gg T_2^4$ the radiation flux $\bar{q}$, for the infinite plates (problem 1.18) and the radiation flux $\frac{\bar{Q}}{2\pi r_1 \ell}$ for the infinite concentric cylinders (problem 1.19) are approximately the same $\left(\bar{q} \approx \frac{\bar{Q}}{2\pi r_1 \ell}\right)$ if the emittances are the same in both cases.

Chapter 2
Maximum Efficiency and Power Density for TPV Energy Conversion

Several properties of TPV energy conversion can be illustrated by considering the efficiency of the simplest possible system, namely an emitter and PV cells. This chapter focuses on the efficiency and output of that simple system.

2.1 Symbols

A	surface area, m^2
c_o	speed of light in a vacuum (2.9979×10^8 m/sec)
E	photon energy, J
e	electron charge (1.602×10^{-19} coul)
e_b	blackbody spectral emissive power, $W/cm^2/\mu m$
$F_{o-\lambda T}$	fraction of total blackbody intensity or emissive power lying in region $0 - \lambda T$
$F(u_g)$	integral defined by equation (2.21)
$G(u_g)$	integral defined by equation (2.22)
h	Plank's constant (6.6262×10^{-34} J.sec)
k	Boltzmann constant (1.3806×10^{-23} J/K)
P_{ELMAX}	electrical power output of TPV system model in figure 2.1, W
$\overline{Q}_n$	total thermal power input to emitter in TPV system, W
q_o	spectral radiant flux leaving a surface, $W/m^2/\mu m$
q_i	spectral radiant flux incident on a surface, $W/m^2/\mu m$
R	parameter defined by equation (2.23)
T	temperature, K
α	spectral absorptance
ε	spectral emittance
λ	wavelength, μm
ρ	spectral reflectance
σ_{sb}	Stefan Boltzmann constant $= \dfrac{2\pi^5 k^4}{15 h^3 c_o^2}$ (5.6696×10^{-8} $W/m^2/K^4$)
η_{MAX}	maximum TPV system efficiency for model in Figure 2.1

Subscripts

b	refers to in-band radiation ($E_g \leq E < \infty$)
c	refers to PV cells
E	refers to emitter
g	corresponding to PV cell bandgap energy
i	refers to incident radiation
l	refers to out-of-band radiation ($0 \leq E < E_g$)
o	refers to outgoing radiation

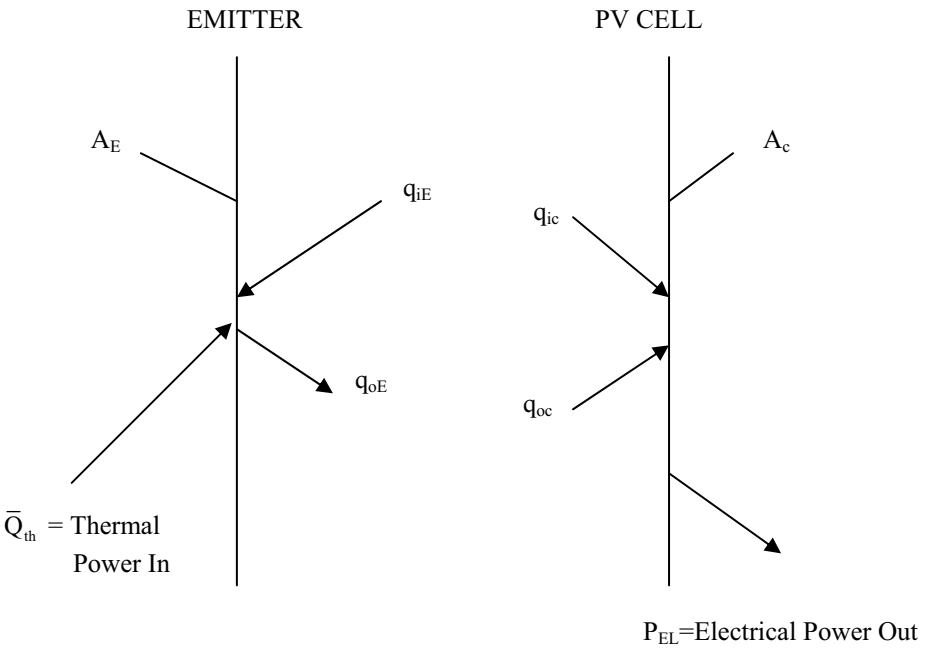

Figure 2.1- Simple TPV model used to calculate the maximum efficiency, η_{MAX}.

2.2 Maximum TPV Efficiency

Consider the TPV system shown in Figure 2.1 which consists of an emitter of area A_E and PV cells of area A_c. Assume the system is in a vacuum so that there is no convective or conductive heat loss. Therefore, the thermal energy, $\bar{Q}_{th}$, supplied to the emitter is just the difference in the total outgoing radiation and the total incident radiation on the emitter. Assuming the radiation fluxes are uniform across the emitter yields the following.

$$\bar{Q}_{th} = A_E \int_0^\infty \left(q_{oE} - q_{iE} \right) d\lambda \tag{2.1}$$

The outgoing radiation flux per unit of wavelength is q_{oE} and the incident radiation flux per unit of wavelength is q_{iE}. The emitter area is A_E and λ is the wavelength. Similarly, q_{oc} is the outgoing radiation flux, and q_{ic} is incident radiation flux at the PV cells.

The outgoing radiation flux is the sum of the emitted radiation and the reflected radiation [equation 1.209)]. Therefore, for the emitter and the PV cells the following is obtained.

$$q_{oE} = \varepsilon_E e_{bE}(\lambda, T_E) + \rho_E q_{iE} \tag{2.2}$$

$$q_{oc} = \varepsilon_c e_{bc}(\lambda, T_c) + \rho_c q_{ic} \tag{2.3}$$

Appearing in these equations are the emittances ε_E and ε_c and reflectances ρ_E and ρ_c of the emitter and PV cells. Also, $e_b(\lambda,T)$ is the blackbody emissive power, which is given by equation (1.120). Since the system is in a vacuum the intensity will be constant everywhere between the emitter and PV cells. In addition, make the critical assumption that all the radiation leaving the emitter goes directly to the PV cells and all radiation leaving the PV cells goes directly to the emitter. Thus any leakage of radiation out of the system is being neglected. In Chapter 7 the consequences of radiation leakage is discussed in detail. Making the no leakage assumption and also the assumption that all q's are uniform, the following conditions apply.

$$q_{oE} = q_{ic} \tag{2.4}$$

$$q_{oc} = q_{iE} \tag{2.5}$$

Using equations (2.4) and (2.5) in (2.2) and (2.3) produces two linear equations for q_{iE} and q_{ic} which can be solved to produce the following.

$$q_{iE} = \frac{\varepsilon_c e_{bc} + \rho_c \varepsilon_E e_{bE}}{1 - \rho_E \rho_c} \tag{2.6}$$

$$q_{ic} = \frac{\varepsilon_E e_{bE} + \rho_E \varepsilon_c e_{bc}}{1 - \rho_E \rho_c} \tag{2.7}$$

Using equations (2.2) and (2.6) in (2.1) yields the following result for the thermal power input.

$$\overline{Q}_{th} = A_E \int_o^\infty \frac{\varepsilon_E (1-\rho) e_{bE} - \varepsilon_c (1-\rho_E) e_{bc}}{1 - \rho_c \rho_E} d\lambda \tag{2.8}$$

In order to calculate the efficiency, the electrical power output must be determined.

$$P_{EL} = \int_{A_c} JV dA \tag{2.9}$$

Where J is the current density (amp/cm^2), V is the electric potential developed by the PV cells and A_c is the surface area of the PV cells. To determine, JV assume the "perfect" PV cell, which is the PV cell model Shockley and Queisser [1] used in calculating what they called the "ultimate" efficiency of a PV cell. In that case, the potential is the largest possible value, namely the bandgap energy of the PV cells in electron-volts, $V = E_g / e = \dfrac{hc_o}{e\lambda_g}$, where e is the electron charge (e = 1.602 × 10^{-19} Coul). The largest possible current density, J, is achieved when each photon with $E > E_g$ that is absorbed produces a current carrier. Thus, the current density produced for the infinitesimal photon energy dE or wavelength dλ is the following.

$$dJ = e\alpha_c \frac{q_{ic}(E)}{E} dE = e\alpha_c q_{ic}(\lambda)\left(\frac{\lambda}{hc_o}\right) d\lambda \tag{2.10}$$

Where α_c is the spectral absorptance. Therefore, assuming the PV cells are *opaque* ($\tau_c = 0$), so that $\alpha_c = 1 - \rho_c$ [equation (1.228)], the maximum possible electrical output is the following since it is assumed that q_{ic} is uniform across A_c.

$$P_{ELMAX} = \frac{A_c}{\lambda_g} \int_o^{\lambda_g} (1 - \rho_c) q_{ic} \lambda \, d\lambda \tag{2.11}$$

Now define the maximum possible efficiency as follows.

$$\eta_{MAX} = \frac{P_{ELMAX}}{\bar{Q}_{th}} \tag{2.12}$$

Therefore, using equations (2.7), (2.8), and (2.11) and assuming $A_E = A_c$ yields the following result for the maximum efficiency.

$$\eta_{MAX} = \frac{1}{\lambda_g} \frac{\int_o^{\lambda_g} (1-\rho_c)\left[\frac{\varepsilon_E e_{bE} + \rho_E \varepsilon_c e_{bc}}{1-\rho_E\rho_c}\right]\lambda d\lambda}{\int_o^{\infty}\left[\frac{\varepsilon_E (1-\rho_c) e_{bE} - \varepsilon_c (1-\rho_E) e_{bc}}{1-\rho_E\rho_c}\right]d\lambda} \tag{2.13}$$

Since the PV cell temperature $T_c \ll T_E$, the PV cell emission is small and the $\varepsilon_c e_{bc}$ term can be neglected in equation (2.13).

$$\eta_{MAX} = \frac{1}{\lambda_g} \frac{\int_o^{\lambda_g}\left[\frac{\varepsilon_E (1-\rho_c) e_{bE}}{1-\rho_E\rho_c}\right]\lambda d\lambda}{\int_o^{\infty}\left[\frac{\varepsilon_E (1-\rho_c) e_{bE}}{1-\rho_E\rho_c}\right]d\lambda} \tag{2.14}$$

Using equation (1.120) for e_{bE} and defining a new integration variable $u = hc_o/k\lambda T_E$ yields the following (problem 2.1),

$$\boxed{\eta_{MAX} = u_g \frac{\int_o^{\infty} \frac{\varepsilon_E (1-\rho_c)}{1-\rho_c(1-\varepsilon_E)}\left[\frac{u^2}{e^u - 1}\right]du}{\int_o^{u_g} \frac{\varepsilon_E (1-\rho_c)}{1-\rho_c(1-\varepsilon_E)}\left[\frac{u^3}{e^u - 1}\right]du}} \tag{2.15}$$

where an opaque, diffuse emitter is assumed so that $\varepsilon_E = \alpha_E = 1 - \rho_E$ and the parameter u_g is defined as,

$$u_g \equiv \frac{hc_o}{k\lambda_g T_E} = \frac{E_g}{kT_E} \tag{2.16}$$

As equation (2.15) shows, η_{MAX} depends upon the emitter emittance, ε_E, the PV cells reflectance, ρ_c, as well as, the parameter, u_g. The parameter, u_g, is defined as the *PV cell dimensionless bandgap energy*. It is the ratio of the PV cell bandgap energy, E_g, to the emitter thermal energy, kT_E. This is an important parameter for determining efficiency for any TPV system, not just the simple model described by equation (2.15).

The simple model also illustrates that the efficiency can be maximized by using the optimum emitter spectral emittance, ε_E, and (or) PV cell spectral reflectance, ρ_c.

2.3 Maximum TPV Efficiency for Constant Emitter Emittance and PV Cell Reflectance

To illustrate the importance of u_g in determining η_{MAX}, assume ε_E and ρ_c are constants so that equation (2.15) becomes the following.

$$\eta_{MAX} = \frac{15}{\pi^4} u_g \int_{u_g}^{\infty} \frac{u^2}{e^u - 1} du \tag{2.17}$$

The following result was used in obtaining equation (2.17).

$$\int_o^{\infty} \frac{u^3}{e^u - 1} du = \frac{\pi^4}{15} \tag{2.18}$$

Equation (2.17) is the "ultimate" efficiency of a PV cell as given by Shockley and Queisser [1]. For $u_g \to \infty$ or $u_g = 0$, η_{MAX} vanishes and for $0 \le u_g < \infty$, η_{MAX} is finite. Thus equation (2.17) will have a maximum value. This is shown in Figure 2.2 where η_{MAX} is shown as a function of u_g. The integral in equation (2.17) was numerically integrated to obtain Figure 2.2. As can be seen, a maximum value of .44 occurs at $u_g = E_g/kT_E = 2.17$. Emitter temperatures in a practical TPV system are in the region $1200 \le T_E \le 2000$ K. Therefore, if $u_g = 2.17$ then $0.22 \le E_g \le .37$ eV. Currently, PV cells with bandgap energies this low are not available. Consider the case where $E_g = .72$ eV, which applies for GaSb, and $T_E = 1700$ K. Therefore, $u_g = 4.9$ and $\eta_{MAX} = 0.2$. Thus, if TPV systems must operate with constant emitter emittance and PV cell reflectance, then efficiency greater than 0.2 is not expected. However, by choosing the proper variation of ε_E and ρ_c, it is possible to achieve an even greater η_{MAX}. The process of controlling the wavelength dependence of ε_E and ρ_c to obtain large efficiency is called *spectral control*.

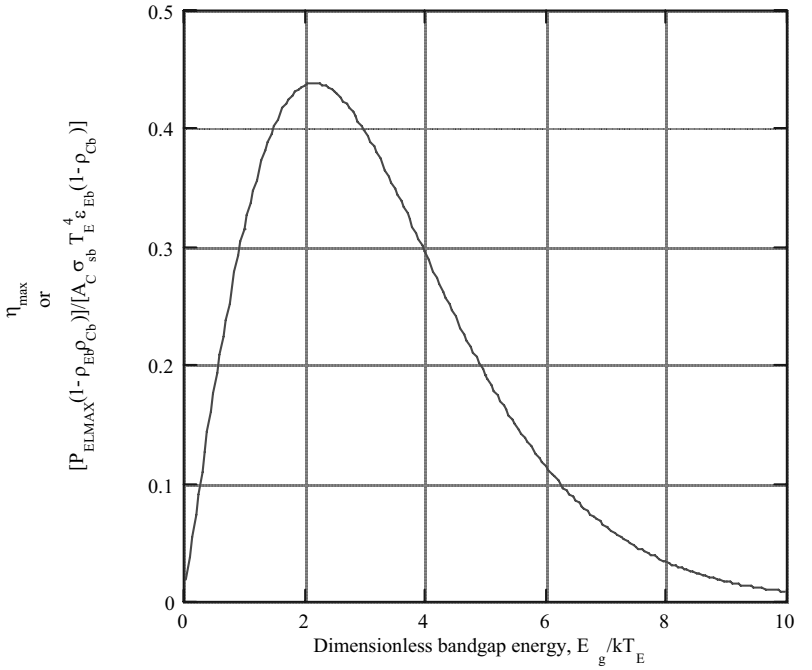

Figure 2.2 - Maximum TPV efficiency for emitter emittance, ε_E, and PV cell reflectance, ρ_C, being constants for the entire spectrum. Also, dimensionless maximum power density for $\varepsilon_E=\varepsilon_{Eb}$ and $\rho_C=\rho_{Cb}$ for $E_g < E=hc_0/k\lambda T_E < \infty$.

2.4 Ideal TPV System

To obtain the largest η_{MAX} possible, the denominator in equation (2.15) should be minimized and the numerator maximized. Obviously, if $\rho_c = 1$ or $\varepsilon_E = 0$ for $0 \le u < \infty$ ($0 \le E < \infty$) both the numerator and denominator vanish. However, if $\rho_c = 1$ or $\varepsilon_E = 0$ for $0 \le u \le u_g$ ($0 \le E < E_g$) then the denominator is greatly reduced while the numerator is unchanged. In addition, if $\varepsilon_E = 1$ and $\rho_c = 0$ for $u_g \le u < \infty$ ($E_g \le E < \infty$), then the numerator is maximized. Physically this means that for photon energies less than the bandgap energy ($E < E_g$), no radiation is being emitted, or all the emitted radiation is being reflected back to the emitter. In addition, for $E > E_g$ the emitter behaves as a blackbody and the PV cells are totally absorbing. Under these conditions, the following result is obtained from equation (2.15).

$$\eta_{MAX} = u_g \frac{\int_{u_g}^{\infty} \frac{u^2}{e^u - 1} du}{\int_{u_g}^{\infty} \frac{u^3}{e^u - 1} du} \qquad \begin{array}{c} \text{Ideal TPV System} \\ \varepsilon_E = 0 \text{ or } \rho_c = 1 \text{ for } 0 \le E \le E_g \\ \varepsilon_E = 1 \text{ and } \rho_c = 0 \text{ for } E_g < E < \infty \end{array} \tag{2.19}$$

If the integrals in equation (2.19) are evaluated numerically, the results are those shown in Figure 2.3. Note that $\eta_{MAX} \to 1$ for $u_g \to \infty$ ($T_E \to 0$ or $E_g \to \infty$). In the previous example (Figure 2.2) there is an optimum $u_g = 2.17$ for maximum η_{MAX}. For $u_g \to \infty$ there is either no thermal input ($T_E \to 0$) or no electrical output ($E_g \to \infty$) so that even though $\eta_{MAX} \to 1$, the electrical power output vanishes (see problem 2.4). Thus for the *ideal TPV system* described by equation (2.19) a paradox for the efficiency and power output occurs. As efficiency of 100% is approached no power is produced!

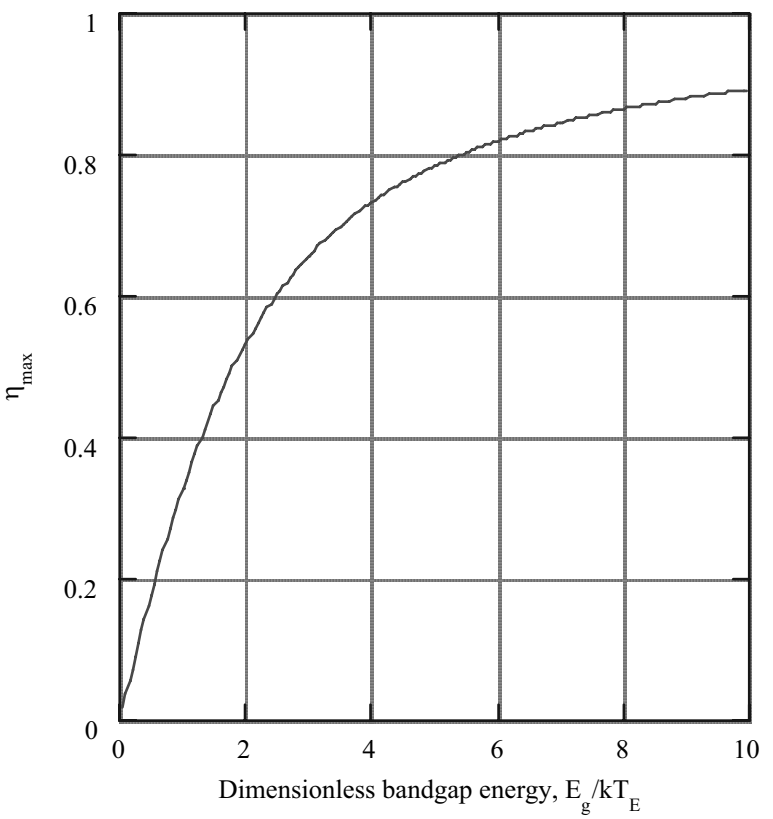

Figure 2.3 - Maximum TPV efficiency for ideal system, ε_E=0 or ρ_C=1. for 0<E<E_g and ε_E=1. and ρ_C=0 for E_g<E<∞

In the previous section the case of GaSb PV cells at T_E = 1700 K (u_g = 4.9) led to the result η_{MAX} = 0.2 for constant ε_E and ρ_c. For the ideal TPV system and u_g = 4.9, Figure 2.3 shows that η_{MAX} = 0.78. Thus, by optimizing the spectral distribution of the radiation, or in other words, utilizing efficient spectral control, large improvements in TPV efficiency can be achieved.

For the ideal TPV system where $\varepsilon_E = 0$ for $0 \le E < E_g$ and $\varepsilon_E = 1$, $\rho_c = 0$ for $E_g \le E < \infty$, all the photons produced by the thermal input, $\overline{Q}_{th}$, create current in the PV cells. For the case where $\rho_c = 1$ for $0 \le E < E_g$ and $\varepsilon_E = 1$, $\rho_c = 0$ for $E_g \le E < \infty$, all the photons emitted create current in the PV cells or are reflected back to the emitter where they can be absorbed and heat the emitter. In both cases, the only loss that occurs in the system is the photon energy in excess of the bandgap energy ($E - E_g$) that is transferred to the lattice of the PV cells and shows up as heat for photon energies $E > E_g$. If the emitter were a monochromatic source (all emitted photons have the same energy) with $E = E_g$ and $\rho_c = 0$, then $\eta_{MAX} = 1$ for all values of u_g (problem 2.5). In other words, all emitted photons produce current in the PV cells and no excess photon energy shows up as heat. Obviously, it would be very desirable to have a thermal monochromatic radiation source where $E = E_g$ in a TPV energy conversion system. As a result, a major part of TPV research is directed at achieving good spectral control. That is, to match the energy of the photons incident on the PV array to PV array bandgap energy. As already mentioned in sections 1.2, there are two methods for producing such radiation. The first is to use so-called selective emitters that have the majority of their emission in a single narrow emission band. The second method is to combine a gray body emitter (ε_E = constant < 1) with a narrow bandpass optical filter so that the combination of emitter and filter performs like a selective emitter. It is also possible to combine both a selective emitter and a filter for spectral control.

2.5 Approximation of Selective Emitter and Filter TPV Systems

Approximate a selective emitter or filter TPV system using the simple model of Figure 2.1 as follows. The PV cell's spectral reflectance, ρ_c, can be used to describe the performance of a filter that is located on the PV cell's surface. Obviously, a selective emitter's performance is determined by the spectral emittance, ε_E. For photon energies, $0 \le E < E_g$, assume the optical properties of the emitter and PV cells are constants, $\varepsilon_E = \varepsilon_{El}$ and $\rho_c = \rho_{cl}$. For $E_g \le E < \infty$ again assume constant optical properties for the emitter and filter, $\varepsilon_E = \varepsilon_{Eb}$ and $\rho_c = \rho_{cb}$. Thus, the spectrum is split into two regions: $0 \le E < E_g$ and $E_g \le E < \infty$. In each region assume constant optical properties. This is called a *two band model* for a TPV system.

Using the approximations for the two band model in equation (2.15) yields the following result (problem 2.6).

$$\eta_{MAX} = u_g \frac{G(u_g)}{F(u_g) + R\left[\frac{\pi^4}{15} - F(u_g)\right]} \qquad \begin{array}{c}\text{Two Band Model} \\ \varepsilon_E = \varepsilon_{El} \text{ and } \rho_c = \rho_{cl} \text{ for } 0 \le E \le E_g \\ \varepsilon_E = \varepsilon_{Eb} \text{ and } \rho_c = \rho_{cb} \text{ for } E_g \le E < \infty\end{array} \tag{2.20}$$

$$F(u_g) \equiv \int_{u_g}^{\infty} \frac{u^3}{e^u - 1} du = \frac{\pi^4}{15} F_{o-\lambda_g T_E} \tag{2.21}$$

$$G(u_g) \equiv \int_{u_g}^{\infty} \frac{u^2}{e^u - 1} du \tag{2.22}$$

$$R \equiv \frac{\varepsilon_{El}(1-\rho_{cl})\left[1-\rho_{cb}(1-\varepsilon_{Eb})\right]}{\varepsilon_{Eb}(1-\rho_{cb})\left[1-\rho_{cl}(1-\varepsilon_{El})\right]} \tag{2.23}$$

Note that $F(u_g)$ is related to the fraction of the blackbody total emissive power that lies in the wavelength range 0 to λ_g, $F_{o-\lambda_g T_E}$, as defined in Chapter One [equation (1.137)].

For the two band model, η_{MAX} is a function of the dimensionless bandgap energy, u_g, as well as the parameter, R. This parameter describes the emitter and (or) filter optical performance. Since η_{MAX} increased as R decreases, it is desirable to make R as small as possible. In a pure selective emitter system with negligible PV cell reflectance ($\rho_{cl} \approx \rho_{cb} \approx 0$), $R = \varepsilon_{El}/\varepsilon_{Eb}$. Thus, R is the ratio of the emittance, ε_{El}, for the low photon energy ($0 \le E < E_g$ or $\lambda_g < \lambda < \infty$) region of the spectrum, which cannot be converted to electrical energy, to the emittance, ε_{Eb}, for the useful photon energy ($E_g \le E < \infty$ or $0 \le \lambda \le \lambda_g$) region of the spectrum. Use the term *out-of-band* to describe the region of the spectrum that cannot be converted to electrical energy ($0 \le E < E_g$ or $\lambda_g < \lambda < \infty$). The term *in-band* is used to describe the region of the spectrum that can be converted to electrical energy ($E_g \le E < \infty$ or $0 \le \lambda \le \lambda_g$). In a selective emitter system, the ratio of the out-of-band emittence, ε_{El}, to the in-band emittance, $\varepsilon_{Eb,}$ is the critical parameter for determining η_{MAX}. For a pure filter system that used a black body emitter ($\rho_{El} = \rho_{Eb} = 1$), $R = (1 - \rho_{cl})/(1 - \rho_{cb})$. Thus, for maximum η_{MAX}, it is desirable for the out-of-band reflectance, ρ_{cl}, to be large and the in-band reflectance to be small. If $\varepsilon_{El} = \varepsilon_{Eb}$, and $\rho_{cl} = \rho_{cb}$, then R = 1 and η_{MAX} [equation (2.20)] reduces to the result in Section 2.3 given by equation (2.17). For the case where R = 0, equation (2.20) reduces to the ideal system described in Section 2.4 where η_{MAX} is given by equation (2.19).

Figure 2.4 shows η_{MAX} as a function u_g for several values of R. Two important results can be noted from Figure 2.4. First, η_{MAX} has a maximum value that increases with decreasing R. Second, the optimum value of u_g for maximum η_{MAX} also increases with decreasing R. Using a GaSb PV cell (E_g = .72 eV) and T_E = 1700 K as typical for a TPV system, u_g = 4.9. Referring to Figure 2.4, if u_g = 4.9 then η_{MAX} will be near its maximum value if R ≤ 0.1. If R = 1, which applies to the case where ε_E and ρ_c are constants for the entire spectrum, then $\eta_{MAX} \approx .2$ and is far from the maximum value. Thus, by reducing R to 0.1 when u_g = 4.9, η_{MAX} will be near its maximum value, which is greater than 0.6. The parameter R is a measure of the spectral control, (how well the spectrum of the radiation is matched to the PV cells bandgap energy). As has just been shown, for typical TPV conditions, $u_g \approx 5.0$. Therefore, it is desirable that R ≤ .1.

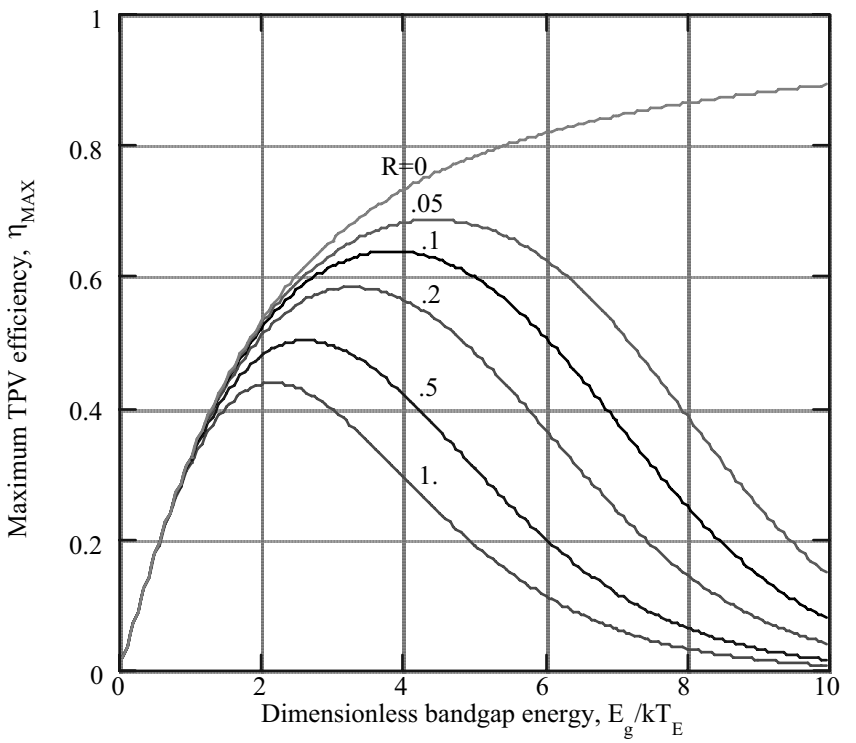

Figure 2.4 - Maximum TPV efficiency for two band model when emitter emittance, $\varepsilon_E=\varepsilon_{El}$ and PV cell reflectance, $\rho_C=\rho_{Cl}$ for $0<E<E_g$ and $\varepsilon_E=\varepsilon_{Eb}$, $\rho_C=\rho_{Cb}$ for $E_g<E<\infty$ and parameter R is given by equation (2.23).

2.6 Power Output

So far only efficiency, η_{MAX}, for the simple TPV system model of Figure 2.1 has been discussed. Yet power output is also a major consideration for a TPV energy conversion system. Substituting equation (2.7) in (2.11) and neglecting $\rho_E\varepsilon_c e_{bc}$ yields the following result.

$$P_{ELMAX} = \frac{A_c}{\lambda_g}\int_o^{\lambda_g} \frac{(1-\rho_c)\varepsilon_E e_{bE}(\lambda, T_E)}{1-\rho_E\rho_c}\lambda d\lambda \tag{2.24}$$

Using equation (1.120) for e_{bE} and defining a new integration variable $u = hc_o/\lambda kT_E$ yields the following,

$$\frac{P_{ELMAX}}{A_c} = \frac{15}{\pi^4}\sigma_{sb}T_E^4 u_g \int_{u_g}^{\infty} \frac{\varepsilon_E(1-\rho_c)}{1-\rho_E\rho_c}\frac{u^2}{e^u-1}du \tag{2.25}$$

where σ_{sb} is the Stefan-Boltzmann constant.

Equation (2.25) shows that the power density (power/area) is proportional to T_E^4. As discussed in Chapter 1, since TPV energy conversion depends upon thermal radiation such a result is expected. Also, the power density only depends upon photons in the energy range $E_g \le E < \infty$, whereas the efficiency [equation (2.15)] depends on all photon energies, $0 \le E < \infty$. As a result, high efficiency does not insure large power density. This has already been pointed out in Section 2.4 for the ideal system. Likewise, large power density does not insure high efficiency since the power density is a monotonically increasing function of temperature whereas efficiency has a maximum value for some optimum value of u_g. Thus to achieve the largest power density, T_E should be as large as possible. However, the resulting value of u_g may not be the optimum for maximum efficiency.

Making the approximations, $\varepsilon_E = \varepsilon_{Eb} = 1 - \rho_{Eb}$ and $\rho_c = \rho_{cb}$ for $E_g \le E < \infty$, just as in Section 2.5, equation (2.25) becomes the following.

$$\frac{(1-\rho_{Eb}\rho_{cb})P_{ELMAX}}{\varepsilon_{Eb}(1-\rho_{cb})A_c\sigma_{sb}T_E^4} = \frac{15}{\pi^4}u_g\int_{u_g}^{\infty}\frac{u^2}{e^u-1}du \qquad \begin{matrix}\varepsilon_E = \varepsilon_{Eb} = 1-\rho_{Eb} \text{ and } \rho_c = \rho_{cb} \\ \text{for } E_g \le E < \infty\end{matrix} \tag{2.26}$$

Thus, the term on the left hand side of equation (2.26), which is a *dimensionless power density*, is identical to η_{MAX} [equation (2.17)] for the case where ε_E and ρ_c are constants for the entire spectrum. Figure 2.2 applies for the dimensionless power density, as well

as, η_{MAX} for the case where ε_E and ρ_c are constants for the entire spectrum. Therefore, both of these quantities have a maximum value at $u_g = 2.17$. As a result, for a fixed emitter temperature, T_E, the optimum bandgap energy, E_{gPMAX}, that yields maximum power density is the following, when T_E is in K and E_{gPMAX} is in eV.

$$E_{gPMAX} = 1.87\times10^{-4} T_E \text{ eV} \qquad \begin{matrix}\varepsilon_E = \varepsilon_{Eb} = 1-\rho_{Eb} \text{ and } \rho_c = \rho_{cb} \\ \text{for } E_g \le E < \infty\end{matrix} \tag{2.27}$$

For a fixed, emitter temperature, equation (2.27) will give the value of E_g that yields maximum power density. However, at a fixed value of E_g, the power density continuously increases with T_E.

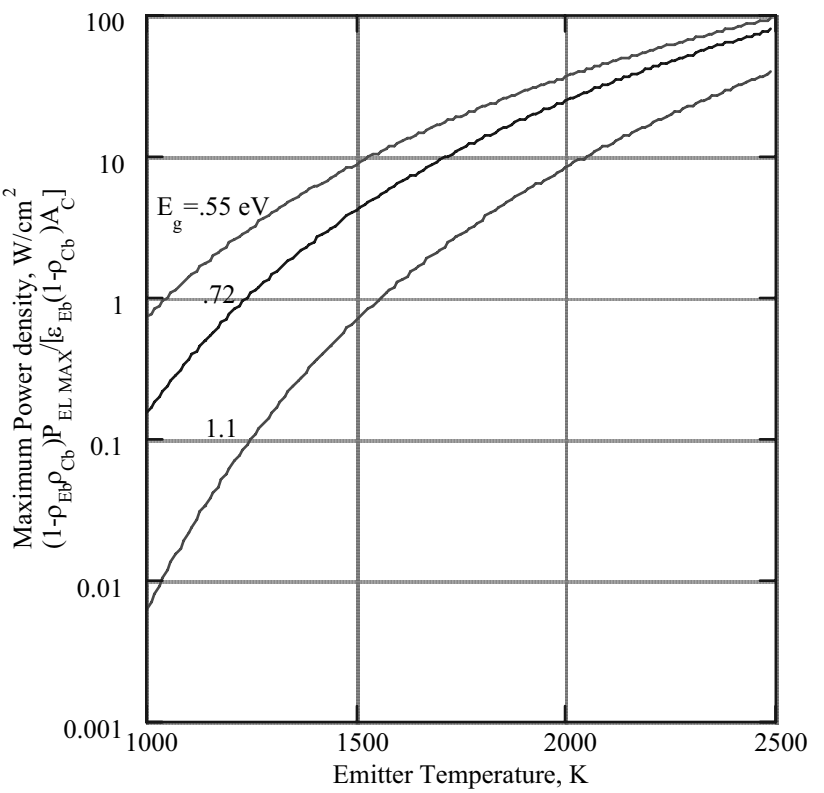

Figure 2.5 - Maximum power density for TPV system when emitter emittance,$\varepsilon_E=\varepsilon_{Eb}=1-\rho_{Eb}$, and PV cell reflectance,$\rho_C=\rho_{Cb}$,for $E_g<E<$ oo for several PV cell bandgap energies,E_g.

This is shown in Figure 2.5 where the power density, is plotted as a function of T_E for E_g = 0.55, 0.72, and 1.1 eV. For silicon PV cells (E_g = 1.1 eV) the simple model indicates that in order to achieve large ($\approx$ 10 W/cm^2) power output, emitter temperatures greater than 2000 K are required. However, for the low bandgap energy PV cells like GaSb (E_g = 0.72 eV) and InGaAs (E_g = 0.55 eV) much lower emitter temperatures yield large power density. Also, for $T_E \leq 1000$ K even for E_g =0.55 eV the output power density is low (< 1 W/cm^2). The T_E^4 power density dependence [equation (2.28)] is a critical issue for a successful TPV energy conversion system. Remember that the simple model of Figure 2.1 yields the maximum possible efficiency and power density. In Chapter 8 the efficiency of a TPV system will be calculated using a realistic model.

2.7 Summary

Using a simple model (Figure 2.1) for a TPV energy conversion system several important conclusions about TPV performance are apparent.

1) There is an optimum value of the dimensionless bandgap energy, $u_g = E_g/kT_E$, to obtain maximum efficiency except for the so-called ideal TPV system. In that case, the efficiency is a monotonically increasing function of u_g and approaches 1 as $u_g \rightarrow \infty$, with the paradoxical result that the power output vanishes as $u_g \rightarrow \infty$.
2) A so-called two-band model is used to approximate selective emitter and filter TPV systems. How well the spectrum of the emitted radiation matches the PV cell bandgap energy is determined by the parameter, R [equation 2.23)]. As R decreases both the optimum value of u_g and the maximum efficiency increase. For typical TPV systems, $u_g \approx 5$, so that $R \leq 0.1$ is required in order to obtain maximum efficiency.
3) High efficiency does not necessarily imply large output power. Likewise, large power density does not insure high efficiency. Efficiency has a maximum value for some optimum u_g, while the power density increases nearly as T_E^4. For the new low bandgap energy PV cells, the simple two-band model predicts output power densities the order of 10 W/cm^2 for $1500 < T_E < 1700$ K.

The simple model used in this chapter includes two critical assumptions. First, the ideal PV cell is assumed. Second, all radiation leaving the emitter goes directly to the PV cells and all radiation leaving the PV cells goes directly to the emitter. Thus, the efficiency and power density calculated with this model are the maximum possible values. In a real TPV system, the PV cells will be less than perfect and all the emitted radiation will not be incident on the PV cells. These issues are addressed in Chapters 6, 7, and 8.

References

[1] W. Shockley and H. J. Queisser , J. Appl. Physics, 32, (1961), 136.

Problems

2.1 Derive equation (2.15) from (2.14).

2.2 Show that the efficiency given by equation (2.17) can be approximated by

$$\eta_{MAX} \approx \frac{15}{\pi^4} u_g \left[u_g^2 + 2u_g + 2 \right] e^{-u_g}, \quad u_g = \frac{E_g}{kT_E} = \frac{hc_o}{\lambda_g kT_E}$$

for $e^{u_g} \gg 1$. For this approximation what value of u_g does the maximum value of η_{MAX} occur and what is the maximum value of η_{MAX}?

2.3 Show that the efficiency given by equation (2.19) can be approximated by

$$\eta_{MAX} \approx \frac{u_g \left(u_g^2 + 2u_g + 2 \right)}{u_g^3 + 3u_g^2 + 6u_g + 6} \qquad u_g = \frac{E_g}{kT_E} = \frac{hc_o}{\lambda_g kT_E}$$

for $e^{u_g} \gg 1$.

2.4 For the same conditions as problem 2.3 ($\rho_c = 0$, $\varepsilon_E = 1$ for $E_g \le E < \infty$ and $e^{u_g} \gg 1$) show that the output power is the following,

$$P_{ELMAX} \approx \frac{15}{\pi_4} A_c \sigma_{sb} T_E^4 u_g \left[u_g^2 + 2u_g + 2 \right] e^{-u_g} \qquad u_g = \frac{E_g}{kT_E} = \frac{hc_o}{\lambda_g kT_E}$$

where $\sigma_{sb} = \frac{2\pi^5}{15} \frac{k^4}{h^3 c_o^2}$ is the Stefan-Boltzmann constant.

2.5 For a monochromatic emitter all emitted photons have the same energy, E. Let N_E be the total number per second per m^2 of monochromatic photons that make up the emitted photon flux and are incident on the PV cells. If $E = E_g$, where E_g is the PV cell's bandgap energy, show that $\eta_{MAX} = 1$ for a TPV system using the "ultimate" PV cell described in section 2.2 with $\rho_c = 0$.

2.6 Derive equation (2.20) from (2.15) using the two band model described as follows.

$$\varepsilon_E = \varepsilon_{El} \text{ and } \rho_c = \rho_{cl} \qquad \text{for} \qquad 0 \le E < E_g$$
$$\varepsilon_E = \varepsilon_{Eb} \text{ and } \rho_c = \rho_{cb} \qquad \text{for} \qquad E_g \le E < \infty$$

2.7 a) For the approximation $e^{u_g} \gg 1$ show that the two band model for η_{MAX} [equation (2.20)] becomes the following,

$$\eta_{MAX} = u_g \frac{G(u_g)}{F(u_g) + R\left[\frac{\pi^4}{15} - F(u_g)\right]} \qquad u_g = \frac{E_g}{kT_E}$$

where

$$F(u_g) \approx e^{-u_g}\left[u_g^3 + 3u_g^2 + 6u_g + 6\right]$$

$$G(u_g) \approx e^{-u_g}\left[u_g^2 + 2u_g + 2\right]$$

b) Calculate η_{MAX} using the approximate expression from a) for T_E = 1700 K, E_g = 0.72 eV and R = .1. For the same conditions, how does this η_{MAX} compare with the maximum value for η_{MAX} shown in Figure 2.4?

2.8 A hypothetical monochromatic emitter at some temperature, T_E, can be described as follows: The emitted photon flux, N_E, (photons/sec m^2) that is also incident on the PV cells will be some fraction, ε_o (< 1.0), of the photon flux emitted by a blackbody at the same temperature, T_E. Also, the power of the emitted monochromatic flux must be some fraction, ε_T, of the total emissive power $\sigma_{sb} T_E^4$, of a blackbody at temperature, T_E. For the TPV system described in problem 2.5, show that the PV bandgap energy, E_g, is related to T_E as follows.

$$E_g = \frac{\pi^4}{15}\left(\frac{\varepsilon_T}{\varepsilon_o}\right)\frac{kT_E}{\int_o^\infty \frac{u^2}{e^u - 1}du}$$

Also show that the output power density is the following.

$$\frac{P_{ELMAX}}{A_c} = \varepsilon_T \sigma_{sb} T_E^4$$

Calculate E_g for T_E = 2000 K and $\varepsilon_T = \varepsilon_o$.

$$\text{Note:} \quad \int_o^\infty \frac{u^2}{e^u - 1}du = 2\sum_{n=1}^{\infty}\frac{1}{n^3}$$

This page intentionally left blank

Chapter 3
Emitter Performances

This chapter concentrates upon the emitter component of a TPV system. Emitters can be split into two groups. First, gray body emitters have a constant spectral emittance. The second group, the selective emitters, have a variable spectral emittance. As already discussed, an efficient selective emitter will have a large emittace for photon energies greater than the PV cell bandgap energy and a negligible spectral emittance for photon energies less than the PV cell bandgap energy. Derivation of the spectral emittance in terms of the fundamental properties, extinction coefficient, and index of refraction take up a major portion of the chapter.

Beginning with a discussion of gray body and selective emitters, the chapter then introduces the important parameters for determining spectral emittance: the extinction coefficient and optical depth. Then the discussion moves to the development of the analysis for the spectral emittance of one-dimensional planar and cylindrical emitters. This analysis shows the significant effect on the spectral emittance caused by temperature changes across the emitter. The effect of radiation scattering on the spectral emittace is also discussed.

3.1 Symbols

a	absorption coefficient, cm^{-1}
c_o	vacuum speed of light (2.998×10^8 m/sec)
E	photon energy, j or eV
h	Plank's constant (6.624×10^{-34} J-sec)
i	radiation intensity, $W/m^2/\mu m$/steradian
j	$\sqrt{-1}$
k	Boltzmann constant (1.38×10^{-23} J/K)
k_{th}	thermal conductivity, W/cm/K
K	extinction coefficient, cm^{-1}
n	index of refraction
q	radiation flux per wavelength per unit area, $W/cm^2/nm$
$\overline{q}$	total radiation flux, W/cm^2
R	directional spectral reflectivity
$\overline{R}$	spectral reflectivity for normal incidence
S	source function, W/m^2/steradian/nm
T	temperature, K

u	dimensionless photon energy $= \frac{hc_o}{\lambda kT} = \frac{1.439 \times 10^7 \left(K \cdot nm\right)}{\lambda T}$
$\varepsilon(\lambda)$	spectral emittance
λ	wavelength, nm or μm
κ	optical depth
Ω	scattering albedo
σ	scattering coefficient, cm^{-1}
ρ	reflectance
σ_{sb}	Stefan-Boltzmann constant, 5.67×10^{-12} W/cm^2K^4
τ	transmittance

Subscripts

b	blackbody
c	denotes beginning of long wavelength region where $\varepsilon \approx 1.0$
I	imaginary part
f	refers to emitting film
g	refers to PV cell bandgap energy
R	real part
s	refers to substrate

Superscripts

+	refers to + x direction
–	refers to – x direction

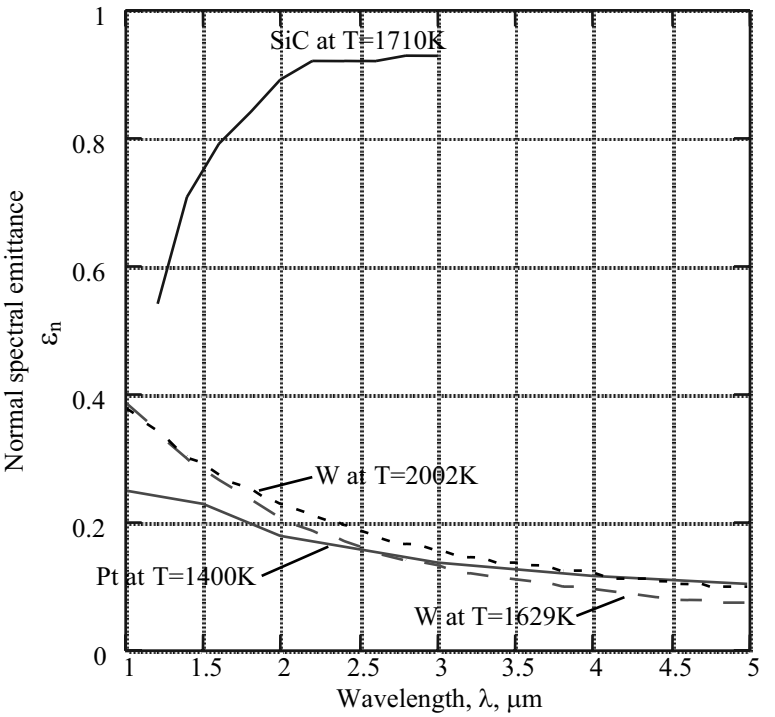

Figure 3.1 - Experimental normal spectral emittance for platinum (Pt), silicon carbide (SiC), and tungsten (W). Pt and W data from [1] and [2].

3.2 Gray Body Emitters

The spectral hemispherical emittance, ε, as defined in Chapter 1 is the optical property which determines the emitted radiation flux for a material. For a *gray body* material, the spectral emittance is the same for all wavelengths (or photon energies). In reality only for a blackbody is ε the same at all wavelengths, namely ε = 1. However, for many metals ε is nearly a constant for a large part of the spectrum. In Figure 3.1 the measured spectral emittances in a vacuum ($n_o = 1$) for platinum (Pt), tungsten (W), and silicon carbide (SiC) are plotted. The Pt and W data are from [1] and the SiC data are from [2]. It should be pointed out that the measured emittance in Figure 3.1 is the normal spectral emittance, defined as follows.

$$\varepsilon_n(\lambda, \theta = 0, T) \equiv \frac{i(\lambda, \theta = 0, T)}{i_b(\lambda, T)} \tag{3.1}$$

Where i is the emitted intensity measured normal to the emitting surface ($\theta = 0$) and i_b is the blackbody intensity. It is assumed that i is independent of the azimuthal angle, ϕ. Obviously, if i is independent of θ, then the normal spectral emittance, ε_n, and the spectral hemispherical emittance, ε, are the same. Generally, the normal emittance is larger than the hemispherical emittance.

All the materials shown in Figure 3.1 have high melting points and are therefore suitable for TPV applications. However, W cannot be operated in air because of oxidation at high temperatures. Although SiC may degrade in air for very high temperatures (> 2000 K, [2]), its large emittance makes it a good candidate for a TPV emitter for lower temperatures. However, ε falls from > .9 at $\lambda = 2.0\mu m$ to $\varepsilon = .54$ at $\lambda = 1.2\mu m$. For high TPV efficiency, the opposite behavior is desirable. In other words, for TPV systems using PV cells with bandgap energies in the range .5 to 1.0 eV, ε should be large for $\lambda < 2.0\mu m$ and small for $\lambda > 2.0\mu m$. Tungsten has the desirable reduction in emittance for long wavelengths. However, the emittance is much lower than SiC emittance for $1 \leq \lambda \leq 2.0\mu m$. One very attractive property of W is its low vapor pressure and thus low evaporation rate at high temperatures. Evaporation may be a serious problem for some emitter materials.

Platinum also has low emittance at long wavelengths; however, its emittance for $\lambda < 1.5\mu m$ is also small. Therefore, its power output, at the shorter wavelengths that can be converted by the PV array, will be low. However, its low emittance and its chemical stability make it an excellent candidate for the substrate of a film selective emitter. The film selective emitter is considered later in this chapter. Generally, spectral emittance increases with temperature. This is illustrated in Figure 3.1 for W where ε_n is shown for T = 1629 K and 2002 K.

3.3 Selective Emitters

As already shown in Chapter 2, matching the emitter radiation to the bandgap energy of the PV cells results in large improvements in TPV efficiency. The ideal selective emitter would emit only photons with energy equal to the bandgap energy of the PV cells. A laser that operates at a single wavelength meets this requirement. However, the processes required to produce lasing from thermal energy input are very inefficient. Thus, a laser emitter is out of the question.

The closest thing to a laser emitter is a group of isolated atoms excited to their lowest excited state and then emit photons of a single energy when they spontaneously decay to the ground state. In a partially ionized gas (or plasma), individual atoms or molecules are excited by collisions with electrons into various excited states. By choosing the proper gas and adjusting the electron temperature, it is possible to produce a plasma where most of the excited atoms are in their lowest excited state. This approach [3] for a selective emitter has been investigated using a cesium plasma. For

cesium, electronic transitions from the first excited state to the ground state result in radiation that is matched to the bandgap energy of gallium arsenide, GaAs (Eg = 1.42 eV, λ_g = .87μm). Thus a cesium plasma emitter is an excellent candidate for a GaAs TPV system. It has been found [3] that radiation efficiencies greater than 70% are possible. However, the cesium plasma emitter has two major drawbacks. First, very high electron temperatures (> 2000 K) are required. Second, since the plasma density is low, the radiation power is low. Solid state densities are required to attain large (> 1 W/cm^2) powers.

58 Ce	**59 Pr**	**60 Nd**	**61 Pm**	**62 Sm**	**63 Eu**	**64 Gd**
Cerium	Praseodymium	Neodymium	Promethium	Samarium	Europium	Gadolinium

65 Tb	**66 Dy**	**67 Ho**	**68 Er**	**69 Tm**	**70 Yb**	**71 Lu**
Terbium	Dysprosium	Holmium	Erbium	Thulium	Ytterbium	Lutetium

Electron structure for rare earth ion, Re^{+++}

$1s^2 2s^2 2p^6 3s^2 3p^6 3d^{10} 4s^2 4p^6 4d^{10} 5s^2 5p^6 4f^N$

N = 1 for Ce, N = 13 for Yb and Lu

Figure 3.2 Lanthanide or rare earth series.

3.3.1 Rare Earth Selective Emitters

The advantage of a low density plasma emitter is that the emitting atoms behave as isolated atoms, emitting narrow line radiation rather than broad gray body radiation associated with most solid state materials. Fortunately, the *lanthanide series* of atoms, Figure 3.2, which begin with cerium (Ce) at atomic number 58 and end with lutetium (Lu) at atomic number 71, behave much like isolated atoms even at solid state densities. The lanthanides or *rare earths*, as they are more commonly called, exist as singly and doubly charged ions when combined with other atoms at solid state densities. The 4f valence electrons of these ions, which account for absorption and emission of radiation, lie in orbits inside the outer 5s and 5p electron shells. As a result, the 5s and 5p electrons shield the 4f electron from neighboring ions. Thus, the rare earth ions at solid state densities behave nearly like isolated atoms and emit radiation in narrow bands, rather than in a continuous gray body fashion. In quantum mechanics terms, the explanation is that the 4f electron wave functions do not overlap with neighboring wave functions.

The above explanation does not fully explain why the rare earth in a host material has distinct emission bands. Non-radiative de-excitation processes for the 4f levels, such as collisions with the host atoms, compete with radiative de-excitation. These non-radiative processes reduce the emission bands. However, in both a theoretical and experimental study, Torsello, et al [4] show that the symmetry of the host crystal around the rare earth atom inhibits the non-radiative decay of the 4f levels. They also demonstrate that the spectral emittance for the rare earths is independent of temperature if there is no temperature gradient across the sample. However, as will be shown in Section 3.8.3, the spectral emittance of the rare earths is very sensitive to temperature gradients across the sample.

Host Material	**Chemical Formula**	**Melting Point of Host, C [19]**
Pure rare earth oxide	R_2O_3	>2200
Yttrium aluminum Garnet (YAG)	$R_xY_{3-x}Al_5O_{12}$ $0<x<3$	1930
Gadolinium gallium Garnet (GGG)	$R_xGd_{3-x}Ga_5O_{12}$ $0<x<3$	1750
Spinel	$R_xMg_{1-x}Al_2O_4$ $0<x<1$	2100
Zirconia	$R_xZr_{1-x}O_2$ $0<x<1$	2700
Yttria	$R_xY_{2-x}O_3$ $0<x<2$	2400

Table 3.1 Possible high temperature host materials for rare earths (Re)

For TPV, the emitter is at temperatures greater than 1000°C so that the rare earth containing material must have a high melting point. There are many possible high temperature host materials for rare earth ions. Several of these are listed in table 3.1. The spectra and energy levels of rare earth ions in crystals have been extensively studied. Most of this work is summarized in the texts of Wyboune [5] and Dieke [6]. As already stated, the rare earth ions behave radiatively similar to isolated atoms. Therefore, the widths and wavelength locations of the rare earth ion emission bands are nearly unaffected by the host material.

The rare earths of most interest for TPV are those with emission bands that match the bandgap energies of the available PV cells. These bandgap energies range from

Eg ≈ 0.5 eV (λ ≈ 2500nm) for InGaAs to Eg ≈ 1.1 eV (λ ≈ 1000nm) for Si. As a result, the rare earths of most interest are ytterbium (Yb), erbium (Er), thulium (Tm), holmium (Ho), and dysprosium (Dy) that have main emission bands in the range $1000 \leq \lambda \leq 2700$nm. Table 3.2 lists the main emission bands of these five rare earths.

Rare Earth Ion	**Yb**	**Er**	**Tm**	**Ho**	**Dy**
Center wavelength, nm for main emission band and energy level designation	960 $^2F_{5/2} - {}^2F_{7/2}$	1500 $^4I_{13/2} - {}^4I_{15/2}$	1700 $^3F_4 - {}^3H_6$	2000 $^5I_7 - {}^5I_8$	2700 $^4H_{13/2} - {}^4H_{15/2}$
Center wavelength, nm for emission band resulting from 2nd excited state manifold and energy level designation		960 $^4I_{11/2} - {}^4I_{15/2}$	1200 $^3H_5 - {}^3H_6$	1100 $^5I_6 - {}^5I_8$	1700 $^4H_{11/2} - {}^4H_{15/2}$
Center wavelength, nm for emission band resulting from 3rd excited state manifold and energy level designation		800 $^4I_{9/2} - {}^4I_{15/2}$	780 $^3H_4 - {}^3H_6$	890 $^5I_5 - {}^5I_8$	1300 $^4H_{9/2} - {}^4H_{15/2}$
Center wavelength, nm for emission band resulting from 4th excited state manifold and energy level designation		650 $^4F_{9/2} - {}^4I_{15/2}$	700 $^3F_2 - {}^3H_6$	750 $^5I_4 - {}^5I_8$	1100 $^4H_{7/2} - {}^4H_{15/2}$

Table 3.2 Rare earth ions for TPV selective emitters

Except for Yb, also shown in Table 3.2, are the next three shorter wavelength bands for these rare earths. The main emission band for each of these rare earths results from transitions from the first excited state manifold to the ground state manifold. Each of the next three shorter wavelength emission bands results from transitions to the ground state manifold from the next three excited state manifolds above the first excited state manifold.

The first rare earth selective emitters were polycrystalline in structure. Guazzoni [7] constructed rare earth oxide (R_2O_3) emitters by sintering the oxide powders. These emitters were the order of 1 mm in thickness. They exhibited large emittance in the emission bands, but undesirably large emittance outside the emission bands. Nelson and Parent [8] and [9] developed a fibrous rare earth oxide emitter consisting of bundles

of small diameter (5-10 μm) fibers. These emitters are similar to the Wesbach mantle used in gas lanterns. The small diameter fibrous bundles have resulted in much lower spectral emittance outside the emission bands. Fibrous emitters are well suited for combustion TPV systems since the flame front can be located within the fibers. The importance of small dimension for obtaining maximum emitter efficiency is discussed in Section 3.10.

3.3.2 Other Selective Emitters

So far the discussion of selective emitters has been confined to the cesium plasma emitter and rare earth containing selective emitters. These emitters have relatively narrow emission bands resulting from electronic transitions from the first excited state to the ground state. However, all solid materials that emit a continuum of radiation rather than band radiation show some selectivity in emission. This is pointed out in Section 3.2, where tungsten is mentioned as a possible TPV emitter. As already mentioned, it is desirable that emittance for a TPV emitter be large for photon energies greater than the PV cell bandgap energy and small for photon energies below the PV cell bandgap energy.

A continuum type emitter, called a "matched emitter" [10], that shows desirable selectivity is cobalt (Co) doped spinel ($Co_xMg_{1-x}Al_3O_4$) that is formed by sintering magnesia (MgO), alumina (Al_2O_3), and Co_3O [10]. The cobalt ion with seven 3d valence electrons is responsible for the emission band.

The spectral emittance of a plasma sprayed film of Co doped spinel on an alumina (Al_2O_3) substrate is presented in [11]. Its spectral emittance has a maximum in the $1000 \leq \lambda \leq 2000$nm region. This is desirable for TPV applications. However, for $\lambda > 2000$nm the emittance is not small (> 0.2); this is not so desirable. It should be pointed out that the emittance in [11] is based upon the emitting surface temperature rather than the alumina substrate temperature. If the substrate temperature, which is higher than the emitting surface temperature, were used, ε would be lower. As pointed out later in Section 3.8.3, the spectral emittance of a film is a sensitive function of temperature change across the film.

Another matched emitter [12] is MgO doped with nickel (Ni) in the form of NiO or cobalt in the form of Co_2O_4. It is the Ni or Co ion that accounts for the emission. Just as for the rare earths, electronic transitions of Ni and Co ions account for the large emission bands. For Ni the emission band is centered a $\lambda \approx 1.4\mu$m. The optimum Ni or Co dopant concentration is small (1-2 mol%). In [12] a maximum of $\varepsilon = .9$ at $\lambda = 1.4\mu$m is measured for a 98% MgO – 2% NiO emitter. In addition, the emittance drops rapidly to $\varepsilon \approx .1$ for $\lambda \approx 3\mu$m and then begins increasing for $\lambda \geq 4\mu$m to $\varepsilon \approx 1.0$ at $\lambda \approx 9\mu$m.

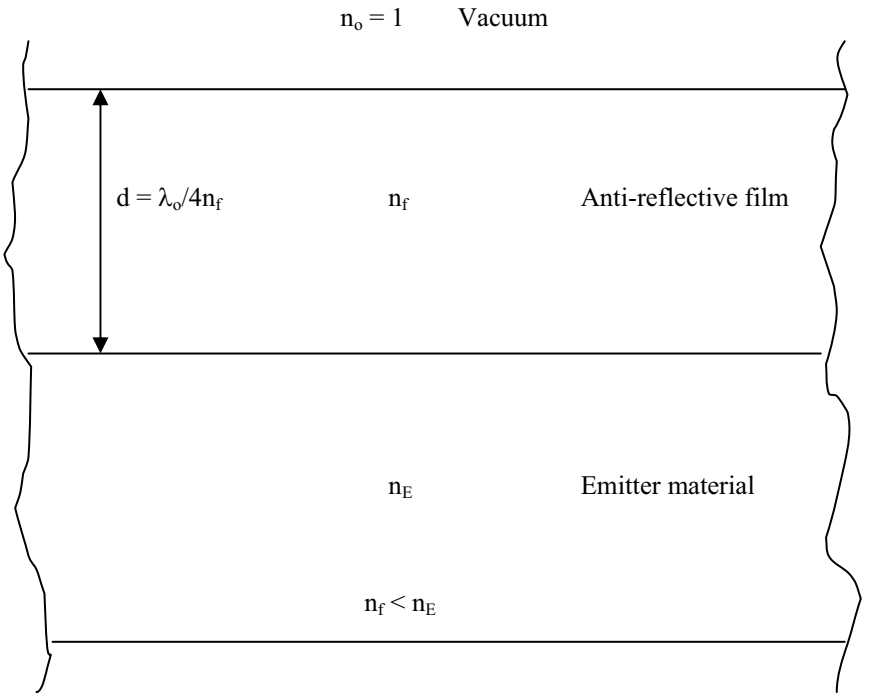

Figure 3.3 - Schematic of selective emitter that uses antireflective film to increase emittance in wavelength region around $\lambda = \lambda_o$.

Another method for producing a selective emitter has been introduced by Fraas [13]. A material such as tungsten has the desirable characteristic of a low emittance at long wavelengths. However, in the wavelength region (1-2μm) where large emittance is desired, the emittance is also low. To increase the emittance in this region, Fraas [13] uses an antireflection film on the tungsten emitter tuned to the desired wavelength. With the appropriate film, reflected radiation at an interface can be greatly reduced. Figure 3.3 is a schematic of a tungsten emitter with an antireflection film. Destructive interference between the light waves reflected at the W-film interface and the film-atmosphere interface results in reduced reflection of radiation back into the W emitter. In order for the destructive interference to occur for normal incidence at some wavelength, λ_o, the film thickness, d, must satisfy the relation $d = \lambda_o/4n_f$, (where n_f is the index of refraction of the antireflection film). To attain the minimum reflectance, the index of refraction of the film, n_f, must satisfy the relation $n_f = \sqrt{n_o n_E}$, where n_o is the surrounding medium (generally vacuum so that $n_o = 1$) and n_E is the emitter index of

refraction. In Chapter 4, where interference filters are discussed, the theory for an antireflection film is presented. In [12] spectral emissive power results for a tungsten emitter at 1300°C with an alumina (Al_2O_3) antireflection film are presented.

A fortuitous advantage of using alumina as the antireflective film is that it also can act as a barrier between the atmosphere and the tungsten emitter. Thus, a tungsten emitter suitable for operation in the atmosphere can be fabricated as suggested in [12]. First, a tungsten film is deposited on a high temperature ceramic substrate, such as silicon carbide. Then the alumina antireflective film is deposited on the tungsten emitter. With tungsten "sandwiched" between the high temperature ceramic materials, atmospheric operation is possible. A major limitation of this emitter is that evaporation of the thin antireflective film results in reduced emittance at $\lambda = \lambda_o$ since the condition $d = \frac{\lambda_o}{4n_f}$ is no longer satisfied.

Two other selective emitters that use tungsten are the periodically structured or grating emitter ([14] and [15]) and the three-dimensional photonic-crystal emitter ([16] and [17]). In the grating type emitter, thermally excited surface electromagnetic waves, called surface plasmons, can be converted to emitted radiation by interaction with the periodically structured tungsten surface. By choosing the proper dimensions of the periodic structure, the emittance can be enhanced in a given wavelength region.

The tungsten photonic crystal emitter, which is three dimensional in structure, also produces enhanced emission at the design wavelength. In addition, if the emitter behaves as theoretical calculations indicate, emission for wavelengths greater than the wavelength corresponding to the photonic bandgap energy is suppressed. Semiconductors are a logical choice for a selective emitter. At room temperature they have large absorptance (and thus large emittance) for photon energies, E, greater than the bandgap energy, E_g, and low absorptance (and thus low emittance) for $E < E_g$. However, as the temperature is increased, free electrons are produced that emit radiation in the energy region $E < E_g$. Thus, at high temperatures a semiconductor does not have low emittance for $E < E_g$. In [18] silicon is investigated as a possible semiconductor selective emitter. For temperatures less than 900 K, the emittance, ε, is less than 0.3 for $E < E_g$ and $\varepsilon > 0.5$ for $E > E_g$. As a result, silicon may be a suitable selective emitter for a low temperature TPV system.

3.4 Extinction Coefficient and Optical Depth

The key atomic property that determines the spectral emittance of a material is the *extinction coefficient*, K, which is introduced in Section 1.6.5. It is the sum of the *absorption coefficient*, a, and the *scattering coefficient*, σ_s. The units for these properties are cm^{-1}. In Section 1.6.5 it was shown that the solution to the equation of radiation transfer for intensity, i, was given in terms of the *optical depth*, κ, given by

equation (1.145). It is shown later in this chapter that optical depth is the major variable for determining spectral emittance.

As noted in Section 1.5.2, the extinction coefficient, K, defined by equation (1.141) should not be confused with the extinction coefficient that is used in describing the attenuation of classical electromagnetic waves in an absorbing medium. For the case of electromagnetic waves, the extinction coefficient is the imaginary part of the index of refraction, n_I, and is dimensionless. It describes the absorption but not scattering of electromagnetic energy or radiation. Thus, in a medium with negligible scattering the two extinction coefficients are related by the following expression.

$$K = a = \frac{4\pi\nu}{c_o} n_I = \frac{4\pi}{\lambda_o} n_I \qquad \sigma_s = 0 \tag{3.1}$$

3.5 Extinction Coefficients of Rare Earth Selective Emitters

As already stated, the spectral emittance, $\varepsilon(\lambda)$, is a function of the extinction coefficient. Therefore, the wavelength dependence of the spectral emittance is similar to the wavelength dependence of the extinction coefficient. Shown in Figure 3.4 is the extinction coefficient, $K(\lambda)$, for erbium aluminum garret ($Er_3Al_5O_{12}$). It is obtained from measured values of reflectance and transmittance at room temperature [19]. Two different instruments are used in measuring the transmittance and reflectance. One instrument covers the wavelength region $600 \le \lambda \le 2500$nm and the other $4000 \le \lambda \le 10{,}000$nm. As a result, in the region $2500 \le \lambda \le 4000$nm a linear variation of $K(\lambda)$ with λ is assumed. Erbium has no emission bands in this region and thus $K(\lambda)$ is small. As a result, the linear approximation should be applicable.

Erbium aluminum garret is similar in atomic structure to yttrium aluminum garret ($Y_3Al_5O_{12}$). Yttrium aluminum garnet, which is used as a host material for rare earth lasers such as the neodymium (Nd) laser, has the acronym YAG. Therefore, the acronym ErAG is used for erbium aluminum garnet. Similarly, RAG is used to identify any rare earth (R) aluminum garnet.

The main emission band for Er is centered around $\lambda \approx 1500$nm and results from transitions from the first excited state manifold to the ground state $\left({}^4I_{13/2} \rightarrow {}^4I_{15/2}\right)$ manifold. Shown in 3.4a) are three other emission bands centered at $\lambda \approx 960$, 800 and 650nm. The band at $\lambda \approx 960$nm results from transitions from the second excited state manifold to the ground state manifold $\left({}^4I_{11/2} \rightarrow {}^4I_{15/2}\right)$.

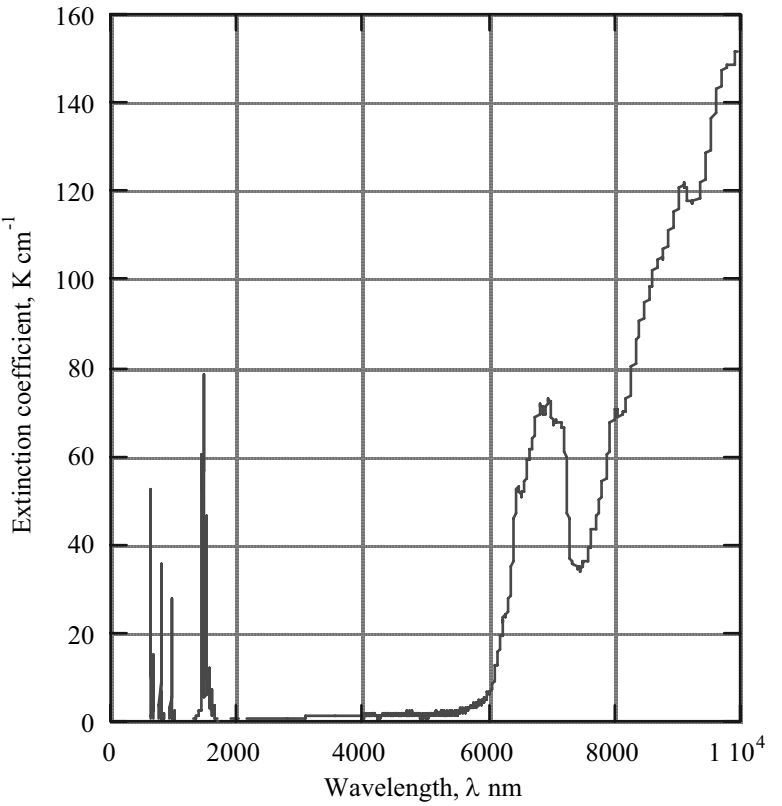

Figure 3.4a) - Extinction coefficient for erbium aluminum garnet (EAG).

The emission bands at $\lambda \approx 800$ and 650nm result from transitions from the third $\left({}^4I_{9/2} \rightarrow {}^4I_{15/2}\right)$ and fourth $\left({}^4F_{9/2} \rightarrow {}^4I_{15/2}\right)$ excited state manifolds to the ground state manifold. Figure 3.4b) is an expanded view of the four emission bands. The power in an infinitesimal wavelength band, $d\lambda$, for emission into a vacuum is $\varepsilon(\lambda)e_b(\lambda,T)d\lambda$, where $e_b(\lambda,T)$ is the blackbody spectral emissive power [equation (1.120)] and $\varepsilon(\lambda)$ is the spectral emittance. For temperatures of interest for TPV, (1000-2000 K) $e_b(\lambda,T)$ will be small for $\lambda \leq 1.0\mu m$ (see Figure 1.9). Therefore, even for $\varepsilon \approx 1$ there is little power in the emission bands below $\lambda \approx 1000nm$ compared to the main emission band at $\lambda = 1500nm$.

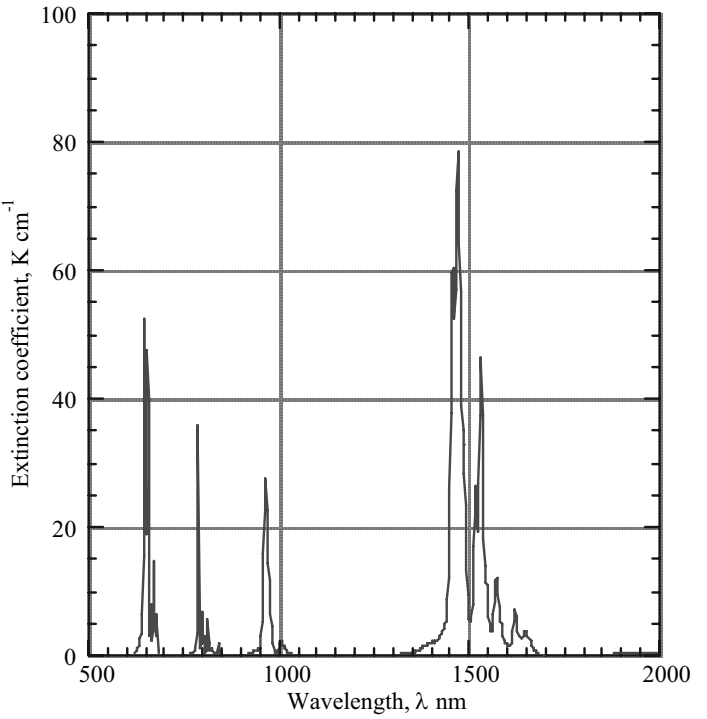

Figure 3.4b) - Extinction coefficient for erbium aluminum garnet (EAG) in emission bands.

As Figure 3.4 indicates, the extinction coefficient remains small outside the emission bands until $\lambda \geq 5500$nm. Thus, ε is also be small in the out of band regions until $\lambda > 5500$nm. For $\lambda > 5500$nm, the extinction coefficient rises rapidly. This increase results from the vibrational modes of the EAG atomic structure. Because of the large extinction coefficient, $\varepsilon \approx 1.0$ for this long wavelength region. Obviously, for TPV this is an undesirable result since this long wavelength radiation cannot be converted to electrical energy by the PV array. However, more than 90% of the total emissive power $\left(\int_0^{\infty} e_b(\lambda, T)\, d\lambda \right)$ lies below $\lambda = 5500$nm if $T > 1700$ K (see Figure 1.9). Therefore, if $T > 1700$K, the power in the long wavelength region is small and is not be a serious loss. This long wavelength region of large extinction coefficient (thus $\varepsilon \approx 1.0$) is characteristic of most high temperature oxide materials. The wavelength where this

region begins will be referred to as the *cutoff wavelength*, λ_c. For most high temperature oxide materials, the cutoff is around 5000nm.

As mentioned earlier, the wavelength dependence of radiation from rare earth ions is not greatly affected by the host material. Thus, the wavelength dependence of K for Er in any of the host materials shown in Table 3.1 will be similar. However, the magnitude of K will depend upon the host material. Extinction coefficient data for all the rare earths shown in Table 3.2 are similar to that for Er as shown in Figure 3.4. The main emission band, which has the largest extinction coefficient resulting from transitions from the first excited state manifold to the ground state manifold, will be in the wavelength region $960 \leq \lambda \leq 2700$nm, depending upon the rare earth ion. Except for Yb, there are three other emission bands for each of the rare earths at the wavelengths shown in Table 3.2.

3.6 Coupled Energy Equation and Radiation Transfer Equation for a Solid Material

It is pointed out in Chapter 1 (Section 1.7) that contrary to the usual belief, spectral emittance is not an intensive property (does not depend upon dimensions of material), but does depend upon dimensions of the emitting material. For rare earth selective emitters, emission that leaves the surface can originate at depths the order of 1mm. Host materials shown in Table 3.1 for the rare earth ions are all dielectrics that have low thermal conductivity ($k_{th} \leq .1$ W/cm K). Therefore, over a distance of 1mm, a significant temperature change will occur. As a result, in calculating the spectral emittance, both thermal conduction and radiation must be included. Radiation and thermal conduction are coupled through the conservation of energy derived in Section 1.6.6 [equation (1.159)]. The radiation intensity, i, is given by equations (1.148) and (1.149) and the radiation flux, $\vec{\vec{q}}$, is given in terms of i by equations (1.151) and (1.154). Thus, in order to calculate the spectral emittance, a rather complicated set of equations must be solved simultaneously.

3.7 One Dimensional Radiation Transfer Equations

Later in this chapter the radiation transfer equation is applied to a planar and cylindrical emitting and scattering material. In these cases, it is assumed that i only depends upon a single dimension.

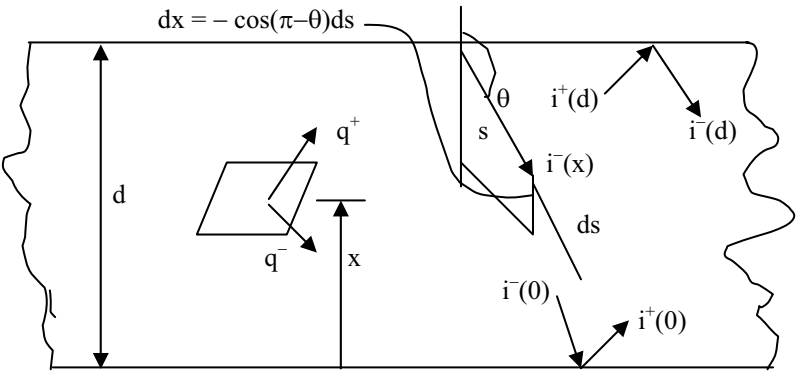

a) Planar radiation between infinite parallel boundaries.

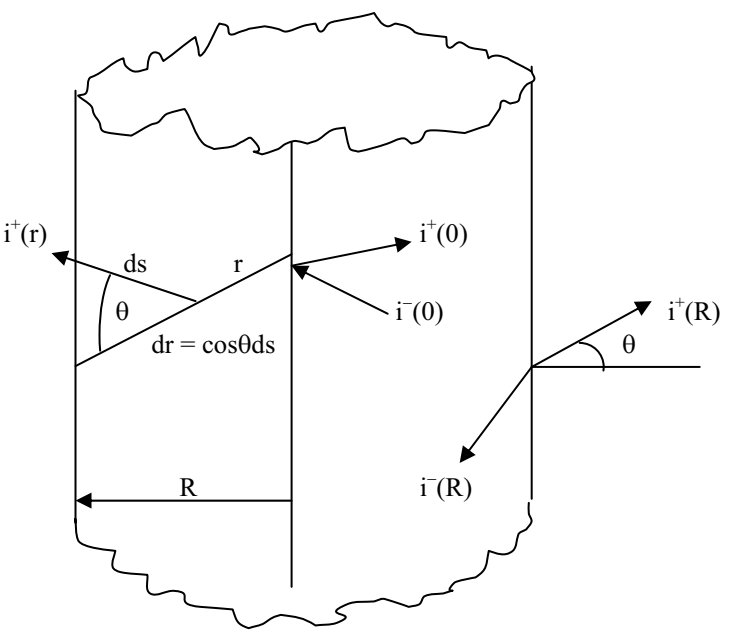

b) Radiation in an infinitely long cylinder.

Figure 3.5 One dimensional radiation in planar and cylindrical geometries.

Consider the planar geometry shown in Figure 3.5a) where i is a function of the x coordinate only. For convenience, the radiation field is split into two parts: radiation

moving in the +x direction ($0 \le \theta \le \frac{\pi}{2}$) is denoted by a + superscript, and radiation moving in the –x direction is denoted by a – superscript. For the +x direction, $ds = \frac{dx}{\cos\theta}$ and the optical depth [equation (1.145)] is the following,

$$\kappa(s) = \frac{\kappa(x)}{\cos\theta} \tag{3.2}$$

where κ(x) is the optical depth in the +x direction.

$$\kappa(x) = \int_o^x K(x^*)dx^* \tag{3.3}$$

For the –x direction, $ds = -\frac{dx}{\cos(\pi-\theta)} = \frac{dx}{\cos\theta}$ so that equations (3.2) and (3.3) again apply. Therefore, from equation (3.2), $d\kappa(s) = \frac{d\kappa(x)}{\cos\theta}$. Thus, the radiation transfer equations for i^+ and i^- are obtained from equation (1.146).

$$\cos\theta \frac{\partial i^+}{\partial \kappa(x)} + i^+\left[\kappa(x),\theta\right] = S\left[\kappa(x)\right] \qquad 0 \le \cos\theta \le 1 \tag{3.4}$$

$$\cos\theta \frac{\partial i^-}{\partial \kappa(x)} + i^-\left[\kappa(x),\theta\right] = S\left[\kappa(x)\right] \qquad -1 \le \cos\theta \le 0 \tag{3.5}$$

Partial derivative notation is used in equations (3.4) and (3.5) because i^+ and i^- depend both upon x and θ.

Now consider the cylindrical geometry, as shown in Figure 3.5b, where i is a function of only the radial coordinate, r. Again split i into positive $i^+(r)$ ($0 \le \cos\theta \le 1$) and negative $i^-(r)$($-1 \le \cos\theta \le 0$) components. Similar to the planar geometry case $ds = \frac{dr}{\cos\theta}$ so that the optical depth is also similar to the planar case.

$$\kappa(s) = \kappa(r)/\cos\theta \tag{3.6}$$

$$\kappa(r) = \int_o^r K(r^*)\,dr^* \tag{3.7}$$

Therefore, the radiation transfer equations for the cylindrical geometry are the same as the planar geometry [equations (3.4) and (3.5)] except that $\kappa(x)$ is replaced by $\kappa(r)$.

The radiation transfer equations can be integrated with the use of an integrating factor. Replace θ in equations (3.4) and (3.5) with a new variable, μ, defined as follows.

$$\mu = \cos\theta \tag{3.8}$$

Multiplying equations (3.4) and (3.5) by the integrating factor, $\exp[\kappa/\mu]$ and then integrating yields the following results.

$$\boxed{i^+(\kappa,\mu) = i^+(0,\mu)\exp\left[-\frac{\kappa}{\mu}\right] + \int_o^{\kappa} S(\kappa^*)\exp\left[-\frac{\kappa-\kappa^*}{\mu}\right]\frac{d\kappa^*}{\mu} \qquad 0 \le \mu \le 1} \tag{3.9}$$

$$\boxed{i^-(\kappa,\mu) = i^-(\kappa_d,\mu)\exp\left[\frac{\kappa_d-\kappa}{\mu}\right] - \int_{\kappa}^{\kappa_d} S(\kappa^*)\exp\left[\frac{\kappa^*-\kappa}{\mu}\right]\frac{d\kappa^*}{\mu} \qquad -1 \le \mu_- \le 0} \tag{3.10}$$

Appearing in these equations are the boundary intensities, $i^+(0, \mu)$ and $i^-(\kappa_d,\mu)$ where κ_d is the following.

$$\kappa_d = \int_o^d K(x^*)\,dx^* \tag{3.11}$$

To obtain the cylindrical form of equations (3.4) and (3.5) replace κ_d with the following.

$$\kappa_R = \int_o^R K(r^*)\,dr^* \tag{3.12}$$

Notice that $\mu \le 0$ in equation (3.10) and that equations (3.9) and (3.10) depend upon the source function, S, and the boundary intensities.

3.7.1 One Dimensional Source Function Equation

Now consider the source function (equation 1.147) for the one-dimensional planar and cylindrical geometries. In terms of i^+ and i^-, the integral in equation (1.147) becomes the following.

$$\int_{\omega=4\pi} i\,d\omega = 2\pi \int_{\theta=0}^{\pi/2} i^+(\kappa,\theta)\sin\theta\,d\theta + 2\pi \int_{\theta=\pi/2}^{\pi} i^-(\kappa,\theta)\sin\theta\,d\theta \tag{3.13}$$

Now substitute $\mu = \cos\theta$ in the first integral and $\mu = -\cos\theta$ in the second integral. Therefore, the source function becomes the following.

$$S(\kappa) = n^2(1-\Omega)i_b(\kappa) + \frac{\Omega}{2}\left[\int_0^1 i^+(\kappa,\mu)\,d\mu + \int_0^1 i^-(\kappa,-\mu)\,d\mu\right] \tag{3.14}$$

Using equations (3.9) and (3.10) for i^+ and i^- in equation (3.14) produces the following result.

$$S(\kappa) = n^2(1-\Omega)i_b(\kappa)$$
$$+\frac{\Omega}{2}\left[\int_0^1 i^+(0,\mu)\exp\left[-\frac{\kappa}{\mu}\right]d\mu + \int_0^1 i^-(\kappa_d,-\mu)\exp\left[\frac{\kappa_d-\kappa}{-\mu}\right]d\mu + \int_0^{\kappa_d} S(\kappa^*)E_1(|\kappa-\kappa^*|)\,d\kappa^*\right] \tag{3.15}$$

Appearing in equation (3.15) is the first order exponential integral, $E_1(x)$, where the *n^{th} order exponential integral* is defined as follows.

$$E_n(x) \equiv \int_0^1 \nu^{n-2}\exp\left(-\frac{x}{\nu}\right)d\nu \tag{3.16}$$

Some useful relations for exponential integral functions are given in Appendix A.

Equation (3.15) is an integral equation for the planar geometry source function, $S(\kappa)$, in terms of the blackbody intensity, i_b, the scattering albedo, Ω, and the boundary intensities $i^+(0,\mu)$ and $i^-(\kappa_d,-\mu)$. For the cylindrical geometry, replace κ_d in equation (3.15) by κ_R. Once the source function is known, the intensities can be calculated using equations (3.9) and (3.10).

3.7.2 One Dimensional Radiation Flux

Solution of the energy equation [equation (1.160)] requires an expression for the total radiation flux, $\overline{q}$ [equations (1.151a) and (1.154)]. The radiation intensity, i, represents energy per unit solid angle crossing an area normal to the direction of i. Therefore, the radiation flux per unit wavelength per unit area, q, is obtained by integrating the i^+ and i^- over the projected area $\cos\theta dA$ and solid angle $2\pi\sin\theta d\theta$ and then dividing the result by dA. For the radiation flux, q^+, moving in the +x direction the following is obtained.

$$q^+(\kappa,\lambda) = 2\pi \int_o^{\pi/2} i^+(\kappa,\theta,\lambda)\cos\theta\sin\theta d\theta \tag{3.17}$$

Similarly, for the radiation flux moving in the -x direction, q^-, the following is obtained.

$$q^-(\kappa,\lambda) = -2\pi \int_{\pi/2}^{\pi} i^-(\kappa,\theta,\lambda)\cos\theta\sin\theta d\theta \tag{3.18}$$

The radiation fluxes q^+ and q^-, as well as the intensities i^+ and i^- are always positive quantities. Therefore, since $\cos\theta < 0$ for $\frac{\pi}{2} \le \theta \le \pi$, the negative sign occurs in the q^- expression. The net radiation flux, q, in the +x direction is the following.

$$q(\kappa,\lambda) = q^+(\kappa,\lambda) - \overline{q}(\kappa,\lambda) = 2\pi\left[\int_o^{\pi/2} i^+(\kappa,\theta,\lambda)\cos\theta\sin\theta d\theta + \int_{\pi/2}^{\pi} i^-(\kappa,\theta,\lambda)\cos\theta\sin\theta d\theta\right] \tag{3.19}$$

Making the substitution $\mu = \cos\theta$ in the first integral and $\mu = -\cos\theta$ in the second integral, the radiation flux becomes the following.

$$q(\kappa,\lambda) = 2\pi \int_o^1 \left[i^+(\kappa,\mu,\lambda) - i^-(\kappa,-\mu,\lambda)\right]\mu d\mu \tag{3.20}$$

If equations (3.9) and (3.10) are substituted for i^+ and i^-, the following is obtained.

$$q(\kappa,\lambda) = 2\pi\left[\int_0^1 i^+(0,\mu,\lambda)\exp\left[-\frac{\kappa}{\mu}\right]\mu d\mu - \int_0^1 i^-(\kappa_d,-\mu,\lambda)\exp\left[\frac{\kappa_d-\kappa}{-\mu}\right]\mu d\mu + \int_0^{\kappa} S(\kappa^*,\lambda)E_2(\kappa-\kappa^*)d\kappa^* - \int_{\kappa}^{\kappa_d} S(\kappa^*,\lambda)E_2(\kappa^*-\kappa)d\kappa^*\right] \tag{3.21}$$

Appearing in this equation is the second order exponential integral, E_2. Equation (3.21) gives q as a function of the source function, S, and the boundary intensities $i^+(0)$ and $i^-(\kappa_d)$. To obtain the total radiation flux, $\bar{q}$, equation (3.21) must be integrated over all λ. Equation (3.21) applies to the one-dimensional planar geometry. The one-dimensional cylindrical case is obtained by substituting κ_R for κ_d.

3.7.3 No Scattering Medium

For an emitter made of a single crystal, such as the rare earth garnets mentioned in Section 3.5, there are few imperfections that can act as scattering centers. As a result, scattering can be neglected compared to absorption in the extinction coefficient. This approximation should be applicable in the emission bands of all rare earth selective emitters where emission and absorption from the lowest excited states of the rare earth ion dominate. However, polycrystalline materials have many grain boundaries that act as scattering centers. Therefore, outside the emission bands scattering may be important for the sintered and fibrous rare earth emitters discussed in Section 3.3.1.

If scattering can be neglected, then a great deal of simplification of the source function equation occurs. For no scattering (Ω = 0), the source function [equation (3.15)] reduces to the blackbody intensity.

$$S(\kappa) = n^2 i_b(\lambda, T(\kappa)) = n^2\frac{e_b(\lambda, T(\kappa))}{\pi} \tag{3.22}$$

Thus, if the temperature and index of refraction are constant throughout the medium, S(κ) is also a constant. In that case, the κ* integrations in equation (3.21) can be completed so that the radiation flux is the following.

$$q(\kappa,\lambda) = 2\pi\left\{\int_0^1 i^+(0,\mu,\lambda)\exp\left[\frac{-\kappa}{\mu}\right]\mu d\mu - \int_0^1 i^-(\kappa_d,-\mu,\lambda)\exp\left[\frac{\kappa_d-\kappa}{-\mu}\right]\mu d\mu + n^2 i_b(\lambda,T)\left[E_3(\kappa_d-\kappa)-E_3(\kappa)\right]\right\} \tag{3.23}$$

For a medium with n = 1 emitting into a vacuum (n_o = 1) there is no reflection at the vacuum-medium interface. As a result, $i^+(0)$ and $i^-(\kappa_d)$ vanish if there is no radiation entering the medium at the boundaries. Therefore, at the boundaries $q(\kappa_d)$ and q(0) become the following.

$$q\left(\kappa_d,\lambda\right) = -q\left(0,\lambda\right) = \pi i_b\left(\lambda,T\right)\left[1-2E_3\left(\kappa_d\right)\right] \tag{3.24}$$

The spectral emittance for the medium is the following.

$$\varepsilon\left(\lambda\right) \equiv \frac{q\left(\kappa_d,\lambda\right)}{\pi i_b\left(\lambda,T\right)} = 1-2E_3\left(\kappa_d\right)$$

planar geometry, constant temperature, no scattering

$$i^+\left(0\right) = i^-\left(\kappa_d\right) = 0$$
$$n = n_o = 1$$

(3.25)

For a cylindrical geometry, replace κ_d with κ_R.

3.8 Spectral Emittance for Planar Emitter

The one-dimensional radiation transfer equations and energy equation are applicable to any emitting, absorbing, and scattering solid state medium. For TPV applications selective emitter materials are of most interest. In this case, the characteristic dimension of the emitter is small (< 1mm). Therefore, a planar selective emitter is a film. Also, for wavelength regions outside the emission bands a selective emitter is nearly transparent to radiation. In these transparent regions, undesirable radiation from the thermal source heating the emitter passes through the selective emitter nearly unattenuated. To block this undesirable radiation, a low emittance metal substrate can be placed between the thermal source and the emitting film.

Figure 3.6 illustrates two configurations for a film emitter with a conducting substrate with index of refraction, $n_s = n_{sR} - jn_{sI}$. In Figure 3.6a, the substrate is in direct contact with the emitter, which applies if the substrate is deposited on the emitter. If there is a gap between the substrate and emitter, such as would occur if the substrate is a metal foil, then Figure 3.6b applies. For the gap case, assume the substrate and backside of the emitter are at the same temperature, T_s. For vacuum conditions, this may be a poor approximation since heat transfer between the substrate and emitter will be by radiation only. In that case, a significant temperature difference between the higher temperature substrate and emitter backside can exist. A significant temperature difference results in reduced radiation from the emitter; therefore, a lower spectral emittance exists compared to the case where emitter and substrate are at the same temperature.

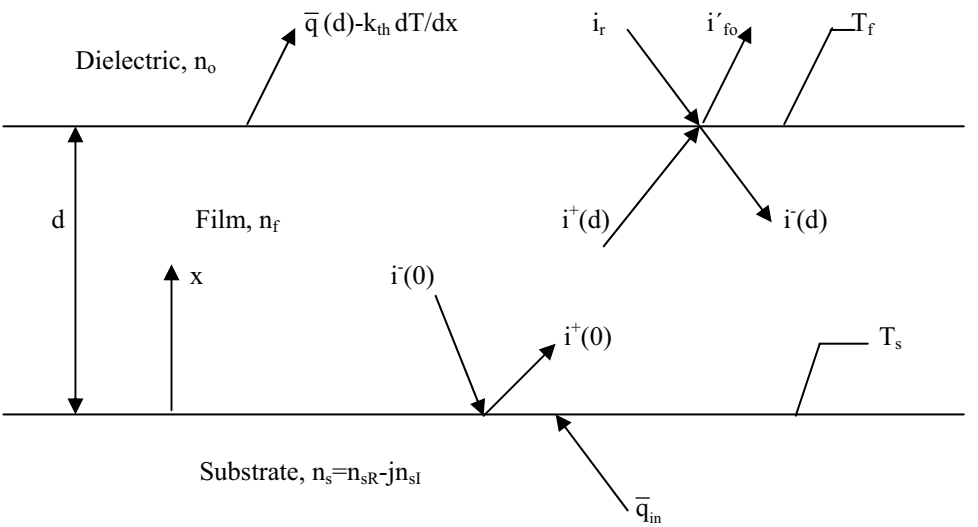

a) Emitter film in direct contact with substrate.

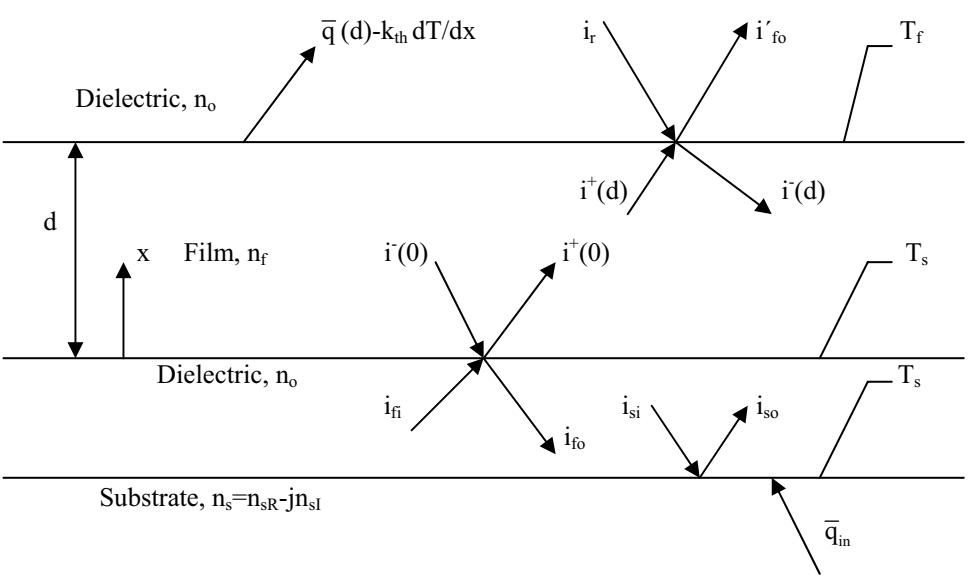

b) Dielectric gap between emitter film and substrate.

Figure 3.6 Schematic diagram of film emittance model.

The thermal energy flux entering the emitter at x = 0 is $\bar{q}_{in}$ and leaving the emitter at x = d is the sum of the radiation flux, $\bar{q}(d)$, and the thermal conduction, $-k_{th}\left.\frac{dT}{dx}\right|_{x-d}$. Therefore, assuming a steady state, the one dimensional energy equation [equation (1.160)] becomes the following.

$$-k_{th}\frac{dT}{dx}+\bar{q}(x)=\bar{q}_{in}=-k_{th}\left.\frac{dT}{dx}\right|_{x=o}+\bar{q}(d) \tag{3.26}$$

The total radiation flux, $\bar{q}(x)$, is the following.

$$\bar{q}(x)=\int_{o}^{\infty}q(x,\lambda)d\lambda \tag{3.27}$$

And q(x,λ) is given by equation (3.21) that in turn, depends upon the source function, S(κ), given by equation (3.15). Thus, equations (3.15), (3.21), (3.26), and (3.27) are a coupled set of equations that must be solved in order to obtain the temperature, T and radiation fluxes, q(x) and $\bar{q}(x)$. Once q(d) is determined, the hemispherical spectral emittance, ε, is obtained. The solution depends on the boundary conditions, the optical depth, κ_d, and the indices of refraction of the film, n_f, surrounding dielectric, n_o, and substrate, $n_{sR} - jn_{sI}$.

The radiation flux, q(κ), at the optical depth κ is obtained using equation (3.21). Assume the intensities leaving the boundaries at x = 0 and x = d, $i^+(0)$ and $i^-(d)$ are independent of angle. As a result, equation (3.21) yields the following result.

$$q(\kappa,\lambda)=2\left[q^{+}(0)E_3(\kappa)-q^{-}(\kappa_d)E_3(\kappa_d-\kappa)\right]+\phi_{+}(\kappa)-\phi_{-}(\kappa) \tag{3.28}$$

Where,

$$q^{+}(0)=\pi i^{+}(0) \tag{3.29}$$

$$q^{-}(\kappa_d)=\pi i^{-}(\kappa_d) \tag{3.30}$$

$$\phi_+(\kappa) = 2\pi \int_o^{\kappa} S(\kappa^*,\lambda) E_2(\kappa - \kappa^*)\, d\kappa^* \tag{3.31}$$

$$\phi_-(\kappa) = 2\pi \int_{\kappa}^{\kappa_d} S(\kappa^*,\lambda) E_2(\kappa^* - \kappa)\, d\kappa^* \tag{3.32}$$

To obtain $q^+(0)$ and $q^-(\kappa_d)$ boundary conditions at x = 0 and x = d must be applied.

Radiation enters the film from the substrate at x = 0 and also from the surroundings at x = d. Therefore, the boundary conditions at x = 0 and x = d are somewhat complicated. First, consider the case where the substrate is in direct contact with the emitter (Figure 3.6a). At the film-substrate interface (x = 0 or κ = 0) the intensity moving in the +x direction is the sum of the reflected intensity and the radiation emitted from the substrate into the film.

$$i^+(0) = n_f^2 \varepsilon'_{fs}(\theta) i_b(\lambda, T_s) + R'_{fs}(\theta) i^-(0) \qquad x = \kappa_d = 0 \tag{3.33}$$

Here $i_b(\lambda,T_s)$ is the black body intensity [equation (1.120)] at the substrate temperature, T_s, R'_{fs} is the directional spectral reflectivity at the film-substrate interface, and ε'_{fs} is the directional spectral emittance. Using equation (3.33), the radiation flux in the +x direction at x = 0 is the following.

$$\begin{aligned} q^+(0) = 2\pi \int_o^{\pi/2} i^+(0) \cos\theta \sin\theta\, d\theta = 2\pi n_f^2 \int_o^{\pi/2} \varepsilon'_{fs}(\theta) i_b(\lambda, T_s) \cos\theta \sin\theta\, d\theta \\ -2\pi \int_{\pi/2}^{\pi} R'_{fs}(\theta) i^-(0) \cos\theta \sin\theta\, d\theta \end{aligned} \tag{3.34}$$

Similar to equation (3.18), the negative sign in front of the second integral is required to make the term positive since cosθ is negative for $\frac{\pi}{2} \le \theta \le \pi$. In Section 1.5.4 Snell's Law is applied to the interface between a dielectric and a conductor. In that case, for angles of incidence $\theta > \theta_{cr} = \sin^{-1}\left(\frac{n_o}{\alpha_{cr}}\right)$ radiation from the conductor into the dielectric is totally reflected when $\alpha_{cr} > n_o$, where α_{cr} is given by equation (1.71) for $\theta_o^+ = \frac{\pi}{2}$, and n_o is the index of refraction for the dielectric. However, for radiation from the dielectric into the conductor [second term on right side of equation (3.34)], there are

no angles of incidence for which total reflection occurs. Thus, $R'_{fs}(\theta) < 1$ for all angles of incidence, $\frac{\pi}{2} \le \theta \le \pi$, in equation (3.34). Now replace πi_b by $e_b(\lambda,T)$ and change the variable of integration in equation (3.34) by substituting $\mu = \cos\theta$.

$$q^+(0) = 2n_f^2 e_b(\lambda,T)\int_o^1 \varepsilon'_{fs}(\mu)\mu d\mu - 2\pi\int_{-1}^{o} R'_{fs}(\mu) i^-(0)\mu d\mu \tag{3.35}$$

As discussed in section 1.9, for emission from a metal into a dielectric, the normal spectral emittance, ε_n given by equation (1.246) is a good approximation for ε'. Therefore, assume $\varepsilon'_s = \varepsilon_{nfs}$. Similarly, assume R'_{fs} can be approximated by the reflectivity for normal incidence, $\overline{R}_{fs}$ [equation 1.110)]. As a result, from equation (1.237) the following is obtained.

$$\varepsilon'_s = 1 - R'_{fs} \approx \varepsilon_{fsn} = 1 - \overline{R}_{fs} \tag{3.36}$$

Also, remember $i^-(\kappa_d)$ is assumed to be independent of θ. Therefore, using equation (3.10) for $i^-(0)$ in equation (3.35), the following is obtained.

$$\boxed{q^+(0) = n_f^2 \varepsilon_{nfs} e_b(\lambda,T_s) + \overline{R}_{fs}\left[2q^-(\kappa_d)E_3(\kappa_d) + \phi_-(0)\right]} \tag{3.37}$$

Appearing in equation (3.37) are the radiation flux in –x direction at x = d, $q^-(\kappa_d)$, and the source function integral, $\phi_-(0)$. As equation (3.37) shows, $q^+(0)$ is related to the boundary value of q^- at $\kappa = \kappa_d (x = d)$. As a result of the radiation boundary condition at $x = d(\kappa = \kappa_d)$, $q^-(\kappa_d)$ becomes a function of $q^+(0)$. Thus the boundary conditions at x = 0 and x = d yield two linear simultaneous equations for $q^+(0)$ and $q^-(\kappa_d)$.

Referring to Figure 3.6, at the emitter-dielectric interface at x = d or $\kappa = \kappa_d$, the intensity moving in the –x direction, $i^-(d)$, is the sum of the reflected intensity, $R'_{fo} i^+(d)$, and the external intensity that passes through the interface, $(1 - R'_{fo}) i_r$.

$$i^-(d) = (1 - R'_{fo}) i_r + R'_{fo} i^+(d) \tag{3.38}$$

Characterize the external radiation intensity, i_r, as follows,

$$i_r = s i_b(\lambda, T_r) + r i'_{fo} \tag{3.39}$$

where the first term is the emitted intensity from the external source at temperature, T_r. The second term is the fraction of the intensity leaving the emitter, i'_{fo}, that is reflected back to the emitter. The quantities s and r are not the emittance and reflectance of the external source. However, they can be approximated as the product of two terms, one of which is the emittance or reflectance. The other term is a geometrical factor that accounts for the fraction of radiation that leaves the external source and impinges upon the emitter. This geometrical factor is called the *configuration or view factor* and will be defined in Chapter 6. The intensity leaving the emitter, i'_{fo}, is the sum of the intensity passing through the interface and the reflected intensity from the external source, $R'_{fo} i_r$. Since the surrounding medium is a dielectric, the intensity passing through the interface is $\left(1 - R'_{fo}\right) i^+(d)$.

$$i'_{fo} = \left(1 - R'_o\right) i^+(d) + R'_{fo} i_r \tag{3.40}$$

Eliminating i_r and i'_{fo} between equations (3.38) through (3.40) yields the following solution for $i^-(d)$.

$$i^-(d) = \frac{1}{1 - r R'_{fo}} \left\{ \left(1 - R'_{fo}\right) s i_b(\lambda, T_r) + \left[R'_{fo} + r\left(1 - 2R'_{fo}\right) \right] i^+(d) \right\} \tag{3.41}$$

Now calculate the radiation flux at x = d, moving in the -x direction, $q^-(d)$. Using equation (3.41) for $i^-(d)$ in equation (3.18) gives the following result.

$$q^-(d) = -2\pi \int_{\pi/2}^{\pi} i^-(d) \cos\theta \sin\theta \, d\theta =$$

$$-2\pi \int_{\pi/2}^{\pi} \frac{\left(1 - R'_{fo}\right)}{1 - r R'_{fo}} s i_b(\lambda, T_r) \cos\theta \sin\theta \, d\theta + 2\pi \int_{o}^{\pi/2} \frac{R'_{fo} + r\left(1 - 2R'_{fo}\right)}{1 - r R'_{fo}} i^+(d) \cos\theta \sin\theta \, d\theta \tag{3.42}$$

Notice that the integration limits differ. The first integral is for radiation moving in the -x direction $\left(\frac{\pi}{2} \le \theta \le \pi\right)$ from the external source while the second integral is for radiation moving in the +x direction $\left(0 \le \theta \le \frac{\pi}{2}\right)$. Snell's Law (Section 1.5.4) applies at the interface at x = d. Therefore, when $n_f > n_o$, which applies for dielectric emitter

films, all the incident radiation $i^+(d)$ is reflected for $\theta_{crfo} \le \theta \le \frac{\pi}{2}$ where θ_{crfo} is given by equation (1.57).

$$\sin\theta_{crfo} = \frac{n_o}{n_f} \tag{3.43}$$

Therefore, for radiation in the +x direction at x = d, $R'_{fo} = 1$ for $\theta_{crfo} \le \theta \le \frac{\pi}{2}$. For $0 \le \theta \le \theta_{crfo}$ assume that R'_{fo} can be approximated by the value for normal incidence, $R'_{fo} = \bar{R}_{fon}$, [equation (1.110)]. Also, assume that r and s are constants. Therefore, making the change of variable, $\mu = \cos\theta$, equation (3.42) becomes the following,

$$q^-(d) = 2\pi s\left[\frac{1-\bar{R}_{fon}}{1-r\bar{R}_{fon}}\right] i_b(\lambda, T_r)\int_o^{-1}\mu d\mu = 2\pi\left\{\frac{\bar{R}_{fon} + r\left(1-2\bar{R}_{fon}\right)}{1-r\bar{R}_{fon}}\int_{\mu_M}^{1} i^+(d)\mu d\mu + \int_o^{\mu_M} i^+(d)\mu d\mu\right\} \tag{3.44}$$

where $\mu_M = \cos\theta_{crfo}$ and $\sin\theta_{crfo}$ is given by equation (3.43). Now substitute equation (3.9) for $i^+(d)$ and assume that $i^+(0)$ is independent of θ. Therefore, equation (3.44) becomes the following,

$$\boxed{q^-(\kappa_d) = 2q^+(0)\left[\bar{\rho}_{fo}E_3(\kappa_d) + \mu_M^2\left(1-\bar{\rho}_{fo}\right)E_3\left(\frac{\kappa_d}{\mu_M}\right)\right] + \bar{\rho}_{fo}\phi_+(\kappa_d) + \left(1-\bar{\rho}_{fo}\right)\phi_{M+}(\kappa_d) + \bar{\tau}_{fo}se_b(\lambda, T_r)} \tag{3.45}$$

where $\bar{\rho}_{fo}$ is an effective reflectance for the emitter-dielectric interface and $\bar{\tau}_{fo}$ is an effective transmittance for the interface.

$$\bar{\rho}_{fo} = \frac{\bar{R}_{fo} + r\left(1-2\bar{R}_{fo}\right)}{1-r\bar{R}_{fo}} \tag{3.46}$$

$$\bar{\tau}_{fo} = \frac{1-\bar{R}_{fo}}{1-r\bar{R}_{fo}} \tag{3.47}$$

If there is no reflected radiation from the surroundings (r = 0), then $\overline{\rho}_{fo} = \overline{R}_{fo}$ and $\overline{\tau}_{fo} = 1 - \overline{R}_{fo}$. Also appearing in equation (3.45) is the radiation flux at x = 0 moving in the +x direction, $q^{+}(0)$ [equation (3.29)] the two source function integrals, $\phi_{+}\left(\kappa_d\right)$ [equation (3.31)] and $\phi_{M+}\left(\kappa_d\right)$ and the parameter, μ_M.

$$\phi_{M+}\left(\kappa\right) = 2\pi\mu_M \int_o^{\kappa} S\left(\kappa^*, \lambda\right) E_2\left(\frac{\kappa - \kappa^*}{\mu_M}\right) d\kappa^* \tag{3.48}$$

$$\mu_M = \cos\theta_{crfo} = \sqrt{1 - \left(\frac{n_o}{n_f}\right)^2} \tag{3.49}$$

Now consider the case where there is a dielectric gap between the substrate and the emitter (Figure 3.6b). The boundary condition at x = d is the same as in the case of no gap (Figure 3.6a). Therefore, the radiation flux $q^{-}(\kappa_d)$ given by equation (3.45) also applies to the case where a gap exists. For the case where a gap exists, the boundary condition at x = 0 is similar to the boundary condition at x = d. This will become evident with the calculation of the radiation flux, $q^{+}(0)$. For the case where the gap exists, the intensity moving in the +x direction at x = 0, $i^{+}(0)$, is the following.

$$i^{+}\left(0\right) = \left(1 - R'_{fo}\right) i_{fi} + R'_{fo} i^{-}\left(0\right) \tag{3.50}$$

The first term is the fraction of the incident intensity, i_{fi}, that is transmitted through the emitter-dielectric interface. The second term is the fraction of the intensity, $i^{-}(0)$, that is reflected into the +x direction. Referring to Figure 3.7b, the following equations apply for the intensity leaving the emitter in the -x direction, i_{fo}, and the intensity leaving the substrate in the +x direction, i_{so}.

$$i_{fo} = \left(1 - R'_{fo}\right) i^{-}\left(0\right) + R'_{fo} i_{fi} \tag{3.51}$$

$$i_{so} = n_o^2 \varepsilon'_{so} i_b\left(\lambda, T_s\right) + R'_{so} i_{si} \tag{3.52}$$

Since the gap is very small, assume that all the radiation leaving the substrate, i_{so}, is incident on the emitter. Similarly, all radiation leaving the emitter, i_{fo}, is incident on the substrate. As a result, $i_{so} = i_{fi}$ and $i_{fo} = i_{si}$. Using this result in equations (3.51) and (3.52) produces the following result for i_{fi}.

$$i_{fi} = \frac{1}{1 - R'_{so} R'_{fo}} \left[n_o^2 \varepsilon'_{so} i_b(\lambda, T_s) + R'_{so} \left(1 - R'_{fo}\right) i^-(0) \right] \tag{3.53}$$

Now substitute equation (3.53) in equation (3.50).

$$i^+(0) = \frac{1}{1 - R'_{so} R'_{fo}} \left\{ n_o^2 \left(1 - R'_{fo}\right) \varepsilon'_{so} i_b(\lambda, T_s) + \left[R'_{fo} + R'_{so} \left(1 - 2R'_{fo}\right) \right] i^-(0) \right\} \tag{3.54}$$

Comparing equations (3.41) and (3.54), the similarity between the boundary conditions at x = 0 and x = d becomes evident. If r is replaced by R'_{so}, s by $n_o^2 \varepsilon'_{so}$, and $i^+(d)$ by $i^-(0)$ in equation (3.41), then equation (3.54) is obtained. The radiation flux moving in the +x direction at x = 0, $q^+(0)$, can now be calculated with the use of equation (3.54).

$$\begin{aligned} q^+(0) = 2\pi \int_0^{\pi/2} i^+(0) \cos\theta \sin\theta \, d\theta &= 2\pi i_b(\lambda, T_s) \int_0^{\pi/2} \frac{n_o^2 \left(1 - R'_{fo}\right)}{1 - R'_{fo} R'_{so}} \varepsilon'_{so} \cos\theta \sin\theta \, d\theta \\ &\quad - 2\pi \int_{\pi/2}^{\pi} \frac{R'_{fo} + R'_{so} \left(1 - 2R'_{fo}\right)}{1 - R'_{fo} R'_{so}} i^-(0) \cos\theta \sin\theta \, d\theta \end{aligned} \tag{3.55}$$

Similar to equation (3.42), the integration limits are different for the two integrals. In the first integral, the radiation is in the +x direction so that $0 \le \theta \le \frac{\pi}{2}$. In the second integral, the radiation is in the -x direction so the $\frac{\pi}{2} \le \theta \le \pi$ and a negative sign multiplies the integral since cos θ < 0. Also, at the film-gap interface (x = 0) Snell's Law applies. Therfore, since $n_f > n_o$, all radiation moving in the -x direction at x = 0 will be reflected for $\frac{\pi}{2} \le \theta \le \theta'_{crfo}$, where $\theta'_{crfo} = \pi - \theta_{crfo}$ and θ_{crfo} is given by equation (3.43). As a result, for radiation in the -x direction at x = 0, $R'_{fo} = 1$ for $\frac{\pi}{2} \le \theta \le \theta'_{crfo}$. For $\theta'_{crfo} < \theta \le \pi$ assume that R'_{fo} can be approximated by the value for normal incidence $R'_{fo} = \overline{R}_{fon}$, [equation (1.110)]. Similar to the case for the ε'_{fs} and R'_{fs} terms in equation (3.35), make the following approximations: $\varepsilon'_{so} \approx \varepsilon_{son}$, $R'_{fo} \approx \overline{R}_{fon}$ and $R'_{so} \approx \overline{R}_{son}$. The normal spectral emittance is ε_{son} and $\overline{R}_{son}$ is the normal spectral reflectivity at the substrate-dielectric interface and $\overline{R}_{fon}$ is the spectral reflectivity at the

film-dielectric interface. With these conditions equation (3.55) becomes the following when the change of variable $\mu = \cos\theta$ is made.

$$q^+(0) = 2\pi\left[\bar{\tau}_{fs}\varepsilon_{son}n_o^2 i_b(\lambda, T_s)\int_o^1 \mu d\mu - \int_{-\mu_M}^{o} i^-(0)\mu d\mu - \bar{\rho}_{fs}\int_{-1}^{-\mu_M} i^-(0)\mu d\mu\right] \tag{3.56}$$

Here $\bar{\tau}_{fs}$ is an effective transmittance and $\bar{\rho}_{fs}$ is an effective reflectance for the emitter-gap-substrate region and μ_M is given by equation (3.49).

$$\bar{\tau}_{fs} = \frac{1-\bar{R}_{fo}}{1-\bar{R}_{fo}\bar{R}_{so}} \tag{3.57}$$

$$\bar{\rho}_{fs} = \frac{\bar{R}_{fo} + \bar{R}_{so}(1-2\bar{R}_{fo})}{1-\bar{R}_{fo}\bar{R}_{so}} \tag{3.58}$$

Now use equation (3.10) for $i^-(0)$ in equation (3.56).

$$\boxed{\begin{aligned} q^+(0) = \bar{\tau}_{fs}n_o^2\varepsilon_{son}e_b(\lambda, T_s) + 2q^-(\kappa_d)\left[\bar{\rho}_{fs}E_3(\kappa_d) + \mu_M^2(1-\bar{\rho}_{fs})E_3\left(\frac{\kappa_d}{\mu_M}\right)\right] \\ +\bar{\rho}_{fs}\phi_-(0) + (1-\bar{\rho}_{fs})\phi_{M-}(\kappa_d) \end{aligned}} \tag{3.59}$$

Appearing in equation (3.59) are the source function integrals $\phi_-(0)$ given by equation (3.32) and $\phi_{M-}(\kappa)$ defined as follows.

$$\phi_{M-}(\kappa) = 2\pi\mu_M\int_o^{\kappa} S(\kappa^*, \lambda)E_2\left(\frac{\kappa^*}{\mu_M}\right)d\kappa^* \tag{3.60}$$

The similarity between the boundary radiation flux, $q^+(0)$ and $q^-(\kappa_d)$ can be seen by comparing equations (3.45) and (3.59). If the subscript fs is replaced by fo, $\phi_-(0)$ by $\phi_+(\kappa_d)$, $\phi_{M-}(\kappa_d)$ by $\phi_{M+}(\kappa_d)$, $n_o^2\varepsilon_{son}$ by s, and $q^-(\kappa_d)$ by $q^+(0)$ in equation (3.59), then equation (3.45) for $q^-(\kappa_d)$ is obtained.

Compare $q^+(0)$ for the no gap case [equation (3.37)] with $q^+(0)$ for the case with a gap [equation (3.59)]. The addition of the dielectric gap results in several changes in

$q^+(0)$. First, the emittance of the substrate is reduced by the effective transmittance of the gap, $\overline{\tau}_{fs}$. Second, the reflectance of the film-substrate interface, $\overline{R}_{fsn}$, is replaced by the effective reflectance of the gap, $\overline{\rho}_{fs}$. Finally, because total reflection of radiation occurs for $\theta > \theta_{cr}$ at the film-gap and substrate-gap interface the additional two terms containing $\left(1-\overline{\rho}_{fs}\right)$ appear in equation (3.59).

Equation (3.45) for $q^-(\kappa_d)$ and equation (3.59) for $q^+(0)$, for the case where a dielectric gap exists, can be solved simultaneously to obtain $q^+(0)$ and $q^-(\kappa_d)$.

$$\begin{aligned} q^+(0) = \frac{1}{D}\Big\{ & 2a_{fs}\left[\overline{\tau}_{fo} s e_b(\lambda, T_r) + \overline{\rho}_{fo}\phi_+(\kappa_d) + \left(1-\overline{\rho}_{fo}\right)\phi_{M+}(\kappa_d)\right] \\ & + \overline{\tau}_{fs} n_o^2 \varepsilon_{son} e_b(\lambda, T_s) + \overline{\rho}_{fs}\phi_-(0) + \left(1-\overline{\rho}_{fs}\right)\phi_{M-}(\kappa_d)\Big\} \end{aligned} \tag{3.61}$$

$$\begin{aligned} q^-(\kappa_d) = \frac{1}{D}\Big\{ & 2a_{fo}\left[\overline{\tau}_{fs} n_o^2 \varepsilon_{son} e_b(\lambda, T_s) + \overline{\rho}_{fs}\phi_-(0) + \left(1-\overline{\rho}_{fs}\right)\phi_{M-}(\kappa_d)\right] \\ & + \overline{\tau}_{fo} s e_b(\lambda, T_r) + \overline{\rho}_{fo}\phi_+(\kappa_d) + \left(1-\overline{\rho}_{fo}\right)\phi_{M+}(\kappa_d)\Big\} \end{aligned} \tag{3.62}$$

These results for $q^+(0)$ and $q^-(\kappa_d)$ can now be used in equation (3.28) to obtain $q(\kappa,\lambda)$, (problem 3.3).

$$\begin{aligned} q(\kappa,\lambda) = \frac{2}{D}\Big\{ & \left[\overline{\tau}_{fs} n_o^2 \varepsilon_{son} e_b(\lambda, T_s) + \overline{\rho}_{fs}\phi_-(0) + \left(1-\overline{\rho}_{fs}\right)\phi_{M-}(\kappa_d)\right] B(\kappa) \\ & - \left[\overline{\tau}_{fo} s e_b(\lambda, T_r) + \overline{\rho}_{fo}\phi_+(\kappa_d) + \left(1-\overline{\rho}_{fo}\right)\phi_{M+}(\kappa_d)\right] A(\kappa)\Big\} + \phi_+(\kappa) - \phi_-(\kappa) \end{aligned} \quad \text{with gap} \tag{3.63}$$

New terms appearing in equations (3.61) – (3.63) are defined as follows:

$$A(\kappa) = E_3(\kappa_d - \kappa) - 2a_{fs}E_3(\kappa) \tag{3.64}$$

$$B(\kappa) = E_3(\kappa) - 2a_{fo}E_3(\kappa_d - \kappa) \tag{3.65}$$

$$D = 1 - 4a_{fo}a_{fs} \tag{3.66}$$

$$a_{fo} = \overline{\rho}_{fo}E_3(\kappa_d) + \left(1-\overline{\rho}_{fo}\right)\mu_M^2 E_3\left(\frac{\kappa_d}{\mu_M}\right) \tag{3.67}$$

$$a_{fs} = \overline{\rho}_{fs}E_3(\kappa_d) + \left(1-\overline{\rho}_{fs}\right)\mu_M^2 E_3\left(\frac{\kappa_d}{\mu_M}\right) \tag{3.68}$$

Equation (3.63) applies for the case where a dielectric gap exists between the substrate and the emitter. If there is no dielectric gap, then $\bar{\tau}_{fs} n_o^2 \varepsilon_{son} \rightarrow n_f^2 \varepsilon_{fsn}$, $\bar{\rho}_{fs} \rightarrow \bar{R}_{fsn}$, and the $\left(1-\bar{\rho}_{fs}\right)$ term in equation (3.63) vanishes.

$$\boxed{\begin{aligned} q(\kappa,\lambda) = \frac{2}{D'}\Big\{ \Big[n_f^2 \varepsilon_{fsn} e_b(\lambda, T_s) + \bar{R}_{fs}\phi_-(0)\Big] B(\kappa) \\ -\Big[\bar{\tau}_{fo} s e_b(\lambda, T_r) + \bar{\rho}_{fo}\phi_+(\kappa_d) + (1-\bar{\rho}_{fo})\phi_{M+}(\kappa_d)\Big] A'(\kappa)\Big\} + \phi_+(\kappa) - \phi_-(\kappa) \end{aligned}} \quad \text{no gap} \tag{3.69}$$

Where the following new terms appear:

$$A'(\kappa) = E_3(\kappa_d - \kappa) - 2a'_{fs} E_3(\kappa) \tag{3.70}$$

$$D' = 1 - 4a_{fo} a'_{fs} \tag{3.71}$$

$$a'_{fs} = \bar{R}_{fs} E_3(\kappa_d) \tag{3.72}$$

Now consider the source function given by equation (3.15). Again, assume that the boundaries are diffuse, so that $i^+(0)$ and $i^-(\kappa_d)$ are independent of angle. Thus, the μ integrations in equation (3.15) can be carried out. Therefore, using equations (3.29) and (3.30), the following is derived for $S(\kappa)$.

$$\begin{aligned} S(\kappa) &= n_f^2 (1-\Omega)\frac{e_b(\lambda, T)}{\pi} \\ &+ \frac{\Omega}{2\pi}\left[q^+(0) E_2(\kappa) + q^-(\kappa_d) E_2(\kappa_d - \kappa) + \pi \int_o^{\kappa_d} S(\kappa^*) E_1\left(|\kappa - \kappa^*|\right) d\kappa^* \right] \end{aligned} \tag{3.73}$$

Substituting equations (3.61) and (3.62) for $q^+(0)$ and $q^-(\kappa_d)$ yields the following result when the definitions of the integral functions $\phi_+(\kappa_d)$, $\phi_-(0)$, $\phi_{M+}(\kappa_d)$, and $\phi_{M-}(\kappa_d)$ are used.

$$
\begin{aligned}
S(\kappa) = n_f^2(1-\Omega)\frac{e_b(\lambda,T)}{\pi} + \frac{\Omega}{2D}\Bigg\{\Bigg[\overline{\tau}_{fs} n_o^2 \varepsilon_{son}\frac{e_b(\lambda,T_s)}{\pi} \\
+2\int_o^{\kappa_d} S(\kappa^*)\left(\overline{\rho}_{fs}E_2(\kappa^*) + \mu_M(1-\overline{\rho}_{fs})E_2\left(\frac{\kappa^*}{\mu_M}\right)\right)d\kappa^*\Bigg] G(\kappa) + \Bigg[\overline{\tau}_{fo} s\frac{e_b(\lambda,T_r)}{\pi} \\
+2\int_o^{\kappa_d} S(\kappa^*)\left(\overline{\rho}_{fo}E_2(\kappa_d-\kappa^*) + \mu_M(1-\overline{\rho}_{fo})E_2\left(\frac{\kappa_d-\kappa^*}{\mu_M}\right)\right)d\kappa^*\Bigg] H(\kappa)\Bigg\} \\
+\frac{\Omega}{2}\int_o^{\kappa_d} S(\kappa^*)E_1(|\kappa^*-\kappa|)d\kappa^* \qquad \text{with gap}
\end{aligned}
\tag{3.74}
$$

Appearing in equation (3.74) are the following two functions of the optical depth, κ.

$$G(\kappa) = E_2(\kappa) + 2a_{fo}E_2(\kappa_d-\kappa) \tag{3.75}$$

$$H(\kappa) = E_2(\kappa_d-\kappa) + 2a_{fs}E_2(\kappa) \tag{3.76}$$

Just as in the case for q(κ), [equation (3.69)], to obtain S(κ) for the case of no dielectric gap, let $\overline{\tau}_{fs} n_o^2 \varepsilon_{son} \to n_f^2 \varepsilon_{fsn}$, $\overline{\rho}_{fs} \to \overline{R}_{fs}$, and remove the $(1-\overline{\rho}_{fs})$ terms in equation (3.74).

$$
\begin{aligned}
S(\kappa) = n_f^2(1-\Omega)\frac{e_b(\lambda,T)}{\pi} + \frac{\Omega}{2D'}\Bigg\{\Bigg[n_f^2\varepsilon_{fsn}\frac{e_b(\lambda,T_s)}{\pi} + 2\overline{R}_{fs}\int_o^{\kappa_d} S(\kappa^*)E_2(\kappa^*)d\kappa^*\Bigg] G(\kappa) \\
+\Bigg[\overline{\tau}_{fo} s\frac{e_b(\lambda,T_r)}{\pi} + 2\int_o^{\kappa_d} S(\kappa^*)\left(\overline{\rho}_{fo}E_2(\kappa_d-\kappa^*) + \mu_M(1-\overline{\rho}_{fo})E_2\left(\frac{\kappa_d-\kappa^*}{\mu_M}\right)\right)d\kappa^*\Bigg] H'(\kappa)\Bigg\} \\
+\frac{\Omega}{2}\int_o^{\kappa_d} S(\kappa^*)E_1(|\kappa^*-\kappa|)d\kappa^* \qquad \text{no gap}
\end{aligned}
\tag{3.77}
$$

Where $H'(\kappa)$ is the following,

$$H'(\kappa) = E_2(\kappa_d-\kappa) + 2a'_{fs}E_2(\kappa) \tag{3.78}$$

and a'_{fs} and D' are given by equations (3.72) and (3.71).

Solution of the source function equation depends upon the temperature, T, and the optical depth, κ_d, as well as the optical properties of the film-vacuum and film-substrate interfaces. Once the source function is known, the radiation flux, $q(\kappa,\lambda)$, can be calculated using either equation (3.63) or (3.69). Solution of the coupled one-dimensional energy equation [equation (3.26)] and source function equation can only be obtained numerically. A numerical solution procedure is presented in Appendix B.

3.8.1 No Scattering Spectral Emittance

As discussed in section 3.7.3, neglecting scattering is an accurate approximation for a single crystal material and not as accurate an approximation for polycrystalline material. However, in regions of the spectrum where emission or absorption is large, scattering can be neglected. Therefore, the spectral emittance, $\varepsilon(\lambda)$, calculated in those regions of the spectrum is applicable for all materials.

To determine the spectral emittance, calculate the radiation flux leaving the film surface, $q_{out}(\kappa_d)$. The intensity that leaves the film surface is $\left(1-R'_{fo}\right)i^{+}\left(d\right)$; therefore, the flux leaving the film is the following.

$$q_{out}\left(\kappa_d\right)=2\pi\int_{o}^{\pi/2}\left(1-R'_{fo}\right)i^{+}\left(\kappa_d\right)\cos\theta\sin\theta d\theta \tag{3.79}$$

Since $n_f > n_o$, Snell's Law applies and $R'_{fo}=1$ for $\theta > \theta_{crfo}$. Therefore, changing the variable to $\mu = \cos\theta$ and assuming $R'_{fo}=\bar{R}_{fo}$ for $0 \le \theta \le \theta_{crfo}$ ($\mu_M \le \mu \le 1$) yields the following.

$$q_{out}\left(\kappa_d\right)=2\pi\left(1-\bar{R}_{fo}\right)\int_{\mu_M}^{1}i^{+}\left(\kappa_d\right)\mu d\mu \tag{3.80}$$

Now use equation (3.9) for $i^{+}(\kappa_d)$ and remember that $i^{+}(0)$ is assumed to be independent of θ so that $q_{out}(\kappa_d)$ is the following,

$$q_{out}\left(\kappa_d\right)=\left(1-\bar{R}_{fo}\right)\left\{2q^{+}\left(0\right)h_{-}+\phi_{+}\left(\kappa_d\right)-\phi_{M+}\left(\kappa_d\right)\right\} \tag{3.81}$$

where,

$$h_{-} = E_3\left(\kappa_d\right) - \mu_M^2 E_3\left(\frac{\kappa_d}{\mu_M}\right) \tag{3.82}$$

Substituting equation (3.61) for $q^{+}(0)$ and using the definition of emittance [equation (1.169)] yields the following result for $\varepsilon(\lambda)$ when a dielectric gap exists between the film and substrate (problem 3.4).

$$\varepsilon\left(\lambda\right) \equiv \frac{q_{out}\left(\kappa_d\right)}{n_o^2 e_b\left(\lambda, T_s\right)} = 2\left(\frac{n_f}{n_o}\right)^2 \frac{\left(1-\overline{R}_{fo}\right)}{D}\left\{\left[\left(\frac{n_o}{n_f}\right)^2 \overline{\tau}_{fs}\varepsilon_{son} + \frac{2\overline{\tau}_{fo} s a_{fs} e_b\left(\lambda, T_r\right)}{n_f^2 e_b\left(\lambda, T_s\right)} + 2\overline{\rho}_{fs}\overline{\phi}_{-}\left(0\right) + 2\left(1-\overline{\rho}_{fs}\right)\overline{\phi}_{M-}\left(\kappa_d\right)\right] h_{-} + h_{+}\overline{\phi}_{+}\left(\kappa_d\right) - h_M\overline{\phi}_{M+}\left(\kappa_d\right)\right\}$$

with gap (3.83)

Notice that $\varepsilon(\lambda)$ is defined in terms of the substrate temperature, T_s. Since emittance is usually thought of as a surface phenomenon, it is normally defined in terms of the surface temperature. This will apply for materials with large extinction coefficients so that κ is large, even for very small d. As a result, emitted radiation originates very near the emitting surface. Generally, metals perform in such a manner. However, for selective emitters where extinction coefficients are not as large, the emitted radiation originates from significant distances from the surface. Thus temperature differences between the substrate and the emitting surface play a significant role in determining the emittance. If $\varepsilon(\lambda)$ were defined in terms of the temperature of the emitting surface, T_f, which will be smaller than the substrate temperature, T_s, it is possible that $\varepsilon(\lambda) > 1$ could occur.

Appearing in equation (3.83) are the dimensionless source function integrals that are obtained using equations (3.31), (3.32), (3.48), and (3.60).

$$\overline{\phi}_{+}\left(\kappa_d\right) \equiv \frac{\phi_{+}\left(\kappa_d\right)}{2n_f^2 e_b\left(\lambda, T_s\right)} = \frac{\pi}{n_f^2 e_b\left(\lambda, T_s\right)} \int_0^{\kappa_d} S\left(\kappa^*\right) E_2\left(\kappa_d - \kappa^*\right) d\kappa^* \tag{3.84}$$

$$\overline{\phi}_{-}\left(0\right) \equiv \frac{\phi_{-}\left(\kappa_d\right)}{2n_f^2 e_b\left(\lambda, T_s\right)} = \frac{\pi}{n_f^2 e_b\left(\lambda, T_s\right)} \int_0^{\kappa_d} S\left(\kappa^*\right) E_2\left(\kappa^*\right) d\kappa^* \tag{3.85}$$

$$\bar{\phi}_{M+}(\kappa_d) \equiv \frac{\phi_{M+}(\kappa_d)}{2n_f^2 e_{bs}(\lambda, T_s)} = \frac{\pi\mu_M}{n_f^2 e_b(\lambda, T_s)} \int_o^{\kappa_d} S(\kappa^*) E_2(\kappa^*) d\kappa^* \tag{3.86}$$

$$\bar{\phi}_{M-}(\kappa_d) \equiv \frac{\phi_{M-}(\kappa_d)}{2n_f^2 e_b(\lambda, T_s)} = \frac{\pi\mu_M}{n_f^2 e_b(\lambda, T_s)} \int_o^{\kappa_d} S(\kappa^*) E_2\left(\frac{\kappa^*}{\mu_M}\right) d\kappa^* \tag{3.87}$$

New terms appearing in equation (3.83) are the following.

$$h_+ = 1 - 4a_{fs}\mu_M^2 E_3\left(\frac{\kappa_d}{\mu_M}\right) \tag{3.88}$$

$$h_M = 1 - 4a_{fs} E_3(\kappa_d) \tag{3.89}$$

To obtain $\varepsilon(\lambda)$ for no dielectric gap, remove the $(1-\bar{\rho}_{fs})$ term in equation (3.83) and let $a_{fs} \to a'_{fs}$, $\bar{\tau}_{fs} n_o^2 \varepsilon_{son} \to n_f^2 \varepsilon_{fsn}$, and $\bar{\rho}_{fs} \to \bar{R}_{fs}$.

$$\boxed{\begin{aligned} &\varepsilon(\lambda) = 2\left(\frac{n_f}{n_o}\right)^2 \frac{(1-\bar{R}_{fo})}{D'} \\ &\left\{\left[\varepsilon_{fsn} + \frac{2\bar{\tau}_{fo} s a'_{fs} e_b(\lambda, T_r)}{n_f^2 e_b(\lambda, T_s)} + 2\bar{R}_{fs}\bar{\phi}_-(0)\right] h_- + h'_+ \bar{\phi}_+(\kappa_d) - h'_M \bar{\phi}_{M+}(\kappa_d)\right\} \text{ no gap} \end{aligned}} \tag{3.90}$$

Where a'_{fs} is given by equation (3.72), D' by equation (3.71), and h'_+ and h'_M as follows.

$$h'_+ = 1 - 4a'_{fs}\mu_M^2 E_3\left(\frac{\kappa_d}{\mu_M}\right) \tag{3.91}$$

$$h'_M = 1 - 4a'_s E_3(\kappa_d) \tag{3.92}$$

Also, remember that $\bar{\rho}_{fo} = \bar{R}_{fo}$ in the expression for a_{fo} [equation (3.67)] for the no gap case.

The spectral emittance includes contributions from the substrate (term proportional to ε_{son} or ε_{fsn}) and also the external source (term proportional to s). Usually the emittance does not include the external source term.

Equations (3.83) and (3.90) show that the emittance is made up of three terms. The first term, which is proportional to h_-, represents the radiation leaving the substrate and the external source, plus the radiation reflected back into the film from the film-substrate interface. The second term, which is proportional to h_+ or h'_+, represents the radiation emitted within the film. The last term in $\varepsilon(\lambda)$ is the negative term h_M or h'_M. It represents the radiation with angle of incidence $\theta > \theta_{crfo}$ that is totally reflected back into the film at the film-dielectric interface.

The quantity, h_-, [equation (3.82)] decreases with increasing optical depth, κ_d. However, the quantities h_+, h_M, h'_+, and h'_M increase with increasing optical depth, κ_d. The dependence on κ_d of each of the three terms in $\varepsilon(\lambda)$ is a function of the four source function integrals, $\overline{\phi}_+$, $\overline{\phi}_-$, $\overline{\phi}_{M+}$, and $\overline{\phi}_{M-}$, as well as the h functions. If there is negligible scattering and the temperature is uniform, then the source function, S, will be independent of κ [see equation (3.22)]. In that case, all the source function integrals will increase with increasing optical depth, κ_d (problem 3.5). Therefore, the terms in $\varepsilon(\lambda)$ that are proportional to h_+, h_M, h'_+, and h'_M will be monotonically increasing functions of κ_d. However, since h_- decreases while $\overline{\phi}_-(0)$ and $\overline{\phi}_{M-}(\kappa_d)$ increase with increasing κ_d, it is possible for the emittance term proportional to h_- to achieve a maximum value at some value of κ_d (problem 3.6). The physical explanation for this maximum is the following. As κ_d increases, the contributions of the substrate emittance, ε_{son} or ε_{fsn}, and external source decrease while the contribution of the reflected radiation at the film-substrate interface [$\overline{\phi}_-(0)$ and $\overline{\phi}_{M-1}(\kappa_d)$ terms)] increases. As a result, when no external source exists, for certain values of $\left(\frac{n_o}{n_f}\right)^2 \overline{\tau}_{fs}\varepsilon_{son}$ and $\overline{\rho}_{fs}$ in equation (3.83) or ε_{fsn} and $\overline{R}_{fs}$ in equation (3.90), it is possible for a maximum to occur.

3.8.2 No Scattering, Linear Temperature Variation Spectral Emittance

As already stated at the end of Section 3.8, for the most general case the source function, $S(\kappa)$, can only be determined by solving the coupled source function equation (3.74) or (3.77) and energy equation (3.26). However, if scattering can be neglected, then the source function equation is greatly simplified and $S(\kappa)$ is given by equation (3.22). As stated at the beginning of the section, neglecting scattering should be a valid approximation for single crystal materials and for all material where emission or

absorption is large. The temperature dependence of $S(\kappa)$ for the no scattering case is given by the blackbody emissive power, $e_b(\lambda,T)$. Temperature variation is determined by the one dimensional energy equation (3.26). The radiation flux, $\bar{q}$, is always less than the blackbody flux, $\sigma_{sb}T_s^4$, therefore, defining the following dimensionless variables,

$$\bar{T} = \frac{T}{T_s}, \qquad \bar{Q} = \frac{\bar{q}}{\sigma_{sb}T_s^4}, \qquad \bar{x} = \frac{x}{d} \tag{3.93}$$

results in the following energy equation.

$$-\frac{d\bar{T}}{d\bar{x}} + \gamma\bar{Q} = \gamma\bar{Q}_{in} = \text{ constant} \tag{3.94}$$

The dimensionless quantity, γ, is the ratio of radiation to thermal conduction.

$$\gamma = \frac{\sigma_{sb}T_s^4}{\frac{k_{th}T_s}{d}} = \frac{\sigma_{sb}T_s^3 d}{k_{th}} \tag{3.95}$$

Thus if $\gamma \ll 1$, the radiation term can be neglected and the solution to equation (3.94) is a linear temperature variation.

$$\bar{T} = 1 - \bar{x}\Delta T \tag{3.96}$$

The fractional temperature drop is the following.

$$\Delta T = \frac{T_s - T_f}{T_s} \tag{3.97}$$

Remember that T_s is the substrate temperature and T_f is the film temperature at the film-dielectric emitting surface.

Except for metallic emitters, most high temperature emitter materials have low thermal conductivity. For example, yttria, which is a possible host material for a rare earth selective emitter (Table 3.1), has $k_{th} \approx .03$ W/cmK at 1273K. Therefore, if $k_{th} > .01$ W/cmK and $d < .1$cm, then γ becomes the following.

$$\gamma < 10\sigma_{sb}T_s^3 = 5.67\times10^{-11}T_s^3 \tag{3.98}$$

As a result, if T_s = 1200K, $\gamma < .1$, and if T_s = 2000K, $\gamma < .5$. Thus, at lower emitter temperatures it appears that the linear temperature variation [equation (3.96)] is a good approximation. However, at high emitter temperatures it appears that the linear approximation may not be a valid approximation. For the present assume the linear approximation is applicable for calculating the spectral emittance, $\varepsilon(\lambda)$. In Appendix B a method is outlined for solving the coupled source function and energy equations to obtain the temperature variation. For a metallic emitter, $k_{th} > 0.1$ W/cmK; therefore, a linear temperature variation across the emitter is certainly applicable.

In the case for no scattering $\left(S = \frac{n_f^2 e_b(\lambda, T)}{\pi} \right)$ and a linear temperature variation $\left(\bar{T} = 1 - \bar{x}\Delta T \right)$, the source function integrals [equations (3.84) through (3.87)] become the following.

$$\bar{\phi}_+(\kappa_d) = \frac{\phi_+(\kappa_d)}{2n_f^2 e_b(\lambda, T_s)} = d\left(e^{u_s} - 1\right) \int_o^1 \frac{K(\bar{x}) E_2\left[\kappa_d - \kappa(\bar{x})\right]}{\exp\left[\frac{u_s}{1 - \bar{x}\Delta T}\right] - 1} d\bar{x} \tag{3.99}$$

$$\bar{\phi}_-(0) = \frac{\phi_-(0)}{2n_f^2 e_b(\lambda, T_s)} = d\left(e^{u_s} - 1\right) \int_o^1 \frac{K(\bar{x}) E_2\left[\kappa(\bar{x})\right]}{\exp\left[\frac{u_s}{1 - \bar{x}\Delta T}\right] - 1} d\bar{x} \tag{3.100}$$

$$\bar{\phi}_{M+}(\kappa_d) = \frac{\phi_+(\kappa_d)}{2n_f^2 e_b(\lambda, T_s)} = \mu_M d\left(e^{u_s} - 1\right) \int_o^1 \frac{K(\bar{x}) E_2\left[\frac{\kappa_d - \kappa(\bar{x})}{\mu_M}\right]}{\exp\left[\frac{u_s}{1 - \bar{x}\Delta T}\right] - 1} d\bar{x} \tag{3.101}$$

$$\bar{\phi}_{M-}(\kappa_d) = \frac{\phi_{M-}(\kappa_d)}{2n_f^2 e_b(\lambda, T_s)} = \mu_M d\left(e^{u_s} - 1\right) \int_o^1 \frac{K(\bar{x}) E_2\left[\kappa(\bar{x})\right]}{\exp\left[\frac{u_s}{1 - \bar{x}\Delta T}\right] - 1} d\bar{x} \tag{3.102}$$

$$u_s = \frac{hc_o}{\lambda k T_s} = \frac{1.439 \times 10^7 \left(K \bullet nm\right)}{\lambda T_s} \tag{3.103}$$

The quantity u_s is the *dimensionless photon energy* based on the substrate temperature, T_s. Also, remember that $\kappa(x)$ is the optical depth given by equation (3.3) so that $\kappa(\bar{x})$ and κ_d are the following.

$$\kappa(\bar{x}) = d\int_o^{\bar{x}} K(\bar{x}^*)\,d\bar{x}^* \tag{3.104}$$

$$\kappa_d = \int_o^d K(x)\,dx = d\int_o^1 K(\bar{x})\,d\bar{x} \tag{3.105}$$

If the emitter material is of uniform composition, then the extinction coefficient, K(x), should be independent of x. In that case, κ_d=Kd and for no scattering and a linear temperature variation, the integral functions $\bar{\phi}_+(\kappa_d)$, $\bar{\phi}_-(0)$, $\bar{\phi}_{M+}(\kappa_d)$, and $\bar{\phi}_{M-}(\kappa_d)$ become the following.

$$\bar{\phi}_+(\kappa_d) = \kappa_d\left(e^{u_s}-1\right)\int_o^1 \frac{E_2\left[\kappa_d(1-\bar{x})\right]}{\exp\left[\dfrac{u_s}{1-\bar{x}\Delta T}\right]-1}\,d\bar{x} \tag{3.106}$$

$$\bar{\phi}_-(0) = \kappa_d\left(e^{u_s}-1\right)\int_o^1 \frac{E_2\left[\kappa_d\bar{x}\right]}{\exp\left[\dfrac{u_s}{1-\bar{x}\Delta T}\right]-1}\,d\bar{x} \tag{3.107}$$

$$\bar{\phi}_{M+}(\kappa_d) = \mu_M\kappa_d\left(e^{u_s}-1\right)\int_o^1 \frac{E_2\left[\dfrac{\kappa_d}{\mu_M}(1-\bar{x})\right]}{\exp\left[\dfrac{u_s}{1-\bar{x}\Delta T}\right]-1}\,d\bar{x} \tag{3.108}$$

$$\bar{\phi}_{M-}(\kappa_d) = \mu_M\kappa_d\left(e^{u_s}-1\right)\int_o^1 \frac{E_2\left[\dfrac{\kappa_d}{\mu_M}\bar{x}\right]}{\exp\left[\dfrac{u_s}{1-\bar{x}\Delta T}\right]-1}\,d\bar{x} \tag{3.109}$$

For the general case, numerical integrations are required to determine the integral functions. However, approximations to the integrals can be obtained for the case of small temperature difference, $\Delta T \ll 1$. For thin (d < 1mm) emitters this should be a valid approximation. Assuming the extinction coefficient is independent of x, the integral functions are given by equations (3.106) through (3.109). Two series expansions of the denominators in these integrals can be carried out for $\Delta T \ll 1$. One expansion applies for the dimensionless photon energy, u_s, being large so that $e^{u_s} \gg 1$ and the other for $u_s \ll 1$. In these two cases the results are the following (problems 3.9 and 3.10).

For $\Delta T \ll 1$ and $u_s \gg 1$ the integral functions are written in terms of the parameter Z.

$$Z = \frac{u_s \Delta T}{\kappa_d} \tag{3.110}$$

$$\bar{\phi}_+ (\kappa_d) = \left(1 - e^{u_s}\right) \sum_{n=o}^{\infty} \left[\frac{e^{-u_s \Delta T}}{n+2} - E_{n+3}(\kappa_d) \right] Z^n \tag{3.111}$$

$$\bar{\phi}_- (0) = \left(1 - e^{u_s}\right) \sum_{n=o}^{\infty} \left[\frac{1}{n+2} - e^{u_2 \Delta T} E_{n+3}(\kappa_d) \right] (-Z)^n \tag{3.112}$$

$$\bar{\phi}_{M+} (\kappa_d) = \mu_M^2 \left(1 - e^{u_s}\right) \sum_{n=o}^{\infty} \left[\frac{e^{-u_s \Delta T}}{n+2} - E_{n+3}\left(\frac{\kappa_d}{\mu_M}\right) \right] (\mu_M Z)^n \tag{3.113}$$

$$\bar{\phi}_{M-} (\kappa_d) = \mu_M^2 \left(1 - e^{u_s}\right) \sum_{n=o}^{\infty} \left[\frac{1}{n+2} - e^{-u_s \Delta T} E_{n+3}\left(\frac{\kappa_d}{\mu_M}\right) \right] (-\mu_M Z)^n \tag{3.114}$$

And for the case where $\Delta T \ll 1$ and $u_s \ll 1$ the integral functions are the following.

$$\bar{\phi}_+ (\kappa_d) \approx \frac{1}{2} - E_3(\kappa_d) - \frac{\Delta T}{2} \left[1 - \frac{2}{3} \frac{\left(1 - 3E_4(\kappa_d)\right)}{\kappa_d} \right] \tag{3.115}$$

$$\overline{\phi}_{-}(0) \approx \frac{1}{2} - E_3(\kappa_d) + \frac{\Delta T}{\kappa_d}\left[\frac{1}{3} + 2E_4(\kappa_d) - e^{-\kappa_d}\right] \tag{3.116}$$

$$\overline{\phi}_{M+}(\kappa_d) \approx \mu_M^2 \left\{ \frac{1}{2} - E_3\left(\frac{\kappa_d}{\mu_M}\right) - \frac{\Delta T}{2}\left[1 - \frac{2\mu_M}{3}\frac{\left(1 - 3E_4\left(\frac{\kappa_d}{\mu_M}\right)\right)}{\kappa_d}\right]\right\} \tag{3.117}$$

$$\overline{\phi}_{M-}(\kappa_d) \approx \mu_M^2 \left\{ \frac{1}{2} - E_3\left(\frac{\kappa_d}{\mu_M}\right) + \frac{\mu_M \Delta T}{\kappa_d}\left[\frac{1}{3} - 2E_4\left(\frac{\kappa_d}{\mu_M}\right) - e^{-\frac{\kappa_d}{\mu_M}}\right]\right\} \tag{3.118}$$

For most TPV applications, $T_s \leq 2000K$. Therefore, for $\lambda < 7200nm$ (7.2μm) equation (3.103) yields $u_s > 1.0$. As a result, the approximations given by equations (3.110) through (3.114) should apply for most TPV applications.

Now consider the spectral emittance, $\varepsilon(\lambda)$, as a function of the optical depth, κ_d, for the two cases given by equations (3.83) and (3.90). Assume no external source ($s = r = 0$ so that $\overline{\rho}_{fo} = \overline{R}_{fo} = 1 - \overline{\tau}_{fo}$). Also assume emission is into a vacuum; therefore, $n_o = 1$. Also, assume the substrate real and imaginary parts of the complex index of refraction are $n_{sR} = 5.0$ and $n_{sI} = 7.0$. These values of n_{sR} and n_{sI} are representative of platinum in the near infrared region of the spectrum [20]. The emittance of the substrate into the film, ε_{fsn} and into the vacuum, ε_{son}, are given by equation (1.246). Assuming $u_s = 5.0$, which is representative of a TPV system, and a temperature variation, $\Delta T = .05$, the source function integrals given by equations (3.99) through (3.102) were numerically integrated. These result are then used in equations (3.83) and (3.90) to calculate $\varepsilon(\lambda)$ for a film index of refraction, $n_f = 1.9$ (representative of a rare earth aluminum garnet emitter). Figure 3.7 shows the calculated values of $\varepsilon(\lambda)$ for the two cases.

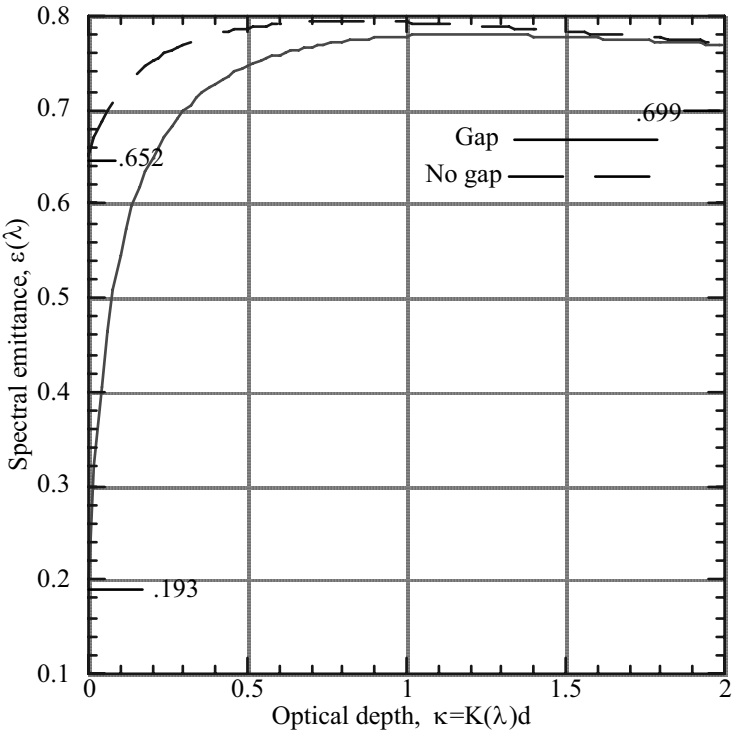

Fig. 3.7 - Comparison of spectral emittance into a vacuum as a function of optical depth of planar emitters with and without a vacuum gap between emitter and substrate. Scattering has been neglected and a linear temperature variation across the emitter is assumed. The temperature change across emitter is $\Delta T=.05$, the thickness of emitter is d, the extinction coefficient is $K(\lambda)$, the dimensionless photon energy is $u_s=5.$ and the index of refraction is $n_f=1.9$. A metal substrate is assumed with index of refraction $n_{sR}=5.$ and $n_{sI}=7.$

As Figure 3.7 indicates, for $\kappa_d > 1$ the spectral emittances for the two cases are nearly the same. However, for small values of κ_d, the no dielectric gap case has a significantly larger $\varepsilon(\lambda)$ than for the case where a dielectric gap exists between the substrate and emitter.

In the short wavelength region where the PV array is able to convert the photon energy to electrical energy ($\lambda < \frac{hc_o}{E_g}$), a large $\varepsilon(\lambda)$ and thus large κ_d is desired. Therefore, either the gap or no gap case can be used since both yield large $\varepsilon(\lambda)$ for $\kappa_d>1$.

However, in the nonconvertible wavelength region ($\lambda > \frac{hc_o}{E_g}$) where small $\varepsilon(\lambda)$ and thus small κ_d is required, the dielectric gap case is considerably better than the no gap case.

The spectral emittance increases rapidly with optical depth and then levels off for $\kappa_d > 1$. The contribution to $\varepsilon(\lambda)$ from the reflected radiation at the film-substrate interface [$\overline{\rho}_{fs}\overline{\phi}_{-}(0)h_{-}$ tern in equation (3.83) and $\overline{R}_{fs}\overline{\phi}_{-}(0)h_{-}$ tern in equation (3.90)] reaches a maximum value and then begins a slow decrease, as discussed earlier. As a result, $\varepsilon(\lambda)$ also has a maximum value. This maximum value is more pronounced for larger values of ΔT.

For a selective emitter, the optical depth, κ_d, will be large within emission bands and small outside emission bands. Therefore, for no external source (s = r =0, $\overline{\rho}_{fo} = \overline{R}_{fo}$, $\overline{\tau}_{fo} = 1 - \overline{R}_{fo}$) consider the two limiting cases for $\varepsilon(\lambda)$, $\kappa_d \ll 1$ and $\kappa_d \to \infty$. For $\kappa_d \ll 1$ equations (3.106) through (3.109) show that $\overline{\phi}_{-}(\kappa_d) = \overline{\phi}_{-}(0) = \overline{\phi}_{M+}(\kappa_d) = \overline{\phi}_{M-}(\kappa_d) \approx 0$. Also, since $E_3(0)$ = ½ equation (3.82) yields $h_{-} \approx \frac{1}{2}\left(1-\mu_M^2\right) = \frac{1}{2}\left(\frac{n_o}{n_f}\right)^2$. Using these results in equations (3.83) and (3.90) yields the following results for $\varepsilon(\lambda)$,

$$\varepsilon(\lambda) = \frac{N_{fo}\overline{\tau}_{fs}\varepsilon_{son}}{N_{fo} + N_{fs}\left(1-N_{fo}\right)} \qquad \text{with gap} \qquad \left.\right\} \kappa_d \ll 1 \qquad (3.119)$$

$$\varepsilon(\lambda) \approx \frac{\left(1-\overline{R}_{fo}\right)\varepsilon_{fsn}}{1-\overline{R}_{fs}\left(1-N_{fo}\right)} \qquad \text{no gap} \qquad \left.\right\} \kappa_d \ll 1 \qquad (3.120)$$

where,

$$N_{fo} = \left(\frac{n_o}{n_f}\right)^2\left(1-\overline{R}_{fo}\right) = \frac{4n_o^3}{n_f\left(n_f+n_o\right)^2} \le 1 \qquad n_o \le n_f \qquad (3.121)$$

$$N_{fs} = \left(\frac{n_o}{n_f}\right)^2\left(1-\overline{\rho}_{fs}\right) \le 1 \qquad n_o \le n_f \qquad (3.122)$$

Equation (1.110), where $n_{oR} = n_o$, $n_{1R} = n_f$, $n_{oI} = 0$, $n_{1I} = 0$, was used to replace $\bar{R}_{fo}$ in equation (3.121). The results at d = 0 for ε(λ) in Figure 3.7 do not apply to a real situation because they include the film index, n_f. In a real case if d = 0 the film must vanish and $n_f = n_o$. As a result, $N_{fo} = \bar{\tau}_{fs} = 1$, $\bar{R}_{fo} = 0$, and $\bar{R}_{fs} = 0$ so that equations (3.119) and (3.120) yield $\varepsilon(\lambda) = \varepsilon_{son}$, as one would expect. However, if d > 0, then equation (3.119) and (3.120) do apply as long as $\kappa_d \ll 1$.

Notice that ε(λ) is independent of ΔT when $\kappa_d \ll 1$. Therefore, in regions of the spectrum where $\kappa_d \ll 1$, such as outside the emission bands of a selective emitter, the spectral emittance will be nearly independent of ΔT. This is not the case for regions of the spectrum where $\kappa_d \gg 1$, such as an emission band of a selective emitter. In that case ε(λ) is very sensitive to ΔT.

Consider ε(λ) when $\kappa_d \to \infty$. For $\Delta T \ll 1$ and $u_s \gg 1$ the source function integrals are given by equations (3.111) through (3.114), and for $\kappa_d \to \infty$ they yield the following result.

$$\lim_{\kappa_d \to \infty} \bar{\phi}_+(\kappa_d) = \frac{1}{2} e^{-u_s \Delta T}\left(1 - e^{-u_s}\right) \tag{3.123}$$

$$\lim_{\kappa_d \to \infty} \bar{\phi}_-(0) = \frac{1}{2}\left(1 - e^{-u_s}\right) \tag{3.124}$$

$$\lim_{\kappa_d \to \infty} \bar{\phi}_{M+}(\kappa_d) = \frac{1}{2}\mu_M^2 e^{-u_s \Delta T}\left(1 - e^{-u_s}\right) \tag{3.125}$$

$$\lim_{\kappa_d \to \infty} \bar{\phi}_{M-}(\kappa_d) = \frac{1}{2}\mu_M^2\left(1 - e^{-u_s}\right) \tag{3.126}$$

$u_s > 1$, $\Delta T \ll 1$

Also, since $E_3(\infty) = 0$ the following results occur: $h_+ = h'_+ = h_M = h'_M = h_- = 0$, and $D = D' = 1$. As a result, equations (3.83) and (3.90) for no external source (r = s = 0) yield the following for ε(λ).

$$\lim_{\kappa_d \to \infty} \varepsilon(\lambda) = \left(1 - \bar{R}_{fo}\right) e^{-u_s \Delta T} \tag{3.127}$$

$r = s = 0$, $u_s > 1$, $\Delta T \ll 1$

This result applies for both the gap and no gap situations. As equation (3.127) indicates, $\varepsilon(\lambda)$ will be an exponential function of ΔT in regions of the spectrum where $\kappa_d \gg 1$, such as an emission band of a selective emitter. The asymptotic values of $\varepsilon(\lambda)$ shown in Figure 3.7 were obtained using equations (3.119), (3.120), and (3.127).

The hemispherical spectral emittance for a metal into a dielectric derived in section 1.9 did not require solution of the radiative transfer equation. For a metal $\kappa_d \gg 1$ and thus the transmittance is zero. Therefore, in section 1.9 the conservation of energy result $\varepsilon' + \rho' = 1$ [equation (1.226)] was used to obtain $\varepsilon_n = 1 - \bar{R}_n$ [equation (1.246)]. That result agrees with equation (3.127) if $\Delta T = 0$ and $u_s \gg 1$.

3.8.3 Importance of Temperature Change Across Planar Emitter

Since emitters are thin (≤ 1mm), only small temperature changes will occur across the emitter. However, as mentioned in the previous section, even small temperature changes will have a significant effect on $\varepsilon(\lambda)$. This is illustrated in Figure 3.8 where $\varepsilon(\lambda)$ is shown as a function of ΔT for two different optical depths, κ_d = .01 and 1. Emittter and substrate properties are the same as in Figure 3.7. Equations (3.83) and (3.90) are used to calculate $\varepsilon(\lambda)$ with the source function integrals $\bar{\phi}_+(\kappa_d)$, $\bar{\phi}_-(0)$, $\bar{\phi}_{M+}(\kappa_d)$, and $\bar{\phi}_{M-}(\kappa_d)$ evaluated by numerical integration. As Figure 3.8 shows, even small values of ΔT cause a significant reduction in $\varepsilon(\lambda)$ for κ_d = 1. However, for κ_d = .01 the reduction in $\varepsilon(\lambda)$ is small for increasing ΔT. In the previous section it has been shown that $\varepsilon(\lambda) \sim e^{-u_s \Delta T}$ for $\kappa_d \gg 1$ and that $\varepsilon(\lambda)$ is independent of ΔT for $\kappa_d \ll 1$. Repeating for emphasis what has already been shown, small values of ΔT will significantly reduce $\varepsilon(\lambda)$ in regions of the spectrum where κ_d is large, but will have negligible effect upon $\varepsilon(\lambda)$ in regions of the spectrum where κ_d is small.

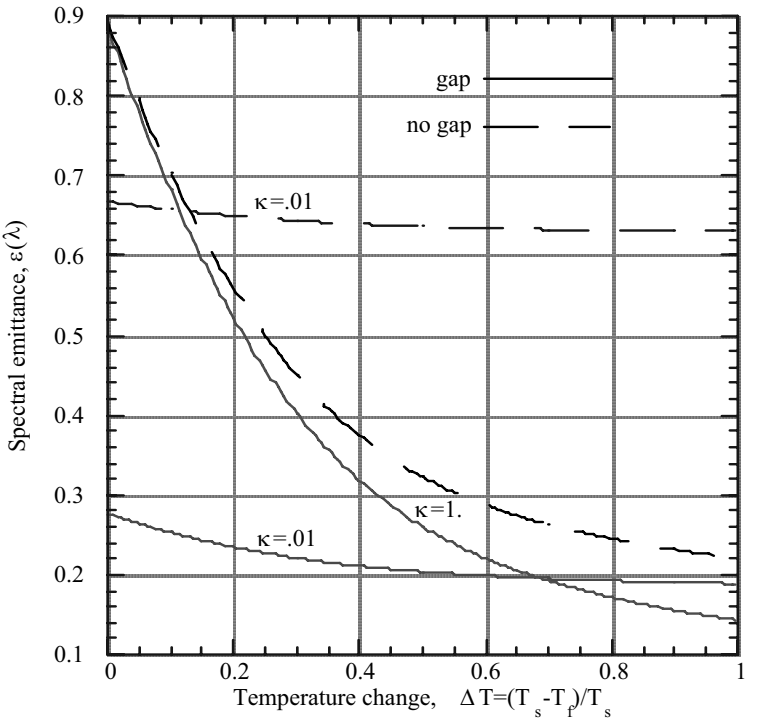

Figure 3.8 - Effect of temperature change, ΔT, across planar emitter on the spectral emittance, $\varepsilon(\lambda)$ at optical depths of κ=.01 and 1. Conditions are the same as for Fig. 3.7, n_f=1.9, n_o=1., n_{sR}=5., n_{sI}=7., u_s=5.

Notice that for both the vacuum gap and no vacuum gap cases, $\varepsilon(\lambda)$ for κ_d = .01 becomes larger than $\varepsilon(\lambda)$ for κ_d = 1 at large ΔT. This may at first seem counter intuitive since large optical depth usually implies large $\varepsilon(\lambda)$. However, increasing ΔT means that the emitter thickness, d, is also increasing. For κ_d = 1 the increased thickness is a region of lower temperature that becomes an absorber of radiation from the higher temperature region near the substrate, thus reducing $\varepsilon(\lambda)$. When κ_d = .01, the increased thickness is also a region of lower temperature; however, since κ_d is small, it is nearly transparent to the radiation being emitted by the higher temperature region near the substrate. Thus $\varepsilon(\lambda)$ is nearly constant for κ_d = .01 but decreases rapidly for κ_d = 1 as ΔT increases. Eventually, as ΔT increases, $\varepsilon(\lambda)$ for κ_d = .01 will exceed $\varepsilon(\lambda)$ for κ_d = 1. As Figure 3.8 shows, this occurs at a much smaller ΔT for the no gap vacuum case than for the vacuum gap case.

The results shown in Figure 3.8 are for a dimensionless photon energy, $u_s = 5.0$. As equation (3.127) shows, increasing u_s at a given ΔT reduces $\varepsilon(\lambda)$ significantly for regions of the spectrum where $\kappa_d \geq 1$ but has negligible effect for regions where $\kappa_d \leq .1$. For $u_s \ll 1$ the source function integrals [equations (3.115) through (3.118)] are independent of u_s and thus $\varepsilon(\lambda)$ will also be independent of u_s.

For rare earth selective emitters, $\kappa_d \geq 1$ in emission bands and in the long wavelength region ($\lambda_c \geq 5000$nm) where λ_c is the cutoff wavelength discussed in Section 3.5. The emission bands occur in the wavelength region $1000 \leq \lambda \leq 2700$nm. Thus, u_s will be at least twice as large in the emission bands as in the long wavelength cutoff region. Therefore, the spectral emittance in emission bands will be more sensitive to ΔT than the cutoff region spectral emittance.

3.8.4 Effect of Scattering on Spectral Emittance of a Planar Emitter

When scattering of radiation must be included ($0 < \Omega \leq 1$) in the source function equation [equation (3.15)], solution of the radiation transfer problem is much more difficult. As stated earlier, scattering should not be significant for emitters made of single crystal materials. However, for polycrystalline emitters scattering may be important.

The effect of scattering on the spectral emittance can be investigated by considering an approximate solution to the source function equation. If there is no scattering, the scattering coefficient, $\sigma = 0$ and also the scattering albedo, $\Omega = 0$. In that case, the source function reduces to the blackbody emissive power term, $S_o(\kappa) = \dfrac{n_f^2 e_b(\lambda, T)}{\pi}$. An iterative approach to solving for $S(\kappa)$ is to begin by substituting the first approximation $S_o(\kappa) = \dfrac{n_f^2 e_b(\lambda, T)}{\pi}$ for $S(\kappa)$ in the integral term in equation (3.15). Then carry out the integration to obtain the next approximation for $S(\kappa) = S_1(\kappa)$. The next approximation, $S_2(\kappa)$, is obtained by substituting $S_1(\kappa)$ for $S(\kappa)$ in the integral. This process can be repeated until $S_n(\kappa)$ converges to the correct solution, $S(\kappa)$. However, to estimate the importance of scattering, the first approximation, $S_1(\kappa)$, for constant temperature ($\Delta T = 0$) can be used. Neglecting the temperature variation means that $\varepsilon(\lambda)$ will be independent of the dimensionless photon energy, u_s, as well as, the temperature.

Consider a planar emitter where a dielectric gap exists between the substrate and the emitter. In this case, the source function is given by equation (3.74). For constant temperature, $T = T_s$, $S_o(\kappa) = \dfrac{n_f^2 e_b(\lambda, T_s)}{\pi}$, and neglecting the external source ($s = r = 0$) equation (3.74) becomes the following.

$$S(\kappa) \approx$$

$$n_f^2 \frac{e_b(\lambda, T_s)}{\pi}\left\{1-\Omega+\frac{\Omega G(\kappa)}{2D}\left[\overline{\tau}_{fs} n_o^2 \varepsilon_{fsn} + 2\int_o^{\kappa_d}\left(\overline{\rho}_{fs} E_2(\kappa^*) + \mu_M\left(1-\overline{\rho}_{fs}\right) E_2\left(\frac{\kappa^*}{\mu_M}\right)\right) d\kappa^*\right]\right.$$

$$\left. + \frac{\Omega H(\kappa)}{2D}\left[\int_o^{\kappa_d}\left(\overline{\rho}_{fo} E_2(\kappa_d - \kappa^*) + \mu_M\left(1-\overline{\rho}_{fo}\right) E_2\left(\frac{\kappa_d-\kappa^*}{\mu_M}\right)\right) d\kappa^*\right] + \frac{\Omega}{2}\int_o^{\kappa_d} E_1\left(\left|\kappa^*-\kappa\right|\right) d\kappa^*\right\} \tag{3.128}$$

The κ* integrations can now be carried out. After a great deal of tedious algebra and using the results, $\left(1-\overline{\rho}_{fs}\right) = \overline{\tau}_{fs}\left(1-\overline{R}_{so}\right) = \overline{\tau}_{fs}\varepsilon_{son}$ and $\left(\frac{n_o}{n_f}\right)^2 = 1-\mu_M^2$, equation (3.128) becomes the following.

$$\boxed{S(\kappa) \approx \frac{n_f^2 e_b(\lambda, T_s)}{\pi}\left\{1-\frac{\Omega}{2D}\left(\frac{n_o}{n_f}\right)^2\left[E_2(\kappa)\left(2a_{fs}\left(1-\overline{\rho}_{fo}\right)-\left(1-\overline{\rho}_{fs}\right)\left(n_f^2-1\right)\right)\right.\right.}$$

$$\boxed{\left.\left. + E_2(\kappa_d-\kappa)\left(1-\overline{\rho}_{fo}-2a_{fo}\left(1-\overline{\rho}_{fs}\right)\left(n_f^2-1\right)\right)\right]\right\}} \tag{3.129}$$

$T = T_s$, with gap

To obtain the case for no dielectric gap between the emitter and substrate, make the following substitutions in equation (3.129): $\left(1-\overline{\rho}_{fs}\right) \to 0$, $D \to D'$, $a_{fs} \to a'_{fs} = \overline{R}_{fs} E_3(\kappa_d)$.

$$\boxed{S(\kappa) \approx \frac{n_f^2 e_b(\lambda, T_s)}{\pi}\left\{1-\frac{\Omega}{2D'}\left(\frac{n_o}{n_f}\right)^2\left(1-\overline{\rho}_{fo}\right)\left[2\overline{R}_{fs} E_3(\kappa_d) E_2(\kappa) + E_2(\kappa_d-\kappa)\right]\right\}} \tag{3.130}$$

$T = T_s$, no gap

For cases where **Ω** is small, equations (3.129) and (3.130) should be good approximations for S(κ).

Equations (3.129) and (3.130) can now be used in equations (3.84) through (3.87) to calculate the source function integrals that appear in the spectral emittance [equations (3.83) and (3.90)].

First, define the following function.

$$F(\kappa,\kappa_d)\equiv c_1E_2(\kappa)+c_2E_2(\kappa_d-\kappa) \tag{3.131}$$

Where for the case when a dielectric gap exists between the emitter and substrate,

$$\left.\begin{aligned} c_1&=\frac{1}{D}\left[2a_{\bar{f}\bar{s}}\left(1-\bar{\rho}_{\bar{f}o}\right)-\left(n_f^2-1\right)\left(1-\bar{\rho}_{\bar{f}\bar{s}}\right)\right] && (3.132)\\ c_2&=\frac{1}{D}\left[1-\bar{\rho}_{\bar{f}o}-2a_{\bar{f}o}\left(n_f^2-1\right)\left(1-\bar{\rho}_{\bar{f}\bar{s}}\right)\right] && (3.133)\end{aligned}\right\}\ \text{with gap}$$

and for no dielectric gap,

$$\left.\begin{aligned} c_1&=\frac{2}{D'}\left[\bar{R}_{\bar{f}\bar{s}}E_3(\kappa_d)\left(1-\bar{\rho}_{\bar{f}o}\right)\right] && (3.134)\\ c_2&=\frac{1}{D'}\left(1-\bar{\rho}_{\bar{f}o}\right) && (3.135)\end{aligned}\right\}\ \text{no gap}$$

Therefore, the source function integrals become the following.

$$\bar{\phi}_+(\kappa_d)\approx\frac{1}{2}\left[1-2E_3(\kappa_d)-\Omega\left(\frac{n_o}{n_f}\right)^2\int_o^{\kappa_d}F(\kappa,\kappa_d)E_2(\kappa_d-\kappa)d\kappa\right] \tag{3.136}$$

$$\bar{\phi}_-(0)\approx\frac{1}{2}\left[1-2E_3(\kappa_d)-\Omega\left(\frac{n_o}{n_f}\right)^2\int_o^{\kappa_d}F(\kappa,\kappa_d)E_2(\kappa)d\kappa\right] \tag{3.137}$$

$$\bar{\phi}_{M+}(\kappa_d)\approx\frac{\mu_M}{2}\left\{\mu_M\left[1-2E_3\left(\frac{\kappa_d}{\mu_M}\right)\right]-\Omega\left(\frac{n_o}{n_f}\right)^2\int_o^{\kappa_d}F(\kappa,\kappa_d)E_2\left(\frac{\kappa_d-\kappa}{\mu_M}\right)d\kappa\right\} \tag{3.138}$$

$$\bar{\phi}_{M-}(\kappa_d)\approx\frac{\mu_M}{2}\left\{\mu_M\left[1-2E_3\left(\frac{\kappa_d}{\mu_M}\right)\right]-\Omega\left(\frac{n_o}{n_f}\right)^2\int_o^{\kappa_d}F(\kappa,\kappa_d)E_2\left(\frac{\kappa}{\mu_M}\right)d\kappa\right\} \tag{3.139}$$

Equations (3.136) through (3.139) can now be used to calculate $\varepsilon(\lambda)$. Figure 3.9 shows $\varepsilon(\lambda)$ as a function of optical depth, κ_d, calculated for no dielectric gap[equation (3.90)].

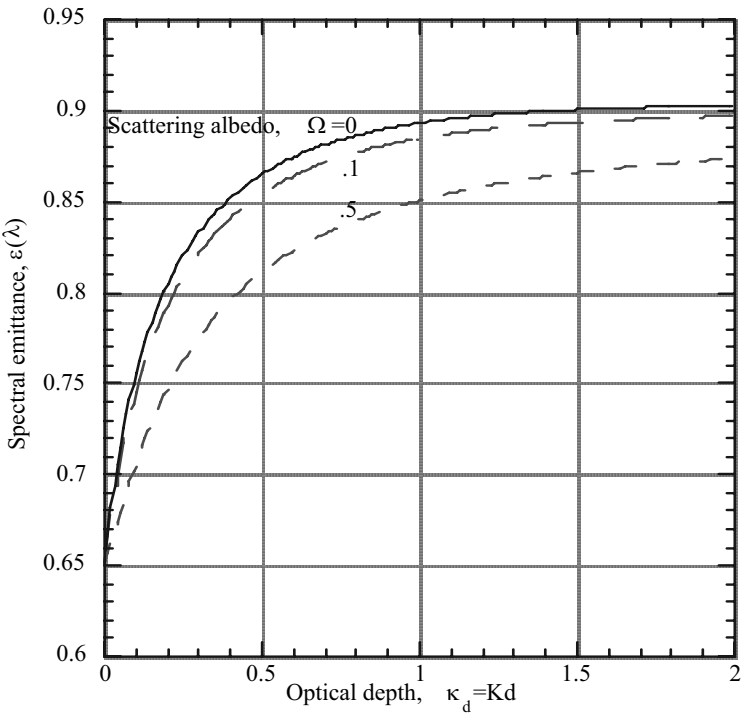

Figure 3.9 - Effect of scattering on spectral emittance, $\varepsilon(\lambda)$, of a planar emitter at constant temperature without a dielectric gap between emitter and substrate. Properties of emitter and substrate are the same as those in Fig. 3.7, n_f=1.9, n_o=1., n_{sR}=5., n_{sI}=7, u_s=5.

The same emitter and substrate properties as in Figure 3.7 have been used. As can be seen, there is only a small reduction in $\varepsilon(\lambda)$ in going from scattering ($\Omega = 0$) to equal scattering and absorption coefficients ($\Omega = 0.5$). For the case with a dielectric gap, the results are similar. For $\kappa_d \ll 1$ there is a negligible reduction in $\varepsilon(\lambda)$.

These results, showing the small reduction in $\varepsilon(\lambda)$ when scattering is included, have been obtained assuming $\Delta T = 0$ and using the lowest order approximation for the source function [equations (3.129) and (3.130)]. Appendix B presents a method for the complete solution of the coupled energy equation, radiation flux equation, and source function equation.

3.9 Cylindrical Emitter

As discussed earlier (Section 3.3.1), fibrous rare earth selective emitters are candidates for a TPV emitter in combustion driven systems. The small 5-10μm diameter fibers are assembled in bundles. This fibrous bundle can be approximated as an infinite cylinder. Such an approximation will not include the effects of the reflectance that occurs when radiation leaves a fiber and enters an adjoining fiber. The whole bundle is approximated as a continuous cylinder.

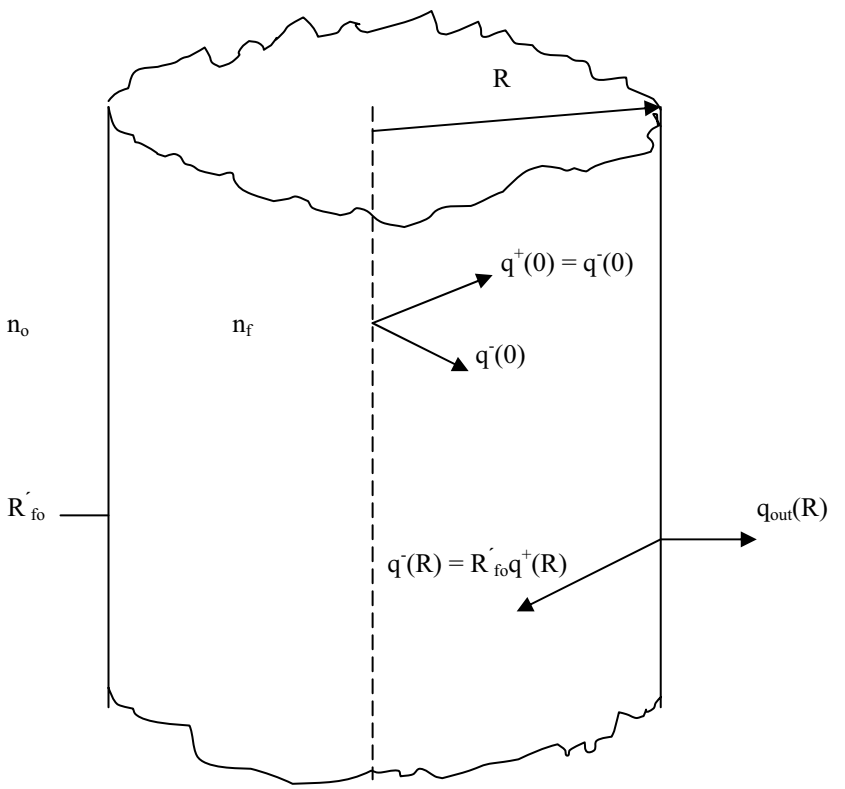

Figure 3.10 Cylindrical emitter showing boundary conditions.

First, consider the steady state energy equation [equation (1.160)] for the infinite cylinder shown in Figure 3.10. Assuming only radial variation, the energy equation is the following.

$$\frac{d}{dr}\left[r\left(k_{th}\frac{dT}{dr} - \overline{q} \right) \right] = 0 \tag{3.140}$$

Integration yields the following result.

$$r\left[k_{th}\frac{dT}{dr}-\bar{q}\right]=\text{constant} \tag{3.141}$$

In order to avoid the term in brackets being singular at r = 0, it must vanish for all r. Thus at all r the conduction and radiation fluxes balance.

$$k_{th}\frac{dT}{dr}=\bar{q} \tag{3.142}$$

In other words, for steady state conditions, all the thermal energy being conducted into the cylinder at the outer radius, r = R, leaves the cylinder as radiation. Similar to the case for the planar emitter (Section 3.8.2), define the following dimensionless variables.

$$\bar{T}=\frac{T}{T_s},\qquad \bar{Q}=\frac{\bar{q}}{\sigma_{sb}T_s^4},\qquad \bar{r}=\frac{r}{R} \tag{3.143}$$

Where T_s is the temperature at r = R. In this case, equation (3.142) becomes the following.

$$\frac{d\bar{T}}{dr}=\gamma\bar{Q} \tag{3.144}$$

Where again γ is the ratio of the radiation flux to the thermal conduction flux.

$$\gamma\equiv\frac{\sigma_{sb}T_s^4}{k_{th}\dfrac{T_s}{R}}=\frac{\sigma_{sb}T_s^3R}{k_{th}} \tag{3.145}$$

As discussed in Section (3.8.2), for TPV applications γ < 0.5 for rare earth selective emitters. Thus for $\gamma \ll 1$ equation (1.144) yields the result, $\bar{T}=\text{constant}\left(T=T_s\right)$. Whereas for a planar emitter, $\gamma \ll 1$ results in a linear temperature variation [equation (3.96)]. Since spectral emittance is a sensitive function of the temperature change, the cylindrical emitter operating at constant temperature will produce a larger spectral emittance than a planar emitter.

We now proceed to develop the spectral emittance, ε(λ), for an infinite cylinder at constant temperature and no external source of radiation. Figure 3.10 shows the infinite

cylinder model with the following boundary conditions. From symmetry conditions, at r = 0 the following boundary condition applies.

$$q^{+}(0) = q^{-}(0) \qquad \text{at } r = 0 \tag{3.146}$$

At r = R, Snell's Law comes into play so that $R'_{fo} = 1$ for $\theta_M \le \theta \le \frac{\pi}{2}$ and the reflected flux at r = R, $q^{-}(\kappa_R)$ is the following.

$$q^{-}(\kappa_R) = 2\pi \int_{o}^{\theta_M} R'_{fo} i^{+}(\kappa_R, \cos\theta)\cos\theta\sin\theta d\theta + \int_{\theta_M}^{\pi/2} i^{+}(\kappa_R, \cos\theta)\cos\theta\sin\theta d\theta \tag{3.147}$$

Where the optical depth, κ_R, is given by equation (3.12) and $\sin\theta_M = \frac{n_o}{n_f}$. Now substitute equation (3.9) for $i^{+}(\kappa_R,\cos\theta)$, where $\mu = \cos\theta$ and assume $R'_{fo} = \bar{R}_{fo}$, just as was assumed for the case of a planar emitter. Also, for a cylindrical emitter we assume the intensity at the origin, $i^{+}(o)$ will be independent of θ, $q^{+}(0) = \pi i^{+}(0)$. As a result, equation (3.147) becomes the following.

$$\begin{aligned} q^{-}(\kappa_R) = 2q^{+}(0)\left[\bar{R}_{fo}E_3(\kappa_R) + (1-\bar{R}_{fo})\mu_M^2 E_3\left(\frac{\kappa_R}{\mu_M}\right)\right] \\ +\bar{R}_{fo}\phi_{+}(\kappa_R) + (1-\bar{R}_{fo})\phi_{M+}(\kappa_R) \end{aligned} \tag{3.148}$$

Where $\phi_{+}(\kappa_R)$ and $\phi_{M+}(\kappa_R)$ are given by equations (3.31) and (3.48) and $\mu_M^2 = 1 - \left(\frac{n_o}{n_f}\right)^2$. Notice that equation (3.148) can be obtained from the planar emitter equation for $q^{-}(\kappa_d)$ by letting $\bar{\rho}_{fo} = \bar{R}_{fo}$ and s = 0 in equation (3.45).

Now use equation (3.10) with κ_d replaced by κ_R to obtain $q^{-}(0)$.

$$\begin{aligned} q^{-}(0) &= -2\pi \int_{\pi/2}^{\pi} i^{-}(0,\cos\theta)\cos\theta\sin\theta d\theta \\ &= -2\pi \int_{-1}^{o} i^{-}(0,\mu)\mu d\mu = 2q^{-}(\kappa_R)E_3(\kappa_R) + \phi_{-}(0) \end{aligned} \tag{3.149}$$

In obtaining equation (3.149) it has been assumed that the boundary at r = R is diffuse so that $i^-(\kappa_R)$ is independent of μ and given by equation (3.32) where κ_d is replaced by κ_R. The boundary condition $q^+(0) = q^-(0)$ can now be used in equation (3.149) so that the following is obtained.

$$q^+(0) = 2q^-(\kappa_R)E_3(\kappa_R) + \phi_-(0) \tag{3.150}$$

Equations (3.148) and (3.150) can now be solved for $q^+(0)$ and $q^-(\kappa_R)$.

$$q^-(\kappa_R) = \frac{1}{D_R}\left\{2\left[\bar{R}_{fo}E_3(\kappa_R) + \mu_M^2\left(1-\bar{R}_{fo}\right)E_3\left(\frac{\kappa_R}{\mu_M}\right)\right]\phi_-(0) + \bar{R}_{fo}\phi_+(\kappa_R) + \left(1-\bar{R}_{fo}\right)\phi_{M+}(\kappa_R)\right\} \tag{3.151}$$

$$q^+(0) = \frac{1}{D_R}\left\{\phi_-(0) + 2\left[\bar{R}_{fo}\phi_+(\kappa_R) + \left(1-\bar{R}_{fo}\right)\phi_{M+}(\kappa_R)\right]E_3(\kappa_R)\right\} \tag{3.152}$$

where,

$$D_R = 1 - 4E_3(\kappa_R)\left[\bar{R}_{fo}E_3(\kappa_R) + \left(1-\bar{R}_{fo}\right)\mu_M^2E_3\left(\frac{\kappa_R}{\mu_M}\right)\right] \tag{3.153}$$

Knowing $q^-(\kappa_R)$ and $q^+(0)$ allows determination of the radiation flux $q(\kappa,\lambda)$ at all values of κ. Equation (3.21) gives the radiation flux for a cylinder if κ_d is replaced by κ_R. Then carrying out the μ integrations for $i^+(\kappa_R)$ being independent of μ results in the following.

$$q(\kappa,\lambda) = 2\left[q^+(0)E_3(\kappa) - q^-(\kappa_R)E_3(\kappa_R - \kappa)\right] + \phi_+(\kappa) - \phi_-(\kappa) \tag{3.154}$$

This is identical to $q(\kappa,\lambda)$ for the planar emitter [equation (3.28)] when κ_d is replaced by κ_R. Substituting equation (3.151) and (3.152) for $q^-(\kappa_R)$ and $q^+(0)$ in equation (3.154) yields the following result.

$$q(\kappa,\lambda) = \frac{2}{D_R}\left\{B_R(\kappa)\phi_-(0) - A_R(\kappa)\left[\bar{R}_{fo}\phi_+(\kappa_R) + \left(1-\bar{R}_{fo}\right)\phi_{M+}(\kappa_R)\right]\right\} + \phi_+(\kappa) - \phi_-(\kappa) \tag{3.155}$$

Where,

$$A_R(\kappa) = E_3(\kappa_R - \kappa) - 2E_3(\kappa_R)E_3(\kappa) \tag{3.156}$$

$$B_R(\kappa) = E_3(\kappa) - 2\left[\bar{R}_{fo}E_3(\kappa_R) + (1-\bar{R}_{fo})\mu_M^2 E_3\left(\frac{\kappa_R}{\mu_M}\right)\right]E_3(\kappa_R - \kappa) \tag{3.157}$$

For the planar emitter in Section 3.8 an external source of radiation was included in the radiation flux, $q(\kappa)$. In that case, the flux at the emitting surface, $q(\kappa_d)$, includes contributions from the external source, as well as, the radiation coming from the planar emitter. Therefore, to calculate the spectral emittance, equation (3.79) was required to determine the emitted radiation. However, for the cylindrical emitter the external source has been neglected thus, $\varepsilon(\lambda)$ can be determined by evaluating equation (3.155) at $\kappa = \kappa_R$. (Problem 3.11)

$$\varepsilon(\lambda) \equiv \frac{q(\kappa_R,\lambda)}{n_o^2 e_b(\lambda,T_s)} = 2\left(\frac{n_f}{n_o}\right)^2 \frac{(1-\bar{R}_{fo})}{D_R}\left[2\bar{\phi}_{-R}(0)h_{-R} + \bar{\phi}_{+R}(\kappa_R)h_{+R} - \bar{\phi}_{MR}(\kappa_R)h_{MR}\right] \tag{3.158}$$

Where,

$$\bar{\phi}_{+R}(\kappa_R) = \frac{\pi}{n_f^2 e_b(\lambda,T_s)}\int_o^{\kappa_R} S(\kappa^*)E_2(\kappa_R - \kappa^*)d\kappa^* \tag{3.159}$$

$$\bar{\phi}_{-R}(0) = \frac{\pi}{n_f^2 e_b(\lambda,T_s)}\int_o^{\kappa_R} S(\kappa^*)E_2(\kappa^*)d\kappa^* \tag{3.160}$$

$$\bar{\phi}_{MR}(\kappa_R) = \frac{\pi\mu_M}{n_f^2 e_b(\lambda,T_s)}\int_o^{\kappa_R} S(\kappa^*)E_2\left(\frac{\kappa_R - \kappa^*}{\mu_M}\right)d\kappa^* \tag{3.161}$$

$$h_{+R} = 1 - 4\mu_M^2 E_3(\kappa_R)E_3\left(\frac{\kappa_R}{\mu_M}\right) \tag{3.162}$$

$$h_{-R} = E_3(\kappa_R) - \mu_M^2 E_3\left(\frac{\kappa_R}{\mu_M}\right) \tag{3.163}$$

$$h_{MR} = 1 - 4E_3^2(\kappa_R) \tag{3.164}$$

Comparing $\varepsilon(\lambda)$ for a planar emitter without a dielectric gap between emitter and the substrate [equation(3.90)] with the cylindrical result for $\varepsilon(\lambda)$ [equation (3.158)], it can be seen that $\varepsilon(\lambda)$ for the cylinder can be obtained from the planar result by setting r = s = 0, $\bar{R}_{fs} = 1$, and as a result $\varepsilon_{fsn} = 1 - \bar{R}_{fs} = 0$. Similar to the case for the planar $\varepsilon(\lambda)$, the result for $\varepsilon(\lambda)$ given by equation (3.158) only assumes isotropic scattering and intensity dependent on r only. However, to proceed further without having to solve the energy and source function equations, the no scattering and constant temperature approximations must be made. Assuming constant temperature and neglecting scattering, $S(\kappa^*) = \dfrac{n_f^2 e_b(\lambda, T_s)}{\pi}$, yields the following result. (Problem 3.12)

$$\boxed{\varepsilon(\lambda) = \frac{(1 - \bar{R}_{fo})}{D_R}\left[1 - 4E_3^2(\kappa_R)\right]}$$
constant temperature and no scattering (3.165)

Consider the two limiting cases, $\kappa_R = 0$ and $\kappa_R \to \infty$. For $\kappa_R = 0$, $E_3 = ½$ and

$$\varepsilon(\lambda) = 0, \qquad \kappa_R = 0 \tag{3.166}$$

For $\kappa_R \to \infty$, $E_3 = 0$, and $D_R = 1$ so that the spectral emittance is the following.

$$\lim_{\kappa_R \to \infty} \varepsilon(\lambda) = 1 - \bar{R}_{fo} \tag{3.167}$$

These results for the cylindrical emitter can be compared to the corresponding results [equations (3.120) and (3.127)] for the planar emitter. For a selective emitter, where $\kappa_R = 0$, for wavelength regions outside emission bands, $\varepsilon(\lambda) \to 0$ for the cylindrical emitter. However, for the planar emitter, where $\kappa_d = 0$, the spectral emittance is determined by the substrate emittance. Within emission bands, where κ_d and κ_R are large, $\varepsilon(\lambda) \approx 1 - \bar{R}_{fo}$ for the cylindrical emitter but $\varepsilon(\lambda)$ for the planar emitter is reduced

by the factor $e^{-u_s \Delta T}$. Thus, because the cylindrical emitter operates at nearly constant temperature and without a substrate, it will have larger $\varepsilon(\lambda)$ within emission bands and lower $\varepsilon(\lambda)$ outside emission bands.

Figure 3.11 shows $\varepsilon(\lambda)$ calculated using equation (3.165) for the cylindrical emitter as a function of optical depth, κ_R, for emission into a vacuum ($n_o = 1$) for three different indices of refraction. The spectral emittance increases rapidly with κ_R and nearly reaches its limiting value when $\kappa_R = 1$. This behavior is similar to the planar emitter (Figure 3.7). Notice also for the cylindrical emitter that for small κ_R the spectral emittance rate of increase grows as n_f increases. This same behavior exists for the planar emitter but is less pronounced.

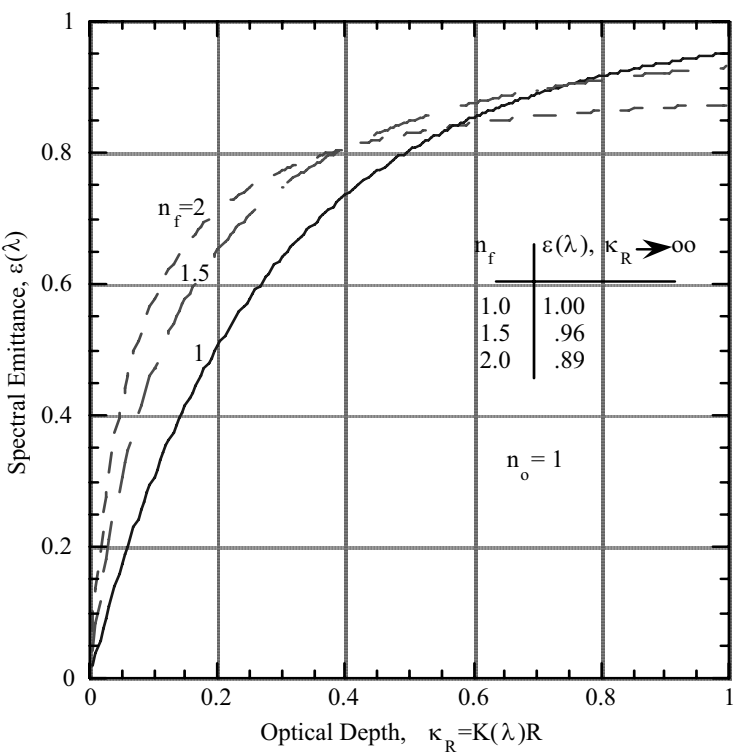

Figure 3.11 - Spectral emittance of cylinder of radius,R, at a constant temperature as a function of optical depth, $\kappa_R = K(\lambda)R$, where $K(\lambda)$ is the extinction coefficient and n_f is the cylinder index of refraction and n_o is the surrounding index of refraction. Scattering has been neglected.

3.10 Emitter Performance

So far in this chapter spectral emittance is the only emitter performance parameter discussed. However, for a TPV system we want to know the emitter efficiency and power output that can be converted to electrical energy by the PV array. These parameters are functions of the spectral emittance, $\varepsilon(\lambda)$. The *emitter efficiency*, η_E, defined below, tells what fraction of the total emitted radiation is useful. In other words, what fraction of emitted radiation can be converted to electrical energy by the PV array. From the definition of spectral emittance [equation (3.169)] and assuming the index of refraction of the surroundings, n_o, is independent of λ, the emitter efficiency becomes the following.

$$\eta_E \equiv \frac{\int_0^{\lambda_g} q_E(\kappa_E,\lambda)\,d\lambda}{\int_0^{\infty} q_E(\kappa_E,\lambda)\,d\lambda} = \frac{n_o^2\int_0^{\lambda_g}\varepsilon(\lambda)e_b(\lambda,T_E)\,d\lambda}{n_o^2\int_0^{\infty}\varepsilon(\lambda)e_b(\lambda,T_E)\,d\lambda} \tag{3.168}$$

Where κ_E is the optical depth of the emitter, T_E is the emitter temperature, and λ_g is the wavelength that corresponds to the PV array bandgap energy, E_g.

$$\lambda_g = \frac{h_{co}}{E_g} = \frac{1.24\times10^3}{E_g(eV)}\,nm \tag{3.169}$$

Note that T_E is the emitter temperature for which $\varepsilon(\lambda)$ is defined. For a planar emitter it is the substrate temperature. The numerator of equation (3.168) is the emitted radiation that can be converted by the PV array and is defined as the *useful power density*, $\overline{q}_b$. The denominator is the *total emitted radiation*, $\overline{q}_E$.

$$\overline{q}_b \equiv n_o^2\int_0^{\lambda_g}\varepsilon(\lambda)e_b(\lambda,T_E)\,d\lambda = \overline{q}_E\eta_E \tag{3.170}$$

$$\overline{q}_b \equiv n_o^2\int_0^{\infty}\varepsilon(\lambda)e_b(\lambda,T_E)\,d\lambda = n_o^2\sigma_{sb}\varepsilon_T(T_E)T_E^4 \tag{3.171}$$

In equation (3.171) the total power density is written in terms of the total hemispherical emittance, $\varepsilon_T(T_E)$, [equation (1.179)]. The useful power density, $\overline{q}_b$, can also be written in terms of the *useful emittance*, $\varepsilon_b(T_E)$, defined as follows.

$$\varepsilon_b\left(T_E\right) \equiv \frac{\int_o^{\lambda_g} q_E\left(\kappa_E,\lambda\right)d\lambda}{n_o^2\int_o^{\lambda_g} e_b\left(\lambda,T_E\right)d\lambda} = \frac{\int_o^{\lambda_g}\varepsilon\left(\lambda\right)e_b\left(\lambda,T_E\right)d\lambda}{\int_o^{\lambda_g} e_b\left(\lambda,T_E\right)d\lambda} = \frac{\int_o^{\lambda_g}\varepsilon\left(\lambda\right)e_b\left(\lambda,T_E\right)d\lambda}{\sigma_{sb}T_E^4F_{o-\lambda_gT_E}} \tag{3.172}$$

In obtaining the last expression in equation (3.172), the definition of the function $F_{o-\lambda_gT_E}$ [equation (1.137)], has been used. Therefore, $\overline{q}_b$, is the following.

$$\overline{q}_b = n_o^2\sigma_{sb}\varepsilon_b\left(T_E\right)T_E^4F_{o-\lambda_gT_E} \tag{3.173}$$

Thus, using equation (3.173) and (3.171) the emitter efficiency can be written as follows.

$$\eta_E = \frac{\overline{q}_b}{\overline{q}_E} = \frac{\varepsilon_b\left(T_E\right)}{\varepsilon_T\left(T_E\right)}F_{o-\lambda_gT_E} \tag{3.174}$$

Obviously, it is desirable that the useful emittance, ε_b, be large while the total emittance, ε_T, be small. For most TPV systems, the ranges of λ_g and T_E are $1.0 < \lambda_g < 2.0\mu m$ and $1200 < T_E < 2000K$. As a result, $1200 < \lambda_gT_E < 4000\mu mK$. In this range of λ_gT_E, the function $F_{o-\lambda_gT_E}$ has the range $.002 < F_{o-\lambda_gT_E} < .48$ (see Figure 1.5). Thus, η_E will be small for a TPV system when $\lambda_gT_E < 2000$ unless $\varepsilon_b \gg \varepsilon_T$. Achieving $\varepsilon_b \gg \varepsilon_T$ requires a very effective selective emitter.

3.10.1 Gray Body Emitter Performance

Consider η_E for a gray body emitter ($\varepsilon(\lambda)$ = constant). In this case, the efficiency reduces to the function $F_{o-\lambda_gT_E}$ defined by equation (1.137).

$$\eta_E = F_{o-\lambda_gT_E} = \frac{\int_o^{\lambda_g} e_b\left(\lambda,T_E\right)d\lambda}{\int_o^{\infty} e_b\left(\lambda,T_E\right)d\lambda} = \frac{15}{\pi^4}\int_{u_g}^{\infty}\frac{x^3}{e^x-1}dx \tag{3.175}$$

The results from problem 1.13 have been used to obtain the last expression in equation (3.175), where $u_g = \frac{hc_\infty}{k\lambda_g T_E} = \frac{E_g}{kT_E}$ is the PV array dimensionless bandgap energy [equation (2.16)].

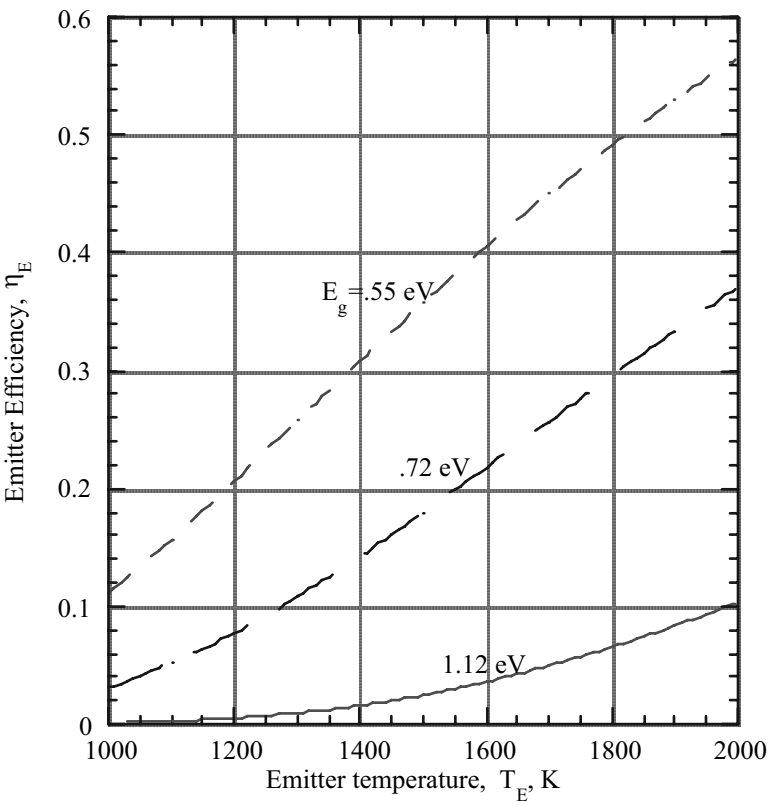

Figure 3.12 - Emitter efficiency for gray body($\varepsilon_E(\lambda)$=constant) emitter at various PV array bandgap energies, E_g.

Figure 3.12 shows η_E as a function of T_E for a gray body emitter for bangap energies of E_g = 1.12eV (silicon), .72eV (GaSb), and .55eV (InGaAs). The first thing to notice is that η_E increases rapidly with temperature. The rate of increase in η_E grows as E_g increases. However, even though the rate of increase in η_E for E_g = 1.12eV is

large, the value of η_E is low (< .10) for T_E < 2000K. The strong temperature dependence of η_E will also be true for a selective emitter.

The useful power density for a gray body emitter with constant spectral emittance, ε_g, is given by equation (3.173). As a result, the quantity $\frac{\overline{q}_b}{n_o^2 \varepsilon_g}$ will be a function of E_g and T_E.

$$\boxed{\frac{\overline{q}_b}{n_o^2 \varepsilon_g} = \sigma_{sb} T_E^4 F_{o-\lambda_g T_E} = \sigma_{sb} T_E^4 \eta_E \qquad \varepsilon(\lambda) = \varepsilon_g = \text{constant}} \tag{3.176}$$

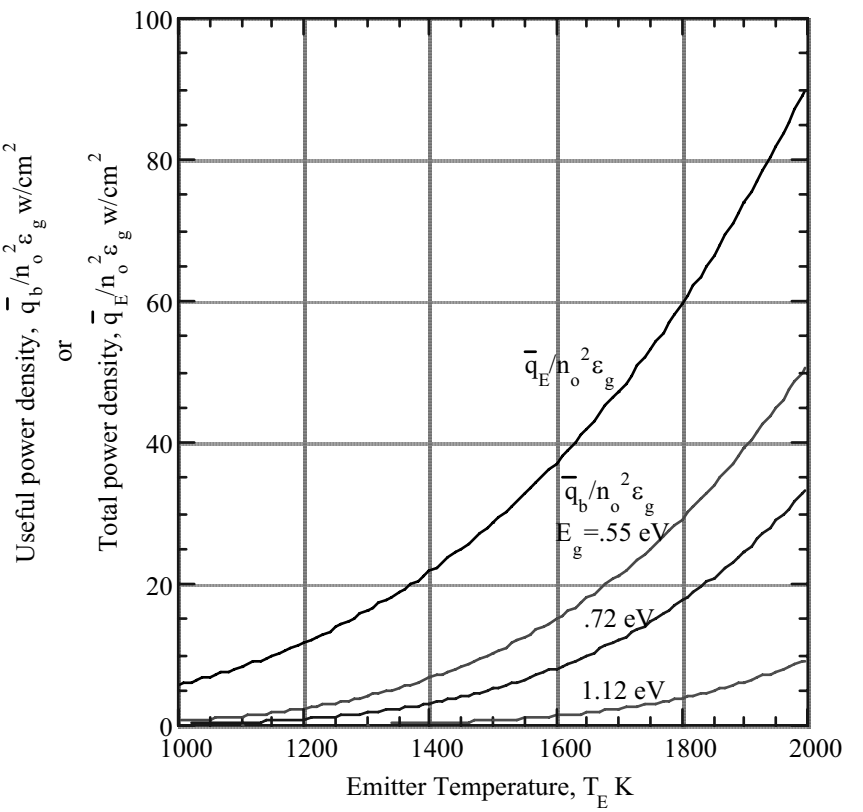

Figure 3.13- Total power density, $\overline{q}_E$, and useful power density, $\overline{q}_b$, for a gray body emitter with emittance, ε_g, and emitting into a media with index of refraction, n_o, for several PV bandgap energies, E_g.

This result is shown in Figure 3.13 for Eg = 0.55, 0.72, and 1.12eV. Also shown in the figure is the quantity $\frac{\overline{q}_E}{n_o^2 \varepsilon_g}$, where $\overline{q}_E$ [equation (3.171)] is the total radiated power. The difference $\overline{q}_E - \overline{q}_b$, which is the radiation flux that cannot be converted to electrical energy, is at least twice the useful power, $\overline{q}_b$, except for E_g = 0.55eV at the highest temperatures. For an efficient TPV system, this radiation flux, $\overline{q}_E - \overline{q}_b$, must be recycled back to the emitter.

Useful power density increases with emitter temperature even faster than the efficiency. Again, however, just as for η_E at E_g = 1.12eV, the useful power density, $\overline{q}_b$, is low (< 10W/cm^2) even for a blackbody (ε_g = 1) emitting into a vacuum (n_o = 1). These efficiency and density results again emphasize the importance of low bandgap energy PV arrays for a successful TPV system.

The emitter efficiency for a gray body emitter is independent of the spectral emittance, ε_g [equation (3.175)]. However, the useful power density, $\overline{q}_b$, is directly proportional to ε_g. Thus, the most desirable gray body emitter for a TPV system would appear to be the one with the maximum ε_g: namely a blackbody. With a blackbody emitter, however, the radiation flux for photon energies that cannot be converted by the PV array $\left(\overline{q}_E - \overline{q}_b\right)$ will also be a maximum. This maximum nonconvertible radiation flux means there will be a very large waste heat removal problem. (see problem 3.13)

3.10.2 Selective Emitter Performance

Now consider efficiency and useful power density for a selective emitter that has considerable variation in spectral emittance. As shown earlier, the spectral emittance, $\varepsilon(\lambda)$, of a planar emitter is a sensitive function of the temperature variation across the emitter and the optical depth, $\kappa(d) = K(\lambda)d$, where $K(\lambda)$ is the extinction coefficient and d is the emitter thickness. In the case of a cylindrical emitter, the temperature was shown to be nearly a constant in Section 3.9. As a result, the cylindrical spectral emittance is independent of temperature. Therefore, the efficiency for a cylindrical emitter can be calculated using equation (3.165) if scattering is neglected. However, for a planar emitter, where $\varepsilon(\lambda)$ depends upon temperature, the energy equation and radiation transfer equations must be solved simultaneously in order to determine the efficiency.

3.10.3 Cylindrical Selective Emitter Performance

First, consider the cylindrical selective emitter that has the added simplification of constant temperature operation. As an example of a selective emitter, the extinction coefficient for erbium aluminum garnet (ErAG) as shown in Figure 3.4 and index of refraction from [19] were used to calculate $\varepsilon(\lambda)$ [equation (3.165)]. Numerical

integrations of the integrals in equation (3.168) for η_E are performed at T_E = 1200, 1700, and 2000K. The upper limit chosen for the integral in the numerator of equation (3.168) is E_g = .72eV, (λ_g = 1722nm), which corresponds to a GaSb or InGaAs PV array. These results are shown in Figure 3.14.

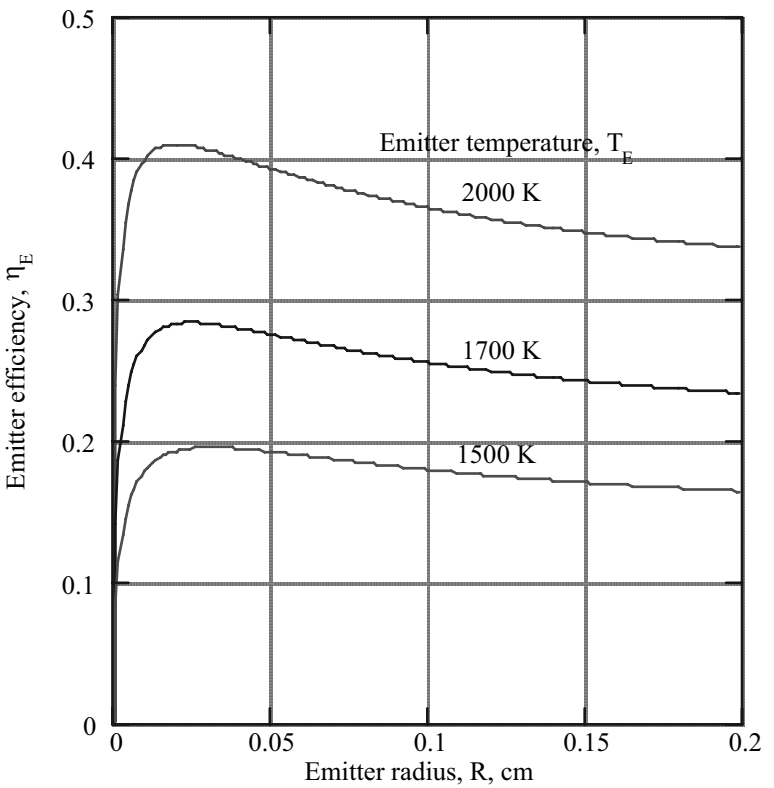

Figure 3.14 - Emitter efficiency, η_E, of cylindrical erbium aluminum garnet based on a PV cell bandgap energy, E_g=.72eV(λ_g=1722 nm). The extinction coefficient shown in Fig. 3.4 and index of refraction from [19] are used to calculate $\varepsilon(\lambda)$. Also, constant temperature and emission into a vacuum are assumed.

The first thing to notice about the results in Figure 3.14 is that there is an optimum radius for maximum emitter efficiency. Also, the optimum radius becomes smaller as T_E increases. In going from T_E = 1500K to T_E = 2000K, the optimum radius decreases from R_{opt} = .025cm at T_E = 1500K, to R_{opt} = .017cm at T_E = 2000K. The nearly exponential dependence of spectral emittance, $\varepsilon(\lambda)$, on optical depth, $\kappa_R(\lambda)$, is the

reason there is an optimum thickness. Referring to equation (3.165) note that $1-4E_3^2(\kappa_R)$ is the major factor in determining ε(λ). Therefore, since $E_3(x)$ can be approximated as $\frac{1}{2}\exp\left[-\frac{3}{2}x\right]$,

$$\varepsilon(\lambda) \sim 1-e^{-3\kappa_R} = 1-e^{-3KR} \tag{3.177}$$

In the emission band where K(λ) is large, ε(λ) will increase rapidly with R. However, outside the emission bands and below the long wavelength cutoff region, where K(λ) is small, the emittance increases nearly linearly with R. As a result, the useful power density, $\bar{q}_b$, will increase rapidly to nearly its maximum value when R ≈ R_{opt}. For R > R_{opt}, $\bar{q}_b$ will show only a small increase. However, the total radiated power, $\bar{q}_E$, continues to increase for R > R_{opt} so that the efficiency decreases from its maximum value.

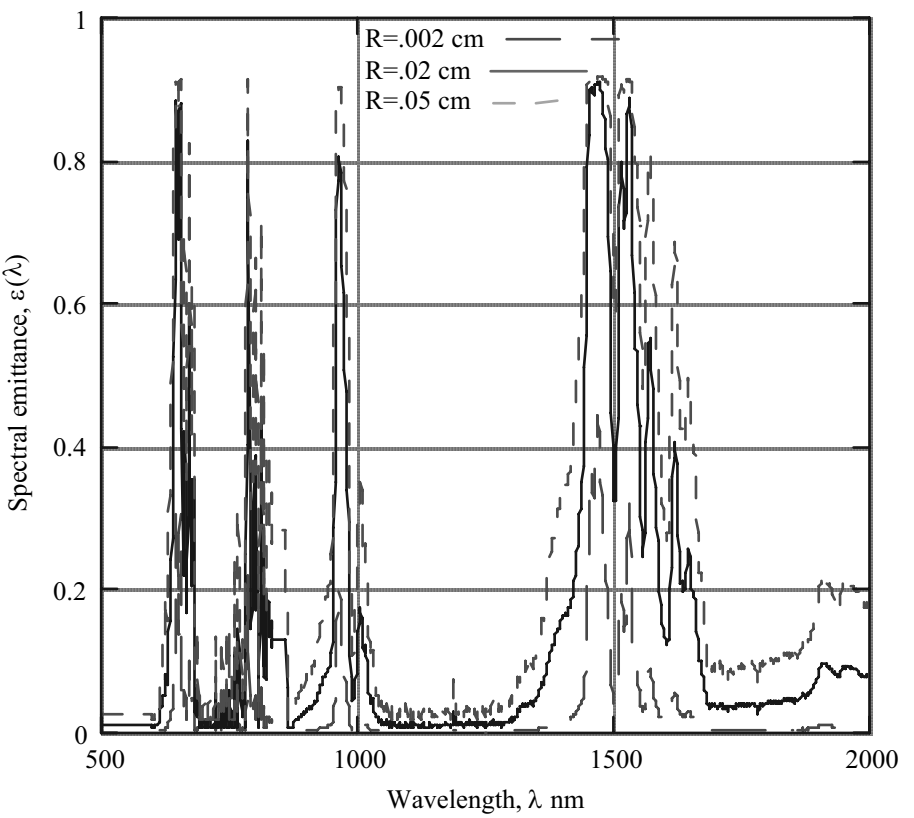

Figure 3.15a) - Effect of radius, R, on the spectral emittance, ε(λ), of constant temperature erbium aluminum garnet(EAG) cylindrical emitter for wavelength range, 500<λ<2000 nm.

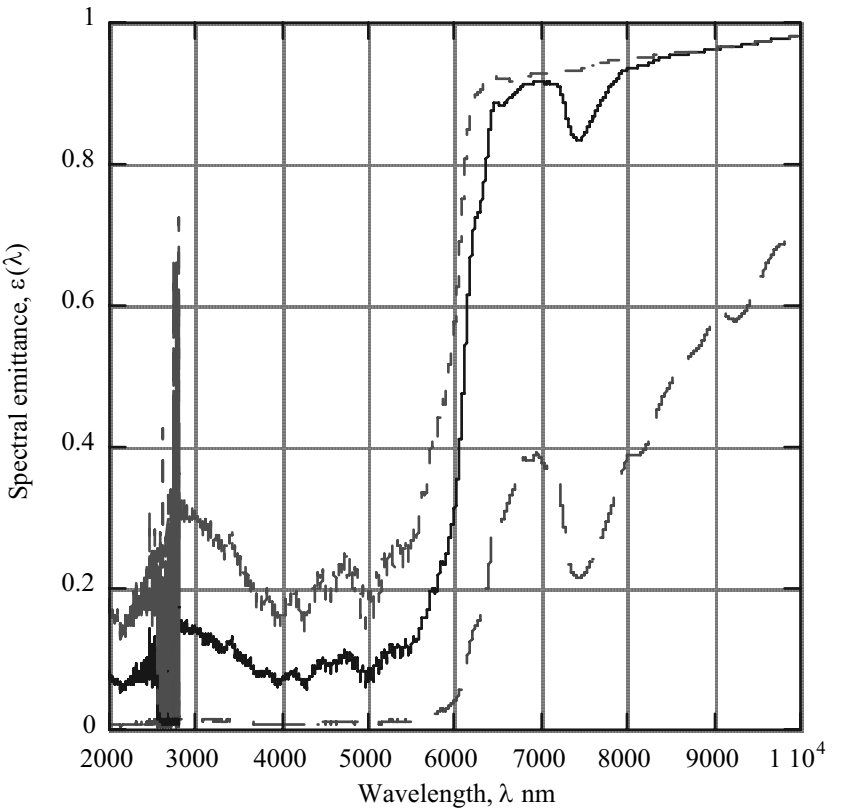

Figure 3.15b) - Effect of radius, R, on the spectral emittance, $\varepsilon(\lambda)$, of constant temperature erbium aluminum garnet(EAG) cylindrical emitter for wavelength range, $2000<\lambda<10{,}000$ nm. Extinction coefficient taken from Fig. 3.4 and index of refraction from [19]. Reflectivity for normal incidence was assumed for cylinder-vacuum($n_o=1$) interface reflectance,ρ_{fo}.

Figure 3.15 shows the spectral emittance at R = .002cm ($R < R_{opt}$), R = .02cm ($R \approx R_{opt}$), and R = .05cm ($R > R_{opt}$). For R = .002cm, the emittance is small everywhere but in the emission bands and beyond the long wavelength ($\lambda > 6000$nm) cutoff region. When R = .02cm ($R \approx R_{opt}$), the emittance in the emittance bands and the long wavelength region have increased nearly to their limiting values. However, outside these regions the emittance is well below the values for R = .05cm. Therefore, the useful radiation, $\overline{q}_b$, has nearly stopped increasing for $R \geq R_{opt}$ while the total radiation, $\overline{q}_E$, continues to increase for $R \geq R_{opt}$, resulting in a decrease in η_E.

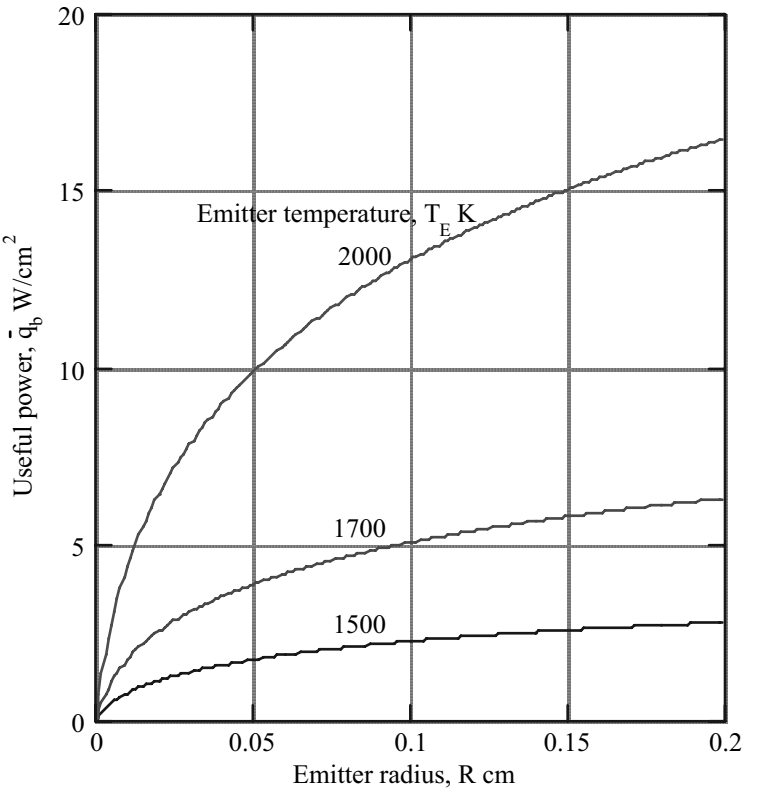

Figure 3.16 - Useful power for cylindrical erbium aluminum garnet emitter for same conditions as Figure 3.14.

Whereas, the cylindrical emitter has an optimum radius for maximum efficiency, there is no optimum radius for maximum useful power, $\bar{q}_b$ [equation (3.170)]. This is illustrated in Figure 3.16 where $\bar{q}_b$ is shown as a function of R for the same ErAG emitter as used for Figures 3.14 and 3.15. The useful power is a monotonically increasing function of R. The limiting value for $\bar{q}_b$ as $R \to \infty$ can be determined using equation (3.165) for $\varepsilon(\lambda)$ in the result for $\bar{q}_b$ [equation (3.170)] for $n_o = 1$.

$$\lim_{R\to\infty} \bar{q}_b = \int_o^{\lambda_g} \left(1 - \bar{R}_{fo}\right) e_b\left(\lambda, T_E\right) d\lambda \tag{3.178}$$

In the range $0 \le \lambda \le \lambda_g$, the index of refraction n_f for EAG (see Figure 3.6c) is nearly a constant, $n_f \approx 1.8$. As a result, $\overline{R}_{fo}$ is also nearly a constant, $\left(\overline{R}_{fo} = \left(\frac{1.8-1}{1.8+1} \right)^2 = .082 \right)$.

$$\lim_{R \to \infty} \overline{q}_b \approx \left(1 - \overline{R}_{fo}\right) \int_o^{\lambda_g} e_b\left(\lambda, T_E\right) d\lambda = \sigma_{sb} T_E^4 \left(1 - \overline{R}_{fo}\right) F_{o-\lambda_g T_E} \tag{3.179}$$

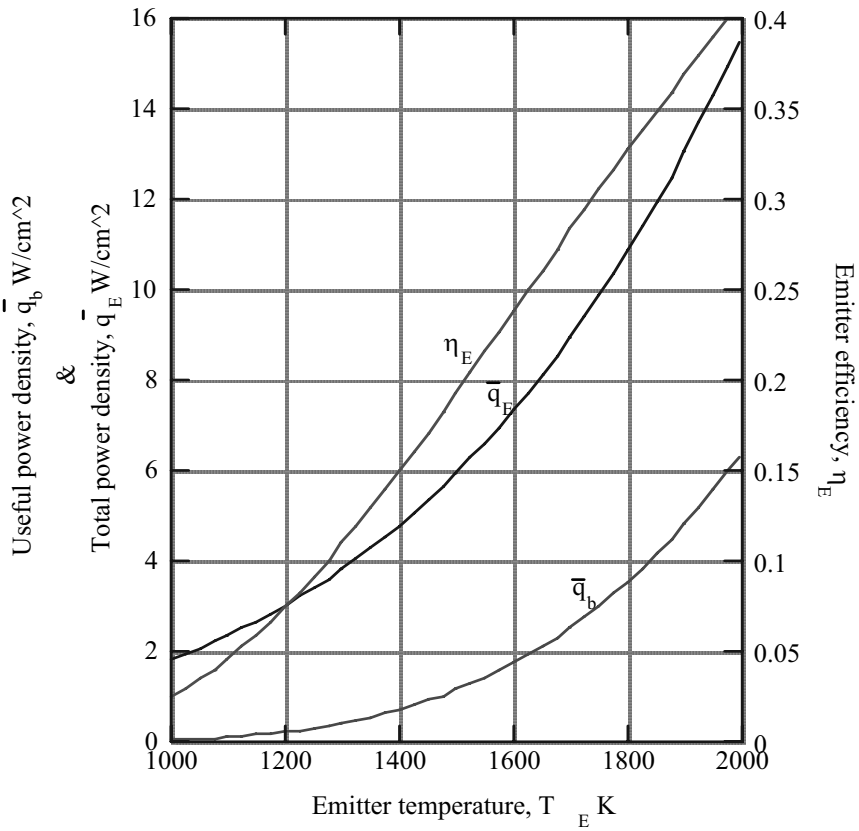

Figure 3.17 Useful and total emitted powers and emitter efficiency for cylindrical EAG selective emitter. Emitter radius, R=.02 cm and same conditions as Fig. 3.16.

Now consider how the efficiency, η_E, useful power density, $\overline{q}_b$, and the total power density, $\overline{q}_E$, for the cylindrical EAG selective emitter depend upon emitter temperature,

T_E. These are calculated using equations (3.170) and (3.171) and the spectral emittance for constant temperature and no scattering given by equation (3.165). Using an emitter radius, R = .02cm, which is close to the optimum radius for maximum efficiency (see Figure 3.14), and the same input quantities as in Figure 3.14 yields the results shown in Figure 3.17. In the range $1200 < T_E < 2000$K, the efficiency is nearly a linear function of T_E. For $T_E < 1400$K, the useful power density, $\bar{q}_b < 1$ w/cm^2. As a result, a TPV system using a EAG emitter with a PV array where $E_g = 0.72$eV at emitter temperatures less than 1400°K requires large emitter area and PV array area to produce significant power output.

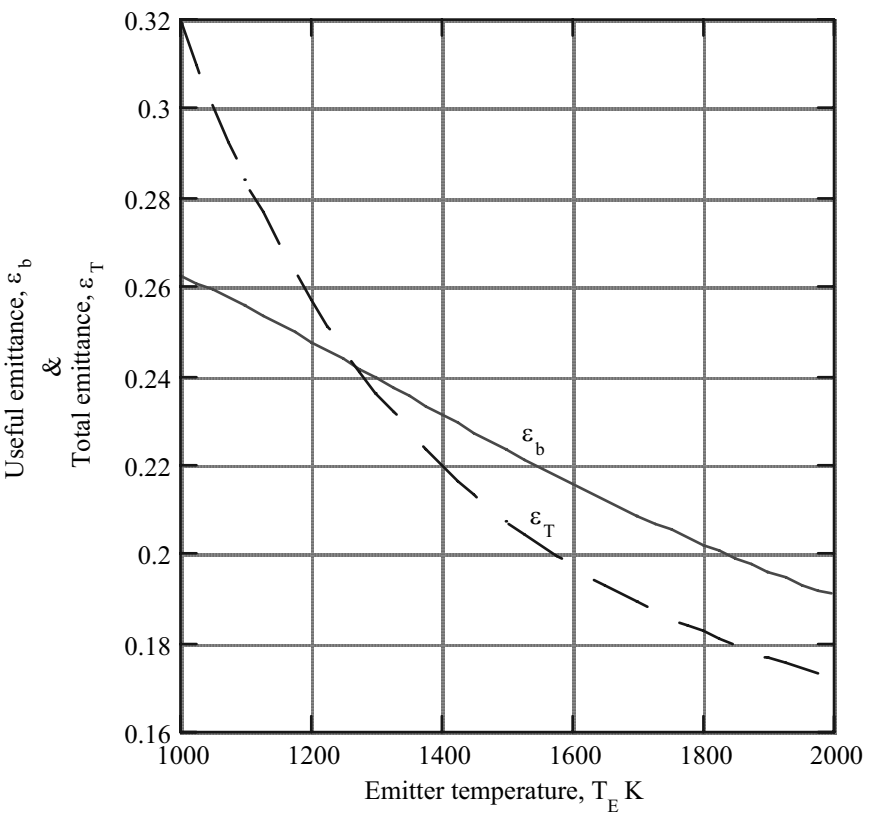

Figure 3.18 - Useful emittance and total emittance for cylindrical erbium aluminum garnet selective emitter. Emitter radius, R=.02 cm and same conditions as Fig. 3.14.

Two other performance parameters for a selective emitter are the useful emittance $\varepsilon_b(T_E)$, equation (3.172), and the total emittance, $\varepsilon_T(T_E)$, equation (1.179). These quantities are shown in Figure 3.18 for the cylindrical EAG emitter. The useful emittance, ε_b, varies nearly linearly with T_E with a small negative slope. However, the total emittance, ε_T, decreases much more rapidly with increasing T_E. This temperature dependence of ε_b and ε_T, plus the increase in $F_{o-\lambda_g T_E}$ with increasing temperature results in the increase of emitter efficiency [see equation (3.174)].

3.10.4 Planar Selective Emitter Performance

The externally heated cylindrical emitter operates at constant temperature, but the planar emitter heated from one side suffers a temperature change across the emitter. As has already been pointed out, even small temperature changes produce a significant reduction in the spectral emittance within emission bands. Therefore, temperature variation across the emitter must be included in calculating the efficiency of a planar emitter.

The temperature variation can be obtained from the solution of the energy equation [equation (1.160)] with appropriate boundary conditions. The one dimensional energy equation [equation (1.160)] for a planar emitter (Figure 3.6) has the following solution.

$$\bar{q}_{in} = k_{th}\frac{dT}{dx} - \bar{q} = k_{th}\left.\frac{dT}{dx}\right|_{x=d} - \bar{q}_E \tag{3.180}$$

This indicates that the heat input, $\bar{q}_{in}$, is the sum of thermal conduction, $-k_{th}\frac{dT}{dx}$, and the radiation flux, $\bar{q}$. In Section 3.8.2, it was shown that in most cases, it is a valid approximation to neglect $\bar{q}$ compared to $k_{th}\frac{dT}{dx}$ so that a linear temperature variation results and $\frac{dT}{dx} = \frac{T_s \Delta T}{d}$. Also, in a TPV system, the emitter will most likely operate in a vacuum. As a result, the conduction term, $\left.k_{th}\frac{dT}{dx}\right|_{x=d} = 0$ and all the energy leaves the emitter as radiation, $\bar{q}_E$. Therefore, neglecting $\bar{q}$ in equation (3.180) and using the linear temperature variation yields the following result.

$$\Delta T = \frac{d\bar{q}_E}{k_{th} T_s} \tag{3.181}$$

Where,

$$\bar{q}_E = n_o^2 \int_o^\infty \varepsilon(\lambda, T_s, \Delta T)\, e_b(\lambda, T_s)\, d\lambda \tag{3.182}$$

and $\varepsilon(\lambda,T_s,\Delta T)$ is the spectral emittance given by equations (3.83) or (3.90).

Obviously, assuming a linear temperature variation is inconsistent with the result $\left.\frac{dT}{dx}\right|_{x=d} = 0$. For emission into a vacuum at a given substrate temperature, T_s, the assumed linear temperature variation will yield larger values for the temperature through the film than the actual values. As a result, ε and $\bar{q}_E$ will also be larger than the actual values. However, the linear temperature variation assumption greatly simplifies the calculation of, η_E, $\bar{q}_b$, $\bar{q}_E$, ε_T, and ε_b.

Since ε is a function of ΔT, equation (3.181) must be solved by an iterative process. An initial guess for ΔT is used to calculate ε and that result is used in equation (3.182) to calculate $\bar{q}_E$. This value of $\bar{q}_E$ is then used in equation (3.182) to calculate a new value for ΔT. The process continues until convergence. Once ΔT is determined, the emitter performance parameters, η_E, $\bar{q}_b$, $\bar{q}_E$, ε_T, and ε_b can be calculated.

Consider an EAG planar selective emitter with a dielectric gap between the emitter and a platinum substrate. The spectral emittance is given by equation (3.83) and the extinction coefficient, $K(\lambda)$, is shown in Figure 3.4. The index of refraction is taken from [19]. For a linear temperature variation and no scattering, the source function integrals are given by equations (3.106) through (3.109). The emitter efficiency, η_E, is given by equation (3.168). Just as for the cylindrical emitter, $\lambda_g = 1720$nm is the upper limit on the integral in equation (3.168). For $T_s = 1700$K the emitter efficiency and temperature change are calculated as a function of emitter thickness. These results are shown in Figure 3.19a. Appearing in Figure 3.19b are the useful radiation power, $\bar{q}_b$, and the total radiated power, $\bar{q}_E$.

The first thing to notice in Figure 3.19a is that η_E decreases with increasing thickness. Maximum η_E occurs when d = 0, which means the emitter consists only of the platinum substrate with $\varepsilon(\lambda) = \varepsilon_{son}$. Thus platinum is a more efficient emitter than an emitter consisting of EAG on a platinum substrate. However, as Figure 3.19b shows, the useful power, $\bar{q}_b$, increases rapidly with increasing d to a maximum $\bar{q}_b = 7.3$ W/cm^2 at $d \approx .2$cm. This maximum $\bar{q}_b$ is more than 2.5 times $\bar{q}_b$ for the platinum substrate alone (d = 0). Thus, to produce the same useful power at a

temperature of 1700K as an ErAG emitter, the platinum emitter area would have to be 2.5 times greater than the ErAG emitter area.

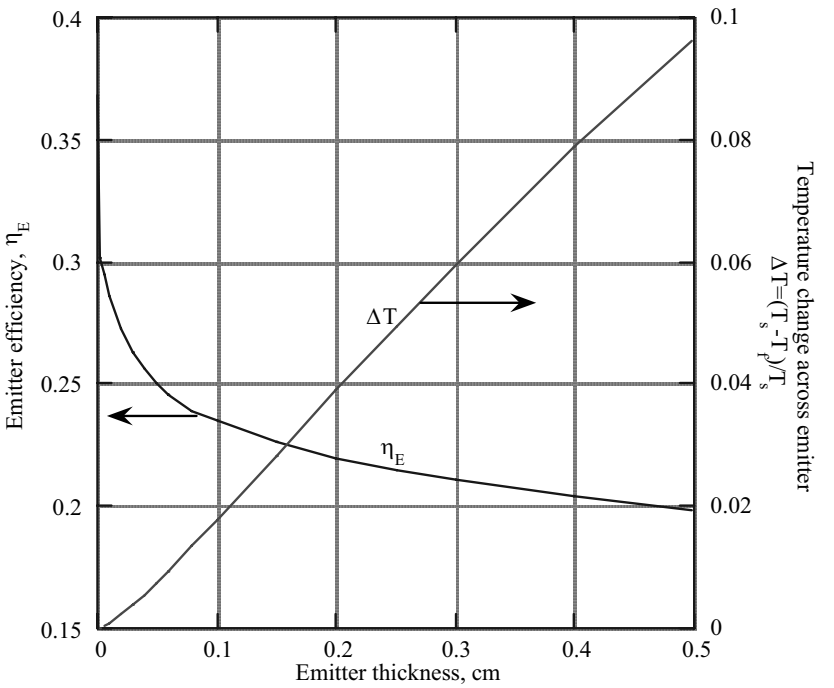

Figure 3.19a) - Emitter efficiency, η_E and temperature change, ΔT of erbium aluminum garnet(EAG) planar emitter with dielectric gap between emitter and Pt substrate as a function of emitter thickness, d at substrate temperature, T_s=1700K. Extinction coefficient, K , taken from Fig. 3.4 and index of refraction from [19]. Results based on PV cell bandgap energy E_g=.72eV(1722 nm). Emission into a vacuum(n_o=1) and values of n_{sR} and n_{sI} for Pt taken from ref. 20.

The very small emittance (< 0.10) of platinum at long wavelengths (see Figure 3.1) compared to the large emittance (> 0.9) of EAG for λ > 5000nm (see Figure 3.15) is the primary reason for platinum having a larger η_E.

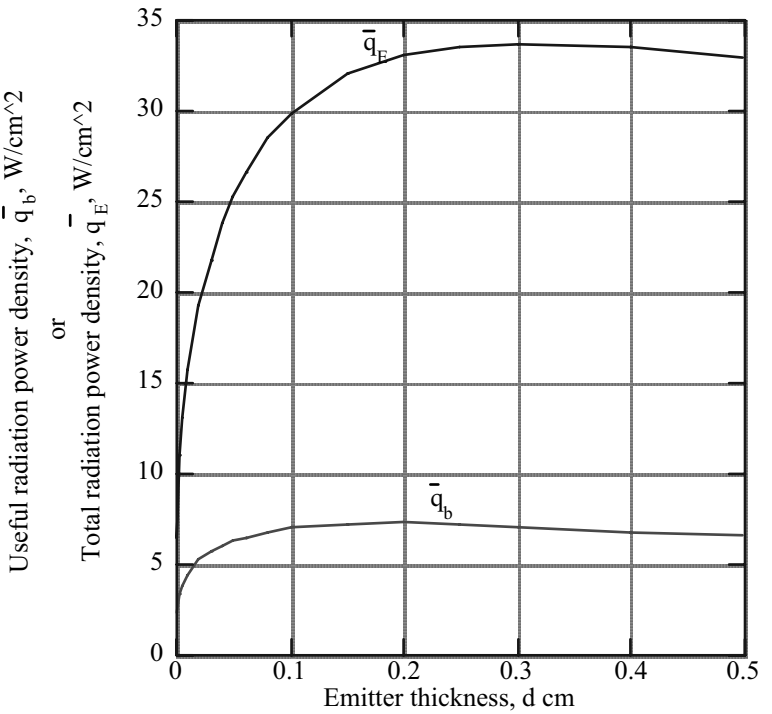

Figure 3.19b) - Useful power and total power of erbium aluminum garnet(EAG) planar emitter with dielectric gap between emitter and Pt substrate as a function of emitter thickness, d at substrate temperature, T_s=1700K. Extinction coefficient, K , taken from Fig. 3.4 and index of refraction from [19]. Results based on PV cell bandgap energy E_g=.72eV(1722 nm). Emission into a vacuum(n_o=1) and values of n_{sR} and n_{sI} for Pt taken from ref. 20.

For the planar film emitter, the temperature change across the emitter is a major factor in determining the emissive behavior of the emitter. As discussed in Section 3.8.3, the primary variables for determining the spectral emittance, ε, are the optical depth, κ_d = Kd, and the temperature change, ΔT. As d increases, both κ_d and ΔT increase. However, increasing κ_d results in an increase in ε, but increasing ΔT results in a decrease in ε. In the case of an emission band where κ_d is large, the spectral emittance is nearly independent of κ_d and is exponentially dependent on ΔT [equation (3.127)]. Thus, the emitter efficiency behavior at constant T_s, which depends upon the spectral emittance in the emission bands, will be determined by ΔT. As a result, the

efficiency decreases with increasing d. Competition between ΔT and κ_d in determining the emittance behavior as a function of d also accounts for both $\bar{q}_b$ and $\bar{q}_E$ having maximum values.

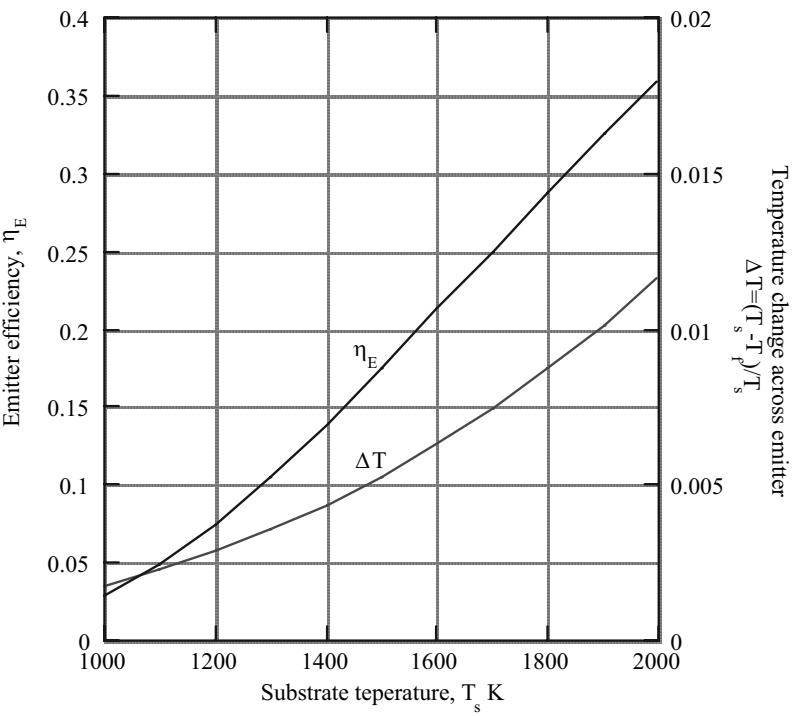

Figure 3.20a) - Emitter efficiency, η_E and temperature change, ΔT, of erbium aluminum garnet(EAG) planar emitter with dielectric gap between emitter and Pt substrate as a function of substrate temperature,T_s, for emitter thickness, d=.05 cm. Extinction coefficient K, taken from Fig. 3.4 and index of refraction from [19], n_o=1. Results based on PV cell bandgap energy, E_g=.72eV(1722 nm).

Now consider the performance of the EAG emitter as a function of the temperature, T_s. Choose the emitter thickness to be d = .05cm, where $\bar{q}_b$ = 6.3 W/cm^2 at T_s = 1700K. This value of $\bar{q}_b$ is close to the maximum $\bar{q}_b$ = 7.3 W/cm^2 and yields an efficiency, η_E = .25. With these conditions calculate η_E, ΔT, $\bar{q}_b$, and $\bar{q}_E$ as a function of T_s. The results are shown in Figure 3.20. The calculation procedure is similar to that used to determine η_E, ΔT, $\bar{q}_b$, and $\bar{q}_E$ shown in Figure 3.19.

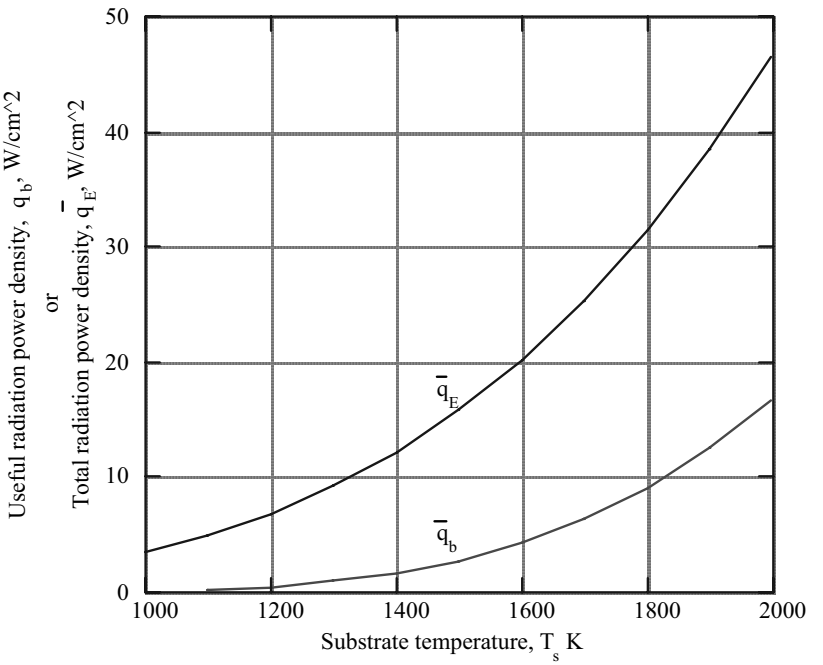

Figure 3.20b) - Useful power and total power of erbium aluminum garnet(ErAG) planar emitter with dielectric gap between emitter and Pt substrate as a function of substrate temperature, T_s for emitter thickness, d=.05 cm. Extinction coefficient K, and index of refraction, n_r, for ErAG taken from Fig. 3.4, n_o=1. Results based on PV cell bandgap energy, E_g=.72eV(1722 nm).

Similar to the results for the constant temperature cylindrical emitter, $\bar{q}_E$ and $\bar{q}_b$ increase rapidly as a result of increasing T_s. For $T_s > 1200K$, η_E is nearly a linear function of T_s, similar to the cylindrical emitter (Figure 3.17). Compare the planar emitter results for $\bar{q}_E$ and $\bar{q}_b$ with the cylindrical emitter results in Figure 3.17. Both show a rapid increase as a result of increasing temperature. However, the magnitudes of $\bar{q}_E$ and $\bar{q}_b$ are much greater for the planar emitter. The greater magnitudes for the planar emitter occur because thermal conduction exists for the planar emitter but does not exist for the cylindrical emitter.

In Figure 3.21, the useful emittance, ε_b, and the total emittance, ε_T, are shown as functions of the substrate temperature, T_s. Compare these results with the cylindrical results shown in Figure 3.18. Notice that $\varepsilon_b > \varepsilon_T$ for $T_E > 1300K$ for the cylindrical

emitter, but $\varepsilon_b < \varepsilon_T$ for all T_s for the planar emitter. Also, the magnitudes for ε_b and ε_T are greater for the planar emitter.

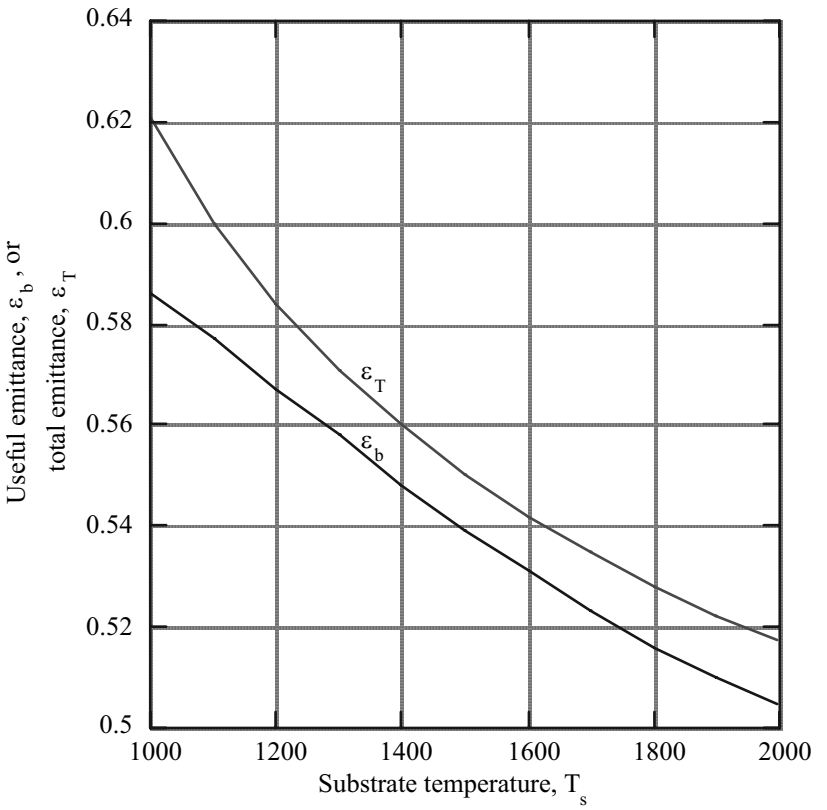

Figure 3.21 - Useful emittance, ε_b, and total emittance, ε_T, of planar EAG selective emitter of thickness, d=.05 cm for the same conditions as Figures 3.19 and 3.20.

3.11 Comparison of Selective Emitters and Gray Body Emitters

At the same temperature, compare the efficiency results for a gray body emitter when E_g=.72eV (Figure 3.12) with the cylindrical (Figure 3.17), or planar (Figure 3.20) EAG selective emitter. The efficiency for the EAG cylindrical emitter is slightly higher than η_E for the gray body emitter, but η_E for the planar emitter is slightly lower than η_E for the gray body emitter. As a result, it might be concluded that there is no advantage to the ErAG selective emitter. However, two other selective emitter properties, besides

efficiency, are advantageous. First, the spectral emittance of a selective emitter can be better matched to the spectral response of the PV array. As a result, the PV efficiency will be higher than with a gray body emitter. Second, the nonconvertible radiation flux, $\overline{q}_L = \overline{q}_E - \overline{q}_b$, in most cases, will be smaller for a selective emitter than for a gray body emitter operating at the same temperature. As pointed out earlier, large values of nonconvertible radiation presents a waste heat removal problem for a TPV system.

Using equation (3.171) for $\overline{q}_E$ and equation (3.170) for $\overline{q}_b$, the nonconvertible radiation flux, $\overline{q}_L$, can be written as follows.

$$\overline{q}_L = \overline{q}_E - \overline{q}_b = \varepsilon_T\left(T_E\right)\sigma_{sb}T_E^4\left(1-\eta_E\right) \tag{3.183}$$

Therefore, for a selective emitter system with nonconvertible flux, $\overline{q}_{Ls}$, and a gray body system with nonconvertible flux, $\overline{q}_{Lg}$, the following result is obtained if both systems are at the same temperature.

$$\frac{\overline{q}_{Ls}}{\overline{q}_{Lg}} = \frac{\varepsilon_{Ts}\left(T_E\right)}{\varepsilon_g}\left(\frac{1-\eta_{Es}}{1-\eta_{Eg}}\right) \tag{3.184}$$

Here ε_{Ts} is the total emittance of the selective emitter system that is a function of T_E, and ε_g is the gray body emittance that is a constant. The efficiency of the selective emitter is η_{Es} and η_{Eg} and is the gray body emitter efficiency. Thus, if $\varepsilon_{Ts}(T_E) < \varepsilon_g$ the selective emitter system has a smaller nonconvertible radiation flux than a gray body system operating at the same temperature if $\eta_{Es} \geq \eta_{Eg}$.

As mentioned earlier, η_{Es} for the EAG selective emitter is nearly the same as η_{Eg} for a gray body emitter. In that case, equation (3.184) yields the following.

$$\frac{\overline{q}_{Lg}}{\overline{q}_{Ls}} \approx \frac{\varepsilon_g}{\varepsilon_{Ts}\left(T_E\right)} \tag{3.185}$$

A black body ($\varepsilon_g = 1$) produces the largest useful power, $\overline{q}_b$. Therefore, comparing the cylindrical EAG emitter (Figure 3.20) with a black body, $\overline{q}_{Lg} > 5\overline{q}_{Ls}$ at $T_E = 2000K$ and $\overline{q}_{Lg} > 3\overline{q}_{Ls}$ at $T_E = 1000K$. Similarly, comparing the planar EAG emitter (Figure 3.21) with a black body we see that $\overline{q}_{Lg} > 1.9\overline{q}_{Ls}$ at $T_s = 2000K$ and $\overline{q}_{Lg} > 1.6$ at $T_s = 1000K$. A filter TPV system utilizing a black body emitter has a significantly greater amount of nonconvertible radiation than a selective emitter system. Therefore, if the

filter has any absorptance, the black body system will have a large amount of waste heat compared to a selective emitter system.

3.12 Summary

Emitters can be split into two groups; gray body emitters that have a nearly constant spectral emittance and selective emitters that have a widely varying spectral emittance. Silicon carbide (SiC) is a gray body emitter with large emittance, $\varepsilon(\lambda)$, while platinum (P_T) is gray body emitter with low emittance. The unique atomic structure of rare earth ions such as ytterbium (Yb^{+++}), erbium (Er^{+++}), thulium ($T_M{}^{+++}$), holmium (Ho^{+++}), and neodymium (Nd^{+++}) in high temperature materials such as $ReAl_5O_{12}$, where Re is a rare earth, result in selective emission in the near infrared. Also, application of an antireflection coating on a metal can produce increased emittance in a desired region of the spectrum. An alumina (Al_2O_3) film on tungsten (W) can significantly increase the W emittance in a desired region of the spectrum. Recent development of grating and photonic-crystal emitters made of tungsten produce emission bands in the near infrared.

Using the conservation of energy and radiative transfer equations and classical electromagnetic theory results for reflectivity developed in Chapter 1, expressions for the spectral emittance, $\varepsilon(\lambda)$, for planar and cylindrical materials are derived. Significant results from that development are the following.

1) For small radius ($\leq$ 1mm) a cylindrical emitter can be assumed to operate at a constant temperature, whereas the temperature of a planar emitter of small thickness ($\leq$ 1mm) can be assumed to vary linearly across the thickness.
2) The material properties that determine $\varepsilon(\lambda)$ are the indices of refraction of the emitting material, n_f, and the surroundings, n_o, and the extinction coefficient, $K(\lambda)$, of the emitting material.
3) Two main parameters determine $\varepsilon(\lambda)$. One is the optical depth, κ, which is the product of the extinction coefficient and the dimension of the emitting material. The other is the temperature change across the emitting material, ΔT. Increasing κ causes an increase in $\varepsilon(\lambda)$ while increasing ΔT results in a decrease in $\varepsilon(\lambda)$. As a result, for a planar emitter there is an optimum thickness for maximum $\varepsilon(\lambda)$.
4) For a planar emitter, in regions of the spectrum where the optical depth, $\kappa_d \gg 1$, such as an emission band of a selective emitter, $\varepsilon(\lambda) \sim e^{-u\Delta T}$, where $u = \dfrac{hc_o}{\lambda k T_s}$. In regions where $\kappa_d \ll 1$, $\varepsilon(\lambda)$ is independent of ΔT.
5) Scattering of radiation, which may be important for polycrystalline materials, reduces $\varepsilon(\lambda)$ a small amount.

Emitter efficiency, η_E, which is the ratio of the emitted radiation, $\overline{q}_b$, with photon energies greater than the PV cell bandgap energy, E_g, to the total emitted radiation, $\overline{q}_E$, is a sensitive function the emitter temperature, T_E. The emitted radiation that cannot be converted to electrical energy ($\overline{q}_E - \overline{q}_b$) is significantly greater for a black body emitter than for a selective emitter.

Other factors besides performance may be the determining factors in choosing what type emitter to use in a TPV system. Two of the most important of these factors are durability and cost. Durability will be determined by the chemical stability and evaporation rate of the emitter material at high temperature. Chemical stability and evaporation rate data will be required to evaluate emitter materials before a successful TPV system can be developed. Determining the cost of new selective emitter materials is not yet possible. However, for gray body emitters such as tungsten and silicon carbide, cost information is available.

References

[1] Y. S. Touloukian, and D. P DeWitt, Thermophysical Properties of Matter, vol 7, Thermal Radiative Properties, Metallic Elements and Alloys, Plenum Press, New York, 1970.

[2] U. C. Pernisz, and C. K. Saha, proceedings of the First NREL Conference on Thermophotovoltaic Generation of Electricity, AIP Conference Proceedings 321, (1995), 99.

[3] R. Lowe, C. Goradia, M. Goradia, and D. L. Chubb, J. Appl. Phys., 68, (1990) 5033.

[4] G. Torsello, M. Lomascolo, A. Licciulli, D. Diso, S. Tundo, and M. Mazzer, Nature Materials, 3, (2004), 632.

[5] B. G. Wybourne, Spectroscopic Properties of Rare Earths, Interscience, New York, 1965.

[6] G. H. Dieke, Spectra and Energy Levels of Rare Earths, Interscience, New York, 1968.

[7] G. E. Guazzoni, Appl. Spectrosc, 26, (1972) 60.

[8] R. E. Nelson, Proc. 32 International Power Sources Symposium (Electrochemical Society, Pennington, NJ), (1986), 95.

[9] C. R. Parent, and R. E. Nelson, Proc. 21st Intersociety Energy Conversion Engineering Conf. (IECEC), (American Chemical Society, Washington, DC, vol. 2, (1986), 1314.

[10] L. Ferguson, and L. Fraas, proceedings of the Third NREL Conference on Thermophotovoltaic Generation of Electricity, AIP Conference Proceedings 401, (1997), 169.

[11] C. J. Crowley, N. A. Elkouh, and P. J. Magari, proceedings of the Fourth NREL Conference on Thermophotovoltaic Generation of Electricity, AIP Conference Proceedings, 460, (1999), 197.

[12] L. G. Ferguson, and F. Dogan, Materials Science and Engineering B83, (2001), 35.

[13] L. Fraas, J. Samaras, J. Avery, and L. Minkin, proceedings of the 28th IEEE Photovoltaic Specialists Conference, (2000), 1020.

[14] A. Heinzel, V. Boerner, A. Gombert, B. Blasi, V. Wittwer, and J. Luther, J. of Modern Optics, 47, (2000), 2399.

[15] C. Schlemmer, J. Aschaber, V. Boerner, and J. Luther, in Proceedings of 5th NREL Conference on Thermophotovoltaic Generation of Electricity, AIP Conference Proceedings 653, (2003), 164.

[16] S. Y. Lin, J. G. Fleming, E. Chow, and J. Bur, Phys. Rev. B, Condensed Matter and Materials Physics, 62, (2000), R2243.

[17] S. Y. Lin, J. Moreno, and J. G. Fleming, Appl. Phys. Lett., 83, (2003). 380.

[18] D. L. Chubb, D. S. Wolford, A. Meulenberg, and R. S. DiMatteo, 5th NREL Conference on Thermophotovoltaic Generation of Electricity, AIP Conference Proceedings 653, (2003), 174.

[19] D. L. Chubb, A. T. Pal, M. O. Patton, and P. P. Jenkins, European Journal of Ceramic Materials, 19, (1999), 2551.

[20] Handbook of Chemistry and Physics, 71st ed., 1990-1991, edited by D. R. Lide, 12.

Problems

3.1 At a given emitter temperature, T_E, a TPV system that uses a black body emitter will produce the maximum power output. Compare the emitter efficiencies, η_E, [equation (3.175)] and useful power outputs, $\overline{q}_b$, [equation (3.173)] for emission into a vacuum ($n_o = 1.0$) of a black body emitter at $T_E = 1500K$ when $\lambda_g = 1720nm$ (GaSb) and when $\lambda_g = 1110nm$ (Si). What conclusions can be made? (Hint: use results of problem 1.14.)

3.2 Present a qualitative argument based on the spectral emittance data shown in Figure 3.1, for silicon carbide (SiC) and tungsten (W), to determine which material will yield the larger emitter efficiency if $\lambda_g \leq 1700nm$.

3.3 Solve equations (3.45) and (3.59) for $q^-(\kappa_d)$ and $q^+(0)$. Use those results in equation (3.28) to obtain equation (3.63) for $q(\kappa,\lambda)$ for a planar emitter with a dielectric gap between the emitter and substrate.

3.4 Use equations (3.63) and (3.69) to obtain the spectral emittance, $\varepsilon(\lambda)$, for a planar emitter with a dielectric gap between the emitter and substrate [equation (3.83)] and for a planar emitter with a deposited substrate [equation (3.90)].

3.5 Evaluate the source function integrals $\overline{\phi}_+(\kappa_d)$, $\overline{\phi}_-(0)$, $\overline{\phi}_{M+}(\kappa_d)$, and $\overline{\phi}_{M-}(\kappa_d)$, given by equations (3.84) through (3.87) for the case of uniform temperature and no scattering. Show that they are all monotonically increasing functions of the optical depth, κ_d.

3.6 In the expressions for the spectral emittance, $\varepsilon(\lambda)$, given by equations (3.83) and (3.90) neglect the external source term. In that case the terms proportional to h_- represent the contribution to $\varepsilon(\lambda)$ resulting from the radiation from the substrate plus the radiation reflected at the film-substrate interface. For the case where $n_f \approx n_o$, the emitter temperature is uniform and scattering is negligible obtain an equation for the optical depth, κ_d, that will maximize the terms proportional to h_- in equations (3.83) and (3.90). Also, show that these

terms will be monotonically decreasing functions of κ_d if $\frac{\tau_{fs}\varepsilon'_{son}}{\bar{\rho}_{fs}} > 1$ in equation (3.83) and $\frac{\varepsilon_{fsn}}{\bar{R}_{fs}} = \frac{1-\bar{R}_{fs}}{\bar{R}_{fs}} > 1$ in equation (3.90).

3.7 For a planar emitter at constant temperature ($\Delta T = 0$), with a deposited metal substrate with index of refraction, $n_{sR} + n_{sI}$, no external source ($r = s = 0$), optical depth, κ_d, index of refraction, n_f, and no scattering emitting into a dielectric with index of refraction, n_o, show that the spectral emittance, $\varepsilon(\lambda)$, is given by the following equation.

$$\varepsilon(\lambda) = \frac{\left(1-\bar{R}_{fo}\right)\left[1-4\bar{R}_{fs}E_3^2\left(\kappa_d\right)\right]}{1-4\bar{R}_{fs}E_3\left(\kappa_d\right)\left[\bar{R}_{fo}E_3\left(\kappa_d\right)+\mu_M^2\left(1-\bar{R}_{fo}\right)E_3\left(\frac{\kappa_d}{\mu_M}\right)\right]}$$

Where,

$$\mu_M^2 = 1-\left(\frac{n_o}{n_f}\right)^2$$

$$\bar{R}_{fo} = \left(\frac{n_f-n_o}{n_f+n_o}\right)^2$$

$$\bar{R}_{fs} = \frac{\left(n_{sR}-n_f\right)^2+n_{sI}^2}{\left(n_{sR}+n_f\right)^2+n_{sI}^2}$$

3.8 The spectral emittance, $\varepsilon(\lambda)$, for a planar emitter is given by equation (3.83) for the case where a dielectric gap exists between the substrate and emitter and by equation (3.90) for the case of no dielectric gap. For both cases, where there is no external source ($r = s = 0$), show that $\varepsilon(\lambda) \approx 0$ for an emitter material where $n_f >> n_o$, ($\mu_M \approx 1$). In other words, all radiation is trapped within the emitter.

3.9 For the case of no scattering ($\Omega = 0$), small temperature change, $\Delta T \ll 1$, and large dimensionless photon energy, u_s, show the integral functions, $\bar{\phi}_+\left(\kappa_d\right)$, $\bar{\phi}_-\left(0\right)$, $\bar{\phi}_{M+}\left(\kappa_d\right)$, and $\bar{\phi}_{M-}\left(\kappa_d\right)$, given by equations (3.106) through (3.109)

reduce to equations (3.110) through (3.114). [Hint: make use of the relation $E_{n-1}(x) = -\frac{dE_n(x)}{dx}$].

3.10 For the case of no scattering ($\Omega = 0$), small temperature change, $\Delta T \ll 1$, and small dimensionless photon energy, $u_s \ll 1$, show that the integral functions, $\bar{\phi}_+(\kappa_d)$, $\bar{\phi}_-(0)$, $\bar{\phi}_{M+}(\kappa_d)$, and $\bar{\phi}_{M-}(\kappa_d)$, given by equations (3.106) through (3.109) reduce to those given by equations (3.115) through (3.118).
[Hint: make use of the relation $xE_n(x) = e^{-x} - nE_{n+1}(x)$].

3.11 Evaluate equation (3.155) at $\kappa = \kappa_R$ in order to arrive at the emittance for a cylinder as given by equation (3.158).

3.12 Show that the spectral emittance for a cylinder at constant temperature [equation (3.158)] reduces to equation (3.165) if scattering is neglected.

3.13 For a gray body emitter at temperature, T_E, with spectral emittance, ε_g, show that the emitted radiation flux that is not convertible to electrical energy by a PV array with bandgap energy, E_g, ($E < E_g$) is the following.

$$\bar{q}_L = n_o^2 \varepsilon_g \sigma_{sb} T_E^4 (1 - \eta_E)$$

Where η_E is the emitter efficiency [equation (3.175)]. Assume a tungsten emitter can be approximated as a gray body with $\varepsilon_g = 0.3$. Calculate $\bar{q}_L$ for tungsten with $E_g = 0.72$eV at $T_E = 1700$K emitting in vacuum ($n_o = 1$), and compare that with $\bar{q}_L$ for a blackbody emitter at the same conditions.

3.14 For no scattering, constant temperature and index of refraction, $n_f = 1$, show that the spectral emittances, $\varepsilon(\lambda)$ for a planar emitter with a deposited metal substrate and a cylindrical emitter emitting into a vacuum, ($n_o = 1$), are the following.

$$\varepsilon(\lambda) = 1 - 4\bar{R}_{fs} E_3^2(\kappa_d) \qquad \text{planar}$$

$$\varepsilon(\lambda) = 1 - 4E_3^2(\kappa_R) \qquad \text{cylindrical}$$

Where $\bar{R}_{fs}$ is the reflectance at the film-substrate interface, $\kappa_d = K(\lambda)d$ is the optical depth of the planar emitter of thickness, d, and $\kappa_R = K(\lambda)R$ is the optical depth of the cylindrical emitter of radius R.

This page intentionally left blank

Chapter 4
Optical Filters for Thermophotovoltaics

As pointed out in Chapter 2, spectral control is a major factor in attaining high efficiency for a TPV energy converter. Placing an optical filter between the emitter and PV array is one method of spectral control. To achieve high TPV system efficiency, the filter must have low absorptance. It must have large transmittance in the useful photon energy region (photon energy, E, greater than the PV cell bandgap energy, E_g, or $\lambda < \lambda_g = \frac{hc_o}{E_g}$) and large reflectance outside this region ($E < E_g$ or $\lambda > \lambda_g$).

In this chapter several types of filters that are applicable to TPV energy conversion are discussed. These include dielectric interference filter, plasma filters, and resonant array filters. Also, spectral control can be achieved using a back side reflector (BSR) on the PV array.

4.1 Symbols

a	absorption coefficient, cm^{-1}
e	electron charge, (1.602×10^{-19} Coul)
E	electric field, V/m or photon energy, J
$\vec{E}^t$	electric field for wave traveling in +z direction
$\vec{E}^r$	electric field for wave traveling in -z direction
H	magnetic field, Amp/m
h	Plank's constant (6.624×10^{-34} J-sec)
k	magnitude of wave vector, m^{-1} or Boltzmann constant (1.38×10^{-23} J/K)
$\vec{k}^t$	wave vector for wave traveling in +z direction
$\vec{k}^r$	wave vector for wave traveling in -z direction
$\hat{k}$	magnitude of wave vector given by equations (1.37) and (4.38)
m*	effective mass, kg
m_e	electron mass, (9.107×10^{-31} kg)
n	index of refraction
t	internal transmittance
v	velocity, m/sec
α	absorptance
ε	permittivity ($amp^2\ sec^4/kg\ m2$)
$\bar{\varepsilon}$	complex dielectric constant

ε_o	vacuum permittivity (8.855×10^{-12} Amp^2 sec^4/kg m2)
λ	wavelength, nm
η	efficiency
μ	mobility, cm^2/V sec or magnetic permeability
μ_o	magnetic permeability of vacuum (1.2556 m kg/sec^2 Amp^2)
ρ	reflectance
τ	transmittance
τ_c	collision time, sec

4.2 Filter Performance Parameters

The performance of a filter will be determined by the transmittance, τ_f, reflectance, ρ_f, and absorptance, α_f, as well as an efficiency, η_f, yet to be defined. In Section 1.7 the total optical properties are defined. Define the filter efficiency as follows.

$$\eta_f \equiv \frac{\text{transmitted radiation that can be converted to electrical energy by PV array}}{\text{total radiation incident on the filter - total radiation reflected by the filter}} \equiv \frac{\text{transmitted radiation that can be converted to electrical energy by PV array}}{\text{total radiation transmitted and absorbed by filter}} \tag{4.1}$$

$$\eta_f = \frac{\int_o^{\lambda_g} \tau_f(\lambda) q_i d\lambda}{\int_o^{\infty} \left[1-\rho_f(\lambda)\right] q_i d\lambda} = \frac{\int_o^{\lambda_g} \tau_f(\lambda) q_i d\lambda}{\int_o^{\infty} \left[\tau_f(\lambda)+\alpha_f(\lambda)\right] q_i d\lambda} \tag{4.2}$$

Where q_i is the incident radiation flux (W/cm^2 nm) and $\lambda_g = \frac{hc_o}{E_g}$ is the wavelength that corresponds to the PV array bandgap energy, E_g. The incident radiation flux, q_i, depends upon the emittance, ε_E, and temperature, T_E, of the emitter, as well as, a factor, F_c, that depends upon the geometry and optical properties of the cavity that contains the emitter and PV array.

$$q_i = F_c \varepsilon_E(\lambda) e_b(\lambda, T_E) \tag{4.3}$$

The term $e_b(\lambda,T_E)$ is the blackbody emissive power [equation (1.127)]. Since the factor, F_c, depends upon the optical properties of the cavity, it is also λ dependent. For the present, neglect the λ dependence of F_c. When discussing the total system efficiency in later chapters, the optical properties of the cavity are included. Therefore, neglecting the λ dependence of F_c results in the following.

$$\eta_f(T_E, \lambda_g) = \frac{\int_o^{\lambda_g} \varepsilon_E(\lambda) \tau_f(\lambda) e_b(\lambda, T_E) d\lambda}{\int_o^{\infty} \varepsilon_E(\lambda) \left[\tau_f(\lambda)+\alpha_f(\lambda)\right] e_b(\lambda, T_E) d\lambda} \tag{4.4a}$$

$$\eta_f\left(T_E,\lambda_g\right)=\frac{\int_0^{\lambda_g}\varepsilon_E\left(\lambda\right)\tau_f\left(\lambda\right)e_b\left(\lambda,T_E\right)d\lambda}{\int_0^{\infty}\varepsilon_E\left(\lambda\right)\left[1-\rho_f\left(\lambda\right)\right]e_b\left(\lambda,T_E\right)d\lambda} \tag{4.4b}$$

If the emitter emittance is independent of λ, which is the case for a blackbody, then ε_E will cancel out in equations (4.4a) and (4.4b).

Again assuming F_c is independent of λ, the total transmittance, reflectance, and absorbtance, as defined in Section 1.7, are the following.

$$\tau_{fT}\left(T_E\right)=\frac{\int_0^{\infty}\varepsilon_E\left(\lambda\right)\tau_f\left(\lambda\right)e_b\left(\lambda,T_E\right)d\lambda}{\int_0^{\infty}\varepsilon_E\left(\lambda\right)e_b\left(\lambda,T_E\right)d\lambda} \tag{4.5}$$

$$\rho_{fT}\left(T_E\right)=\frac{\int_0^{\infty}\varepsilon_E\left(\lambda\right)\rho_f\left(\lambda\right)e_b\left(\lambda,T_E\right)d\lambda}{\int_0^{\infty}\varepsilon_E\left(\lambda\right)e_b\left(\lambda,T_E\right)d\lambda} \tag{4.6}$$

$$\alpha_{fT}\left(T_E\right)=\frac{\int_0^{\infty}\varepsilon_E\left(\lambda\right)\alpha_f\left(\lambda\right)e_b\left(\lambda,T_E\right)d\lambda}{\int_0^{\infty}\varepsilon_E\left(\lambda\right)e_b\left(\lambda,T_E\right)d\lambda} \tag{4.7}$$

It can be shown (problem 4.13) that,

$$\eta_f\approx\frac{\tau_{fT}}{\tau_{fT}+\alpha_{fT}} \tag{4.8}$$

If $\dfrac{\int_{\lambda_g}^{\infty} \varepsilon_E(\lambda)\tau_f(\lambda)e_b(\lambda,T_E)\,d\lambda}{\int_{o}^{\infty} \varepsilon_E(\lambda)e_b(\lambda,T_E)\,d\lambda} \ll \tau_{fT}$. Thus, if $\tau_f(\lambda) \approx 0$ for $\lambda > \lambda_g$, then η_f can be approximated by equation (4.8).

4.3 Interference Filters

4.3.1 Introduction

The objective of this section is to develop the analysis necessary to calculate the spectral reflectance, transmittance, and absorbtance of an interference filter. Such an analysis is available in several references [1-4]. However, to maintain the self-contained principle of this text, the detailed analysis is presented in a manner similar to that in reference [3]. Although the physics of interference is easily explained, the analysis to calculate the optical properties of an interference filter is somewhat tedious.

4.3.2 Interference

In Section 1.5.1 it was shown that for a linear, homogeneous, stationary, isotropic medium with no space charge, the electric field is determined by a linear second order partial differential equation [equation (1.17)] known as the wave equation. Solutions to this equation are harmonic plane waves given by equation (1.10). A characteristic of plane waves is that they can interact to increase or decrease the electromagnetic field. This process is called *interference*. Using interference, it is possible to produce optical bandpass filters that have large transmission in a specified region of the spectrum and large reflectance outside that region. Obviously, such a device has application as a spectral control component of a TPV energy conversion system.

Interference is achieved by controlling the path length of the plane waves and the wave vector, k, or index of refraction, $n = \dfrac{\lambda}{2\pi}k$, of the media. Therefore, an interference filter consists of layers of thin films with the indices of refraction changing between adjacent layers. The film thicknesses are selected to give the desired optical path lengths.

Interference of plane waves can be demonstrated in the following manner. Suppose there is a phase difference, $k\delta$, or path length difference, δ, between plane wave $\vec{E}_a$ and plane wave $\vec{E}_b$. Thus, from equation (1.10b) for both waves moving in the +z direction,

$$\vec{E}_a = \vec{a}e^{j(\omega t - kz)} \tag{4.9}$$

$$\vec{E}_b = \vec{b}e^{j\left[\omega t - k(z+\delta)\right]} \tag{4.10}$$

and the sum is the following.

$$\vec{E}_a + \vec{E}_b = e^{j(\omega t - kz)}\left[\vec{a} + \vec{b}e^{-jk\delta}\right] \tag{4.11}$$

Now, let $k\delta = m\pi$, where m is a constant. Therefore,

$$\vec{E}_a + \vec{E}_b = e^{j(\omega t - kz)}\left[\vec{a} + \vec{b}e^{-jm\pi}\right] = e^{j(\omega t - kz)}\left[\vec{a} + \vec{b}\left(\cos m\pi - j\sin m\pi\right)\right] \tag{4.12}$$

Thus, if m is an even integer,

$$\vec{E}_a + \vec{E}_b = \left(\vec{a} + \vec{b}\right)e^{j(\omega t - kz)} \qquad m = 0, 2, 4, 6... \tag{4.13}$$

and if m is an odd integer.

$$\vec{E}_a + \vec{E}_b = \left(\vec{a} - \vec{b}\right)e^{j(\omega t - kz)} \qquad m = 1, 3, 5, 7... \tag{4.14}$$

Equation (4.13), where the wave amplitudes add, is a case of *constructive interference*, and equation (4.14), where the amplitudes subtract, is a case of *destructive interference*. Remember, the actual electric field is the real part of equation (4.13) or (4.14).

As just shown, for interference to occur, the following condition must be satisfied in terms of the wavelength, λ, and index of refraction, n.

$$k\delta = \frac{2\pi}{\lambda}n\delta = m\pi \tag{4.15}$$

or

$$\delta = \frac{m}{2}\frac{\lambda}{n} \tag{4.16}$$

where m is an integer. If m = 0, 2, 4..., constructive interference occurs, and if m = 1, 3, 5..., destructive interference occurs.

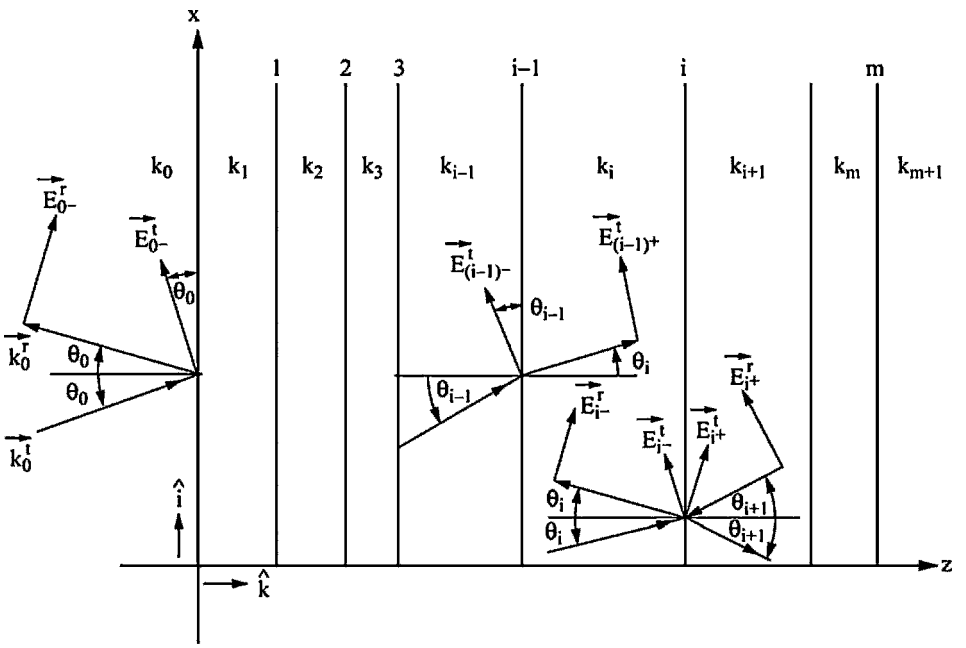

Figure 4.1.—Notation used for multi-layer interference filter model.

4.3.3 Interference Filter Model

Figure 4.1 shows the notation used for the multi-later interference filter model. The ith layer is characterized by its wave vector, $k_i = \frac{2\pi n_i}{\lambda}$, where n_i is the index of refraction, which is complex if the layer is absorbing, and λ is the vacuum wavelength. Also, the ith layer lies between the i – 1 and i interfaces, as shown in Figure 4.1. The last layer, m, is the substrate which will be some transparent material such as quartz or sapphire. Surrounding the filter is the medium, k_o, which in most cases is vacuum $\left(k_o = \frac{2\pi}{\lambda}\right)$.

Light enters the filter at z = 0 at some given angle of incidence, θ_o. Since Snell's Law [equation (1.56)] must be satisfied at each interface, the following condition applies.

$$n_0 \sin\theta_0 = n_1 \sin\theta_1 = n_2 \sin\theta_2 \ldots \quad = n_i \sin\theta_i \tag{4.17}$$

If n_i is complex, then θ_i must also be complex and θ_i is not the angle of incidence at the ith interface or the refraction angle at the (i – 1) interface. To satisfy both Snell's Law and the law of reflection [equation (1.55)], the reflected light leaving the film at z = 0 is also at angle θ_o.

As discussed in Section 1.5.5, the direction of the electric field for so-called natural light encountered in a TPV system is random. Therefore, the intensity is the average of the p (electric field in the plane of incidence) polarized intensity and the s (electric field perpendicular to the plane of incidence) polarized intensity. As a result, both p and s polarization must be included in the model.

Within each layer of the filter, the electric field is the sum of plane waves traveling in the +z and -z directions. Therefore, in the ith layer the electric field is the following,

$$\begin{aligned}\vec{E}(x,z,t) &= \vec{E}(x,z)e^{j\omega t} = \vec{E}_i^{+}e^{j\left(\omega t-\vec{k}_i\bullet\vec{r}+\alpha_i\right)} + \vec{E}_i^{-}e^{j\left(\omega t+\vec{k}_i\bullet\vec{r}+\beta_i\right)} \\ &= \left\{\vec{E}_i^{+}e^{j\left[-k_i\left(x\sin\theta_i+z\cos\theta_i\right)+\alpha_i\right]} + \vec{E}_i^{-}e^{j\left[k_i\left(x\sin\theta_i+z\cos\theta_i\right)+\beta_i\right]}\right\}e^{j\omega t}\end{aligned} \tag{4.18}$$

where $\vec{E}_i^{+}$, $\vec{E}_i^{-}$, α_i, and β_i are constants that are determined by boundary conditions. Equation (4.18) applies to both s and p polarization with the constant vectors $\vec{E}_i^{+}$ and $\vec{E}_i^{-}$ giving the direction of polarization. For plane waves the magnetic field is given by equation (1.34).

$$\begin{aligned}\vec{H}(x,z,t) &= \vec{H}(x,z)e^{j\omega t} = \frac{1}{\omega\mu_i}\left[\vec{k}_i\times\vec{E}\right] \\ &= \frac{e^{j\omega t}}{\omega\mu_i}\left\{\left[\vec{k}_i^{\,t}\times\vec{E}_i^{+}\right]e^{j\left[-k_i\left(x\sin\theta_i+z\cos\theta_i\right)+\alpha_i\right]} + \left[\vec{k}_i^{\,r}\times\vec{E}_i^{-}\right]e^{j\left[k_i\left(x\sin\theta_i+z\cos\theta_i\right)+\beta_i\right]}\right\}\end{aligned} \tag{4.19}$$

The wave vector notation $\vec{k}^{\,t}$ refers to a wave traveling in the +z direction and $\vec{k}^{\,r}$ to a wave traveling the -z direction. To determine the constants, boundary conditions on $\vec{E}$ and $\vec{H}$ at each interface must be applied.

To simplify the algebra in the application of the boundary conditions make the following definitions of the electric fields at an interface, i. For the plane wave moving in the +z direction on the – side of interface i ($z = z_i$),

$$\vec{E}_{i-}^{\,t} = \vec{E}_i^{+}e^{j\left[-k_i\left(x\sin\theta_i+z_i\cos\theta_i\right)+\alpha_i\right]} \tag{4.20}$$

and for a plane wave moving in the –z direction on the – side of interface i,

$$\vec{E}_{i-}^{\,r} = \vec{E}_i^{-} e^{j\left[k_i\left(x\sin\theta_i + z_i\cos\theta_i\right)+\beta_i\right]} \tag{4.21}$$

The superscript t denotes a wave moving in the +z direction (the transmitted direction) and the superscript r denotes a wave moving in the -z direction (the reflected direction). Similarly, for plane waves moving in the ±z directions on the + side of interface i – 1 ($z = z_{i-1}$) make the following definitions.

$$\vec{E}_{(i-1)+}^{\,t} = \vec{E}_i^{+} e^{j\left[-k_i\left(x\sin\theta_i + z_{i-1}\cos\theta_i\right)+\alpha_i\right]} \tag{4.22}$$

$$\vec{E}_{(i-1)+}^{\,r} = \vec{E}_i^{-} e^{j\left[k_i\left(x\sin\theta_i + z_{(i-1)}\cos\theta_i\right)+\beta_i\right]} \tag{4.23}$$

From equations (4.20) and (4.22) the following is obtained,

$$\vec{E}_{(i-1)+}^{\,t} = \vec{E}_{i-}^{\,t} e^{j\phi_i} \tag{4.24}$$

$$\vec{E}_{(i-1)+}^{\,r} = \vec{E}_{i-}^{\,r} e^{j\phi_i} \tag{4.25}$$

where

$$\boxed{\phi_i = k_i\left(z_i - z_{i-1}\right)\cos\theta_i = \frac{2\pi}{\lambda} n_i\left(z_i - z_{i-1}\right)\cos\theta_i} \tag{4.26}$$

is called the *phase thickness* of the ith layer.

Evaluating equation (4.18) on the + and – sides of interface i, using the definitions given by equations (4.20) through (4.23), yields the following results for the electric and magnetic fields on each side of interface i.

$$\vec{E}_{i-}\left(x, z_i^{-}\right) = \left[\vec{E}_{i-}^{\,t} + \vec{E}_{i-}^{\,r}\right] \tag{4.27a}$$

$$\vec{H}_{i-}\left(x, z_i^{-}\right) = \frac{1}{\omega\mu_i}\left[\left(\vec{k}_i^{\,t} \times \vec{E}_{i-}^{\,t}\right) + \left(\vec{k}_i^{\,r} \times \vec{E}_{i-}^{\,r}\right)\right] \tag{4.27b}$$

$$\vec{E}_{i+}\left(x, z_i^{+}\right) = \left[\vec{E}_{i+}^{\,t} + \vec{E}_{i+}^{\,r}\right] \tag{4.28a}$$

$$\vec{H}_{i+}\left(x, z_i^+\right) = \frac{1}{\omega\mu_{i+1}}\left[\left(\vec{k}^t_{i+1} \times \vec{E}^t_{i+}\right) + \left(\vec{k}^r_{i+1} \times \vec{E}^r_{i+}\right)\right] \tag{4.28b}$$

Now apply the boundary conditions at interface i. Neglecting any surface currents at the interface, the tangential E_{tan} and H_{tan} fields must be continuous across the interface [see equations (1.48) and (1.49)]. In calculating the optical properties, the tangential E and H fields are also required to calculate the intensity from the Poynting vector [equation (1.30)]. Both p and s polarization must be considered. For p polarization as shown in Figure 4.1, the boundary condition on the E and H fields at interface i are the following,

$$\left.\begin{aligned} \left(E^t_{i-} + E^r_{i-}\right)\cos\theta &= \left(E^t_{i+} + E^r_{i+}\right)\cos\theta_{i+1} && (4.29)\\ \frac{k_i}{\mu_i}\left(E^t_{i-} - E^r_{i-}\right) &= \frac{k_{i+1}}{\mu_{i+1}}\left(E^t_{i+} - E^r_{i+}\right) && (4.30) \end{aligned}\right\} \text{ p polarization}$$

where equations (4.27b) and (4.28b) were used to obtain equation (4.30). For s polarization, $\vec{E}$ is in the +y direction. Therefore, the boundary conditions on E and H are the following.

$$\left.\begin{aligned} E^t_{i-} + E^r_{i-} &= E^t_{i+} + E^r_{i+} && (4.31)\\ \frac{k_i}{\mu_i}\cos\theta_i\left(-E^t_{i-} + E^r_{i-}\right) &= \frac{k_{i+1}}{\mu_{i+1}}\cos\theta_{i+1}\left(-E^t_{i+} + E^r_{i+}\right) && (4.32) \end{aligned}\right\} \text{ s polarization}$$

Solving equations (4.29) and (4.30) for $E^t_{i-}\cos\theta_i$ and $E^r_{i-}\cos\theta_i$, the tangential components of the electric field for p polarization on the – side of interface i, yields the following.

$$\left.\begin{aligned} E^t_{i-}\cos\theta_i &= \frac{1}{2}\left[1 + \frac{\mu_i k_{i+1}\cos\theta_i}{\mu_{i+1} k_i \cos\theta_{i+1}}\right]E^t_{i+}\cos\theta_{i+1} + \frac{1}{2}\left[1 - \frac{\mu_i k_{i+1}\cos\theta_i}{\mu_{i+1} k_i \cos\theta_{i+1}}\right]E^r_{i+}\cos\theta_{i+1} && (4.33)\\ E^r_{i-}\cos\theta_i &= \frac{1}{2}\left[1 - \frac{\mu_i k_{i+1}\cos\theta_i}{\mu_{i+1} k_i \cos\theta_{i+1}}\right]E^t_{i+}\cos\theta_{i+1} + \frac{1}{2}\left[1 + \frac{\mu_i k_{i+1}\cos\theta_i}{\mu_{i+1} k_i \cos\theta_{i+1}}\right]E^r_{i+}\cos\theta_{i+1} && (4.34) \end{aligned}\right\} \text{ p polar-ization}$$

Similarly, solving equations (4.31) and (4.32) for E_{i-}^{t} and E_{i-}^{r}, the tangential components of the electric field for s polarization on the – side of interface i, yields the following.

$$\left.\begin{aligned} E_{i-}^{t} &= \frac{1}{2}\left[1+\frac{\mu_i k_{i+1}\cos\theta_{i+1}}{\mu_{i+1}k_i\cos\theta_i}\right]E_{i+}^{t}+\frac{1}{2}\left[1-\frac{\mu_i k_{i+1}\cos\theta_{i+1}}{\mu_{i+1}k_i\cos\theta_i}\right]E_{i+}^{r} && (4.35)\\ E_{i-}^{r} &= \frac{1}{2}\left[1-\frac{\mu_i k_{i+1}\cos\theta_{i+1}}{\mu_{i+1}k_i\cos\theta_i}\right]E_{i+}^{t}+\frac{1}{2}\left[1+\frac{\mu_i k_{i+1}\cos\theta_{i+1}}{\mu_{i+1}k_i\cos\theta_i}\right]E_{i+}^{r} && (4.36)\end{aligned}\right\}\ \text{s polarization}$$

There is a similarity between equations (4.33) and 4.34) and equations (4.35) and (4.36). Define an effective wave vector, $\hat{k}_i$, for p polarization

$$\hat{k}_i = \frac{k_i}{\mu_i\cos\theta_i} = \frac{2\pi}{\lambda}\frac{n_i}{\mu_i\cos\theta_i} \qquad \text{p polarization} \qquad (4.37)$$

and for s polarization

$$\hat{k}_i = \frac{k_i}{\mu_i}\cos\theta_i = \frac{2\pi}{\lambda}\frac{n_i\cos\theta_i}{\mu_i} \qquad \text{s polarization} \qquad (4.38)$$

then the equations for the tangential electric field components for both p and s polarization are the same,

$$\hat{E}_{i-}^{t} = \frac{1}{2}\left[1+\frac{\hat{k}_{i+1}}{\hat{k}_i}\right]\hat{E}_{i+}^{t}+\frac{1}{2}\left[1-\frac{\hat{k}_{i+1}}{\hat{k}_i}\right]\hat{E}_{i+}^{r} \qquad (4.39)$$

$$\hat{E}_{i-}^{r} = \frac{1}{2}\left[1-\frac{\hat{k}_{i+1}}{\hat{k}_i}\right]\hat{E}_{i+}^{t}+\frac{1}{2}\left[1+\frac{\hat{k}_{i+1}}{\hat{k}_i}\right]\hat{E}_{i+}^{r} \qquad (4.40)$$

where for p polarization the tangential electric fields are the following.

$$\hat{E}_{i-}^{t} = E_{i-}^{t}\cos\theta_i, \quad \hat{E}_{i-}^{r} = E_{i-}^{r}\cos\theta_i \qquad \text{p polarization} \qquad (4.41)$$

and for s polarization,

$$\hat{E}_{i-}^{t} = E_{i-}^{t}, \qquad \hat{E}_{i-}^{r} = E_{i-}^{r} \qquad \text{s polarization} \qquad (4.42)$$

Let i = i – 1 in equations (4.39) and (4.40) and use equations (4.25) and (4.26). Therefore, the following recursion relations for the tangential electric fields on the – side of the i – 1 interface in terms of the tangential electric fields on the – side of the ith interface are obtained.

$$\hat{E}^{t}_{(i-1)-} = \frac{1}{2}\left[1+\frac{\hat{k}_i}{\hat{k}_{i-1}}\right]\hat{E}^{t}_{i-}e^{j\phi_i} + \frac{1}{2}\left[1-\frac{\hat{k}_i}{\hat{k}_{i-1}}\right]\hat{E}^{r}_{i-}e^{-j\phi_i} \tag{4.43}$$

$$\hat{E}^{r}_{(i-1)-} = \frac{1}{2}\left[1-\frac{\hat{k}_i}{\hat{k}_{i-1}}\right]\hat{E}^{t}_{i-}e^{j\phi_i} + \frac{1}{2}\left[1+\frac{\hat{k}_i}{\hat{k}_{i-1}}\right]\hat{E}^{r}_{i-}e^{-j\phi_i} \tag{4.44}$$

At the last interface (i = m) there is no reflected E field so that $\hat{E}^{r}_{m+} = 0$. Also, the transmitted E field at i = m can be arbitrarily set at $\hat{E}^{t}_{m+} = 1$. Therefore, from equations (4.39) and (4.40)

$$\hat{E}^{t}_{m-} = \frac{1}{2}\left[1+\frac{\hat{k}_{m+1}}{k_m}\right] \tag{4.45}$$

$$\hat{E}^{r}_{m-} = \frac{1}{2}\left[1-\frac{\hat{k}_{m+1}}{k_m}\right] \tag{4.46}$$

Thus, using the recursion relations [equations (4.43) and (4.44)] $\hat{E}^{t}_{o-}$ and $\hat{E}^{r}_{o-}$ can be determined. Using these electric fields, the reflectance and transmittance can be calculated.

Equations (4.43) and (4.44) can be rewritten as follows,

$$\boxed{\hat{E}^{t}_{(i-1)-} = \frac{1}{\hat{t}_{i-1}}\left[e^{j\phi_i}\hat{E}^{t}_{i-} + \hat{r}_{i-1}e^{-j\phi_i}\hat{E}^{r}_{i-}\right]} \tag{4.47}$$

$$\boxed{\hat{E}^{r}_{(i-1)-} = \frac{1}{\hat{t}_{i-1}}\left[\hat{r}_{i-1}e^{j\phi_i}\hat{E}^{t}_{i-} + e^{-j\phi_i}\hat{E}^{r}_{i-}\right]} \tag{4.48}$$

where $\hat{r}$ and $\hat{t}$ are the Fresnel coefficients [equations (1.83) and (1.84)].

$$\hat{t}_{i-1} = \frac{2\hat{n}_{i-1}}{\hat{n}_{i-1} + \hat{n}_i} \tag{4.49}$$

$$\hat{r}_{i-1} = \frac{\hat{n}_{i-1} - \hat{n}_i}{\hat{n}_{i-1} + \hat{n}_i} \tag{4.50}$$

$$\hat{n}_i = \frac{n_i}{\mu_i \cos\theta_i} \qquad \text{p polarization} \tag{4.51a}$$

$$\hat{n}_i = \frac{n_i \cos\theta_i}{\mu_i} \qquad \text{s polarization} \tag{4.51b}$$

Since the recursion relations are linear algebraic equations, they can be written in matrix form.

$$\begin{bmatrix} \hat{E}^t_{(i-1)-} \\ \hat{E}^r_{(i-1)-} \end{bmatrix} = \begin{bmatrix} \dfrac{e^{j\phi_i}}{\hat{t}_{i-1}} & \dfrac{\hat{r}_{i-1}e^{-j\phi_i}}{\hat{t}_{i-1}} \\ \dfrac{\hat{r}_{i-1}}{\hat{t}_{i-1}}e^{j\phi_i} & \dfrac{e^{-j\phi_i}}{\hat{t}_{i-1}} \end{bmatrix} \begin{bmatrix} \hat{E}^t_{i-} \\ \hat{E}^r_{i-} \end{bmatrix} = [M] \begin{bmatrix} \hat{E}^t_i \\ \hat{E}^r_{i-} \end{bmatrix} \tag{4.52}$$

The use of matrix form greatly simplifies the algebra and is ideal for computer calculation of the optical properties. All the necessary matrix algebra is presented in Appendix C. As can be seen, the matrix [M] contains properties of both the i and i – 1 layers. However, by changing variables from $\hat{E}^t_{i-}$ and $\hat{E}^r_{i-}$ to the magnitude of the total tangential electric field $\hat{E}_i$ and the magnitude of the total tangential magnetic field $\hat{H}_i$ then the defining matrix will only depend upon properties of the ith layer. Since the boundary conditions require $\hat{E}_i$ and $\hat{H}_i$ to be the same on each side of an interface the following is obtained,

$$\hat{E}_i = \hat{E}^t_{i-} + \hat{E}^r_{i-} = \hat{E}^t_{i+} + \hat{E}^r_{i+} \tag{4.53}$$

$$\hat{H}_i = \frac{\hat{n}_i}{c_o}\left[\hat{E}^t_{i-} - \hat{E}^r_{i-}\right] = \frac{\hat{n}_{i+1}}{c_o}\left[\hat{E}^t_{i+} - \hat{E}^r_{i+}\right] \tag{4.54}$$

where equations (4.27b) and (4.28b) were used to calculate $\hat{H}_i$. Remember, $\hat{k}_i$, $\hat{n}_i$, $\hat{E}^t_{i-}$, and $\hat{E}^r_{i-}$ depend upon the polarization [equations (4.41), (4.42), (4.51a), and (4.51b).

Equations (4.53) and (4.54) can be written in matrix form.

$$\begin{bmatrix} \hat{E}_i \\ \hat{H}_i \end{bmatrix} = \begin{bmatrix} 1 & 1 \\ \dfrac{\hat{n}_i}{c_o} & -\dfrac{\hat{n}_i}{c_o} \end{bmatrix} \begin{bmatrix} \hat{E}^t_{i-} \\ \hat{E}^r_{i-} \end{bmatrix} \tag{4.55}$$

Therefore,

$$\begin{bmatrix} \hat{E}^t_{i-} \\ \hat{E}^r_{i-} \end{bmatrix} = \begin{bmatrix} 1 & 1 \\ \dfrac{\hat{n}_i}{c_o} & -\dfrac{\hat{n}_i}{c_o} \end{bmatrix}^{-1} \begin{bmatrix} \hat{E}_i \\ \hat{H}_i \end{bmatrix} = \begin{bmatrix} \dfrac{1}{2} & \dfrac{c_o}{2\hat{n}_i} \\ \dfrac{1}{2} & -\dfrac{c_o}{2\hat{n}_i} \end{bmatrix} \begin{bmatrix} \hat{E}_i \\ \hat{H}_i \end{bmatrix} \tag{4.56}$$

Now evaluate equation (4.55) at i – 1 and use equations (4.52) and (4.56) to obtain the following expression (problem 4.1).

$$\begin{bmatrix} \hat{E}_{(i-1)} \\ \hat{H}_{(i-1)} \end{bmatrix} = \begin{bmatrix} \cos\phi_i & \dfrac{jc_o \sin\phi_i}{\hat{n}_i} \\ \dfrac{j\hat{n}_i}{c_o}\sin\phi_i & \cos\phi_i \end{bmatrix} \begin{bmatrix} \hat{E}_i \\ \hat{H}_i \end{bmatrix} = [M_i] \begin{bmatrix} \hat{E}_i \\ \hat{H}_i \end{bmatrix} \tag{4.57}$$

Equation (4.57) is a relation for $\hat{E}_{(i-1)}$ and $\hat{H}_{(i-1)}$ in terms of $\hat{E}_i$ and $\hat{H}_i$ where the $[M_i]$ matrix is a function only of the properties of layer i. Also notice that the determinant of $[M_i]$ is unity. Since the determinant of a product of matrices equals the product of the individual determinants, the determinant of the product matrix, $[M] = [M_i]\,[M_{i-1}]\ldots[M_1]$, will also be unity. This is a useful check for computer calculations.

By matrix multiplication the fields at z = 0 ($\hat{E}_o$ and $\hat{H}_o$) can be calculated in terms of the fields at $z = z_m$ ($\hat{E}_m$ and $\hat{H}_m$). Using equation (4.57)

$$\begin{bmatrix} \hat{E}_{m-1} \\ \hat{H}_{m-1} \end{bmatrix} = [M_m] \begin{bmatrix} \hat{E}_m \\ \hat{H}_m \end{bmatrix}$$
$$\begin{bmatrix} \hat{E}_{m-2} \\ \hat{H}_{m-2} \end{bmatrix} = [M_{m-1}] \begin{bmatrix} \hat{E}_{m-1} \\ \hat{H}_{m-1} \end{bmatrix} = [M_{m-1}][M_m] \begin{bmatrix} \hat{E}_m \\ \hat{H}_m \end{bmatrix}$$
$$\begin{bmatrix} \hat{E}_o \\ \hat{H}_o \end{bmatrix} = [M_1][M_2][M_3]\ldots[M_m] \begin{bmatrix} \hat{E}_m \\ \hat{H}_m \end{bmatrix} \tag{4.58}$$
$$\boxed{\begin{bmatrix} \hat{E}_o \\ \hat{H}_o \end{bmatrix} = [M] \begin{bmatrix} \hat{E}_m \\ \hat{H}_m \end{bmatrix}}$$

where

$$\boxed{[M_i] = \begin{bmatrix} \cos\phi_i & \dfrac{jc_o \sin\phi_i}{\hat{n}_i} \\ \dfrac{j\hat{n}_i}{c_o}\sin\phi_i & \cos\phi_i \end{bmatrix}} \tag{4.59}$$

and

$$[M] = [M_1][M_2]\ldots[M_m] \tag{4.60}$$

At $z = z_m^+$ only the transmitted field, $\hat{E}_{m+}^t$, exists and can arbitrarily be given the value $\hat{E}_{m+}^t = 1$. Therefore, from equations (4.53) and (4.54) the following are obtained.

$$\hat{E}_m = \hat{E}_{m+}^t = 1 \tag{4.61a}$$

$$\hat{H}_m = \frac{\hat{n}_{m+1}}{c_o}\hat{E}_{m+}^t = \frac{\hat{n}_{m+1}}{c_o} \tag{4.61b}$$

4.3.4 Reflectance, Transmittance, and Absorptance

With the expressions for $\hat{E}_o$ and $\hat{H}_o$ in terms of $\hat{E}_m$ and the properties of each of the layers the reflectance, transmittance, and absorptance can be calculated. As shown in Section 1.5.5, only when the medium surrounding the filter is non-absorbing (n_o is a real number) can the intensity at z = 0 be separated into transmitted and reflected parts.

Since in TPV applications $n_o = 1$, the intensity at $z = 0$ can be separated into transmitted and reflected parts. As a result, the reflectance is defined as follows,

$$\rho = \frac{\hat{I}^r_{o-}}{\hat{I}^t_{o-}} \tag{4.62}$$

where $\hat{I}^r_{o-}$ is the reflected intensity leaving the filter in the –z direction at $z = 0$ and $\hat{I}^t_{o-}$ is the intensity incident on the film moving in the +z direction at $z = 0$. Notice that ρ is defined in terms of the intensity moving in the $\pm z$ directions; thus, it is determined by the tangential components $\hat{E}^r_{o-}$ and $\hat{E}^t_{o-}$. Even if ρ were defined in terms of the total reflected and incident intensities, which are determined by the total electric fields E^r_{o-} and E^t_{o-}, the result will be the same as equation (4.62) (problem 4.2).

The intensity is the time average of the Poynting vector and is given by equation (1.39), which is given in terms of the total E field. In terms of the tangential E field, the intensities are the following.

$$\hat{I}^r_{o-} = \frac{1}{2}\frac{\hat{n}_{oR}}{c_o}\hat{E}^r_{o-}\hat{E}^{r*}_{o-} \tag{4.63a}$$

$$\hat{I}^t_{o-} = \frac{1}{2}\frac{\hat{n}_{oR}}{c_o}\hat{E}^t_{o-}\hat{E}^{t*}_{o-} \tag{4.63b}$$

Therefore,

$$\rho = \frac{\hat{E}^r_{o-}\hat{E}^{r*}_{o-}}{\hat{E}^t_{o-}\hat{E}^{t*}_{o-}} \tag{4.64}$$

From equations (4.53) and (4.54),

$$\hat{E}^r_{o-} = \frac{1}{2}\left[\hat{E}_o - \frac{c_o}{\hat{n}_o}\hat{H}_o\right] \tag{4.65a}$$

$$\hat{E}^t_{o-} = \frac{1}{2}\left[\hat{E}_o + \frac{c_o}{\hat{n}_o}\hat{H}_o\right] \tag{4.65b}$$

so that the reflectance is the following.

$$\rho = \frac{\left[\hat{E}_o - \frac{c_o}{\hat{n}_o}\hat{H}_o\right]\left[\hat{E}_o - \frac{c_o}{\hat{n}_o}\hat{H}_o\right]^*}{\left[\hat{E}_o + \frac{c_o}{\hat{n}_o}\hat{H}_o\right]\left[\hat{E}_o + \frac{c_o}{\hat{n}_o}\hat{H}_o\right]^*} \tag{4.66}$$

Remember equation (4.66) applies for both p and s polarizations. For p polarization, $\hat{n}_i$ is given by equation (4.51a) and for s polarization, $\hat{n}_i$ is given by equation (4.51b).

The transmittance, $\hat{\tau}$, defined in terms of the intensity leaving the filter in the +z direction, $\hat{I}^t_{m+}$, and the incident intensity moving in the +z direction, $\hat{I}^t_{o-}$, is the following,

$$\hat{\tau} \equiv \frac{\hat{I}^t_{m+}}{\hat{I}^t_{o-}} = \frac{\hat{n}_{(m+1)R}\hat{E}^t_{m+}\hat{E}^{t*}_{m+}}{\hat{n}_{oR}\hat{E}^t_{o-}\hat{E}^{t*}_{o-}} \tag{4.67}$$

where $\hat{n}_{oR}$ and $\hat{n}_{(m+1)R}$ are the real parts of the index of refraction. Thus, $\hat{\tau}$ is determined by the tangential electric fields. However, if the transmittance, τ, is defined in terms of the total transmitted intensity, which is moving in the θ_{m+1} direction, then the following is obtained (problem 4.3).

$$\tau \equiv \frac{I^t_{m+}}{I^t_{o-}} = \frac{\hat{n}_{(m+1)R}E^t_{m+}E^{t*}_{m+}}{\hat{n}_{oR}E^t_oE^{t*}_o} = \frac{\cos\theta_o}{\cos\theta_{m+1}}\hat{\tau} \tag{4.68}$$

Since $\hat{E}^t_{m+} = 1$, and $\hat{E}^t_{o-}$ is given by equation (4.65b) the following is obtained for $\hat{\tau}$.

$$\hat{\tau} = \frac{4\hat{n}_{(m+1)R}}{\hat{n}_o\left[\hat{E}_o + \frac{c_o}{\hat{n}_o}\hat{H}_o\right]\left[\hat{E}_o + \frac{c_o}{\hat{n}_o}\hat{H}_o\right]^*} \tag{4.69}$$

If all layers of the filter are non-absorbing, then conservation of energy requires that $\rho + \hat{\tau} = 1$. However, if a layer is absorbing, then conservation of energy yields the following,

$$\rho + \hat{\tau} + \sum_i \alpha_i = 1 \tag{4.70}$$

where α_i is the absorptance of layer i and the summation is over all the absorbing layers. The absorptance of layer i is defined as follows,

$$\alpha_i = \frac{\hat{I}_{i-1} - \hat{I}_i}{\hat{I}^t_{o-}} \tag{4.71}$$

where, from equation (1.86) the intensity in the z direction at interface i is the following.

$$\hat{I}_i = \frac{1}{2} \mathrm{Re}\left[\hat{E}_i \hat{H}_i^*\right] \tag{4.72}$$

Since $\hat{I}_i$, as well as the tangential E and H fields, are continuous at an interface there is no need for + or – subscripts. Therefore, using equations (4.63b), (4.65b), and (4.72), the absorbtance of layer i is the following.

$$\boxed{\alpha_i = \frac{4c_o \left\{\mathrm{Re}\left[\hat{E}_{i-1}\hat{H}^*_{i-1}\right] - \mathrm{Re}\left[\hat{E}_i \hat{H}_i^*\right]\right\}}{\hat{n}_o \left[\hat{E}_o + \frac{c_o}{\hat{n}_o}\hat{H}_o\right]\left[\hat{E}_o + \frac{c_o}{\hat{n}_o}\right]^*}} \tag{4.73}$$

Using the matrix equation (4.58) for the electric and magnetic fields, the reflectance, transmittance, and total absorptance, $\alpha_T = \sum_i \alpha_i$ can then be calculated using equations (4.66), (4.67), and (4.70).

In the case of an absorbing layer, i, the angle θ_i is complex. From Snell's Law

$$\sin\theta_i = s_{iR} + j s_{iI} = \frac{n_o \sin\theta_o}{n_i} = \frac{n_o \sin\theta_o}{n_{iR} - j n_{iI}} \tag{4.74}$$

where n_{iR} and n_{iI} are the real and imaginary parts of n_i. s_{iR} and s_{iI} are the real and imaginary parts of $\sin\theta_i$. Therefore,

$$\boxed{\sin\theta_i = s_{iR} + js_{iI} = \frac{n_o n_{iR}}{n_{iR}^2 + n_{iI}^2}\sin\theta_o + j\frac{n_o n_{iI}}{n_{iR}^2 + n_{iI}^2}\sin\theta_o} \tag{4.75}$$

Also required is $\cos\theta_i$.

$$\cos\theta_i = c_{iR} + c_{iI} = \sqrt{1 - \sin^2\theta_i} \tag{4.76}$$

Substituting equation (4.75) for $\sin\theta_i$ yields the following result for $\cos\theta_i$ (problem 4.5),

$$\boxed{\cos\theta_i = c_{iR} + c_{iI} = \sqrt{\frac{1}{2}\left[\sqrt{p_i^2 + q_i^2} + p_i\right]} - j\sqrt{\frac{1}{2}\left[\sqrt{p_i^2 + q_i^2} - p_i\right]}} \tag{4.77}$$

where

$$p_i = 1 - \left(n_{iR}^2 - n_{iI}^2\right)\left(\frac{n_o \sin\theta_o}{n_{iR}^2 + n_{iI}^2}\right)^2 \tag{4.78a}$$

$$q_i = -2n_{iR}n_{iI}\left(\frac{n_o \sin\theta_o}{n_{iR}^2 + n_{iI}^2}\right)^2 \tag{4.78b}$$

Now consider the field described by $\exp\left[j\left(\omega t - \vec{k}_i\vec{r}\right)\right]$ when k is complex.

$$\vec{k}_i \bullet \vec{r} = \frac{2\pi}{\lambda}\left(n_{iR} - jn_{iI}\right)\left(x\sin\theta_i + z\cos\theta_i\right) \tag{4.79}$$

Using equations (4.75) and (4.77),

$$\vec{k}_i \bullet \vec{r} = \frac{2\pi}{\lambda}\left\{\left[\left(n_{iR}s_{iR} + n_{iI}s_{iI}\right)x + \left(n_{iR}c_{iR} + n_{iI}c_{iI}\right)z\right] - j\left(n_{iI}c_{iR} - n_{iR}c_{iI}\right)z\right\} \tag{4.80}$$

where the result $\left(n_{iI}s_{iR} - n_{iR}s_{iI}\right) = 0$ was used. Thus, obtain the following,

$$\exp\left[j\left(\omega t - \vec{k}_i \cdot \vec{r}\right)\right] = \exp\left[j\left(\omega t - \frac{2\pi}{\lambda}\vec{\alpha}_i \cdot \vec{r}\right)\right]e^{-\frac{2\pi}{\lambda}\beta_i z} \tag{4.81}$$

where

$$\vec{\alpha}_i = \left(n_{iR}s_{iR} + n_{iI}s_{iI}\right)\hat{i} + \left(n_{iR}c_{iR} + n_{iI}c_{iI}\right)\hat{k} \tag{4.82}$$

$$\beta_i = n_{iI}c_{iR} - n_{iR}c_{iI} \tag{4.83}$$

Equation (4.81) represents a wave that is moving in the $\vec{\alpha}_i$ direction and is being dissipated in the z direction. Thus, in a layer where absorption exists, the refraction angle, γ_i, the wave makes with the + side of the i – 1 interface is the following.

$$\vec{\alpha}_i \cdot \hat{k} = \alpha_i \cos\gamma_i = n_{iR}c_{iR} + n_{iI}c_{iI} \tag{4.84}$$

The angle γ_i is also the angle of incidence on – side of the i interface.

In Section 1.5.4 wave propagation into an absorptive medium is treated using the wave equation [equation (1.62)]. Both that analysis and the present analysis yield the same result for α and β, as they must. Values for α_i^2 and β_i^2 are given by equations (1.71) and (1.72), where $n_{1R} = n_{iR}$, $n_{1I} = n_{iI}$, and $\theta_o^+ = \theta_o$.

All the tools necessary to calculate the optical properties of an interference filter consisting of m layers have now been developed. In the next section these tools are used to calculate the optical properties of a single layer system.

4.3.5 Single Film System

Figure 4.2 is a schematic drawing of a single film system. Light is incident from a medium with index of refraction, n_o, at angle of incidence, θ_o, on to a film of index of refraction, n_1, and thickness, d. The film is attached to a medium of refractive index, n_2.

The matrix equation [equation (4.58)] that relates the tangential E and H fields at interfaces 0 and 1 is the following.

$$\begin{bmatrix} \hat{E}_o \\ \hat{H}_o \end{bmatrix} = \begin{bmatrix} \cos\phi_1 & \dfrac{jc_o \sin\phi_1}{\hat{n}_1} \\ \dfrac{j\hat{n}_1 \sin\phi_1}{c_o} & \cos\phi_1 \end{bmatrix} \begin{bmatrix} \hat{E}_1 \\ \hat{H}_1 \end{bmatrix} \tag{4.85}$$

Therefore, carrying out matrix multiplication,

$$\hat{E}_o = \hat{E}_1 \cos\phi_1 + j\hat{H}_1 \frac{c_o \sin\phi_1}{\hat{n}_1} \tag{4.86a}$$

$$\hat{H}_o = \hat{H}_1 \cos\phi_1 + j\hat{E}_1 \frac{n_1 \sin\phi_1}{c_o} \tag{4.86b}$$

where

$$\phi_1 = \frac{2\pi}{\lambda} n_1 d \cos\theta_1 \tag{4.87}$$

And $\cos\theta_1$ is given by equation (4.77) with $n_{iR} = n_{1R}$ and $n_{iI} = n_{1I}$. If medium 1 is non-absorbing so that n_1 is a real number, $\cos\theta_1 = \sqrt{1 - \left(\frac{n_o}{n_1}\right)^2 \sin^2\theta_o}$.

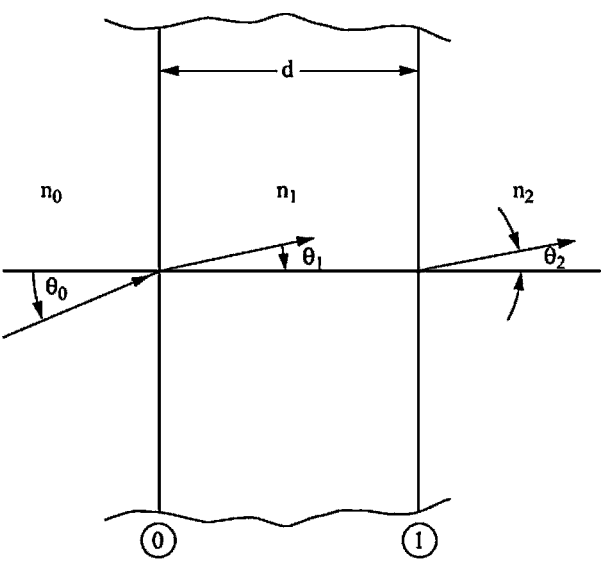

Figure 4.2.—Single film system.

The magnitude of $\hat{E}_1$ can be arbitrarily set at $\hat{E}_1 = 1$ so that from equation (4.61b), $\hat{H}_1 = \frac{\hat{n}_2}{c_o}$. From equations (4.86a) and (4.86b) the following results are obtained.

$$\hat{E}_o - \frac{c_o}{\hat{n}_o}\hat{H}_o = \left(1 - \frac{\hat{n}_2}{\hat{n}_o}\right)\cos\phi_1 + j\left(\frac{\hat{n}_2}{\hat{n}_1} - \frac{\hat{n}_1}{\hat{n}_o}\right)\sin\phi_1 \tag{4.88a}$$

$$\hat{E}_o + \frac{c_o}{\hat{n}_o}\hat{H}_o = \left(1 + \frac{\hat{n}_2}{\hat{n}_o}\right)\cos\phi_1 + j\left(\frac{\hat{n}_2}{\hat{n}_1} + \frac{\hat{n}_1}{\hat{n}_o}\right)\sin\phi_1 \tag{4.88b}$$

Thus, using equation (4.66), the reflectance is the following for $\hat{n}_o$, $\hat{n}_1$, and $\hat{n}_2$ all being real numbers (all three layers are non-absorbing).

$$\rho = \frac{\hat{n}_1^2\left(\hat{n}_o - \hat{n}_2\right)^2\cos^2\phi_1 + \left(\hat{n}_o\hat{n}_2 - \hat{n}_1^2\right)^2\sin^2\phi_1}{\hat{n}_1^2\left(\hat{n}_o + \hat{n}_2\right)^2\cos^2\phi_1 + \left(\hat{n}_o\hat{n}_2 + \hat{n}_1^2\right)^2\sin^2\phi_1} \tag{4.89}$$

Using the identities $\cos^2\phi_1 = \frac{1}{2}\left(1 + \cos 2\phi_1\right)$ and $\sin^2\phi_1 = \frac{1}{2}\left(1 - \cos 2\phi_1\right)$ equation (4.89) becomes the following.

$$\rho = \frac{\hat{n}_1^2\left(\hat{n}_o - \hat{n}_2\right)^2 + \left(\hat{n}_o\hat{n}_2 - \hat{n}_1^2\right)^2 + \left(\hat{n}_1^2 - \hat{n}_o^2\right)\left(\hat{n}_2^2 - \hat{n}_1^2\right)\cos 2\phi_1}{\hat{n}_1^2\left(\hat{n}_o + \hat{n}_2\right)^2 + \left(\hat{n}_o\hat{n}_2 + \hat{n}_1^2\right)^2 + \left(\hat{n}_1^2 - \hat{n}_o^2\right)\left(\hat{n}_2^2 - \hat{n}_1^2\right)\cos 2\phi_1} \tag{4.90}$$

Remember, equation (4.90) applies for both p and s polarization where $\hat{n}$ is given by equation (4.51a) for p polarization and (4.51b) for s polarization.

Now investigate how ρ depends upon the phase thickness, ϕ_1. Assume medium 0 is vacuum ($n_o = 1$) and that medium 1, the film, and medium 2, the substrate, are non-absorbing so that n_1 and n_2 are real numbers. Also, assume $n_2 = 1.5$, which approximates silica glass and normal incidence ($\theta_o = \theta_1 = \theta_2 = 0$). For normal incidence, $\hat{n}_i = \frac{n_i}{\mu_i}$, for both p and s polarization. Further, assume all three media are non-magnetic so that $\mu_o = \mu_1 = \mu_2$. As a result, the $\wedge$ is removed from all the n's in equation (4.90) for the reflectance, ρ. For these conditions, results from equation (4.90) for ρ are shown in Figure 4.3 as a function of $\frac{2\pi n_1 d}{\lambda}$ for several values of n_1.

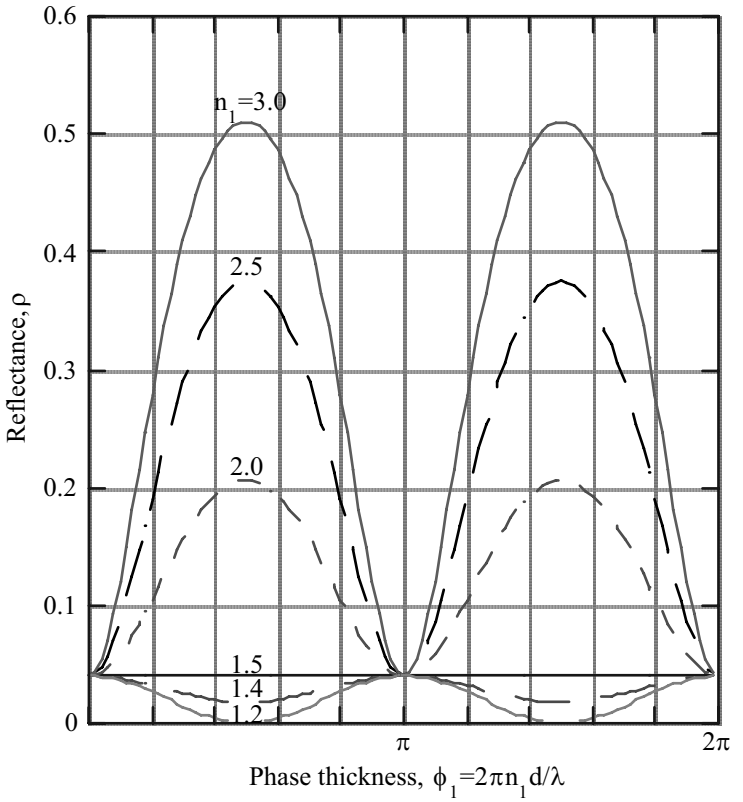

Figure 4.3 - Reflectance for normal incidence(θ_o=0) into a vacuum(n_o=1) of a nonabsorbing single film with real index of refraction, n_1 and thickness, d on a nonabsorbing substrate with index of refraction, n_2=1.5 .

The first thing to notice in the results for ρ in Figure 4.3 are the maxima and minima that occur at $\frac{n_1 d}{\lambda} = \frac{m}{4}$, where m = 0, 1, 2, 3,… If $n_1 > n_2$ then ρ has a maximum for $\frac{n_1 d}{\lambda} = \frac{m}{4}$ where m = 1, 3, 5,… and a minimum for $\frac{n_1 d}{\lambda} = \frac{m}{2}$ where m = 0, 1, 2, 3,… If $n_1 < n_2$, then the location of the maxima and minima are opposite those for the case of $n_1 > n_2$. The reflectance has a minimum for $\frac{n_1 d}{\lambda} = \frac{m}{4}$ where

m = 1, 3, 5,… and a maximum for $\frac{n_1 d}{\lambda} = \frac{m}{2}$ where m = 0, 1, 2, 3,… Also, for $n_1 < n_2$ the reflectance is always less than or equal to the reflectance for $n_1 > n_2$. When $n_1 = n_2$, the reflectance is independent of ϕ_1 [see equation (4.90)]. It can be shown that $\rho = 0$ can be obtained when $\frac{n_1 d \cos\theta_1}{\lambda} = \frac{m}{4}$, m being an odd integer, if $n_1 = \sqrt{n_o n_2}$ (problem 4.6). Thus, with a single film it is possible to obtain $\rho = 0$ ($\tau = 1$) at a series of wavelengths $\lambda = \frac{n_1 d \cos\theta_1}{m}$ where m is an odd integer and $n_1 = \sqrt{n_o n_2}$.

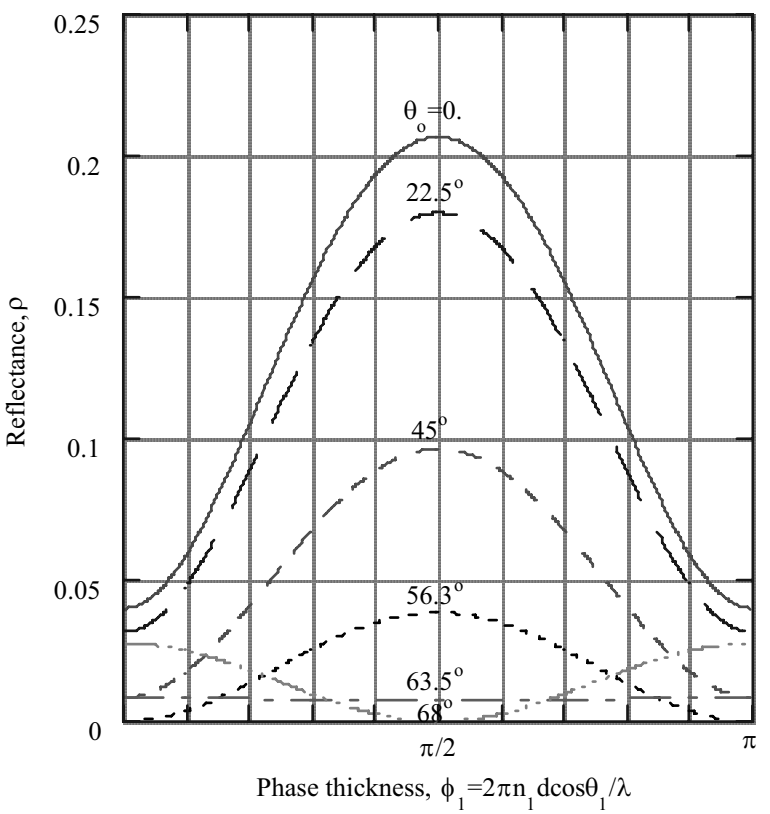

Figure 4.4a) - Effect of angle of incidence, θ_o on p polarization reflectance into a vacuum(n_o=1.) of a nonabsorbing film with index of refraction, n_1=2. and thickness, d on a substrate with index of refraction, n_2=1.5. $\cos\theta_1 = [1.-(n_o/n_1)^2 \sin^2\theta_o]^{1/2}$

As Figure 4.3 shows, large reflectance can be obtained for $n_1 > n_2$ if n_1 is large. However, currently there are no non-absorptive materials with n much greater than 2. Therefore, the only way to achieve large reflectance at a series of wavelengths and large transmittance at another series of wavelengths is by using several layers of materials with different indices of refraction.

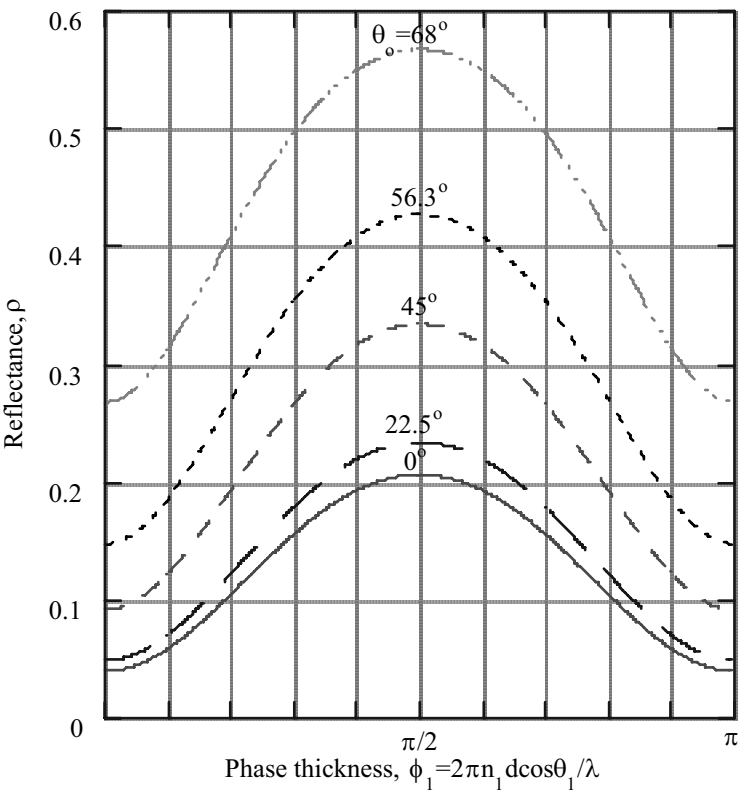

Figure 4.4b) - Effect of angle of incidence, θ_o on s polarization reflectance into a vacuum(n_o=1.) of a nonabsorbing film with index of refraction, n_1=2. and thickness, d on a substrate with index of refraction, n_2=1.5. $\cos\theta_1=[1.-(n_o/n_1)^2\sin^2\theta_o]^{1/2}$

Now consider how the angle of incidence, θ_o, affects the reflectance for the non-absorbing single film system when $n_1 > n_2$. Figure 4.4 shows ρ for both p and s

polarizations as a function of the phase thickness, $\phi_1 = \frac{2\pi n_1 d \cos\theta_1}{\lambda}$, for $n_o = 1.0$, $n_1 = 2.0$, $n_2 = 1.5$, and several angles of incidence, θ_o.

Comparing Figure 4.4a and 4.4b notice that as θ_o increases, the reflectance for s polarization increases while the reflectance for p polarization decreases. For $\theta_o = 63.5°$, p is nearly a constant for p polarization, and for $\theta_o > 63.5°$ the dependence on ϕ_1 changes. Minima of ρ occur where maxima occurred for smaller angles of incidence. For p polarization at $\theta_o = 68°$ and $\phi_1 = \frac{m\pi}{2}$, where m is an odd integer, the reflectance vanishes ($\rho = 0$). While for s polarization, ρ is a maximum. For p polarization at $\theta_o = 56.3°$ and $\phi_1 = m\pi$, where m is an integer, $\rho = 0$. While for s polarization, ρ is a minimum (problem 4.7).

As just shown, when $n_1 > n_2$, and $\phi_1 = \frac{m\pi}{2}$, where m is an odd integer, ρ is a maximum for s polarization, while $\rho = 0$ for p polarization at some angle of incidence, θ_{os}. Thus, the single film system can be used as a polarizer. All the reflected light will be s polarized when $\theta_o = \theta_{os}$ if $n_1 > n_2$. If $n_1 < n_2$ and $\phi_1 = \frac{m\pi}{2}$ where m is an odd integer, then ρ will be a minimum for both p and s polarization. Therefore, n_1 must be greater than n_2 for an effective polarizer.

As Figures 4.3 and 4.4 show, when $n_1 > n_2$ and $\phi_1 = \frac{m\pi}{2}$, where m is an odd integer, the reflectance can be greatly enhanced. Therefore, the single film system can also be used as a beam splitter.

When the film is absorptive, the analysis is more complex. Again, the reflectance is given by equation (4.66). However, now $\hat{n}_1$ will be a complex number and thus ϕ_1 is also complex. Also, the transmittance, $\hat{\tau}$, must be calculated using equation (4.69). Using computer software that is capable of treating complex numbers, equations (4.66), (4.69), and (4.88) can be used to calculate ρ and $\hat{\tau}$. However, if $\hat{n}_1$ and ϕ_1 are written in terms of their real and imaginary parts then ρ and $\hat{\tau}$ are given in terms of only real numbers. Thus, after a great deal of painful algebra, the following is obtained for ρ and $\hat{\tau}$ for the absorbing film,

$$\rho = \frac{a_1 \cosh 2\phi_{1I} - a_2 \cos 2\phi_{1R} - 2\left[a_3 \sin 2\phi_{1R} + a_4 \sinh 2\phi_{1I}\right]}{b_1 \cosh 2\phi_{1I} - b_2 \cos 2\phi_{1R} - 2\left[b_3 \sin 2\phi_{1R} + b_4 \sinh 2\phi_{1I}\right]} \tag{4.91}$$

$$\hat{\tau} = \frac{8\hat{n}_o\hat{n}_2\left(\hat{n}_1\hat{n}_1^*\right)^2}{b_1\cosh 2\phi_{1I} - b_2\cos 2\phi_{1R} - 2\left[b_3\sin 2\phi_{1R} + b_4\sinh 2\phi_{1I}\right]} \tag{4.92}$$

where,

$$a_1 = \hat{n}_{1I}^2 p_+^2 + \hat{n}_{1R}^2 p_-^2 + \left(\hat{n}_1\hat{n}_1^* t_-\right)^2 \tag{4.93a}$$

$$a_2 = a_1 - 2\left(\hat{n}_1\hat{n}_1^* t_-\right)^2 \tag{4.93b}$$

$$a_3 = \hat{n}_{1I}\hat{n}_1\hat{n}_1^* t_- p_+ \tag{4.93c}$$

$$a_4 = \hat{n}_{1R}\hat{n}_1\hat{n}_1^* t_- p_- \tag{4.93d}$$

$$b_1 = \hat{n}_{1I}^2 p_-^2 + \hat{n}_{1R}^2 p_+^2 + \left(\hat{n}_1\hat{n}_1^* t_+\right)^2 \tag{4.94a}$$

$$b_2 = b_1 - 2\left(\hat{n}_1\hat{n}_1^* t_+\right)^2 \tag{4.94b}$$

$$b_3 = \hat{n}_{1I}\hat{n}_1\hat{n}_1^* t_+ p_- \tag{4.94c}$$

$$b_4 = \hat{n}_{1R}\hat{n}_1\hat{n}_1^* t_+ p_+ \tag{4.94d}$$

$$\hat{n}_1\hat{n}_1^* = \hat{n}_{1R}^2 + \hat{n}_{1I}^2 \tag{4.95}$$

$$p_+ = \hat{n}_o\hat{n}_2 + \hat{n}_1\hat{n}_1^* \tag{4.96a}$$

$$p_- = \hat{n}_o\hat{n}_2 - \hat{n}_1\hat{n}_1^* \tag{4.96b}$$

$$t_+ = \hat{n}_o + \hat{n}_2 \tag{4.97a}$$

$$t_- = \hat{n}_o - \hat{n}_2 \tag{4.97b}$$

$$\phi_{1R} = \frac{2\pi d}{\lambda}\left[n_{1R}c_{1R} + n_{1I}c_{1I}\right] \tag{4.98a}$$

$$\phi_{1I} = \frac{2\pi d}{\lambda}\left[n_{1R}c_{1I} - n_{1I}c_{1R}\right] \tag{4.98b}$$

$$\left.\begin{aligned} &\hat{n}_{1R} = \frac{n_{1R}c_{1R} - n_{1I}c_{1I}}{\mu_1\left(c_{1R}^2 + c_{1I}^2\right)}, \qquad \hat{n}_{1I} = -\frac{n_{1R}c_{1I} + n_{1I}c_{1R}}{\mu_1\left(c_{1R}^2 + c_{1I}^2\right)} \\ &\hat{n}_o = \frac{n_o}{\mu_o \cos\theta_o}, \qquad \hat{n}_2 = \frac{n_2}{\mu_2\left[1 - \left(\frac{n_o}{n_2}\right)^2 \sin\theta_o\right]^{\frac{1}{2}}} \end{aligned}\right\} \text{p polarization} \tag{4.99}$$

$$\left.\begin{aligned} &\hat{n}_{1R} = \frac{1}{\mu_1}\left(n_{1R}c_{1R} + n_{1I}c_{1I}\right), \qquad \hat{n}_{1I} = \frac{1}{\mu_1}\left(n_{1R}c_{1I} - n_{1I}c_{1R}\right) \\ &\hat{n}_o = \frac{n_o \cos\theta_o}{\mu_o}, \qquad \hat{n}_2 = \frac{n_2\left[1 - \left(\frac{n_o}{n_2}\right)^2 \sin\theta_o\right]^{\frac{1}{2}}}{\mu_2} \end{aligned}\right\} \text{s polarization} \tag{4.100}$$

and $c_{1R} = \mathrm{Re}[\cos\theta_1]$ and $c_{1I} = I_M[\cos\theta_1]$ are given by equation (4.77) where i = 1. If the materials in regions 0, 1, and 2 are non-magnetic, then $\mu_o = \mu_1 = \mu_2$ and the μ terms will cancel in equations (4.91) and (4.92).

The imaginary part of the index of refraction is a measure of the absorptance of a material. However, physically the absorption coefficient, $a(cm^{-1})$, is a more useful measure of the absorptance since intensity $\sim e^{-ax}$ [see equations (1.40) and (1.41)]. From equation (1.41), the following is obtained.

$$n_I = \frac{\lambda}{4\pi}a \tag{4.101}$$

Thus if $a \approx 1cm^{-1}$ and $\lambda \approx 2\mu m$, then $n_I \approx 1.6 \times 10^{-5}$. Thus, n_I is negligible for $a \leq 1cm^{-1}$ for wavelengths in the near infrared, where a TPV system operates.

Equations (4.91) and (4.92) can be used to calculate ρ and $\hat{\tau}$ and $\alpha_T = 1 - \rho - \hat{\tau}$ as functions of the phase thickness, $\overline{\phi}_1 = \frac{2\pi\overline{n}_1 d\overline{\cos\theta}_1}{\lambda}$. In this expression $\overline{n}_1 = \sqrt{n_{1R}^2 + n_{1I}^2}$ is the magnitude of n_1 and $\overline{\cos\theta}_1 = \sqrt{c_{1R}^2 + c_{1I}^2}$ is the magnitude of $\cos\theta_1$. The phase

thickness can also be expressed in a different manner. For a single film system to yield maximum reflectance at some wavelength, λ_o, when $n_1 > n_2$ the following condition must be satisfied.

$$\frac{2\pi\bar{n}_1 d\overline{\cos\theta_1}}{\lambda_o} = \frac{\pi}{2} \tag{4.102}$$

As a result,

$$\bar{\phi}_1 = \frac{\pi}{2}\frac{\lambda_o}{\lambda} \tag{4.103}$$

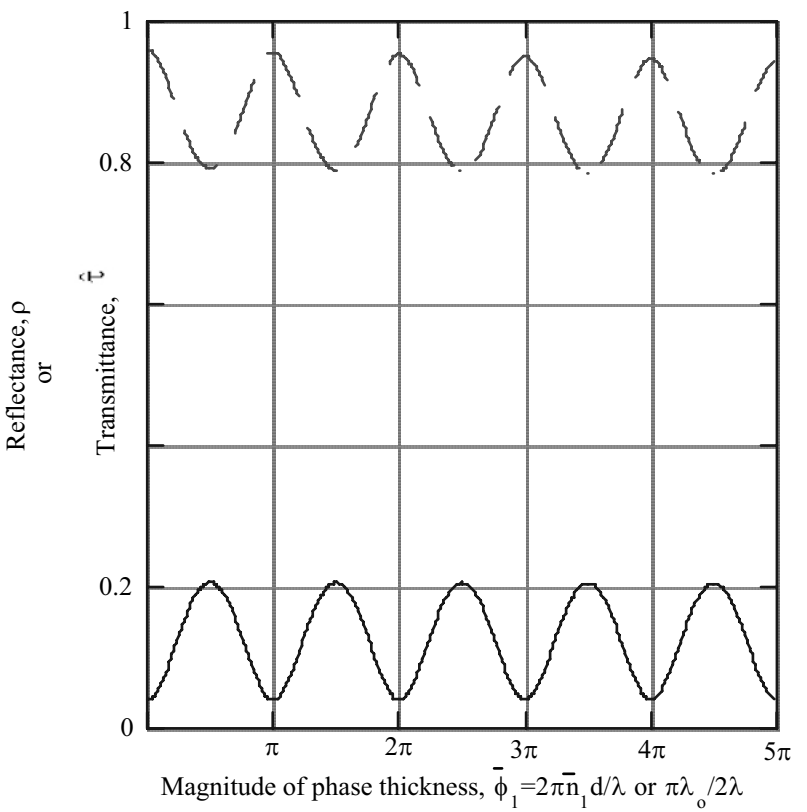

Figure 4.5a) - Effect of absorption on reflectance and transmittance of a single film system for normal incidence (θ_o=0), n_o=1., n_1=2.-.001j, n_2=1.5. Reflectance ρ, solid line and transmittance, $\hat{\tau}$, dashed line.

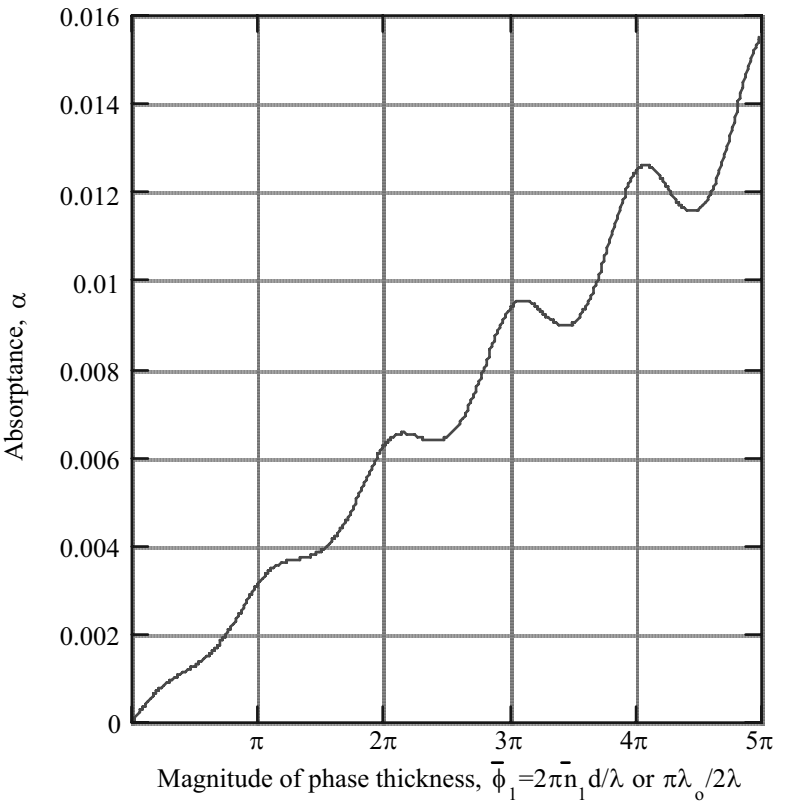

Figure 4.5b) - Effect of absorption on absorptance of single film system for normal incidence(θ_o=0), n_o=1., n_1=2.-.001j, n_2=1.5.

For normal incidence ($\theta_o = \theta_1 = \theta_2 = 0$) ρ, $\hat{\tau}$, and α are shown in Figure 4.5 as functions of $\bar{\phi}_1$ for $n_o = 1.0$, $n_1 = 2.0 - .001j$, and $n_2 = 1.5$. These results apply for both p and s polarization. Comparing Figure 4.5a with Figure 4.4, notice that the reflectance is nearly unchanged by the addition of the small imaginary part ($n_{1I} = .001$) to the film index of refraction, n_1. The transmittance decreases with increasing $\bar{\phi}_1$, which shows up as an increase in absorptance. The absorptance does not reach .01 until $\bar{\phi}_1 = \frac{\pi\lambda_o}{2\lambda} \approx 3.7\pi$. Thus for $\lambda > \lambda_o/7.4$, the absorptance will be less than .01. Only at

very small λ is there significant absorptance. Also, this result is for $n_{1I} = .001$, which corresponds to an absorption coefficient, $\alpha > 60\text{cm}^{-1}$ for $\lambda = 2.0\mu\text{m}$. This is a rather large absorption coefficient for a non-conducting material. Thus, an interference filter made of several layers of thin film dielectric materials should have small absorptance. For conductors where $n_I > 1$, however, absorptance will be large.

For $\theta_o > 0$ the effect of absorptance is similar to the $\theta_o = 0$ case. The reflectance remains nearly constant while the transmittance decreases as the absorptance increases for increasing phase thickness, $\bar{\phi}_1$. This result applies to both p and s polarization. Also, just as in the case of no absorptance (Figure 4.4), the reflectance increases and the transmittance decreases as θ_o increases for s polarization. For p polarization, the opposite occurs. The reflectance decreases and the transmittance increases for increasing θ_o.

When $\theta_o > 0$ the sinusoidal dependence of ρ and $\hat{\tau}$ on the phase thickness remains the same as when $\theta_o = 0$, if n_{1I} is small. For both p and s polarization, ρ and $\hat{\tau}$ have maxima or minima occurring for $\bar{\phi}_I = \dfrac{m\pi}{2}$, where m = 1, 3, 5, 7,… regardless of the value of θ_o when n_{1I} is small. However, if n_{1I} is large, as is the case for conductors at long wavelengths, then ρ and $\hat{\tau}$ no longer behave in a sinusoidal manner as functions of the phase thickness. If the film is a conductor such as gold or copper, where $n_{1I} \gg n_{1R}$ at long wavelengths; then $n_1 \approx -jn_{1I}$. In that case the reflectance is the following (problem 4.12),

$$\rho = \frac{a_1 \cosh 2\phi_I - a_2}{a_1 \cosh 2\phi_I - b_2} \qquad n_1 = -jn_{1I} \tag{4.104}$$

where, $\phi_I = -\dfrac{2\pi d_1}{\lambda}\sqrt{n_{1I}^2 + n_o^2 \sin^2\theta_o}$ and

$$a_1 = \left(\hat{n}_2^2 + \hat{n}_{1I}^2\right)\left(\hat{n}_o^2 + \hat{n}_{1I}^2\right) \tag{4.105a}$$

$$a_2 = \left(\hat{n}_2^2 - \hat{n}_{1I}^2\right)\left(\hat{n}_o^2 - \hat{n}_{1I}^2\right) + 4\hat{n}_o\hat{n}_2\hat{n}_{1I}^2 \tag{4.105b}$$

$$b_2 = \left(\hat{n}_2^2 - \hat{n}_{1I}^2\right)\left(\hat{n}_o^2 - \hat{n}_{1I}^2\right) - 4\hat{n}_o\hat{n}_2\hat{n}_{1I}^2 \tag{4.105c}$$

It can be shown that $a_1 > a_2$. Therefore, since $\cosh 2\phi_I \geq 1$ for all ϕ_I, the reflectance can never be zero.

4.3.6 Many Layer System for $\phi_i = N\pi$ or $\phi_i = N\pi/2$ and N Is an Odd Integer

As stated in the last section, since n_R is limited to values not much larger than 2, the only way to achieve large reflectance is to use several layers of alternating high and low indices of refraction. The analysis of the many layer system is algebraically very complex as the results for ρ and $\hat{\tau}$ for even the single layer indicate [equations (4.91) and (4.92)]. However, with the use of computer software that is capable of matrix multiplication and complex number algebra, the analysis is greatly simplified.

The tangential electric, $\hat{E}_o$, and magnetic, $\hat{H}_o$, fields at the front interface are given in terms of the electric $\hat{E}_m\,(=1)$, and magnetic, $H_m\left(=\dfrac{\hat{n}_{m+1}}{c_o}\right)$, fields at the last interface by equation (4.58). Each layer, i, of the system is characterized by the matrix, M_i, given by equation (4.59). Appearing in M_i is the phase thickness, ϕ_i, given by equation (4.26) and the effective index of refraction, $\hat{n}_i$, given by equation (4.51a) for p polarization and by equation (4.51b) for s polarization. Also, $\cos\theta_i$, which appears in the expression for ϕ_i, is given by equation (4.77). Once the M_i matrix for each layer is established, then matrix multiplication will yield the matrix M, which can be used in equation (4.58) to obtain E_o and H_o. The optical properties are then calculated using equations (4.66), (4.69), and (4.70).

Ideally, the starting point for the design of an interference filter would be the desired reflectance, ρ, (or transmittance) dependence on wavelength for a particular application. Conceivably, once $\rho(\lambda)$ is known, a set on 2N algebraic equations could be derived for n_i and d_i (thickness of layer i) for the N layer system as functions of $\rho(\lambda)$ at 2N values of λ. However, the system of equations would be non-linear so that obtaining a solution would be difficult. In addition, as already stated, there are only limited values of n_i to choose from for non-absorptive materials. Therefore, the starting point is to choose at least two non-absorptive materials; one with a large index of refraction and the other with a low index of refraction. Besides the index of refraction requirement, the materials must be capable of operating in the environment of the application. In the case of TPV, it is desirable to have low vapor pressure materials so that evaporation is not a problem.

Once the materials are chosen, then some sort of an optimization procedure must be used to yield $\rho(\lambda)$ and $\tau(\lambda)$ that are as close to the desired $\rho(\lambda)$ and $\tau(\lambda)$ as possible. Thelen[4,5] describes several of these procedures. The commercial software program TFCALC™ from Software Spectra of Portland, Oregon, includes optimization procedures. The so-called equivalent layer procedure is described later. However, for non-absorptive media $\left(\hat{n}_{iI} = 0\right)$, there are two cases where the matrix $[M_i]$ is greatly simplified and thus ρ and τ can easily be determined. In the first case, if $\phi_i = N\pi$, where

N is an integer, then $\sin\phi_i = 0$ and $\cos\phi_i = \pm 1$. Thus [M] = ±[I] so that $\hat{E}_o = \pm\hat{E}_m = \pm 1$, and $\hat{H}_o = \pm\hat{H}_m = \frac{\hat{n}_{m+1}}{c_o}\hat{E}_m = \pm\frac{\hat{n}_{m+1}}{c_o}$. As a result, ρ reduces to the same result as a single layer system [equation (4.89) or (4.90)] where $\phi_1 = N\pi$ and $\hat{n}_2 = \hat{n}_{m+1}$. Also in this case, ρ is independent of the indices of refraction, $\hat{n}_i$, of the layers that make up the filter. The reflectance depends only on the index of refraction of the surroundings, n_o, and the substrate, n_{m+1}. If $n_o \approx n_{m+1}$ then $\rho \approx 0$ and $\tau \approx 1$ so that a multi-layer where $\phi_i = 0, \pi, 2\pi, \ldots$ will have large transmittance.

Now consider the case for m non-absorptive layers on substrate, m+1. If $\phi_i = \frac{2\pi n_i d_i \cos\theta_i}{\lambda} = \frac{N\pi}{2}$, where d_i is the thickness of layer i and N is an odd integer, then $\sin\phi_i = \pm 1$ and $\cos\phi_i = 0$. As a result, $[M_i]$ [equation (4.59)] is the following.

$$[M_i] = \begin{bmatrix} 0 & \pm\frac{jc_o}{\hat{n}_i} \\ \pm\frac{j\hat{n}_i}{c_o} & 0 \end{bmatrix} \tag{4.106}$$

Therefore, by repeated matrix multiplication the following are obtained,

$$[M] = [M_1][M_2]\ldots[M_m] = \begin{bmatrix} \frac{1}{P_m} & 0 \\ 0 & P_m \end{bmatrix} \quad \text{m an even integer} \tag{4.107a}$$

$$[M] = [M_1][M_2]\ldots[M_m] = \begin{bmatrix} 0 & \pm j\frac{\hat{n}_{m+1}}{c_o P_{m+1}} \\ \pm j\frac{c_o P_{m+1}}{\hat{n}_{m+1}} & 0 \end{bmatrix} \quad \text{m an odd integer} \tag{4.107b}$$

where,

$$P_m = \frac{\hat{n}_{m-1}\hat{n}_{m-3}\hat{n}_{m-5}\ldots\hat{n}_1}{\hat{n}_m\hat{n}_{m-2}\hat{n}_{m-4}\ldots\hat{n}_2} \tag{4.108}$$

Now use equations (4.58), (4.61), and (4.66) to obtain the reflectance, ρ.

$$\rho = \left[\frac{1 - \frac{\hat{n}_{m+1}}{\hat{n}_o} P_m^2}{1 + \frac{\hat{n}_{m+1}}{\hat{n}_o} P_m^2} \right] \qquad \phi_i = \frac{N\pi}{2},\ N = 1, 3,... \quad \text{and m is even} \tag{4.109a}$$

$$\rho = \left[\frac{1 - \frac{\hat{n}_{m+1}}{\hat{n}_o} P_{m+1}^2}{1 + \frac{\hat{n}_{m+1}}{\hat{n}_o} P_{m+1}^2} \right] \qquad \phi_i = \frac{N\pi}{2},\ N = 1, 3,... \quad \text{and m is odd} \tag{4.109b}$$

As equations (4.109) show, $\rho \to 1$ for either $P^2 \to \infty$ or $P^2 \to 0$. From equation (4.108), P^2 can be made to approach either zero or infinity if the indices of refraction of adjacent layers alternate between high and low values.

Consider the case where every other layer has the same index of refraction when m is an even integer. Thus, $\hat{n}_{m-1} = \hat{n}_{m-3} = \hat{n}_{m-5} = ... \hat{n}_1$, and $\hat{n}_m = \hat{n}_{m-2} = \hat{n}_{m-4} = ... \hat{n}_2$, and $P_m = \left(\frac{\hat{n}_1}{\hat{n}_2} \right)^{m/2}$ so the reflectance is the following.

$$\rho = \left[\frac{1 - \frac{\hat{n}_{m+1}}{\hat{n}_o} \left(\frac{\hat{n}_1}{\hat{n}_2} \right)^m}{1 + \frac{\hat{n}_{m+1}}{\hat{n}_o} \left(\frac{\hat{n}_1}{\hat{n}_2} \right)^m} \right]^2 \qquad \text{m even} \tag{4.110}$$

Therefore, by increasing the number of layers, m, the reflectance can be made to approach one for either $\hat{n}_1 > \hat{n}_2$ or $\hat{n}_1 < \hat{n}_2$. If m is an odd integer and every other layer has the same index of refraction, the reflectance is the following (problem 4.9).

$$\rho = \left[\frac{1 - \frac{\hat{n}_1}{\hat{n}_o} \frac{\hat{n}_2}{\hat{n}_{m+1}} \left(\frac{\hat{n}_1}{\hat{n}_2} \right)^m}{1 + \frac{\hat{n}_1}{\hat{n}_o} \frac{\hat{n}_2}{\hat{n}_{m+1}} \left(\frac{\hat{n}_1}{\hat{n}_2} \right)^m} \right]^2 \qquad \text{m odd} \tag{4.111}$$

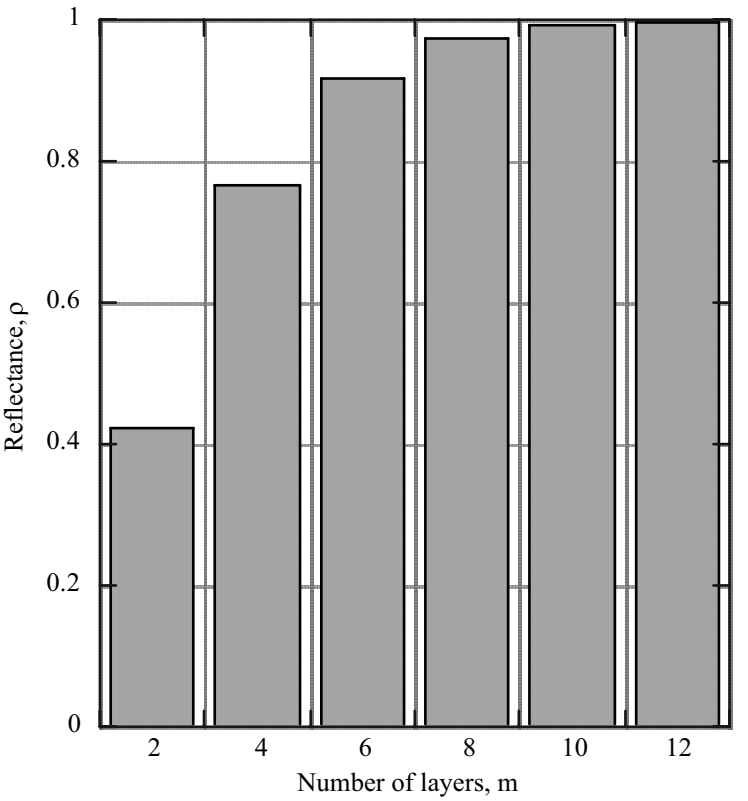

Figure 4.6 - Effect of even number of layers with alternating indicies of refraction, n_1=2.4 and n_2=1.35 on reflectance into a vacuum(n_o=1) at normal incidence for an interference filter with $n_1d_1=n_2d_2=N\lambda/4$,where N is an odd integer. Substrate index of refraction, n_s=1.5.

Again, by increasing m, the reflectance can be made to approach one. Figure 4.6 is obtained using equation (4.110) with $\theta_o = 0$. It shows the rapid increase in ρ as the number of layers, m, is increased for the case of m being an even integer. A similar result would be obtained for m being an odd integer. In Figure 4.6, $n_1 = 2.4$, which approximates zinc selenide (ZnSe), and $n_2 = 1.35$, which approximates magnesium fluoride (MgF_2). If $n_1 = 1.35$ and $n_2 = 2.4$, then $\rho = 0.13$ for m = 2, and $\rho = 0.55$ for m = 4, compared to $\rho = 0.42$ and 0.77, when $n_1 = 2.4$ and $n_2 = 1.35$. However, for $m \geq 8$, the reflectances are nearly the same for both cases ($n_1 > n_2$ or $n_1 < n_2$).

The reflectances given by equations (4.109a) and (4.109b) apply only when $\phi_i = \frac{N\pi}{2}$ or $n_i d_i \cos\theta_i = N\frac{\lambda}{4}$, where N is an odd integer, λ is the wavelength, n_i is the index of refraction, d_i the thickness, and θ_i the angle of incidence for layer i. Thus for a given value of $4n_i d_i \cos\theta_i$, the reflectance at a series of wavelengths,

$$\lambda_N = \frac{4n_i d_i \cos\theta_i}{N} \qquad N = 1, 3, 5,... \tag{4.112}$$

will be the same. If a multi-layer film satisfying $\phi_i = \frac{N\pi}{2}$ is designed to yield large reflectance at a specific wavelength λ_o, then large reflectance will also occur at $\lambda_N < \lambda_o$ given by equation (4.112).

4.3.7 Equivalent Layer Procedure

No matter whether a single layer or a multi-layer filter is being considered, the characteristic matrix [M] is always 2 × 2.

$$[M] = \begin{bmatrix} m_{11} & jm_{12} \\ jm_{21} & m_{22} \end{bmatrix} \tag{4.113}$$

Also, the determinant, DET[M] = $m_{11}m_{22} + m_{12}m_{21} = 1$. Therefore, if $m_{11} = m_{22}$, then [M] for a multi-layer is of the same form as for a single layer [equation (4.59)]. Define an *equivalent index of refraction*, *N*, and *phase thickness*, γ, for the multi-layer as follows.

$$\cos\gamma = m_{11} = m_{22} \tag{4.114}$$

$$\hat{N} = c_o\sqrt{\frac{m_{21}}{m_{12}}} \tag{4.115}$$

Remember, $\hat{n}$ depends on the polarization and magnetic permeability, μ, [equations (4.51a) and (4.51b)]. However, $\hat{N}$ can be interpreted as an equivalent index of refraction for a non-magnetic material ($\mu = \mu_o$) at normal incidence ($\theta = 0$). As a result,

$$N = \mu_o\hat{N} = c_o\mu_o\sqrt{\frac{m_{21}}{m_{12}}} \tag{4.116}$$

Using equations (4.114), (4.115), and DET[M] = 1 the *equivalent single layer* matrix becomes the following,

$$[M]=\begin{bmatrix} \cos\gamma & \dfrac{jc_o \sin\gamma}{\hat{N}} \\ \dfrac{j\hat{N}\sin\gamma}{c_o} & \cos\gamma \end{bmatrix} \tag{4.117}$$

where

$$\sin^2\gamma = 1-\cos^2\gamma = m_{12}m_{21} = 1-m_{11}^2 = 1-m_{22}^2 \tag{4.118}$$

The equivalent single layer applies only if $m_{11} = m_{22}$ for the multi-layer. What conditions must be satisfied for $m_{11} = m_{22}$? Consider a multi-layer made of layers 1, 2, 3,…, which has the following structure.

1234… 4321

This is called a *symmetrical multi-layer*. In this case, the characteristic matrix [M] obtained by matrix multiplication beginning at the m layer will be the same as the matrix [M′] obtained by matrix multiplication beginning at layer 1. Also, for each layer, i, the matrix elements m_{11}^i and m_{22}^i are the same (= $\cos\phi_i$). If $m_{11}^1 = m_{22}^i$, the following is obtained.(problem 4.4)

$$\begin{aligned} [M] &= [M_m][M_{m-1}]\ldots[M_1] = \begin{bmatrix} m_{11}^m & m_{12}^m \\ m_{21}^m & m_{22}^m \end{bmatrix}\begin{bmatrix} m_{11}^{m-1} & m_{12}^{m-1} \\ m_{21}^{m-1} & m_{22}^{m-1} \end{bmatrix}\ldots = \begin{bmatrix} m_{22} & m_{12} \\ m_{21} & m_{11} \end{bmatrix} \\ [M'] &= [M_1][M_2]\ldots[M_m] = \begin{bmatrix} m_{11}^1 & m_{12}^1 \\ m_{21}^1 & m_{22}^1 \end{bmatrix}\begin{bmatrix} m_{11}^2 & m_{12}^2 \\ m_{21}^2 & m_{22}^2 \end{bmatrix}\ldots = \begin{bmatrix} m_{11} & m_{12} \\ m_{21} & m_{22} \end{bmatrix} \end{aligned} \tag{4.119}$$

For a symmetrical multi-layer, [M′] = [M]. The only way for this to be true is if $m_{11} = m_{22}$. Thus, a symmetrical multi-layer can be characterized by an equivalent single layer where the equivalent phase thickness and index of refraction are given by equations (4.114) and (4.115). The equivalent index of refraction, N, will be a function of wavelength even if the indices of refraction of the individual layers are constants.

Consider the simplest symmetric layer systems LHL and HLH where L signifies a low index of refraction material and H a high index of refraction material. Also, the

phase thicknesses of the layers at wavelength λ_o are $\phi_i = \frac{2\pi n_i d_i \cos\theta_i}{\lambda_o} = \frac{\pi}{2}$, so that $n_i d_i \cos\theta_i = \frac{\lambda_o}{4}$. The wavelength λ_o is called the *design wavelength*. As shown in Section 4.3.5, for a single layer with $\phi = \frac{\pi}{2}$ the reflectance will be a maximum if $n > n_s$ or a minimum if $n < n_s$ where n_s is the substrate index of refraction. Since $n_i d_i \cos\theta_i = \frac{\lambda_o}{4}$ the phase thickness of each layer is $\phi_i = \frac{2\pi}{\lambda} n_i d_i \cos\theta_i = \frac{\pi}{2}\frac{\lambda_o}{\lambda}$. Thus, the characteristic matrix [M], and therefore the equivalent index of refraction, N, and phase thickness, γ, will be functions of $\bar{\lambda} = \frac{\lambda_o}{\lambda}$ and $\frac{n_H}{n_L}$.

In Figure 4.7, the equivalent index of refraction, N is shown as a function of $\bar{\lambda}$ for the [LHL] and [HLH] systems for $\frac{n_H}{n_L} = 3$ and $1.78 \left(\frac{n_H}{n_L} = \frac{2.4}{1.35} = 1.78\right)$. Figure 4.7 shows N for only a single cycle of $\bar{\lambda}$. The period is 2 so that $N(\bar{\lambda} + 2) = N(\bar{\lambda})$. Notice that $N \to \pm\infty$ for certain ranges of $\bar{\lambda}$. Between the regions where $N \to +\infty$ and $N \to -\infty$ the value of N is imaginary. As a result, the reflectance, ρ, approaches one for $\bar{\lambda}$ in this range. For both the [HLH] and [LHL] case in Figure 4.7, $0.56 \le \bar{\lambda} \le 0.76$ when $\frac{n_H}{n_L} = 1.78$ and $0.47 \le \bar{\lambda} \le 0.83$ when $\frac{n_H}{n_L} = 3.0$ are regions where $\rho \to 1$. These regions are called *stop bands* since the reflectance approaches one in these $\bar{\lambda}$ ranges. As the ratio $\frac{n_H}{n_L}$ increases the stop bands also increase in size.

Now apply the equivalent layer procedure to design a bandpass filter. For a TPV system that uses GaSb or InGaAs PV arrays, a bandpass filter that has large transmittance around $\lambda \approx 1.5\mu m$ is desirable. Therefore, choose the center wavelength of the filter to be $\lambda_c \approx 1.5\mu m$ and require the transmittance to be large for $1.0 \le \lambda \le 2.0\mu m$. Use the symmetric three-layer systems, [HLH] and [LHL], with $n_L = 1.35(ZnSe)$ and $n_H = 2.4(MgF_2)$ to design the filter. From Figure 4.7 for $\frac{n_H}{n_L} = \frac{2.4}{1.35} = 1.78$, the stop bands are defined by $0.56 \le \bar{\lambda} \le 0.76$. Therefore, to achieve large reflectance at $\lambda = 1.0\mu m$, $\bar{\lambda} = \frac{\lambda_o}{1.0} = 0.56$ and thus $\lambda_o = .56\mu m$ for either the HLH or LHL system.

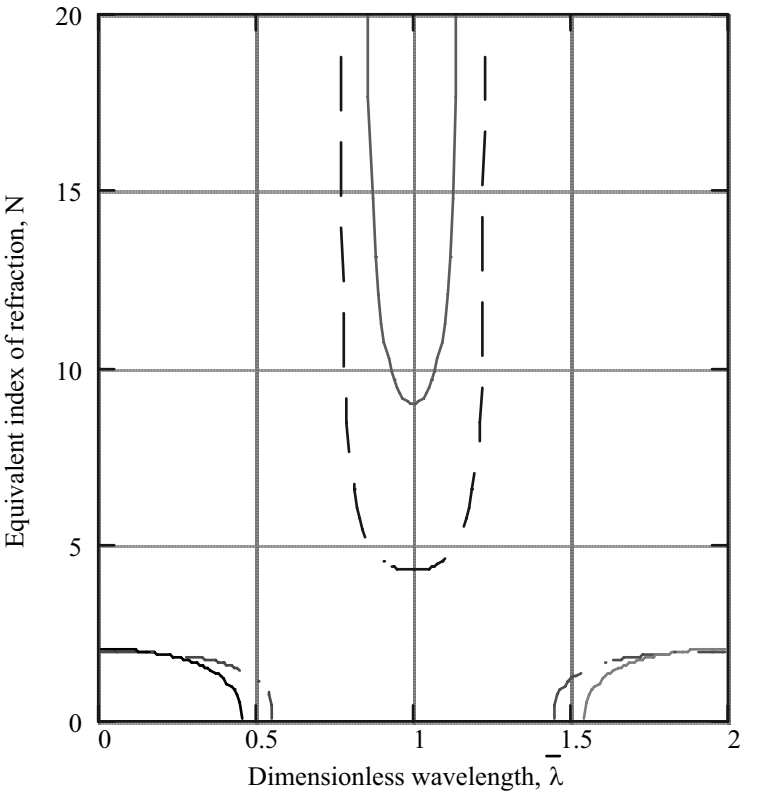

Figure 4.7a) - Equivalent index of refraction, N for symmetric HLH, nonabsorbing systems as a function of $\bar{\lambda} = \lambda_o/\lambda$, where λ_o is the design wavelength, and ndcos $\theta = \lambda_o/4$ for each layer, where n is the index of refraction, d the thickness and θ the angle of incidence of each layer. Solid curve; $n_H/n_L = 3$, dashed curve; $n_H/n_L = 1.78$.

Similarly, for large reflectance at λ = 2.0μm, $\bar{\lambda} = \frac{\lambda_o}{2.0} = 0.76$ and thus λ_o = 1.52μm. Thus if λ_o = 0.56μm the stop band covers the range $\lambda \leq \frac{\lambda_o}{\bar{\lambda}} = \frac{0.56}{0.76} = 0.73\mu m$ to $\lambda \leq 1.0\mu m$.

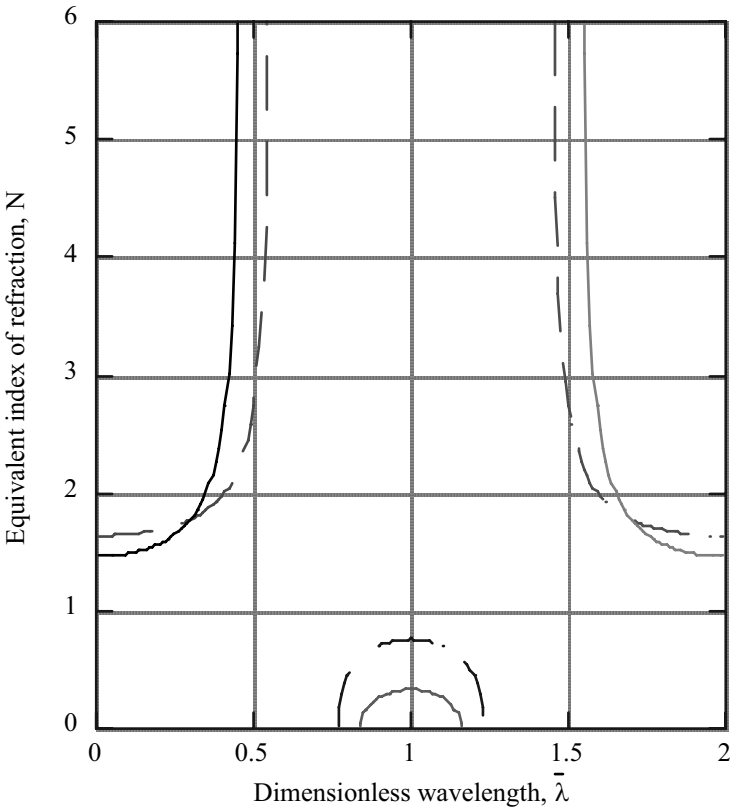

Figure 4.7b) - Equivalent index of refraction, N for symmetric LHL, nonabsorbing systems as a function of $\bar{\lambda}=\lambda_o/\lambda$, where λ_o is the design wavelength, and $ndcos\theta=\lambda_o/4$ for each layer, where n is the index of refraction, d the thickness and θ the angle of incidence of each layer. Solid curve; $n_H/n_L=3$, dashed curve; $n_H/n_L=1.78$.

Similarly, if λ_o = 1.52μm the stop band covers the range $\lambda \geq$ 2.0μm to $\lambda \leq \frac{\lambda_o}{\bar{\lambda}} = \frac{1.52}{0.56} = 2.71\mu m$. Now choose the following layer configuration,

$$s\left|1.01\left[LHL\right]0.37\left[HLH\right]\right|o \qquad \lambda_c = 1.5\mu m \qquad (4.120)$$

where s is the substrate (n_s = 1.52) and o is the surrounding medium (n_o = 1.0). The numbers1.01 and 0.37 give the design wavelengths of the [LHL] and [HLH] groups in terms of the center wavelength (λ_c = 1.5μm) of the filter. For the [LHL] group λ_o = 1.01(1.5) = 1.52μm and for the [HLH] group λ_o = 0.37(1.5) = 0.56μm. Each layer must satisfy the condition,

$$nd\cos\theta = \frac{\lambda_o}{4} \tag{4.121}$$

To calculate the reflectance, ρ, transmittance, $\hat{\tau}$, and total absorptance, α_T, of the configuration given by equation (4.120), equations (4.58), (4.61), (4.66), (4.69), and (4.70) are applied. A Mathematica [6] computer program, included on the enclosed CD-R disk, has been written to carry out the calculations. A description of this program is in Appendix D. For the configuration given by equation (4.120) the reflectance in the stop bands ($0.73 \le \lambda \le 1.0$ and $2.0 \le \lambda \le 2.7$) is not large. However, by repeating the [LHL] and [HLH] groups several times the reflectance increases in the stop bands. If each group is repeated five times, so that the configuration is the following,

$$s\left|1.01\left[LHL\right]^5\ 0.37\left[HLH\right]^5\right|o \tag{4.122}$$

then the reflectance is large in the stop bands and the transmittance is large between them, as Figure 4.8a shows for θ_o = 0.

To increase τ in the bandpass region ($1.0 \le \lambda \le 2.0$), additional [HLH] groups can be added between the $[LHL]^5$ and $[HLH]^5$ groups, between the substrate, s, and $[LHL]^5$ and between $[HLH]^5$ and the surrounding media, o. These additional [HLH] groups act as anti-reflection films at λ_c = 1.5μm. Consider the interface between $[HLH]^5$ and o. The design wavelength for [HLH] is λ_o = 0.56μm. For λ_c = 1.5μm, $\bar{\lambda} = \frac{\lambda_o}{\lambda_c} = 0.373$ and N ≈ 1.7 (Figure 4.7a). As discussed earlier in Section 4.2.5 and also problem 4.5, ρ = 0 if the anti-reflection film index of refraction is given by $\sqrt{n_o N}$. Therefore, if $N_{anti} = \sqrt{1(1.7)} = 1.3$, ρ = 0 between $[HLH]^5$ and o when λ = 1.5μm. For $N_{anti} = 1.3$, $\bar{\lambda} = \frac{\lambda_o}{\lambda} \approx 0.48$ (Figure 4.7a) so that the desired design wavelength, λ_o, for the [HLH] anti-reflection film is λ_o = 0.48(1.5) = 0.72μm. Repeating the same procedure for the $[LHL]^5$– s and $[LHL]^5$ – $[HLH]^5$, interfaces the design wavelength for a [HLH] group between $[LHL]^5$ and s is λ_o = 0.78μm and between $[LHL]^5$ and $[HLH]^5$ is

λ_o = 0.765μm. Thus the multi-layer interference filter with λ_c = 1.5μm has the following configuration.

$$s\left|0.52[HLH]1.01[LHL]^5\ 0.51[HLH]0.37[HLH]^5\ 0.47[HLH]\right|o \qquad \lambda_c = 1.5\mu m \tag{4.123}$$

Using the program described in Appendix D, the transmittance and reflectance for θ_o = 0 have been calculated and the results for $\hat{\tau}$ are shown in Figure 4.8b. Comparing Figure 4.8a and 4.8b it can be seen that the additional [HLH] groups make only a modest improvement in the transmittance in the bandpass region.

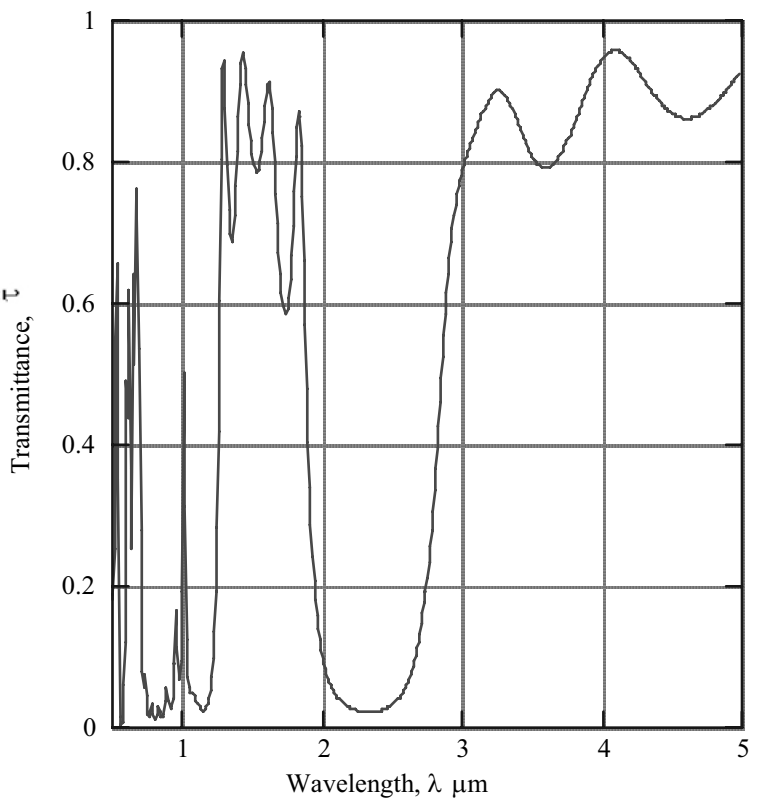

Figure 4.8a) - Transmittance, $\hat{\tau}$, at θ_o = 0 of a multi-layer bandpass filter with center wavelength, λ_c = 1.5 μm and configuration

s|1.01[LHL]^5.37[HLH]^5|o based on the equivalent layer procedure using the groups [HLH] and [LHL] where n_L=1.35 and n_H=2.4. For the substrate, n_s=1.52 and for the surroundings n_o=1.0.

The results in Figure 4.8 point out a problem for TPV energy conversion that all non-absorping interference filters have. Similar to the problem for rare-earth selective emitters discussed in Chapter 3, at long wavelengths the transmittance becomes large just as the emittance for the rare-earth emitters also becomes large. Thus, in both cases the long wavelength radiation, which cannot be converted to electrical energy by the PV array is a significant loss for the TPV system. Increasing the stop band regions will extend the regions of large reflectance (problem 4.10). As Figure 4.7 shows the stop bands increase with increasing $\frac{n_H}{n_L}$.

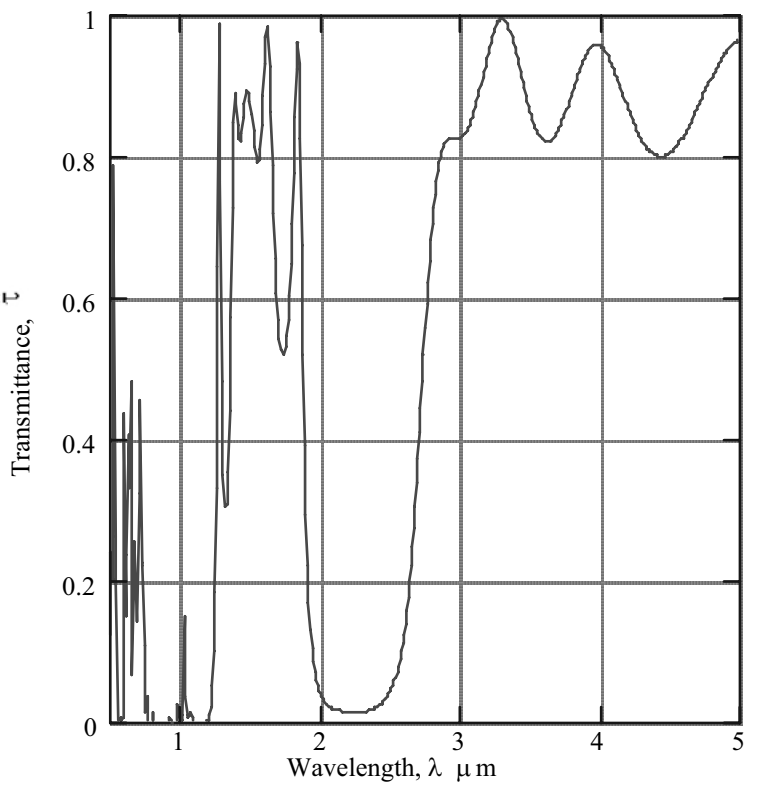

Figure 4.8b) - Transmittance, $\hat{\tau}$, at $\theta_o = 0$ of a multi-layer bandpass filter with center wavelength, $\lambda_c = 1.5$ μm and configuration

s|.52[HLH]1.01[LHL]^5.51{HLH].37[HLH]^5.47[HLH]|o based on the equivalent layer procedure using the groups [HLH]and [LHL] where n_L=1.35 and n_H=2.4. For the substrate, n_s=1.52 and for the surroundings n_o=1.0.

However, as stated earlier, presently no known dielectric materials with large index of refraction exist. Reflectance and transmittance resulting from the interference effect have sinusoidal-like behavior. As a result, either large or small ρ or τ within some wavelength region, $\Delta\lambda$, means that ρ or τ will be large or small at π multiples of $\frac{1}{\lambda}$ for wavelengths within $\Delta\lambda$. Thus, it is impossible to design an interference filter that will have $\hat{\tau} \rightarrow 1$ in some bandpass wavelength region and $\rho \rightarrow 1$ everywhere outside this region.

4.3.8 Interference Filter with Embedded Metallic Layer

One method for obtaining large reflectance at the long wavelengths is to use a highly reflecting metallic layer embedded within dielectric anti-reflecting layers. This approach has been proposed by Demichelis, et al. [7,8] In [9] this type of filter was used to compare a solar TPV (STPV) system to a conventional directly solar illuminated PV system.

For most metals, the imaginary part of the index of refraction, n_I, becomes large (> 10) at infrared wavelengths. As a result, the reflectivity into a dielectric is large [equation (1.110)] at long wavelengths. However, if n_I is large the absorptance will also be large. The absorptance can be minimized by making the metallic layer very thin. For a TPV filter, the wavelength region, 1-3μm, is where large transmittance is required. In this wavelength region, metals do not have large transmittance. However, by placing anti-reflecting layers, designed for a particular wavelength, on each side of the metal, the required large transmittance in a wavelength band around the design wavelength can be achieved.

Consider a filter designed to have large transmittance in the wavelength region around $\lambda_c = 1.5\mu m$. Since gold has very large reflectivity (> 0.9) for long wavelengths, choose it for the metal layer. To attain large transmittance around $\lambda_c = 1.5\mu m$ requires anti-reflecting layers with indices of refraction that match the index of refraction of gold at $\lambda_c = 1.5\mu m$. If the indices of refraction are the same, no reflection at the metal-anti-reflecting layer interfaces will occur. Using the equivalent layer procedure, suitable anti-reflecting layers can be determined.

Using the index of refraction data for gold [10], the following curve fits are obtained.

$$n_R = 1.8717 - 3.5607\lambda + 2.7027\lambda^2 - 0.81284\lambda^3 + 0.12732\lambda^4 - 0.0097148\lambda^5 + 0.00028705\lambda^6 \quad (4.124a)$$

$$n_I = -0.54737 + 6.9109\lambda - 0.13307\lambda^2 \quad (4.124b)$$

Where λ is in micrometers (μm). Equations (4.124a) and (4.124b) are close fits to the data of [10] except in the region λ < 1.0μm. At λ_c = 1.5μm, $|n| = \sqrt{n_R^2 + n_I^2} \approx 10$. For the symmetric layer group [HLH] in Figure 4.7a where $\frac{n_H}{n_L} = 1.78$, the equivalent index of refraction, N ≈ 10 when $\bar{\lambda} = \frac{\lambda_o}{\lambda} \approx 0.78$. Thus, if λ = 1.5μm, then the design wavelength, λ_o = 0.78(1.5) = 1.17μm. Therefore, placing a gold layer between two [HLH] groups, with λ_o = 1.17μm for both groups, should yield a bandpass filter centered at λ_c = 1.5μm with large reflectance for long wavelengths. Using the Mathematica program described in Appendix D, the optical properties for the filter on a glass substrate (n_s = 1.52) at normal angle of incidence (θ_o = 0) are calculated. It is found that λ_o = 1.17μm yields a bandpass region where λ_c < 1.5μm. However, by changing λ_o to 1.38μm the bandpass region is centered at λ_c = 1.5μm. Therefore, the filter is designated as follows.

$$s\left|0.92[HLH][m]0.92[HLH]\right|o \tag{4.125}$$

CONFIGURATION	FILM THICKNESS, nm
o Vacuum, n_o=1.0	
H	143.8
L	255.6
H	143.8
M Gold	25.0
H	143.8
L	255.6
H	143.8
s Substrate, Glass n_s=1.52	

Table 4.1 Layer thickness for embedded metal interference filter of configuration s|.92[HLH][M].92[HLH]|0. with center wavelength, λ_c=1.5μm. H is ZnSe(n_H=2.4), L is MgF_2(n_L=1.35) and M is gold. Wavelength dependence of gold index of refraction is given by equations 4.124.

The thicknesses of each layer are listed in Table 4.1. Magnesium fluoride (MgF_2) is the low index material (n_L = 1.35) and zinc selenide (ZnSe) is the high index material (n_H = 2.4).

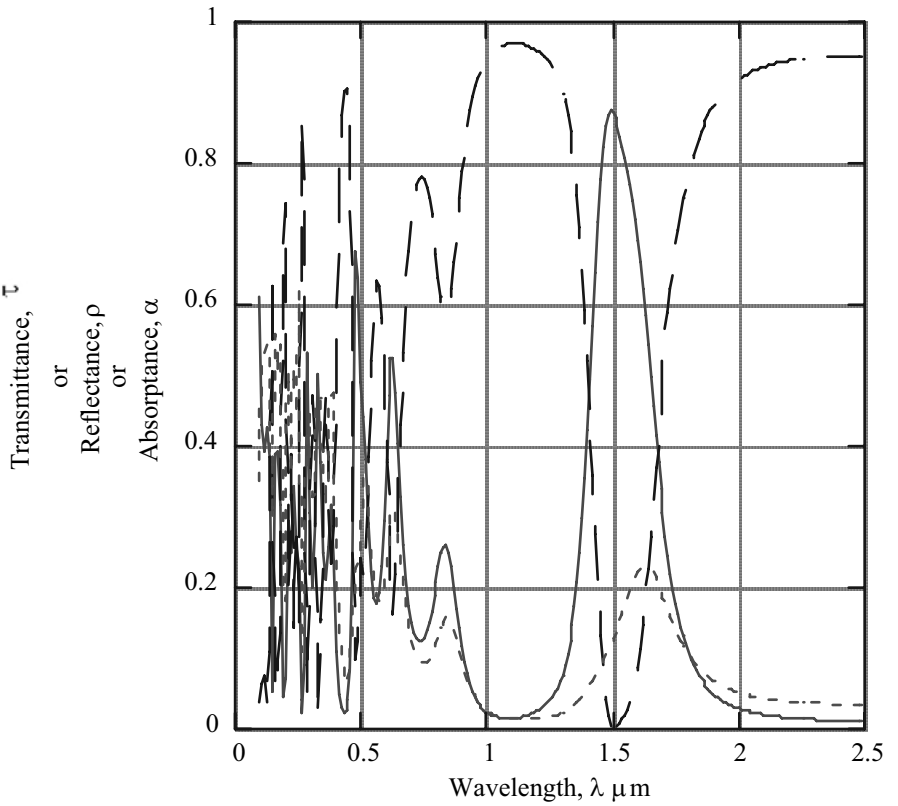

Figure 9a) Transmittance, absorptance and reflectance for $0<\lambda<2.5$ μm

The optical properties as a function of wavelength are shown in Figure 4.9. The first thing to notice is the large reflectance ($\rho \geq 0.85$) for long wavelengths ($\lambda \geq 2.0\mu m$), which is the desired result. This compares to the opposite, undesirable result of small reflectance for the long wavelengths of the filter in Figure 4.8. The undesirable feature of the embedded metal filter is the absorptance resulting from the gold layer. The bandpass region of the embedded metal filter is also rather narrow, which limits the amount of convertible radiation that reaches the PV array, thus limiting the power density of the TPV system.

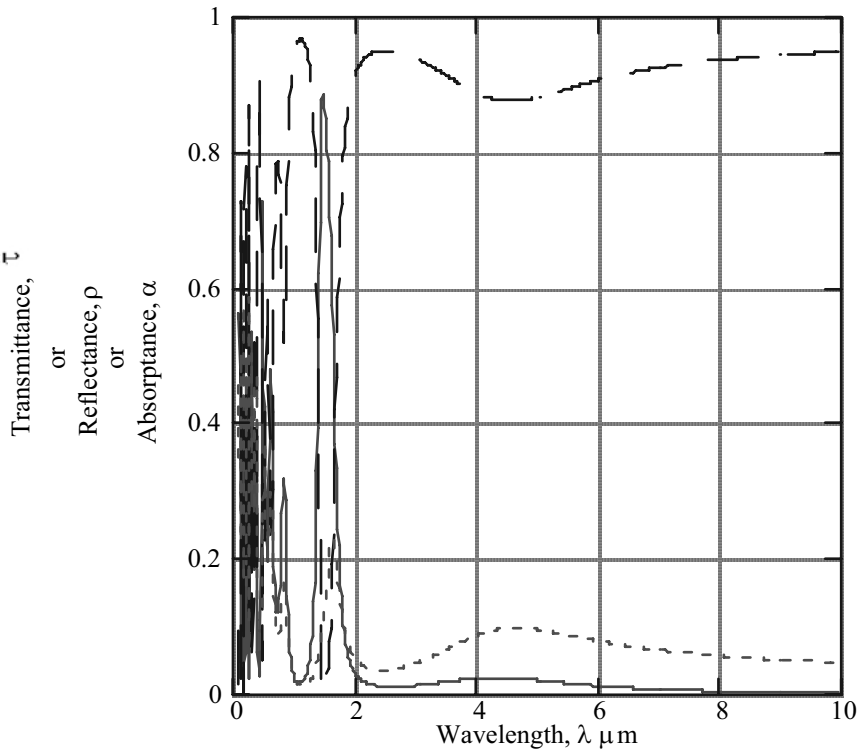

b) Transmittance, absorptance and reflectance for $0<\lambda<10$ μm

Figure 4.9 - Performance of embedded metal interference filter of configuration [HLH]m[HLH] with center wavelength, λ_c=1.5 μm at normal incidence, θ_o=0. H has index of refraction, n_H=2.4, L has index of refraction, n_L=1.35. Index of refraction of gold given by equations 4.124a) and b). Thicknesses of layers given in Table 4.1. For the substrate n_s=1.52 and for the surroundings n_o=1.0. $\hat{\tau}$ ——, ρ —— —, α - - - - -

Now consider the filter efficiency, η_f, and total optical properties, τ_{fT}, ρ_{fT}, and α_{fT}. Apply equations (4.4) through (4.7) to the embedded metal filter of Figure 4.9. Although the emitter spectral emittance, $\varepsilon_E(\lambda)$, is an important variable in equations (4.4) through (4.7), assume ε_E is a constant (a blackbody for example) so that it drops out of the equations. In that case η_f, τ_{fT}, ρ_{fT}, and α_{fT} can be calculated using the $\tau_f(\lambda)$, $\rho_f(\lambda)$, and $\alpha_f(\lambda)$ data of Figure 4.9. These results are shown in Figure 4.10 as a function of the emitter temperature, T_E. Numerical integration with λ_g = 1.9μm (E_g = 0.65eV) has been used to calculate η_f. As Figure 4.10 shows the filter efficiency, $\eta_f > 0.5$ for $T_E \geq 1500$K, while the total absorptance remains at $\alpha_{fT} \approx 0.07$ over the entire

temperature range. The embedded gold produces the desired large reflectance (>0.85) for long wavelengths at the expense of the absorptance loss.

Remember, the embedded metal filter has been designed using the rather simple equivalent layer method. Using a more precise optimization method would yield thicknesses for the various layers that would produce a better performing filter.

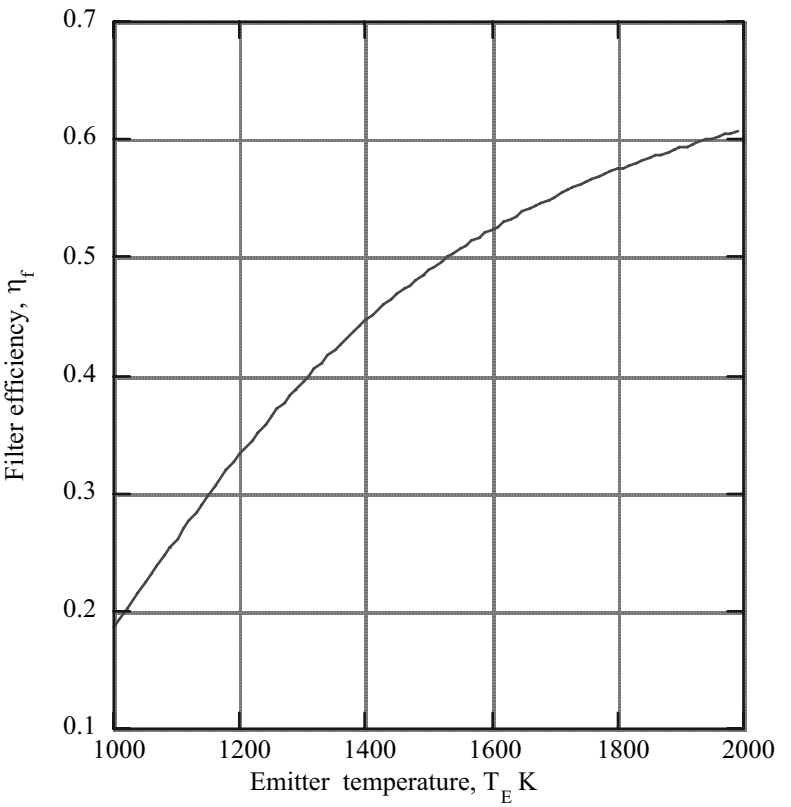

Figure 4.10a) - Filter efficiency of embedded metal interference filter of Fig. 4.9 for constant emitter emittance, ε_E. Limit wavelength for filter efficiency calculation, λ_g=1.9 μm.

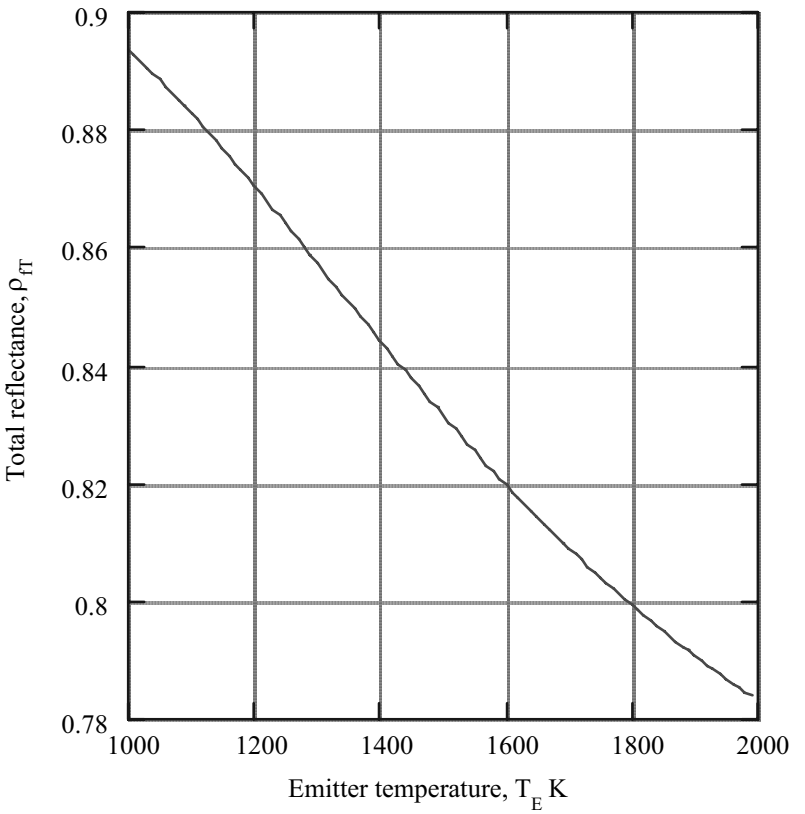

Figure 4.10b) - Total reflectance of embedded metal interference filter of Fig. 4.9 for constant emitter emittance, ε_E. Limit wavelength for filter efficiency calculation, λ_g=1.9 μm.

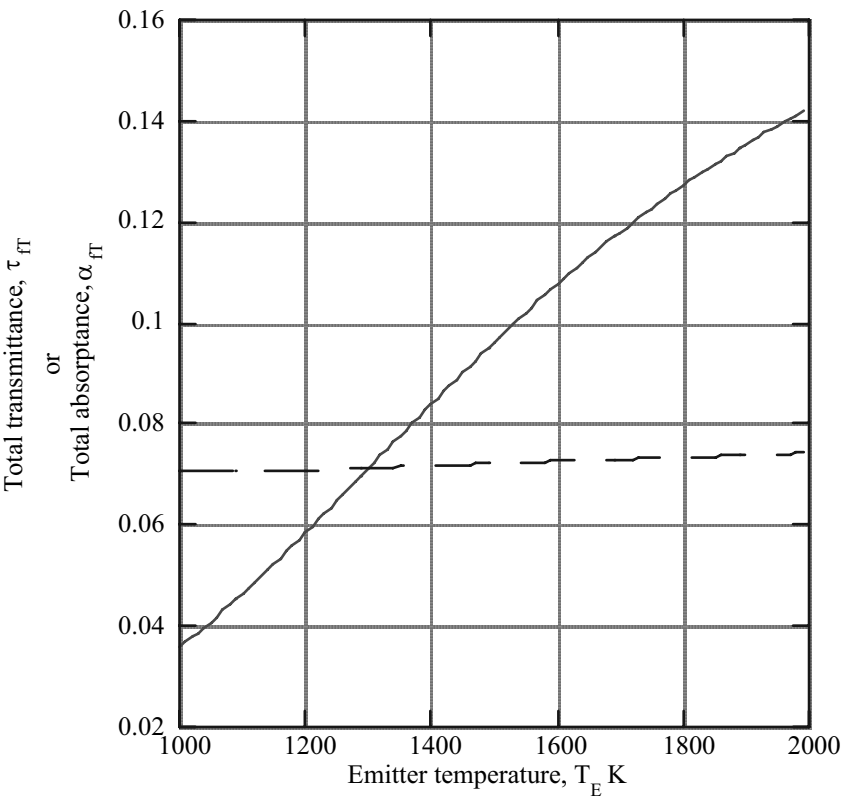

Figure 4.10c) - Total transmittance and absorptance of embedded metal interference filter of Fig. 4.9 for constant emitter emittance, ε_E. Limit wavelength for filter efficiency calculation, λ_g=1.9 μm.

τ_{fT} ———— , α_{fT} — —

4.3.9 Interference Filter Performance for Angles of Incidence Greater than Zero

In a TPV system, the radiation incident on a filter will arrive at all angles of incidence. Obviously, if the filter is designed for $\theta^o = 0$, then the optical performance at $\theta_o > 0$ will not be as good as at $\theta_o = 0$. Consider the embedded metal interference filter of Figure 4.9. For $\theta_o = 45^o$ the spectral performance of this filter for s polarization is shown in Figure 4.11.

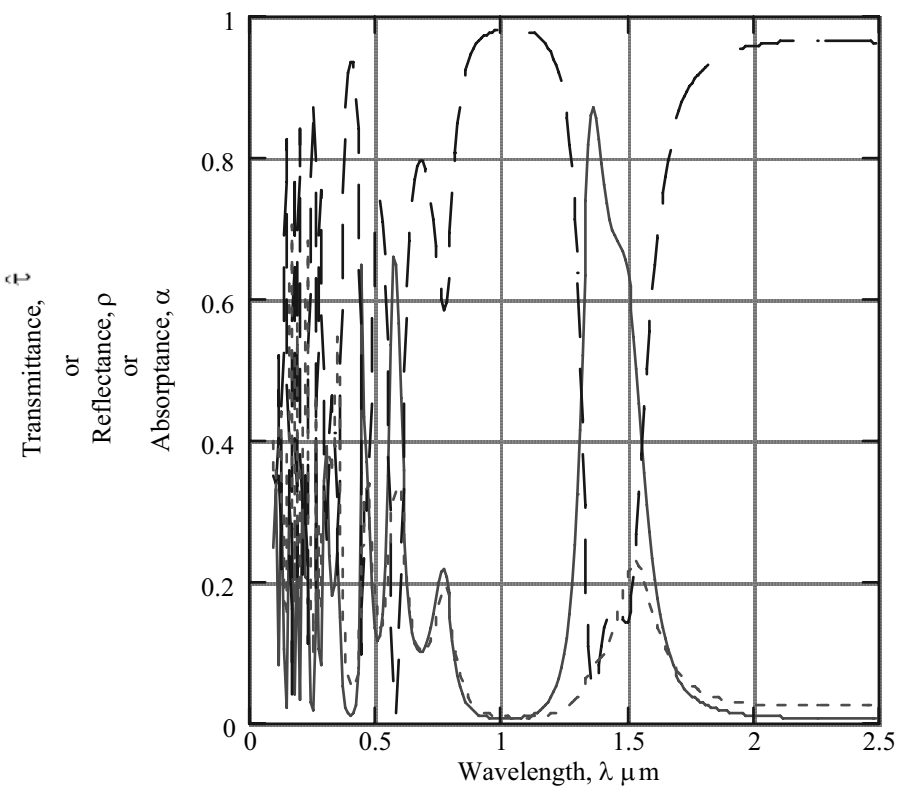

Figure 4.11a) - Transmittance, absorptance and reflectance for $0<\lambda<2.5$ μm of embedded metal interference filter of Fig. 4.9 for s polarization at angle of incidence, $\theta_o = 45^0$. $\hat{\tau}$ ——, ρ ——, α — — —

As Figure 4.11a shows, the center wavelength, λ_c, moves to a shorter wavelength but the transmittance in the bandpass region is changed only slightly from the $\theta_o = 0$ case (Figure 4.9). In addition, the long wavelength performance at $\theta_o = 0$ and $\theta_o = 45^o$ is nearly the same. As θ_o is increased beyond 45º, the degradation of performance is more pronounced.

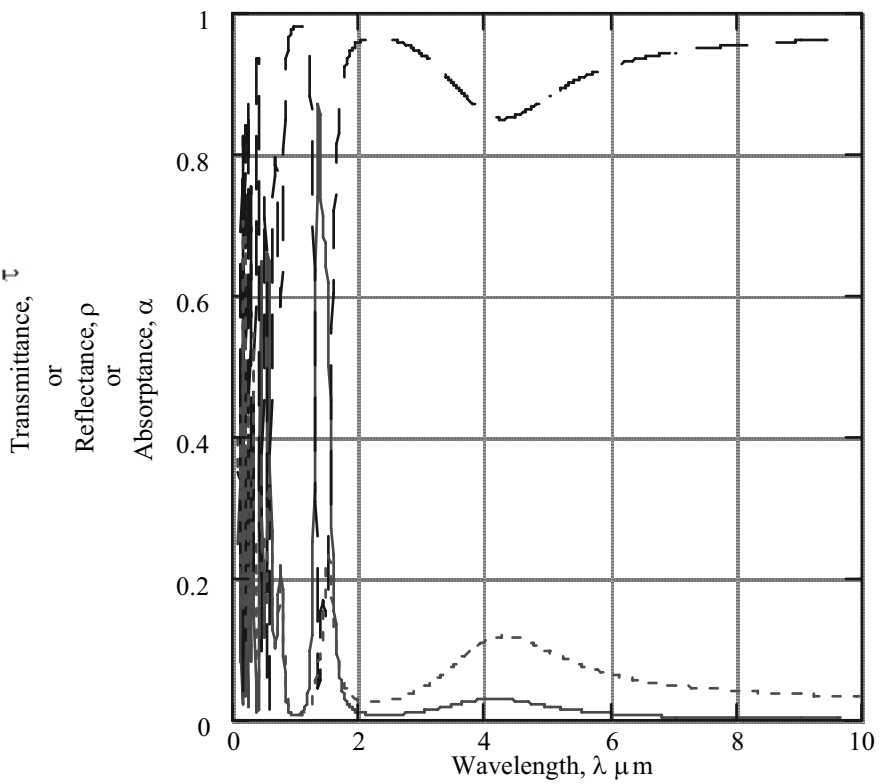

Figure 4.11b) - Transmittance, absorptance and reflectance for 0< λ<10 μm of embedded metal interference filter of Fig. 4.9 for s polarization at angle of incidence, $\theta_o = 45^0$. $\hat{\tau}$ —— ρ —— —— α - - - -

This is illustrated in Figure 4.12 where the filter efficiency, η_f, is shown at a function of θ_o for both s and p polarization. These calculations are performed using λ_g = 1.9μm and T_E = 1500K. In the case of p polarization, η_f actually increases for $\theta_o > 80^o$. For s polarization, η_f decreases rapidly for $\theta_o > 50^o$.

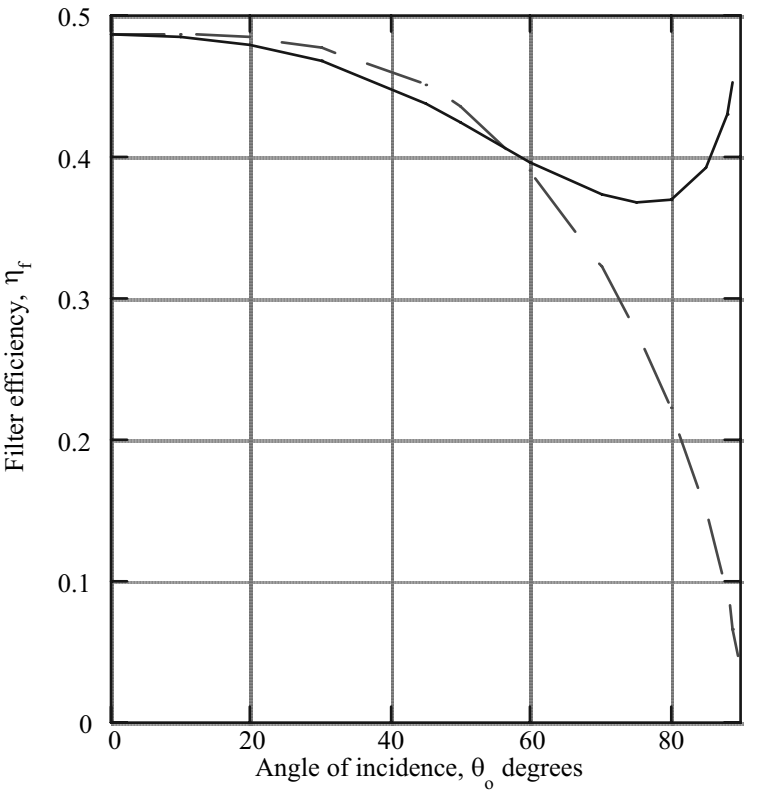

Figure 4.12 - Effect of angle of incidence, θ_o on filter efficiency, η_f for the embedded metal interference filter of figure 4.9 at T_E=1500 K. Solid line p polarization, dashed line s polarization. Limit wavelength for filter efficiency calculation, λ_g=1.9 μm.

Figure 4.12 shows that $\eta_f \approx 0.5$ for p polarization at $\theta_o = 90^o$. It should be pointed out, however, that $\hat{\tau} \to 0$ and $\rho \to 1$ as $\theta_o \to 90^o$. Therefore, even though η_f remains finite, the amount of transmitted radiation is negligible.

4.4 Plasma Filters

Interference filters generally consist of dielectric materials that have nearly constant real indices of refraction and negligible absorptance. In this section consider so-called plasma filters that are made from conductors and semiconductors, which have both real and imaginary indices of refraction and thus are absorptive. However, the virtues of a plasma filter are its simplicity and large reflectance.

Semiconductors such as silicon [14], indium gallium arsenide [15], and transparent conducting oxides, such as indium oxide [16], tin oxide, indium tin oxide, zinc oxide, and cadium stamnate [17,18] are some possible plasma filter materials. The transparent conducting oxides have large bandgap energies (> 3eV), which account for their transparency.

4.4.1 Drude Model

The term plasma filter applies to a class of optical filters whose electrical and optical properties are approximated by the so-called Drude model. The Drude model applies when the valence electrons of an atom are considered to be free of the ion core. The model approximates metals and doped semiconductors where electrons in the conduction band are essentially free of the ion cores.

The Drude model, will be used to calculate the complex index of refraction, n. Once n is known the reflectance, ρ, transmittance, τ, and absorptance, α, will be calculated.

In the Drude model, electrons are treated as a gas of free particles, similar to a *plasma*, which is an ionized gas. In a plasma, the electrons have high mobility compared to the nearly stationary ions. Therefore, results of the Drude model are also applicable to a plasma. Thus, some of the terms such as plasma frequency, are used in both the Drude model and in plasma theory.

To quantify the model, apply a transverse electromagnetic wave with electric field, $\vec{E}$, to the electron gas. The electric field causes an acceleration of an electron given by the equation of motion.

$$m^* \frac{d\vec{v}}{dt} = m^* \frac{d^2\vec{r}}{dt^2} = -e\vec{E} \tag{4.126}$$

Where $\vec{v} = \frac{d\vec{r}}{dt}$ is the electron velocity, $\vec{r}$ is the electron location, e is the magnitude of the electron charge, and m^* is the *effective mass* of the electron. The effective mass accounts for the fact that the electrons are not really free but are affected by the ion cores. This is discussed in Chapter 5. In addition to the electric field force, the electron momentum, $m^*\vec{v}$, is changed by collisions. This momentum change is $m^*\vec{v}/\tau_c$, where

τ_c is the time between collisions. Since collisions reduce the electron momentum the equation of motion becomes the following.

$$m^* \frac{d^2\vec{r}}{dt^2} = -e\vec{E} - \frac{m^*}{\tau_c}\frac{d\vec{r}}{dt} \tag{4.127}$$

For a plane wave, the electric field is given by equation (1.10). For wavelengths in the visible and near infrared part of the spectrum, the electron movement will be much smaller than the wavelength. Therefore, since $k \sim \frac{1}{\lambda}$ the $\vec{k}\bullet\vec{x}$ term in equation (1.10) can be neglected. As a result, equation (4.127) becomes the following,

$$\frac{d^2\vec{r}}{dt^2} + \frac{1}{\tau_c}\frac{d\vec{r}}{dt} = -\frac{e}{m^*}\vec{E}_o e^{j\omega t} \tag{4.128}$$

where the electron location is the real part of the solution to equation (4.128). As a trial solution, assume $\vec{r} = \vec{r}_o e^{j\omega t}$ and substitute it in equation (4.128). As a result the following is obtained.

$$\vec{r}_o = \frac{e\tau_c}{\omega m^*}\frac{\vec{E}_o}{\omega\tau_c - j} \tag{4.129}$$

The electron displacement $\vec{r}_o$ produces an electric dipole moment, $-e\vec{r}_o$. If the electron number density is N(m^{-3}), the dipole moment per unit volume is the following,

$$\vec{P} = -eN\vec{r}_o = -\frac{\omega_p^2 \varepsilon_o \vec{E}_o}{\omega^2 - \frac{j\omega}{\tau_c}} \tag{4.130}$$

where ε_o is the vacuum permittivity and ω_p is the so-called *plasma frequency*.

$$\omega_p^2 = \frac{e^2 N}{\varepsilon_o m^*} = 3.182\times10^9 \frac{N\left(cm^{-3}\right)}{\frac{m^*}{m_e}} \qquad sec^{-2} \tag{4.131}$$

In a plasma this is the frequency of the oscillation that electrons experience when they are displaced from their equilibrium position. It is the Coulomb force between the electrons and ions that causes the oscillations.

In Chapter 1 [equation (1.5)] the permittivity, ε, for a linear medium has been defined as

$$\varepsilon = \varepsilon_o + \chi \tag{4.132}$$

where χ is the electric susceptibility.

$$\vec{P} = \chi \vec{E}_o \tag{4.133}$$

Thus, combining equations (4.130), (4.132), and (4.133) the following result for the *dielectric constant*, $\overline{\varepsilon}$, is obtained.

$$\overline{\varepsilon} = \frac{\varepsilon}{\varepsilon_o} = 1 - \frac{\omega_p^2}{\omega^2 - \frac{j\omega}{\tau_c}} \tag{4.134}$$

Separating $\overline{\varepsilon}$ into real and imaginary parts yields the following,

$$\overline{\varepsilon} = \overline{\varepsilon}_R - j\overline{\varepsilon}_I \tag{4.135}$$

where

$$\overline{\varepsilon}_R = 1 - \frac{\left(\omega_p \tau_c\right)^2}{\left(\omega\tau_c\right)^2 + 1} \tag{4.136}$$

$$\overline{\varepsilon}_I = \frac{\omega_p^2 \tau_c}{\omega\left[\left(\omega\tau_c\right)^2 + 1\right]} \tag{4.137}$$

For a non-magnetic medium [equation (1.26)], the following relation between $\overline{\varepsilon}$ and the index of refraction, n, applies,

$$n = \sqrt{\overline{\varepsilon}} = n_R - jn_I \tag{4.138}$$

and from equations (1.30),

$$n_R = \left[\frac{1}{2} \sqrt{\bar{\varepsilon}_R^2 + \bar{\varepsilon}_I^2} + \frac{\bar{\varepsilon}_R}{2} \right]^{1/2} \tag{4.139}$$

$$n_I = \left[\frac{1}{2} \sqrt{\bar{\varepsilon}_R^2 + \bar{\varepsilon}_I^2} - \frac{\bar{\varepsilon}_R}{2} \right]^{1/2} \tag{4.140}$$

In order for $\bar{\varepsilon}$ and n to have closer agreement with experimental results, make the following change to $\bar{\varepsilon}_R$. Replace the quantity 1 by $\bar{\varepsilon}_\infty$ in the equation for $\bar{\varepsilon}_R$. The ∞ subscript is used because this is the value for $\bar{\varepsilon}_R$ for $\omega \to \infty$, or $\lambda = \frac{2\pi c_o}{\omega} = 0$. The justification for this alteration is the following. For $\omega \to \infty$, or $\lambda = 0$, equation (4.137) implies that $\bar{\varepsilon}_I = 0$ and $\bar{\varepsilon}_R = \bar{\varepsilon}_\infty$, so that $n_R = \sqrt{\bar{\varepsilon}_\infty}$ and $n_I = 0$. Therefore, if $\bar{\varepsilon}_\infty = 1$, the normal reflectivity, $\bar{R}$, [equation (1.110)] at the medium-vacuum interface, $\bar{R} = \frac{(1 - n_R)^2}{(1 + n_R)^2} = 0$. Experimental results for $\bar{R}$ for $\omega \to \infty$ are finite, therefore justifying the approximation, $\bar{\varepsilon}_\infty > 1$. As a result, $\bar{\varepsilon}_R$ becomes the following.

$$\bar{\varepsilon}_R = \bar{\varepsilon}_\infty \left[1 - \frac{(\omega_p' \tau_c)^2}{(\omega \tau_c)^2 + 1} \right] \tag{4.141}$$

where a new plasma frequency, ω_p', that includes $\bar{\varepsilon}_\infty$ is defined as follows.

$$\omega_p'^2 = \frac{e^2 N}{\varepsilon_o \bar{\varepsilon}_\infty m^*} = \frac{\omega_p^2}{\bar{\varepsilon}_\infty} \tag{4.142}$$

Now consider typical values for ω_p and τ_c for metals and doped semiconductors, which can be described by the Drude model. For metals such as copper and the alkali metals at room temperature, $N \approx 10^{22} cm^{-3}$ so that for $m^* = m_e$, where m_e is the electron mass, $\omega_p \approx 5 \times 10^{15} sec^{-1}$. Also, for metals $\tau_c \approx 10^{-14} sec$. Therefore, for these conditions $(\omega_p \tau_c)^2 \approx 2.5 \times 10^3 \gg 1$. For doped semiconductors, the free carrier density, N, will be less than for metals. However, $N \approx 10^{21} cm^{-3}$ is possible, and since $m^* < 0.5 m_e$ and τ_c

for semiconductors is much large than τ_c for metals, the approximation $\omega_p\tau_c \gg 1$ is also applicable to semiconductors.

Consider the dielectric constant when $(\omega\tau_c)^2 \gg 1$. From equations (4.141) and (4.137) the following results are obtained.

$$\left.\begin{aligned} \overline{\varepsilon}_R &\approx \overline{\varepsilon}_\infty\left[1-\left(\frac{\omega_p'}{\omega}\right)^2\right] = \overline{\varepsilon}_\infty\left[1-\left(\frac{\lambda}{\lambda_p}\right)^2\right] && (4.143a)\\ \overline{\varepsilon}_I &\approx \left(\frac{\omega_p'}{\omega}\right)^2\frac{1}{\omega\tau_c} = \overline{\varepsilon}_\infty\left(\frac{\lambda}{\lambda_p}\right)^2\frac{\lambda}{2\pi c_o\tau_c} && (4.143b)\end{aligned}\right\} \quad (\omega\tau_c)^2 = \left(\frac{2\pi c_o\tau_c}{\lambda}\right)^2 \gg 1$$

where

$$\lambda_p = \frac{2\pi c_o}{\omega_p'} \tag{4.144}$$

is the wavelength corresponding to the frequency ω_p'. As equations (4.143a) and (4.143b) indicate, for $\left(\frac{\lambda}{\lambda_p}\right)^2 \gg 1$ and $\frac{\lambda}{2\pi c_o\tau_c} \ll 1$ the following approximation results.

$$\overline{\varepsilon}_R \approx -\overline{\varepsilon}_\infty\left(\frac{\lambda}{\lambda_p}\right)^2 \quad \text{and} \quad \left|\overline{\varepsilon}_R\right| \gg \overline{\varepsilon}_I \quad \text{for} \quad \left(\frac{\lambda}{\lambda_p}\right)^2 \gg 1 \quad \text{and} \quad \frac{\lambda}{2\pi c_o\tau_c} \ll 1 \tag{4.145}$$

Therefore, for this approximation, equations (4.139) and (4.140) yield the following.

$$n_R \approx 0, \qquad n_I \approx \sqrt{\varepsilon_\infty}\left(\frac{\lambda}{\lambda_p}\right) \tag{4.146}$$

Thus, the real part of the index of refraction vanishes while the imaginary part of the index of refraction is a linear function of wavelength. This approximation applies to most conductors for wavelengths beyond the visible.

An important feature of the Drude model is that $\overline{\varepsilon}_R$ changes sign from – to + at some frequency, ω_o. This frequency is found by setting equation (4.141) equal to zero.

$$\omega_o^2 = \omega_p'^2 - \frac{1}{\tau_c^2} \tag{4.147}$$

For most plasma filters, the approximation $\left(\omega_p'\tau_c\right)^2 \gg 1$ is applicable. As a result,

$$\omega_o \approx \omega_p' \qquad \text{for} \left(\omega_p'\tau_c\right)^2 \gg 1 \tag{4.148}$$

This is a resonance condition. When the frequency of the wave, ω, is the same as the natural frequency of the electrons, ω_p', energy will be transferred from the wave to the electrons. Thus the absorption will be highest when $\omega = \omega_o \approx \omega_p'$, as will be shown in the next section.

Now consider how the normal vacuum reflectivity, $\overline{R}$, behaves in the vicinity of the frequency $\omega = \omega_p'$. Again assume $\left(\omega_p'\tau_c\right)^2 \gg 1$. Therefore, for $\omega = \omega_p'$, equations (4.137) and (4.141) yield the following result.

$$\overline{\varepsilon}_R = 0 \quad \text{and} \quad \overline{\varepsilon}_I \ll 1 \qquad \text{for} \left(\omega_p'\tau_c\right)^2 \gg 1 \tag{4.149}$$

As a result, from equations (4.139) and (4.140) $n_R = n_I = \sqrt{\overline{\varepsilon}_I/2} \ll 1$ and $\overline{R} \approx 1$. Now increase or decrease ω a small increment away from ω_p' so that $\omega = \omega_p' \pm \Delta\omega$. In this case, equation (4.141) yields the following result for $\left(\omega_p'\tau_c\right)^2 \gg 1$.

$$\overline{\varepsilon}_R = \overline{\varepsilon}_\infty - \left(\frac{\omega_p}{\omega_p' \pm \Delta\omega}\right)^2 = \overline{\varepsilon}_\infty - \overline{\varepsilon}_\infty \left[1 \mp 2\frac{\Delta\omega}{\omega_p'} + 3\left(\frac{\Delta\omega}{\omega'}\right)^2 \mp \ldots\right] \tag{4.150}$$

Retaining only the linear $\frac{\Delta\omega}{\omega_p}$ term,

$$\overline{\varepsilon}_R = \pm 2\overline{\varepsilon}_\infty \frac{\Delta\omega}{\omega_p'} \tag{4.151}$$

Thus, if ω is greater than ω_p', then $\overline{\varepsilon}_R > 0$ and if ω is less than ω_p' then $\overline{\varepsilon}_R < 0$. Again for $\left(\tau_c\Delta\omega\right)^2 \gg 1$ and $\omega = \omega_p \pm \Delta\omega$, $\overline{\varepsilon}_I \ll \overline{\varepsilon}_R$ so that

$$\left.\begin{aligned} n_R &\approx \left[\frac{\sqrt{\bar{\varepsilon}_R^2}}{2}+\frac{\bar{\varepsilon}_R}{2}\right]^{1/2} \qquad (4.152a)\\ n_I &\approx \left[\frac{\sqrt{\bar{\varepsilon}_R^2}}{2}-\frac{\bar{\varepsilon}_R}{2}\right]^{1/2} \qquad (4.152b)\end{aligned}\right\} \quad \omega = \omega_p' \pm \Delta\omega$$

Using equation (4.151) in (4.152), yields the following results. For $\omega = \omega_p' + \Delta\omega$, $n_R \approx \sqrt{\frac{2\bar{\varepsilon}_\infty \Delta\omega}{\omega_p'}}$, $n_I \approx 0$, and $\bar{R} = \left(\frac{n_R - 1}{n_R + 1}\right)^2 < 1$; and for $\omega = \omega_p' - \Delta\omega$, $n_R \approx 0$, $n_I \approx \sqrt{\frac{2\bar{\varepsilon}_\infty \Delta\omega}{\omega_p'}}$, and $\bar{R} \approx \frac{n_I^2}{n_I^2} = 1$. Thus, as the wave frequency decreases (wavelength increases) from ω_p', the reflectivity $\bar{R} \approx 1$. But if the wave frequency increases (wavelength decreases) from ω_p', the reflectivity becomes less than one.

Now consider the rate of change of $\bar{R}$ for $\omega = \omega_p' + \Delta\omega$. That is, in the frequency region where $n_R \approx 0$ and $\bar{R}$ is decreasing from one.

$$\frac{d\bar{R}}{d\omega} = \frac{d\bar{R}}{d\Delta\omega} = \frac{d\bar{R}}{dn_R}\frac{dn_R}{d\Delta\omega} \approx \frac{2\bar{R}}{1 - n_R}\sqrt{\frac{2\bar{\varepsilon}_\infty}{\omega_p' \Delta\omega}} \qquad (4.153)$$

Thus, for $\Delta\omega \to 0$ $\left(\omega = \omega_p'\right)$ the reflectivity is decreasing at nearly an infinite rate. This is a desirable characteristic for a plasma filter since it will change from $\bar{R} = 1$ to a low value of $\bar{R}$ within a small frequency range around $\omega = \omega_p'$.

For a plasma filter, the frequency $\omega = \omega_p'$ or wavelength $\lambda = \lambda_p = \frac{2\pi c_o}{\omega_p'}$ becomes a design point. In a TPV application, the plasma filter should have $\bar{R} = 1$ for $\lambda > \lambda_g = \frac{hc_o}{E_g}$, where E_g is the PV array bandgap energy, and $\bar{R} = 0$ for $\lambda < \lambda_g$. Thus, to match the plasma filter to the PV array, the following design condition applies.

$$\lambda_p = \frac{2\pi c_o}{\omega_p'} \approx \lambda_g = \frac{hc_o}{E_g} \tag{4.154a}$$

So that,

$$\frac{hc_o}{\lambda_p} = \frac{h\omega_p'}{2\pi} = \frac{h}{2\pi}\sqrt{\frac{e^2 N}{\bar{\varepsilon}_o \bar{\varepsilon}_\infty m^*}} \approx E_g \tag{4.154b}$$

becomes the design condition for the plasma filter. Using the result, $\omega = \frac{2\pi c_o}{\lambda}$, equations (4.137) and (4.141) can be rewritten as follows,

$$\bar{\varepsilon}_R = \bar{\varepsilon}_\infty \left[1 - \frac{u^2}{u_p^2\left(1+u^2\right)}\right] \tag{4.155}$$

$$\bar{\varepsilon}_I = \frac{\bar{\varepsilon}_\infty u^2}{u_p^2\left(1+u^2\right)} \tag{4.156}$$

Where

$$u = \frac{1}{\omega\tau_c} = \frac{\lambda}{2\pi c_o \tau_c} = 5.31\times10^{-19}\frac{\lambda(\text{nm})}{\tau_c(\text{sec})} \tag{4.157}$$

$$u_p = \frac{1}{\omega_p'\tau_c} = \frac{\lambda_p}{2\pi c_o \tau_c} = 5.31\times10^{-19}\frac{\lambda_p(\text{nm})}{\tau_c(\text{sec})} \tag{4.158}$$

Thus, $\bar{\varepsilon}_R$ and $\bar{\varepsilon}_I$ are functions of the single variable, u, and the two parameters, $\bar{\varepsilon}_\infty$ and u_p. Similarly, the real and imaginary parts of the index of refraction, n_R and n_I, and the reflectivity, $\bar{R}$, are determined by the single variable, u, and the parameters, $u_p = \frac{1}{\omega_p\tau_c}$ and $\bar{\varepsilon}_\infty$. Consider the range of the parameter, u_p, for a plasma filter to be used in a TPV system. For TPV systems, the PV bandgap energies, E_g, of interest are $0.5 \le E_g \le 1.1$eV ($2500 \ge \lambda_g \ge 1100$nm). As a result, equations (4.154) yield the following results.

$$\begin{aligned} 7.6\times10^{14} \le \omega_p \le 1.7\times10^{15} \qquad & \text{sec}^{-1} \\ 2500 \ge \lambda_p \ge 1100 \qquad & \text{nm} \end{aligned} \tag{4.159}$$

In addition from equation (4.154b) the following is obtained.

$$1.8\times10^{20} \le \frac{N}{\bar{\varepsilon}_\infty \left(\frac{m^*}{m_e}\right)} \le 8.8\times10^{20} \qquad \text{cm}^{-3} \tag{4.160}$$

The quantity $\bar{\varepsilon}_\infty \left(\frac{m^*}{m_e}\right)$ is the order of 1 for semiconductors. Thus $10^{20} \le N \le 10^{21}$ cm^{-3}, which is within the range attainable with highly doped semiconductors.

Rather than the collision time, τ_c, the more commonly used semiconductor property is the *mobility*, μ. If the charge carrier (electron or hole) motion is dominated by collisions, then the acceleration term in the equation of motion [equation (4.127)] can be neglected and the following results,

$$\vec{v} = \frac{d\vec{r}}{dt} = -\mu\vec{E} \tag{4.161}$$

where

$$\mu = \frac{e\tau_c}{m^*} \qquad \frac{m^2}{V\,\text{sec}} \tag{4.162}$$

The equation of motion given by equation (4.161) applies to both electrons and holes in a semiconductor when a steady DC electric field is applied. The collision time or mobility is determined by the scattering mechanisms the electrons or holes experience. Collisions with *phonons* (quanta of lattice vibration, just as the photon is the quanta of electromagnetic vibration) and collisions with the ionized impurity used to dope the semiconductor are the two major scattering mechanisms. For a discussion of scattering mechanisms in solids, see Chapter 9 of [11].

Semiconductor mobilities range from 10 cm^2/Vsec to 1000 cm^2/Vsec [12]. As a result, from equation (4.158)

$$5.7\times10^{-15} \le \frac{\tau_c}{\frac{m^*}{m_e}} \le 5.7\times10^{-13} \qquad \text{sec} \tag{4.163}$$

for

$$10 \le \mu \le 1000 \qquad \frac{\text{cm}^2}{V\,\text{sec}}$$

Since $\frac{m^*}{m_e} < 1$, equations (4.158) and (4.163) yield the following.

$$\begin{aligned} 5 \le \omega_p' \tau_c \le 1000 \\ 0.2 \ge u_p \ge 10^{-3} \end{aligned} \tag{4.164}$$

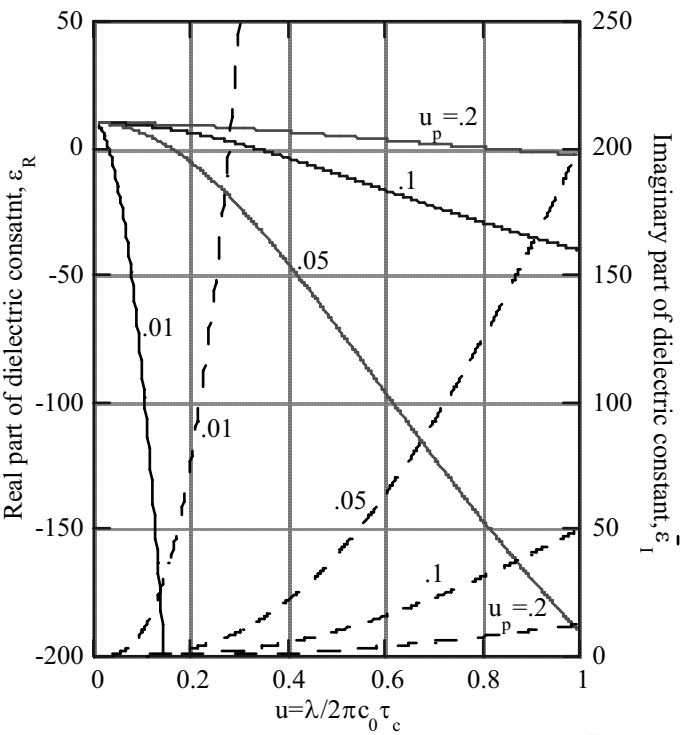

Figure 4.13 - Drude model of the dielectric constant, $\bar{\varepsilon}$, as a function of $u=\lambda/2\pi c_0\tau_c$ for several values of the parameter $u_p=\lambda_p/2\pi c_0\tau_c$. Solid lines are the real part of $\bar{\varepsilon}$ and dashed lines are the imaginary part of $\bar{\varepsilon}$. $\bar{\varepsilon}_\infty = 10$.

In Figure 13 the real and imaginary part of the dielectric constant, calculated using equations (4.155) and (4.156), are shown as a function of u for several values of the parameter, up. As up decreases, the rate of change of both $\bar{\varepsilon}_R$ and $\bar{\varepsilon}_I$ increases.

Now consider the reflectivity for normal incidence, $\bar{R}$, as a function of u. Using equations (4.139) and (4.140) for the index of refraction and equations (4.155) and (4.156) for $\bar{\varepsilon}_R$ and $\bar{\varepsilon}_I$ in equation (1.110) for $\bar{R}$, yields the results shown in Figure 4.14 for the same values of u_p and $\bar{\varepsilon}_\infty$ as used in Figure 4.13. For $u_p \le 0.05$ the reflectivity increases to $\bar{R} > 0.9$ rapidly in the region where $\varepsilon_R = 0$, as has already been shown [equation (4.149)]. This is the desired result for a TPV plasma filter. However, for $u_p > 0.1$, the rate of increase is less; also, the maximum value of $\bar{R}$ is much smaller. Obviously, for a TPV application it is desirable that $u_p \le 0.05$. Thus, if λ_p = 2500nm (E_g = .5eV), and $u_p \le 0.05$, equations (4.158) and (4.162) yield $\mu \ge 46.7 \Big/ \frac{m^*}{m_e}$ cm^2/Vsec. Also, for λ_p = 2500nm equations (4.143a) and (4.144) yield $N = 1.8 \times 10^{20}\ \bar{\varepsilon}_\infty \left(\frac{m^*}{m_e}\right)$. If λ_p = 1100nm (E_g = 1.1eV) and $u_p \le 0.05$, equations (4.158) and (4.162) yield $\mu \ge 20.5 \Big/ \frac{m^*}{m_e}$ cm^2/Vsec and equation (4.154b yields $N = 8.8 \times 10^{20}\ \bar{\varepsilon}_\infty \left(\frac{m^*}{m_e}\right)$ cm^{-3}. The effective mass, $\frac{m^*}{m_e}$, can vary greatly depending upon the semiconductor (see table 2.2 of [12]). For electrons, $0.01 < \frac{m^*}{m_e} < 0.5$ and for holes $0.1 \le \frac{m^*}{m_e} \le 1$. The dielectric constant, $\bar{\varepsilon}_\infty$, is the order of 10 for most semiconductors. Therefore, to achieve $u_p \le 0.05$ for $2500 \ge \lambda_p \ge 1100$nm requires large mobility ($\mu > 100$ cm^2/Vsec) and large doping ($N > 10^{20}$ cm^{-3}). At high doping levels the primary scattering mechanism for the electrons or holes will be collisions with the impurity dopant. Thus, the collision time, τ_c, and mobility, μ, become inversely proportional to N [12,13]. This makes it difficult to achieve both large N and μ simultaneously.

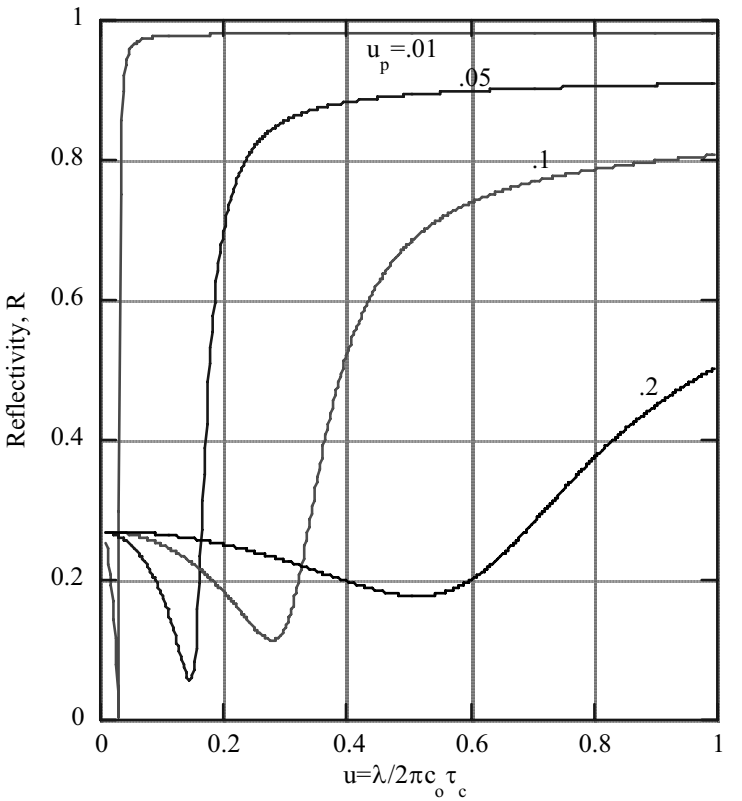

Figure 4.14 - Drude model reflectivity for normal incidence, $\bar{R}$, as a function of $u=\lambda/2\pi c_o \tau_c$ for several values of the parameter $u_p=\lambda_p/2\pi c_o \tau_c$. $\bar{\varepsilon}_\infty = 10$.

Now consider the effect of $\bar{\varepsilon}_\infty$ on the reflectivity for normal incidence. Figure 4.15 shows $\bar{R}$ as a function of u for several values of $\bar{\varepsilon}_\infty$. As $\bar{\varepsilon}_\infty$ increases, the transition region for low to high $\bar{R}$ moves to larger values of u. The rate of change of $\bar{R}$ in the transition region decreases only slightly as $\bar{\varepsilon}_\infty$ increases. Also, the asymototic value for $u \to \infty$ is not affected by $\bar{\varepsilon}_\infty$. As far as TPV applications are concerned, the only major disadvantage of increasing $\bar{\varepsilon}_\infty$ is the increase in $\bar{R}$ in the area before the transition region. The desirable result is $\bar{R} = 0$ in this area.

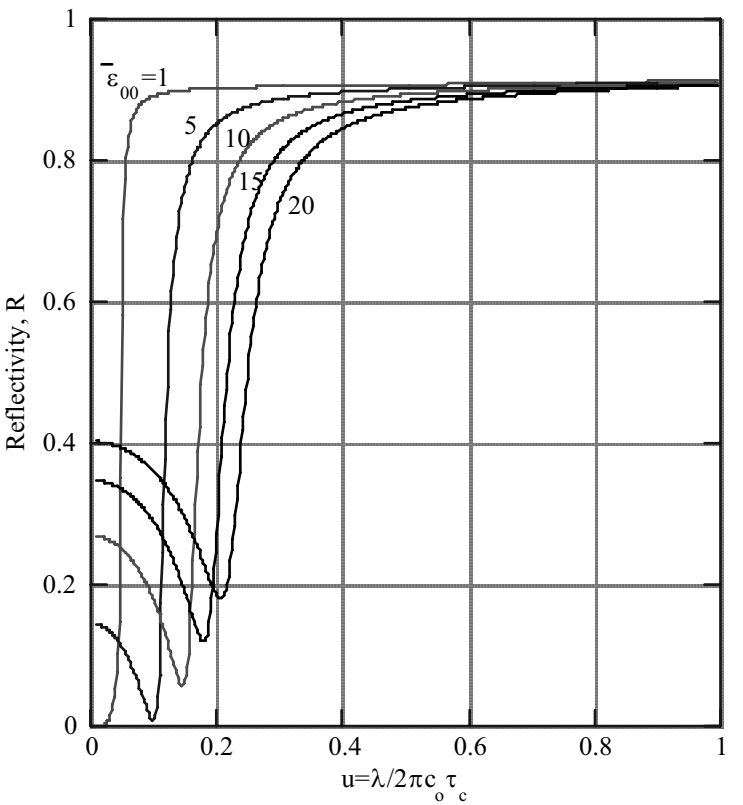

Figure 4.15 – Effect of dielectric constant at infinite frequency ($\lambda = 0$), $\bar{\varepsilon}_\infty$, on the Drude model reflectivity at normal incidence, $\bar{R}$, for $u_p = \lambda_p / 2\pi c_o \tau_c = .05$.

4.4.2 Reflectance, Transmittance, and Absorptance of a Plasma Filter

The structure of a plasma filter consists of two layers. A simple plasma filter consists of a thin film of a conductor or semiconductor on a transparent dielectric substrate such as glass, which provides the mechanical strength for the filter. For a TPV application, the film layer has a plasma frequency, ω_p', that satisfies the design criteria given by equations (4.154). It is also possible to combine a plasma filter and an interference filter, as is discussed later.

Since the film layer is thin, interference effects exist. Thus, the same analysis used in calculating the spectral transmittance, $\hat{\tau}(\lambda)$, reflectance, $\rho(\lambda)$, and absorptance, $\alpha(\lambda)$, of an interference filter must be applied to the plasma filter. The single film system treated in Section 4.3.5 applies to the plasma filter. For a single film with a complex index of refraction, $n_1 = n_{1R} - jn_{1I}$, the spectral reflectance, $\rho(\lambda)$ and transmittance, $\hat{\tau}(\lambda)$, are given by equations (4.91) and (4.92). Figure 4.16 shows the reflectance, ρ, as a function of wavelength, λ, for several values of the charge carrier density, N.

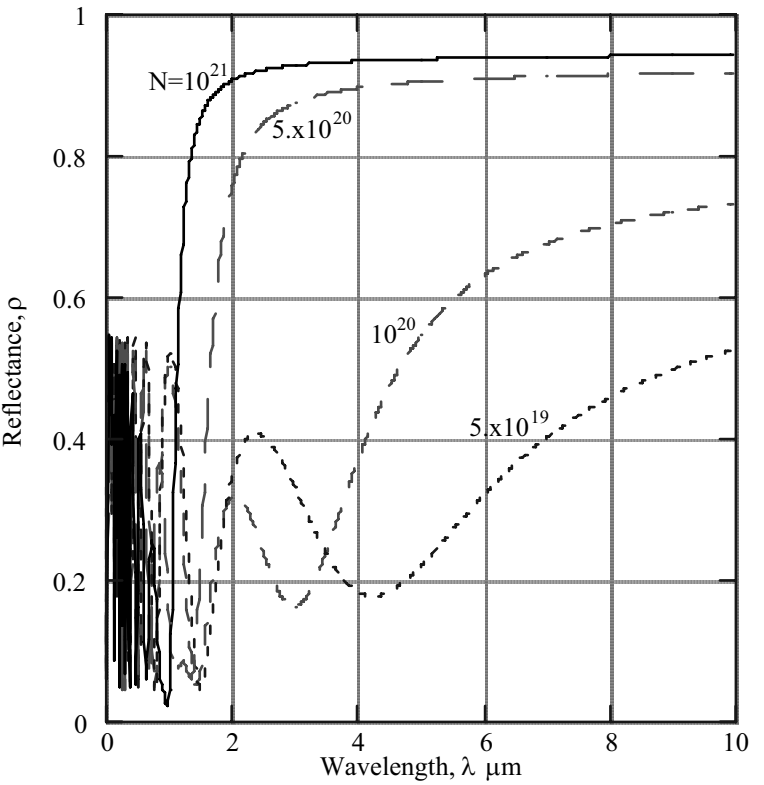

Figure 4.16 - Reflectance, ρ of a plasma filter at normal incidence for several charge densities, N as a function of wavelength, λ. Filter mobility, μ=100 $cm^2V^{-1}sec^{-1}$, film thickness, d=.25 μm, dielectric constant for $\lambda = 0$, $\bar{\varepsilon}_\infty = 10$, effective mass of charge carriers, m^*/m_e=.1, index of refraction of surroundings, n_o=1., index of refraction of substrate, n_s=1.5.

The other parameters used to calculate the results in Figure 4.16 are the following; film thickness, d = 0.25μm, film mobility, μ = 100 cm2/Vsec, dielectric constant for λ = 0, $\bar{\varepsilon}_\infty$ = 10, effective mass, $\frac{m^*}{m_e}$ = 0.1, index of refraction of surroundings, n_o = 1, and index of refraction of substrate, n_s = 1.5. As Figure 4.16 shows, to achieve large reflectance at the long wavelengths requires large charge carrier density (N >10^{20} cm^{-3}). Large N also yields the desirable result of a sharp transition at $\lambda \approx \lambda_p$ from small reflectance to large reflectance. Notice the oscillations in ρ resulting from interference effects.

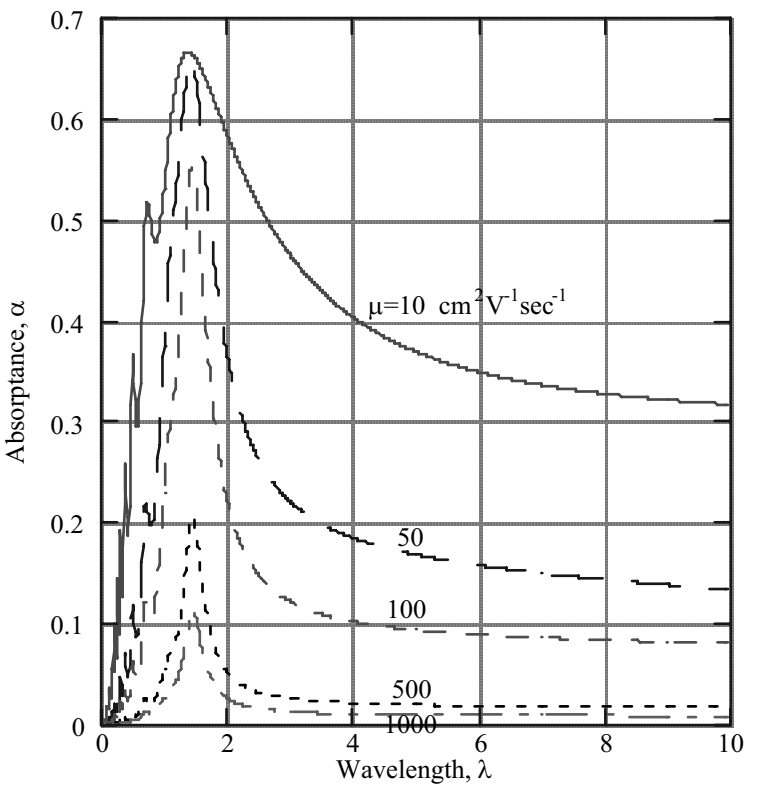

Figure 4.17 -Effect of mobility, μ on the absorptance of a plasma filter for normal incidence. Charge carrier density, N = 5 × $10^{20}$$cm^{-3}$, film thickness, d = .25 μm, dielectric constant for λ = 0, $\bar{\varepsilon}_\infty$ = 10 effective mass of charge carriers, m^*/m_e =.1, index of refraction of surroundings, n_o =1., index of refraction of substrate, n_s =1.5.

In the previous section it has been noted that the Drude model for the dielectric constant results in a resonance condition where $\bar{\varepsilon}_R = 0$ when $\omega = \omega_p'$ ($\lambda = \lambda_p$). For $\lambda \approx \lambda_p$, energy is transferred from the radiation field to the charge carriers of the media at a fast rate. This result is illustrated in Figure 4.17 where the absorptance, $\alpha(\lambda) = 1 - \rho(\lambda) - \hat{\tau}(\lambda)$ is shown as a function of wavelength, λ, for several values of the mobility, μ, and charge carrier density, $N = 5 \times 10^{20}$ cm^{-3}. The absorptance has been calculated using equations (4.91) and (4.92). Figure 4.17 shows that the absorptance is significant for $\mu < 500 \text{cm}^2\text{V}^{-1}\text{sec}^{-1}$. Also, the largest absorptance occurs at $\lambda = \lambda_p$. For the parameters used to calculate Figure 4.17, $\lambda_p = 1.49\mu$m.

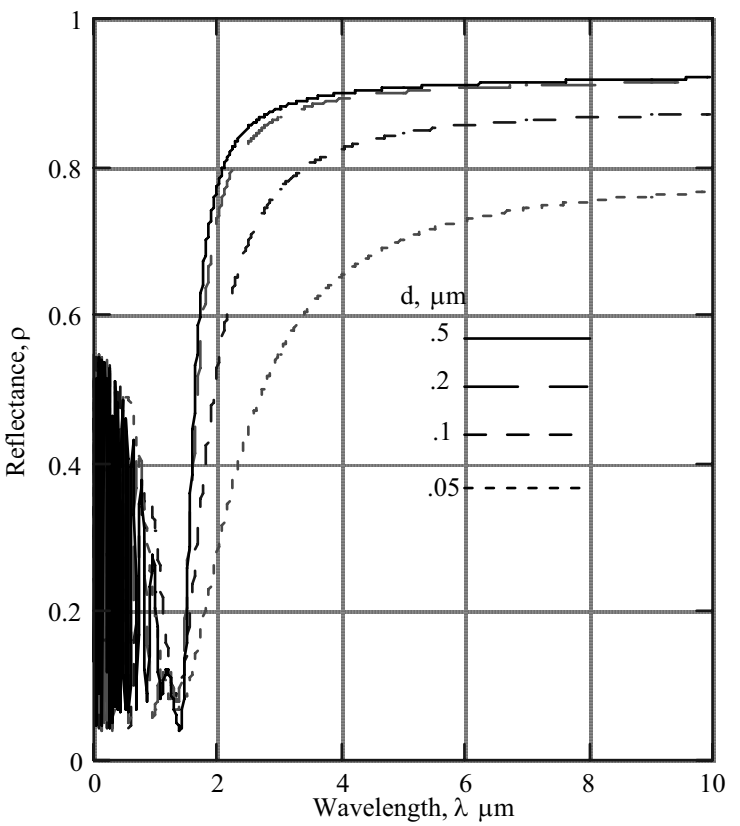

Figure 4.18 - Effect of film thickness, d on the reflectance at normal incidence of a plasma filter. Charge carrier density, $N=5\text{x}10^{20}\text{cm}^{-3}$, mobility, $\mu=100\ \text{cm}^2\text{V}^{-1}\text{sec}^{-1}$, dielectric constant for $\lambda=0$, $\bar{\varepsilon}_\infty = 10$ effective mass of charge carriers, $m^*/m=.1$, index of refraction of surrounds, $n_o=1$, index of refraction of substrate, $n_s=1.5$.

Besides mobility, the film thickness, d, also has a significant effect on the optical properties. Figure 4.18 illustrates the film thickness effect on reflectance, ρ. As d increases, the reflectance increases in the region $\lambda \geq \lambda_p = 1.49\mu m$, reaching a maximum for $d \approx 0.5\mu m$. Also, increasing d produces the desirable sharper transition from small ρ to large ρ in the region around $\lambda \approx \lambda_p$. Increasing film thickness results in larger reflectance; however, it also results in increased absoptance, α, in the transition region ($\lambda \approx \lambda_p = 1.49\mu m$). This is illustrated in Figure 4.19, where α is shown for the same conditions as in Figure 4.18. Notice that in the region $\lambda > \lambda_p$, the absorptance decreases with increasing thickness, reaching a minimum for $d \approx 0.5\mu m$.

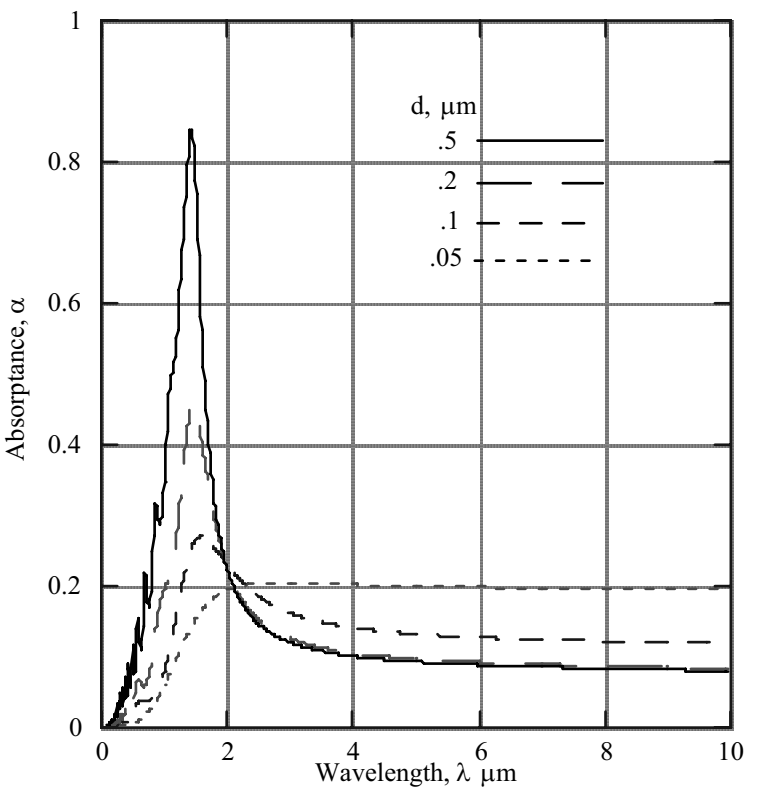

Figure 4.19 - Effect of film thickness, d on the absorptance of a plasma filter at normal incidence. Charge carrier density, $N=5*10^{20} cm^{-3}$, mobility, $\mu=100\ cm^2V^{-1}sec^{-1}$, dielectric constant for $\lambda=0$, $\bar{\varepsilon}_\infty = 10$ effective mass of charge carriers, $m^*/m=.1$, index of refraction of surrounds, $n_o=1$, index of refraction of substrate, $n_s=1.5$.

For a TPV application, a plasma filter should have the following characteristics: a sharp transition from small to large reflectance for $\lambda \approx \lambda_p$, low absorptance for all λ's, and large transmittance for $\lambda < \lambda_p$. As Figure 4.18 indicates, the sharp transition and large reflectance for $\lambda > \lambda_p$ can be achieved. However, as Figure 4.19 shows, significant absorptance occurs at all λ's and significant, undesirable reflectance occurs for $\lambda < \lambda_p$. For the parameters used to calculate Figures 4.18 and 4.19, it appears that $d \approx 0.2\mu m$ is the optimum film thickness for satisfying the conditions for a TPV system.

4.4.3 Efficiency and Total Transmittance, Reflectance, and Absorptance of a Plasma Filter

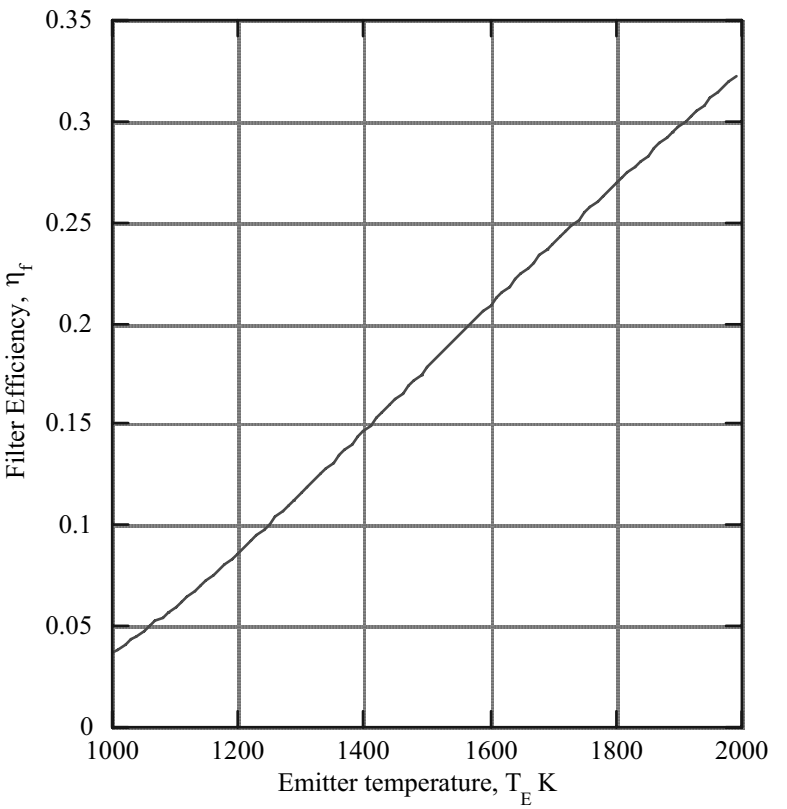

Figure 4.20a) - Filter efficiency, η_f

For a constant emitter emittance, ε_E, consider the filter efficiency, η_f, defined by equations 4.4, for a plasma filter with the following characteristics: angle of incidence, $\theta_o = 0$, charge carrier density, $N = 3.60 \times 10^{20}$ cm^{-3}, mobility, $\mu = 100 cm^2 V^{-1} sec^{-1}$, film thickness, $d = 0.25\mu m$, dielectric constant for $\lambda = 0$, $\bar{\varepsilon}_\infty = 10$, effective mass of charge carriers, $\frac{m^*}{m_e} = 0.1$, index of refraction of surroundings, $n_o = 1.0$, and index of refraction of substrate, $n_s = 1.5$. For these conditions, $\lambda_p = 1.75\mu m$ [equation (4.144)]. Using the design condition $\lambda_g = \lambda_p = 1.75\mu m$, where λ_g is the wavelength corresponding to the PV array bandgap energy, numerical integration has been used to evaluate equation (4.4b).

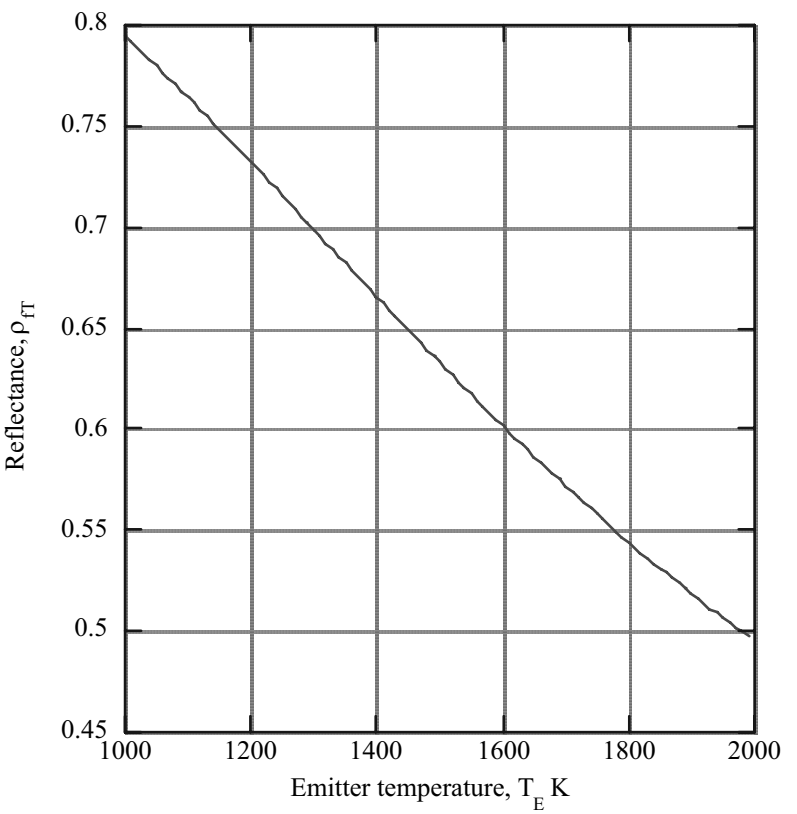

Figure 4.20b) - Total reflectance, ρ_{fT}

Those results are shown in Figure 4.20a. As can be seen, the filter efficiency increases with temperature but remains low compared to the imbedded metal interference filter of Figure 4.10. A rather large total absorptance, α_{fT}, as shown in Figure 4.20c, accounts for the low efficiency. Also, shown in Figure 4.20b and 4.20c are the total reflectance, ρ_{fT} [equation (4.6)] and total trasmittance, τ_{fT} [equation (4.5)]. The total absorptance is considerably larger than the imbedded metal interference filter of Figure 4.10c.

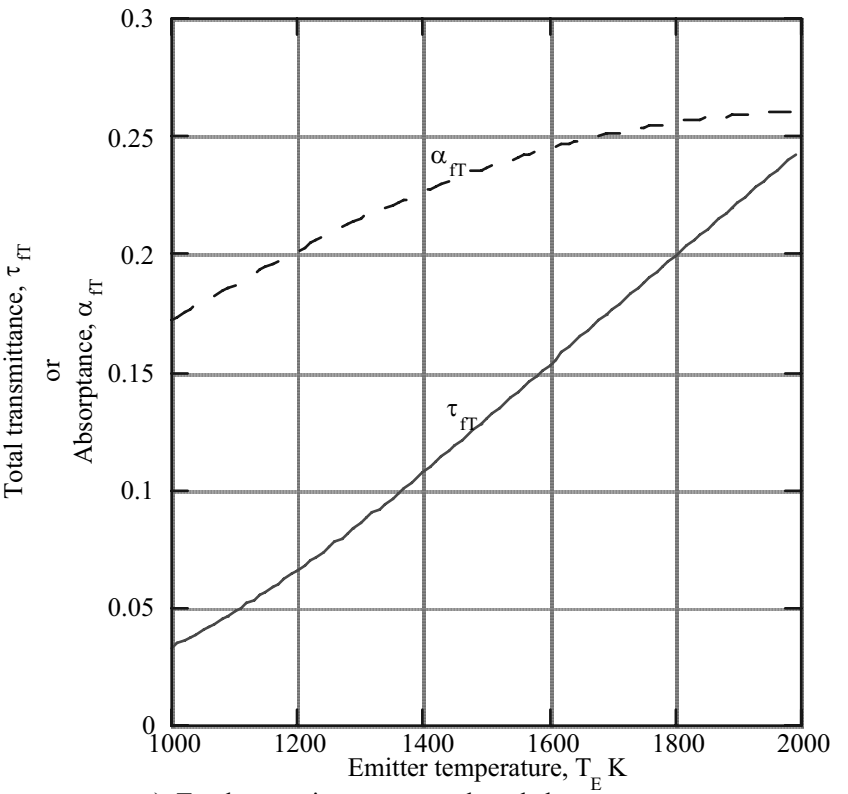

c) Total transmittance, τ_{fT} and total absorptance, α_{fT}

Figure 4.20 - Optical performance of a plasma filter at normal incidence for the following filter parameters. Charge carrier density, $N=3.61\times10^{20}$, mobility, $\mu=100\ cm^2V^{-1}sec^{-1}$, film thickness, d = .25 μm, dielectric constant for $\lambda = 0$, $\bar{\varepsilon}_\infty = 10$, effective mass of charge carriers, $m^*/m = 1$, index of refraction of surrounds, $n_o = 1$, index of refraction of substrate, $n_s = 1.5$. Limit wavelength for filter efficiency calculation, $\lambda_g = \lambda_p = 1.75\mu m$.

Finally, consider how the efficiency varies with angle of incidence, θ_o. Figure 4.21 shows η_f as a function of θ_o for the same filter parameters as those used in Figure 4.20. For s polarization, η_f actually increases with incrasing θ_o. However, similar to the embedded metal interference filter (Section 4.3.9) as $\theta_o \to 90°$, $\rho \to 1$, and $\tau \to 0$. As a result, even though η_f remains finite, the amount of transmitted radiation is negligible.

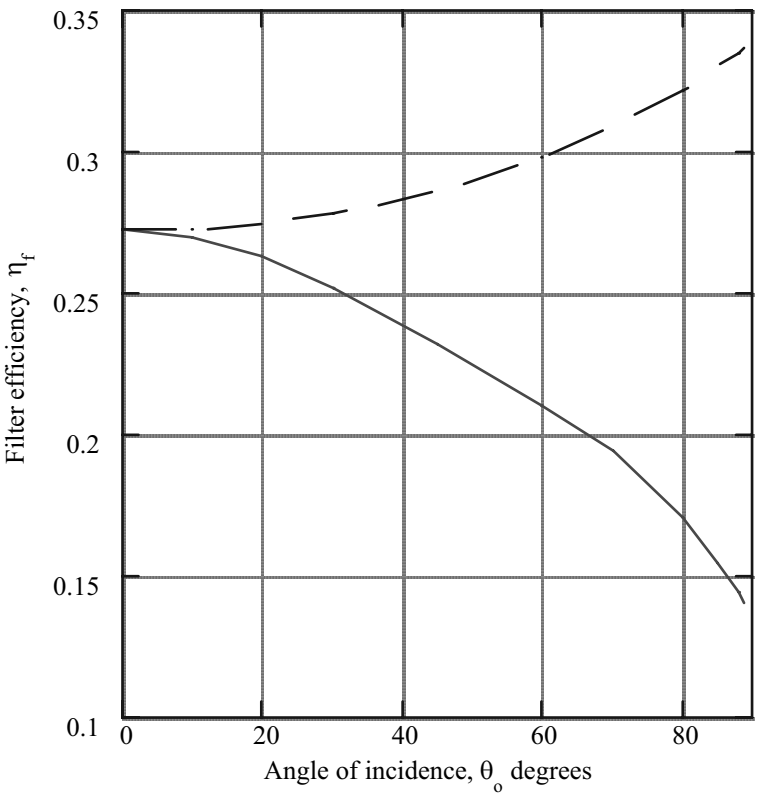

Figure 4.21 - Effect of angle of incidence, θ_o on the filter efficiency, η_f of a plasma filter for the same filter parameters as Fig. 4.20. Solid line p polarization, dashed line s polarization.

4.5 Combined Interference-Plasma Filter

As shown earlier, dielectric interference filters have large transmittance in their band-pass region with negligible absorptance for all wavelengths. However, at long wavelengths, where large reflectance is required for a TPV filter, dielectric interference filters fail to meet that requirement. In contrast, plasma filters yield large reflectance for long wavelengths but also have significant absorptance for wavelengths where large transmittance is required. If the best aspects of both the dielectric interference filter and the plasma filter can be combined in a single filter, then a suitable TPV filter results.

By placing a dielectric interference filter in front of a plasma filter, large transmittance in the band-pass region and large reflectance at long wavelengths can be achieved. The dielectric interference filter provides the large transmittance band-pass region and also gives large reflectance in the wavelength region immediately above the band-pass region where a plasma filter has large absorptance. A properly designed plasma filter then provides large reflectance in the long wavelength region where it has much smaller absorptance. The dielectric interference filter acts to "block" the large absorptance wavelength region from reaching the plasma filter. Such a combined filter for TPV application was introduced by researchers at Knolls Atomic Power[15,19,20]. Referring to Figure 4.1, the plasma filter is layer m, which lies next to the substrate, and the interference filter is made up of layers $1 \le m \le m-1$.

Consider an interference-plasma filter that uses the [LHL] and [HLH] groups discussed in Section 4.3.7 for the dielectric interference filter and a plasma filter based on the Drude model. Select the center of the band-pass to be $\lambda_c = 1.5\mu m$. To produce a band-pass region for $1 \le \lambda \le 2\mu m$ it is shown in Section 4.3.7 that the design wavelengths for the [LHL] and [HLH] groups are $\lambda_o = 1.52\mu m$ and $\lambda_o = 0.56\mu m$ if $n_H = 2.4$(ZnSe) and $n_L = 1.35$(MgF2). Also, adding an anti-reflection [HLH] group with $\lambda_o = 0.765\mu m$ between the [LHL] and [HLH] group improves the transmittance in the band-pass region. Therefore, use the following configuration for the interference filter.

$$s\left|1.01[\mathrm{LHL}]^5\ 0.51[\mathrm{HLH}]0.37[\mathrm{HLH}]^5\right|o \qquad \lambda_c = 1.5\mu m \tag{4.165}$$

For the plasma filter, select the charge carrier density $N = 5 \times 10^{20}\ cm^{-3}$. As Figures 4.16 and 4.17 show, this will produce large reflectance for $\lambda > 2\mu m$ and also confine the large absorptance region to $\lambda < 2\mu m$ where the interference filter "blocks" the radiation from reaching the plasma filter. In order to have as small absorptance as possible, select the mobility $\mu = 1000 cm^2 V^{-1} sec^{-1}$, which is difficult to achieve for semiconductors. Also, choose the dielectric constant for $\lambda = 0$ to be $\bar{\varepsilon}_\infty = 10$ and charge carrier effective mass $\frac{m^*}{m_e} = 0.1$. The thickness of the plasma layer, d_p, can be

varied to yield the maximum filter efficiency. For the interference filter given by equation (4.165), the plasma filter thickness that maximizes the filter efficiency is $d_p = 0.15\mu m$. The various film thicknesses are given in Table 2.

CONFIGURATION	FILM THICKNESS, nm
$(H\ L\ H)^5$	58.3 103.7 58.3
$(H\ L\ H)$	79.7 141.7 79.7
$(L\ H\ L)^5$	281.5 158.3 281.5
Plasma	150.0
s Substrate, glass n_s=1.52	

Table 4.2 Layer thickness for interference-plasma filter where the center wavelength, λ_c=1.5μm and H is ZnSe(n_H=2.4), L is MgF_2(n_L=1.35). The plasma layer has a charge carrier density, $N=5x10^{20}$ cm^{-3}, a mobility, $\mu=1000cm^2V^{-1}sec^{-1}$, a dielectric constant for $\lambda=0$, $\varepsilon_\infty=10$ and an effective mass for charge carriers, $m^*/m_e=.1$.

Figure 4.22 shows the spectral optical performance of the interference-plasma filter described in Table 2. The plasma layer produces the desired large reflectance at long wavelengths, which is even greater than the long wavelength reflectance of the embedded metal interference filter of Figure 4.9. Also, transmittance in the band-pass region (λ_c = 1.5μm) reaches 0.9 and the absorptance remains low for $\lambda > 2\mu m$. The calculations have been made using the Mathematica program described in Appendix D.

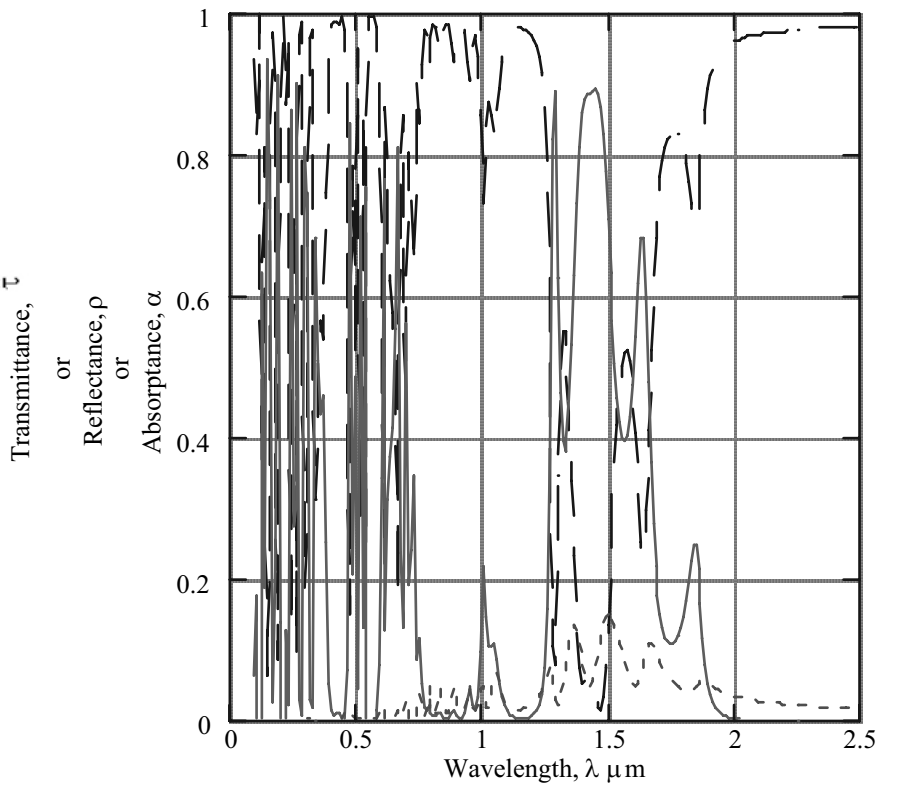

Figure 4.22a) - Transmittance, absorptance and reflectance for $0<\lambda<2.5$ μm

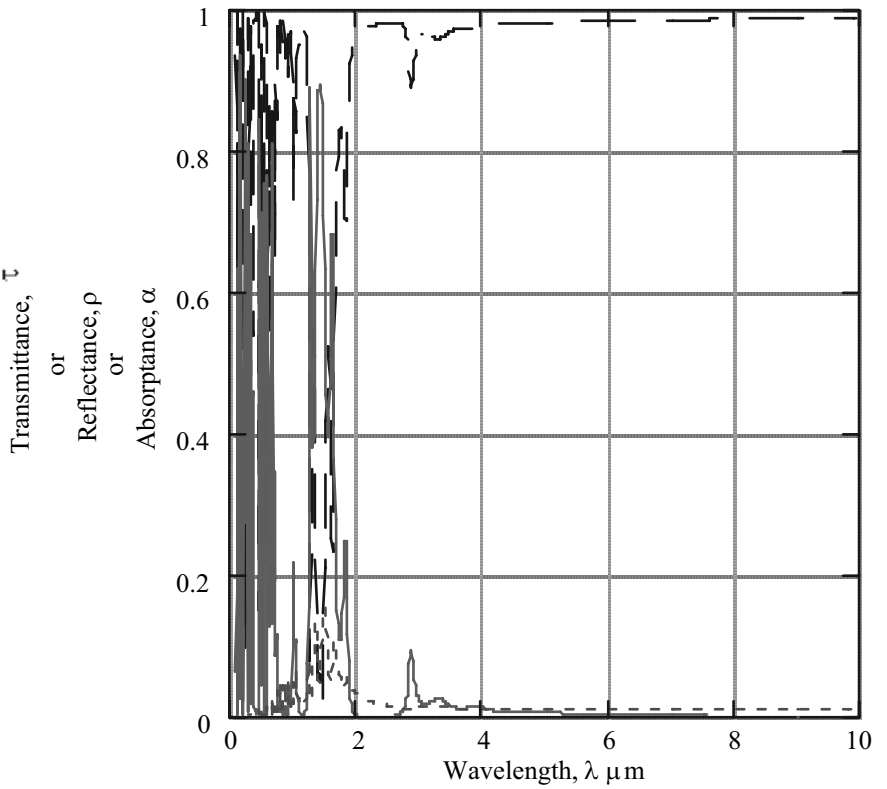

b) Transmittance, absorptance and reflectance for $0<\lambda<10$ μm

Figure 4.22 - Performance of interference-plasma filter of configuration given in Table 4.2 with center wavelength, λ_c=1.5 μm at normal incidence, θ_o=0. For the substrate n_s=1.52 and for the surroundings n_o=1.0. $\hat{\tau}$ —— ρ—— —— α - - - - -

Using the optical spectral properties of Figure 4.22, the filter efficiency, η_f, and total optical properties have been calculated using equations (4.4) through (4.7). Figure 4.23 shows these results. The filter efficiency has been calculated using λ_g = 1.9μm as the wavelength limit for the integration in equation (4.4) and the emitter emittance, ε_E, is assumed constant. As Figure 4.23a shows, the filter efficiency reaches nearly 0.7 for T_E = 1500K. Even at T_E = 1200K the efficiency is greater than 0.55. To obtain these large efficiencies means that most of the incident radiation is reflected back to the emitter, as the large reflectance values shown in Figure 4.23b indicate. Note also that the total absorptance is less than 0.04 for all values of T_E.

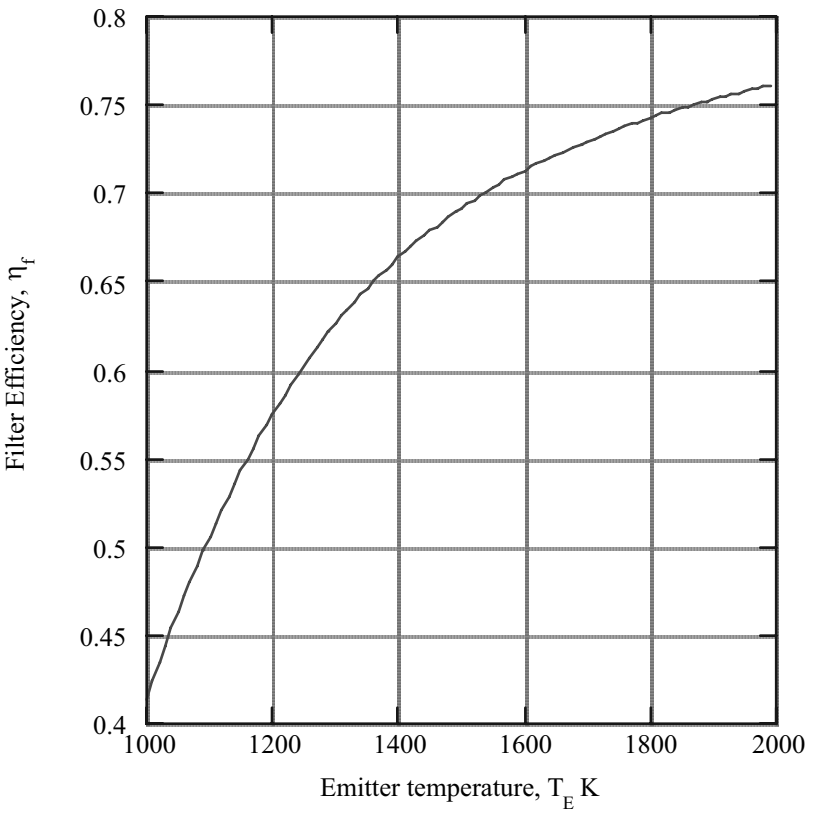

Figure 4.23a) - Filter efficiency, η_f, of interference-plasma filter of Fig. 4.22 for constant emitter emittance, ε_E. Limit wavelength for filter efficiency calculation, λ

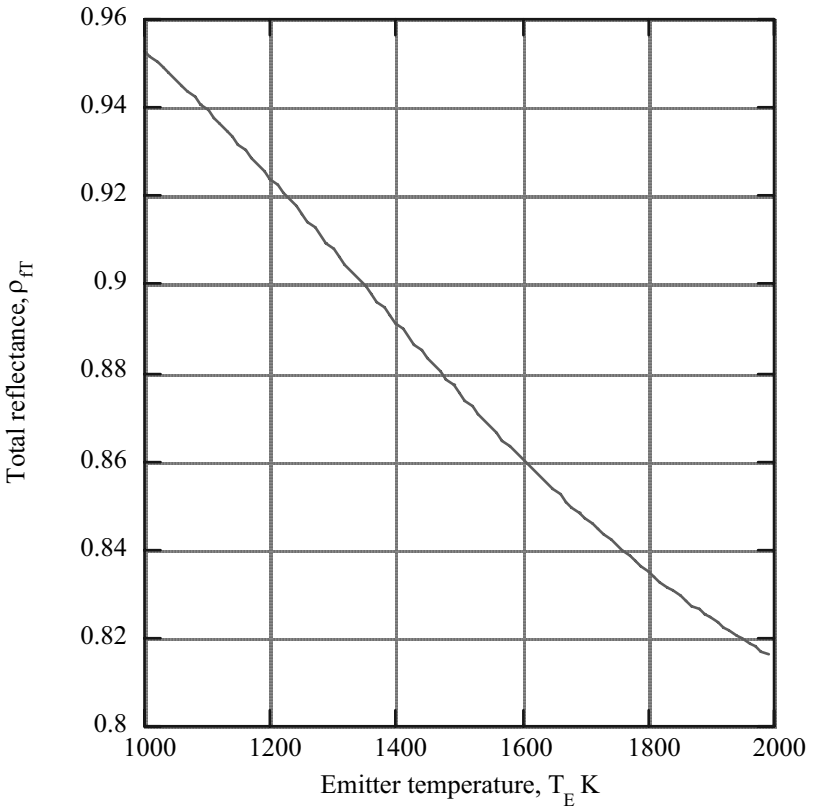

Figure 4.23b) - Total reflectance, ρ_{fT}, of interference-plasma filter of Fig. 4.22 for constant emitter emittance, ε_E. Limit wavelength for filter efficiency calculation, $\lambda_g = 1.9\,\mu m$.

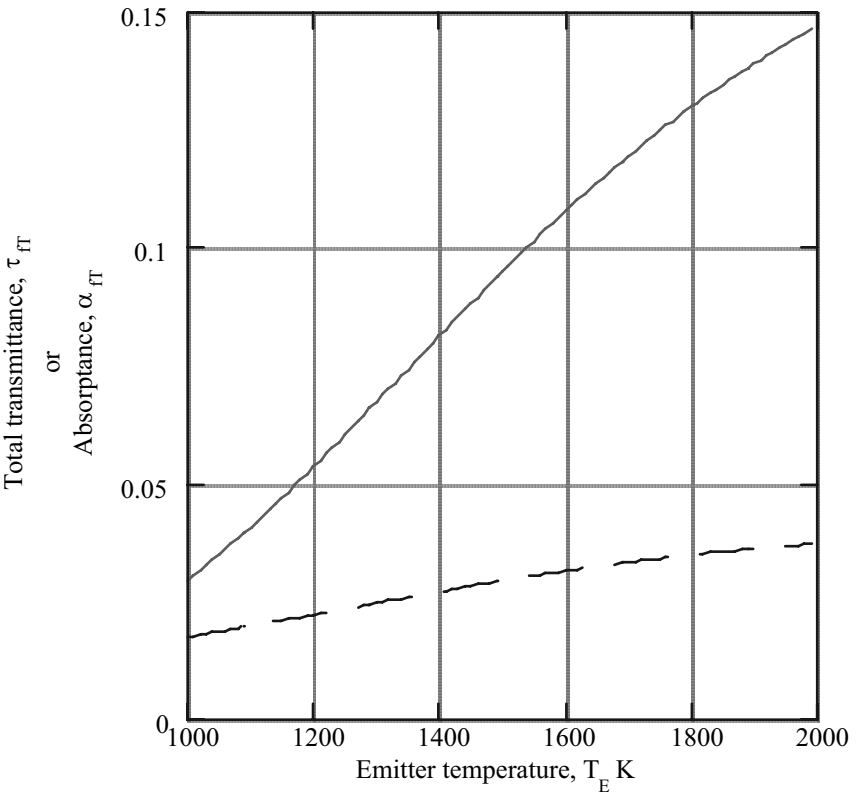

Figure 4.23c) - Total transmittance, τ_{fT}, and total absorptance, α_{fT} of interference-plasma filter of Fig. 4.22 for constant emitter emittance, ε_E. Limit wavelength for filter efficiency calculation, $\lambda_g = 1.9\,\mu m$. τ_{fT} ———, α_{fT} — —

Comparing the filter efficiencies of the three filters (embedded metal, plasma, and interference-plasma) one would conclude that the interference-plasma filter is superior. However, the plasma portion of the interference-plasma filter uses a fictitious semiconductor material with an optimistic mobility of $\mu = 1000\ cm^2V^{-1}sec^{-1}$. Whereas, the embedded metal filter consists of real materials. If μ is reduced, then absorptance will increase and efficiency will decrease for the interference-plasma filter. For

$\mu = 500\ cm^2V^{-1}sec^{-1}$, $\eta_f = 0.55$ and for $\mu = 100\ cm^2V^{-1}cm^{-1}$, $\eta_f = 0.18$ at $T_E = 1500K$. This compares to $\eta_f = 0.49$ at $T_E = 1500K$ for the embedded metal filter. In addition, the interference-plasma filter is a much more complex structure, consisting of 34 layers, whereas the embedded metal filter contains only 7 layers.

There are major issues with the fabrication of all interference type filters. Two of these issues are precision growth and adherence of the various layers. Whether the filters discussed in this chapter can be successfully fabricated is a question that cannot be easily answered and is beyond the scope of this text. However, there is a vast amount of literature on the growth of thin films such as references [21-23].

4.6 Resonant Array Filters

A periodic distribution of small openings in a highly reflecting material such as gold is a simple description of a resonant array filter. The characteristic dimension and spacing of the openings are less than the wavelength of the incident radiation.

In the early 1960's, metallic meshes with a thickness smaller than the wavelength were used as filters in the far infrared. Ulrich [24,25] predicted the performance of these filters with a semi-empirical theory. He found that the measured transmittance could be fitted with the transmittance calculated for an equivalent transmission line. This work was extended by several other researchers (for example, references [26-28]). In the following sections, the transmission line theory is developed and applied to the resonant array filter. Such filters, which have transmission bands in the near infrared, are being developed for TPV applications [29].

A complete explanation for a resonant array filter requires a solution to equation (1.9) with appropriate boundary conditions. This is a difficult problem to solve analytically. For a single hole in a metallic film where the wavelength, λ, is greater than the hole diameter, d, the transmittance scales [30] as $(d/\lambda)^4$. Therefore, the transmittance should be small for a metallic film with a periodic distribution of openings when $d/\lambda < 1$. However, when an electromagnetic wave is incident on a metallic film with a periodic pattern of openings, oscillating currents or surface waves are induced in the film. These oscillating or surface waves then emit radiation, which has a maximum at a resonance condition $\lambda \approx p$, where p is the period of the opening distribution. In this case the metallic film behaves like an inductor. Therefore, Ulrich [24] modeled metallic mesh filters in the far infrared with a transmission line shunted by an impedance that represents the metallic mesh. Thus, the transmission line voltage reflectance and transmittance yield the optical transmittance and reflectance of the metallic mesh.

Complementary to an inductive metallic mesh resonant array filter is a capacitive resonant array filter [24,25]. In this case, a periodic metallic array is deposited on a

dielectric substrate. The capacitive array acts as a band rejection filter. In other words, at the resonant condition, $\lambda \approx p$, the capacitive array is highly reflecting.

Recent theoretical and experimental research [31-33] has been conducted with metallic films on dielectric substrates containing a periodic pattern of sub-wavelength holes or slits. This work has been done in the visible and near infrared and has yielded an explanation for the optical properties of these films. For narrow slits [33] the transmission process occurs by two different mechanisms. For very thin films, surface electromagnetic waves (surface plasmons) are produced as a result of the periodic distribution of the slits when radiation at the resonant wavelength is incident. At the resonant wavelength, which is determined by the period of the slit distribution and the index of refraction of the substrate, the surface waves on each side of the film are coupled. The surface waves on the substrate side of film then radiate to produce large transmittance.

For thick films, the slits act as waveguides. At the resonant wavelength incident light induces currents that flow parallel to the slit walls, having different directions on the two opposite sides of the slits. At the substrate these waves then account for the large transmittance. Unlike the surface wave case, the resonant wavelength is not sensitive to the substrate index of refraction.

Recent research [33] has used an exact solution to equation (1.9) to explain the optical performance of these filters. However, as stated earlier, the transmission line model is presented here to obtain the optical properties.

4.6.1 Transmission Line Theory

In a media of permittivity, ε, transverse electromagnetic waves are produced between current carrying conductors. Such a configuration is called a transmission line. Probably the most common example of a transmission line is a coaxial cable. A coaxial cable consists of a center conductor surrounded by an outer coaxial conductor with a dielectric material between the two conductors. All the necessary results required to analyze a resonant array filter can be obtained by considering the transmission line shown in Figure 4.24. It consists of two infinite parallel conductors with a media of constant electric permittivity, ε, and magnetic permeability, μ, between them. A current of magnitude, $I(z)$ flows in the $+z$ direction in the top conductor and the same magnitude current flows in the $-z$ direction in the bottom conductor.

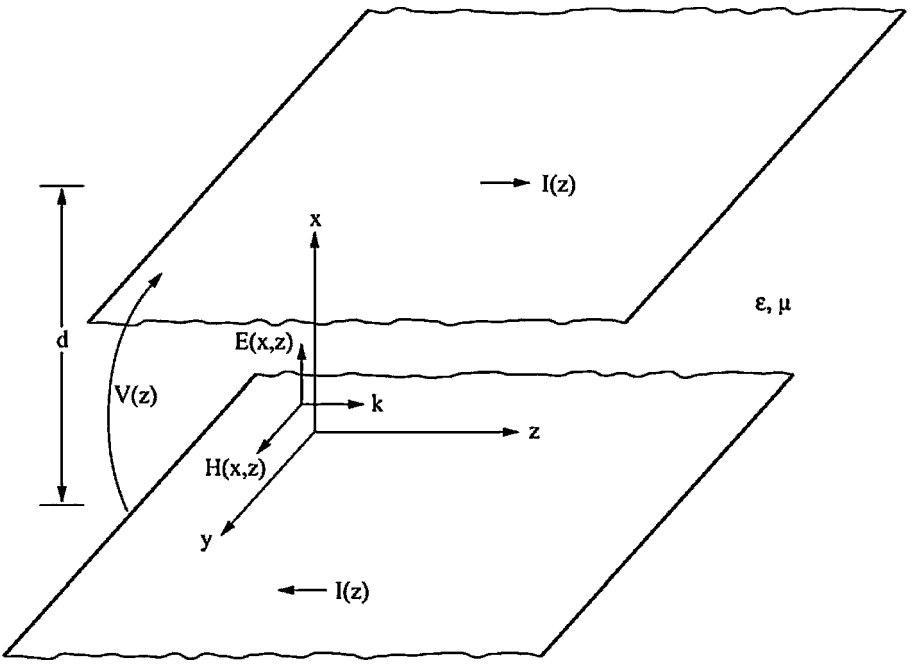

Figure 4.24.—Transmission line consisting of two infinite parallel conductors with a media of electric permittivity, ε, and magnetic permeability, μ, between the conductors.

In the media between the conductors, there is no space change or current. As a result, the electric and magnetic fields must satisfy the wave equation [equation (1.29)]. For the transverse guided waves, assume the following solutions.

$$E(x,z) = E_o^{\pm}(x)e^{j(\omega t \mp kz)} \tag{4.166}$$

$$H(x,z) = H_o^{\pm}(x)e^{j(\omega t \mp kz)} \tag{4.167}$$

The negative sign in the exponent is for a wave moving in the +z direction and the positive sign for a wave moving in the –z direction. For a wave moving in the +z direction, E_o^+ and H_o^+ apply, and for a wave moving in the –z direction, E_o^- and H_o^- apply.

Notice that these solutions differ from the plane wave solutions in Chapter 1 [equation (1.106)] where the wave amplitudes $E_o^{\pm}$ and $H_o^{\pm}$ are constants. For the guided waves, the amplitude varies in the x direction. The electric field has only an x component for the region between the conductors. As a result, Coulomb's Law [equation (1.3)], yields the following result.

$$\nabla \bullet \vec{D} = \varepsilon \nabla \bullet \vec{E} = \varepsilon \frac{\partial E}{\partial x} = 0 \tag{4.168}$$

Thus, the wave equation is the following.

$$\frac{\partial^2 E}{\partial z^2} = \mu\varepsilon \frac{\partial^2 E}{\partial t^2} \tag{4.169}$$

Substituting equation (4.166) for E yields the following dispersion relation.

$$k = \omega\sqrt{\mu\varepsilon} = \frac{\omega}{v_\phi} = n\frac{\omega}{c_o} \tag{4.170}$$

Similar to plane waves, $v_\phi = \frac{1}{\sqrt{\mu\varepsilon}}$ is the phase velocity of the wave and n is the index of refraction, $n = \frac{c_o}{v_\phi}$.

For equations (4.166) and (4.168) to be satisfied, $E_o(x)$ = constant. Thus, the potential, V(z), is the following,

$$V(z) = \int_o^d E^{\pm}(x,z)\,dx = \int_o^d E_o^{\pm} e^{j(\omega t \mp kz)} dx = V_o^{\pm} e^{j(\omega t \mp kz)} \tag{4.171}$$

where $V_o^{\pm} = E_o^{\pm} d$.

Using Faraday's Law [equation (1.2)] and equations (4.166) and (4.167), the following result is obtained,

$$\frac{E}{H} = \pm\frac{\omega\mu}{k} = \pm\frac{c_o\mu}{n} \equiv \pm Z_o \tag{4.172}$$

where Z_o is the *impedance* of the media between the conductors. It is the reciprocal of the optical admittance [equation (1.35)]. The positive sign refers to a wave moving in the +z direction and the negative sign refers to a wave moving in the –z direction.

Now consider the capacitance and inductance of the transmission line. The capacitance is defined as follows,

$$C \equiv \frac{Q}{V} \tag{4.173}$$

where Q is the charge (coulombs) on either of the conductors. From the boundary condition on the normal electric field at a surface [equation (1.43)], the following is obtained,

$$\varepsilon \Delta E = q \tag{4.174}$$

where ΔE is the change in the electric field across the conductor and q is the surface charge density (coul/cm^2). Also the boundary condition on the tangential magnetic field at a surface [equation (1.48)] yields the following,

$$\Delta H = J \tag{4.175}$$

where ΔH is the change in the tangential magnetic field across the conductor and J is the current flowing in the conductor per unit length in the y direction.

The capacitance for the infinitesimal length dz is the following.

$$dC = \frac{\int_{-\infty}^{\infty} q dy}{V} dz \tag{4.176}$$

Using equations (4.174), (4.172), and (4.175), the capacitance per unit length in the z direction is the following,

$$\frac{dC}{dz} = \pm \varepsilon Z_o \frac{\int_{-\infty}^{\infty} J dy}{V} = \pm \varepsilon Z_o \frac{I}{V} \tag{4.177}$$

where I(amps) is the current flowing in either conductor. The positive sign applies for the wave moving in the +z direction and the negative sign applies for the wave moving in the –z direction.

The inductance of the transmission line for an infinitesimal length dz is the following.

$$dL = \frac{d\phi}{I} \tag{4.178}$$

The magnetic flux, $d\phi$, contained between the conductors is

$$d\phi = dz \int_o^d B dx = \mu dz \int_o^d H dx \tag{4.179}$$

Substituting equation (4.172) for H yields the following result for the inductance per unit length.

$$\frac{dL}{dz} = \pm \frac{\mu}{Z_o I} \int_o^d E dx = \pm \frac{\mu}{Z_o} \frac{V}{I} \tag{4.180}$$

The ratio of equations (4.180) and (4.177) yields the following key transmission line result.

$$\frac{\dfrac{dL}{dz}}{\dfrac{dC}{dz}} = \frac{\mu}{\varepsilon Z_o^2} \left(\frac{V}{I} \right)^2 = \left(\frac{V}{I} \right)^2 \equiv Z^2 \tag{4.181}$$

The ratio of the potential, V, to the current, I, is the characteristic impedance of the transmission line. Thus,

$$\frac{V}{I} = \pm Z \tag{4.182}$$

where the positive sign refers to the wave moving in the +z direction and the negative sign refers to the wave moving in the –z direction. Using equation (4.171) in (4.182), the following result is obtained for the current.

$$I(z) = \frac{V_o^+}{Z} e^{j(\omega t - kz)} \tag{4.183a}$$

$$I(z) = -\frac{V_o^-}{Z} e^{j(\omega t + kz)} \tag{4.183b}$$

Equation (4.183a) applies for a wave moving in the +direction and equation (4.183b) applies for a wave moving in the –z direction.

Equations (4.171) and (4.183) are the voltage and current solutions for a transmission line that are required to determine the optical properties of a resonant array filter. In the next section, these solutions are applied to the equivalent electrical circuit for a resonant array filter.

4.6.2 Transmission Line Equivalent Circuit for Resonant Array Filter

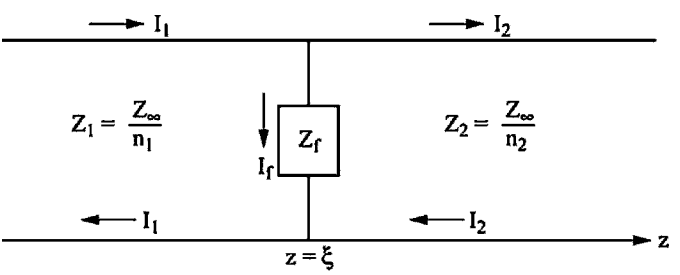

Figure 4.25.—Equivalent circuit for resonant array filter.

As discussed earlier, the resonant array filter can be modeled by a transmission line that is shunted by an impedance, Z_f, representative of the filter. Thus, the equivalent circuit for the filter is shown in Figure 4.25. To the left of Z_f the transmission line has impedance Z_1. This impedance represents the dielectric media that contains the incident radiation. Referring to equation (4.172), the impedance can be written as $Z_1 = \frac{Z_\infty}{n_1}$ where Z_∞ is the impedance of a vacuum. To the right of Z_f the transmission line has impedance $Z_2 = \frac{Z_\infty}{n_2}$. In this case, Z_2 represents the dielectric media that contains the transmitted radiation.

In media 1 there is both an incident wave and a reflected wave. Thus, using equations (4.171) and (4.183), the voltage and current in media 1 are the following.

$$V_1(Z) = V_{o1}^{+} e^{j(\omega t - k_1 z)} + V_{o1}^{-} e^{j(\omega t + k_1 z)} \tag{4.184}$$

$$I_1(Z) = \frac{V_{o1}^{+}}{Z_1} e^{j(\omega t - k_1 z)} - \frac{V_{o1}^{-}}{Z_1} e^{j(\omega t + k_1 z)} \tag{4.185}$$

In media 2 there is only a transmitted wave that originates at z = ξ. Therefore, the voltage and current are the following.

$$V_2(Z) = V_{o2}^{+} e^{j[\omega t - k_2 (z - \xi)]} \qquad z \geq \xi \tag{4.186}$$

$$I_2(Z) = \frac{V_{o2}^{+}}{Z_2} e^{j[\omega t - k_2 (z - \xi)]} \qquad z \geq \xi \tag{4.187}$$

At z = ξ the voltage must be continuous. As a result,

$$V_{o1}^{+} e^{-jk_1 \xi} + V_{o1}^{-} e^{+jk_1 \xi} = V_{o2}^{+} = Z_f I_f e^{-j\omega t} \tag{4.188}$$

where $Z_f I_f$ is the voltage across Z_f. Also, at z = ξ current continuity must exist so that,

$$\begin{gathered} I_1(\xi) = I_2(\xi) + I_f \\ \frac{V_{o1}^{+}}{Z_1} e^{-jk_1 \xi} - \frac{V_{o1}^{-}}{Z_1} e^{-jk_1 \xi} = \frac{V_{o2}^{+}}{Z_2} + I_f e^{-j\omega t} \end{gathered} \tag{4.189}$$

Combining equations (4.188) and (4.189) and using $Z_1 = \frac{Z_\infty}{n_1}$ and $Z_2 = \frac{Z_\infty}{n_2}$, the following result is obtained for the voltage transmission coefficient, t.

$$t \equiv \frac{V_{o2}^{+}}{V_{o1}^{+}} = \frac{2n_1 \left(\frac{Z_f}{Z_\infty} \right)}{1 + (n_1 + n_2) \frac{Z_f}{Z_\infty}} e^{-jk_1 \xi} \tag{4.190}$$

This is also the electric field transmission coefficient [see equation (4.171)]. As a result, using equation (4.67), the filter transmittance is the following,

$$\tau \equiv \frac{n_2 E_{o2}^{+}\left(E_{o2}^{+}\right)^{*}}{n_1 E_{o1}^{+}\left(E_{o1}^{+}\right)^{*}} = \frac{n_2}{n_1} tt^{*} \tag{4.191}$$

where * denotes the complex conjugate. The impedance can be split into real (resistance), R_f and imaginary (reactance), X_f, parts so that $Z_f = R_f + jX_f$. Therefore, substitution of equation (4.190) in (4.191) yields the filter transmittance.

$$\boxed{\tau = \frac{4n_1 n_2\left[\left(\frac{R_f}{Z_\infty}\right)^2 + \left(\frac{X_f}{Z_\infty}\right)^2\right]}{\left[1+\left(n_1+n_2\right)\left(\frac{R_f}{Z_\infty}\right)\right]^2 + \left(n_1+n_2\right)^2\left(\frac{X_f}{Z_\infty}\right)^2}} \tag{4.192}$$

Similar to the transmittance, the reflectance can be obtained from solving equations (4.188) for $\frac{V_{o1}^{-}}{V_{o1}^{+}}$ (problem 4.16).

$$\rho_{12} \equiv \frac{E_{o1}^{-}\left(E_{o1}^{-}\right)^{*}}{E_{o1}^{+}\left(E_{o1}^{+}\right)^{*}} = \frac{V_{o1}^{-}\left(V_{o1}^{-}\right)^{*}}{V_{o1}^{+}\left(V_{o1}^{+}\right)^{*}} = \frac{\left[1+\left(n_2-n_1\right)\frac{R_f}{Z_\infty}\right]^2 + \left(n_2-n_1\right)^2\left(\frac{X_f}{Z_\infty}\right)^2}{\left[1+\left(n_2+n_1\right)\frac{R_f}{Z_\infty}\right]^2 + \left(n_2+n_1\right)^2\left(\frac{X_f}{Z_\infty}\right)^2} \tag{4.193}$$

Notice that the symbol for reflectance has the subscript 12, since this is the reflectance when the incident radiation is in media 1. From equation (4.193) it can be seen that $\rho_{12} \neq \rho_{21}$, where ρ_{21} is the reflectance if the incident radiation is in media 2. Equation (4.192) shows that the transmittance is the same in both directions. Using equations (4.192) and (4.193), the absorptance can be calculated.

$$\boxed{\alpha_{12} = 1-\tau-\rho_{12} = \frac{4n_1\left(\frac{R_f}{Z_\infty}\right)}{\left[1+\left(n_2+n_1\right)\frac{R_f}{Z_\infty}\right]^2 + \left(n_2+n_1\right)^2\left(\frac{X_f}{Z_\infty}\right)^2}} \tag{4.194}$$

Thus, if the filter impedance is only reactance ($R_f = 0$) there is no absorptance. This is similar to an electrical circuit that has no I^2R resistance loss if $R = 0$.

Equations (4.192) through (4.194) give the optical properties in terms of the filter resistance, R_f, and reactance, X_f. For a metallic mesh like that shown in Figure 4.26, where the mesh thickness is much less than the wavelength, resistance and reactance results are given in [28].

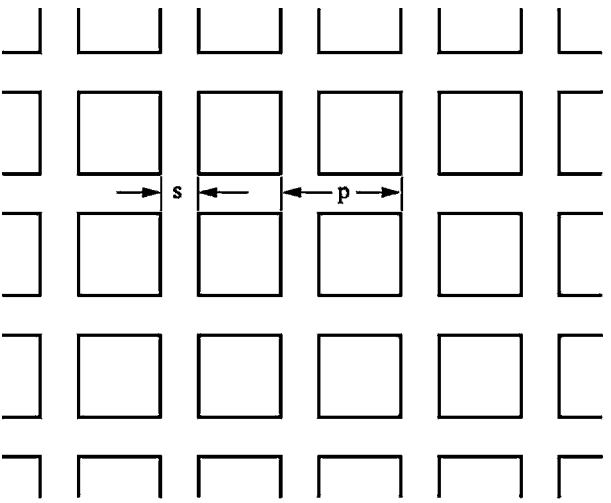

Figure 4.26.—Metallic mesh filter with period, p, and hole spacing, s, and thickness, d.

$$\left.\begin{aligned} \frac{X_f}{Z_\infty} &= -\frac{p}{\lambda}\ln\left[\operatorname{cosec}\frac{\pi s}{2p}\right]\left[\frac{\lambda_o}{\lambda}-\frac{\lambda}{\lambda_o}\right]^{-1} \qquad (4.195)\\ \frac{R_f}{Z_\infty} &= \sqrt{\frac{16\pi\varepsilon_o c_o}{\lambda\sigma}}\frac{p}{4s} = \frac{289}{\sqrt{\lambda\sigma}}\frac{p}{s} \qquad (4.196)\end{aligned}\right\} \quad \begin{array}{l}\lambda \gg d\\ \lambda > p > s\end{array}$$

$$\lambda(\text{nm}) \qquad \sigma\left(\frac{1}{\text{ohm}-\text{cm}}\right)$$

Appearing in equations (4.195) and (4.196) are the gird period, p, and the mesh spacing, s, the permittivity of vacuum, ε_o, the vacuum speed of light, c_o, the conductivity of the metal, σ, and the wavelength, λ. As equation (4.195) shows, when

$\lambda = \lambda_o$ the reactance, $\frac{X_f}{Z_\infty} \to \infty$. This is the resonant condition for the filter. The resonant wavelength of the mesh, λ_o, is the following,

$$\lambda_o = \lambda_\infty \sqrt{\frac{n_1^2 + n_2^2}{2}} \tag{4.197}$$

where λ_∞ is the resonant wavelength for a metallic mesh in a vacuum. For this case Ulrich [25] found that $\lambda_\infty \approx p$. Therefore, the resonant condition can be approximated as follows.

$$\boxed{\lambda_o \approx p \sqrt{\frac{n_1^2 + n_2^2}{2}}} \tag{4.198}$$

At resonance the transmittance is a maximum. Equation (4.192) yields the following result when $\frac{X_f}{Z_\infty} \to \infty$.

$$\tau_{MAX} = \frac{4 n_1 n_2}{(n_1 + n_2)^2} \qquad \text{for } \lambda = \lambda_o \tag{4.199}$$

This is just the transmissivity that occurs for normal incidence at an interface between two dielectrics with indices of refraction n_1 and n_2 [equation (1.111)].

4.6.3 Metallic Mesh Filter

Consider a metallic mesh filter like that shown in Figure 4.26. The starting point to design a filter is the resonant wavelength condition [equation (4.198)]. Maximum transmittance occurs at the resonant wavelength, λ_o. As a result, for a bandpass filter with a center wavelength, λ_o, equation (4.198) determines the period, p, of the filter. Consider a bandpass filter in vacuum centered at $\lambda_o = 1.5\mu m$ consisting of a metallic film on a sapphire substrate. For vacuum $n_1 = 1$ and for sapphire, $n_2 \approx 1.75$. As a result, equation (4.198) yields $p = 1.05\mu m$. Assume that the spacing, $s = \frac{p}{2}$. Therefore, $s = 0.53\mu m$.

Figure 4.27 shows the transmittance reflectance and absorptance for this filter using a gold conductivity of $\sigma = 4.55 \times 10^5 ohm^{-1}cm^{-1}$. Equations (4.192) through (4.196) are used to make the calculations. Large reflectance (> 0.9) for $\lambda > \lambda_f$ and low

absorptance are major virtues of this filter. The transmission bandwidth is larger than the embedded metal interference filter (Figure 4.11) or the interference-plasma filter (Figure 4.22).

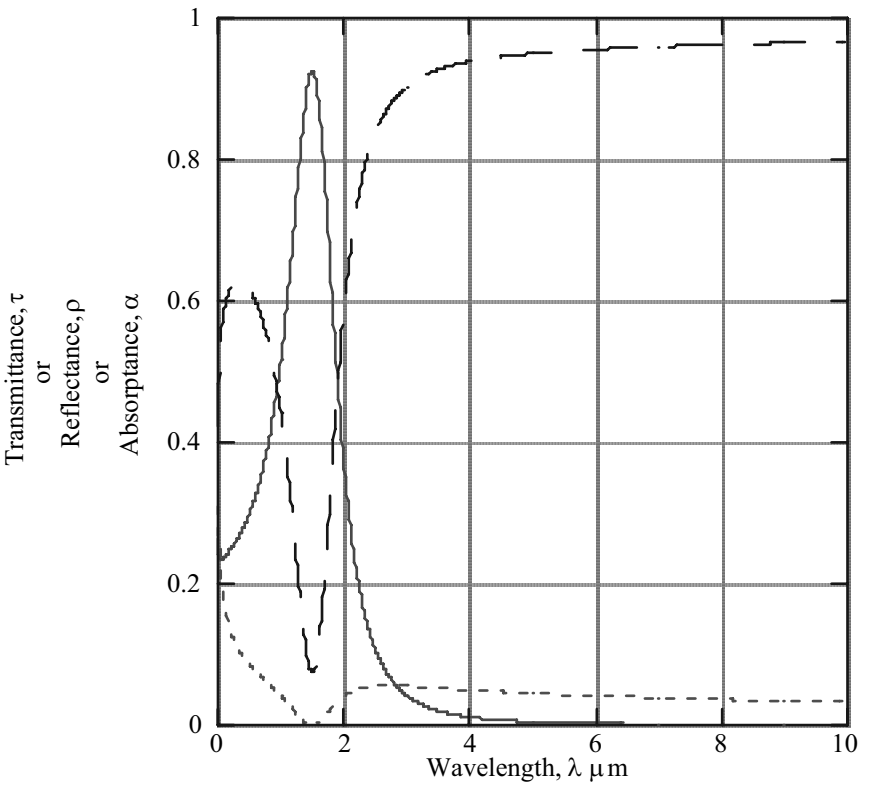

Figure 4.27 - Optical properties in vacuum of resonant array bandpass filter consisting of a gold film(σ=4.55x10^5 ohm^{-1}cm^{-1}) on a sapphire substrate(n_2=1.75). Center wavelength of filter, λ_f=1.5 μm so that hole period, p=1.05 μm. Assumed hole spacing, s=p/2. τ ——— ρ—— —— α— — —

This bandwidth can be reduced by increasing the ratio $\frac{s}{p}$. This is illustrated in Figure 4.28, where the transmittance is shown for three values of $\frac{s}{p}$ (0.25, 0.5, 0.75) for the

same filter design as in Figure 4.27. With $\frac{s}{p}$ = 0.75 the bandwidth becomes comparable to the bandwidth of the embedded metal and interference-plasma filters.

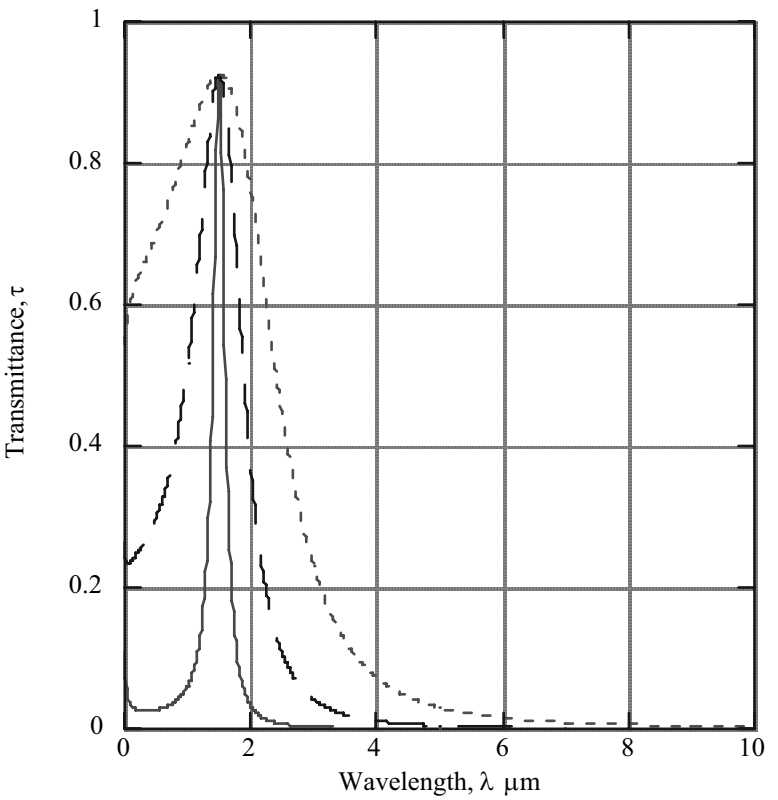

Figure 4.28 - Effect of hole spacing, s on the transmittance, τ, in vacuum for a resonant array gold(σ=4.55x10^5 ohm^{-1}cm^{-1}) film on a sapphire substrate(n_2=1.75). Hole period, p=1.05 μm(λ_f=1.5 μm).

s/p=.75 ——— s/p=.5 —— —— s/p=.25 - - - - -

With $\frac{s}{p}$ = 0.75, the hole size, h = p – s = 0.25p. Thus, if p ≈ 1μm, then h ≈ 0.25μm. Producing a metal film with holes this small in a regular pattern with a period, p ≈ 1μm is a formidable fabrication problem. One method for making the array film is to

fabricate a silicon stencil using ion-bean lithography. Then, using this stencil to mask a gold film the array pattern is etched with a proton beam[29].

The resonant array in Figure 4.26 consists of square holes. However, most resonant array filters in the mid to far infrared have used cross-shaped openings [27,34,35]. In this case it has been found experimentally [34,35] that the resonant condition can be approximated as follows,

$$\lambda_o = 2L\sqrt{\frac{n_1^2 + n_2^2}{2}} \tag{4.200}$$

where L is the length of each arm of the cross. Comparing equation (4.200) with equation (4.198), 2L has replaced the period p in the resonant condition. The bandwidth for the cross configuration depends upon the ratio of the cross thickness to the spacing distance of the crosses [35]; whereas for the square hole configuration the bandwidth depends upon the ratio $\frac{s}{p}$ (Figure 4.28).

For TPV applications [29] in the near infrared, the cross configuration is being developed. So far, in the TPV resonant array filter research, peak transmission has been less than 0.7[36] for narrow bandwidth filters. This compares to theoretical maximums greater than 0.9 (Figure 4.28).

Now consider the film efficiency and total transmittance, reflectance, and absorptance of the resonant array filter of Figure 4.26. Assume a constant emitter emittance, ε_E, and the spectral properties shown in Figure 4.27. Then use equations (4.4) through (4.7) to calculate the total optical properties. These results are shown in Figure 4.29. Compare the efficiencies of the embedded metal interference filter (Figure 4.10a) and the interference-plasma filter (Figure 4.23a) with the resonant array filter efficiency. The resonant array filter has a greater efficiency than the embedded metal interference filter but a smaller efficiency than the plasma-interference filter. Remember, however, that these are theoretical results. The real efficiency of the filter will be strongly dependent upon the fabrication process.

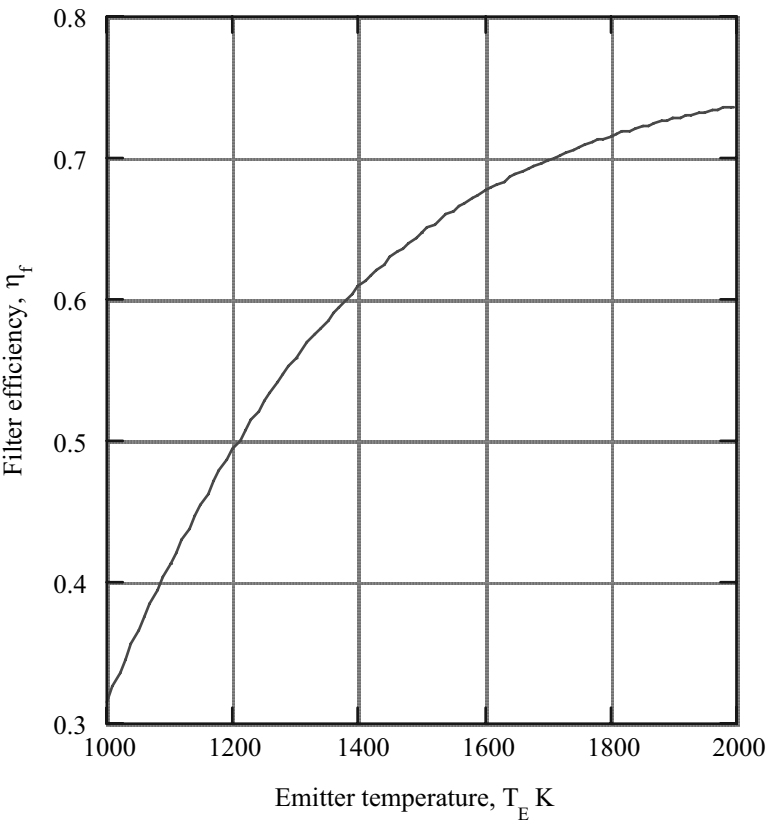

Figure 4.29a) - Filter efficiency, η_f, of resonant array filter of Fig. 4.27 for constant emitter emittance, ε_E. Limit wavelength for filter efficiency calculation, $\lambda_g = 1.9\,\mu m$.

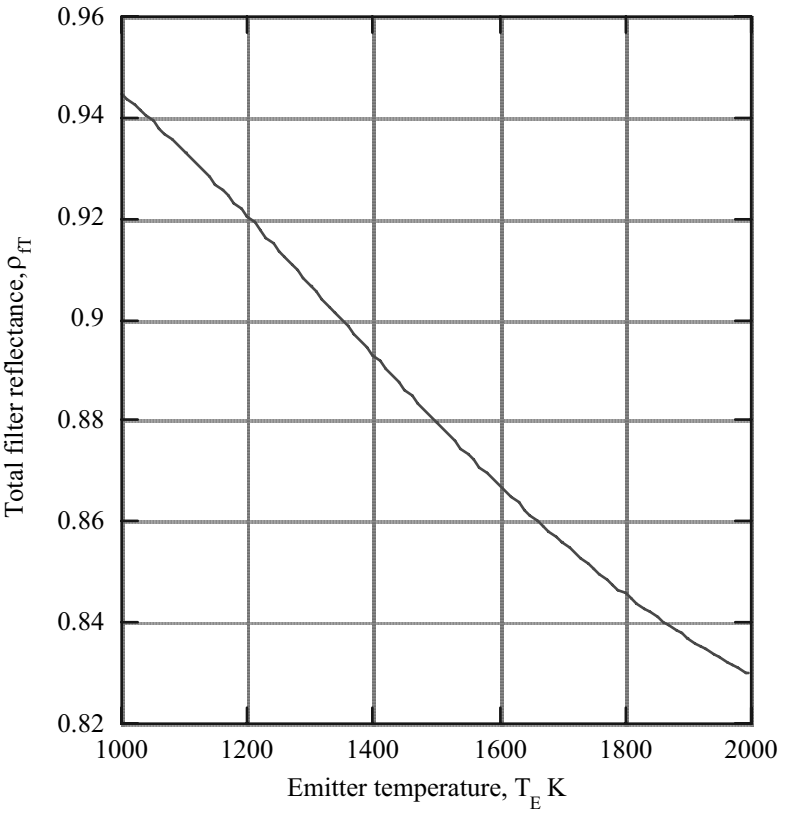

Figure 4.29b) - Total filter reflectance, ρ_{fT}, of resonant array filter of Fig. 4.27 for constant emitter emittance, ε_E. Limit wavelength for filter efficiency calculation, λ_g =1.9 μm.

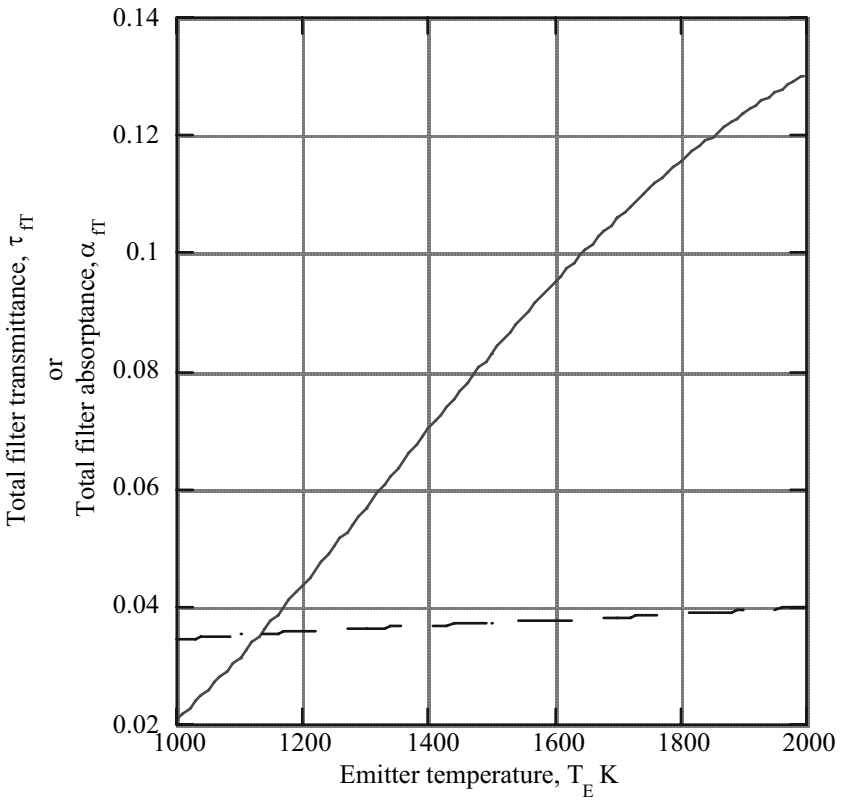

Figure 4.29c) - Total filter transmittance, τ_{fT} and total filter absorptance of resonant array filter of Fig. 4.27 for constant emitter emittance, ε_E. Limit wavelength for filter efficiency calculation, λ_g=1.9 μm.

τ_{fT} ———— α_{fT} —— ——

4.7 Spectral Control Using a Back Surface Reflector (BSR)

Probably the simplest method of spectral control is the use of a highly reflecting surface, such as gold, behind the PV array. The back surface reflector (BSR) reflects the photons not absorbed by the PV array back toward the emitter in a TPV system. For the BSR method to be successful, the PV material must have low absorptance for photon energies less than the PV material bandgap energy, E_g. These are the photon energies that cannot be converted to electrical energy by the PV array and must be reflected back to the emitter for an efficient system. As a result, the BSR method is only applicable to PV cells that are fabricated on non-absorbing substrates.

In a conventional PV cell the substrate serves as an electrical contact and must, therefore, have large electrical conductivity. For a semiconductor, large electrical conductivity is achieved by adding charge carriers (electrons or holes), which is called doping and is discussed in Chapter 5. However, the added charge carriers results in free carrier absorptance. In section 4.4.1, the Drude model is applied to doped semiconductors to obtain an index of refraction that has an imaginary part, n_I. Thus, the semiconductor is absorptive [equation (1.41)].

One method for eliminating the use of a conducting substrate is to make electrical contact to the PV array on the front surface. Thus, an insulating substrate can be used that has small absorptance. This scheme is used in the so-called monolithic interconnected module (MIM) device [37, 38].

4.7.1 Efficiency of a Back Surface Reflector (BSR) for Spectral Control

The filter efficiency expression given by equation (4.4) does not apply when a BSR is used for spectral control. However, the general definition given by equation (4.1) still applies if the word "filter" is replaced by "PV array" in the denominator and the word "transmitted" is replaced by "incident" in the numerator of equation (4.1). Therefore, the BSR efficiency is the following,

$$\eta_{BSR} = \frac{\int_0^{\lambda_g} q_i \, d\lambda}{\int_0^{\infty} q_i \, d\lambda - \int_0^{\infty} q_o \, d\lambda} \tag{4.201}$$

where q_i is the incident radiation flux and q_o is the radiation flux reflected back toward the emitter. The incident radiation is given by equation (4.3). However, to determine q_o, a radiation transfer analysis must be performed.

In Chapter 6 radiation transfer theory is presented and applied to a TPV system. One of the results [equation (6.22)] can be used to calculate the reflected flux, q_o, for the BSR model shown in Figure 4.30.

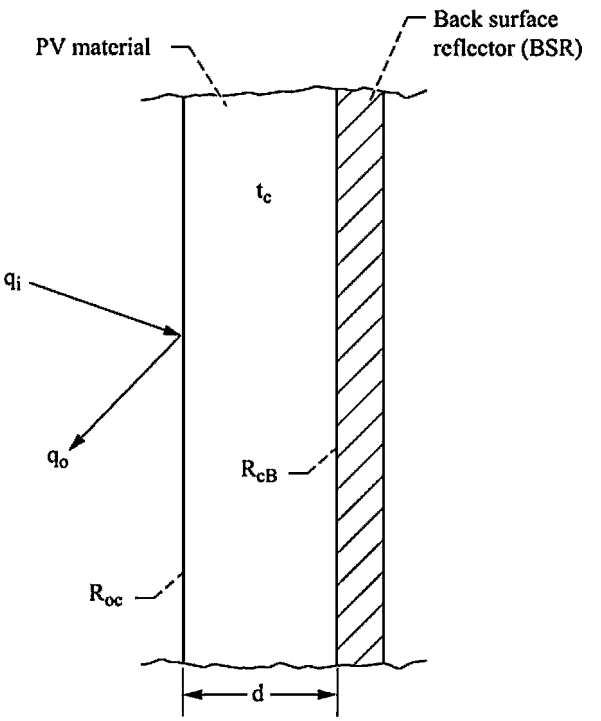

Figure 4.30.—Model used to calculate efficiency of back surface reflector (BSR) for spectral control.

The PV cell consists of several layers of different materials deposited on a substrate. However, the model lumps the optical properties of the PV cell into three quantities: R_{oc}, the reflectivity at the vacuum-PV interface; R_{cB}, the reflectivity at the PV-BSR interface; and t_c, the internal transmittance of the PV material. From equation (6.22) the following is obtained for q_o,

$$q_o = q_i \left[R_{oc} + \frac{R_{cB}\left(1-R_{oc}\right)^2 t_c^2}{1-R_{oc}R_{cB}t_c^2} \right] \tag{4.202a}$$

where the internal transmittance, t_c, is given by equation (6.21),

$$t_c = 2E_3\left(K_c d\right) = 2E_3\left(\kappa_c\right) \tag{4.202b}$$

where $E_3(x)$ is the third order exponential integral [equation (3.16)], K_c is the extinction coefficient of the PV material of thickness, d, and optical depth $\kappa_c = K_c d$.

Substituting equation (4.202) in (4.201) yields the following.

$$\eta_{BSR} = \frac{\int_0^{\lambda_g} q_i d\lambda}{\int_0^{\infty} q_i \left[1 - R_{oc} - \frac{R_{cB} t_c^2 \left(1 - R_{oc}\right)^2}{1 - R_{oc} R_{cB} t_c^2}\right] d\lambda} \tag{4.203}$$

For an efficient PV cell, all the photons with energy greater than the bandgap energy, $E_g = \frac{hc_o}{\lambda_g}$, will be absorbed. As a result, for $0 \le \lambda \le \lambda_g$, $t_c \approx 0$. Also, for an efficient PV cell, $R_{oc} \ll 1$. As a result, equation (4.203) can be approximated as follows.

$$\eta_{BSR} \approx \frac{\int_0^{\lambda_g} q_i d\lambda}{\int_0^{\lambda_g} q_i d\lambda + \int_{\lambda_g}^{\infty} q_i \left[1 - R_{cB} t_c^2\right] d\lambda} \tag{4.204}$$

Notice that η_{BSR} depends upon $1 - R_{cB} t_c^2$, which must be small if η_{BSR} is to be large. However, since $R_{cB} \le 1$ and $t_c \le 1$, the product $R_{cB} t_c^2$ does not approach 1 unless $t_c \approx 1$ and $R_{cB} \approx 1$. Thus, for $\lambda_g \le \lambda \le \infty$, the PV material must be nearly transparent ($t_c \approx 1$) and the reflectivity at the PV-BSR interface must be large ($R_{cB} \approx 1$) in order for η_{BSR} to be large. The radiation that is incident and then is reflected back to the emitter passes through the PV material twice. As a result, the t_c term is raised to the second power.

If equation (4.3) is used for q_i in equation (4.204) and constant emitter emittance, ε_E, is assumed, then η_{BSR} is the following.

$$\eta_{BSR} = \frac{\int_0^{\lambda_g} e_b(\lambda, T_E)\, d\lambda}{\int_0^{\lambda_g} e_b(\lambda, T_E)\, d\lambda + \int_{\lambda_g}^{\infty} \left[1 - R_{cB} t_c^2\right] e_b(\lambda, T_E)\, d\lambda} \qquad \begin{array}{l} \varepsilon_E = \text{constant} \\ t_c = 0 \text{ for } 0 \le \lambda \le \lambda_g \\ R_{oc} \ll 1 \end{array} \qquad (4.205)$$

Although R_{cB} and t_c depend upon λ, assume they are constant for $\lambda_g \le \lambda \le \infty$. As a result,

$$\eta_{BSR} = \frac{F_{o-\lambda_g T_E}}{1 - R_{cB} t_c^2 \left[1 - F_{o-\lambda_g T_E}\right]} = \frac{F_{o-\lambda_g T_E}}{1 - 4R_{cB} E_3^2(\kappa_c)\left[1 - F_{o-\lambda_g T_E}\right]} \qquad (4.206)$$

where $F_{o-\lambda_g T_E}$ is defined by equation (1.137).

Figure 4.31 shows η_{BSR} as a function of the dimensionless bandgap energy, $\frac{E_g}{kT_E} = \frac{hc_o}{k\lambda_g T_E}$, for $\kappa_c = 0.01$ and several values of R_{cB}. In most cases, the range of dimensionless bandgap energies is $4 < \frac{E_g}{kT_E} < 6$. As Figure 4.31 indicates, for this range of $\frac{E_g}{kT_E}$, the efficiency decreases rapidly with increasing $\frac{E_g}{kT_E}$. The rate of decrease increases as R_{cB} decreases. In order to achieve $\eta_{BSR} > 0.6$ for $\frac{E_g}{kT_E} \approx 6$, the reflectivity at the substrate-BSR interface must be greater than 0.9.

The results in Figure 4.31 are calculated using a small value of the optical depth, $\kappa_c = 0.01$. In Figure 4.32, the dependence of η_{BSR} on κ_c is shown for $\frac{E_g}{kT_E} = 5$ at several values of R_{cB}. As R_{cB} increases, the efficiency becomes more sensitive to the optical depth. To achieve $\eta_{BSR} > 0.6$ requires $R_{cB} > 0.9$ for $\kappa_c = 0.04$. If $\kappa_c = 0.01$, then $\eta_{BSR} > 0.6$ can be attained for $R_{cB} \approx 0.8$.

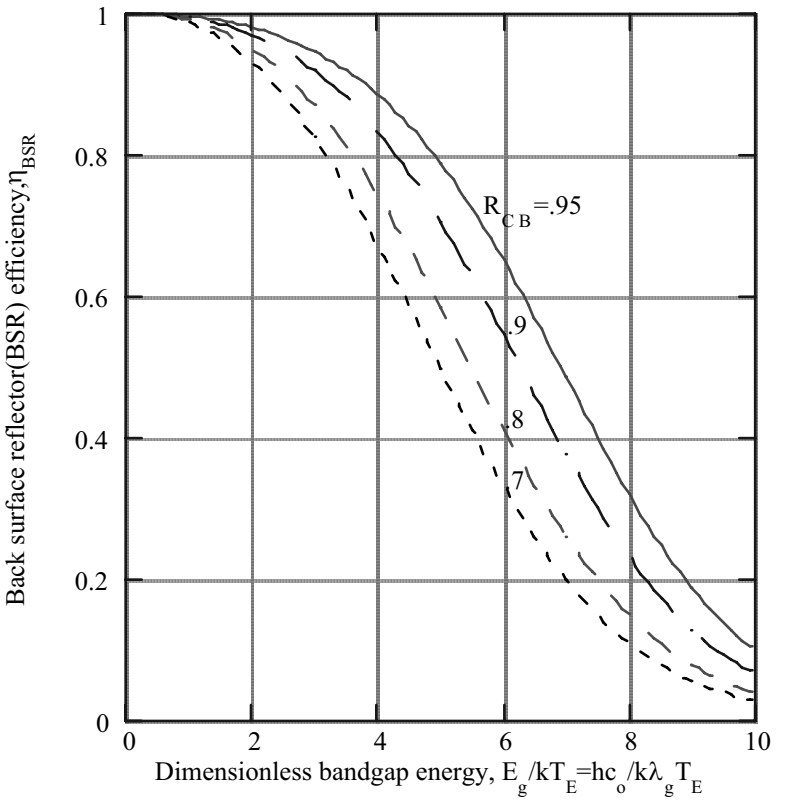

Figure 4.31 Effect of reflectivity at substrate-BSR interface, R_{CB} on back surface reflector(BSR) efficiency, η_{BSR} for optical depth of PV material, κ_c=.01. Results assume ε_E, R_{CB} and κ_C are independent of wavelength, λ.

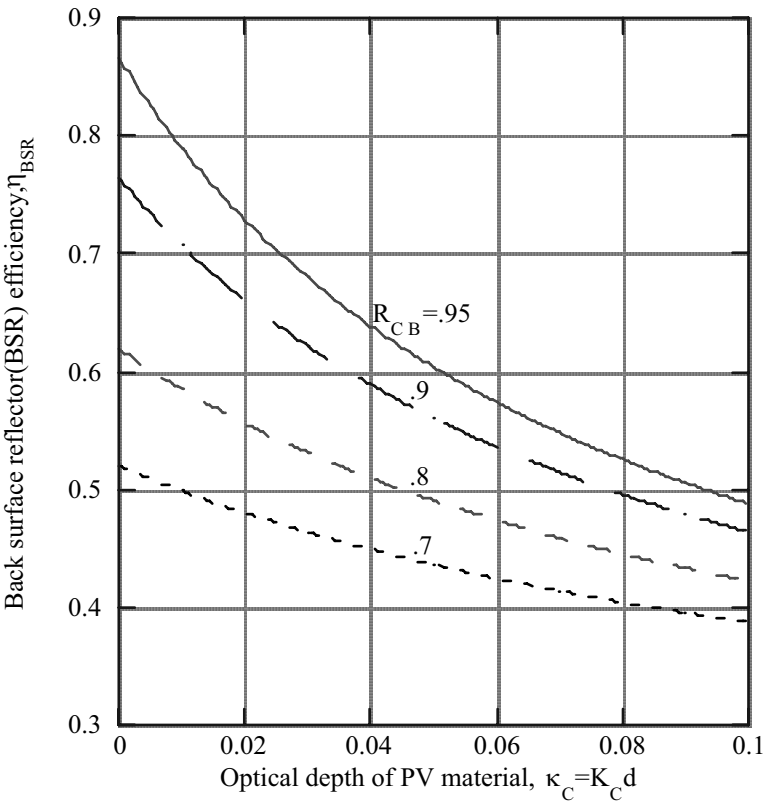

Figure 4.32 Dependence of back surface reflector(BSR) efficiency, η_{BSR} on the optical depth of PV material, $\kappa_C=K_Cd$ for dimensionless bandgap energy, $E_g/kT_E=5$ at several values of the reflectivity at the substrate-BSR interface, R_{CB}. Where K_C is the extinction coefficient and d is the thickness of the PV material. Results assume emitter emittance, ε_E, R_{CB} and κ_C are independent of wavelength, λ.

4.8 Summary

Spectral control by reflecting photons with energy, $E < E_g$, where E_g is the bandgap energy of the PV array, back to the emitter is discussed in this chapter. In particular, five different filters plus a back surface reflector (BSR) on the PV array are considered. The chapter begins by defining a filter efficiency, η_f, [equation (4.1)] and then proceeds to develop the theoretical tools necessary to calculate the optical performance of each of the six methods of spectral control.

For multi-layer interference filters, a matrix theory has been developed. Results for the transmitted and reflected electric and magnetic fields are derived in matrix form by satisfying boundary conditions at the interfaces between layers. The final matrix results that relate incident fields to transmitted fields are given by equations (4.58) through (4.60). These results for the electric and magnetic fields can then be used to calculate the optical properties [equations (4.66), (4.69), (4.70)].

The equivalent layer procedure for designing an interference filter has been presented [equations (4.114) through (4.116)]. It has been used to design an all-dielectric interference filter and also a dielectric interference filter with an embedded metal. The all-dielectric filter suffers from low reflectance for long wavelengths, whereas, the addition of a metallic layer produces large reflectance at the long wavelengths.

So-called plasma filters, which are made from metals and doped semiconductors, has been treated using the Drude model. This model is used to determine the dielectric constant, $\overline{\varepsilon}$ [equations (4.137) and (4.141)] and the index of refraction, n [equations (4.139) and (4.140)]. The optical properties of the plasma filter are calculated using equations (4.91) and (4.92). The virtue of a plasma filter is large reflectance for long wavelengths. However, plasma filters also have significant absorptance. By combining a dielectric interference filter with a plasma filter, large transmittance within a prescribed wavelength band can be obtained as well as large reflectance in the long wavelength region (Figure 4.22).

Interference filters have fabrication issues. Two significant ones are precision growth and adherence of the various layers.

Resonant array filters consist of a metallic film with a periodic pattern with period, p, of small holes or crosses with characteristic dimension, L. The condition of $p < \lambda$ and $L < \lambda$ makes fabrication of these filters difficult. A transmission line theory has been presented for calculating the optical properties.

A back surface reflector (BSR) on the PV array is the simplest spectral control method. However, a non-absorbing substrate for the PV array is required to make a BSR feasible. High efficiency requires large reflectivity at the substrate-BSR interface ($R_{cB} > 0.9$) and small optical depth of the PV material ($\kappa_c < 0.01$).

The theoretical filters for spectral control discussed in this chapter are all candidates for TPV application. Remember, however, it is the fabrication process that will determine if experimental performance can be attained that matches the theoretical performance presented here.

References

[1] O. S. Heavens, Optical Properties of Thin Solid Films, Dover Publications, New York, 1991.

[2] Z. Knittl, Optics of Thin Films, John Wiley and Sons, London, 1976.

[3] P. H. Berning, Theory and Calculations of Optical Thin Films, in Physics of Thin Films, vol. 1, edited by George Hass, Academic Press, New York, 1963.

[4] A. Thelen, Physics of Thin Films 5 (1969) 47.

[5] A. Thelen, Optical Soc. of America 53 (1963) 1266.

[6] S. Wolfram, The Mathematica Book, third ed., Cambridge University Press, 1996.

[7] F. Demichelis, E. Minetti-Mezzetti, M. Agnello, and V. Perotto Solar Cells, 5 (1982) 135.

[8] F. Demichelis, E. Minetti-Mezzetti, and V. Perotto Solar Cells, 6 (1982) 323.

[9] H. Höfler, H. J. Paul, W. Ruppel, and P. Würfel Solar Cells, 10 (1983) 273.

[10] D. W. Lynch, and W. R. Hunter, Comments on the Optical Constants of Metals and an Introduction to the Data for Several Metals in Handbook of Optical Constants of Solids, edited by E. D. Palik, Academic Press, 1998.

[11] K. F. Brennan, The Physics of Semiconductors with Applications to Optoelectronic Devices, Cambridge University Press, New York, 1999.

[12] S. M. Sze, Physics of Semiconductor Devices, Wiley-Interscience, New York, 1969.

[13] E. Conwell, and V. F. Weisskopf, Phys. Rev. 77(1950) 388.

[14] H. Ehsani, I. Bhat, J. Borrego, and R. Gutmann in proceedings of The Second NREL Conference on Thermophotovoltaic Generation of Electricity, AIP Conference Proceedings 358 (1996) 312.

[15] G. W. Charache, et. al., in proceedings of The Third NREL Conference on Thermophotovoltaic Generation of Electricity, AIP Conference Proceedings, 401 (1997) 215.

[16] S. D. Murthy, E. Langlois, I. Bhat, R. Gutmann, E. Brown, R. Dzeindziel, M. Freeman, and N. Choudhuryin in proceedings of The Second NREL Conference on Thermophotovoltaic Generation of Electricity, AIP Conference Proceedings, 358(1996) 290.

[17] X. Wu, W. P. MulliganJ. D. Webb, J. D., and T. J. Coutts in proceedings of The Second NREL Conference on Thermophotovoltaic Generation of Electricity, AIP Conference Proceedings, 358 (1996) 329.

[18] T. J. Coutts, X. Wu, W. P. Mulligan, and J. M. Webb, J. of Electronic Materials, 259 (1996) 935.

[19] P. F. Baldasaro, E. J. Brown, D. M. Depoy, B. C. Campbell, and J. Parrington, in proceedings of The First NREL Conference on Thermophotovoltaic Generation of Electricity, AIP Conference Proceedings, 321 (1995) 29.

[20] P. M. Martin, L. C. Olsen, J. W. Johnston, D. M. DePoy, Appl. Optics, 41 (2002) 6702.

[21] H. A. Macleod, Thin-Film Optical Filters, 3rd Edition, Institute of Physics Publishing, 2001.

[22] K. K. Schuegraf, editor, Handbook of Thin Film Deposition Process and Techniques: Principles, Methods, Equipment, and Applications, Noyes Publications, 1998.

[23] D. L. Smith, Thin Film Deposition: Principles and Practice, McGraw-Hill, 1995.

[24] R. Ulrich, Infrared Physics, 7 (1967) 37.

[25] R. Ulrich, Infrared Physics, 7 (1967) 65.

[26] I. Anderson, The Bell System Technical Journal, 549 (1975) 1725.

[27] V. P. Tomaselli, D. C. Edewaard, P. Gillan, and K. D. Möller, Applied Optics, 20 (1981) 1361.

[28] L. B. Whithourn, and R. C. Compton, Applied Optics, 24 (1985) 217.

[29] W. E. Horne, M. D. Morgan, and V. S. Sundaram, in proceedings of The Second NREL Conference on Thermophotovoltaic Generation of Electricity, AIP Conference Proceedings, 358 (1996) 35.

[30] H. A. Bethe, Phys. Rev., 66 (1944) 163.

[31] H. F. Ghaemi, T. Thio, D. E. Grupp, T. W. Ebbesen, and H. J. Lezec, Phys. Rev. B, 58 (1998) 6779.

[32] T. J. Kim, T. Thio, T. W. Ebbesen, D. E. Grupp, and H. J. Lezec, Optics Letters, 24(1999) 256.

[33] J. A. Porto, F. J. Garcia-Vidal, and J. B. Pendry, Phys. Rev. Lett., 83 (1999) 2845.

[34] C. M. Rhoads, E. K. Damon, and B. A. Munk, Applied Optics, 21 (1982) 2814.

[35] S. T. Chassand and R. D. Joseph, Applied Optics, 22 (1983) 1775.

[36] V. S. Sundaram, et. al., in proceedings of The Third NREL Conference on Thermophotovoltaic Generation of Electricity, AIP Conference Proceedings, 401 (1997) 1121.

[37] D. M. Wilt, et. al., "in proceedings of The Third NREL Conference on Thermophotovoltaic Generation of Electricity, AIP Conference Proceedings, 401 (1997) 237.

[38] J. S. Ward, et. al., "in proceedings of The Third NREL Conference on Thermophotovoltaic Generation of Electricity, AIP Conference Proceedings, 401 (1997) 227.

Problems

4.1 Derive the matrix relation for $\hat{E}_{(i-1)}$ and $\hat{H}_{(i-1)}$ in terms of $\hat{E}_i$ and $\hat{H}_i$ given by equation (4.57).

4.2 Show that the reflectance defined in terms of the tangential fields $\hat{E}^r_{o-}$ and $\hat{E}^t_{o-}$ and the reflectance defined in terms of the total fields E^r_{o-} and E^t_{o-} are equal for a multi-layer filter.

4.3 Show that the transmittance, τ, defined in terms of the total fields E^t_{m+} and E^t_{o-} and the transmittance, $\hat{\tau}$, defined in terms of the tangential fields $\hat{E}_{m+}$ and $\hat{E}_{o-}$ are related as follows for a multi-layer filter,

$$\tau \cos\theta_{m+1} = \hat{\tau} \cos\theta_o$$

where θ_o is the angle of incidence for the incident light and θ_{m+1} is the angle of the transmitted light.

4.4 For N 2 × 2 matrices of the following form,

$$A_i = \begin{bmatrix} a^i_{11} & a^i_{12} \\ a^i_{21} & a^i_{22} \end{bmatrix} \quad \text{where} \quad a^i_{11} = a^i_{22}$$

show that

$$A_N A_{N-1} \ldots A_1 = \begin{bmatrix} a_{22} & a_{12} \\ a_{21} & a_{11} \end{bmatrix}$$

where

$$A_1 A_2 A_3 \ldots A_N = \begin{bmatrix} a_{11} & a_{12} \\ a_{21} & a_{22} \end{bmatrix}$$

4.5 Using equations (4.74) and (4.76) obtain the result given by equation (4.77).

4.6 For a single, non-absorptive film with index of refraction, n_1, and thickness, d, on a non-absorptive substrate with index of refraction, n_2, where $n_1 < n_2$, the reflectance, ρ, into a vacuum ($n_o = 1$) at normal incidence ($\theta_o = 0$) has a minimum for $n_1 \frac{d}{\lambda} = \frac{m}{4}$ where m is an odd integer and d is the film thickness and λ is the wavelength (see Figure 4.3). Show that if $n_1 \frac{d}{\lambda} = \frac{m}{4}$, where m is an odd, integer, that $\rho = 0$ if $n_1 = \sqrt{n_o n_2}$.

4.7 Show that for a single non-absorptive film with index of refraction, n_1, on a non-absorptive substrate with index of refraction, n_2, that the reflectance, for p polarization into a non-absorptive medium with index of refraction, n_o, vanishes ($\rho = 0$) for the following conditions.

a) $$\phi_1 = \frac{2\pi n_1 d \cos\theta_1}{\lambda} = m\pi \qquad m = 0, 1, 2, 3,\ldots$$

for the angle of incidence, θ_o, $\sin\theta_o = \frac{n_2}{\sqrt{n_o^2 + n_2^2}}$.

For $n_o = 1$ and $n_2 = 1.5$, calculate θ_o.

b) $$\phi_1 = \frac{2\pi n_1 d \cos\theta_1}{\lambda} = \frac{\pi}{2} m \qquad m = 1, 3, 5, 7,\ldots$$

and

$$\cos^2\theta_o = \frac{\sqrt{b^2 - 4ac} - b}{2a}$$

where

$$a = n_{o2}^2 - n_{o1}^6 n_{21}^2$$

$$b = 1 - n_{o2}^2 - 2n_{o1}^4 n_{21}^2 \left(1 - n_{o1}^2\right)$$

$$c = -n_{o1}^2 n_{21}^2 \left(1 - n_{o1}^2\right)^2$$

$$n_{o1} = \frac{n_o}{n_1}, \qquad n_{o2} = \frac{n_o}{n_2}, \qquad n_{21} = \frac{n_2}{n_1}$$

For $n_o = 1$, $n_1 = 2$, and $n_2 = 1.5$, calculate θ_o.

4.8 For a single non-absorptive film of index of refraction, n_1, and thickness, d, on a non-absorptive substrate of index of refraction, n_2, show that the reflectance, ρ, into a non-absorptive medium of index of refraction, n_o, vanishes ($\rho = 0$) for all phase thicknesses, $\phi_1 = \frac{2\pi n_1 d \cos\theta_1}{\lambda}$ for p polarization if $n_1 = n_2$ and $\tan\theta_o = \frac{n_2}{n_o}$, where θ_o is the angle of incidence at the film-medium interface. In this case, θ_o is just the Brewster angle, which is the angle of incidence for a single interface that yields $\rho = 0$ for p polarization and $\rho \neq 0$ for s polarization.

4.9 Consider a multi-layer interference filter of m non-absorptive ($n_{iI} = 0$) layers, where m is an odd integer and alternating layers have the same index of refraction ($n_1 = n_3 = n_5 = \ldots$, $n_2 = n_4 = n_6 = \ldots$). For the phase thickness, $\phi_i = \frac{N\pi}{2}$, for all layers, where N is an odd integer, show that the reflectance is given by equation (4.111).

4.10 A multi-layer bandpass interference filter uses the layer groups [HLH] and [LHL] where H indicates a high index of refraction material, n_H, and L a low index of refraction material, n_L. Using Figure 4.7, estimate the design wavelengths, λ_o for the [HLH] and [LHL] groups if $\frac{n_H}{n_L} = 3$ and the center wavelength of the filter is $\lambda_c = 1.5\mu m$.

4.11 Calculate the thicknesses for normal incidence ($\theta_o = 0$) of each of the layers of the [HLH] and [LHL] groups that make up the interference filter given by equation (4.123). The indices of refraction of $n_L = 1.35$ and $n_H = 2.4$.

4.12 For good conductors at long wavelengths, such as gold and copper, the index of refraction can be approximated as purely imaginary, $n = -jn_I$. If $n_1 = -jn_{1I}$ for a film on a non-absorptive substrate show that the reflectance is given by equation (4.104).

4.13 Show that the filter efficiency, η_f, defined by equation (4.4) can be approximated as follows,

$$\eta_f \approx \frac{\tau_{fT}}{\tau_{fT} + \alpha_{fT}} = \frac{\tau_{fT}}{1 - \rho_{fT}}$$

if the ratio of the power transmitted in the wavelength region $\lambda_g \leq \lambda \leq \infty$ to the total incident power is much less than τ_{fT}. Where τ_{fT}, ρ_{fT} and α_{fT} are given by equations (4.5) through (4.7) and λ_g is the wavelength corresponding to the PV array bandgap energy, E_g

4.14 Use the Drude model results for the dielectric constant $\bar{\varepsilon}$ [equations (4.135), (4.137), (4.141)] to obtain the vacuum normal reflectivity, $\bar{R}$, for the two limiting cases, $\omega \to 0$ ($\lambda \to \infty$) and $\omega \to \infty$ ($\lambda \to 0$).

4.15 Derive the result given by equation (4.153),

$$\frac{d\bar{R}}{d\omega} \approx -\frac{2\bar{R}}{1-n_R^2}\sqrt{\frac{2\varepsilon_\infty}{\omega_p'\Delta\omega}}$$

where $\omega = \omega_p' + \Delta\omega$.

4.16 Determine the reflectance, ρ [equation (4.193)], for a resonant array filter by solving equations (4.188) and (4.189) for $\frac{V_{o1}^-}{V_{o1}^+}$ and using the definition of reflectance, $\rho_{12} = \frac{V_{o1}^-\left(V_{o1}^-\right)^*}{V_{o1}^+\left(V_{o1}^+\right)^*}$, and $Z_f = R_f + jX_f$.

4.17 A major fabrication problem for a resonant array filter is the very small sized periodic pattern required. The period, p, and spacing, s, must be smaller than the wavelength, λ. For the metallic mesh filter of Figure 4.27, a sapphire substrate ($n_2 = 1.75$) is used. If a magnesium fluoride substrate ($n_2 = 1.35$) is used, how much larger would p and the maximum transmittance, τ_{MAX}, be than p and τ_{MAX} for the sapphire substrate used?

4.18 Using equation (4.205) derive the efficiency, $\eta_{BSR,}$ for a back surface reflector (BSR) in terms of the $F_{o\text{-}\lambda T}$ function [equation (1.137)] for the case where $\left(1-R_{cB}t_c^2\right)$ is a constant for $\lambda_g \le \lambda \le \lambda_c$ and $R_{cB}t_c^2 \ll 1$ for $\lambda_c < \lambda < \infty$. Use the result given in problem 1.14 for Fo-λT to calculate η_{BSR} for $u_g = \frac{hc_o}{k\lambda_g T_E} = 5$ and $u_c = \frac{hc_o}{k\lambda_c T_E} = 2$ when $R_{cB}t_c^2 = 0.9$ for $\lambda_g \le \lambda \le \lambda_c$. Compare this result for η_{BSR} to the result for η_{BSR} when $R_{cB}t_c^2 = 0.9$ for $\lambda_g \le \lambda \le \infty$ [equation (4.206)] and $u_g = 5$. What conclusion can be made based upon this comparison?

This page intentionally left blank

Chapter 5
Photovoltaic Cells

In a TPV system, the PV array is the major component since it converts the thermal radiation into electrical energy. In 1839, the photovoltaic effect was discovered by Becquerel [1] who observed that a voltage was produced by the action of light on an electrode in an electrolyte solution. Modern photovoltaic research began in 1954 when Chopin, et. al. [2] reported 6% conversion efficiency for a silicon PV cell under solar illumination. Since then there has been a numerous amount of solar PV research. Much of this solar PV research has been reported in the Proceedings of IEEE Photovoltaics Specialists Conferences that began in 1962. Many books have also been written on PV fundamentals and applications. Several are listed in references [3] through [8].

The solar PV research has concentrated on semiconductors such as silicon, Si, and gallium arsenide, GaAs, all of which have large (> 1eV) bandgap energies. However, TPV applications require low bandgap semiconductors. Therefore, most of TPV photovoltaic research has concentrated on semiconductors such as gallium antimonide, GaSb, indium gallium arsenide, InGaAs, indium gallium arsenic antimonide, InGaAsSb, and indium arsenic antimony phosphide, InAsSbP.

As already mentioned, the fundamentals of solar photovoltaics are covered in many textbooks. Therefore, the emphasis of this chapter will be to develop the material necessary to calculate the PV array performance in a TPV system. The chapter begins with a discussion of the solid state theory that explains the energy band structure of semiconductors.

5.1 Symbols

a	absorption coefficient, cm^{-1}
A_o	ideality factor
A_c	total PV array area, cm^2
A_j	area of a single cell in the PV array, cm^2
A_{ja}	active area of a single cell in the PV array, cm^2
b_o & b_1	parameters in approximation of second order exponential integral $E_2(x) = b_o e^{-b_1 x}$
c_o	vacuum speed of light (2.9979×10^{10} cm/sec)
e	electron charge, (1.602×10^{-19} Coul)
E	electron or photon energy, J
E_g	bandgap energy, eV

FF	PV cell fill factor
G	generation rate of electron-hole pairs, pairs/cm^{3}sec
I	current, A
I_{sc}	PV cell short circuit current, A
h	Plank's constant (6.624×10^{-34} J-sec)
$\hbar$	$h/2\pi$
J	current density, A/cm^2
J_s	dark saturation current density, A/cm^2
J'	current density per wavelength, A/cm^{2}nm
J_F	maximum possible photon produced current density, eq. (5.161)
J_{sc}	short circuit current, A/cm^2
J_{ph}	photon produced current density, A/cm^2
k_B	Boltzmann constant (1.3805×10^{-34} J/K)
L	diffusion length, cm
m^*	effective mass, kg
m_e	electron mass, (9.107×10^{-31} kg)
n	electron density, cm^{-3}, or index of refraction
n_i	intrinsic carrier density, , $n_i^2 = np$ cm^{-3}
N_A	density of acceptor dopant, cm^{-3}
N_c	effective density of states in the conduction band, cm^{-3}
N_D	density of donor dopant, cm^{-3}
N_V	effective density of states in the valence band, cm^{-3}
p	hole density, cm^{-3}
p_{EL}	PV cell output power density, W/cm^2
P_{EL}	PV cell output power, W
R_c	reflectivity at PV cell surface
R_e	recombination rate of electron-hole pairs, pairs/cm^3 sec
R_s	series resistance, ohms
R_{sh}	shunt resistance, ohms
S	surface recombination velocity, cm/sec
S_r	spectral response, A/W
$\bar{v}$	thermal speed $\sqrt{\frac{k_B T}{m^*}}$, cm/sec
V	voltage, V
V_{oc}	PV cell open circuit voltage, V
V_M	PV cell voltage at maximum power output, V
β	optical depth
ε_E	emitter spectral emittance
ϕ	surface recombination parameter

λ	wavelength, nm
η	efficiency
μ	mobility, Coul sec/kg or cm^2/V
ρ	reflectance
τ	average collision time, sec
τ'	lifetime, sec

Subscripts

d	refers to depletion region of p-n junction
n	refers to electrons or region of p-n junction where electrons are the majority charge carrier
p	refers to holes or region of p-n junction where holes are the majority charge carrier

5.2 Energy Bands (Kronig-Penney Model) and Current in Semiconductors

In Chapter 4, the Drude model is used to approximate electron motion in metals and highly doped semiconductors where electrons are essentially free. However, for most crystalline semiconductors, electrons are not free but are influenced by the ion cores that are located in a periodic fashion at the *lattice points* of the crystal. The periodic nature of a crystal lattice results in a band structure for electron energies. There are regions of nearly continuous electron energies separated by regions where there are no allowed electron energies. Quantum mechanics is required to show how this occurs. So in keeping with the self contained aim of this text the necessary quantum mechanics to present the Kronig-Penney [10] model for a periodic structure is given in Appendix E.

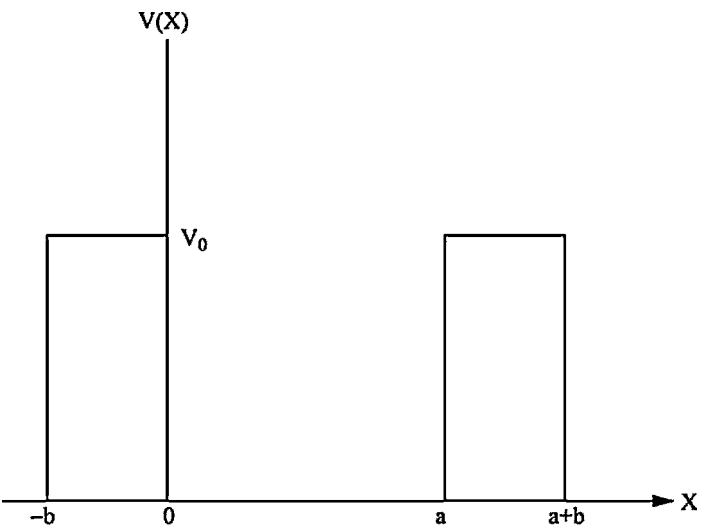

Figure 5.1.—One-dimensional model for crystal with periodic potential of height V_0 and width b and period a+b.

The model is restricted to a single space dimension, x, but the results apply to three dimensions as well. Consider the one-dimensional periodic structure shown in Figure 5.1. The ion cores are represented by the periodic rectangular potential of height, V_o, and width, b, with a period, a + b. The one-dimensional form of the Schrödinger equation [equation (E – 5)] for the wave function, $\psi(x,t)$, that describes the system is the following,

$$\frac{d^2\psi}{dx^2}+\frac{2m_e}{\hbar^2}\left[E-V(x)\right]\psi=0 \tag{5.1}$$

where E is the electron energy, m_e the electron mass, and $\hbar = \frac{h}{2\pi}$ where h is the Planck Constant. To satisfy the periodic potential, V(x) = V[x + (a + b)] the wave function must be of the so-called Bloch form[10],

$$\psi(x) = e^{jkx} u(x) \tag{5.2}$$

where u(x) = u[x + (a + b)] is a periodic function. The term e^{ikx} is the wave function for a free electron [equation (E – 8)]. Thus, the periodic potential that represents the effect of the ion cares results in the system wave function being the free electron wave function modified by the periodic function u(x).

Using equation (5.2) in (5.1) will lead to a relationship between the wave number k and the energy, E. This is the desired result since it will show that for certain values of k there are discontinuities in the energy, which are the forbidden energy bands for a semiconductor.

Substituting equation (5.2) in (5.1) yields the following,

$$\frac{d^2u}{dx^2} + 2jk\frac{du}{dx} - \left[k^2 - \alpha^2 + \frac{2m_e V(x)}{\hbar^2}\right]u = 0 \tag{5.3}$$

where for convenience, α is defined as follows.

$$\alpha = \sqrt{\frac{2m_e E}{\hbar^2}} \tag{5.4}$$

In the region $0 \le x \le a$, V(x) = 0 so that equation (5.3) becomes the following.

$$\frac{d^2u_1}{dx^2} + 2jk\frac{du_1}{dx} - \left(k^2 - \alpha^2\right)u_1 = 0 \tag{5.5}$$

In the regions $-b \le x \le 0$ and $a \le x \le a + b$, the potential is $V(x) = V_o$. Therefore, in those regions the following equation applies,

$$\frac{d^2u_2}{dx^2} + 2jk\frac{du_2}{dx} - \left(k^2 - \beta^2\right)u_2 = 0 \tag{5.6}$$

where for convenience, β is defined as follows.

$$\beta = \sqrt{\frac{2m_e\left(E - V_o\right)}{\hbar^2}} \tag{5.7}$$

The solutions to equations (5.5) and (5.7) are plane waves of the following form.

$$u_1\left(x\right) = Ae^{j(\alpha - k)x} + Be^{-j(\alpha + k)x} \qquad 0 \le x \le a \tag{5.8}$$

$$u_2\left(x\right) = Ce^{j(\beta - k)x} + De^{-j(\beta + k)x} \qquad \begin{matrix} -b \le x \le 0 \\ a \le x \le a + b \end{matrix} \tag{5.9}$$

The constants A, B, C, and D are determined by satisfying boundary conditions. The boundary conditions are that the wave function and its first derivative must be continuous at x = –b, x = 0, and x = a. Also, the periodic condition, u(x) = u[x + (a + b)] must be satisfied so that the boundary conditions are the following.

$$u_1\left(a\right) = u_2\left(-b\right) \tag{5.10a}$$

$$u_1\left(0\right) = u_2\left(0\right) \tag{5.10b}$$

$$\left.\frac{du_1}{dx}\right|_{x=a} = \left.\frac{du_2}{dx}\right|_{x=-b} \tag{5.10c}$$

$$\left.\frac{du_1}{dx}\right|_{x=o} = \left.\frac{du_2}{dx}\right|_{x=o} \tag{5.10d}$$

Using equations (5.8) and (5.9) in equations (5.10) yields the following.

$$Ae^{j(\alpha - k)a} + Be^{-j(\alpha + k)a} - Ce^{-j(\beta - k)b} - De^{j(\beta + k)b} = 0 \tag{5.11a}$$

$$A + B - C - D = 0 \tag{5.11b}$$

$$A\left(\alpha - k\right)e^{j(\alpha - k)a} - B\left(\alpha + k\right)e^{-j(\alpha + k)a} - C\left(\beta - k\right)e^{-j(\beta - k)b} + D\left(\beta + k\right)e^{j(\beta + k)b} = 0 \tag{5.11c}$$

$$A\left(\alpha - k\right) - B\left(\alpha + k\right) - C\left(\beta - k\right) + D\left(\beta + k\right) = 0 \tag{5.11d}$$

Equations (5.11) are a set of linear homogeneous equations for the constant A, B, C, and D. Only if the determinant, DET, of the coefficients of A, B, C, and D is zero, can a nontrivial solution be obtained [11].

$$\mathrm{DET} = \begin{vmatrix} 1 & 1 & -1 & -1 \\ \alpha_- & -\alpha_+ & -\beta_- & \beta_+ \\ e^{j\alpha_- a} & e^{-j\alpha_+ a} & -e^{-j\beta_- b} & -e^{j\beta_+ b} \\ \alpha_- e^{j\alpha_- a} & -\alpha_+ e^{-j\alpha_+ a} & -\beta_- e^{-j\beta_- b} & \beta_+ e^{j\beta_+ b} \end{vmatrix} = 0 \tag{5.12}$$

Where,

$$\alpha_+ = \alpha + k \qquad \alpha_- = \alpha - k \tag{5.13}$$

$$\beta_+ = \beta + k \qquad \beta_- = \beta - k \tag{5.14}$$

By expanding this determinant, the relation between the wave number, k, and the energy, E, is obtained. Expanding DET on the first row in equation (5.12) results in the following [11].

$$\begin{aligned} \mathrm{DET} = 4\alpha\beta\left[e^{2jkb} + e^{-2kja}\right] - (\alpha+\beta)^2\left[e^{j(\alpha_- a+\beta_+ b)} + e^{-j(\alpha_+ a+\beta_- b)}\right] \\ + (\beta-\alpha)^2\left[e^{-j(\alpha_+ a-\beta_+ b)} + e^{j(\alpha_- a-\beta_- b)}\right] = 0 \end{aligned} \tag{5.15}$$

Using equations (5.13) and (5.14) and the definition $\cos x = \frac{1}{2}\left(e^{jx} + e^{-jx}\right)$ in equation (5.15) results in the following.

$$\mathrm{DET} = 4\alpha\beta\cos\left[k(a+b)\right] - (\alpha+\beta)^2\cos(\alpha a + \beta b) + (\beta-\alpha)^2\cos(\alpha a - \beta b) = 0 \tag{5.16}$$

Using the identity, $\cos(x \pm y) = \cos x \cos y \mp \sin x \sin y$, yields the final result.

$$\cos\left[k(a+b)\right] = -\frac{\alpha^2+\beta^2}{2\alpha\beta}\sin\alpha a \sin\beta b + \cos\alpha a \cos\beta b \tag{5.17}$$

Remember that $\alpha \sim \sqrt{E}$ and $\beta \sim \sqrt{E - V_o}$. Thus, if $V_o > E$, then β is purely imaginary. Assume V_o is a delta function such that as $V_o \to \infty$, $b \to 0$, and the product bV_o is finite. This is a reasonable approximation because as an electron comes very close to

an ion core it will be repelled by the electrons surrounding the positive nucleus, thus resulting in $V \to \infty$. Thus, if $\beta = J\sqrt{\frac{2m_e(V_o - E)}{\hbar^2}}$, equation (5.17) becomes the following if the identities sin jx = j sin hx, and cos jx = coshx are used.

$$\cos\left[k(a+b)\right] = \frac{V_o}{2\sqrt{E(V_o - E)}}\sin\left(a\sqrt{\frac{2m_eE}{\hbar^2}}\right)\sinh\left(b\sqrt{\frac{2m_e(V_o - E)}{\hbar^2}}\right) + \cos\left(a\sqrt{\frac{2m_eE}{\hbar^2}}\right)\cosh\left(b\sqrt{\frac{2m_e(V_o - E)}{\hbar^2}}\right) \tag{5.18}$$

Now take the limits $V_o \to \infty$ and $b \to 0$ as bV_o remains finite.

$$\begin{aligned}\frac{V_o}{2\sqrt{E(V_o - E)}}\sinh\left(b\sqrt{\frac{2m_e(V_o - E)}{\hbar^2}}\right) &\to \frac{1}{2}\sqrt{\frac{V_o}{E}}\sinh\left(\sqrt{b}\sqrt{\frac{2m_eV_ob}{\hbar^2}}\right) \\ &= \frac{1}{2}\sqrt{\frac{V_o}{E}}\left[\sqrt{\frac{2m_eb(V_ob)}{\hbar^2}} + \frac{1}{3!}\left(\sqrt{\frac{2m_eb(V_ob)}{\hbar^2}}\right)^{3/2} + \ldots\right] \\ &= \frac{1}{2}V_ob\sqrt{\frac{2m_e}{\hbar^2E}}\left[1 + \frac{m_eb(V_ob)}{3\hbar^2} + \ldots\right] = \frac{V_ob}{2}\sqrt{\frac{2m_e}{\hbar^2E}}\end{aligned} \tag{5.19}$$

$$\cosh\left(b\sqrt{\frac{2m_e(V_o - E)}{\hbar^2}}\right) \to \cosh\left(\sqrt{b}\sqrt{\frac{2m_eV_ob}{\hbar^2}}\right) = 1 \tag{5.20}$$

Therefore, equation (5.18) becomes the following,

$$\cos ka = \cos\left(a\sqrt{\frac{2m_eE}{\hbar^2}}\right) + P\frac{\sin\left(a\sqrt{\frac{2m_eE}{\hbar^2}}\right)}{a\sqrt{\frac{2m_eE}{\hbar^2}}} \tag{5.21}$$

where

$$P = \frac{m_ea(V_ob)}{\hbar^2} \tag{5.22}$$

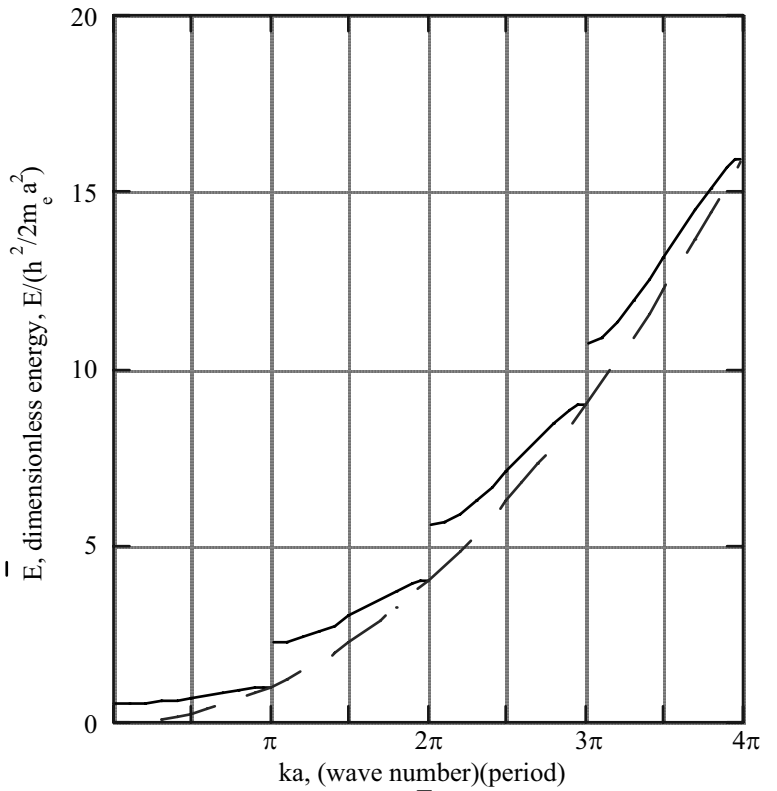

Figure 5.2 Dimensionless energy, $\bar{E}$, as a function of the product of wave number, k, and period, a, for Kronig-Penney model of a semiconductor showing forbidden energy bands at ka=π, 2π, 3π, ... P=3π/2 in eq. (5.24). Dashed line is dimensioless energy for a free electron.

Equation (5.21) is the relationship between the energy, E, and the wave number, k. Now define a dimensionless energy, $\bar{E}$.

$$\bar{E} = \frac{E}{\left(\frac{\pi^2 \hbar^2}{2m_e a^2}\right)} \tag{5.23}$$

Therefore, equation (5.21) becomes

$$\cos ka = \cos \pi\sqrt{\bar{E}} + \frac{P \sin \pi\sqrt{\bar{E}}}{\pi\sqrt{\bar{E}}} \tag{5.24}$$

For certain values of $\bar{E}$, the right hand side of equation (5.24) will be greater than 1 or less than –1. In that case, in order to satisfy the equation k will be imaginary. However, only real values of k are possible. As a result, the values of $\bar{E}$ where the right hand side of the equation is greater than 1 or less than –1 are forbidden. This is illustrated in Figure 5.2 where the forbidden energy bands occur at ka = π, 2π, 3π, 4π,… Also shown by the dashed line in Figure 5.2 is the dimensionless energy for a free electron, which is a given by equation (E – 9). The periodic behavior of the potential results in the electron energy having forbidden regions compared to the free electron continuous energy dependence upon k.

The allowed energy bands are either *conduction bands* or *valence bands*. In a conduction band, there are vacant energy states that an electron can move into if accelerated to higher energy by an external force such as an electric field. Thus, the electrons are essentially free in a conduction band. However, in a valence band all the energy states are occupied. Thus, if an external force is applied to an electron, there are no vacant energy states for the electron to move into within that valence band. If this valence band is separated from an empty higher energy conduction band by a forbidden energy band (the bandgap energy) of sufficient magnitude, then there are no available energy states for the electron to move into and no electron motion is possible. Such a material is an *insulator*. If the bandgap energy, E_g, is small ($E_g \sim 1$eV), then electrons can be thermally or optically excited into the empty conduction band where there are available energy states. Thus, a current can flow in such a material, which is called a *semiconductor*. A *conductor*, such as a metal, has a conduction band that is partially filled with electrons or the conduction band overlaps ($E_g \leq 0$) the valence band so that there are available energy states for electrons.

In a semiconductor, both electrons and *holes* contribute to the current conduction process. When an electron is excited from an energy level in the filled valence band it leaves a vacant energy state which has a +e charge called a hole, where e is the magnitude of the electron charge. When an electric field is applied, as electrons are excited into the conduction band there will be vacant energy states in the valence band for the positively charged holes to move and thus produce a hole current in the valence band. Holes are not real particles, but are a means of representing current flow in a partially filled valence band. When an electric field is applied to a semiconductor the current flows in the same direction as the positively charged holes and in the opposite direction of negatively charged electrons.

An interesting question about current conduction in a semiconductor is the following. What is the amount of current delivered to the outside circuit when an

electron-hole pair is created, as for example, by absorption of a photon? When the electron-hole pair is created, it delivers a charge, e, to the external circuit, not 2e, as one might expect. Current flow is defined as the passage of charge through a complete circuit. Thus, when a electron-hole pair is created, the total path is partly traveled by the electron and partly by the hole (electrons and holes move in opposite directions). Thus, only a charge equal to, e, travels the total semiconductor length.

For a free electron, the momentum is given by p = ħk [equation (E – 11)]. Analogous to the free electron case, the k vector for a semiconductor is called the *crystalline momentum*. For a free electron, the motion is determined by Newton's Second Law, $\frac{dp}{dt} = F_{ext}$, where F_{ext} is an external force, such as an electric field. What is the equation of motion for an electron or hole in a semiconductor where the motion is affected by the potential of the ion cores? To determine the equation of motion in this case consider the following derivation. The incremental change in energy, dE, of an electron is equal to the work done on the electron by the external electric field, $\vec{\varepsilon}$,

$$dE = -e\vec{\varepsilon} \bullet d\vec{x} = -e\vec{\varepsilon} \bullet \vec{v}dt \tag{5.25}$$

where $\vec{v}$ is the electron velocity and t is time. Also,

$$dE = \frac{2E}{dk_x}dk_x + \frac{2E}{dk_y}dk_y = \frac{2E}{dk_z}dk_z = \nabla_k E \bullet d\vec{k} \tag{5.26}$$

It can be shown [12] that for a particle moving in a periodic potential, the average velocity is the following.

$$\vec{v} = \frac{1}{\hbar}\nabla_k E \tag{5.27}$$

Combining equations (5.25) through (5.27)

$$\begin{gathered} dE = \nabla_k E \bullet d\vec{k} = -\frac{e}{\hbar}\nabla_k E \bullet \vec{\varepsilon}dt \\ \therefore \frac{d\vec{k}}{dt} = -\frac{e}{\hbar}\vec{\varepsilon} \end{gathered} \tag{5.28}$$

Also, from equations (5.27) and (5.26)

$$\frac{d\vec{v}}{dt} = \frac{1}{\hbar}\frac{d}{dt}\nabla_k E = \frac{1}{\hbar}\nabla_k\left(\frac{dE}{dt}\right) = \frac{1}{\hbar}\nabla_k\left(\frac{d\vec{k}}{dt}\bullet\nabla_k E\right) \tag{5.29}$$

Now substitute equation (5.28) in (5.29) to obtain the following,

$$\frac{d\vec{v}}{dt} = -\frac{1}{\hbar^2}\nabla_k\left(e\vec{\varepsilon}\bullet\nabla_k E\right) = -\frac{1}{\hbar^2}\left(e\vec{\varepsilon}\bullet\nabla_k\right)\nabla_k E \tag{5.30}$$

which can be written in tensor notion as follows.

$$\frac{dv_i}{dt} = -\frac{1}{\hbar^2}\frac{\partial^2 E}{\partial k_i \partial k_j}e\varepsilon_j = -\frac{e\varepsilon_j}{m^*_{nij}} \tag{5.31}$$

This is analogous to Newton's Second Law where $\frac{d\vec{v}}{dt}$ is the acceleration, and the right hand side of equation (5.31) is the ratio of the force to the mass where

$$\frac{1}{m^*_{nij}} \equiv \frac{1}{\hbar^2}\frac{\partial^2 E}{\partial k_i \partial k_i} \tag{5.32}$$

and m^*_{nij} is the *effective mass* of the electron.

If the energy is an isotropic function of $\vec{k}$ so that E depends upon only a single component of $\vec{k}$, such as in the Kronig-Penney model, then

$$\frac{1}{m^*_n} = \frac{1}{\hbar}\frac{\partial^2 E}{\partial k^2} \tag{5.33}$$

A similar result for the effective mass applies to holes as well. Thus the electron or hole motion in a semiconductor satisfies a modified Newton's Second Law. The effect of the crystalline potential on the electron and hole motion is accounted for by the effective mass. It is the effective mass that is used to determine the electron and hole mobility and diffusion constants. This is discussed further when the electron and hole transport equations are presented.

5.3 Density of Electrons and Holes and Mass Action Law

In the previous section it has been shown that a semiconductor has a bandgap structure of allowable energies. Within the conduction, band the electron energies are a

continuous function of the wave vector, k. Similarly, within the valence band hole energies are continuous. Now calculate the density of electrons and holes that exist for equilibrium conditions.

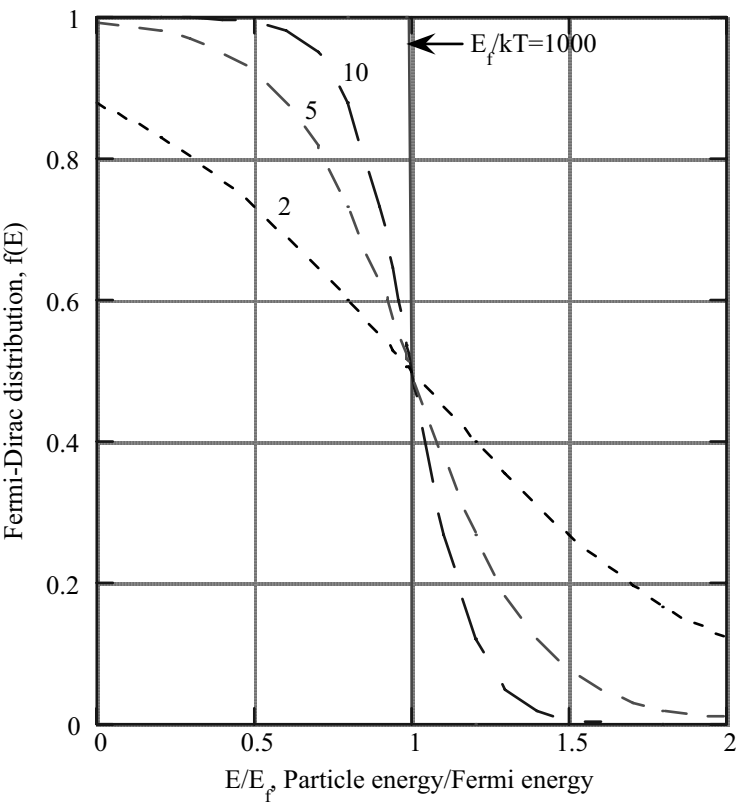

Figure 5.3 Fermi-Dirac distribution for various values of the ratio of the Fermi energy, E_f, to the thermal energy, kT.

In a conduction band, the electron energy is a continuous function of the wave vector or crystalline momentum, k. At equilibriumm the probability that an energy state will be occupied is given by the *Fermi-Dirac distribution function*. The Fermi-Dirac distribution applies to particles (called *fermions*) that obey the Pauli exclusion principle; no two quantum-mechanical particles of half-integral spin can occupy the same quantum state simultaneously. Examples of fermions are electrons, protons, and

neutrons. The Fermi-Dirac distribution, which is a result derived using equilibrium statistical mechanics [12], is the following,

$$f(E)=\frac{1}{\exp\left(\frac{E-E_f}{k_BT}\right)+1}=\frac{1}{\exp\left[\frac{E_f}{k_BT}\left(\frac{E}{E_f}-1\right)\right]+1} \tag{5.34a}$$

where E_f is the Fermi energy, T is the temperature, and k_B is the Botzmann constant. Figure 5.3 shows f(E) as a function of $\frac{E}{E_f}$ for several values of $\frac{E_f}{k_BT}$. For large $\frac{E_f}{k_BT}$ ($T \to 0$) the probability for the occupation of a state with $E < E_f$ is one and zero for $E > E_f$. As $\frac{E_f}{k_BT}$ decreases, the occupation probability for $E > E_f$ increases while the occupation probability decreases for $E < E_f$. For $k_BT \to \infty$ the occupation probability is ½ for all energies. If $E - E_f \gg k_BT$, then f(E) can be approximated by the Maxwell-Boltzmann distribution.

$$f(E)\approx \exp\left[-\frac{E-E_f}{k_BT}\right] \qquad E-E_f \gg k_BT \tag{5.34b}$$

The Fermi-Dirac distribution applies to electrons in a conduction band. A hole in a valence band signifies an empty energy state. Therefore, if the probability that a particular energy state is occupied by an electron is 0.4, the probability that it is empty (occupied by a hole) is 0.6. Thus, the Fermi-Dirac distribution for holes is the following.

$$1-f(E)=\frac{\exp\left[\frac{E-E_f}{k_BT}\right]}{\exp\left[\frac{E-E_f}{k_BT}\right]+1} \tag{5.35a}$$

For holes, the range of energies is $-\infty < E \le E_v$ where E_v is the energy at the top of the valence band and $E_v < E_f$. Thus, for $E_f - E \gg k_BT$, equation (5.35a) is the following.

$$1-f(E)\approx \exp\left[-\frac{E_f-E}{k_BT}\right] \qquad E_f-E \gg k_BT \tag{5.35b}$$

Because only a single fermion can occupy a given quantum state, the Fermi energy depends upon the fermion density. At T = 0, where f(E) = 1 for $E < E_f$ and f(E) = 0, for $E > E_f$, each fermion occupies a single energy state beginning at E = 0 with the last fermion being at the Fermi energy, E_f.

The Fermi-Dirac distribution gives the occupation probability for a particular energy state. In order to calculate the electron or hole density, the number of energy states available must be known; this is called the *density of states*, D(E). Thus, the density of electrons for an infinitesimal energy band dE is

$$dn = f(E)D(E)dE \tag{5.36}$$

The density of states function is derived in Appendix E [equation (E – 23)]. The electron energy in equation (5.36) is measured with respect to the energy at the bottom of the conduction band, E_c. Therefore, E in equation (E – 23) must be replaced by $E - E_c$ to determine D(E) that is used in equation (5.36). For semiconductors, such as PV cells, that operate near room temperature, $E_c - E_f \gg k_B T$ so that f(E) can be approximated by equation (5.34b). Thus,

$$dn = \gamma\sqrt{E - E_c}\,\exp\left[-\frac{E - E_f}{k_B T}\right]dE \tag{5.37}$$

where,

$$\gamma = 4\pi\left(\frac{2m_n^*}{h^2}\right)^{3/2} \tag{5.38}$$

and m_n^* is the electron effective mass. Equation (5.37) must be integrated from E_c to the energy at the top of the conduction band in order to calculate the electron density. However, extending the integration to infinity will introduce only a small error since the exponential term in equation (5.37) is very small for large E. Therefore,

$$n \approx \gamma\int_{E_c}^{\infty}\sqrt{E - E_c}\,\exp\left[-\frac{E - E_f}{k_B T}\right]dE \tag{5.39}$$

Let $x = \dfrac{E - E_c}{k_B T}$. Therefore,

$$n = \frac{1}{2}\gamma\sqrt{\pi\left(k_B T\right)^3}\,\exp\left[-\frac{\left(E_c - E_f\right)}{k_B T}\right]\int_o^\infty \sqrt{x}\,e^{-x}dx \tag{5.40}$$

The integral has the value $\frac{\sqrt{\pi}}{2}$, so that

$$n = N_c \exp\left[-\frac{\left(E_c - E_f\right)}{k_B T}\right] \tag{5.41}$$

where

$$N_c = 2\left(\frac{2\pi m_n^* k_B T}{h^2}\right)^{3/2} \tag{5.42}$$

is called the *effective density of states in the conduction band*. At room temperature $N_c = 2.8 \times 10^{19}\text{cm}^{-3}$ for silicon. In a similar manner, the density of holes, p, in the valence band can be derived (problem 5.2),

$$p = N_V \exp\left[-\frac{\left(E_f - E_V\right)}{k_B T}\right] \tag{5.43}$$

where N_V is called the *effective density of states in the valence band*,

$$N_V = 2\left(\frac{2\pi m_p^* k_B T}{h^2}\right)^{3/2} \tag{5.44}$$

where m_p^* is the effective mass of the holes. At room temperature $N_V = 1.04 \times 10^{19}\text{cm}^{-3}$ for silicon.

Remember, equations (5.41) and (5.43) apply for equilibrium conditions. They will not apply where an applied electric field exists or where incident radiation is present. To maintain charge neutrality in an *intrinsic semiconductor*, $n = p = n_i$, where n_i is the *intrinsic charge carrier density*. An intrinsic semiconductor has no intentionally introduced *dopants* that can add electrons or holes to the conduction and valence bands. By equating equations (5.41) and (5.44) an expression for the *intrinsic Fermi energy*, E_i, is obtained.

$$N_c \exp\left[-\frac{E_c - E_i}{k_B T}\right] = N_V \exp\left[-\frac{E_i - E_V}{k_B T}\right]$$
$$E_i = \frac{E_V + E_c}{2} + \frac{k_B T}{2} \ln\left(\frac{N_V}{N_c}\right) = \frac{E_V + E_c}{2} + \frac{3k_B T}{4} \ln\left(\frac{m_p^*}{m_n^*}\right) \quad (5.45)$$

At room temperature, the last term in equation (5.45) is much smaller than the first term. As a result, the intrinsic Fermi energy lies nearly in the middle of the *bandgap energy*, $E_g = E_c - E_V$.

The *intrinsic carrier density*, n_i, is obtained by taking the product of equations (5.41) and (5.43).

$$\boxed{n_i^2 = np} \quad (5.46)$$

$$n_i^2 = N_c N_V \exp\left[-\frac{E_g}{k_B T}\right]$$
$$n_i = \sqrt{N_c N_V} \exp\left[-\frac{E_g}{2k_B T}\right] \quad (5.47)$$

Equation (5.46) is called the *mass action law*. It applies to both intrinsic and extrinsic semiconductors for equilibrium conditions. An extrinsic semiconductor contains dopants that contribute either electrons to the conduction band or holes to the valence band. A semiconductor that contains a dopant that contributes electrons to the conduction band is called an *n-type semiconductor* and the dopant is called a *donor*. A semiconductor that contains a dopant that contributes holes to the valence band is called a *p-type semiconductor*. Since the dopant accepts an electron, thus creating a hole in the valence band, it is called an *acceptor*.

For an n-type semiconductor, the donor dopant can be easily ionized at room temperature. Therefore, the electron density that it contributes to the conduction band is just equal to the donor density, N_D. Similarly, for a p-type semiconductor, the hole density that the acceptor dopant contributes is equal to the acceptor density, N_A. It is possible to dope a semiconductor with both donors and acceptors. Thus, for equilibrium conditions, charge neutrality requires that the total density of negative charges (electrons + ionized acceptors) equals the total density of positive charges (holes + ionized donors).

$$n + N_A = p + N_D \quad (5.48)$$

For an n-type semiconductor at room temperature, $N_D \gg p$, and $N_A = 0$, so that

$$n = p + N_D \approx N_D \qquad \text{n-type} \tag{5.49}$$

and for a p-type semiconductor at room temperature, $N_A \gg n$, and $N_D = 0$, so that

$$p = n + N_A \approx N_A \qquad \text{p-type} \tag{5.50}$$

As equations (5.41) and (5.43) indicate, n and p densities increase exponentially as the temperature increases. Therefore, for high temperature $n \gg N_D$ and $p \gg N_A$. Therefore, n = p and a doped semiconductor behaves like an intrinsic semiconductor at high temperature.

Combining equations (5.41) and (5.49) leads to an expression for E_c - E_f in terms of N_D, N_c, and T for an n-type semiconductor when the donor is fully ionized.

$$E_c - E_f = k_B T \ln\left(\frac{N_c}{N_D}\right) \tag{5.51}$$

Similarly, combining equations (5.43) and (5.50) leads to an expression for $E_f - E_V$ for a p-type semiconductor when the acceptor is fully ionized.

$$E_f - E_V = k_B T \ln\left(\frac{N_V}{N_A}\right) \tag{5.52}$$

Thus, as equation (5.51) shows, the Fermi energy, E_f, will move closer to the energy at the bottom of the conduction band, E_c, as the donor density, N_D, increases for an n-type semiconductor. Also, as equation (5.52) shows, the Fermi energy moves closer to the energy at the top of the valence band, E_V, as the acceptor density, N_A, increases for a p-type semiconductor.

Figure 5.4 reviews the conditions that exist at room temperature for the three types of semiconductors: intrinsic (Figure 5.4a), n-type (Figure 5.4b), and p-type (Figure 5.4c). The first part is a schematic energy band diagram. The second part is the density of states, D(E), for electrons in the conduction band and holes in valence band. Similarly, the third part is the Fermi-Dirac distribution, F(E), for electrons and holes. The last part is the product D(E)F(E), the electron and hole density as a function of energy.

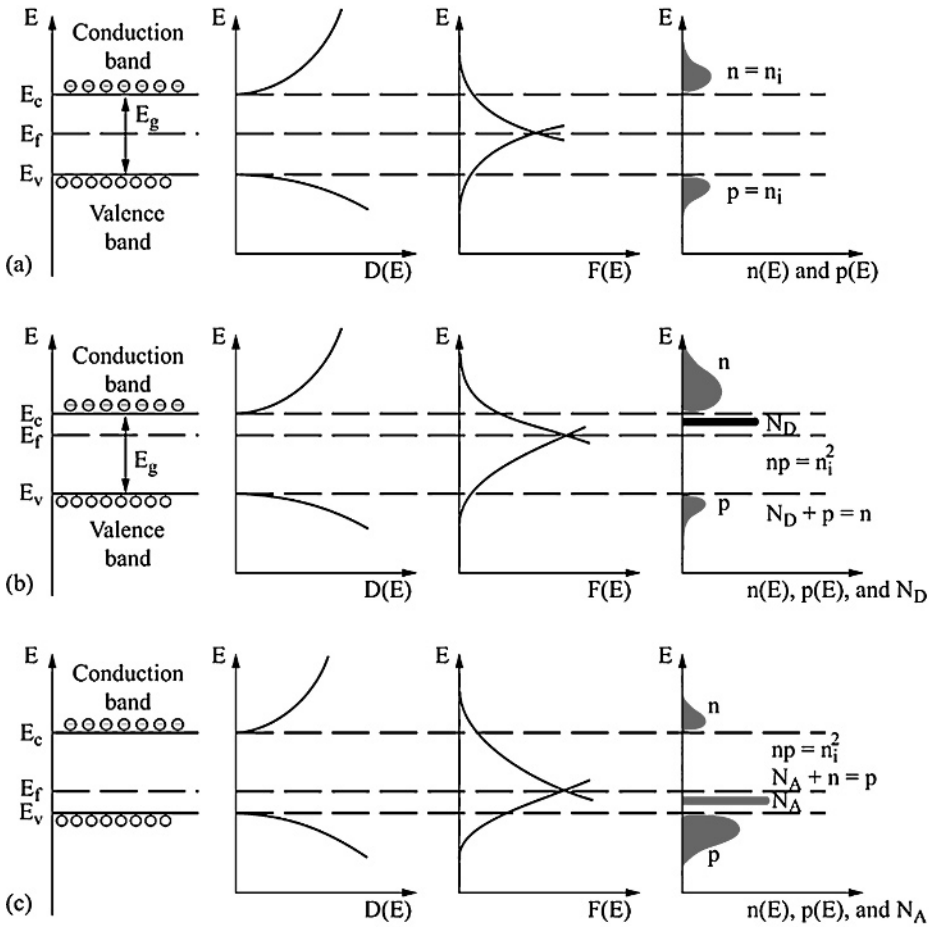

Figure 5.4.—Schematic band diagram, density of states, Fermi-Dirac distribution and charge carrier densities for the three types of semiconductors at room temperature. (a) Intrinsic semiconductor. (b) n-type semiconductor. (c) p-type semiconductor.

For each type semiconductor at room temperature, the electrons all have energies close to the conduction band energy, E_c. In a similar manner, the holes all have energies close to the valence band energy, E_V. Also, charge neutrality requires $n = p$ for an intrinsic semiconductor, $n = p + N_D$ for an n-type semiconductor, and $p = n + N_A$ for a p-type semiconductor. In addition, the mass action law requires $np = n_i^2$ for all semiconductors.

5.4 Transport Equations

In the previous section, the electron and hole densities and the mass action law are derived using the Fermi-Dirac distribution function that applies for equilibrium conditions. However, to determine the performance of a PV cell, the non-equilibrium situation that occurs when incident photons create electrons and holes must be considered. Creation of the electrons and holes results in a non-equilibrium current flow. Transport equations give the dependence of the current on the electric field and density gradients of electrons and holes.

Derivation of the transport equations for the electrons and holes begins with the Boltzmann Equation [12]. The Boltzmann Equation determines the non-equilibrium distribution function that replaces the Fermi-Dirac equilibrium distribution function. A procedure known as the method of moments [12], applied to the Boltzmann Equation, yields the transport equations. Two important approximations are made when using the Boltzmann Equation: first, it assumes that both position and momentum can be specified simultaneously; this is a violation of the Heisenberg Uncertainty Principle. Therefore, the Boltzmann Equation is not valid when quantum mechanical effects are evident. Second, it neglects the effect of external forces, such as an electric field, on collisions that the electrons and holes have with the crystal lattice, impurity atoms, or each other. In other words, it is assumed that negligible acceleration, caused by an external force, occurs during the time of collision.

The first moment of the Boltzmann Equation yields the continuity equation. For electrons it is the following.

$$\boxed{\frac{\partial n}{\partial t} - \frac{1}{e}\nabla \bullet \vec{J}_n = G - Re} \tag{5.53}$$

And for holes, it is the following,

$$\boxed{\frac{\partial p}{\partial t} + \frac{1}{e}\nabla \bullet \vec{J}_p = G - Re} \tag{5.54}$$

where the electron and hole *current densities* and total current density are defined as follows,

$$\vec{J}_n = -en\vec{v}_n \tag{5.55a}$$

$$\vec{J}_p = ep\vec{v}_p \tag{5.55b}$$

$$\vec{J} = \vec{J}_n + \vec{J}_p \tag{5.55c}$$

where e is the magnitude of the electron charge, and $\vec{v}_n$ and $\vec{v}_p$ are the average velocities of the electrons and holes. The G term is the generation rate of electrons and holes. In a PV cell electrons and holes are generated in pairs by the incident photons and by thermal excitation. The Re term is the recombination rate for electrons and holes. Generation and recombination rates will be discussed in the next section.

Taking the second moment of the Boltzmann equation yields the so-called *drift-diffusion equations* for electrons and holes.

$$\boxed{\tau_n \frac{\partial \vec{J}_n}{\partial t} + \vec{J}_n = e\mu_n n\vec{\varepsilon} + eD_n \nabla n} \tag{5.56}$$

$$\boxed{\tau_p \frac{\partial \vec{J}_p}{\partial t} + \vec{J}_p = e\mu_p p\vec{\varepsilon} - eD_p \nabla p} \tag{5.57}$$

Where τ_n and τ_p are *average collision times* for electrons and holes, μ_n and μ_p are electron and hole *mobilities*, D_n and D_p are electron and hole *diffusion coefficients*, and $\vec{\varepsilon}$ is the electric field.

$$\mu_n = \frac{e\tau_n}{m_n^*} \tag{5.58a}$$

$$\mu_p = \frac{e\tau_p}{m_p^*} \tag{5.58b}$$

$$D_n = \mu_n \frac{k_B T}{e} \tag{5.58c}$$

$$D_p = \mu_p \frac{k_B T}{e} \tag{5.58d}$$

The $\tau \frac{\partial \vec{J}}{\partial t}$ terms in equations (5.56) and (5.57) can usually be neglected since the average collision times are very small (10^{-14} – 10^{-13} sec). The current terms proportional to the electric field, $\vec{\varepsilon}$ are called the *drift currents* and the current terms proportional to ∇n and ∇p are called *diffusion currents*.

The four equations (5.53), (5.54), (5.56), and (5.57) contain five unknown quantities, n, p, $\vec{J}_n$, $\vec{J}_p$, and $\vec{\varepsilon}$, that are functions of the semiconductor mobilities and diffusion coefficients. Coulomb's Law [equation (1.3)] completes the system of equations for the five unknowns,

$$\nabla \bullet \vec{\varepsilon} = \frac{e\left(p + N_A - n - N_D\right)}{\varepsilon_s} \tag{5.59}$$

where ε_s is the electric permittivity of the semiconductor.

The key parameter in the drift-diffusion equations is the mobility, which is proportional to the average collision time. The average collision time is determined by the scattering mechanisms for electrons and holes. For intrinsic or lightly doped semiconductors, the most probable scattering mechanism results from thermal vibrations (acoustic phonons) of the crystal lattice. Since the lattice vibrations (phonon density) and electron and hole thermal speed increase with temperature, the collision frequency, ν, which is the inverse of the collision time, τ, also increases with temperature. For phonon collisions [13]

$$\frac{1}{\tau_{phonon}} = \nu_{phonon} \sim \left(m^* k_B T\right)^{3/2} \qquad \text{phonon collisions} \tag{5.60a}$$

For doped semiconductors, scattering of electrons and holes by the ionized dopants becomes significant. In this case, the Coulomb force, which is inversely proportional to the square of the distance between the collision pairs, determines the collision frequency. This is the same scattering mechanism that determines the collision frequency in a fully ionized plasma. In this case, the collision frequency is directly proportional to the dopant density, N. The electron and hole thermal speed increase with temperature implies an increase in collision frequency. However, the $\frac{1}{r^2}$ dependence of the Coulomb force results in the collision frequency decreasing with increasing temperature [13].

$$\frac{1}{\tau_{dopant}} = \nu_{dopant} \sim N m^{*-1/2} \left(k_B T\right)^{-3/2} \qquad \text{dopant collisions} \tag{5.60b}$$

Notice that the phonon collision frequency increases with temperature whereas the dopant collision frequency decreases with temperature. Also, the phonon collision

frequency increases with increasing effective mass, whereas the dopant collision frequency decreases with increasing effective mass.

Other scattering mechanisms such as optical phonon scattering [13] can also be significant. The total average collision frequency, ν, is the sum of the individual collision frequencies.

$$\frac{1}{\tau} = \nu = \sum_i \nu_i = \sum_i \frac{1}{\tau_i} \tag{5.61}$$

Thus, the mobilities defined by equations (5.58a) and (5.58b) are the following.

$$\mu_n = \frac{e}{m_n^*} \frac{1}{\sum_i \nu_{ni}} \tag{5.62a}$$

$$\mu_p = \frac{e}{m_p^*} \frac{1}{\sum_i \nu_{pi}} \tag{5.62b}$$

Electron mobilities are greater than hole mobilities since the effective mass for electrons is smaller than hole effective mass. At room temperature electron mobilities are the order of $\left(10^3 \frac{cm^2}{V-sec}\right)$ and hole mobilities are the order of $\left(10^2 \frac{cm^2}{V-sec}\right)$.

5.5 Generation and Recombination of Electrons and Holes

5.5.1 Generation of Electrons and Holes

Generation of electrons and holes by the absorption of photons is the essential step in producing a photovoltaic current. A photon with energy $h\nu > E_g$, where E_g is the bandgap energy, can excite an electron from the valence band into the conduction band. As a result, a hole is left in the valence band. The resulting electron-hole pair results in electron and hole currents. At the same time that electrons and holes are being generated, they are also recombining. Obviously, it is desirable to have a small recombination rate.

The intensity, i, of radiation in a material where emission and scattering can be neglected is given by equation (1.144). Since each photon has energy $h\nu = \frac{hc_o}{\lambda}$, the photon flux, ϕ_{ph} is the following,

$$\phi_{ph}(\lambda,s)=\frac{i(\nu,s)}{h\nu}=\frac{\lambda i(\lambda,0)}{hc_o}e^{-a(\lambda)s} \tag{5.63}$$

where $\phi_{ph}(\lambda,s)$ has the dimensions, $\frac{\text{photons}}{\text{sec}\cdot\text{area}\cdot\text{wavelength}\cdot\text{steradian}}$, $a(\lambda)$ is the absorption coefficient and, s, is the distance in the direction of the radiation. The intensity that enters the material, $i(\lambda,0)$, is the product of incident intensity, $i_i(\lambda)$, and $(1 - R_c)$ where R_c is the reflectivity. Therefore, assuming each photon with energy, $h\nu > E_g$ produces an electron-hole pair, the rate of decrease, $-\frac{d\phi_{ph}}{ds}$, is the generation rate of electron-hole pairs per sec per volume per steradian at wavelength, λ. Thus at wavelength λ, the generation rate of electron-hole pairs is the following,

$$G(s,\lambda)=\int_{\omega}(1-R_c)\frac{\lambda i_i(\lambda)}{hc_o}a(\lambda)e^{-as}d\omega \qquad \lambda\le\frac{hc_o}{E_g} \tag{5.64}$$

where ω is the solid angle. Remember, the intensity depends upon the direction, s. For a PV cell illuminated by the sun the direction is perpendicular to the surface of the PV cell. However, in a TPV application, where the emitter is very close to the PV cell, the incident radiation arrives at all incident angles from 0 to $\frac{\pi}{2}$.

Assume that the intensity varies only in the x direction (the direction perpendicular to the PV cell surface) and that the intensity is isotropic (independent of angle). Therefore, $x = s\cos\theta$ and $d\omega = \sin\theta d\theta d\psi$ so that the generation rate at x is the following.

$$G(x,\lambda)=\frac{\lambda i_i(\lambda)}{hc_o}a(\lambda)\int_{\psi=o}^{2\pi}\int_{\theta}(1-R_c)e^{-\frac{ax}{\cos\theta}}\sin\theta d\theta d\psi \qquad \lambda\le\frac{hc_o}{E_g} \tag{5.65}$$

The reflectivity, R_c, depends upon θ and the indices of refraction. To produce the largest possible generation rate, R_c must be a minimum. A minimum value for R_c is obtained by applying an anti-reflecting film to the PV cell surface. This can be a single film with an index of refraction, n_1, that is less than the index of refraction of the PV material, n_c. As discussed in Section 4.3.5, the reflectivity is zero if $n_1=\sqrt{n_o n_c}$ for a series of wavelengths $\lambda=\frac{4n_1 d\cos\theta_1}{m}$. Where m is an odd integer, d is the film

thickness, $\cos\theta_1 = \sqrt{1-\left(\frac{n_o}{n_1}\right)^2 \sin^2\theta_o}$, $n_o = 1$ (vacuum) and θ_o is the angle of incidence at the vacuum-film interface.

In order to simplify the integration in equation (5.65), assume R_c is independent of θ. However, the upper integration limit, θ_M, on the θ integral is determined by Snell's Law, $n_o \sin\frac{\pi}{2} = n_c \sin\theta_M$. This applies for both the anti-reflecting film case or when no anti-reflecting film is used. Defining a new variable $u = \cos\theta$, equation (5.65) becomes the following,

$$G(x,\lambda) = 2a(\lambda)(1-R_c)\frac{\pi i_i(\lambda)\lambda}{hc_o}\int_{u_M}^{1} e^{-\frac{ax}{u}}du$$

$$= 2a(\lambda)(1-R_c)\frac{q_i(\lambda)\lambda}{hc_o}\left[E_2(ax) - u_M E_2\left(\frac{ax}{u_M}\right)\right] \qquad (5.66a)$$

$$R_c \text{ independent of } \theta,\ i_i(\lambda) \text{ isotropic},\ \lambda \le \frac{hc_o}{E_g}$$

where $u_M = \cos\theta_M = \sqrt{1-\left(\frac{n_o}{n_c}\right)^2}$, $E_2(x)$ is the second order exponential integral (Appendix A), and $q_i(\lambda) = \pi i_i(\lambda)$ is the incident radiation power per unit area per unit wavelength when $i_i(\lambda)$ is isotropic [equation (1.114)].

If all the incident radiation is at zero angle of incidence, as in the case of a solar PV cell, then the generation rate is the following,

$$G(x,\lambda) = a(\lambda)(1-R_\perp)\frac{q_i(\lambda)\lambda}{hc_o}e^{-ax} \qquad \theta_o = 0, \lambda \le \frac{hc_o}{E_g} \qquad (5.66b)$$

where $R_\perp$ is the reflectivity for normal incidence.

The absorption coefficient, $a(\lambda)$, increases rapidly from nearly zero for $\frac{hc_o}{\lambda} = h\nu \le E_g$ to values in the range of $10^4 - 10^6$ cm^{-1} for $h\nu > E_g$. Such large values for $a(\lambda)$ mean that the PV cell thickness, x, will be small [$E_2(1) = 0.15$] in order to absorb all of the incident light when $h\nu \ge E_g$.

How large the absorption coefficient is depends upon the type of semiconductor. The largest values for $a(\lambda)$ occur for so-called *direct bandgap* semiconductors. In a

direct bandgap semiconductor, the minimum of the electron energy, E_c, in the conduction band occurs at the same value of the crystalline momentum, $k_c(E_c) = k_V(E_V)$ as the maximum of the hole energy, E_V, in the valence band. As a result, during the formation of an electron-hole pair by absorption of a photon of energy $h\nu = E_g = E_c - E_V$, both energy and momentum are conserved. For a so-called *indirect bandgap* semiconductor, E_c and E_V occur at different values of crystalline momentum, k. As as result, during the formation of an electron-hole pair by absorption of a photon of energy $h\nu = E_g = E_c - E_V$, energy and momentum will be conserved only by absorbing or emitting a phonon. Thus, conservation of energy requires $h\nu = E_g \pm E_p$, where $+E_p$ is the energy of an emitted phonon and $-E_p$ is the energy of an absorbed phonon. Similarly, conservation of momentum requires $k_c - k_V = k_p$ where k_p is the phonon momentum. Absorption coefficients for indirect bandgap semiconductors for $h\nu \approx E_g$ are on the order of a factor of 10 less than for direct bandgap semiconductors. Thus, indirect bandgap PV cells will be nearly a factor of 10 thicker than direct bandgap cells. Silicon and germanium are the most common indirect bandgap semiconductors. Gallium arsenide (GaAs), indium phosphide (InP) and the low bandgap energy TPV cell semiconductors InGaAs, GaSb, InGaAsSb, and InAsSbP are all direct bandgap semiconductors.

A theoretical calculation [14] of the absorption coefficient for a direct bandgap semiconductor yields the following result,

$$a(\lambda) = a_o\left(E - E_g\right)^{1/2} = a_o\sqrt{hc_o}\left(\frac{1}{\lambda} - \frac{1}{\lambda_g}\right)^{1/2} \qquad E_g \le E < \infty, 0 \le \lambda \le \lambda_g \qquad (5.67)$$

where a_o is a constant, E is the photon energy, and E_g is the bandgap energy. In reference [5], a_o is given as $2\times10^4 \dfrac{1}{\mathrm{cm}(\mathrm{eV})^{1/2}}$. The absorption coefficient given by equation (5.67) applies when a photon with $E > E_g$ excites an electron directly from the valence band into the conduction band resulting in the production of an electron-hole pair. In addition, photons with energy, $E < E_g$ can also be absorbed by exciting electrons or holes to higher energy levels within the conduction and valence bands. This so-called *free carrier absorption* can become significant for large free carrier concentrations.

5.5.2 Recombination of Electrons and Holes

At equilibrium, the generation rate, G, and the recombination rate, Re, are equal and the mass action law $pn = n_i^2$ is maintained. However, if electron-hole pairs are

being generated by incident radiation, the equilibrium condition no longer exists and $G \neq Re$.

The most probable recombination process in a direct bandgap semiconductor occurs between an electron at or near the bottom of the conduction band and a hole at or near the top of the valence band. Since both the electron and hole have the same momentum, k, a large probability for recombination will occur. In this case, the recombination rate, Re, is proportional to the electron and hole densities,

$$Re = \beta np \qquad \frac{1}{cm^3\,sec} \tag{5.68a}$$

where β is a proportionality constant with the units $\frac{cm^3}{sec}$. When charge carriers (electrons and holes) are *injected* by incident radiation, their densities increase from the equilibrium values n_o and p_o by the amounts $\Delta n = n - n_o$ and $\Delta p = p - p_o$. Therefore,

$$Re = \beta\left(n_o + \Delta n\right)\left(p_o + \Delta p\right) \tag{5.68b}$$

To maintain charge neutrality $\Delta n = \Delta p \equiv \delta$. As a result,

$$Re = \beta\left[n_o p_o + \delta\left(n_o + p_o\right) + \delta^2\right] \tag{5.69}$$

At equilibrium, the generation rate, G_{th}, and recombination rate, Re_{th}, are equal.

$$G_{th} = Re_{th} = \beta n_o p_o \tag{5.70}$$

Therefore, equation (5.69) can be written as follows.

$$Re = Re_{th} + \beta\left[\delta\left(n_o + p_o\right) + \delta^2\right] \tag{5.71}$$

Thus, the net recombination rate or the recombination rate resulting from the departure from equilibrium is the following.

$$Re_{net} = Re - Re_{th} = \beta\left[\delta\left(n_o + p_o\right) + \delta^2\right] \tag{5.72}$$

For low-level injection $\delta \ll \left(n_o + p_o\right)$ and

$$Re_{net} = \beta\delta\left(n_o + p_o\right) \tag{5.73}$$

For an n-type semiconductor, $n_o \gg p_o$, and using $\delta = p_n - p_{no} = n_o - n_{no}$

$$Re_{net} = \frac{p_n - p_{no}}{\tau'_p} = \frac{n_n - n_{no}}{\tau'_p} \qquad \text{n-type} \tag{5.74}$$

where

$$\tau'_p = \frac{1}{\beta n_{no}} \tag{5.75}$$

is called the *lifetime* of the excess minority carriers, in this case the holes. Similarly for a p-type semiconductor, $p_o \gg n_o$ and

$$Re_{net} = \frac{n_p - n_{po}}{\tau'_n} = \frac{p_p - p_{po}}{\tau'_n} \qquad \text{p-type} \tag{5.76}$$

where

$$\tau'_n = \frac{1}{\beta p_{po}} \tag{5.77}$$

is the lifetime of the minority carrier electrons. Thus, the recombination rate depends upon the lifetime of the minority carriers; these lifetimes are inversely proportional to the majority carrier density.

The recombination rates given by equations (5.74) and (5.76) apply to direct bandgap semiconductors. Since an electron at or near the bottom of the conduction band and a hole at or near the top of the valence band have different crystalline momentum for indirect bandgap semiconductors, a direct recombination is not possible. As a result, the dominant recombination process is an indirect transition via localized energy states in the forbidden energy band. These energy states result from impurities and lattice defects. For indirect recombination at low-level carrier injection, the recombination rate [13] is similar to equations (5.74) and (5.76),

$$Re_{net} = \frac{p_n - p_{no}}{\tau'_p} \qquad \text{n-type} \tag{5.78}$$

where τ_p' is the minority carrier (hole) lifetime. For p-type

$$Re_{net} = \frac{n_p - n_{po}}{\tau_n'} \qquad \text{p-type} \qquad (5.79)$$

where τ_n' is the minority carrier (electron) lifetime. In the case of indirect recombination, the lifetime is inversely proportional to the density of impurities and lattice defects that make up so-called *recombination centers.*

The recombination mechanisms described occur in the bulk of the semiconductor. However, significant recombination, known as *surface recombination*, also occurs at surfaces of a semiconductor. Surface recombination occurs because the abrupt discontinuity in the crystal lattice at the surface creates a large number of localized energy states or recombination centers. For low carrier injection, the rate per unit area and unit time that carriers recombine on the surface, is the following [13],

$$Re_s = S_p\left(p_s - p_{no}\right) \qquad \text{n-type} \qquad (5.80)$$

$$Re_s = S_n\left(n_s - n_{po}\right) \qquad \text{p-type} \qquad (5.81)$$

where S_p for minority carrier holes, and S_n for minority carrier electrons, have velocity units and are called *surface recombination velocities*. The subscript s denotes conditions at the surface. Surface recombination velocities are directly proportional to the number of recombination centers per unit area on the surface. Notice that the surface recombination rates are per unit of surface area while the bulk recombination rates are per unit volume.

Surface recombination is a boundary condition upon the minority carrier diffusion current. At a surface in a p-type semiconductor $\left|D_n \hat{t} \bullet \nabla n_p\right| = S_n\left(n_p - n_{po}\right)$ where $\hat{t}$ is a unit vector normal to the surface. Similarly, for an n-type semiconductor at a surface $\left|D_p \hat{t} \bullet \nabla p_n\right| = S_p\left(p_n - p_{no}\right)$. Recombination velocities range from $10^2 \frac{cm}{sec}$ to $10^6 \frac{cm}{sec}$.

All the recombination rates discussed are obtained using the low minority carrier injection approximation (injected minority carrier density much less than the equilibrium majority carrier density). However, in a TPV application at high emitter temperature the photon flux may be large enough that the injected minority carrier density is no longer small compared to the equilibrium majority carrier density.

5.6 p-n Junction

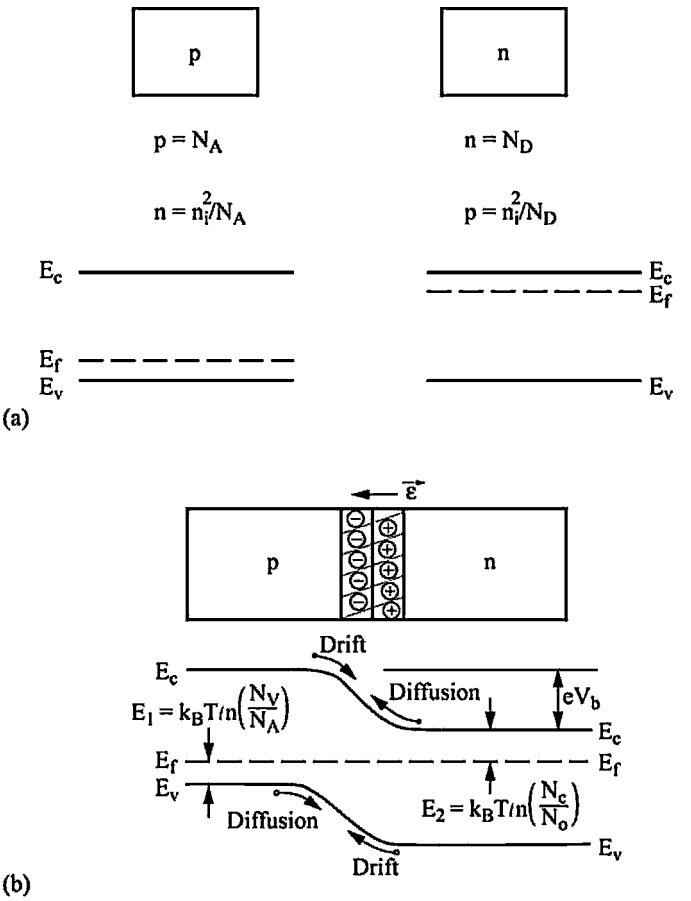

Figure 5.5.—Formation of a p-n junction. (a) Isolated uniformly doped p and n semiconductors and associated energy band diagrams. (b) p-n junction at equilibrium and associated energy band diagram.

To this point, the discussion has been concerned with the general properties of semiconductors. However, the primary subject of this chapter is a semiconductor device, namely the photovoltaic cell. The basis for most semiconductor devices is the *p-n junction*, which forms between p and n-type semiconductors. A p-n junction can be formed in a p-type semiconductor by diffusing an n-type donor dopant into the p semiconductor. Similarly, a p-n junction can be formed in an n-type semiconductor by diffusing a p-type acceptor into the n semiconductor.

Figure 5.5 illustrates what happens when a junction is formed between p and n-type semiconductors. When the semiconductors are isolated, as in Figure 5.5a, the Fermi level, E_f, of the uniformly doped p-type semiconductor lies near the top of the valence band energy, E_V. Similarly, the Fermi level of the uniformly doped n-type material lies close to the bottom of the conduction band, E_c. When the two materials are joined the large carrier density gradients (∇n and ∇p) cause carrier diffusion. Holes from the p-type material diffuse into the n-type material leaving behind negative acceptor ions, N_A, near the junction. At the same time, electrons diffuse from the n-type material into the p-type material leaving behind positive donor ions, N_D, near the junction. Thus, an electric field is produced in the direction of the p-type material as shown in Figure 5.5b. As a result of the junction formation, the energy band diagram is as shown in Figure 5.5b. The Fermi energy, E_f, remains constant throughout the junction for steady state, equilibrium conditions as can be shown as follows.

At steady state, equilibrium conditions the net current flow for electrons and holes must be zero. Hence, the electrons that diffuse from n to p, are balanced by electrons that drift from p to n. Similarly, holes that diffuse from p to n are balanced by holes that drift n to p. For electrons from equation (5.56),

$$\vec{J}_n = e\mu_n \vec{\varepsilon} + \mu_n k_B T \nabla n = 0 \tag{5.82a}$$

where equation (5.59a) is used for D_n. Hence,

$$-e\vec{\varepsilon} = k_B T \frac{\nabla n}{n} \tag{5.82b}$$

where $-e\vec{\varepsilon}$ is the force acting on the electron. The force is also equal to minus the gradient in the potential energy of the electrons in the conduction band, E_n.

$$-e\vec{\varepsilon} = -\nabla E_n = -\nabla E_c \tag{5.83}$$

Since the force is the same for all electrons in the conduction band $\nabla E_n = \nabla E_c$, where E_c is the energy at the bottom of the conduction band. Now use equation (5.41) to calculate $\frac{\nabla n}{n}$. Substituting that result and equation (5.83) in equation (5.82) produces the following result.

$$\nabla E_f = 0 \tag{5.84}$$

Therefore, E_f is a constant. The same result can be obtained based upon the hole current condition, $\vec{J}_p = 0$ (problem 5.4).

Because of the electric field, $\vec{\varepsilon}$, there is an electric potential difference across the junction. This potential difference, V_b, is called the *built-in potential*. For steady state conditions or no magnetic field, Faraday's Law [equation (1.2)] allows the electric field to be defined as,

$$\vec{\varepsilon} = -\nabla V \tag{5.85}$$

where V is the electric potential. From equations (5.83) and (5.85) the following is obtained.

$$V = -\frac{E}{e} \tag{5.86}$$

Thus, referring to Figure 5.5b the built-in potential, V_b, is the following,

$$eV_b = E_c - E_v - E_1 - E_2 = E_g - E_1 - E_2 \tag{5.87}$$

where E_g is the bandgap energy, $E_1 = E_f - E_V$ and $E_2 = E_c - E_f$. E_1 is given by equation (5.51). Therefore,

$$eV_b = E_g - k_B T \ln\left(\frac{N_V}{N_A}\right) - k_B T \ln\left(\frac{N_c}{N_D}\right) = E_g - k_B T \ln\left(\frac{N_V N_c}{N_A N_D}\right) \tag{5.88}$$

Also, E_g can be expressed in terms of n_i, N_V, N_c, and k_BT by using equation (5.47). Hence, V_B can also be written as follows.

$$V_b = \frac{k_B T}{e} \ln\left(\frac{N_A N_D}{n_i^2}\right) \tag{5.89}$$

As equation (5.88) indicates, p-n junctions in semiconductors with the largest bandgap energies and the highest doping levels have the largest built-in potentials. For Si, V_b ranges from 0.4 to 1 eV, and for GaAs, V_b ranges from 1 to 1.4 eV in going from dopant levels from 10^{14} to 10^{18}cm^{-3}. It is the electric field resulting from the built-in potential that sweeps minority carriers produced by incident radiation across the junction in a PV cell. Minority electrons in the p region are injected into the n region,

and minority holes in the n region are injected into the p region. These minority electron and hole currents make up the total current that is supplied to the load.

The region around the junction is called the *space charge region* or *depletion region*. It this region that fixed positively charged donor and negatively charged acceptor ions produce the space charge electric field. Nearly all mobile charge carrier electrons and holes are depleted from this region.

5.7 Current-Voltage Relation for an Ideal Junction in the Dark

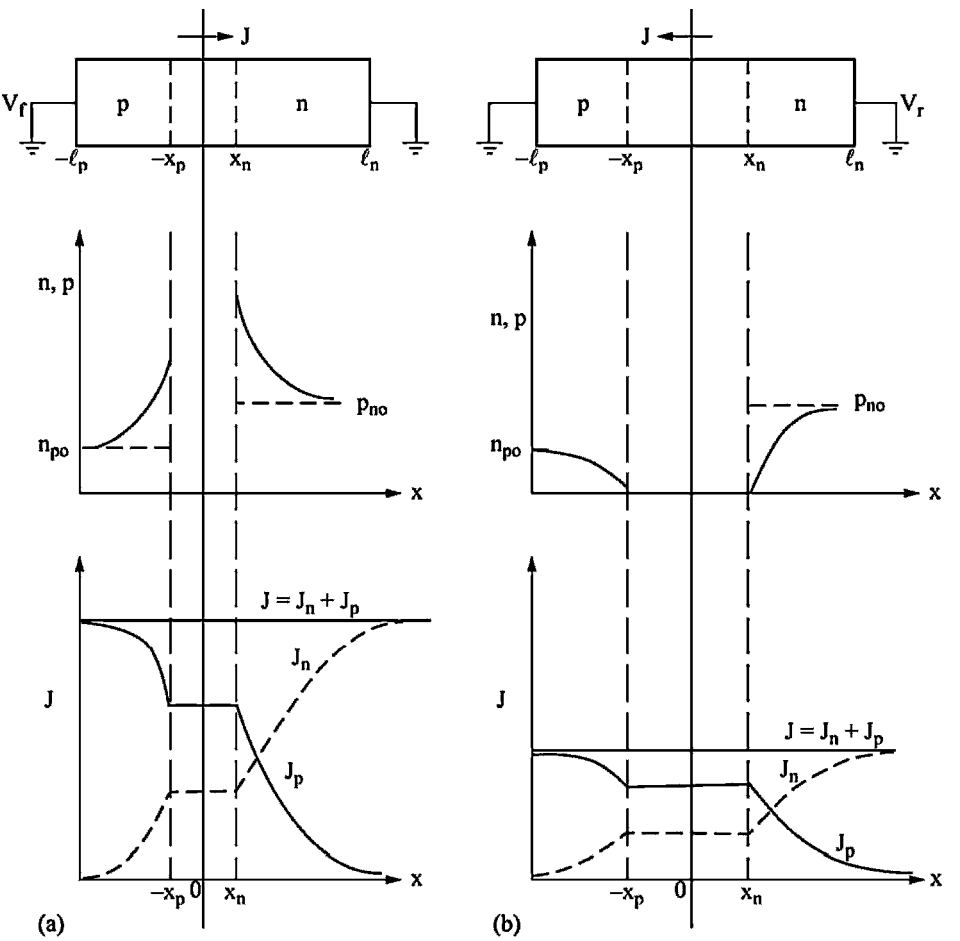

Figure 5.6.—p-n junction charge carrier distribution and current distribution under forward and reverse bias. (a) Forward bias. (b) Reverse bias.

Consider how a p-n junction, as shown in Figure 5.6, behaves if an electric potential is applied. If a potential V_f is applied to the p side of the junction, as shown in Figure 5.6a, it is called *forward bias*. If a potential V_r is applied to the n side of the junction, as shown in Figure 5.6b, it is called *reverse bias*. For the forward bias condition, the net potential across the junction will be $V_b - V_f$. The applied V_f reduces the built-in electric field, which reduces the drift currents of electrons and holes. Thus, the balance between diffusion current and drift current existing at equilibrium is disturbed. As a result, holes from the p side diffuse into the n side and electrons diffuse from the n side into the p side. Thus, minority *carrier injection* occurs. Minority electrons are injected into the p side, and minority holes are injected into the n side. This results in a current flow from the p side to the n side. Under reverse bias, V_r, the potential across the junction increases to $V_r + V_b$ from V_b under equilibrium conditions. The resulting increased electric field increases the electron and hole drift currents moving from the n side to the p side so that they exceed the electron and hole diffusion currents moving in the opposite direction. As a result, reverse bias produces a small reverse current moving from the n to the p side.

5.7.1 Assumptions for Ideal p-n Junction

Making use of several assumptions for a p-n junction, the transport equations yield the ideal current-voltage or Shockley equation. The ideal p-n junction assumptions are the following:

1) One-dimensional, steady state transport equations apply with no carrier generation (G = 0) and constant mobilities and lifetimes.
2) Depletion region has abrupt boundaries and no electric field and equilibrium conditions exist outside these boundaries.
3) Within the depletion region, the diffusion and drift currents for both electrons and holes are approximately equal.
4) There are low injected minority densities p_n and n_p compared to majority carrier densities, $n_{no} \approx N_D$ and $p_{po} \approx N_A$, which remain unchanged at the depletion region boundaries.
5) No generation or recombination in depletion region so that electron current density, J_n, and hole current density, J_p, remain constant through the depletion region.

Consider the consequences of assumptions 1) and 3). If the electron diffusion current is balanced by the electron drift current, then equation (5.82b) applies. Using equation (5.85) in equation (5.82b) produces the following result for the one-dimensional case.

$$e\frac{dV}{dx} = \frac{k_{BT}}{n}\frac{dn}{dx} = k_B T\frac{d\ln n}{dx} \tag{5.90}$$

Hence,

$$\int_{o}^{V_b - V_a} dV = V_b - V_a = k_B T \int_{n(-x_p)}^{n(x_n)} \ln n = \frac{k_B T}{e} \ln\left[\frac{n(x_n)}{n(-x_p)}\right]$$

where V_b, is the built-in potential and V_a is the applied potential across the junction. Also, as shown in Figure 5.6, $x = x_p$ and $x = x_n$ are the boundaries of the depletions region. Therefore,

$$\frac{n(x_n)}{n(-x_p)} = e^{\frac{eV_b}{k_B T}} e^{-\frac{eV_a}{k_B T}} \tag{5.91}$$

At $x = x_n$, $n(x_n) = N_D + p_n(x_n)$. However, from approximation 4), $p_n(x_n) \ll N_D$, so that $n(x_n) = n_{no} \approx N_D$. Also, from equation (5.89)

$$\frac{N_A N_D}{n_i^2} = e^{\frac{eV_b}{k_B T}} \tag{5.92}$$

Substitute equation (5.92) in equation (5.91), using the conditions $n(x_n) = N_D$ and the law of mass action for the equilibrium region far from the junction, $n_i^2 = p_{po} n_{po} \approx N_A n_{po}$ yields the following.

$$\boxed{n(-x_p) \equiv n_p(-x_p) = n_{po} e^{\frac{eV_a}{k_B T}}} \tag{5.93}$$

Note that the subscript p denotes the region in the p-type material and that the subscript po denotes the region in the p-type material far from the junction where equilibrium exists. Similarly, the subscripts n and no refer to n-type material.

Starting with $\vec{J}_p = 0$ and in a manner similar to that used to obtain equation (5.93), the following result for the injected hole density at the junction boundary in the n-type semiconductor is obtained (problem 5.5).

$$\boxed{p(x_n) \equiv p_n(x_n) = p_{no} e^{\frac{eV_a}{k_B T}}} \tag{5.94}$$

Equations (5.93) and (5.94) are sometimes referred to as the *law of the junction*. They show that the injected minority carrier densities at the junction boundaries are exponentially dependent upon the applied potential, V_a. As a result, since $eV_a > k_BT$ for room temperature conditions, $p_n(x_n)$ and $n_p(-x_p)$ are much greater than their equilibrium values, p_{no}, and n_{po}.

5.7.2 Current-Voltage Relation for Infinite Neutral Regions

The law of the junction equations is the boundary conditions on the minority carrier densities at the p-n junction boundaries. They are used in the solution of the transport equations. Substituting the electron and hole drift-diffusion equations [equations (5.56) and (5.57)] into their respective continuity equations [equations (5.53) and (5.54)] under assumption 1) yields the following.

$$D_n \frac{d^2n}{dx^2} + \mu_n \varepsilon \frac{dn}{dx} + \mu_n n \frac{d\varepsilon}{dx} = Re \tag{5.95}$$

$$D_p \frac{d^2p}{dx^2} - \mu_p \varepsilon \frac{dp}{dx} - \mu_p p \frac{d\varepsilon}{dx} = Re \tag{5.96}$$

If equation (5.95) is multiplied by $p\mu_p$, and equation (5.96) is multiplied by $n\mu_n$, and the resulting equations are added using the result $\mu = \frac{e}{k_BT} D$, then the following results.

$$\frac{D_n D_p}{pD_p + nD_n}\left[p\frac{d^2n}{dx^2} + n\frac{d^2p}{dx^2} + \frac{e\varepsilon}{k_BT}\left(p\frac{dn}{dx} - n\frac{dp}{dx} \right) \right] = Re \tag{5.97}$$

Now apply equation (5.97) to the p region of the p-n junction shown in Figure 5.6. From assumption 4) for $x \le -x_p$, $n_p \ll p_p = p_{po} \approx N_A$. Also in the region $x \le -x_p$ charge neutrality exists and the electric field vanishes. In addition, the departure from equilibrium for carrier densities, $n_p - n_{po}$ and $p_p - p_{po}$ will be of the same order of magnitude. As a result, $\frac{d^2n_p}{dx^2} \sim \frac{d^2p_p}{dx^2}$. With these approximations, the transport equation in the p neutral region reduces to the transport equation for the minority electrons,

$$D_n \frac{d^2n_p}{dx^2} = Re = \frac{n_p - n_{po}}{\tau_n'} \qquad x \le -x_p \tag{5.98}$$

where equation (5.79) has been used for the recombination rate.

Applying equation (5.97) to the neutral region of the n-type semiconductor ($x \geq x_n$) using the same approximations, yields the transport equation for minority holes,

$$D_p \frac{d^2 p_n}{dx^2} = Re = \frac{p_n - p_{no}}{\tau'_p} \qquad x \geq x_n \tag{5.99}$$

where equation (5.78) has been used for the recombination rate.

The solutions to equations (5.98) and (5.99) with appropriate boundary conditions yields the minority carrier density distributions in the neutral regions of the p-n junction. From the minority carrier density distributions, the minority carrier diffusion currents can be calculated at the depletion region boundaries ($x = -x_p$ and $x = x_n$). By assumption 5) the electron and hole currents are constant through the depletion region. Hence, the sum of the minority electron diffusion current at $x = -x_p$ and the minority hole current at $x = x_n$ yields the total current, which is constant throughout the semiconductor.

The boundary conditions at $x = -x_p$ and $x = x_n$ are given by equations (5.93) and (5.94). If the lengths of the p and n neutral regions are large, compared to the width of the depletion region, then the boundary condition at $x \to \infty$ is $p_n = p_{no}$, and $x = -\infty$ is $n_p = n_{po}$. However, for a PV cell the top and bottom surfaces are close to the junction. As a result, surface recombination is important and the minority carrier diffusion into the surfaces is given by the surface recombination rates [equations (5.80) and (5.81)]. In this case at $x = \ell_p$ (surface of p region where $\frac{dn_p}{dx} > 0$)

$$D_n \left.\frac{dn_p}{dx}\right|_{x=-\ell_p} = S_n \left[n_p\left(-\ell_p\right) - n_{po} \right] \tag{5.100}$$

and at $x = \ell_n$ (surface of n region where $\frac{dp_n}{dx} < 0$)

$$-D_p \left.\frac{dp_n}{dx}\right|_{x=\ell_p} = S_p \left[p_n\left(\ell_n\right) - p_{no} \right] \tag{5.101}$$

Let $N_p = p_n - p_{no}$, and $P_n = n_p - n_{po}$. As a result, since n_{po} and p_{no} are constants, equations (5.98) and (5.99) are the following.

$$\frac{d^2N_p}{dx^2} - \frac{N_p}{D_n\tau'_n} = 0 \qquad x \le -x_p \tag{5.102}$$

$$\frac{d^2P_n n}{dx^2} - \frac{P_n}{D_p\tau'_p} = 0 \qquad x \ge x_n \tag{5.103}$$

These are linear, second order, homogenous differential equations with constant coefficients. Solutions are the sum of two exponential terms of the following form [11],

$$N_p = A_p e^{\alpha_1 x} + B_p e^{\alpha_2 x} \qquad x \le -x_p \tag{5.104}$$

$$P_n = A_n e^{\beta_1 x} + B_n e^{\beta_2 x} \qquad x \ge x_n \tag{5.105}$$

where A and B are constants and the α's and β's are roots of the characteristic equations.

$$\alpha^2 - \frac{1}{D_p\tau'_p} = 0 \Rightarrow \alpha = \pm\frac{1}{\sqrt{D_p\tau_p}}$$

$$\beta^2 - \frac{1}{D_n\tau'_n} = 0 \Rightarrow \beta = \pm\frac{1}{\sqrt{D_n\tau_n}}$$

Hence,

$$N_p = A_p e^{\frac{x}{L_n}} + B_p e^{-\frac{x}{L_n}} \qquad x \le -x_p \tag{5.106}$$

$$P_n = A_n e^{\frac{x}{L_n}} + B_n e^{-\frac{x}{L_n}} \qquad x \ge x_n \tag{5.107}$$

where

$$L_p = \sqrt{D_p\tau'_p} = \sqrt{\frac{k_B T}{e}\mu_p\tau'_p} = \sqrt{\frac{k_B T}{m_p^*}\tau_p\tau'_p} \tag{5.108}$$

and

$$L_n = \sqrt{D_n \tau_n'} = \sqrt{\frac{k_B T}{e} \mu_n \tau_n'} = \sqrt{\frac{k_B T}{m_n^*} \tau_n \tau_n'} \tag{5.109}$$

are called the *diffusion lengths*: L_p for the minority holes in the n region and L_n for the minority electrons in the p region.

The constants A and B are determined by using the boundary conditions. First consider the case where the neutral regions are long. Thus, for $x \to -\infty$, $N_p \to 0$ so that B_p must be zero Similarly, for $x \to \infty$, $P_n \to 0$ so that A_n must be zero. Also, at $x = -x_p$, $N_p(-x_p)$ is given by equation (5.93).

$$n_{po}\left(e^{\frac{eV_a}{k_B T}} - 1\right) = A_p e^{-\frac{x_p}{L_n}} \tag{5.110}$$

Similarly at $x = x_n$, $P_n(x_n)$ is given by equation (5.94) and

$$p_{no}\left(e^{\frac{eV_a}{k_B T}} - 1\right) = B_n e^{-\frac{x_n}{L_p}} \tag{5.111}$$

Using equations (5.110) and (5.111) for A_p and B_n in equations (5.106) and (5.107) yields the following results.

$$N_p = n_p - n_{po} = n_{po}\left(e^{\frac{eV_a}{k_B T}} - 1\right) e^{\frac{(x+x_p)}{L_n}} \qquad x \le -x_p \tag{5.112}$$

$$P_n = p_n - p_{no} = p_{no}\left(e^{\frac{eV_a}{k_B T}} - 1\right) e^{\frac{-(x-x_n)}{L_p}} \qquad x \ge x_n \tag{5.113}$$

Using equations (5.112) and (5.113) to calculate the minority diffusion currents at $x = -x_p$ and $x = x_n$ yields the *current-voltage relation* or *Shockley equation* for an ideal p-n junction,

$$\boxed{J = e\left[D_n \left.\frac{dn_p}{dx}\right|_{x=-x_p} + D_p \left.\frac{dp_n}{dx}\right|_{x=x_n}\right] = J_s\left(e^{\frac{eV_a}{k_B T}} - 1\right)} \tag{5.114}$$

where J_s is called the *saturation current density*.

$$J_s = \frac{en_{po}D_n}{L_n} + \frac{ep_{no}D_p}{L_p} = en_{po}\sqrt{\frac{D_n}{\tau_n'}} + ep_{no}\sqrt{\frac{D_p}{\tau_p'}} = en_{po}\bar{v}_n\sqrt{\frac{\tau_n}{\tau_n'}} + ep_{no}\bar{v}_p\sqrt{\frac{\tau_p}{\tau_p'}} \tag{5.115}$$

and $\bar{v} = \sqrt{\frac{k_B T}{m^*}}$ is the thermal speed. For an efficient PV cell, the saturation current must be small. As a result the minority carrier lifetimes, τ', must be large compared to the average collision times, τ.

5.7.3 Current-Voltage Relation for Finite Neutral Regions

Note that the saturation current density in equation (5.115) is independent of the dimensions of the semiconductor. However, if the assumption that the neutral regions are long does not apply, then dimensions will enter the current-voltage relation. In that case the boundary conditions given by equations (5.100) and (5.101) must be applied. Again, the solutions for the minority carrier densities are given by equations (5.106) and (5.107). Applying the boundary condition at $x = -\ell_p$ given by equation (5.100) to equation (5.106) yields the following.

$$\begin{aligned} D_n \left.\frac{dn_p}{dx}\right|_{x=-x_p} &= S_n\left[n_p\left(-\ell_p\right) - n_{po}\right] \\ \frac{D_n}{L_n}\left[A_p e^{-\frac{\ell_p}{L_n}} - B_p e^{\frac{\ell_p}{L_n}}\right] &= S_n\left[A_p e^{-\frac{\ell_p}{L_n}} + B_p e^{\frac{\ell_p}{L_n}}\right] \end{aligned} \tag{5.116}$$

Also, at $x = -x_p$ the boundary condition is given by equation (5.93).

$$\begin{aligned} N_p\left(-x_p\right) = n_p\left(-x_p\right) - n_{po} &= n_{po}\left(e^{\frac{eV_a}{k_B T}} - 1\right) \\ A_p e^{-\frac{x_p}{L_n}} + B_p e^{\frac{x_p}{L_n}} &= n_{po}\left(e^{\frac{eV_a}{k_B T}} - 1\right) \end{aligned} \tag{5.117}$$

Equations (5.116) and (5.117) can be solved for A_p and B_p so that

$$N_p(x) = n_p(x) - n_{po} = n_{po}\left(e^{\frac{eV_a}{k_BT}} - 1\right)\left[\frac{\left(1+\frac{S_nL_n}{D_n}\right)e^{\frac{\ell_p+x}{L_n}} + \left(1-\frac{S_nL_n}{D_n}\right)e^{\frac{-(\ell_p+x)}{L_n}}}{\left(1+\frac{S_nL_n}{D_n}\right)e^{\frac{\ell_p-x_p}{L_n}} + \left(1-\frac{S_nL_n}{D_n}\right)e^{\frac{-(\ell_p+x_p)}{L_n}}}\right] \quad (5.118)$$

$$-\ell_p \le x \le -x_p$$

As a result, the electron diffusion current at $x = x_p$ is the following,

$$J_n(-x_p) = eD_n\left.\frac{dn_p}{dx}\right|_{x=-x_p} = J_{sn}\left[e^{\frac{eV_a}{k_BT}} - 1\right] \quad (5.119)$$

where

$$J_{sn} = \frac{en_{po}D_n}{L_n}\left[\frac{\left(1+\frac{S_nL_n}{D_n}\right)e^{\frac{(\ell_p-x_p)}{L_n}} - \left(1-\frac{S_nL_n}{D_n}\right)e^{\frac{-(\ell_p-x_p)}{L_n}}}{\left(1+\frac{S_nL_n}{D_n}\right)e^{\frac{(\ell_p-x_p)}{L_n}} + \left(1-\frac{S_nL_n}{D_n}\right)e^{\frac{-(\ell_p-x_p)}{L_n}}}\right] \quad (5.120a)$$

$$J_{sn} = \frac{en_{po}D_n}{L_n}\left[\frac{\frac{S_nL_n}{D_n}\cosh\left(\frac{\ell_p-x_p}{L_n}\right) + \sinh\left(\frac{\ell_p-x_p}{L_n}\right)}{\frac{S_nL_n}{D_n}\sinh\left(\frac{\ell_p-x_p}{L_n}\right) + \cosh\left(\frac{\ell_p-x_p}{L_n}\right)}\right] \quad (5.120b)$$

is the electron saturation current density. Solving the hole transport equation [equation (5.103)] in the n region with the boundary conditions given by equations (5.94 and (5.101) yields the following result for the hole diffusion current at $x = x_n$.

$$J_p(x_n) = -eD_p\left.\frac{dp_n}{dx}\right|_{x=x_n} = J_{sp}\left[e^{\frac{eV_a}{k_BT}} - 1\right] \quad (5.121)$$

$$J_{sp} = \frac{ep_{no}D_p}{L_p}\left[\frac{\left(1+\frac{S_pL_p}{D_p}\right)e^{\frac{(\ell_n - x_n)}{L_p}} - \left(1-\frac{S_pL_p}{D_p}\right)e^{\frac{-(\ell_n - x_n)}{L_p}}}{\left(1+\frac{S_pL_p}{D_p}\right)e^{\frac{(\ell_n - x_n)}{L_p}} + \left(1-\frac{S_pL_p}{D_p}\right)e^{\frac{-(\ell_n - x_n)}{L_p}}}\right] \tag{5.122a}$$

$$J_{sp} = \frac{ep_{no}D_p}{L_p}\left[\frac{\frac{S_pL_p}{D_p}\cosh\left(\frac{\ell_n - x_n}{L_p}\right) + \sinh\left(\frac{\ell_n - x_n}{L_p}\right)}{\frac{S_pL_p}{D_p}\sinh\left(\frac{\ell_n - x_n}{L_p}\right) + \cosh\left(\frac{\ell_n - x_n}{L_p}\right)}\right] \tag{5.122b}$$

Thus, the total current density is the following.

$$\boxed{J = \left(J_{sn} + J_{sp}\right)\left[e^{\frac{eV_a}{k_BT}} - 1\right]} \tag{5.123}$$

Comparing equations (5.114) and (5.123), the addition of surface recombination and finite dimensions changes only the saturation current. If the neutral regions are large ($l_p \to \infty$ and $l_n \to \infty$) then the saturation current $J_{sn} + J_{sp}$ reduces to the result given by equation (5.115). The *surface recombination parameter*, ϕ, in equations (5.120) and (5.122) can be written as follows,

$$\phi \equiv \frac{SL}{D} = S\sqrt{\frac{\tau'}{D}} = S\sqrt{\frac{e\tau'}{\mu k_B T}} = S\sqrt{\frac{m^*}{k_B T}\frac{\tau'}{\tau}} = \frac{S}{\bar{v}}\sqrt{\frac{\tau'}{\tau}} \tag{5.124}$$

where $\bar{v} = \sqrt{\frac{k_B T}{m^*}}$ is the thermal speed. Thus, the surface recombination parameter is proportional to $\sqrt{\frac{\tau'}{\tau}}$. If $\frac{en_{po}D_n}{L_n}$ and $\frac{ep_{no}D_p}{L_p}$ are written in terms of $\frac{\tau'}{\tau}$, then dimensionless current densities $\bar{J}_{sn}$ or $\bar{J}_{sp}$ can be defined as follows,

$$\bar{J}_{sn} \equiv \frac{\bar{J}_{sn}}{en_{po}\bar{v}_n} = \sqrt{\frac{\tau_n}{\tau'_n}}\frac{(1+\phi_n)e^{u_p} - (1-\phi_n)e^{-u_p}}{(1+\phi_n)e^{u_p} + (1-\phi_n)e^{-u_p}} \tag{5.125}$$

$$\bar{J}_{sp} \equiv \frac{\bar{J}_{sp}}{ep_{no}\bar{v}_p} = \sqrt{\frac{\tau_p}{\tau'_p}}\,\frac{\left(1+\phi_p\right)e^{u_n} - \left(1-\phi_p\right)e^{-u_n}}{\left(1+\phi_p\right)e^{u_n} + \left(1-\phi_p\right)e^{-u_n}} \tag{5.126}$$

where

$$u_p \equiv \frac{\ell_p - x_p}{L_n} \tag{5.127}$$

and

$$u_n \equiv \frac{\ell_n - x_n}{L_p} \tag{5.128}$$

are the dimensionless widths of the neutral regions in the p and n type semiconductors. For an efficient PV cell, u_p and u_n should be less than one. In that case, minority electrons in the p region generated by incident photon absorption will have a high probability of being injected into the n region by the built-in potential. Similarly, minority holes in the n region have a high probability of being injected into the p region.

In Figure 5.7, $\bar{J}_{sn}$ and $\bar{J}_{sp}$ are plotted as functions of $\frac{\tau'_n}{\tau_n}$ and $\frac{\tau'_p}{\tau_p}$ for $u_n = u_p = 1$ and $\frac{S_n}{\bar{v}_n} = \frac{S_p}{\bar{v}_p} = 0.01,1$. The dimensionless saturation current densities decrease rapidly with increasing $\frac{\tau'}{\tau}$. Also, $\bar{J}_{sn}$ and $\bar{J}_{sp}$ are nearly independent of the speed ratio, $\frac{S}{\bar{v}}$. Thus, an important parameter for controlling the saturation current density is the ratio of minority carrier lifetime to minority carrier average collision time.

For large values of $\frac{\tau'}{\tau}$ $\left(\phi \gg 1\right)$, equations (5.125) and (5.126) become the following.

$$\bar{J}_{sn} = \sqrt{\frac{\tau_n}{\tau'_n}}\coth u_p \to 0 \qquad \text{for } \frac{\tau'_n}{\tau_n} \to \infty \tag{5.129}$$

$$\bar{J}_{sp} = \sqrt{\frac{\tau_p}{\tau'_p}}\coth u_n \to 0 \qquad \text{for } \frac{\tau'_p}{\tau_p} \to \infty \tag{5.130}$$

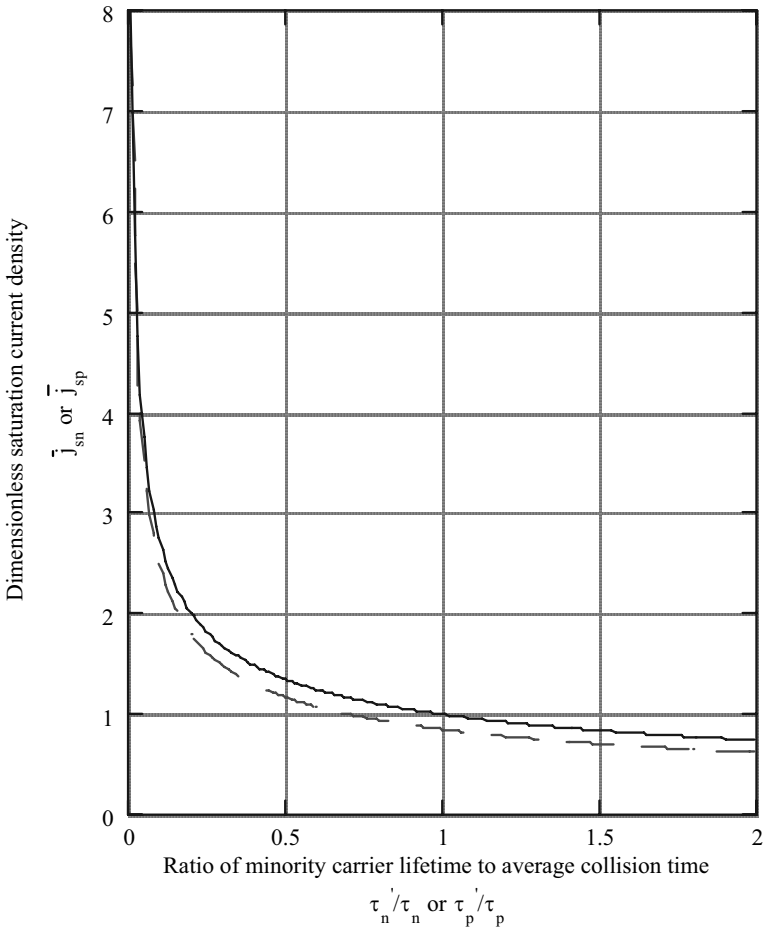

Figure 5.7 Dependence of dimensionless saturation current densities of an ideal p-n junction on the ratio of minority carrier lifetime to minority carrier average collision time for the ratio of neutral region width to diffusion length, $(\ell_p - x_p)/L_n = (\ell_n - x_n)/L_p = 1$, and two ratios of recombination velocity to thermal speed, $S/\overline{v}$. Solid line, $S_n/\overline{v}_n = S_p/\overline{v}_p = .01$ and $S_n/\overline{v}_n = S_p/\overline{v}_p = 1$ for dashed line.□

For small values of $\dfrac{\tau'}{\tau}$ $(\phi \ll 1)$, equations (5.125) and (5.126) are the following.

$$\bar{J}_{sn} = \sqrt{\frac{\tau_n}{\tau_n'}} \tanh u_p \to \infty \qquad \text{for } \frac{\tau_n'}{\tau_n} = 0 \tag{5.131a}$$

$$\bar{J}_{sp} = \sqrt{\frac{\tau_p}{\tau_p'}} \tanh u_p \to \infty \qquad \text{for } \frac{\tau_p'}{\tau_p} = 0 \tag{5.131b}$$

Just as in the case for infinite neutral regions [equation (5.115)], the lowest saturation current densities are obtained for large values of $\frac{\tau'}{\tau}$.

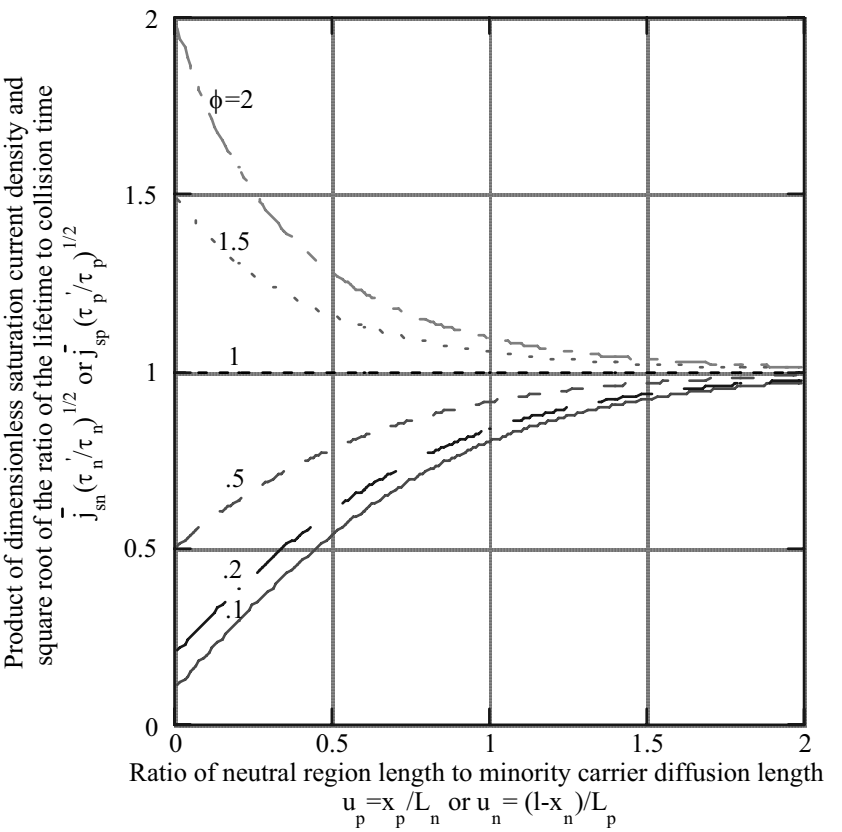

Figure 5.8 Dependence of the dimensionless saturation current densities of an ideal p-n junction on the dimensionless neutral region lengths for several values of the surface recombination parameter, $\phi = SL/D$

The dimensionless length of the neutral regions, u_p and u_n are important in determining $\overline{J}_{sn}$ and $\overline{J}_{sp}$. This is illustrated in Figure 5.8, where $\overline{J}_{sn}\sqrt{\frac{\tau_n'}{\tau_n}}$ and $\overline{J}_{sp}\sqrt{\frac{\tau_p'}{\tau_p}}$ are shown as functions of u_n and u_p for several values of ϕ_p and ϕ_n. Notice that the minority electron and hole saturation current densities are decreasing functions of u_p and u_n if $\phi_n > 1$ or $\phi_p > 1$, and increasing functions of u_p or u_n if $\phi_n < 1$ or $\phi_p<1$. Also, in all cases, for large u_p or u_n the sum of the saturation current densities are equal to the result given by equation (5.115), which applies for infinite neutral regions. Obviously, to obtain the smallest possible saturation current density, the surface recombination velocity parameters, ϕ_n and ϕ_p, and the neutral region length, u_p and u_n must be small.

As Figures 5.7 and 5.8 show $\overline{J}_{sn} = \overline{J}_{sp} \approx 1$, if $\frac{\tau_n'}{\tau_n} > 1$ and $\frac{\tau_p'}{\tau_p} > 1$ and if $u_p > 1$ and $u_n > 1$. Therefore, in this case $\overline{J}_{sn} \approx en_{po}\overline{v}_n$ and $\overline{J}_{sp} \approx ep_{no}\overline{v}_p$. Using the mass action law [equation (5.46)] and $n_{no} = N_D$, $p_{po} = N_A$, the following relation results for the saturation current density.

$$J_s = J_{sn} + J_{sp} \approx e\left(\frac{N_c N_v}{N_A}\right)\sqrt{\frac{k_B T}{m_n^*}}\left[1+\frac{N_A}{N_D}\sqrt{\frac{m_n^*}{m_p^*}}\right]\exp\left[-\frac{E_g}{k_B T}\right]$$

$$J_s = 1.46\times10^{18}\left(\frac{m_n^*}{m_e}\right)\left(\frac{m_p^*}{m_e}\right)^{3/2}\frac{T^{7/2}}{N_A}\left[1+\frac{N_A}{N_D}\sqrt{\frac{m_n^*}{m_p^*}}\right]\exp\left[-\frac{1.16\times10^4 E_g}{T}\right] \tag{5.132}$$

$$T(\mathrm{K}),\ N_A\left(\mathrm{cm}^{-3}\right),\ E_g(\mathrm{eV})$$

Thus, the saturation current density is exponentially dependent upon the bandgap energy, E_g. This strong dependence on E_g means that the low bandgap energy TPV cells have significant saturation current densities, a detrimental effect.

5.7.4 Depletion Region Contribution to Current and High-Injection Effects

In obtaining the ideal current-voltage relation, it has been assumed that recombination does not occur in the depletion region so that electron and hole currents are constant through the depletion region. However, in reality recombination does occur in the depletion region so that there is a recombination contribution to the current from the depletion region. It is also possible for electrons and holes to "tunnel" through the depletion region by moving from the conduction band or valence band to energy states within the bandgap. From these energy states, the electrons and holes can tunnel into the opposite band or recombine thus resulting in a contribution to the current. The

energy states within the bandgap result from impurities and lattice defects. Generally, recombination will be the major contributor to current generation in the depletion region.

In the case of reverse basis, where the applied potential adds to the built-in potential, the electric field will be large. As a result, free carrier electrons and holes are swept out of the depletion region before they can recombine. In forward basis, however, the density of electrons and holes will exceed their equilibrium values. Thus, they attempt to return to their equilibrium values by recombining. In this case, it can be shown that the current density generated in the depletion region, J_d, is the following.

$$J_d \sim n_i e^{\frac{eV_a}{2k_B T}} \tag{5.133}$$

Where n_i is the intrinsic carrier density [equation (5.47)], which is exponentially dependent upon the bandgap energy, E_g. In previously derived current-voltage relations [equations (5.114) and (5.123)], the current is proportional to $\exp\left[\frac{eV_a}{k_B T}\right]$.

The low injected minority carrier density assumption has been used in deriving the current-voltage relations. However, in a TPV application at large emitter temperature, minority carrier densities may become comparable to the majority carrier densities; this is called *high injection*.

Consider the neutral regions of the p-n junction for high injection. The transport equations for minority carriers in the p and n neutral regions are the same as in the low injection case. The only differences are the boundary conditions at boundaries of the neutral regions and the depletion region [equations (5.93) and (5.94)]. If the low injection assumption is not made, then equations (5.91) and (5.92) can be combined to yield the following result for minority electrons at the boundary between the p neutral region and the depletion region, $n_p(-x_p)$,

$$n_p\left(-x_p\right) = \frac{n_i^2}{N_A N_D} n_n\left(x_n\right) e^{\frac{eV_a}{k_B T}} \tag{5.134}$$

where $n_n(x_n) \approx N_D$ is the electron density at the boundary between the depletion region and the n neutral region. If high injection occurs so that $n_p(-x_p) \approx p_p(-x_p) \approx N_A$ and $n_n(x_n) \approx N_D$, then equation (5.134) yields the following.

$$n_p\left(-x_p\right) \approx n_i e^{\frac{eV_a}{2k_B T}} \tag{5.135}$$

ith this boundary condition, the solution for the electron diffusion current density at $x = -x_p$ is the following,

$$J_n\left(-x_p\right) = J_{sn}\left[e^{\frac{eV_a}{2k_BT}} - 1\right] \tag{5.136}$$

where J_{sn} is given by equation (5.120) with n_{po} replaced by n_i. Similar to recombination current in the depletion region [equation (5.133)], the current density is proportional to $e^{\frac{eV_a}{2k_BT}}$ rather than $e^{\frac{eV_a}{k_BT}}$ as is the case for low injection. A similar result for the hole diffusion current density at $x = x_n$ occurs if the boundary condition $p_n\left(x_n\right) \approx n_i e^{\frac{eV_a}{2k_BT}}$ is applied,

$$J_p\left(x_n\right) = J_{sp}\left[e^{\frac{eV_a}{2k_BT}} - 1\right] \tag{5.137}$$

where J_{sp} is given by equation (5.122) with p_{no} replaced by n_i. Thus, for the high injection boundary condition, the current-voltage relation is the following.

$$J = \left(J_{sn} + J_{sp}\right)\left[e^{\frac{eV_a}{2k_BT}} - 1\right] \tag{5.138}$$

5.8 Ideality Factor and Empirical Current-Voltage Relation of p-n Junction in the Dark

Under the ideal p-n junction assumptions, the current density is proportional to $e^{\frac{eV_a}{k_BT}}$ [equation (5.123)]. If depletions region recombination and high injection are included, then the current density will be proportional to $e^{\frac{eV_a}{2k_BT}}$. To approximate all these effects in the J vs. V_a relation for a real p-n junction in the dark, the following relation is used.

$$\boxed{J = J_s\left[e^{\frac{eV_a}{A_o k_B T}} - 1\right]} \tag{5.139}$$

The term A_o is called the *junction perfection factor* or *ideality factor* and J_s, is the saturation current, which includes the effects of depletion region recombination and high injection.

If the p-n junction behaves as an ideal junction, then $A_o = 1$. If high injection and depletion region recombination are dominate, then $A_o = 2$. The ideality factor, A_o, and saturation current, J_s, can be determined from experimental J vs. V_a data taken in the dark. For $\frac{eV_a}{k_B T} \gg 1$, $\ln J = \ln J_s + \frac{eV_a}{A_o k_B T}$ so that the slope of lnJ vs. V_a yields the value of A_o. The value of J_s is the asymptotic value of J for $\frac{eV_a}{k_B T} \ll 0$.

5.9 Current-Voltage Relation for an Ideal p-n Junction Under Illumination

Now consider a p-n junction with incident radiation, $q_i(\lambda)$, on the p side of the junction. In this case, electron-hole pairs are generated throughout the semiconductor for photon energies, $E = \frac{hc_o}{\lambda} > E_g$, where E_g is the bandgap energy. For the ideal p-n junction in the dark, it is assumed there is no generation or recombination in the depletion region. Therefore, the electron and hole currents are constant through the depletion region. As a result, the total current density, J, is the sum of the minority electron current density, J_n, at the boundary between the p region and the depletion region and the minority hole current density, J_p, at the boundary between the depletion region and the n region.

For the illuminated p-n junction, electron-hole pair production occurs in the depletion region. In this case, the total current density, J, is calculated by taking the sum of J_n and J_p at the p region-depletion region boundary or the sum of J_n and J_p at the depletion region-n region boundary.

Except for assumption 5), the same approximations used to obtain the J–V_a relation [equation (5.114)] for the p-n junction in the dark are used to obtain the J–V_a relation for the illuminated case. To simplify the algebra in deriving a solution to the transport equation, the origin of the coordinate system is located at the surface of the p region. This is illustrated in Figure 5.9.

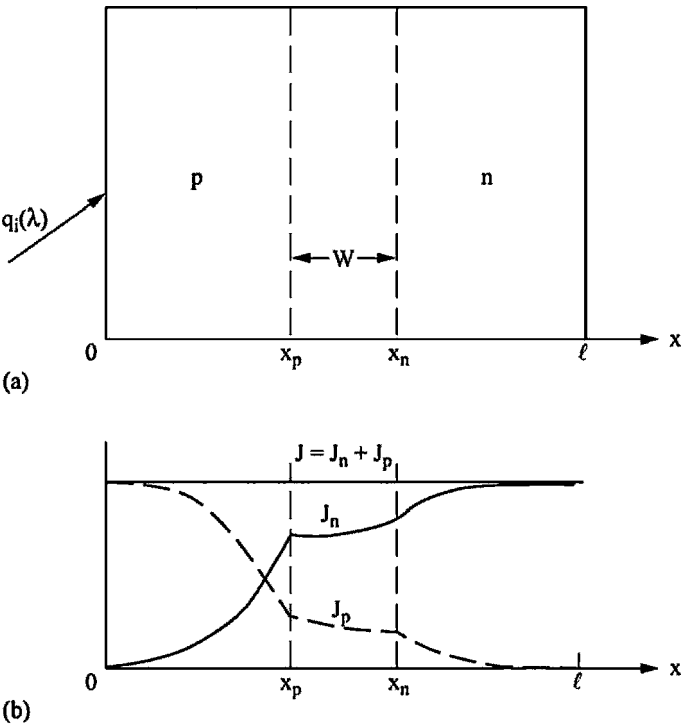

Figure 5.9.—p-n junction with incident radiation, $q_i(\lambda)$.
(a) Schematic of p-n junction. (b) Current distribution.

5.9.1 Electron Current Density in p Region

The transport equation for the minority electrons in the neutral p region now includes the generation term given by equation (5.66a). The generation rate is the number of electrons and holes produced per unit wavelength. Therefore, the minority electron density appearing in the transport equation will be the electron density per unit wavelength, which is denoted as n'_p. The total density is therefore $n_p = \int_o^\infty n'_p d\lambda$. And the transport equation is the following,

$$D_n \frac{d^2 n'_p}{dx^2} = \frac{n'_p - n'_{po}}{\tau'_n} - 2\left[1 - R_p(\lambda)\right] a_p(\lambda) \frac{\lambda q_i(\lambda)}{hc_o} \left[E_2(a_p x) - u_M E_2\left(\frac{a_p x}{u_M}\right) \right] \qquad (5.140a)$$

where $R_p(\lambda)$ is the reflectivity at the surface of the p region, $a_p(\lambda)$ is the absorption coefficient in the p region, and $u_M = \sqrt{1-\left(\frac{n_o}{n_p}\right)^2}$ where $n_o = 1$ is the index of refraction of vacuum and n_p is the index of refraction of the p region.

Rewrite equation (5.140a) as follows,

$$\frac{d^2N'_p}{dx^2} - \frac{N'_p}{L_n^2} = -\frac{2a_p(\lambda)F_p(\lambda)}{D_n}\left[E_2(a_p x) - u_M E_2\left(\frac{a_p x}{u_M}\right)\right] \tag{5.140b}$$

where $N'_p \equiv n'_p - n'_{po}$, $L_n = \sqrt{\tau'_n D_n}$, and $F_p(\lambda)$ is the photon flux that enters the p region.

$$F_p(\lambda) = (1-R_p)\frac{\lambda q_i(\lambda)}{hc_o} \tag{5.141}$$

Equation (5.140b) is an inhomogenous, second order, linear differential equation with constant coefficients. The solution consists of the sum of the solution to the homogenous equation [equation (5.102)] and a particular solution, f(x).

$$N'_p = A_p e^{\frac{x}{L_n}} + B_p e^{-\frac{x}{L_n}} + f(x) \tag{5.142}$$

If the right hand side of equation (5.140b) (the inhomogenous part) is the sum of two exponential functions of x, then the particular solution [11] is the following.

$$f(x) = C_1 e^{C_2 x} + C_3 e^{C_4 x} \tag{5.143}$$

It turns out that $E_2(x)$ in equation (5.140b) can be approximated by a simple exponential function (Appendix A).

$$E_2(x) \approx b_o e^{-b_1 x} \tag{5.144}$$

In equation (5.140b) the incident radiation is isotropic. If the incident radiation is normal, then b_o=1/2 and, b_1=1 in equation (5.144) and u_m=0

Using equation (5.144) for $E_2(a_p x)$ and , $E_2\left(\frac{a_p x}{u_M}\right)$ and substituting the trial solution

$$N'_p = C_1 e^{-b_1 a_p x} + C_2 e^{\frac{-b_1 a_p x}{u_M}} \tag{5.145}$$

in equation (5.140b) yields the following equations for C_1 and C_2.

$$\frac{C_1}{L_n^2}\left[\left(a_p b_1 L_n\right)^2 - 1\right] = -\frac{2a_p F_p b_o}{D_n}$$

$$\frac{C_1}{u_M^2 L_n^2}\left[\left(a_p b_1 L_n\right)^2 - u_M^2\right] = \frac{2a_p F_p b_o}{D_n} u_M$$

Thus, the solution is the following.

$$N'_p = A_p e^{\frac{x}{L_n}} + B_p e^{-\frac{x}{L_n}} - 2a_p(\lambda)F_p(\lambda)b_o\tau'_n\left[\frac{e^{-a_p b_1 x}}{\left(a_p b_1 L_n\right)^2 - 1} - \frac{u_M^3 e^{\frac{-a_p b_1 x}{u_M}}}{\left(a_p b_1 L_n\right)^2 - u_M^2}\right] \tag{5.146}$$

The contribution to the solution of the incident radiation is uncoupled from the in-the-dark solution. Hence, for the perfect p-n junction, the current density is just the sum of in-the-dark current density and the radiation caused current density. This becomes evident in the following development.

The boundary conditions that must be applied to determine A_p and B_p are the following.

$$N'_p(x_p) = n'_{po}\left(e^{\frac{eV_a}{k_B T}} - 1\right) \qquad \text{at } x = x_p \tag{5.147}$$

$$D_n \left.\frac{dN'_p}{dx}\right|_{x=o} = S_n N'_p(0) \qquad \text{at } x = 0 \tag{5.148}$$

Substituting equation (5.146) in (5.148) yields the following,

$$(1-\phi_n)A_p - (1+\phi_n)B_p = -\theta_{p1}\left[a_p(\lambda)b_1 L_n + \phi_n\right] + \theta_{p2}\left[\frac{a_p(\lambda)b_1 L_n}{u_M} + \phi_n\right] \tag{5.149}$$

where,

$$\theta_{p1}(\lambda)=\frac{2b_o a_p(\lambda)\tau_n' F_p(\lambda)}{\left(a_p b_1 L_n\right)^2-1}=\frac{2b_o\tau_n'\left(1-R_p\right)\lambda q_i(\lambda)}{hc_o\left[\left(a_p b_1 L_n\right)^2-1\right]}a_p(\lambda) \tag{5.150a}$$

$$\theta_{p2}(\lambda)=\frac{2b_o a_p(\lambda)\tau_n' F_p(\lambda)}{\left(a_p b_1 L_n\right)^2-u_M^2}u_M^3=\frac{2b_o\tau_n'\left(1-R_p\right)\lambda q_i(\lambda)}{hc_o\left[\left(a_p b_1 L_n\right)^2-u_M^2\right]}u_M^3 a_p(\lambda) \tag{5.150b}$$

$$\phi_n=\frac{S_n L_n}{D_n}=\frac{S_n}{\overline{v}_n}\sqrt{\frac{\tau_n'}{\tau_n}} \tag{5.151}$$

$$\overline{v}_n=\sqrt{\frac{k_B T}{m_n^*}} \tag{5.152}$$

Substituting equation (5.146) in (5.147) yields the following,

$$A_p e^{\frac{x_p}{L_n}}+B_p e^{-\frac{x_p}{L_n}}=\gamma_p'+\theta_{p1}e^{-a_p b_1 x_p}-\theta_{p2}e^{\frac{-a_p b_1 x_p}{u_M}} \tag{5.153}$$

where,

$$\gamma_p'=n_{po}'\left(e^{\frac{eV_a}{k_B T}}-1\right) \tag{5.154}$$

Solving equations (5.149) and (5.153) for A_p and B_p and using those results in equation (5.146) gives the following result for $N_p'(x)$,

$$\begin{aligned}N_p'(x)=\frac{1}{2DEN_p}\Bigg\{&\theta_{p1}\left[\left(a_p b_1 L_n+\phi_n\right)\left(e^{u_p-u}-e^{-(u_p-u)}\right)+\left(\left[1+\phi_n\right]e^{u}+\left[1-\phi_n\right]e^{-u}\right)e^{-a_p b_1 x_p}\right]\\&-\theta_{p2}\left[\left(\frac{a_p b_1 L_n}{u_M}+\phi_n\right)\left(e^{u_p-u}-e^{-(u_p-u)}\right)+\left(\left[1+\phi_n\right]e^{u}+\left[1-\phi_n\right]e^{-u}\right)e^{\frac{-a_p b_1 x_p}{u_M}}\right]\\&+\gamma_p'\left[\left(1+\phi_n\right)e^{u}+\left(1-\phi_n\right)e^{-u}\right]\Bigg\}-\theta_{p1}e^{-a_p b_1 x}+\theta_{p2}e^{\frac{-a_p b_1 x}{u_M}}\end{aligned} \tag{5.155a}$$

$$N'_p(x) = \frac{1}{2DEN_p}\left\{\theta_{p1}\left[\left(a_p b_1 L_n + \phi_n\right)\sinh\left(u_p - u\right) + \left(\cosh u + \phi_n \sinh u\right)e^{-a_p b_1 x_p}\right]\right.$$
$$-\theta_{p2}\left[\left(\frac{a_p b_1 L_n}{u_M} + \phi_n\right)\sinh\left(u_p - u\right) + \left(\cosh u + \phi_n \sinh u\right)e^{\frac{-a_p b_1 x_p}{u_M}}\right]$$
$$\left.+\gamma'_p\left[\phi_n \sinh u + \cosh u\right]\right\} - \theta_{p1}e^{a_p b_1 x} + \theta_{p2}e^{\frac{a_p b_1 x}{u_M}} \tag{5.155b}$$

where,

$$u = \frac{x}{L_n} \qquad u_p = \frac{x_p}{L_n} \tag{5.156}$$

$$DEN_p = \frac{1}{2}\left[\left(1+\phi_n\right)e^{u_p} + \left(1-\phi_n\right)e^{-u_p}\right] \tag{5.157a}$$

$$DEN_p = \cosh u_p + \phi_n \sinh u_p \tag{5.157b}$$

Hence, the electron diffusion current per unit wavelength, J'_n at $x = x_p$ is the following,

$$J'_n\left(x_p\right) = eD_n \left.\frac{dN'_p}{dx}\right|_{x=x_p} = J'_{sn}\left[e^{\frac{eV_a}{k_B T}} - 1\right] - J'_{qn} \tag{5.158}$$

where J'_{sn} is the electron saturation current density without illumination and is given by equation (5.120) where $u_p = \frac{\left(\ell_p - x_p\right)}{L_n}$, $n'_{po} = n_{po}$, and J'_{qn} is the current density per unit wavelength resulting from the incident photons. It is given in dimensionless form by the following equations,

$$\overline{J}'_{qn} \equiv \frac{J'_{qn}}{J_F} = \frac{\beta_n}{b_1 DEN_p}\left\{\frac{1}{\beta_n^2 - 1}\left[\beta_n + \phi_n - \left(\left[\beta_n + \phi_n\right]\cosh u_p + \left[\beta_n\phi_n + 1\right]\sinh u_p\right)e^{-\beta_n u_p}\right]\right.$$
$$\left.-\frac{u_M^3}{\beta_n^2 - u_M^2}\left[\frac{\beta_n}{u_M} + \phi_n - \left(\left[\frac{\beta_n}{u_M} + \phi_n\right]\cosh u_p + \left[\frac{\beta_n\phi_n}{u_M} + 1\right]\sinh u_p\right)e^{\frac{-\beta_n u_p}{u_M}}\right]\right\} \tag{5.159a}$$

$$\overline{J}'_{qn} = \frac{\beta_n}{2b_l DEN_p}\left\{\frac{1}{\beta_n^2-1}\left[2(\beta_n+\phi_n)-(\beta_n+1)(1+\phi_n)e^{-u_p(\beta_n-1)}-(\beta_n-1)(1-\phi_n)e^{-u_p(\beta_n+1)}\right]\right.$$
$$\left.-\frac{u_M^3}{\beta_n^2-u_M^2}\left[2\left(\frac{\beta_n}{u_M}+\phi_n\right)-\left(\frac{\beta_n}{u_M}+1\right)(1+\phi_n)e^{-u_p\left(\frac{\beta_n}{u_M}-1\right)}-\left(\frac{\beta_n}{u_M}-1\right)(1-\phi_n)e^{-u_p\left(\frac{\beta_n}{u_M}+1\right)}\right]\right\} \tag{5.159b}$$

where,

$$\beta_n = b_l L_n a_p(\lambda) \tag{5.160}$$

and

$$J_F(\lambda) = 2eb_o F_p(\lambda) = 2eb_o(1-R_p)\frac{\lambda q_i(\lambda)}{hc_o} \tag{5.161}$$

The parameter, β_n, is the *optical depth* based on the minority carrier electron diffusion length, L_n. The current density per unit wavelength, J_F, is the current density that would result if every absorbed photon of wavelength, λ, produced current. In other words, it is the maximum possible current density that can be attained under illumination. Thus, $\overline{J}'_{qn} \le 1$.

In the following sections, expressions for the dimensionless photon generated currents in the n region, $\overline{J}'_{qp}$, and depletions region, $\overline{J}'_d$, are developed. The sum, $\overline{J}'_{qn} + \overline{J}'_{qp} + \overline{J}'_d$ is called the *internal quantum efficiency* and is discussed in detail in Section 5.10.

As mentioned in Section 5.7, for an efficient PV cell, $u_p = \frac{x_p}{L_n} < 1$. Therefore, if $\left|u_p(\beta_n \pm 1)\right| < 1$, and $\left|u_p\left(\frac{\beta_n}{u_M} \pm 1\right)\right| < 1$, then the exponential terms and DEN_p in equation (5.159b) can be approximated by power series. If only the linear term in u_p is retained, then equation (5.159b) reduces to the following result.

$$\overline{J}'_{qn} \approx \frac{u_p\beta_n}{b_l}(1-u_M) = a_p(\lambda)x_p(1-u_M) \qquad u_p = \frac{x_p}{L_n} \ll 1 \tag{5.162}$$

Hence, the photon produced current is a linear function of $a_p(\lambda)$ so that a large absorption coefficient is desirable in this case. Note also that $\bar{J}'_{qn}$ is independent of the surface recombination parameter, ϕ_n, and the parameter, b_1. Thus, for $u_p \ll 1$ the photon generated current is the same for both isotropic and normal incidence radiation[see discussion following equation (5.144)].

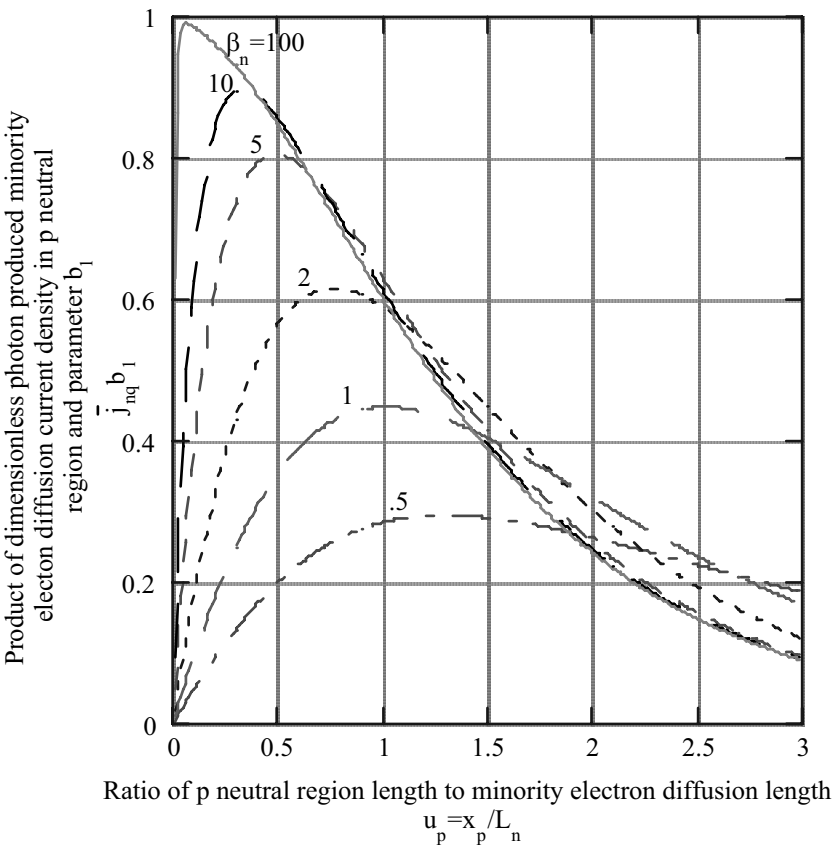

Figure 5.10a) - Effect of dimensionless neutral p region length, x_p/L_n on the photon produced minority electron diffusion current for several values of $\beta_n = b_1 L_n a_p(\lambda)$ and $\phi_n = S_n L_n / D_n = .1$.

In general, there is an optimum value of u_p for producing a maximum value of $\bar{J}'_{qn}$. This is illustrated in Figure 5.10, where $b_1 \bar{J}'_{nq}$ is shown as a function of u_p for several values of β_n when $u_M = 0$. In part a), $\phi_n = 0.1$, and in part b), $\phi_n = 1$. Increasing β_n

results in larger values for $b_1\overline{J}'_{qn}$, as well as, smaller values for u_p where the maximum occurs. For $\beta \to \infty$, equation (5.159b) yields the following.

$$\lim_{\beta_n \to \infty} \overline{J}'_{qn} = \frac{1}{b_1 DEN_p}\left[1 - u_M^2\right] = \frac{1 - u_M^2}{b_1\left(\cosh u_p + \phi_n \sinh u_p\right)} \tag{5.163}$$

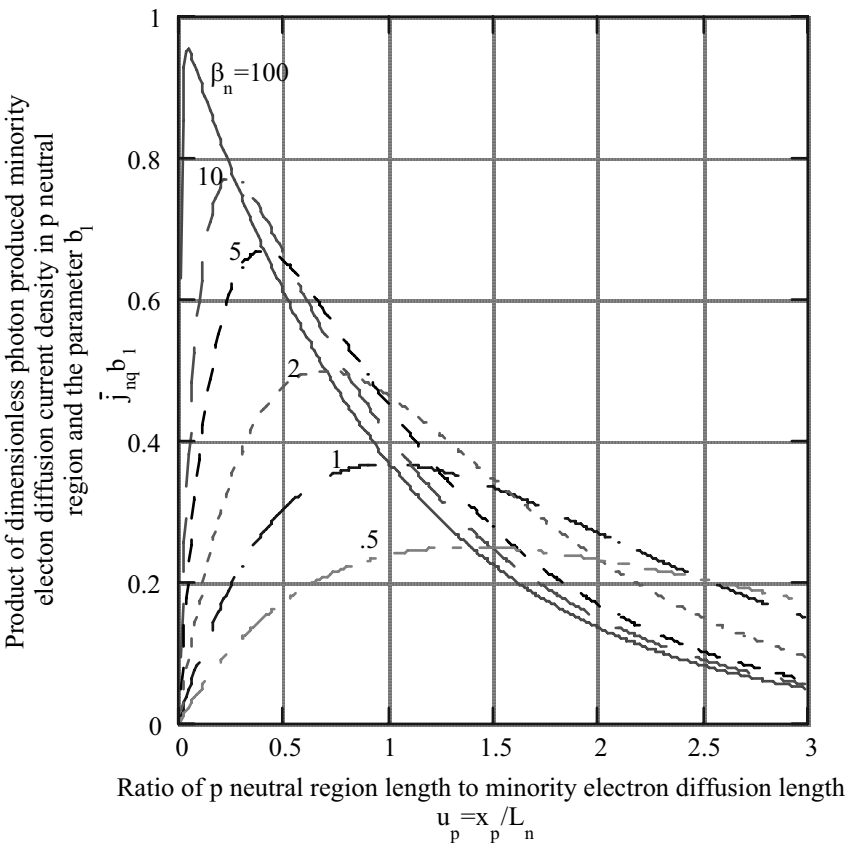

Figure 5.10b) - Effect of dimensionless neutral p region length, x_p/L_n on the photon produced minority electron diffusion current for several values of $\beta_n = b_1 L_n a_p(\lambda)$ and $\phi_n = S_n L_n / D_n = 1$.

In this case, $\overline{J}'_{qn}$ has a maximum value of $\frac{\left(1-u_M^2\right)}{b_1}$ at $u_p = 0$. As ϕ_n increases, $\overline{J}'_{qn}$ decreases (problem 5.8). Thus, large surface recombination velocity, S_n, is detrimental. However, the value of u_p for maximum $\overline{J}'_{qn}$ is not greatly affected.

Equation (5.159) applies for isotropic incident radiation, such as in a TPV system. The dimensionless current when the incident radiation is at zero angle of incidence, such as in a solar PV application, is obtained by setting $b_o = ½$, $b_1 = 1$ [see equation (5.144)], and $u_M = 0$ in equation (5.159).

$$\overline{J}'_{qn} = \frac{\beta'_n}{DEN_p}\frac{1}{\beta'^2_n - 1}\left\{\beta'_n + \phi_n - \left[\left(\beta'_n + \phi_n\right)\cosh u_p + \left(\beta'_n\phi_n + 1\right)\sinh u_p\right]e^{-\beta'_n u_p}\right\} \tag{5.164a}$$

Where,

$$\beta'_n = L_n a_p\left(x\right) \tag{5.164b}$$

and for $\beta'_n \to \infty$,

$$\lim_{\beta'_n\to\infty}\overline{J}'_{qn} = \frac{1}{\cosh u_p + \phi_n \sinh u_p} \tag{5.164c}$$

Now compare $\overline{J}'_{qn}$ for isotropic incident radiation to the zero angle of incidence case for large β_n and β'_n when the photon flux, $\frac{\lambda q_i\left(\lambda\right)}{hc_o}$ and the PV cell properties are the same. Under these conditions, equations (5.163) and (5.154c) yield the following result(b_o= ½ for zero angle of incidence).

$$\frac{J'_{qn}\big|_{isotropic}}{J'_{qn}\big|_{\theta_i=0}} = \frac{\left(1-R_{\perp p}\right)\overline{J}'_{qn}\big|_{isotropic}}{2b_o\left(1-R_p\right)\overline{J}'_{qn}\big|_{\theta_i=0}} = \left(\frac{1-R_{\perp p}}{1-R_p}\right)\frac{1-u_M^2}{2b_o b_1} \tag{5.165a}$$

For efficient PV cells, $R_{\perp p}$ and R_p are small compared to 1. Therefore,

$$\frac{J'_{qn}\big|_{isotropic}}{J'_{qn}\big|_{\theta_i=0}} \approx \frac{1-u_M^2}{2b_o b_1} \tag{5.165b}$$

Values of the constants b_o and b_1 depend upon the exponential approximation used for $E_2(ax)$. The approximations in Appendix A [equations (A-13) and (A-14)] give $b_o = \frac{3}{4}$, $b_1 = \frac{3}{2}$, or $b_o = 0.9$, $b_1 = 1.8$. Therefore, assuming $u_M^2 \ll 1$

$$\frac{J'_{qn}\big|_{isotropic}}{J'_{qn}\big|_{\theta_i=0}} \approx \frac{1}{2b_o b_1} = \frac{4}{9} \quad \text{or} \quad \frac{1}{3.24} \qquad \text{for} \begin{cases} \beta_n \to \infty \\ \beta'_n \to \infty \end{cases} \tag{5.165c}$$

It is possible, therefore, that a PV cell in a TPV application, where the incident radiation is isotropic, produces a significantly lower photon current density than when it is used in a solar application, where the incident photon radiation is at zero angle of incidence. In both cases, incident photon flux is assumed to be the same. However, as mentioned in the discussion of equation (5.162), if $u_p \ll 1$, then the photon generated current is the same for both isotropic and normal incidence radiation when the incident photon flux is the same for both cases. Thus, depending upon the optical depth, β_n, and the ratio of the neutral region length, x_p, to the minority carrier diffusion length, L_n, the photon produced current for a PV array in a TPV application may or may not be affected by the isotropic nature of the incident radiation.

Before proceeding to calculate the photon generated minority hole current density in the n region of the p-n junction, the solution to equation (5.140) when $\beta_n = b_1 a_p(\lambda) L_n = 1$, or $\beta_n = u_M$, is considered. As equations (5.146) and (5.159) show, there are singularities in the solutions for N'_p and J'_{nq} when $\beta_n = 1$, or $\beta_n = u_M$. Thus the particular solution given by equation (5.145) does not apply for $\beta_n = 1$ or $\beta_n = u_M$. If $\beta_n = 1$ or $\beta_n = u_M$, the particular solution is of the form $C_o x e^{-b_1 a_p x}$ or $C'_o x e^{\frac{-b_1 a_p x}{u_M}}$ [11]. Using those particular solutions for N_p, the results for J'_{sn} and J'_{qn} can be determined (problem 5.7). Thus for $\beta_n = 1$ and $u_M = 0$, the solution for $\overline{J}'_{qn}$ is the following.

$$\overline{J}'_{qn} = \frac{1}{2b_1 DEN_p}\left\{(1-\phi_n)e^{-u_p}\sinh u_p + (1+\phi_n)u_p\right\} \tag{5.166}$$

5.9.2 Hole Current Density in n Region

Now consider the minority hole current density, J'_p, in the n region. Again, if the assumptions of section 5.7.1 are applied, the transport equation for minority holes in the

n region is similar to equation (5.140). Also, p'_n is the hole density per unit of wavelength and $p_n = \int_o^\infty p'_n d\lambda$. The hole transport equation is,

$$D_p \frac{d^2 p'_n}{dx^2} = \frac{p'_n - p'_{no}}{\tau'_p} - G(\lambda, x) \tag{5.167}$$

where derivation of the generation term, G(λ,x) is left as an exercise (problem 5.9). In that derivation it is assumed that the p, n, and depletion regions all have the same index of refraction, n_c. Therefore, the generation rate is the following.

$$\begin{aligned} G(\lambda, x) = 2F_p(\lambda) a_n(\lambda) \Bigg\{ & E_2\left[(a_p - a_d) x_p + (a_d - a_n) x_p + a_n x \right] \\ & - u_M E_2 \left[\frac{(a_p - a_d) x_p}{u_M} + \frac{(a_d - a_n) x_p}{u_M} + \frac{a_n x}{u_M} \right] \Bigg\} \qquad x_n \le x \le \ell \end{aligned} \tag{5.168}$$

where $a_d(\lambda)$ is the absorption coefficient in the depletion region, $a_n(\lambda)$ is the absorption coefficient in the n region, $u_M = \sqrt{1 - \left(\frac{n_o}{n_c}\right)^2}$ and $F_p(\lambda)$ is given by equation (5.141). Again, approximate the exponential integral, $E_2(x)$ by equation (5.144). As a result, the hole transport equation is the following,

$$\begin{aligned} \frac{d^2 P'_n}{dx^2} - \frac{P'_n}{L_p^2} = -\frac{2 b_o F_p(\lambda) a_n(\lambda)}{D_p} \Bigg\{ & \mathrm{Exp}\left[-b_1 x_p (a_p - a_d) - b_1 x_n (a_p - a_n) \right] e^{-b_1 a_n x} \\ & - u_M \mathrm{Exp}\left[-\frac{b_1}{u_M} x_p (a_p - a_d) - \frac{b_1}{u_M} x_n (a_p - a_n) \right] e^{\frac{-b_1 a_n x}{u_M}} \Bigg\} \qquad x_n \le x \le \ell \end{aligned} \tag{5.169}$$

where $P'_n = p'_n - p'_{no}$ and $L_p = \sqrt{\tau'_p D_p}$ is the diffusion length of holes in the n region. Similar to the solution for N'_p [equation (5.146)], the solution for P'_n is the following,

$$P'_n = A_n e^{\frac{x}{L_p}} + B_n e^{-\frac{x}{L_p}} - \theta_{n1} e^{-b_1 a_n x} + \theta_{n2} e^{\frac{-b_1 a_n x}{u_M}} \tag{5.170}$$

where

$$\theta_{n1} = \frac{2b_o\tau'_p F_p(\lambda)a_n(\lambda)}{\beta_p^2 - 1}\mathrm{Exp}\left[-b_1 x_p\left(a_p - a_d\right) - b_1 x_n\left(a_p - a_n\right)\right] \tag{5.171a}$$

$$\theta_{n12} = \frac{2b_o\tau'_p F_p(\lambda)a_n(\lambda)}{\beta_p^2 - u_M^2}u_M^3\,\mathrm{Exp}\left[-\frac{b_1 x_p}{u_M}\left(a_p - a_d\right) - \frac{b_1 x_n}{u_M}\left(a_p - a_n\right)\right] \tag{5.171b}$$

$$\beta_p = b_1 a_n(\lambda)L_p \tag{5.171c}$$

The constants A_n and B_n are determined by the boundary conditions.

At $x = x_n$,

$$P'_n(x_n) = p'_{no}\left(e^{\frac{eV_a}{k_B T}} - 1\right) \equiv \gamma'_n \tag{5.172}$$

and at $x = \ell$,

$$-D_p\left.\frac{dP'_n}{dx}\right|_{x=\ell} = S_p P'_n(\ell) \tag{5.173}$$

Applying equation (5.173) to equation (5.170) yields the following.

$$\left(1+\phi_p\right)A_n e^{u_\ell} - \left(1-\phi_p\right)B_n e^{-u_\ell} = \theta_{n1}\left(\phi_p - \beta_p\right)e^{-b_1 a_n \ell} - \theta_{n2}\left(\phi_p - \frac{\beta_p}{u_M}\right)e^{\frac{-b_1 a_n \ell}{u_M}} \tag{5.174}$$

Where

$$u_1 = \frac{\ell}{L_p} \tag{5.175}$$

and

$$\phi_p \equiv \frac{S_p L_p}{D_p} = \frac{S_p}{\overline{v}_p}\sqrt{\frac{\tau'_p}{\tau_p}} \tag{5.176}$$

$$\overline{v}_p = \sqrt{\frac{k_B T}{m_p^*}} \tag{5.177}$$

Applying equation (5.172) to equation (5.170) yields the following result.

$$A_n e^{\frac{x_n}{L_p}} + B_n e^{-\frac{x_n}{L_p}} - \theta_{n1} e^{-b_1 a_n x_n} + \theta_{n2} e^{\frac{-b_1 a_n x_n}{u_M}} = \gamma'_n \tag{5.178}$$

Solving equations (5.174) and (5.178) for A_n and B_n using those results in equation (5.170), the solution for $P'_n(x)$ is obtained,

$$\begin{aligned} P'_n(x) = \frac{1}{2DEN_n}\Bigg\{ & \theta_{n1}\Bigg[e^{-b_1 a_n x_n}\left(\left[1+\phi_p\right]e^{(u_\ell - u)} + \left[1-\phi_p\right]e^{-(u_\ell - u)}\right) \\ & - e^{-b_1 a_n \ell}\left(\beta_p - \phi_p\right)\left(e^{u-\frac{x_n}{L_p}} - e^{-\left(u-\frac{x_n}{L_p}\right)}\right)\Bigg] - \theta_{n2}\Bigg[e^{\frac{-b_1 a_n x_n}{u_M}}\left(\left[1+\phi_p\right]e^{(u_\ell - u)} + \left[1-\phi_p\right]e^{-(u_\ell - u)}\right) \\ & - e^{\frac{-b_1 a_n \ell}{u_M}}\left(\beta_p - \phi_p\right)\left(e^{u-\frac{x_n}{L_p}} - e^{-\left(u-\frac{x_n}{L_p}\right)}\right)\Bigg] + \gamma'_n\left[\left(1+\phi_p\right)e^{(u_\ell - u)} + \left(1-\phi_p\right)e^{-(u_\ell - u)}\right]\Bigg\} \\ & - \theta_{n1} e^{-\beta_p u} + \theta_{n2} e^{\frac{-\beta_p u}{u_M}} \end{aligned} \tag{5.179a}$$

$$\begin{aligned} P'_n(x) = \frac{1}{DEN_n}\Bigg\{ & \theta_{n1}\Bigg[\left(\cosh\left[u_\ell - u\right] + \phi_p \sinh\left[u_\ell - u\right]\right)e^{-b_1 a_n x_n} - \left(\beta_p - \phi_p\right)e^{-b_1 a_n \ell}\sinh\left(u - \frac{x_n}{L_p}\right)\Bigg] \\ & - \theta_{n2}\Bigg[\left(\cosh\left[u_\ell - u\right] + \phi_p \sinh\left[u_\ell - u\right]\right)e^{\frac{-b_1 a_n x_n}{u_M}} - \left(\beta_p - \phi_p\right)e^{\frac{-b_1 a_n \ell}{u_M}}\sinh\left(u - \frac{x_n}{L_p}\right)\Bigg] \\ & + \gamma'_n\left[\cosh\left(u_\ell - u\right) + \phi_p \sinh\left(u_\ell - u\right)\right]\Bigg\} - \theta_{n1} e^{-\beta_p u} + \theta_{n2} e^{\frac{-\beta_p u}{u_M}} \end{aligned} \tag{5.179b}$$

where,

$$DEN_n = \cosh u_n + \phi_p \sinh u_n \tag{5.180a}$$

$$\mathrm{DEN_n} = \frac{1}{2}\left[\left(1+\phi_p\right)e^{u_n} + \left(1-\phi_p\right)e^{-u_n}\right] \tag{5.180b}$$

and

$$u = \frac{x}{L_p} \tag{5.181}$$

$$u_n = \frac{\ell - x_n}{L_p} = u_l - \frac{x_n}{L_p} \tag{5.182}$$

Now calculate the hole diffusion current at the edge of the depletion region ($x = x_n$),

$$J'_p\left(x_n\right) = -eD_p\left.\frac{dP'_n}{dx}\right|_{x=x_n} = J'_{sp}\left[e^{\frac{eV_a}{k_BT}} - 1\right] - J'_{qp} \tag{5.183}$$

where J'_{sp} is the hole saturation current density without illumination and is given by equation (5.122) where $u_n = \frac{\ell_n - x_n}{L_p}$, and $p'_{no} = p_{no}$. The photon produced hole current density is J'_{qp} and is given in dimensionless form by the following expressions.

$$\overline{J}'_{qp} \equiv \frac{J'_{qp}}{J_F} = \frac{\beta_p}{b_l \mathrm{DEN_n}}\left\{\frac{\exp\left[-b_l x_p\left(a_p - a_d\right)\right]}{\beta_p^2 - 1}e^{-b_l a_d x_n}\left[\left(\beta_p\phi_p - 1\right)\sinh u_n\right.\right.$$
$$\left. + \left(\beta_p - \phi_p\right)\left(\cosh u_n - e^{-\beta_p u_n}\right)\right] - \frac{\exp\left[\frac{-b_l x_p}{u_M}\left(a_p - a_d\right)\right]}{\beta_p^2 - u_M^2}u_M^3 e^{\frac{-b_l a_d x_n}{u_M}}\left[\left(\frac{\beta_p\phi_p}{u_M} - 1\right)\sinh u_n\right.$$
$$\left.\left. + \left(\frac{\beta_p}{u_M} - \phi_p\right)\left(\cosh u_n - e^{\frac{-\beta_p u_n}{u_M}}\right)\right]\right\} \tag{5.184a}$$

$$\overline{J}'_{qp} = \frac{\beta_p}{2b_1 DEN_n}\left\{\frac{\exp\left[-b_1 x_p\left(a_p - a_d\right)\right]}{\beta_p^2 - 1} e^{-b_1 a_d x_n}\left[\left(\beta_p + 1\right)\left(1 - \phi_p\right)e^{-u_n} + \left(\beta_p - 1\right)\left(1 + \phi_p\right)e^{u_n}\right.\right.$$

$$\left. -2\left(\beta_p - \phi_p\right)e^{-\beta_p u_n}\right] - \frac{\exp\left[\dfrac{-b_1 x_p}{u_M}\left(a_p - a_d\right)\right]}{\beta_p^2 - u_M^2} u_M^3 e^{\frac{-b_1 a_d x_n}{u_M}}\left[\left(\frac{\beta_p \phi_p}{u_M} + 1\right)\left(1 - \phi_p\right)e^{-u_n}\right.$$

$$\left.\left. + \left(\frac{\beta_p}{u_M} - 1\right)\left(1 + \phi_p\right)e^{u_n} - 2\left(\frac{\beta_p}{u_M} - \phi_p\right)e^{\frac{-\beta_p u_n}{u_M}}\right]\right\} \tag{5.184b}$$

The photon produced hole current density in the n region, $\overline{J}'_{qp}$, is significantly less than the photon produced electron current density, $\overline{J}'_{qn}$, in the p region. This occurs because most of the photon flux is absorbed in the p and depletion regions. The terms $\exp\left[-b_1 x_p\left(a_p - a_d\right)\right]e^{-b_1 a_d x_n}$ and $\exp\left[\dfrac{-b_1 x_p}{u_M}\left(a_p - a_d\right)\right]e^{\frac{-b_1 a_d x_n}{u_M}}$ in equations (5.184a) and (5.184b) account for the photon absorption in the p and depletion regions.

Just as in the case for N'_p, there are singularities in the solutions for P'_n at $\beta_p = 1$, and $\beta_p = u_M$. For $\beta_p = 1$, the particular solution to equation (5.169) is of the form $C_o x e^{-b_1 a_n x}$. Using that result and assuming $u_M = 0$, P'_n can be determined. Thus, the following result for the dimensionless photon saturation current density (problem 5.10) is obtained.

$$\overline{J}'_{qp} = \frac{Exp\left[-b_1 x_p\left(a_p - a_n\right) - b_1 a_d x_n\right]}{2b_1 DEN}\left\{\cosh u_n + \phi_p \sinh u_n - \left[1 - u_n\left(1 - \phi_p\right)\right]e^{-u_n}\right\}$$

$$\beta_p = 1,\ u_M = 0 \tag{5.185}$$

For a thick n region ($u_n \to \infty$), equation (5.184b) has the following asymptotic value.

$$\lim_{u_n \to \infty} = \overline{J}'_{qp} = a_n L_p\left\{\frac{\exp\left[-b_1 x_p\left(a_p - a_d\right)\right]}{\beta_p + 1} e^{-b_1 a x_n} - \frac{\exp\left[-\dfrac{b_1 x_p}{u_M}\left(a_p - a_d\right)\right]}{\dfrac{\beta_p}{u_M} + 1} u_M e^{\frac{-b_1 a_n x_n}{u_M}}\right\} \tag{5.186}$$

Obviously, if the dimensionless width of the n region, u_n, becomes large the photon produced hole current density is independent of the surface recombination parameter, ϕ_p, as equation (5.186) indicates.

Under certain conditions, similar to the photon produced electron current density, $\overline{J}'_{nq}$ in the p region, there is an optimum value of the neutral region length, u_n, for producing maximum $\overline{J}'_{pq}$. This is illustrated in Figure 5.11 where $\overline{J}'_{qp} b_1 \exp\left[b_1 x_p \left(a_p - a_d\right)\right] e^{-b_1 a_d x_n}$ is shown as a function of u_n for $u_M = 0$ and several values of β_p with $\phi_p = 0.1$ in part a) and $\phi_p = 1$ in part b).

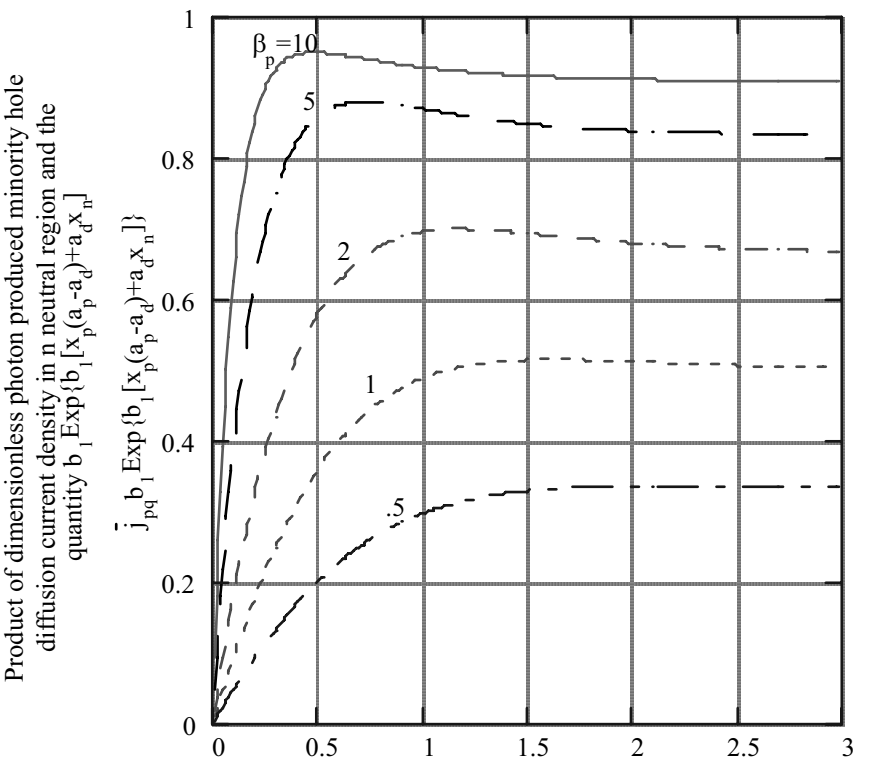

Figure 5.11a) - Effect of dimensionless neutral n region length on the photon generated minority hole diffusion current for u_m=0, several values of the optical depth, $\beta_p = b_1 L_p a_n(\lambda)$ and surface recombination parameter, $\phi_p = S_p L_p / D_p = .1$.

As can be seen, for large β_p and $\phi_p = 1$, the photon produced hole current density has a maximum value greater than the asymptotic value given by equation (5.186). However, for $\beta_p < 1$ and $\phi_p = 0.1$ and also for all β_p when $\phi_p = 1$, the maximum value of $\overline{J}'_{qp}$ is the asymptotic value. It would, therefore, appear that a large (> 1) value of the neutral p region length, u_n, is desirable. However, $u_n > 1$ for $\phi_p \leq 1$ means the saturation current density, J_{sp}, is near its maximum value (Figure 5.8). Whereas, the desired result is that J_{sp} should be as small as possible.

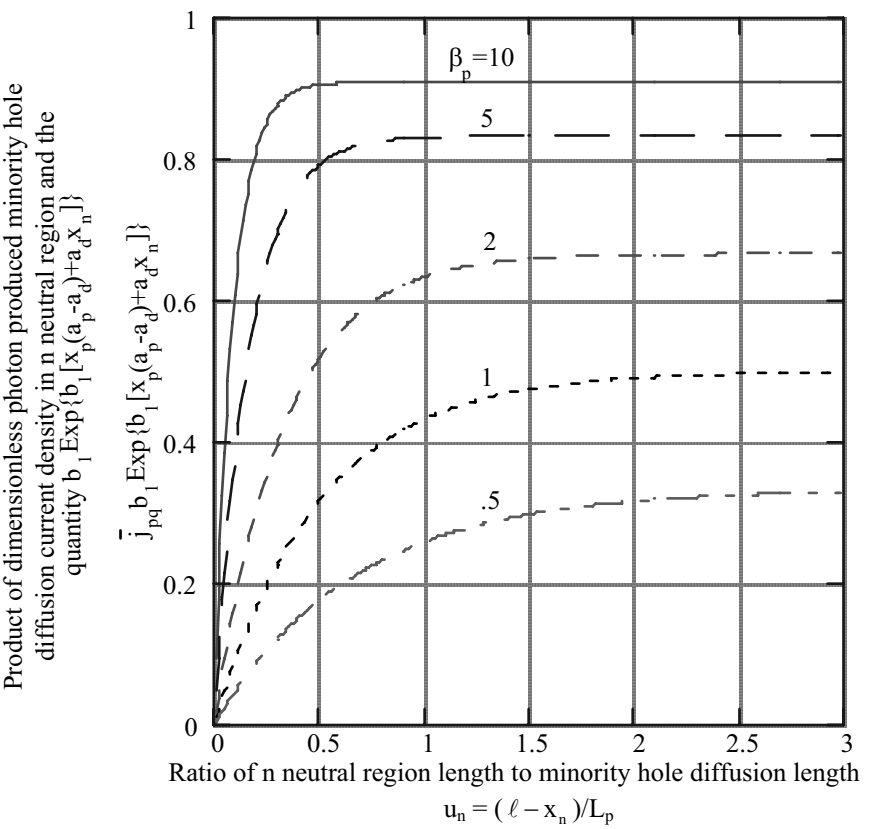

Figure 5.11b) - Effect of dimensionless neutral n region length on the photon generated minority hole diffusion current for u_m=0, several values of the optical depth, $\beta_p = b_1 L_p a_n(\lambda)$ and surface recombination parameter, $\phi_p = S_p L_p / D_p = 1$.

The results for J'_{qn} and J'_{qp} have been derived for the case where the photons are incident on the p side of the junction. Results for J'_{qp} and J'_{qn} when photons are incident on the n side of the junction are obtained as follows. To obtain J'_{qp}, replace β_n by β_p, ϕ_n by ϕ_p, R_p by R_n, and u_p by u_n, in equation (5.159). To obtain J'_{qn}, replace β_p by β_n, ϕ_p by ϕ_n, R_p by R_n, and u_n by u_p, in equation (5.184).

5.9.3 Current Generation in Depletion Region

To obtain the total current, the current density generated in the depletion region must be included along with the minority current densities at the depletion region boundaries. In the depletion region, the electric field will accelerate electrons and holes out of the region. Since the depletion region is narrow, it is reasonable to assume that the electrons and holes leave the depletion region before they can recombine. As a result, the steady state continuity equations for the electrons and holes are the following.

$$\frac{1}{e}\frac{dJ'_n}{dx} = -G(\lambda, x) \qquad (5.187a)$$

$$x_p \le x \le x_n$$

$$\frac{1}{e}\frac{dJ'_p}{dx} = G(\lambda, x) \qquad (5.187b)$$

Similar to equation (5.168), the generation rate in the depletion region is the following,

$$G(\lambda, x) = 2F_p(\lambda)a_d(\lambda)\left\{E_2\left[a_p x_p + a_d(x - x_p)\right] - u_M E_2\left[\frac{a_p x_p}{u_M} + \frac{a_d(x - x_p)}{u_M}\right]\right\}$$

$$x_p \le x \le x_n \qquad (5.188)$$

where $a_d(\lambda)$ is the absorption coefficient for the depletion region. As stated earlier, to determine the total current density, J', the sum of the electron, J'_n, and hole, J'_p, currents at $x = x_p$ or $x = x_n$. are required. The currents J'_n at $x = x_p$, and J'_p at $x = x_n$ have already been calculated. Therefore, either equation (5.187a) can be solved to obtain J'_n at $x = x_n$. Or equation (5.187b) can be solved to obtain J'_p at $x = x_p$ in order to obtain $J' = J'_n(x_n) + J'_p(x_n) = J'_n(x_p) + J'_p(x_p)$. Consider the solution of equation

(5.187a). The boundary condition to be satisfied is that at $x = x_p$, $J'_n = J'_{sn}\left[e^{\frac{eV_a}{k_B T}} - 1\right] - J'_{qn}$, [equation (5.158)].

Using the approximation, $E_2(x) = b_o e^{-b_1 x}$ in equation (5.188) for G(λ,x), equation (5.187a) can be integrated.

$$J'_n(x) = \frac{J_F}{b_1}\left\{\exp\left[-b_1 x_p\left(a_p - a_d\right)\right]e^{-b_1 a_d x} - u_M^2 \exp\left[\frac{-b_1 x_p\left(a_p - a_d\right)}{u_M}\right]e^{\frac{-b_1 a_d x}{u_M}}\right\} + C \tag{5.189}$$

Apply the boundary condition to obtain C. As a result, $J'_n(x)$ is the following.

$$J'_n(x) = J'_{sn}\left[e^{\frac{eV_a}{k_B T}} - 1\right] - J_F\left[J'_{qn} + \frac{e^{\beta_n u_p}}{b_1}\left(1 - e^{-b_1 a_d\left(x - x_p\right)}\right) - u_M^2 \frac{e^{-\beta_n u_p}}{b_1}\left(1 - e^{\frac{-b_1 a_d\left(x - x_p\right)}{u_M}}\right)\right] \tag{5.190}$$

Thus, the electron current density per unit wavelength at $x = x_n$ is the following,

$$J'_n(x_n) = J'_{sn}\left[e^{\frac{eV_a}{k_B T}} - 1\right] - J_F\left[\overline{J}'_{qn} + \overline{J}'_d\right] \tag{5.191}$$

where $\overline{J}'_d$ is the dimensionless photon produced current density per wavelength in the depletion region,

$$\overline{J}'_d = \frac{1}{b_1}\left[e^{-\beta_n u_p}\left(1 - e^{-b_1 a_d W}\right) - u_M^2 e^{\frac{-\beta_n u_p}{u_M}}\left(1 - e^{\frac{-b_1 a_d W}{u_M}}\right)\right] \tag{5.192}$$

where $W = x_n - x_p$ is the width of the depletion region and $\beta_n u_p = b_1 a_p(\lambda) x_p$. Just as in the case of the photon produced hole current density in the n region, $\overline{J}'_{qp}$, the depletion region current density, $\overline{J}'_d$, is small compared to $\overline{J}'_{qn}$ because $e^{-\beta_n u_p} \ll 1$ and $e^{\frac{-\beta_n u_p}{u_M}} \ll 1$, if $\beta_n u_p > 1$.

5.9.4 Current-Voltage Relation

Now that $J'_n(x_n)$ [equation (5.191)] and $J'_p(x_n)$ [equation (5.183)] are known, the current density per wavelength is the following.

$$J' = \left(J'_{sn} + J'_{sp}\right)\left(e^{\frac{eV_a}{k_B T}} - 1\right) - J_F\left(\overline{J}'_{qn} + \overline{J}'_{qp} + \overline{J}'_d\right) \tag{5.193}$$

The total current density is obtained by integrating equation (5.193) over all wavelengths,

$$J = J_s\left(e^{\frac{eV_a}{k_B T}} - 1\right) - J_{ph} \tag{5.194}$$

where J_{ph} is the *total photon generated current density*.

$$J_{ph} = \int_o^{\lambda_g} J_F\left[\overline{J}'_{qn} + \overline{J}'_{qp} + \overline{J}'_d\right]d\lambda \tag{5.195a}$$

$$J'_{ph}(\lambda) = J_F\left[\overline{J}'_{qn} + \overline{J}'_{qp} + \overline{J}'_d\right] \tag{5.195b}$$

The upper limit on the integral in equation (5.195a), λ_g corresponds to the bandgap energy, E_g.

$$\lambda_g = \frac{hc_o}{E_g} \tag{5.196}$$

For $\lambda > \lambda_g$, the photons do not have sufficient energy to produce an electron-hole pair so that $J'_{qn}(\lambda) = J'_{qp}(\lambda) = \overline{J}'_d(\lambda) = 0$, for $\lambda > \lambda_g$. Also,

$$J_s = J_{sn} + J_{sp} \tag{5.197}$$

$$J_{sn} = \int_o^{\infty} J'_{sn}\,d\lambda \tag{5.198}$$

$$J_{sp} = \int_{o}^{\infty} J'_{sp}\, d\lambda \tag{5.199}$$

where J_{sn} is given by equation (5.120), where $u_p = \dfrac{\ell_p - x_p}{L_n}$, and J_{sp} is given by equation (5.122), where $u_n = \dfrac{\ell_n - x_n}{L_p}$.

The λ integration in equation (5.195) is complicated because the β parameters in equation (5.159) for $\overline{J}'_{qn}$, and equation (5.184) for $\overline{J}'_{qp}$, and equation (5.192) for $\overline{J}'_{d}$, depend upon the absorption coefficient, which is a function of wavelength. Therefore, a numerical integration is required.

The total current density consists of the current density resulting from the potential, V_a, which is the first term in equation (5.194). This is the current density that occurs for the unilluminated case and is called the *dark current*. The current density, J_{ph}, is the photon produced current density and is in the opposite direction to the dark current. As stated earlier, this separation of the total current density into two independent parts is a property of the governing second order, linear differential equation [equation (5.140) or 5.168)] with constant coefficients. The solution consists of the homogeneous equation solution, which produces the dark current result, and the particular solution, which produces the photon generated current result.

In equation (5.194) the dark current is for the ideal p-n junction. However, for a real p-n junction, the empirical J–V_a relation [equation (5.139)] for the dark current should be used. Thus, the current-voltage relation for an illuminated p-n junction is the following.

$$\boxed{J = J_s\left[e^{\frac{eV_a}{A_o k_B T}} - 1\right] - J_{ph}} \tag{5.200}$$

The only difference between the current density-voltage relation for a p-n junction in the dark [equation (5.123)] and under illumination [equation (5.194)] is the additional photon generated current term. In Figure 5.12, $\dfrac{J}{J_s}$ is shown as a function of $\dfrac{eV_a}{A_o k_B T}$ for several values of $\dfrac{J_{ph}}{J_s}$. The unilluminated case is described by the $\dfrac{J_{ph}}{J_s} = 0$

curve. When $\frac{J_{ph}}{J_s} > 0$, a portion of the $\frac{J}{J_s}$ curve occurs in the fourth guardant. In this quadrant, the current is moving in the opposite direction to the potential drop or in other words, opposite to the electric field. Thus, work is being done and as a result, electrical power output occurs. The usual way for presenting the current-voltage curve for a PV cell is to plot –J as a function of V_a. Thus, for a PV cell the J vs. V_a result is presented as shown in Figure 5.12b.

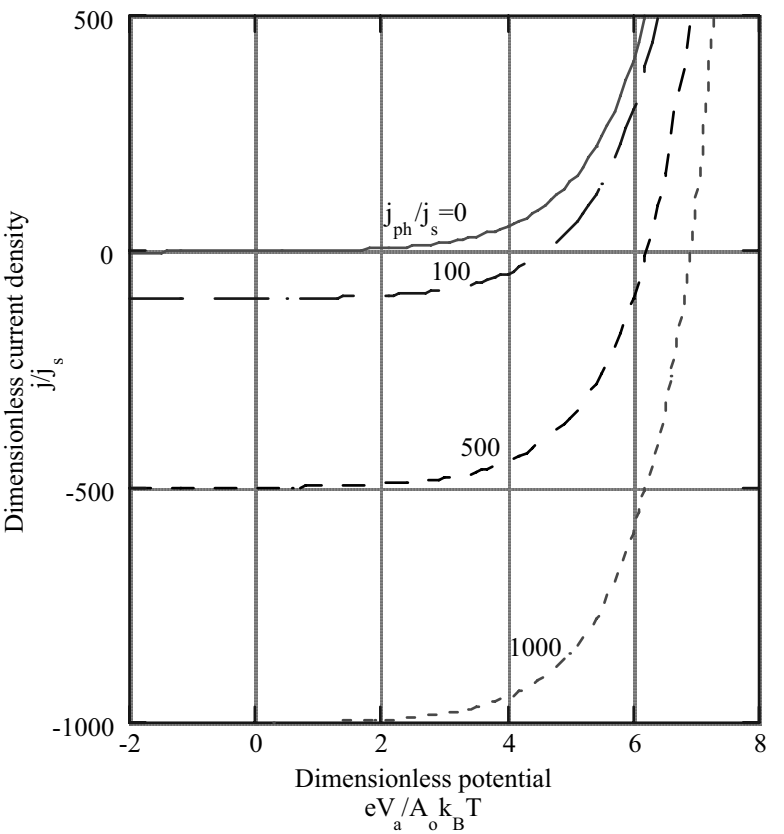

Figure 5.12a) - Non-PV presentation of current-voltage relation for ideal p-n junction with and without illumination at several values of the ratio of the photon generated current density to the saturation current density, j_{ph}/j_s.

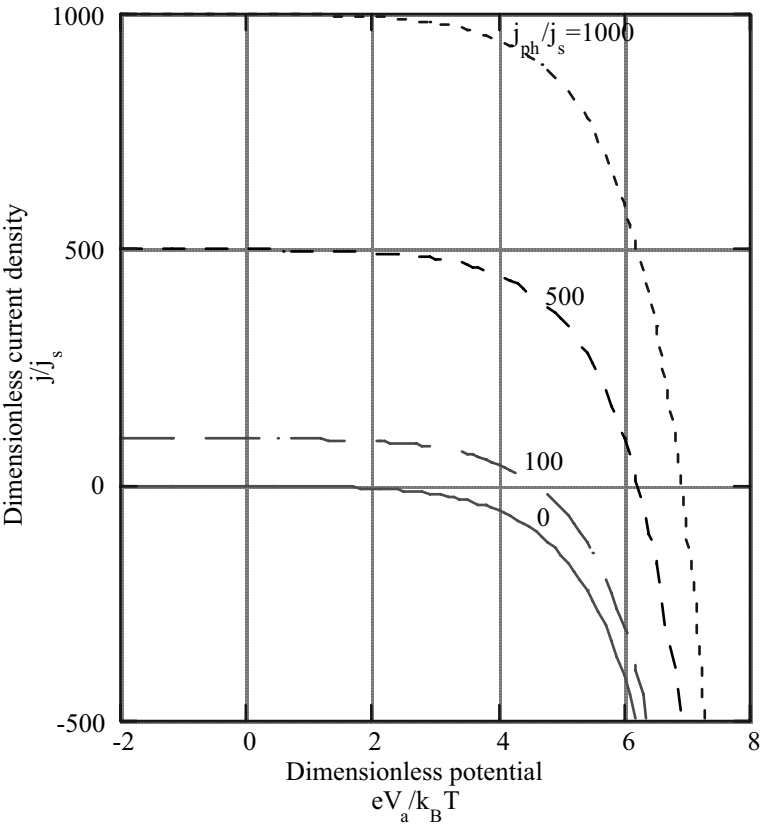

Figure 5.12b) - PV presentation of current-voltage relation for ideal p-n junction with and without illumination at several values of the ratio of the photon generated current density to the saturation current density, j_{ph}/j_s.

5.10 Quantum Efficiency and Spectral Response

Two important and related quantities used to describe the performance of a PV cell are the *quantum efficiency*, η_Q, and the *spectral response*, Sr. These wavelength dependent quantities can be used to calculate the PV array power output and efficiency, as shown in Section 5.12.

In section 5.9.1, the quantity, J_F [equation (5.161)] is introduced. It is the maximum possible current density that can be produced by the incident photon flux. The ratio, $\frac{J'_{ph}}{J_F}$, is the *internal quantum efficiency*,

$$\eta_Q(\lambda) \equiv \frac{J'_{ph}}{J_F} = \frac{hc_o J'_{ph}(\lambda)}{e(1-R_i)\lambda q_i(\lambda)} \tag{5.201}$$

where $R_i = R_n$ if photons are incident on the n side of the junction, and $R_i = R_p$ is photons are incident on the p side of the junction. Also, $b_o = ½$ has been used in equation (5.161). Equation (5.201) is called the internal quantum efficiency since it is based upon the photon flux that enters the semiconductor. Obviously, $\eta_Q(\lambda) \le 1$. The *external quantum efficiency*, η'_Q, is based upon the photon flux that is incident on the semiconductor.

$$\eta'_Q(\lambda) \equiv \frac{hc_o J'_{ph}(\lambda)}{e\lambda q_i(\lambda)} = (1-R_i)\eta_Q(\lambda) \tag{5.202}$$

The spectral response, Sr, is defined as the ratio of the photon produced current density per wavelength, J'_{ph}, to the incident power density per wavelength, q_i.

$$Sr(\lambda) \equiv \frac{J'_{ph}}{q_i(\lambda)} \quad \frac{\text{amps}}{\text{watt}} \tag{5.203a}$$

Thus,

$$Sr(\lambda) = \frac{e\lambda}{hc_o}\eta'_Q(\lambda) = \frac{e\lambda}{hc_o}(1-R_i)\eta_Q(\lambda) \tag{5.203b}$$

If every incident photon at wavelength λ produced current, then $\eta'_Q(\lambda) = 1$, and $Sr(\lambda) \sim \lambda$.

As has been shown, the photon produced current density is made up of the photon generated current density in the neutral regions and the depletion region; it is given by equation (5.195b). Therefore,

$$\eta_Q(\lambda) = \overline{J}'_{qn} + \overline{J}'_{qp} + \overline{J}'_d \tag{5.204}$$

where $\overline{J}'_{qn}$ is given by equation (5.159), $\overline{J}'_{qp}$ by equation (5.184), and $\overline{J}'_{d}$ by equation (5.192). It is the absorption coefficient, a(λ), that determines the wavelength dependence of η_Q. The absorption coefficient appears in the parameters β_n and β_p in equations (5.159) and (5.184). If equation (5.67) is used to approximate the absorption coefficient for a direct bandgap semiconductor, then the optical depth parameters are the following,

$$\beta_n = b_l L_n a_o \sqrt{E_g}\left(\frac{E}{E_g}-1\right)^{1/2} = \beta_{no}\left(\frac{E}{E_g}-1\right)^{1/2} \tag{5.205a}$$

$$\beta_p = b_l L_p a_o \sqrt{E_g}\left(\frac{E}{E_g}-1\right)^{1/2} = \beta_{po}\left(\frac{E}{E_g}-1\right)^{1/2} \tag{5.205b}$$

where

$$\beta_{no} = b_l L_n a_o \sqrt{E_g} \tag{5.206a}$$

$$\beta_{po} = b_l L_p a_o \sqrt{E_g} \tag{5.206b}$$

Equations (5.205) assume that the absorption coefficient is the same in both the p and n regions. Also assuming the absorption coefficient is the same in the depletion region the quantum efficiency can be calculated as a function $\frac{E}{E_g}$ for given values of β_{no}, β_{po}, ϕ_n, ϕ_p, u_p, u_n, and $\frac{W}{L_n}$. In Figure 5.13 the contribution to η_Q from each region of the p-n junction is shown as a function of $\frac{E}{E_g} = \frac{\lambda}{\lambda_g}$. The values chosen for the various parameters are given in the figure caption. Part a) applies for a TPV cell where the incident radiation is isotropic and $b_l = 1.5$. Part b) applies for a solar cell where all the incident radiation is at zero angle of incidence and $b_l = 1$. Obviously, in this case, a significant reduction in the quantum efficiency occurs for the TPV cell under isotropic illumination. However, as pointed out earlier, if u_p and u_n are reduced, the quantum efficiencies for the two radiation conditions are the same.

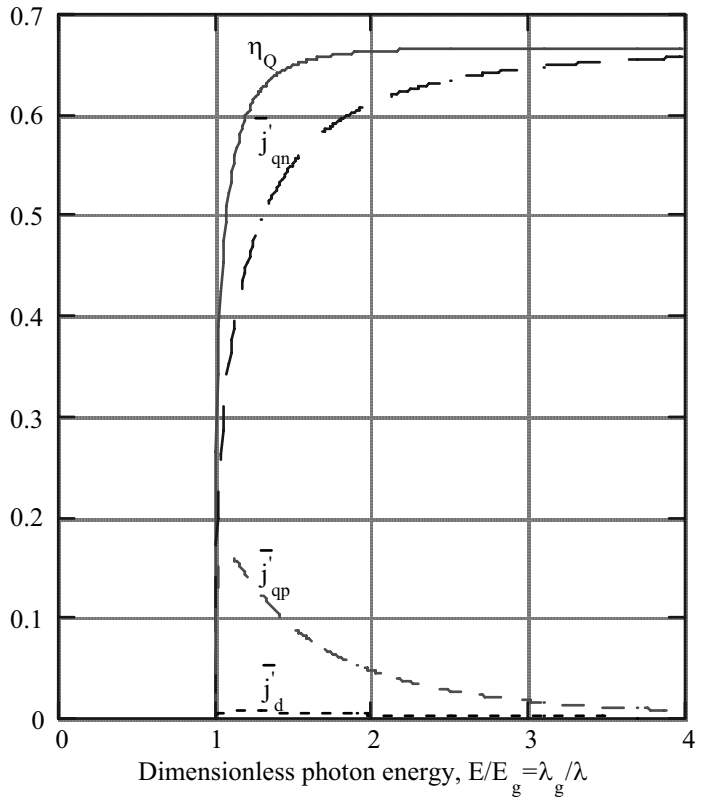

Figure 5.13a) - Contribution to the internal quantum efficiency, η_Q, of the top p region, $\bar{j}'_{qn}$, the depletion region, $\bar{j}'_{d}$, and the bottom n region, $\bar{j}'_{qp}$ of an illuminated p-n junction for isotropic intensity, (b=1.5). Parameters are the following, u_p=.05, u_n=.1, w/L_n=.001, $\phi_n=\phi_p=0$, β_{no}=50., β_{po}=25.

It is the top region, in this case the p region, that is the major contributor to the quantum efficiency even though its dimensionless thickness, u_p, is less than the bottom n region dimensionless thickness, u_n. Reducing u_p even further results in a slight increase in η_Q since the n region contribution increases. For the parameters used in Figure 5.13, the depletion region contribution is negligible. Increasing the absorption coefficient parameters β_{no} and β_{po} from those in Figure 5.13 results in a negligible increase in η_Q.

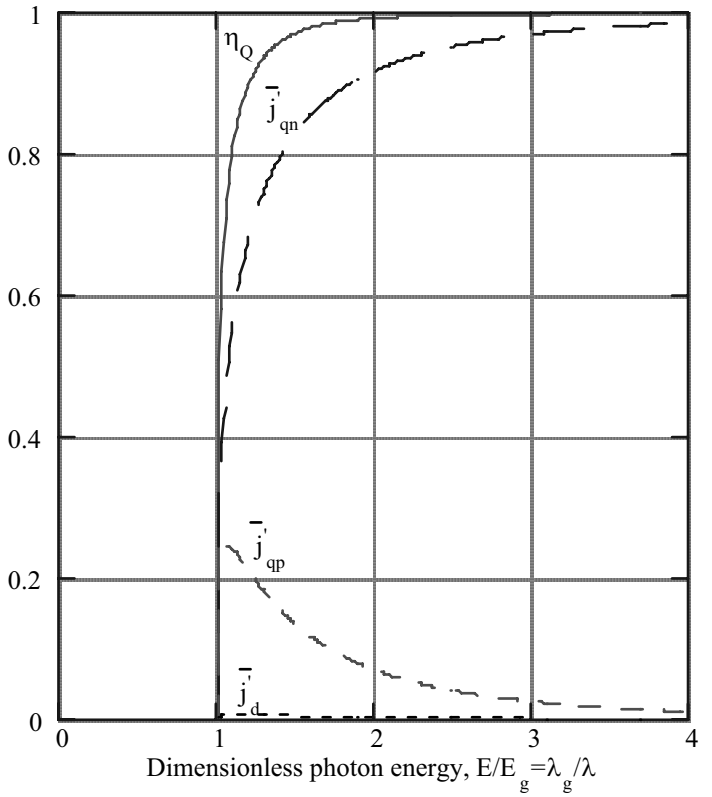

Figure 5.13b) - Contribution to the internal quantum efficiency, η_Q, of the top p region, $\bar{j}'_{qn}$, the depletion region, $\bar{j}'_{d}$, and the bottom n region, $\bar{j}'_{qp}$ of an illuminated p-n junction for normal incident intensity (b_l=1.). Parameters are the following, u_p=.05, u_n=.1, w/L_n=.001, $\phi_n=\phi_p=0$, β_{no}=50., β_{po}=25.

In Figure 5.13, the surface recombination parameters ϕ_n and ϕ_p are zero. However, if surface recombination is important, there is a significant reduction in the quantum efficiency. This is illustrated in Figure 5.14 where ϕ_n = 10, and ϕ_p = 0. For $\phi_p > 0$ there is a negligible affect on η_Q. The major cause of the reduction in η_Q is the front surface recombination.

As Figure 5.13 and Figure 5.14 show, the asymptotic value for η_Q is the asymptotic value of $\bar{J}'_{qn}$, which is given by equation (5.163).

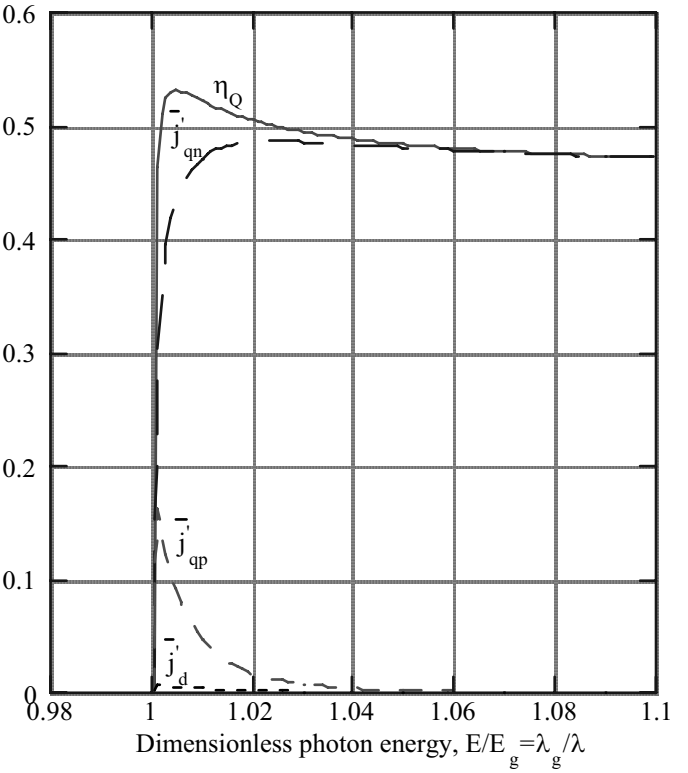

Figure 5.14 Effect of front surface recombination on the internal quantum efficiency, η_Q, of p-n junction illuminated with isotropic radiation, $b_1=1.5$. Contributions from the p top region, $\bar{j}'_{qn}$, from depletion region, $\bar{j}'_{d}$ and from bottom n region, $\bar{j}'_{qp}$. All parameters are the same as figure 5.13 except the front surface recombination parameter which is $\phi_n=10$.

$$\lim_{\frac{E}{E_g}\to\infty} \eta_Q = \frac{1}{b_1\left(\cosh u_p + \phi_n \sinh u_p\right)} \tag{5.207}$$

Thus, for large values of the absorption coefficient ($\frac{E}{E_g} \to \infty$), the quantum efficiency depends upon only the top surface p region properties and the condition of the incident intensity, which is determined by the value of b_1.

As discussed in Section 5.8, the current-voltage relation for a PV cell in the dark depends upon the ideality factor, A_o, and the saturation current density, J_s. Both of these parameters can be determined experimentally. For an illuminated PV cell, the spectral response, $Sr(\lambda)$ can also be measured experimentally. The experimentally measured parameters A_o, J_s, and $Sr(\lambda)$ along with two additional resistance parameters that also can be determined experimentally, provide all the necessary information required to compute the power output and efficiency of a PV cell. The resistances are defined in the next section. Following that the power output and efficiency are calculated in terms of these parameters.

5.11 Equivalent Circuit for PV Cells

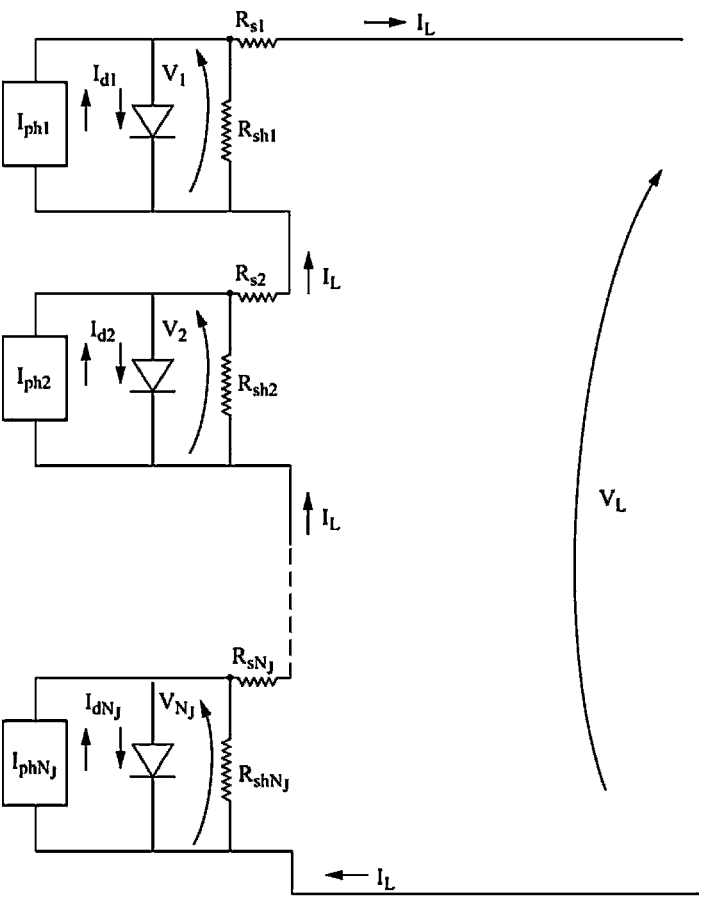

Figure 5.15.—Electrical equivalent circuit for a photovoltaic array of N_J series connected junctions including series, R_s, and shunt, R_{sh}, resistances.

So far, electrical resistance losses have been neglected in the discussion of PV cell performance. However, for low bandgap energy TPV cells, I^2R resistance losses are significant since photon generated current densities are large. Resistance losses result from the finite conductivity of the semiconductor, the resistance associated with contacts between the semiconductor and the metal electrical leads and shunt resistance paths at the cell edges or along defects within the semiconductor. These resistance losses can be accounted for by using an electrical equivalent circuit as shown in Figure 5.15.

For most TPV applications, a number of p-n junctions are connected in series to form a PV array. This array is formed on a single piece of semiconductor material. An example of such an array is the monolithic interconnected module (MIM) [15]. The equivalent circuit in Figure 5.15 is a model of such an array consisting of N_J junctions.

The photon generated current for each junction is represented by the current source $I_{ph} = A_a J_{ph}$, where A_a is the junction *active area*, and J_{ph} is the photon generated current density. The active area is the total area, A_c, minus the area of the metal grids on the top surface that conduct the current. The dark current for each junction, I_d, which is the product of the dark current density [equation (5.139)] and the total junction area, A_c, is given by the diode equation.

$$I_d = A_c J_s \left[\exp\left(\frac{eV}{A_o k_B T} \right) - 1 \right] \tag{5.208}$$

Series resistance losses are represented by the *series resistance*, R_s, and shunt resistance losses are represented by the *shunt resistance*, R_{sh}.

Applying Kirchhoff's voltage law to the current loop of the equivalent circuit yields the following result.

$$\sum_{i=1}^{N_J} V_i - I_L \sum_{i=1}^{N_J} R_{si} - V_L = 0 \tag{5.209}$$

Also, for current continuity,

$$I_L = I_{ph1} - I_{d1} - \frac{V_1}{R_{sh1}} = I_{ph2} - I_{d2} - \frac{V_2}{R_{sh2}} \ldots = I_{phN_J} - I_{dV_J} - \frac{V_{N_J}}{R_{shN_J}} \tag{5.210}$$

Now assume that all junctions are identical so that $A_{c1} = A_{c2} = \ldots A_{cN_J} = A_J$, $R_{s1} = R_{s2} = \ldots R_{sN_J} = R_s$, $R_{sh1} = R_{sh2} = \ldots R_{shN_J} = R_{sh}$, $J_{s1} = J_{s2} = \ldots J_{sN_J} = J_s$,

$A_{o1} = A_{o2} = ... A_{oN_J} = A_o$, $T_1 = T_2 = ... T_{N_J} = T_J$, and $I_{ph1} = I_{ph2} = ... I_{phN_J} = I_{ph}$. As a result, $I_{d1} = I_{d2} = ... I_{dN_J} = I_d$, and $V_1 = V_2 = ... V_{N_J} = V$, so that $\sum_{i=1}^{N_J} V_i = N_J V$, and $\sum_{i=1}^{N_J} R_{si} = N_J R_s$. Using equation (5.208) for I_d in equation (5.210) yields the following.

$$I_L = I_{ph} - I_s\left[\exp\left(\frac{eV}{A_o kT}\right) - 1\right] - \frac{V}{R_{sh}} \tag{5.211}$$

Now use $\sum_{i=1}^{N_J} V_i = N_J V$ and $\sum_{i=1}^{N_J} R_{si} = N_J R_s$ in equation (5.209) to obtain an expression for V and then substitute that expression in equation (5.211) to obtain the current-voltage relation for the array.

$$\boxed{\bar{I}_L \equiv \frac{I_L}{I_s} = \frac{\bar{R}_{sh}}{\bar{R}_s + \bar{R}_{sh}}\left[\frac{I_{ph}}{I_s} - \exp\left(\frac{\bar{V}_L}{N_J} + \bar{R}_s \bar{I}_L\right) + 1\right] - \frac{\bar{V}_L}{N_J\left(\bar{R}_s + \bar{R}_{sh}\right)}} \tag{5.212}$$

Where $\bar{V}_L$ is the dimensionless voltage, $\bar{R}_s$ is the dimensionless series resistance, and I_s is the saturation current.

$$\bar{V}_L = \frac{eV_L}{A_o k_B T} \tag{5.213a}$$

$$I_s = A_J J_s \tag{5.213b}$$

$$\bar{R}_s = \frac{eR_s I_s}{A_o k_B T} \tag{5.213c}$$

$$\bar{R}_{sh} = \frac{eR_{sh} I_s}{A_o k_B T} \tag{5.213d}$$

Equation (5.212) is the current-voltage relation used to describe an illuminated PV array. In the next section it is used to calculate the PV array electrical output power and efficiency. For a single junction ($N_J = 1$), and if $R_s = 0$, $R_{sh} \to \infty$, and $A_c = A_a$, then

equation (5.212) reduces to the current-voltage relation for a PV cell without resistance losses given by equation (5.200).

The series resistance, R_s, and shunt resistance, R_{sh}, can be determined experimentally. With the PV cell under illumination, measured values of I_L vs. V_L can be used to calculate R_s and R_{sh}. And, as stated earlier, I_L vs. V_L data taken in the dark can be used to obtain values for A_o and J_s.

If $R_{sh} \to \infty$, then equation (5.212) can be rewritten as follows.

$$\bar{I}_L = \frac{I_{ph}}{I_s} - \exp\left(\frac{\bar{V}_L}{N_J} + \bar{R}_s \bar{I}_L\right) + 1 \qquad R_{sh} \to \infty \tag{5.214}$$

When $\bar{I}_L \bar{R}_s$ becomes significant in equation (5.214), both the $\frac{I_{ph}}{I_s}$ term and the exponential term are large and their difference is much smaller. As a result, the following approximation can be made.

$$\frac{I_{ph}}{I_s} - \exp\left(\frac{\bar{V}_L}{N_J} + \bar{R}_s \bar{I}_L\right) \approx 0 \tag{5.215}$$

As a result, equation (5.215) yields the following current voltage relation.

$$\bar{I}_L = \frac{1}{\bar{R}_s}\left[\ln\left(\frac{I_{ph}}{I_s}\right) - \frac{\bar{V}_L}{N_J}\right] \tag{5.216}$$

Thus, for significant R_s the PV array behaves like a resistor ($I = \frac{V}{R}$) where the resistance is a negative number. This is illustrated in Figure 5.16, where equation (5.212) is shown for infinite R_{sh}, $N_J = 1$, $\frac{I_{ph}}{I_s} = 10^6$, and several values of $\bar{R}_s$. As can be seen, even for rather small values of $\bar{R}_s$, the PV cell begins to behave like a negative resistor.

In addition, the current for $V_L = 0$, which is called the *short circuit current*, I_{sc}, decreases as R_s increases. An expression for the short circuit current is found by setting $\bar{V}_L = 0$ in equation (5.212).

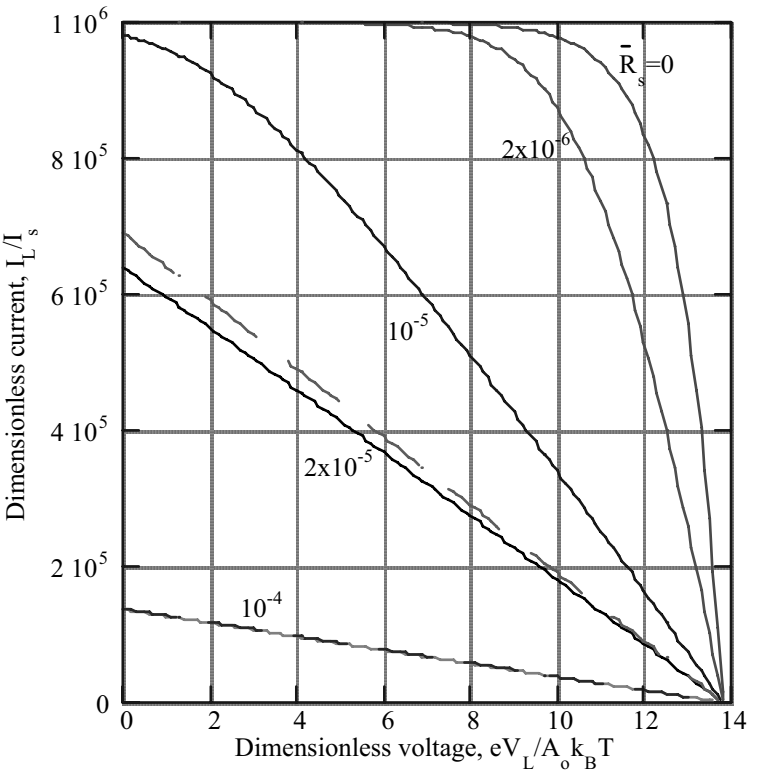

Figure 5.16 Effect of series resistance, R_s on the current-voltage relation of illuminated p-n junction for $N_j=1$, $I_{ph}/I_s=10^6$ and several values of the dimensionless series resistance, $\bar{R}_s=eR_sI_s/A_ok_BT$. The dashed lines are given by Equation (5.216) and the shunt resistance is infinite.

$$\bar{I}_{sc}=\frac{\bar{R}_{sh}}{\bar{R}_s+\bar{R}_{sh}}\left[\frac{I_{ph}}{I_s}-\exp\left(\bar{R}_s\bar{I}_{sc}\right)+1\right] \tag{5.217a}$$

Thus, if $\bar{R}_{sh}\gg\bar{R}_s$ then $\bar{I}_{sc}$ is independent of $\bar{R}_{sh}$. If $\bar{R}_s=0$ then,

$$\bar{I}_{sc}=\frac{I_{ph}}{I_s}\qquad\qquad \bar{R}_s=0 \tag{5.217b}$$

As already mentioned, series resistance is a critical issue for low bandgap energy TPV cells since the photon generated current density, J_{ph}, is large. As a result, the $I_L^2 R_s$ loss is significant unless $R_s \to 0$.

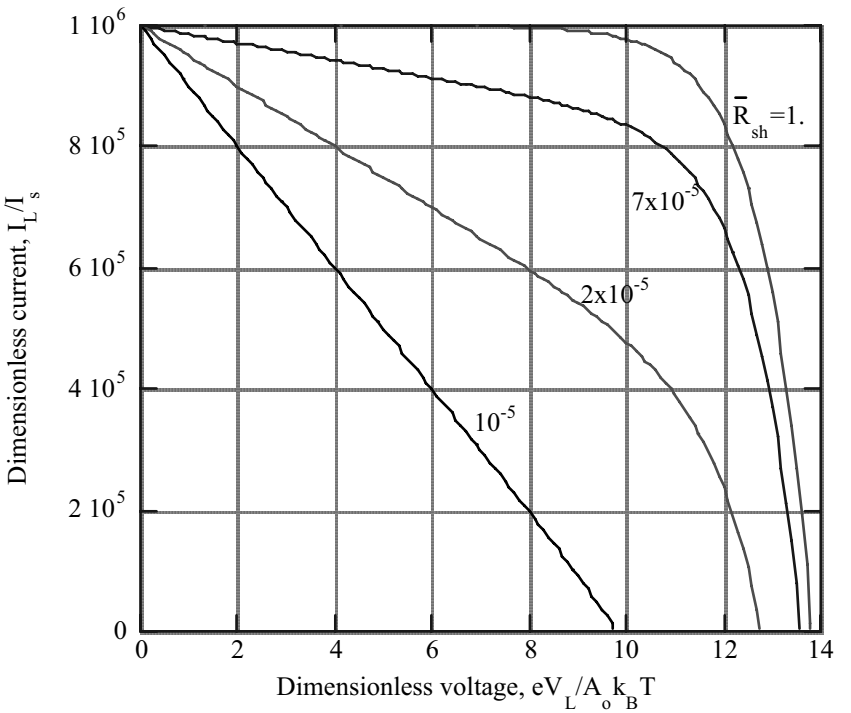

Figure 5.17 - Effect of shunt resistance, R_{sh} on the current-voltage relation of illuminated p-n junction for N_j=1, $I_{ph}/I_s=10^6$ and several values of the dimensionless shunt resistance, $\bar{R}_{sh}=eR_{sh}I_s/A_o k_B T$. The series resistance is zero.

Figure 5.17 shows the effect of shunt resistance, R_{sh}, on the current-voltage relation for $R_s = 0$, and $N_J = 1$. As $\bar{R}_{sh}$ decreases, the voltage at $I_L = 0$, which is called the *open circuit* voltage, V_{oc}, decreases. Eventually, the $\dfrac{\bar{V}_L}{(R_s + R_{sh})}$ term in equation (5.212)

dominates, and the PV cell behaves like a resistor with negative resistance similar to the case for large series resistance.

A relation for the dimensionless open circuit voltage, $\bar{V}_{oc}$, is found by setting $\bar{I}_L = 0$ in equation (5.212).

$$\bar{V}_{oc} \equiv \frac{eV_{oc}}{A_o kT} = N_J \bar{R}_{sh} \left[\frac{I_{ph}}{I_s} - \exp\left(\frac{\bar{V}_{oc}}{N_J} \right) + 1 \right] \tag{5.218a}$$

Thus, $\bar{V}_{oc}$ is independent of the series resistance. For $\bar{R}_{sh} \to \infty$, the term in brackets must vanish. As a result,

$$\bar{V}_{oc} = N_J \ln\left[\frac{I_{ph}}{I_s} + 1 \right] \qquad \bar{R}_{sh} \to \infty \tag{5.218b}$$

To summarize, large series resistance reduces the short circuit current but does not affect the open circuit voltage. Small shunt resistance reduces the open circuit voltage but does not affect the short circuit current. Both large series resistance and small shunt resistance reduce the PV cell efficiency.

5.12 PV Cell Efficiency and Power Output

Efficiency and power output are the two PV cell parameters required to calculate the performance of a TPV system. The electrical power output is the product of the voltage, V_L, and current, I_L, that is supplied to the load,

$$P_{EL} = V_L I_L \tag{5.219}$$

where I_L is a function of V_L. To determine the condition for maximum P_{EL}, the standard maximization procedure is used. Namely, differentiate equation (5.219) with respect to V_L and set the result equal to zero.

$$\frac{dP_{EL}}{dV_L} = \frac{dP_{EL}}{dV} \frac{dV}{dV_L} = 0 \tag{5.220}$$

It can be shown (problem 5.11) that $\frac{dV}{dV_L} > 0$ for all V_L. As a result, to satisfy equation (5.220)

$$\frac{dP_{EL}}{dV} = 0 \tag{5.221}$$

for a maximum P_{EL}. Therefore, using equation (5.209) for V_L in equation (5.219) for identical junctions yields the following result.

$$\frac{dP_{EL}}{dV} = N_J\left[\left(V - 2I_L R_s\right)\frac{dI_L}{dV} + I_L\right] \tag{5.222}$$

Using equation (5.211) for I_L, the equation for the voltage, V_M, to obtain maximum power is obtained after a great deal of algebra.

$$\left[\left(1+\gamma_2\right)\left(\frac{I_{ph}}{I_s}+1\right) - \gamma_3\bar{V}_M\right]e^{-\bar{V}_M} + \gamma_1\left[\frac{I_{ph}}{I_s}+1-e^{\bar{V}_M}\right] - \left[1+\gamma_2\right]\left[\bar{V}_M+1\right] = 0 \tag{5.223a}$$

Equation (5.223a) can be written in terms of $\bar{V}_{oc}$ by replacing $(\frac{I_{ph}}{I_s}+1)$ using equation (5.218a),

$$\left[\left(1+\gamma_2\right)\left(\frac{\bar{V}_{oc}}{N_J\bar{R}_{sh}} + e^{\frac{\bar{V}_{oc}}{N_J}}\right) - \gamma_3\bar{V}_M\right]e^{-\bar{V}_M} + \gamma_1\left[\frac{\bar{V}_{oc}}{N_J\bar{R}_{sh}} + e^{\frac{\bar{V}_{oc}}{N_J}} - e^{\bar{V}_M}\right] - \left[1+\gamma_2\right]\left[\bar{V}_M+1\right] = 0 \tag{5.223b}$$

where

$$\bar{V}_M = \frac{eV_M}{A_o k_B T} \tag{5.224}$$

$$\gamma_1 = \frac{2eR_s I_s}{A_o k_B T} = 2\bar{R}_s \tag{5.225}$$

$$\gamma_2 = \frac{2R_s}{R_{sh}}N_J \tag{5.226}$$

$$\gamma_3 = \frac{2A_o k_B T\left(R_s + R_{sh}\right)}{eI_s R_{sh}^2} = \frac{2}{\bar{R}_{sh}}\frac{\left(R_s + R_{sh}\right)}{R_{sh}} \tag{5.227}$$

Once $\bar{V}_M$ is obtained from the solution to equation (5.223), the power output, P_{EL} can be determined,

$$P_{EL} = V_{LM} I_{LM} = N_J \left(V_M - R_s I_{LM} \right) I_{LM} \tag{5.228}$$

where V_{LM} is obtained from equation (5.209) and I_{LM} is the load current when $V = V_M$. From equation (5.211)

$$\bar{I}_{LM} \equiv \frac{I_{LM}}{I_s} = \frac{I_{ph}}{I_s} - e^{\bar{V}_M} + 1 - \frac{\bar{V}_M}{\bar{R}_{sh}} \tag{5.229a}$$

Equation (5.229a) can be written in terms of $\bar{V}_{oc}$ by using equation (5.218a).

$$\bar{I}_{LM} = \frac{\bar{V}_{oc}}{N_J \bar{R}_{sh}} + e^{\frac{\bar{V}_{oc}}{N_J}} + e^{\bar{V}_m} - \frac{\bar{V}_m}{\bar{R}_{sh}} \tag{5.229b}$$

Equation (5.228) can be rewritten as a function of $\bar{V}_M$ and $\bar{I}_{LM}$ as follows.

$$p_{EL} \equiv \frac{P_{EL}}{A_c} = \frac{A_o k_B T}{e} \frac{I_{LM}}{A_c} N_J \left[\bar{V}_M - \bar{R}_s \bar{I}_{LM} \right] \tag{5.230}$$

The quantity p_{EL} is the *output power density* in units of watts per cm^2 of PV array area, where A_c is the array total area. A dimensionless power density can be defined as follows.

$$\bar{p}_{EL} \equiv \frac{e p_{EL} A_c}{A_o k_B T I_s} = \bar{I}_{LM} N_J \left[\bar{V}_M - \bar{R}_s \bar{I}_{LM} \right] \tag{5.231}$$

The quantity $\bar{I}_{LM}$ is a function of $\bar{V}_M$ [equation (5.229)] and $\bar{V}_M$ is a function of $\frac{I_{ph}}{I_s}$ and the three γ parameters [equation (5.223)]. Thus, $\bar{p}_{EL}$ is a function of $\frac{I_{ph}}{I_s}$ and the three γ parameters, which are functions of $\bar{R}_s$ and $\bar{R}_{sh}$.

Figure 5.18 shows the solution to equation (5.223) for $\bar{V}_M$ as a function of $\frac{I_{ph}}{I_s}$ on a logarithmic scale for several values of $\bar{R}_s$ with $\bar{R}_{sh} \to \infty$ and $N_J = 1$. As can be seen $\bar{V}_M$ is nearly a linear function of $\ln(\frac{I_{ph}}{I_s})$ for $\bar{R}_s = 0$. For increasing $\bar{R}_s$ the PV cell begins to behave as a negative resistor, as already noted in the discussion of Figure 5.16.

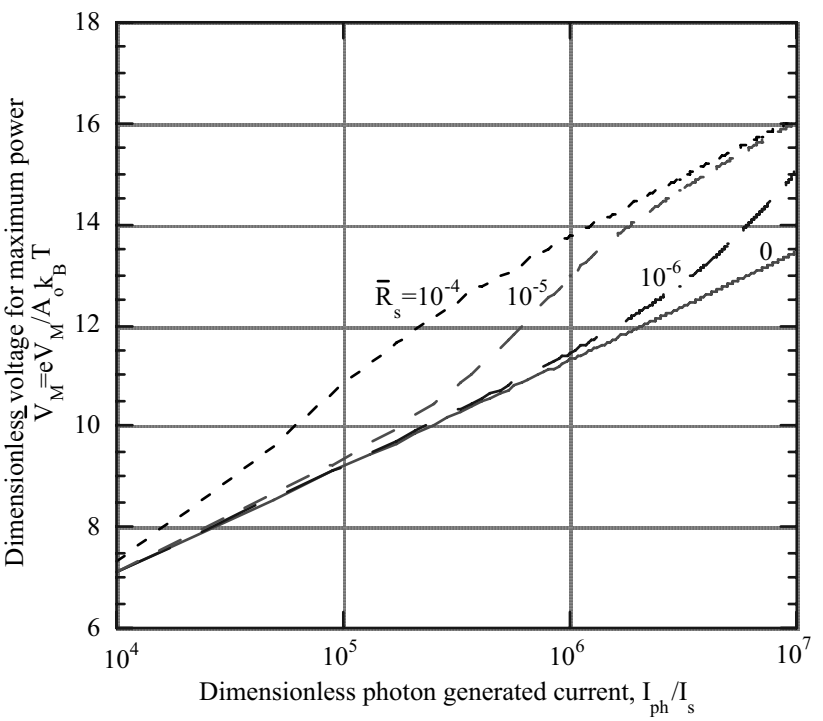

Figure 5.18 - Dimensionless voltage, $\bar{V}_M$ for maximum power output as a function of the dimensionless photon generated current, I_{ph}/I_s for several values of the dimensionless series resistance, $\bar{R}_s$, with shunt resistance, $\bar{R}_{sh} \to \infty$, and $N_j = 1$.

For large series resistance, equation (5.216) applies so that (problem 5.12)

$$\bar{V}_{LM} \approx \frac{N_J}{2} \ln\left(\frac{I_{ph}}{I_s}\right) \approx \frac{\bar{V}_{oc}}{2} \qquad \begin{matrix} \bar{R}_{sh} > 10^{-3} \\ \bar{R}_s > 10^{-5} \end{matrix} \tag{5.232}$$

and

$$\bar{p}_{EL} \approx \frac{N_J}{4} \frac{\left[\ln\left(\frac{I_{ph}}{I_s}\right)\right]^2}{\bar{R}_s} \approx \frac{N_J}{4} \frac{\bar{V}_{oc}^2}{\bar{R}_s} \tag{5.233}$$

The shunt resistance has no effect on $\bar{V}_{LM}$ until $\bar{R}_{sh} < 10^{-3}$. For $\bar{R}_{sh} \to 0$, the last term in equation (5.212) becomes large and $\frac{I_L}{I_s}$ can be approximated as a negative resistor, just as the case for large $\bar{R}_s$.

$$\frac{I_L}{I_s} \approx \frac{I_{ph}}{I_s} - \frac{\bar{V}_L}{N_J \bar{R}_{sh}} \qquad \begin{matrix} \bar{R}_s = 0 \\ \bar{R}_{sh} \ll 1 \end{matrix} \tag{5.234}$$

Thus, the dimensionless maximum power density is the following (problem 5.13).

$$\bar{p}_{EL} = \frac{N_J}{4}\left(\frac{I_{ph}}{I_s}\right)^2 \bar{R}_{sh} \qquad \begin{matrix} \bar{R}_s = 0 \\ \bar{R}_{sh} \ll 1 \end{matrix} \tag{5.235}$$

For a TPV system, the photovoltaic efficiency is defined as follows (see Section 6.5),

$$\boxed{\eta_{PV} \equiv \frac{P_{EL}}{\bar{Q}_c} = \frac{V_{LM} I_{LM}}{\bar{Q}_c}} \tag{5.236}$$

where P_{EL} is the electrical power output and $\bar{Q}_c$ is the useful radiation incident on the PV array. Assuming the incident flux, $q_i(\lambda)$ is uniform over the array area A_c, then $\bar{Q}_c$ is the following.

$$\bar{Q}_c = A_c \int_o^{\lambda_g} q_i(\lambda)\, d\lambda \tag{5.237}$$

Since the upper limit on the integration is $\lambda_g = \frac{hc_o}{E_g}$, $\bar{Q}_c$ includes only photons that can produce electron-hole pairs. For solar PV application, the efficiency is based upon all incident photons. In that case, the upper limit on the integration is infinity. However, in a TPV system, spectral control is employed to produce only incident photons that can produce electron-hole pairs. Thus, the efficiency for producing these useful photons is attributed to the method of spectral control, rather than the PV array (see Section 6.5).

In calculating P_{EL}, it is useful to define a quantity called the *fill factor*, FF, as follows,

$$FF \equiv \frac{V_{LM} I_{LM}}{V_{oc} I_{sc}} \le 1 \tag{5.238}$$

where V_{oc} is the open circuit voltage and I_{sc} is the short circuit current. The maximum possible value of P_{EL} occurs when $I_{LM} = I_{sc}$ for $V_{LM} = V_{oc}$ or FF = 1. In that case the I_L vs. V_L plot (Figures 5.16 and 5.17, for example) would be shaped like a rectangle with I_{sc} the height, and V_{oc} the width. Thus, the value of FF approaches 1 as the shape of the I_L vs. V_L plot becomes rectangular.

Using the definition of the fill factor, P_{EL} can be expressed as follows.

$$P_{EL} = FF V_{oc} I_{sc} \tag{5.239}$$

Using equation (5.228), the fill factor can be expressed as follows.

$$FF = \frac{N_J \bar{I}_{LM} \left[\bar{V}_M - \bar{R}_s \bar{I}_{LM} \right]}{\bar{V}_{oc} \bar{I}_{sc}} \tag{5.240}$$

The maximum load current, $\bar{I}_{LM}$, is given by equation (5.229) and $\bar{V}_M$ is obtained from the solution of equation (5.223). Both of these quantities are functions of $\frac{I_{ph}}{I_s}$, $\bar{R}_s$, and $\bar{R}_{sh}$. The open circuit voltage, $\bar{V}_{oc}$, is given by equation (5.218) and the short circuit current, $\bar{I}_{sc}$, is given by equation (5.217), which are also functions of $\frac{I_{ph}}{I_s}$, $\bar{R}_s$, and

$\bar{R}_{sh}$. For most useful PV cells, R_{sh} is large so that the approximation $\bar{R}_{sh} \to \infty$ can be made. In that case $\bar{V}_{oc}$ is given by equation (5.218b) and from equation (5.217a) for $\bar{R}_{sh} \gg \bar{R}_s$,

$$\bar{I}_{sc} = \frac{I_{ph}}{I_s} + 1 - \exp\left(\bar{R}_s \bar{I}_{sc}\right) \qquad R_{sh} \gg R_s \tag{5.241}$$

Thus equation (5.241) is a transcendental equation for I_{sc} as a function of $\frac{I_{ph}}{I_s}$ and $\bar{R}_s$.

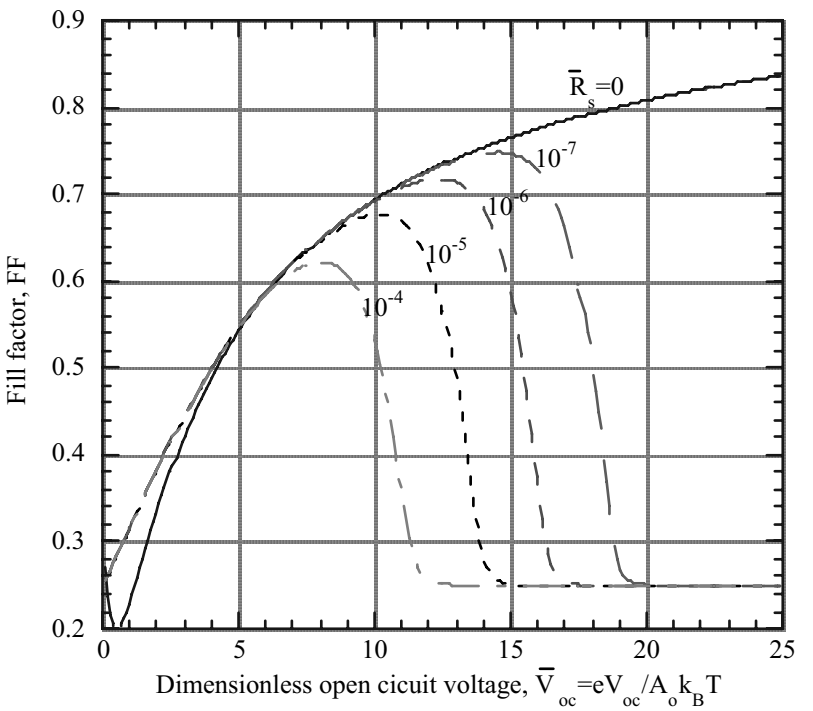

Figure 5.19 - Fill factor, FF, as a function of dimensionless open circuit voltage, $\bar{V}_{oc}$, for infinite shunt resistance, R_{sh}, N_j=1 and various dimensionless series resistances, $\bar{R}_s$. Solid line is approximate result for $\bar{R}_s$=0 given by equataion (5.242).

Since $\frac{I_{ph}}{I_s}+1=\exp\left(\frac{\overline{V}_{oc}}{N_J}\right)$ for $R_{sh}\to\infty$, all the quantities that appear in the equation for FF can be expressed as functions of $\frac{I_{ph}}{I_s}$ and $\overline{R}_s$, or $\frac{\overline{V}_{oc}}{N_J}$ and $\overline{R}_s$. In solar PV applications, FF is generally given as a function of V_{oc}.

In Figure 5.19 the fill factor, FF, is shown as a function of $\overline{V}_{oc}$ for $N_J = 1$. It has been calculated using equation (5.240) where $\overline{I}_{sc}$ is obtained from the solution of equation (5.241), $\overline{V}_n$ from the solution of equation (5.223), and $\overline{I}_{LM}$ from equation (5.229b). As can be seen, the series resistance has a significant negative effect upon the fill factor. For increasing $\overline{V}_{oc}$, the resistance loss term, $\overline{R}_s\overline{I}_{LM}^2$, in equation (5.240) becomes significant and the fill factor begins to decrease. As $\overline{V}_{oc}$ increases further, the PV cell begins to behave as a negative resistor, and the fill factor reaches its asymptotic value of ¼ (problem 5.14). For $\overline{R}_s=0$, $N_J = 1$, and $\overline{V}_{oc} > 5$, the fill factor is closely approximated by the following expression [5].

$$FF=\frac{\overline{V}_{oc}-\ln\left(\overline{V}_{oc}+0.72\right)}{\overline{V}_{oc}+1}\qquad \begin{matrix} N_J=1 \\ \overline{R}_{sh}\to\infty,\ \overline{R}_s=0 \\ \overline{V}_{oc}>5 \end{matrix} \tag{5.242}$$

Consider the low bandgap energy PV cells that are used for TPV applications. For T = 300K, the dimensionless open circuit voltage is the following.

$$\overline{V}_{oc}=38.7\frac{V_{oc}}{A_o}\qquad T=300K \tag{5.243}$$

For TPV cells where $0.5 \le E_g \le 0.75$eV, the open circuit voltage range is approximately $0.2 \le V_{oc} \le 0.6$V. Thus, at T = 300K

$$\frac{7.7}{A_o}\le\overline{V}_{oc}\le\frac{23}{A_o}\qquad T=300K \tag{5.244}$$

Since $1 \le A_o \le 2$, Figure 5.19 shows that for the lowest bandgap energy cells the fill factor will not be affected by $\overline{R}_s$ until $\overline{R}_s \ge 10^{-4}$. However, for the highest bandgap energy cells, $\overline{R}_s$ must be less than 10^{-7} in order to avoid a reduction from the $\overline{R}_s = 0$ fill factor.

Return to the PV efficiency as defined by equation (5.236). Using equation (5.238) η_{PV} becomes the following.

$$\eta_{PV} = \frac{FF V_{oc} I_{sc}}{\bar{Q}_c} \tag{5.245}$$

As will be shown in Chapter 6, the incident flux, q_i, can be written as follows,

$$q_i(\lambda) = g(\lambda)\varepsilon_E(\lambda)e_b(\lambda, T_E) \tag{5.246}$$

where $g < 1$ is a function of the optical cavity geometry and optical properties. If the optical properties of the cavity are independent of λ, then g will also be independent of λ. The emitter spectral emittance is ε_E, and e_b is the black body emissive power. Assume g and ε_E are constants in the range $0 \le \lambda \le \lambda_g$. Therefore,

$$\bar{Q}_c = A_c g \varepsilon_E \int_o^{\lambda_g} e_b(\lambda, T_E)\, d\lambda = A_c g \varepsilon_E \sigma_{sb} F_{o-\lambda_g T_E} T_E^4 \tag{5.247}$$

where $F_{o-\lambda_g T_E}$ is a function of the dimensionless bandgap energy $u_g = \dfrac{E_g}{k_B T_E} = \dfrac{hc_o}{k_B \lambda_g T_E}$ and is given by equation (1.137). The emitter temperature is T_E, and σ_{sb} is the Stefan-Boltzmann constant. Thus, the PV efficiency is the following.

$$\begin{aligned} \eta_{PV} &= \frac{V_{LM} I_{LM}}{A_c g \varepsilon_E \sigma_{sb} F_{o-\lambda_g T_E} T_E^4} = \frac{A_o k_B T I_s \bar{I}_{LM} N_J \left(\bar{V}_M - \bar{R}\bar{I}_{LM}\right)}{e A_c g \varepsilon_E \sigma_{sb} F_{o-\lambda_g T_E} T_E^4} \\ &= \frac{A_o k_B T I_s}{e A_c} \frac{FF \bar{V}_{oc} \bar{I}_{sc}}{g \varepsilon_E \sigma_{sb} F_{o-\lambda_g T_E} T_E^4} \end{aligned} \tag{5.248}$$

The quantities FF, $\bar{V}_{oc}$, and $\bar{I}_{sc}$ are functions of $\dfrac{I_{ph}}{I_s}$, $\bar{R}_s$, and $\bar{R}_{sh}$. Again assume $\bar{R}_{sh} \to \infty$ so that $\bar{V}_{oc}$ and $\bar{I}_{sc}$ are given by equations (5.218b) and (5.241). The photon generated current, I_{ph}, is given in terms of the internal quantum efficiency, $\eta_Q(\lambda)$ [equation (5.201)],

$$I_{ph} = A_{Ja}\frac{e}{hc_o}\int_o^{\lambda_g}(1-R_c)\lambda\eta_Q q_i d\lambda \tag{5.249}$$

where A_{Ja} is the active area of a single junction in the array, and R_c is the reflectivity. Figures 5.13 and 5.14 show that η_Q is nearly a constant for $0 \le \lambda \le \lambda_g$. Therefore, assuming η_Q and R_c, as well and g and ε_E, are constants for $0 \le \lambda \le \lambda_g$, then using equation (5.246) for $q_i(\lambda)$ the following results.

$$I_{ph} = \frac{eA_{Ja}}{hc_o}(1-R_c)g\varepsilon_E\eta_Q\int_o^{\lambda_g}\lambda e_b(\lambda, T_E)d\lambda \tag{5.250}$$

The integral can be written in terms of the dimensionless bandgap energy, $u_g = \dfrac{E_g}{k_B T_E}$ so that equation (5.250) becomes the following,

$$I_{ph} = \frac{15}{\pi^4}\frac{e\sigma_{sb}}{k_B}A_{Ja}(1-R_c)g\varepsilon_E\eta_Q T_E^3 G(u_g) \tag{5.251}$$

where $G(u_g)$ is given by equation (2.22). Equation (5.251) and given values of $\bar{R}_s$ are used to calculate FF, $\bar{V}_{oc}$, and $\bar{I}_{sc}$ in the numerator of the efficiency equation (5.248).

Consider the case where $\bar{R}_s = 0$. Therefore, $I_{sc} = I_{ph}$ and the efficiency is the following,

$$\eta_{PV} = \frac{A_{Ja}}{A_c}(1-R_c)\eta_Q FF\left(\frac{eV_{oc}}{k_B T_E}\right)\frac{\displaystyle\int_{u_g}^{\infty}\frac{u^2}{e^u-1}du}{\displaystyle\int_{u_g}^{\infty}\frac{u^3}{e^u-1}du} \tag{5.252}$$

$\bar{R}_{sh} \to \infty$
$\bar{R}_s = 0$
$R_c(\lambda), \eta_Q(\lambda), g(\lambda)$ and
$\varepsilon_E(\lambda)$ constant for $0 < \lambda < \lambda_g$

where equations (1.137) and (2.22) have been used for $F_{o-\lambda_g T_E}$ and $G(u_g)$. Thus, if $\bar{R}_s = 0$, there is no direct dependence of η_{PV} upon the cavity parameters g and ε_E. Dependence upon g and ε_E occurs only through FF and V_{oc} that are functions of I_{ph},

which, in turn, is a function of g and ε_E. Since $\overline{V}_{oc} = \ln\left(\frac{I_{ph}}{I_s}+1\right)$, V_{oc} is a slowly varying function of I_{ph}. And since FF is a function of $\overline{V}_{oc}$, FF will also be a slowly varying function of I_{ph}. Therefore, if $\overline{R}_s = 0$, the PV efficiency will be nearly independent of g and ε_E. For the "perfect" PV cell, $\eta_Q = 1$, FF = 1, $eV_{oc} = N_J E_g$, $R_c = 0$, and $\frac{A_{Ja}}{A_c} = \frac{A_{Ja}}{N_J A_{Ja}} = \frac{1}{N_J}$. In this case, η_{PV} [equation (5.252)] reduces to the maximum possible TPV efficiency derived in Chapter 2 [equation (2.19)]. In that case η_{PV} is only a function of the dimensionless bandgap energy, $u_g = \frac{E_g}{kT_E}$.

When η_Q, R_c, g, and ε_E are constants for $0 < \lambda < \lambda_g$, the PV efficiency [equation (5.248)], power density, p_{EL}, and dimensionless photon generated current, $\overline{I}_{ph} = \frac{I_{ph}}{I_s}$ [equation (5.251)] can be written as follows,

$$\eta_{PV} = A_o \alpha_{PV} \frac{\overline{I}_{LM} N_J \left(\overline{V}_M - \overline{I}_{LM}\overline{R}_s\right)}{\int_{u_g}^{\infty} \frac{u^3}{e^u - 1} du} \tag{5.253}$$

$$p_{EL} \equiv \frac{P_{EL}}{A_c} = A_o \overline{I}_{LM} N_J \left(\overline{V}_M - \overline{I}_{LM}\overline{R}_s\right) \tag{5.254}$$

$$\overline{I}_{ph} \equiv \frac{I_{ph}}{I_s} = \frac{J_{ph}}{J_s} = \beta_{PV} \int_{u_g}^{\infty} \frac{u^2}{e^u - 1} du \tag{5.255}$$

where,

$$u_g = \frac{E_g}{k_B T_E} \tag{5.256}$$

$$\alpha_{PV} = \frac{\pi^4 k_B T I_s}{15 e g \varepsilon_E \sigma_{sb} T_E^4 A_c} = 9.87 \times 10^7 \frac{T J_s A_J}{g \varepsilon_E T_E^4 A_c} \qquad \begin{matrix} J_s - \frac{amp}{cm^2} \\ T - K \end{matrix} \tag{5.257}$$

$$\beta_{PV} = \frac{15}{\pi^4}\frac{A_{Ja}}{A_c}\eta_Q\left(1-R_c\right)\frac{eg\varepsilon_E\sigma_{sb}T_E^3}{kJ_s} = 1.01\times10^{-8}\left(\frac{A_{Ja}}{A_c}\right)\eta_Q\left(1-R_c\right)\frac{T_E^3}{J_s} \qquad (5.258)$$

Notice that η_{PV} and p_{EL} are directly proportional to the ideality factor, A_o.

The following procedure calculates the efficiency and power density. For given values of u_g and β_{PV}, equation (5.255) produces $\overline{I}_{ph}$. Using that $\overline{I}_{ph}$ and $\overline{R}_s$ [equation (5.213c)] in equation (5.223a) gives $\overline{V}_M$.

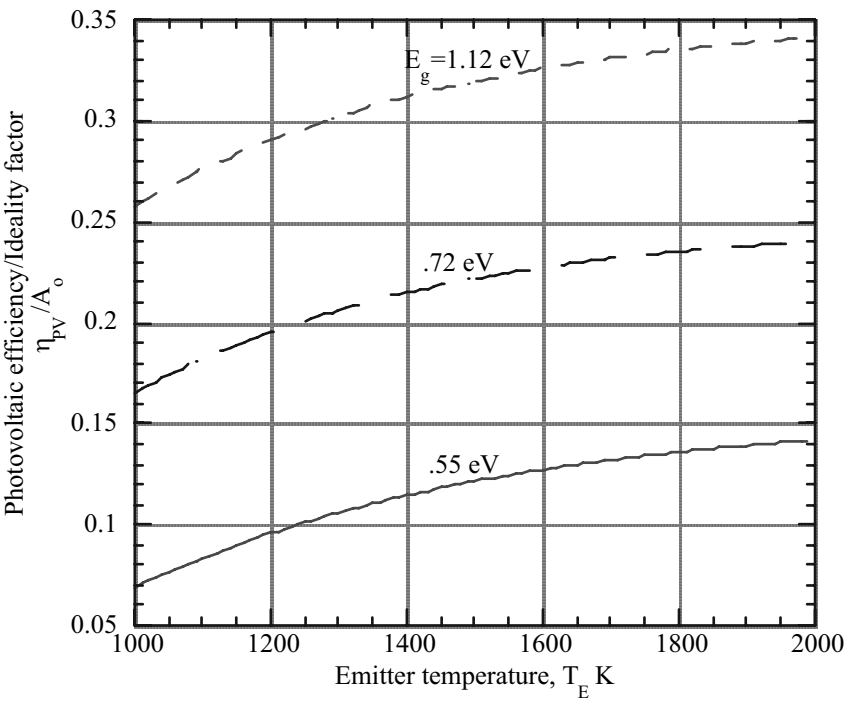

Figure 5.20 - Photovoltaic efficiency, η_{PV}, as a function of emitter temperature, T_E for bandgap energies, E_g=.55, .72 and 1.12 eV and no series resistance(R_s=0). The quantum efficiency,η_Q, cell reflectivity, R_i, emitter emittance, ε_E, and cavity parameter, g, are assumed constant for E_g<E. $\varepsilon_E g$=.6, $A_{ca}/A_c(1-R_i)\eta_Q$=.8, N_j=1 and cell properties to calculate the saturation current density, j_s, given in table 5.1.

The dimensionless maximum load current, $\overline{I}_{LM}$, is then obtained from equation (5.229a). Using these values for $\overline{V}_M$ and $\overline{I}_{LM}$ in equations (5.253) and (5.254) yields $\frac{\eta_{PV}}{A_o}$. To calculate α_{PV} and $\beta_{PV,}$ the saturation current density, J_s, which is an exponential function of $\frac{E_g}{k_B T}$ must be known. An approximate expression for J_s is given by equation (5.132).

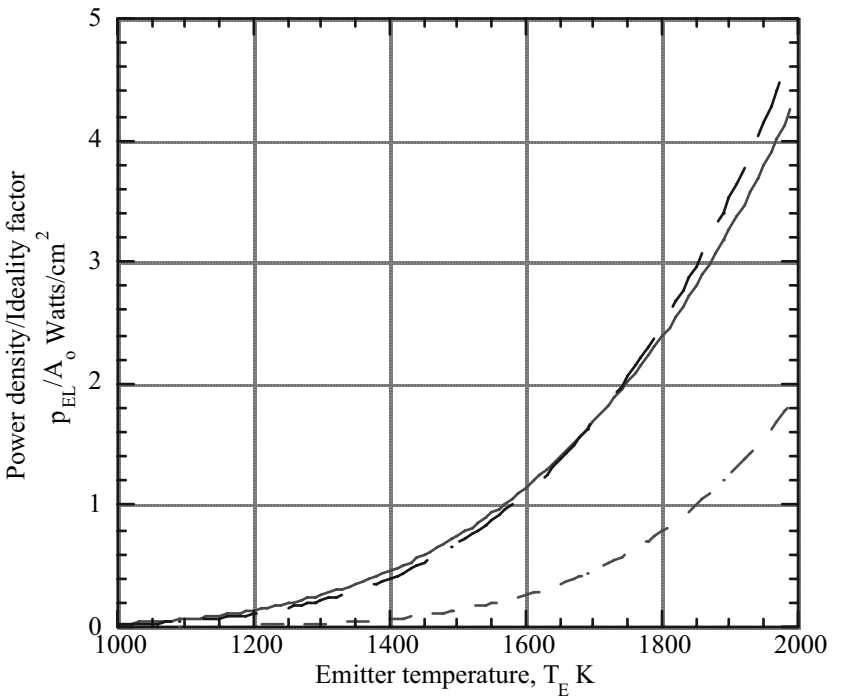

Figure 5.21 - Power density, p_{EL}, as a function of emitter temperature, T_E for three bandgap energies, E_g and the same conditions as Figure 5.20.
E_g =.55 eV ——— E_g =.72 eV—— — E_g =1.12 eV— — —

Using the procedure just described yields the results for $\frac{\eta_{PV}}{A_o}$ and $\frac{p_{EL}}{A_o}$ shown in Figures 5.20 and 5.21. These results are shown as a function of emitter temperature, T_E, for three bandgap energies, E_g = 0.55, 0.72, and 1.12 eV for a single junction (N_J = 1), with no series resistance (R_s = 0), and infinite shunt resistance ($R_{sh} \to \infty$). Other quantities used are the following; $g\varepsilon_E = 0.6$, $\frac{A_{ca}}{A_c}(1-R_c)\eta_Q = 0.8$, and PV cell temperature, T = 300K. The saturation current density, J_s, has been calculated using equation (5.132) for PV cell properties shown in Table 5.1.

Bandgap Energy E_g, eV	Electron Effective Mass, m_n^*/m_e	Hole Effective Mass, m_p^*/m_e	Dopant Density $N_A=N_D$, cm^{-3}	Saturation Current Density, j_s mA/cm^2
0.55 InGaAs	0.041	0.45	10^{18}	6.32
0.72 GaSb	0.042	0.36	10^{18}	$6.65x10^{-3}$
1.12 Si	0.19	0.54	10^{18}	$1.25x10^{-11}$

Table 5.1 PV cell properties used in Figures 5.20 and 5.21. Saturation current densities are calculated using equation 5.132.

The first thing to notice is that $\frac{\eta_{PV}}{A_o}$ increases with increasing bandgap energy, E_g. This occurs because the denominator of the PV efficiency definition [equation (5.236)] includes only photons with energy $E > E_g$. Therefore, for a fixed value of T_E, even though the ratio of the integral terms in equation (5.252) decreases as E_g increases, the increase in open circuit voltage, V_{oc}, and thus fill factor, FF, is greater than the decrease in the integral quotient term. Even though η_{PV} increases with E_g this does not mean that the overall TPV efficiency will increase with E_g. As already shown in Chapter 2, even for the "perfect" PV, cell the overall TPV efficiency is strongly dependent upon the quality of the spectral control. As shown in Chapter 2, to produce maximum overall efficiency there is an optimum value of $\frac{E_g}{kT_E}$. This optimum occurs because η_{PV} increases with increasing $\frac{E_g}{kT_E}$ as the quality of the spectral control, (the *cavity efficiency*, η_c) decreases with increasing $\frac{E_g}{kT_E}$. The second important result is that $\frac{\eta_{PV}}{A_o}$ increases with increasing T_E. This occurs for a given E_g because the fraction of useful photons ($E > E_g$) increases with increasing T_E. Thus, the integral in equation (5.255)

for $\overline{I}_{ph}$ increases; this results in increased values for $\overline{I}_{sc}$, $\overline{V}_{oc}$, and FF. However, if $R_s \neq 0$ there will be an optimum T_E for maximum because as $\overline{I}_{ph}$ increases, the ohmic loss term $\overline{I}_{LM}\overline{R}_s$ in equation (5.253) becomes significant and the efficiency parameter starts to decrease with increasing T_E.

As pointed out earlier, when $R_s = 0$, the PV efficiency is nearly independent of the geometry parameter, g, and the spectral emittance ε_E. Therefore, the results in Figure 20 change very little for $0.4 < g\varepsilon_E < 0.8$. The efficiency drops less than 10% in going from $g\varepsilon_E = 0.8$ to $g\varepsilon_E = 0.4$.

Although for a given T_E, the efficiency parameter, $\frac{\eta_{PV}}{A_o}$, increases with E_g this is not the case for the power density parameter, $\frac{p_{EL}}{A_o}$. As Figure 5.21 shows, $\frac{p_{EL}}{A_o}$ decreases with increasing E_g at the lowest temperatures. However, for $T_E > 1700K$, $\frac{p_{EL}}{A_o}$ is greater for $E_g = 0.72eV$ than for $E_g = 0.55eV$.

5.13 Summary

The chapter began with a presentation of the Kronig-Penney model to explain the energy band structure of a semiconductor. In a conduction band, electrons are essentially free to move under the action of an external electric field. In a valence band, an electron has no vacant energy states to move into. However, in a semiconductor, the valence band and the conduction band are separated by a relatively small bandgap energy, E_g. Thus, an electron can be thermally or optically, as in a photovoltaic cell, excited into the conduction band. When the electron leaves the valence band, it leaves a vacant energy state with a +e charge called a hole. As electrons are excited into the conduction band, the vacated energy states allow for the holes to produce a hole current in the valence band.

Quantum mechanics is required to determine the motion of electrons and holes in a semiconductor. However, by introducing an effective mass for the electrons and holes, their motion can be approximated by Newtonian mechanics. This leads to the so-called transport equations.

The current density of the electrons in the conduction band and holes in the valence band is determined by the transport equations. These are given by equations (5.53), (5.54), (5.56), and (5.57). There are two parts to the current densities; drift current resulting from the electric field and diffusion current produced by spatial gradients in the electron and hole densities.

Several macroscopic properties must be supplied to the transport equations. These are the mobilities and lifetimes of the electrons and holes and the absorption coefficient of the semiconductor. The mobilities determine the current densities while the lifetime and absorption coefficient determine the recombination and generation rates of electrons and holes.

The basis for a PV cell is the p-n junction. On the p side of the junction, a dopant atom is added resulting in holes being the major charge carrier and electrons being the minority charge carrier. On the n side of the junction a dopant atom resulting in electrons being the major charge carrier and holes being the minority charge carrier. By solving the transport equations with the proper boundary conditions for the minority carriers in the neutral p and n regions of the junction, the current vs. voltage relation is obtained. For the unilluminated case, this is given by equation (5.123), where the current density, J, is an exponential function of the applied voltage, V_a. This result does no include recombination in the depletions region or high injection of carriers, which may occur in TPV cells under high intensity illumination. To account for these effects, an empirical current vs. voltage relation is used [equation (5.139)]. In this case the exponential dependence is now $\frac{V_a}{A_o}$, where A_o is the ideality or junction perfection factor.

When the p-n junction is illuminated, a photon produced current results that moves in the opposite direction to the dark current resulting from V_a. Therefore, the photon produced current is moving against the applied electric field. As a result, electrical power is produced when a load is connected across the junction. Under illumination, solutions to the transport equations for the minority current densities separate into two parts. One part is the current produced by an applied field in the dark and the second part is the current produced by the incident photons that have energy greater than the bandgap energy. Combining the empirical dark current relation and the photon produced current yields the current-voltage relation for an illuminated p-n junction [equation (5.200)].

Two related parameters used to evaluate PV cell performance are the quantum efficiency and the spectral response. Internal quantum efficiency, $\eta_Q(\lambda)$, is the ratio of the actual current density produced by incident photons of wavelength, λ, to the maximum possible current density that can be produced by the incident photons of wavelength, λ. The spectral response, $Sr(\lambda)$, is the ratio of the actual current density produced by incident photons of wavelength, λ, to the incident power density of photons of wavelength, λ. The units of $Sr(\lambda)$ are $\frac{A}{W}$.

To include resistance losses and shorting losses that are neglected in the transport equation solutions for the current-voltage relation, an equivalent circuit model for the

PV cell is used (Figure 5.15). A series resistance, R_s, and a shunt resistance, R_{sh}, account for resistance and shorting losses. Combining the experimentally determined values of R_s and R_{sh}, the spectral response, ideality factor, and dark saturation current yields the PV cell efficiency and output power density. Thus, the PV array performance in a TPV system can be calculated using experimentally determined parameters for any given incident spectral photon power density.

Application of the equivalent circuit model yields the following important results. The series resistance reduces the short circuit current but does not affect the open circuit voltage. Whereas, the shunt resistance reduces the open circuit voltage, but does not affect the short circuit current. As the series resistance increases or the shunt resistance decreases, the illuminated p-n junction behaves like a resistor with a negative resistance. If there is negligible series resistance, the photovoltaic efficiency is nearly independent of the optical properties of the optical cavity.

The transport equation solutions for an ideal p-n junction in the dark and under illumination have yielded several important results. Several of these are listed below.

1) Dark saturation current density, J_s, decreases rapidly as $\frac{\tau'}{\tau} \to 1$, where τ' is the minority carrier lifetime and τ is the minority carrier average collision time. For $\frac{\tau'}{\tau} > 1$, J_s decreases at a much lower rate.
2) Surface recombination of electrons and holes increases the dark saturation current, J_s, and decreases the photon produced current density. As a result, the quantum efficiency is reduced.
3) An optimum value of the ratio of the neutral region length to minority carrier diffusion length exists for maximum photon produced minority current density. This maximum increases with increasing values of the optical depth, $La(\lambda)$, where L is the minority carrier diffusion length and $a(\lambda)$ is the absorption coefficient.
4) For $\frac{E}{E_g} > 1$, where E is the photon energy and E_g is the bandgap energy, the quantum efficiency, η_Q, is nearly a constant.

The performance of a PV cell is strongly dependent upon the cell temperature. It is the dark saturation current density, which is proportional to $\exp\left(-\frac{E_g}{kT}\right)$, that causes the strong temperature dependence. Thus, for TPV systems, where E_g is small, detrimental large dark saturation currents exist. Also, in a TPV application, the incident radiation is isotropic rather than at zero incidence angle as in a solar application. If the ratio of the

neutral region length to minority carrier diffusion length is very small, the internal quantum efficiency will be the same for isotropic and normal incident radiation.

References

[1] E. Becquerel, C. R. Hebd. Seances Acad. Sci., 9 (1839) 561.

[2] D. M. Chapin, C. S. Fuller, and G. L. Pearson, J. Appl. Phys., 25(1954) 676

[3] A. Ambroziak, Semiconductor Photoelectric Devices,translated by E. Lepa and edited by O. H. Hughes, Gordon and Breach Science Publishers, New York, 1969.

[4] H. J. Hovel, Semiconductors and Semimetals, vol. 2, Solar Cells, Academic Press, New York, 1975.

[5] M. A. Green, Solar Cells, Operating Principles Technology and System Applications, Prentice-Hall Series in Solid State Physical Electronics, Englewood Cliffs, New Jersey, 1982.

[6] A. L. Fahrenbruch and R. H. Bube, Fundamentals of Solar Cells, Photovoltaic Solar Energy Conversion, Academic Press, New York, 1983.

[7] C. Hu and R. M White, Solar Cells, from Basics to Advanced Systems, McGraw Hill Book Company, New York, 1983.

[8] S. R. Wenham, M. A. Green and M. E. Watt, Applied Photovoltaics, Centre for Photovoltaic Devices and Systems at the University of New South Wales, Australia.

[9] V. M. Andreev, Proceedings of 5th Conference on Thermophotovoltaic Generation of Electricity, AIP Conference Proceedings 653 (2003) 289.

[10] C. Kittel, Introduction to Solid State Physics, 5th Edition, John Wiley and Sons, Inc., New York, 1976, Chapter 7.

[11] I. S. Sokolnikoff and R. M. Refheffer, Mathematics of Physics and Modern Engineering, McGraw-Hill, New York, 1958, Appendix A, Chapter 1.

[12] K. F. Brennan, The Physics of Semiconductors with Applications to Optoelectronic Devices, Cambridge University Press, 1999.

[13] S. M. Sze, Physics of Semiconductor Devices, Wiley-Interscience, New York, 1969.

[14] M., Fox, Optical Properties of Solids, Oxford University Press, New York, 2001.

[15] D. M. Wilt, N. S. Fatemi, P. P. Jenkins, V. G. Weizer, R. W. Hoffman, Jr. , R. K., Jain, C. S., Murray, and D. R. Riley, Proceedings of Third NREL Conference on Thermophotovoltaic Generation of Electricity, AIP Conference Proceedings, 401(1997)237.

Problems

5.1 Use the Kronig-Penney model [equation (5.24)] to estimate the bandgap energy that occurs at k = 0 if P = $\frac{\pi}{2}$, a = 0.5nm, and $m_e = 0.19m_o$, where $m_o = 9.107 \times 10^{-13}$kg is the rest mass of the electron. The values a = 0.534nm and $m_e = 0.19m_o$ are the lattice constant and electron effective mass for silicon, which has a bandgap energy of 1.12eV.

5.2 Derive equation (5.43) for the equilibrium hole density for an intrinsic semiconductor.

5.3 Using the electron and hole continuity equations, obtain the current continuity equation,

$$\frac{\partial \sigma}{\partial t} + \nabla \bullet \vec{J} = 0$$

where $\sigma = e(p-n)$ is the charge density.

5.4 For a p-n junction at equilibrium, the hole current, $\vec{J}_p$ must vanish. Based on $\vec{J}_p = 0$, show that the Fermi-energy, E_f, remains a constant through the junction.

5.5 Using the approximation that the hole diffusion and drift currents are equal ($\vec{J}_p = 0$) when a potential, V_a, is applied across a p-n junction, derive equation (5.94).

5.6 The electron saturation current for an ideal p-n junction in the dark is given by equation (5.120). For $u_p = \frac{\left(\ell_p - x_p\right)}{L_n} < 1$ retain only terms through the first order in the series expansions of the exponential terms in equation (5.120) to obtain an expression for J_{sn}. In this case, what is J_{sn} when $\frac{S_n L_n}{D_n} \to 0$ and when $\frac{S_n L_n}{D_n} \to \infty$?

5.7 Solve equation (5.140b) for N_p when $E_2(ax) \approx b_o e^{-b_1 ax}$, $\beta_n = b_1 a_p L_n = 1$, and $u_M = 0$ for the boundary conditions given by equations (5.147) and (5.148). Using the solution for $N_p(x)$, show that the photon produced electron diffusion current density, $\overline{J}_{qn}$, at $x = x_p$ is the following,

$$\bar{J}'_{qn}\,\frac{1}{2b_1 DEN_p}\left\{(1-\phi_n)\,e^{-u_p}\sinh u_p+(1+\phi_n)\,u_p\right\}$$

where $u_p=\dfrac{x_p}{L_n}$, $\phi_n=\dfrac{S_nL_n}{D_n}$, and DEN_p is given by equation (5.157b). Hint: A particular solution of the form $N_p=C_o x e^{-b_1 a x}$ applies for this case.

5.8 The dimensionless minority electron diffusion current, $\bar{J}'_{nq}$, resulting from incident radiation on the p region of a perfect p-n junction is given by equation (5.159b). For $\beta_n = b_1L_n a(\lambda) > 1$, $u_p(\beta_n-1)\gg 1$, and $u_M = 0$ obtain an expression for $\bar{J}'_{nq}$ and show that $\bar{J}'_{nq}$ decreases with increasing $\phi_n=\dfrac{S_nL_n}{D_n}$ as long as $\beta_n \tanh u_p > 1$. Also, for $\beta_n > 1$, $u_p(\beta-1)\gg 1$, and $\phi_n \ll 1$, show that $\bar{J}_{nq}$ is independent of ϕ_n.

5.9 Derive the generation rate $G_n(\lambda,x)$ [equation (5.168)], for electron-hole pairs in the n region of an ideal p-n junction where the radiation is incident on the p side. Assume that the radiation intensity, $i(\lambda)$, is isotropic, that the reflectivity at the p region surface, R_p, is independent of direction, and that the indices of refraction of the p, n, and depletion regions all have the same value, n_c. The absorption coefficient for the p neutral region, depletion region, and n neutral region are a_p, a_d, and a_n.

5.10 Solve equation (5.169) for $P'_n(x)$ when $\beta_p = b_1a_nL_p = 1$, and $u_M = 0$ for the boundary conditions given by equations (5.172) and (5.173). Using the solution for $P'_n(x)$, calculate the hole diffusion current density, J'_p, at the edge of the depletion region next to the n region and the dimensionless photon produced hole current density, $\bar{J}'_{pq}$, at the depletion region edge.

5.11 Using equations (5.209) and (5.212), show that $\dfrac{dV}{dV_L}>0$ for all V_L for N_J identical p-n junctions in series.

5.12 For large dimensionless series resistance, $\bar{R}_s > 10^{-5}$, a PV cell has the characteristics of a negative resistor with the current-voltage relation given by equation (5.216). Using equation (5.216) show that the maximum dimensionless power density is given by equation (5.233).

5.13 For small shunt resistance, $\bar{R}_{sh}$, and series resistance, $\bar{R}_s = 0$, a PV cell has the characteristics of a negative resistor with the current-voltage relation given by equation (5.234). Using equation (5.234), show that the maximum dimensionless power density is given by equation (5.235).

5.14 For infinite shunt resistance, $R_{sh} \to \infty$, and finite series resistance, R_s, a PV cell begins to behave like a negative resistor as the dimensionless open circuit voltage, $\bar{V}_{oc}$, becomes large. For these conditions show that the asymptotic value of the fill factor, FF, is ¼.

Chapter 6
Governing Equations for Radiation Fluxes in Optical Cavity

In the previous chapters, the primary components (emitter, filter, PV cells) of a TPV system are considered. It is the optical properties of these components that determine the TPV system performance. Knowing the optical properties of the components allows the calculation of the efficiency and power output of the TPV portion of the energy conversion system. However, it should be remembered that the overall performance of a TPV energy conversion system will also depend upon the efficiencies of the thermal energy source, the waste heat removal system, and the power conditioning.

Chapter 6 develops the system of equations that must be solved in order to obtain the radiation fluxes incident on the various components of the system. The general TPV system considered consists of an emitter, a window, a filter, and PV cells. In addition to the component optical properties, the component temperatures and geometries are the other variables that determine the system performance. Thus, the system of equations that determine the radiation fluxes depend upon the component optical properties, geometry, and temperature.

The chapter begins by introducing the radiation transfer theory required to develop the radiation flux equation. That theory is then applied to a general TPV system of either a planar or cylindrical geometry. The definitions of the important efficiencies that make up the overall system efficiency conclude Chapter 6.

It is appropriate at this time to introduce the symbol notation that will be used for radiation energy fluxes. An energy flux per unit area per unit wavelength (watts/cm^2 nm) is denoted by lower-case q. If q is integrated over wavelength, the result is denoted by $\bar{q}$ (watts/nm). If q is integrated over area the result is denoted by Q (watts/nm). Finally, if q is integrated over both area and wavelength it is denoted by $\bar{Q}$ (watts).

6.1 Symbols

A	surface area, cm^2
c_o	vacuum speed of light, 2.9979×10^{10} cm/sec
e_b	blackbody emissive power, watts/cm^2 nm
E	photon energy, j
E_g	PV cell bandgap energy, J

F_{ij}	view factor for radiation leaving element i and impinging on element J
F_{ij}^{lm}	view factor for radiation leaving element i that passes through elements l and m and impinges on element J
h	Plank's constant, 6.62×10^{-34} J-sec
i	radiation intensity, watts/cm^2 steradian nm
J_{sc}	PV cell short circuit current density, Amps/cm^2
k	Boltzmann constant (1.38×10^{-34} J/K)
n	index of refraction
R	reflectivity at interface between two media
t	internal transmission
T_E	emitter temperature, K
r	radius
u_g	dimensionless PV cell bandgap energy, E_g/kT_E
q	radiation energy flux at wavelength, λ, watts/cm^2 nm
$\overline{q}$	total radiation energy flux, watts/cm^2
Q	radiation power at wavelength, λ, watts/nm
$\overline{Q}$	total radiation power, watts
α	absorptance
ε	emittance
ρ	reflectance
τ	transmittance
σ_{sb}	Stefan-Boltzmann constant, 5.67×10^8 watts/cm^2 K^4
ω	solid angle, steradians

Subscripts

C	denotes PV cells or cavity or cylindrical geometry
E	denotes emitter
f	denotes filter
p	denotes planar geometry
W	denotes window

6.2 Radiation Transfer Theory

6.2.1 Radiation Transfer for Uniform Intensity

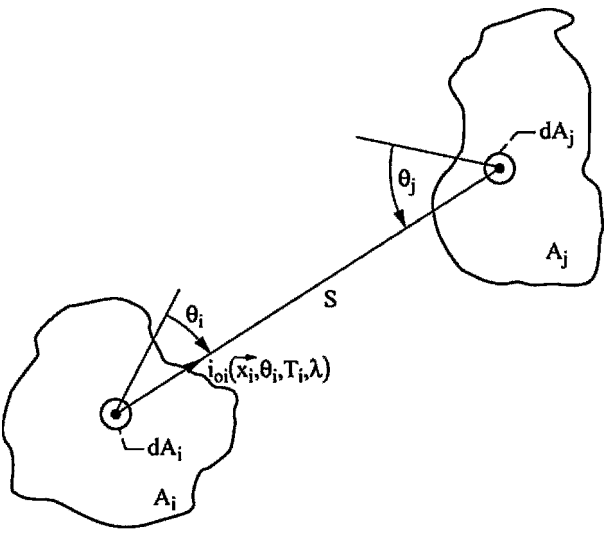

Figure 6.1.—Radiative transfer from area A_i to area A_j.

Consider the transfer of energy by radiation from area A_i to area A_j as shown in Figure 6.1. The intensity of radiation leaving the infinitesimal area dA_1 is i_{oi}, which in general is a function of location, $\vec{x}_i$, direction, θ_i, temperature, T_i, and wavelength, λ. If an absorbing medium that does not alter the direction of the radiation (as a lens would, for example) exists between A_i and A_j, then the radiation energy reaching area dA_j from the area dA_i is the following.

$$dq_{dA_i \to dA_j} = \tau_{ij} i_{oi}\left(\theta_i, \vec{x}_i, \lambda, T_i\right) \cos\theta_i dA_i d\omega_{dA_j} \tag{6.1}$$

Where τ_{ij} is the transmittance of the medium between A_i and A_j, and $d\omega_{dA_j}$ is the solid angle subtended by dA_j at dA_i.

$$d\omega_{dA_j} = \frac{\cos\theta_j dA_j}{S^2} \tag{6.2}$$

Therefore,

$$dq_{dA_i \to dA_j} = \tau_{ij} i_{oi}\left(\theta_i, \vec{x}_i, \lambda, T_i\right) \frac{\cos\theta_i \cos\theta_j}{S^2} dA_i dA_j \tag{6.3}$$

Assuming τ_{ij} is a constant, the total radiative energy at wavelength, λ, reaching A_j from A_i is the following.

$$Q_{ij} = \tau_{ij} \int_{A_i} \int_{A_j} i_{oi} \frac{\cos\theta_i \cos\theta_j}{S^2} dA_j dA_i \tag{6.4}$$

If i_{oi} is independent of $\vec{x}_i$ and θ_i, then $i_{oi}(\lambda,T_i)$ can be removed from the integrals. In that case, Q_{ij} is just the product of $\tau_{ij} i_{oi}$ and a geometrical factor, $F_{ij}A_i$, where F_{ij} is the *view-factor or configuration-factor* ([1], Chapter 7),

$$\boxed{Q_{ij} = \tau_{ij} q_{oi} F_{ij} A_i} \tag{6.5}$$

where the view-factor is defined as follows.

$$\boxed{F_{ij} = \frac{1}{\pi A_i} \int_{A_i} \int_{A_j} \frac{\cos\theta_i \cos\theta_j}{S^2} dA_j dA_i} \tag{6.6}$$

Obviously, from the definition given by equation (6.6), the following is true.

$$\boxed{A_i F_{ij} = A_j F_{ji}} \tag{6.7}$$

Also, q_{oi} is the radiative energy flux leaving A_i, and since i_{oi} is assumed independent of θ_i,

$$q_{oi} = \int i_{oi} \cos\theta_i d\omega = i_{oi} 2\pi \int_0^{\pi/2} \cos\theta_i \sin\theta_i d\theta_i = \pi i_{oi} \qquad \text{watts/cm}^2\,\text{nm} \tag{6.8}$$

Also, q_{oi} is independent of $\vec{x}_i$ since i_{oi} is assumed independent of $\vec{x}_i$. View-factors for many simple geometries are tabulated in Appendix B of [1]. For a complex geometry, numerical integration of equation (6.6) is required.

6.2.2 View-Factors for TPV Systems

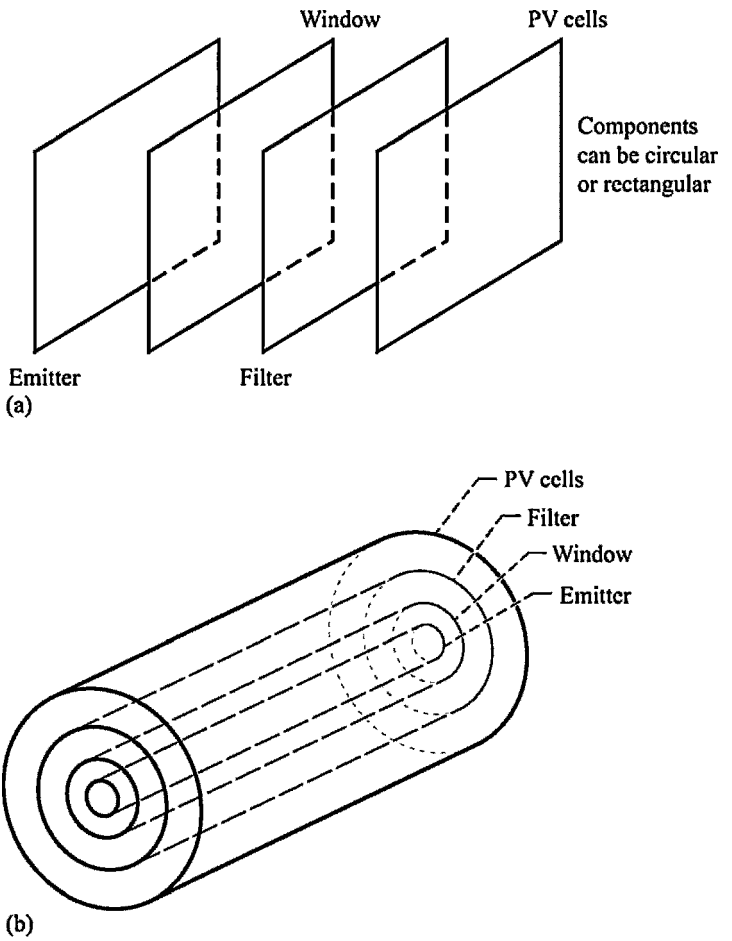

Figure 6.2.—Basic TPV system geometries. (a) Planar. (b) Concentric cylinder.

Two basic geometries are most likely for a TPV system. The first such geometry is a planar one as shown in Figure 6.2a, where each of the components are circular or rectangular disks aligned parallel to each other. The second geometry is a cylindrical one, where each component is a concentric cylinder as shown in Figure 6.2b. Most likely, the inner cylinder is the emitter and the outer cylinder contains the PV cells. However, the reverse case, where the emitter is the outermost cylinder and the PV cells are on the inner most cylinder, is also possible.

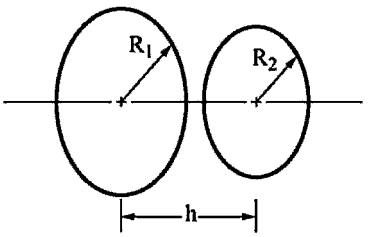

$$Z_1 = \frac{R_1}{h} \qquad Z_2 = \frac{R_2}{h}$$

$$X = 1 + \frac{1 + z_2^2}{z_1^2}$$

$$F_{12} = \frac{1}{2}\left[X - \sqrt{X^2 - 4\left(\frac{z_2}{z_1}\right)^2}\right]$$

(a)

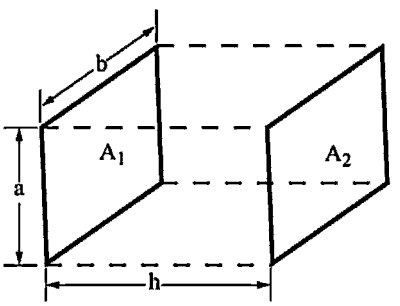

$$X = \frac{a}{h} \qquad Y = \frac{b}{h}$$

$$F_{12} = \frac{2}{\pi XY}\left\{\ln\left[\frac{(1+X^2)(1+Y^2)}{1+X^2+Y^2}\right]^{1/2} + X\sqrt{1+Y^2}\tan^{-1}\left[\frac{X}{\sqrt{1+Y^2}}\right] + Y\sqrt{1+X^2}\tan^{-1}\left[\frac{Y}{\sqrt{1+X^2}}\right] - X\tan^{-1}X - Y\tan^{-1}Y\right\}$$

(b)

Figure 6.3.—View factors for TPV system geometries. (a) Parallel circular disks with centers along the same normal. (b) Identical, parallel, directly opposed rectangles. (c) Unequal, parallel, coaxial squares (ref. 4). (d) Two concentric cylinders of the same length. (e) Differing-diameter coaxial disks blocked by a coaxial cylinder (ref. 2).

View-factors for circular and rectangular disks and concentric cylinders are shown in Figure 6.3. Note that in the case of the cylindrical geometry, the concave inner surface of the outer cylinder has a "self" view-factor, F_{22}. Also, for a cylindrical TPV system with transmitting elements such as a window, radiation from the concave side of an outer cylinder is incident on both the convex and concave sides of an inner transmitting element. In the planar geometry case, incident radiation on a transmitting element from another element only occurs on the side of the transmitting element that faces the radiating element.

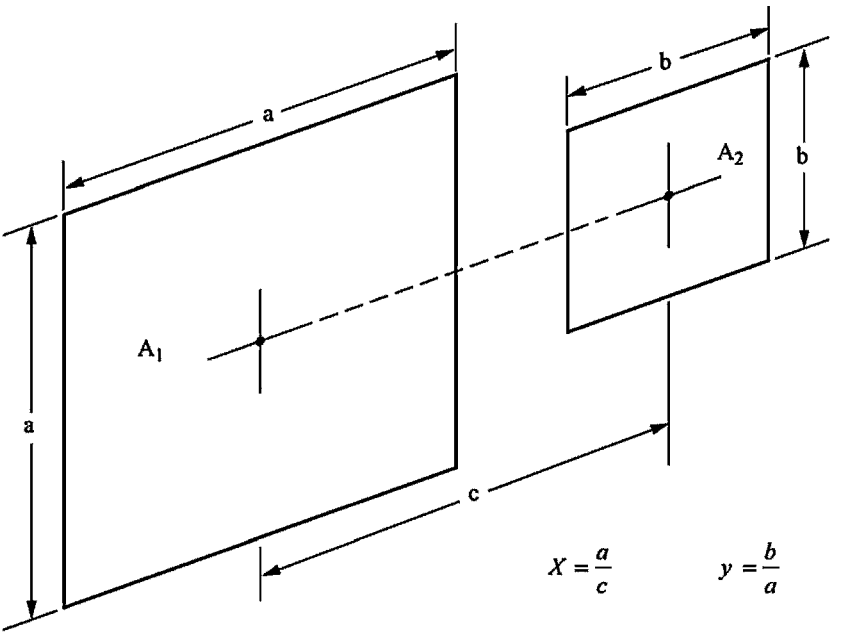

$$F_{12} = \frac{1}{\pi X^2}\left\{ \ln \frac{\left[X^2\left(1+y^2\right)+2\right]^2}{\left[X^2\left(1-y^2\right)+2\right]\left[X^2\left(1+y\right)^2+2\right]} \right.$$

$$+\left[X^2\left(1-y^2\right)+4\right]^{1/2}\left[X\left(1-y\right)\tan^{-1}\frac{X\left(1-y\right)}{\sqrt{X^2\left(1-y\right)^2+4}} - X\left(1+y\right)\tan^{-1}\frac{X\left(1+y\right)}{\sqrt{X^2\left(1-y\right)^2+4}}\right]$$

$$\left. +\left[X^2\left(1+y\right)^2+4\right]^{1/2}\left[X\left(1+y\right)\tan^{-1}\frac{X\left(1+y\right)}{\sqrt{X^2\left(1+y\right)^2+4}} - X\left(1-y\right)\tan^{-1}\frac{X\left(1-y\right)}{\sqrt{X^2\left(1+y\right)^2+4}}\right]\right\}$$

Figure 6.3.—Continued. (c) Unequal, parallel, coaxial squares [4].

Consider the view-factor for the radiation leaving the concave side of the PV cells in a cylindrical TPV system and incident on the concave side of the window, filter, or PV cells as shown in Figure 6.2b. Since the filter is a transmitting element, a portion of the radiation leaving the concave side of the PV cells can pass through the filter and impinge upon the concave sides of the filter and PV cells. Also, a portion of the PV cell radiation passes through both the filter and the window, impinging on the concave sides of the window, filter, and PV cells.

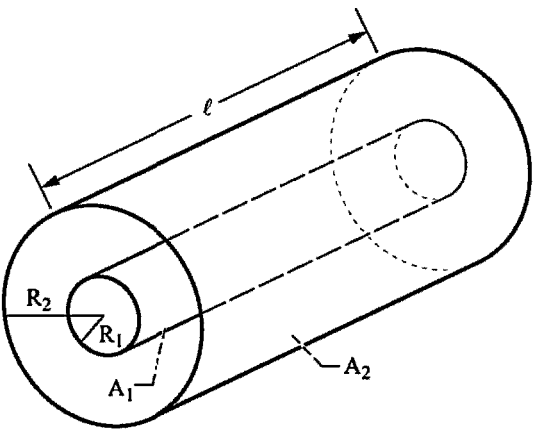

$$Z = \frac{R_2}{R_1}$$

$$L = \frac{\ell}{R_1}$$

$$A = L^2 + z^2 - 1$$

$$B = L^2 - z^2 + 1$$

$$F_{21} = \frac{1}{z} - \frac{1}{\pi z}\left\{\cos^{-1}\frac{B}{A} - \frac{1}{2L}\left[\sqrt{(A+2)^2 - 4z^2}\,\cos^{-1}\frac{B}{zA} + B\sin^{-1}\frac{1}{z} - \frac{\pi A}{2}\right]\right\}$$

$$F_{22} = 1 - \frac{1}{z} + \frac{2}{\pi z}\tan^{-1}\frac{2\sqrt{z^2-1}}{L} - \frac{L}{2\pi z}\left[\frac{\sqrt{4z^2+L^2}}{L}\sin^{-1}\frac{4\left(z^2-1\right)+L^2/z^2\left(z^2-2\right)}{L^2+4\left(z^2-1\right)}\right.$$

$$\left. - \sin^{-1}\frac{z^2-2}{z^2} + \frac{\pi}{2}\left(\frac{\sqrt{4z^2+L^2}}{L} - 1\right)\right]$$

where for any argument X:

$$-\frac{\pi}{2} \le \sin^{-1} X \le \frac{\pi}{2}$$

$$0 \le \cos^{-1} X \le \pi$$

Figure 6.3.—Continued. (d) Two concentric cylinders of the same length.

This is illustrated in Figure 6.4, where the view factors for the concave side of the PV cells to the concave sides of the window, filter, and PV cells are given for radiation that passes through the filter and window. The view-factor for the radiation leaving the concave side of the PV cells that passes through both the filter and the window, and impinges upon the concave side of the PV cells is denoted by F_{cc}^{fw}.

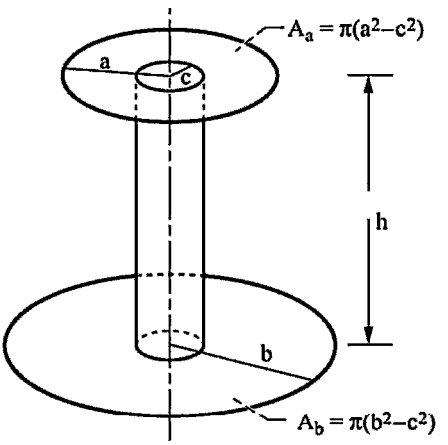

$$A_a F_{ab} = A_b F_{ba} = \frac{a^2-c^2}{2}\cos^{-1}\frac{c}{b} + \frac{b^2-c^2}{2}\cos^{-1}\frac{c}{a}$$

$$-\sqrt{\left(a^2+b^2+h^2\right)^2-4a^2b^2}\,\tan^{-1}\left[\sqrt{\frac{\left(a^2+b^2+h^2+2ab\right)\left(ba-c^2+\sqrt{b^2-c^2}\sqrt{a^2-c^2}\right)}{\left(a^2+b^2+h^2-2ab\right)\left(ba+c^2-\sqrt{b^2-c^2}\sqrt{a^2-c^2}\right)}}\right]$$

$$+\frac{1}{2}\sqrt{\left(a^2+c^2+h^2\right)^2-4a^2c^2}\,\cos^{-1}\left[\frac{c\left(h^2-a^2+c^2\right)}{a\left(h^2+a^2-c^2\right)}\right]$$

$$+\frac{1}{2}\sqrt{\left(b^2+c^2+h^2\right)^2-4b^2c^2}\,\cos^{-1}\left[\frac{c\left(h^2-b^2+c^2\right)}{b\left(h^2+b^2-c^2\right)}\right]$$

$$+2ch\left[\tan^{-1}\left(\frac{\sqrt{b^2-c^2}+\sqrt{a^2-c^2}}{h}\right)-\tan^{-1}\left(\frac{\sqrt{b^2-c^2}}{h}\right)-\tan^{-1}\left(\frac{\sqrt{a^2-c^2}}{h}\right)\right]$$

Figure 6.3.—Concluded. (e) Differing-diameter coaxial disks blocked by a coaxial cylinder [2].

Similarly, F_{cf}^{fw} denotes the view-factor for radiation that leaves the concave side of the PV cells and impinges upon the concave side of the filter after passing through the filter and window. Superscripts denote the elements through which the radiation passes and the subscripts have the same meaning as explained in Section 6.2.1.

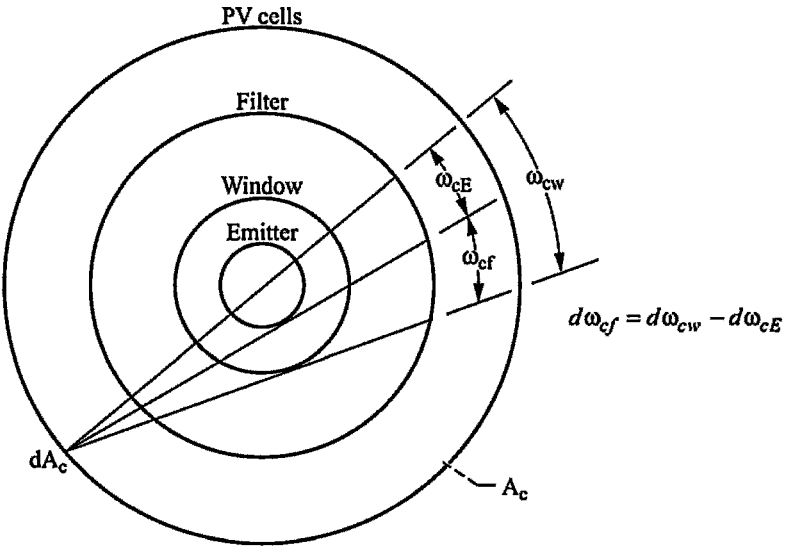

$$F_{cw}^{fw} = F_{cf}^{fw} = F_{cc}^{fw} = \frac{1}{\pi A_c}\int_{A_c} dA_c \int_{\omega_{cf}} \cos\theta_c d\omega_{cf} =$$

$$\frac{2}{\pi A_c}\left[\int_{A_c} dA_c \int_{\omega_{cw}} \cos\theta_c d\omega_{cw} - \int_{A_c} dA_c \int_{\omega_{cE}} \cos\theta_c d\omega_{cE}\right] = F_{cw'} - F_{cE'}$$

similarly,

$$F_{cf}^{f} = F_{cc}^{f} = F_{cf'} - F_{cw'}$$

$$F_{fw}^{w} = F_{ff}^{w} = F_{fw'} - F_{fE'}$$

Figure 6.4.—View factors for concave side of PV cells and filter to concave sides of window, filter, and PV cells in cylindrical TPV system.

As illustrated in Figure 6.4, $F_{cw}^{fw} = F_{cf}^{fw} = F_{cc}^{fw}$. In addition, these view-factors are just the difference in view-factors for the PV cells to the convex side of the window, $F_{cw'}$, and the view-factor for the PV cells to the convex side of the opaque emitter, $F_{cE'}$.

$$F_{cw}^{fw} = F_{cf}^{fw} = F_{cc}^{fw} = F_{cw'} - F_{cE'} \tag{6.9}$$

The view-factors $F_{cw'}$ and $F_{cE'}$ are given by F_{21} in Figure 6.3c. The prime is used to denote the convex side of an element. Similar to equation (6.9), the view-factors for the PV cells to the concave side of the filter and PV cells for radiation leaving the PV cells and passing through the filter is the following.

$$F_{cf}^{f} = F_{cc}^{f} = F_{cf'} - F_{cw'} \tag{6.10}$$

Also, the view-factors for the concave side of the filter to the concave sides of the window and filter for radiation passing through the window are the following.

$$F_{fw}^{w} = F_{ff}^{w} = F_{fw'} - F_{fE'} \tag{6.11}$$

Remember that for the left hand side of equations (6.9), (6.10), and (6.11), the superscripts denote the transmitting elements through which the radiation passes in traveling between the elements given by the subscripts. Also, the inverse of view-factor F_{ij}^{m} is F_{ji}^{m} and is given by equation (6.7).

6.2.3 Optical Properties of Components

To obtain the equations that govern the TPV system performance, it is necessary to perform an energy balance on each of the elements in the system. Each of the elements is characterized by the optical properties: emittance, ε; absorptance, α; reflectance, ρ; and transmittance,τ. In general, these properties are functions of direction and wavelength.

Interference effects are neglected in the following analysis so that the results do not apply for interference filters, which are treated in Chapter 4. However, it is assumed that the components behave in a diffuse manner so that the optical properties are independent of direction and that the radiation field is also independent of direction. The diffuse approximation is also used in deriving equation (6.5). For such TPV system components as an interference filter, the assumption of diffuse behavior may be a poor approximation. Also, as shown in Chapter 1 [equation (1.178)] for a diffuse surface the hemispherical absorptance and emittance are equal.

$$\alpha = \varepsilon \tag{6.12}$$

The optical properties are usually considered to be properties of the material surface. However, as already shown in Chapter 3, the spectral emittance depends upon the dimensions and bulk properties of the material as well. Consider the generic

component as shown in Figure 6.5. The component has two interfaces (1-2 and 3-4) with the surrounding media.

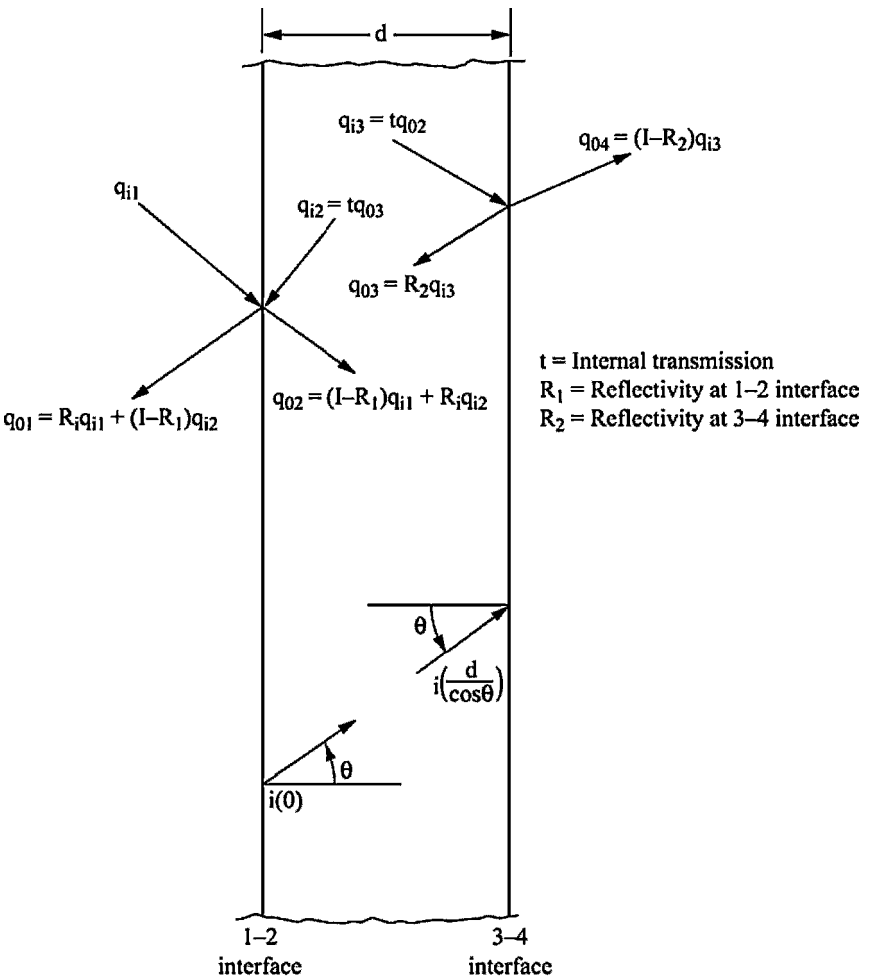

Figure 6.5.—Optical model for a nonradiating TPV component.

The overall optical properties (ρ, τ, α) of the element are determined by the reflectivity at the two interfaces (R_1, R_2) and the internal transmission, t, of the material. In general, R_1 and R_2 are functions of angle and the polarization of the radiation. However, as already stated, it is assumed that the components behave in a diffuse manner (no angle dependence). The reflectivities, R_1 and R_2, depend upon the indexes of refraction, n, of the material on either side of the interface, as well as, the interface

condition (polished, rough, etc.). For the case of normal incidence ($\theta = 0$) between two dielectric materials, the reflectivity is given by equation (1.110).

$$R = \left(\frac{n_1 - n_2}{n_1 + n_2} \right)^2 \tag{1.110}$$

Here n_1 and n_2 are the indices of refraction for the media on either side of the interface. Equation (1.110) is used to approximate the interface reflectivities in the emittance theory of Chapter 3.

For the case where the thickness, $d > \lambda$, interference effects can be neglected. Thus, the internal transmittance of the material, t, is obtained from the solution to the radiative transfer equation [equation (1.143)]. For the case where the media is not emitting and there is no scattering into the direction of propagation, the radiative transfer equation becomes the following,

$$\frac{di}{ds} = Ki \tag{6.13}$$

where K is the extinction coefficient and s is the distance in the direction of propagation. The solution to equation (6.13) is the following,

$$i(s) = i(0)e^{-\kappa} \tag{6.14}$$

where κ is the optical depth.

$$\kappa = \int_o^s K(s')ds' \tag{6.15}$$

Assuming K is independent of s yields the following.

$$i(s) = i(0)e^{-Ks} \tag{6.16}$$

Since no angular dependence is assumed, the flux, q_{o2}, is the following.

$$q_{o2} = \int_{\phi=o}^{2\pi} d\phi \int_{\phi=o}^{\pi/2} i(0)\cos\theta \sin\theta d\theta = \pi i(0) \tag{6.17}$$

Similarly, at the right side of the component where $s = \frac{d}{\cos\theta}$, and using equation (6.16) the flux, q_{i3}, is the following.

$$q_{i3} = \int_{\phi=o}^{2\pi} d\phi \int_{\phi=o}^{\pi/2} i\left(\frac{d}{\cos\theta}\right)\cos\theta\sin\theta d\theta = \pi i(0)\int_{o}^{\pi/2} e^{-\frac{Kd}{\cos\theta}}\cos\theta\sin\theta d\theta \qquad (6.18)$$

Let $x = \cos\theta$, therefore,

$$q_{i3} = 2\pi i(0)\int_{o}^{1} x e^{-\frac{Kd}{x}} dx = 2\pi i(0) E_3(Kd) \qquad (6.19)$$

where $E_3(x)$ is the third order exponential integral.

$$E_3(x) = \int_{o}^{1} \mu e^{-\frac{x}{\mu}} d\mu \qquad (6.20)$$

In obtaining q_{o2} and q_{i3} it is assumed that the thickness, d, is small compared to the dimensions perpendicular to d. Therefore, the integration limit on ϕ is 2π and on θ is $\frac{\pi}{2}$, in equations (6.17) and (6.18). Knowing q_{o2} and q_{i3} (or q_{o3} and q_{i2}), the total internal transmission is determined.

$$t \equiv \frac{q_{i3}}{q_{o2}} = \frac{q_{i2}}{q_{o3}} = 2E_3(Kd) \qquad (6.21)$$

Given the reflectivities R_1 and R_2 and the total internal transmission, t, the overall optical properties (ρ, τ, α) can be determined by making radiation energy balances at the interfaces as shown in Figure 6.5. Diffuse radiation, q_i, is incident on interface 1-2. A portion of q_{1i} is reflected, $R_1 q_{1i}$, and the remainder, $(1 - R)q_{1i}$, is transmitted through the interface. The radiation flux, q_{o1}, leaving the 1-2 interface is made up of the reflected incident radiation, $R_1 q_{i1}$, plus the radiation transmitted through the interface, $(1 - R_1)q_{i2}$. Similar expressions apply for q_{o2}, q_{o3}, and q_{o4}. The internal incident fluxes are $q_{i2} = tq_{o3}$, and $q_{i3} = tq_{o2}$. As a result, there are six equations for the six unknown q's in terms of the incident flux, q_{i1}. If this system of equations is solved (problem 6.6), the following results are obtained for radiation incident on the 1-2 interface.

$$\rho_{12} \equiv \frac{q_{o1}}{q_{i1}} = R_1 + \frac{R_2 (1-R_1)^2 t^2}{1-R_1 R_2 t^2} \tag{6.22}$$

$$\tau \equiv \frac{q_{o4}}{q_{i1}} = \frac{(1-R_1)(1-R_2)t}{1-R_1 R_2 t^2} \tag{6.23}$$

$$\alpha_{12} \equiv \frac{q_{i1} - q_{o1} - q_{o4}}{qi1} = 1 - \rho_{12} - \tau = \frac{(1-R_1)(1-t)(1+tR_2)}{1-R_1 R_2 t^2} \tag{6.24}$$

Equation (6.24), when written as $\alpha_{12} + \rho_{12} + \tau = 1$, is a statement of the conservation of energy.

As can be seen by interchanging R_1 and R_2 in equations (6.22) and (6.24), ρ and α depend upon the direction of the incident radiation. In other words, the overall reflectance and absorptance for radiation incident on the left side is different from ρ and α for radiation incident on the right side if $R_1 \neq R_2$. As is expected, by interchanging R_1 and R_2 in equation (6.23), the overall transmittance, τ, is seen to be independent of the direction of the incident radiation.

The results derived for ρ, α, and τ assume diffuse radiation. However, the q fluxes can be replaced by directionally depend intensities, i, and by a ray-tracing method [1], the same results for ρ, α, and τ are obtained. However, in that case ρ, α, and τ are not be the total hemispherical reflectance, absorptance, and transmittance, but are functions of the incident angle. To obtain the overall total optical properties, solid angle integrations of the product of the intensity and the angular depend properties must be performed. Since equations (6.22) through (6.24) apply for both diffuse and specular (angle dependence) radiation, the unsymmetrical behavior of ρ and α and the symmetrical behavior of τ discussed above applies for both diffuse and specular radiation. For the case where $R_1 \neq R_2$, equations (6.22) through (6.24) imply the following,

$$\alpha_{12} + \rho_{12} = \alpha_{34} + \rho_{34} \quad \text{and} \quad \tau_{12} = \tau_{34} \tag{6.25}$$

where subscript 12 denotes incident radiation on the 1-2 interface, and subscript 34 denotes incident radiation on the 3-4 interface in Figure 6.5.

Although equations (6.22) through (6.24) apply for both diffuse and specular radiation, the total internal transmittance as given by equation (6.21) applies only for diffuse radiation. In the case of specular radiation, the intensity, i(0), in equation (6.17) and (6.18) is a function of θ and must be included in the integrations in order to

determine the total internal transmission. For transmission in a specific direction, equation (6.16) yields the following for the internal transmission.

$$t(\theta) \equiv \frac{i\left(\frac{d}{\cos\theta}\right)}{i(0)} = e^{-\frac{Kd}{\cos\theta}} \tag{6.26}$$

As discussed in Chapter 3, by measuring ρ and τ, the reflectivities, R_1 and R_2, and the internal transmission, τ, can be determined. The first step in this process is to invert equations (6.22) through (6.24) so that R_1, R_2, and t are written as functions of τ and ρ, which has two values depending upon which side the incident radiation occurs. For the case where $R_1 = R_2$ (ρ independent of direction of incident radiation) the following results are obtained (problem 6.7).

$$t = \frac{1}{2}\left[\sqrt{\beta^2 + 4} - \beta\right] \tag{6.27}$$

$$R_1 = R_2 = \frac{2\rho}{2 + \tau\left[\sqrt{\beta^2 + 4} - \beta\right]} \tag{6.28}$$

Where

$$\beta = \frac{(1-\rho)^2 - \tau^2}{\tau} \tag{6.29}$$

6.2.4 Energy Balance on a Component of a TPV System

Remember that the radiative energy reaching A_j from A_i, given by equation (6.5), assumes that i_{oi} is uniform across A_i and is also independent of θ_i. As already stated, a surface that emits and reflects independent of angle θ, is called a diffuse surface. If i_{oi} is a function of $\vec{x}_i$ and θ_i, then it must be included in the integration of equation (6.4). In that case, the integration yields a complicated function of A_i and A_j geometry, as well as temperature, T_i, and wavelength, λ. However, if i_{oi} is uniform across A_i and independent of θ_I, then the rather simple expression given by equation (6.5) is obtained for Q_{ij}. Also, note that Q_{ij} is the radiation that reaches A_j from A_i. It is not the radiation energy absorbed by A_j.

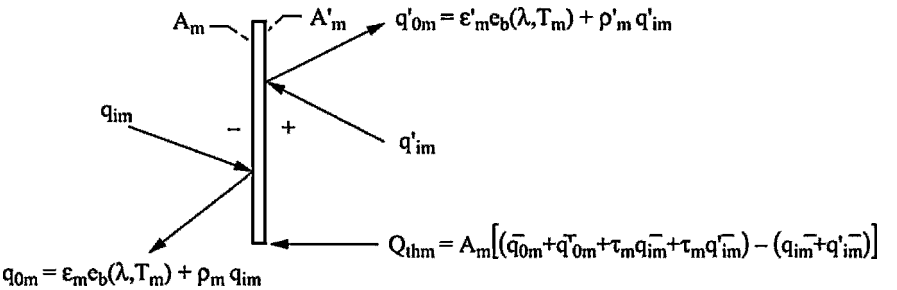

Figure 6.6.—Energy balance on element m of area, A_m.

Now consider a single element, m, of the system as shown in Figure 6.6. Radiation on the left side (negative side) of the element is denoted without a prime, and radiation on the right side (positive side) with a prime. The radiation energy q_{om} and q'_{om} that originate from each side of element m per unit area at wavelength λ are the sum of the emitted radiation and the reflected radiation. The transmitted radiation originates from the other elements in the system and, therefore, is not included in q_{om} and q'_{om}. For radiation leaving the negative side of the element,

$$q_{om} = \varepsilon_m e_b(\lambda, T_m) + \rho_m q_{im} \tag{6.30}$$

and similarly, for the positive side the result is the following.

$$q'_{om} = \varepsilon'_m e_b(\lambda, T_m) + \rho'_m q'_{im} \tag{6.31}$$

where ε_m and ρ_m are the spectral emittance and reflectance for the negative side and ε'_m and ρ'_m are the corresponding quantities for the positive side. The quantity $e_b(\lambda, T_m)$ is the blackbody emissive power. It is assumed that element m is at a uniform temperature, T_m.

Using equations (6.30) and (6.31), an energy balance can be performed on element m. The total energy supplied to element m is just the difference between the total radiant energy leaving m and the total radiant energy incident on m. Assume the q's are uniform across the element. In order to use equation (6.5) for the q_i's, it is necessary to make this approximation. Therefore, the total radiant energy leaving m is the sum of the q_o's and the transmitted radiation integrated over all wavelengths and multiplied by A_m.

$$\bar{Q}_{om} = A_m \int_o^\infty \left[q_{om} + q'_{om} + \tau_m \left(q_{im} + q'_{im} \right) \right] d\lambda \tag{6.32}$$

Note that the emittance (absorptance) and reflectance may be different for each side of m. However, transmittance, τ_m, is the same for both sides.

Similarly, the total radiant energy incident on m is the following.

$$\bar{Q}_{im} = A_m \int_o^\infty \left[q_{im} + q'_{im} \right] d\lambda \tag{6.33}$$

Therefore, using equations (6.24), (6.30), and (6.31), the energy supplied to m is the following,

$$\bar{Q}_m = \bar{Q}_{om} - \bar{Q}_{im} = A_m \int_o^\infty \left[\left(\varepsilon_m + \varepsilon'_m \right) e_b \left(\lambda, T_m \right) - \left(\alpha_m q_{im} + \alpha'_m q'_{im} \right) \right] d\lambda \tag{6.34a}$$

and since $\varepsilon = \alpha$,

$$\bar{Q}_m = A_m \int_o^\infty \left[\varepsilon_m \left(e_b \left(\lambda, T_m \right) - q_{im} \right) + \varepsilon'_m \left(e_b \left(\lambda, T_m \right) - q'_{im} \right) \right] d\lambda \tag{6.34b}$$

Thus, see from equation (6.34a) that $\bar{Q}_m$ is just the difference between the total emitted energy and the total absorbed energy. If the absorbed energy is greater than the emitted energy, then $\bar{Q}_m < 0$. In that case $\bar{Q}_m$ is the amount of thermal energy that must be removed from element m. For the window and filter, this is an absorptive thermal energy loss, $\bar{Q}_{Lm}$. For the PV cells, it is the sum of the electrical power produced $\bar{Q}_{EL}$, and the absorption loss for the PV cells, $\bar{Q}_{LC}$. In the case of the emitter, $\bar{Q}_m > 0$, since energy is always being supplied.

Equations (6.34a) and (6.34b) are written in terms of the incident radiation, q_{im} and q'_{im}. They can also be expressed in terms of the outgoing radiation, q_{om} and q'_{om}, by using equations (6.30) and (6.31) for q_{im} and q'_{im}. In that case, using equations (6.12) and (6.24), $\bar{Q}_m$ becomes the following.

$$\bar{Q}_m = A_m \int_o^\infty \left\{ \frac{\varepsilon_m}{1-\tau_m-\varepsilon_m}\left[(1-\tau_m)e_b(\lambda,T_m)-q_{om}\right] + \frac{\varepsilon'_m}{1-\tau_m-\varepsilon'_m}\left[(1-\tau_m)e_b(\lambda,T_m)-q'_{om}\right]\right\} d\lambda \tag{6.34c}$$

6.3 Radiation Energy Transfer in Planar TPV System

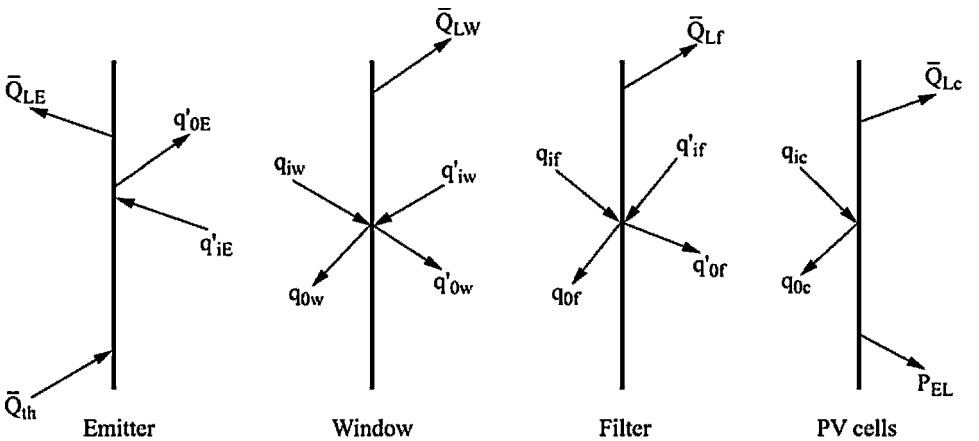

P_{EL} = Total electrical power output, W
$\bar{Q}_{th}$ = Total power input, W
$\bar{Q}_{Lm}$ = Total power loss for component m, W

Figure 6.7.—Schematic representation of general planar TPV system.

Consider a general planar TPV system consisting of an emitter, window, filter, and PV cells shown schematically in Figure 6.7. The efficiency of the system is the following.

$$\eta_T = \frac{P_{EL}}{\bar{Q}_{th}} = 1 - \frac{\bar{Q}_{LE}+\bar{Q}_{Ls}+\bar{Q}_{LW}+\bar{Q}_{Lf}+\bar{Q}_{LC}}{\bar{Q}_{th}} \tag{6.35}$$

Where P_{EL} is the total electrical power output from the PV cells and $\bar{Q}_{th}$ is the total thermal power input to the emitter. The $\bar{Q}_L$ terms are the power losses in the system. The term $\bar{Q}_{LE}$ is the thermal loss from the emitter plus all losses that occur between the source, $\bar{Q}_{th}$, and the emitter. $\bar{Q}_{Ls}$ is the radiation that escapes between the components

of the system. $\bar{Q}_{LW}$ is the absorption loss of the window. $\bar{Q}_{Lf}$ is the absorption loss of the filter , and $\bar{Q}_{LC}$ is absorption loss of the PV cells. In order to determine η_T, all the radiation fluxes shown in Figure 6.7 must first be calculated. To obtain these fluxes the radiation transfer equations for the system must be solved. The radiation transfer equations are obtained using the results of Section 6.2. Consider any of the four components shown in Figure 6.7. Give that component the designation, m. The radiation energy originating from the negative side of m per unit area at wavelength, λ, is the sum of the emitted radiation and the reflected radiation; it is given by equation (6.30).

The radiation incident on the negative side of m per unit area at wavelength λ is q_{im}. If it is assumed that q_{im} is uniform across m, then the total radiation at wavelength λ reaching m from all other elements to the left of m is obtained by using equation (6.5).

$$Q_{im} = A_m q_{im} = \sum_{n-1}^{m-1} \tau_{nm} q'_{on} F_{nm} A_n \qquad m > 1 \tag{6.36}$$

$$\tau_{nm} = \tau_{n+1}\tau_{n+2}\cdots\tau_{m-1} \qquad n < m-1 \tag{6.37a}$$

$$\tau_{nm} = 1 \qquad n = m-1 \tag{6.37b}$$

Note that in using equation (6.5), it has been assumed that q_{on} is uniform across element n. Also note that q'_{on} radiation passes through the negative side of adjoining elements.

Similarly, for the positive side, the results are the following,

$$Q'_{im} = A_m q'_{im} = \sum_{n=m+1}^{N} \tau_{mn} q_{on} F_{nm} A_n \tag{6.38}$$

where N is the total number of components in the system and τ_{mn} is defined by equations (6.37a) and (6.37b). Again, in using equation (6.5) it has been assumed that the q_o's are uniform across each element.

Using equation (6.7), equations (6.36) and (6.37) can be written as follows.

$$q_{im} = \sum_{n=1}^{m-1} \tau_{nm} q'_{on} F_{mn} \tag{6.39}$$

$$q'_{im} = \sum_{n=m+1}^{N} \tau_{nm} q_{on} F_{mn} \tag{6.40}$$

If equation (6.30) is used for q_{im} in equation (6.39), and equation (6.31) is used for q'_{im} in equation (6.40), the following results.

$$q_{om} - \rho_m \sum_{n-1}^{m-1} \tau_{nm} q'_{on} F_{mn} = \varepsilon_m e_b(\lambda, T_m) \equiv q_m(\lambda, T_m) \tag{6.41}$$

$$q'_{om} - \rho'_m \sum_{n=m+1}^{N} \tau_{nm} q_{on} F_{mn} = \varepsilon'_m e_b(\lambda, T_m) \equiv q'_m(\lambda, T_m) \tag{6.42}$$

Notice that two new terms, q_m and q'_m, have been defined. They are the emissive powers of element m. For each element of the system, equations (6.41) and (6.42) can be applied. Thus, a system of 2N linear algebraic equations for the q_o's and the q'_o's result. However, the temperature, T_m, of each element must be given in order to obtain a solution. Once the q_o's are known, the q_i's can be determined using equations (6.30) and (6.31).

For the planar TPV system of Figure 6.7, which contains four elements, there are six equations to be solved for the q_o's (six rather than eight since $q_{oE} = q_{iE} = q'_{oC} = q'_{iC} = 0$). Applying equations (6.41) and (6.42), the following six equations are obtained.

$$q_{oW} - \rho_W q'_{oE} F_{WE'} = q_W \tag{6.43}$$

$$q_{of} - \rho_f \left[\tau_W q'_{oE} F_{fE'} + q'_{oW} F_{fW'} \right] = q_f \tag{6.44}$$

$$q_{oC} - \rho_C \left[\tau_W \tau_f q'_{oE} F_{CE'} + \tau_f q'_{oW} F_{CW'} + q'_{of} F_{Cf'} \right] = q_C \tag{6.45}$$

$$q'_{oE} - \rho'_E \left[q_{oW} F_{E'W} + \tau_W q_{of} F_{E'f} + \tau_W \tau_f q_{oC} F_{E'C} \right] = q'_E \tag{6.46}$$

$$q'_{oW} - \rho'_W \left[q_{of} F_{W'f} + \tau_f q_{oc} F_{W'C} \right] = q'_W \tag{6.47}$$

$$q'_{of} - \rho'_f q_{oC} F_{f'C} = q'_f \tag{6.48}$$

The quantities q_{oW} and q'_{of} can be eliminated from the system of equations by using (6.43) in (6.46), and equation (6.48) in (6.45) to yield the following.

$$\left[1-\rho'_E\rho_W F_{E'W}F_{WE'}\right]q'_{oE}-\rho'_E\left[q_W F_{E'W}+\tau_W F_{E'f}q_{of}+\tau_W\tau_f F_{E'C}q_{oC}\right]=q'_E \tag{6.49}$$

$$\left[1-\rho'_f\rho_C F_{fC}F_{Cf'}\right]q_{oC}-\rho_C\left[\tau_W\tau_f F_{CE'}q'_{oE}+\tau_f F_{CW'}q'_{oW}+q'_f F_{Cf'}\right]=q_C \tag{6.50}$$

Now substitute (6.47) for q'_{oW} in (6.44) and (6.50) to eliminate q'_{oW} from the system of equations.

$$\left[1-\rho'_W\rho_f F_{W'f}F_{fW'}\right]q_{of}-\rho_f\left[\tau_W F_{fE'}q'_{oE}+F_{fW'}\left(q'_W+\rho'_W\tau_f q_{oC}F_{W'C}\right)\right]=q_f \tag{6.51}$$

$$\begin{gathered}\left[1-\rho'_f\rho_c F_{fC}F_{Cf'}-\rho'_W\rho_C\tau_f^2 F_{W'C}F_{CW'}\right]q_{oC}\\ -\rho_C\left[\tau_W\tau_f F_{CE'}q'_{oE}+\rho'_W\tau_f F_{W'f}F_{CW'}q_{of}+\tau_f F_{CW'}q'_W+F_{Cf'}q'_f\right]=q_C\end{gathered} \tag{6.52}$$

Equations (6.49), (6.51), and (6.52) are three linear simultaneous equations for q'_{oE}, q_{of}, and q_{oC}. The filter term, q_{of}, can be eliminated by multiplying equation (6.49) by $1-\rho'_W\rho_f F_{W'f}F_{fW'}$, and equation (6.51) by $\rho'_E\tau_W F_{E'f}$, and adding the resulting two equations. Then multiply equation (6.52) by $1-\rho'_W\rho_f F_{W'f}F_{fW'}$, and multiply equation (6.51) by $\rho'_W\rho_C\tau_f F_{W'f}F_{CW'}$, and add the results. Thus, the following two equations for q'_{oE} and q_{oC} are derived,

$$a_E q'_{oE}-a_C q_{oC}=S_E \tag{6.53}$$

$$-b_E q'_{oE}+b_C q_{oC}=S_C \tag{6.54}$$

where

$$a_E=\left(1-\rho'_E\rho_W F_{E'W}F_{WE'}\right)\left(1-\rho'_W\rho_f F_{W'f}F_{fW'}\right)-\rho'_E\rho_f\tau_W^2 F_{E'f}F_{fE'} \tag{6.55}$$

$$a_C=\rho'_E\tau_W\tau_f\left[F_{E'C}+\rho'_W\rho_f F_{fW'}\left(F_{E'f}F_{W'C}-F_{E'C}F_{W'f}\right)\right] \tag{6.56}$$

$$b_E=\rho_C\tau_W\tau_f\left[F_{CE'}+\rho'_W\rho_f F_{W'f}\left(F_{CW'}F_{fE'}-F_{fW'}F_{CE'}\right)\right] \tag{6.57}$$

$$b_C = \left(1-\rho'_W\rho_f F_{W'f}F_{fW'}\right)\left(1-\rho'_f\rho_C F_{f'C}F_{Cf'}\right)-\rho'_W\rho_C\tau_f^2 F_{CW'}F_{W'C} \tag{6.58}$$

$$S_E = \left(1-\rho'_W\rho_f F_{W'f}F_{fW'}\right)\left(q'_E+\rho'_E F_{E'W}q_W\right)+\rho'_E\tau_W F_{E'f}\left(\rho_f F_{fW'}q'_W+q_f\right) \tag{6.59}$$

$$S_C = \left(1-\rho'_W\rho_f F_{W'f}F_{fW'}\right)\left(q_C+\rho_C F_{Cf}q'_f\right)+\rho_C\tau_f F_{CW'}\left(q'_W+\rho'_W F_{W'f}q_f\right) \tag{6.60}$$

Equations (6.53) and (6.54) give q'_{oE} and q_{oC} in terms of the parameters a, b andS. In turn, the a, b, and S parameters are functions of the component optical properties and view-factors, and the radiation sources (q'_E, q_W, q'_W, q_f, q'_f, q_C). Since the optical properties are functions of the wavelength, λ, these equations must be solved at each λ to obtain $q'_{oE}(\lambda)$ and $q_{oC}(\lambda)$. Therefore, only with the aid of a computer can the general case be easily solved. However, assuming the optical properties are constants within a limited number of wavelength ranges (or bands) greatly reduces the complexity. A four-band model is used in [3].

6.4 Radiation Energy Transfer in Cylindrical TPV System

Figure 6.8 shows a general cylindrical TPV system consisting of the same four elements as the planar system in Figure 6.7. The cylindrical geometry results in additional view-factors not present in a planar system. As already mentioned, the concave inner surface has a "self" view-factor. In addition, transmission through adjoining elements allows radiation from the concave side of an element, q_{om}, to be incident on an adjoining element's concave side. Therefore, the simple results for q_{im} and q'_{im} for a planar system given by equations (6.39) and (6.40) are no longer applicable. However, the same relations [equations (6.30) and (6.31)] between q_{om} and q_{im} and q'_{om} and q'_{im} that apply for the planar geometry also apply for the cylindrical geometry.

First, consider the window in Figure 6.8. Applying equation (6.5) to the concave side and remembering that the emitter is opaque ($\tau_E = 0$) results in the following equation for q_{iW}.

$$A_W q_{iW} = q'_{oE}F_{E'W}A_E + q_{oW}F_{WW}A_W + \tau_W q_{of}F_{fW}^{W}A_f + \tau_f\tau_W q_{oc}F_{CW}^{fW}A_C \tag{6.61}$$

Note that the prime denotes the convex side and the unprimed denotes the concave side of an element. Also, in equation (6.61) view-factors with superscripts have been introduced. These are the view-factors discussed in Section 6.2.2, between the concave side of element i, and the concave side of element j, for radiation passing through

elements m and n. The superscripted view-factors F_{CW}^{fW} and F_{fW}^{W} are given by equations (6.9) and (6.11). The view-factor $F_{E'W}$ is given by $\frac{A_W}{A_E}F_{WE'}$, where $F_{WE'}$ is given by F_{21} in Figure 6.3d with $r_2 = r_W$ and $r_1 = r_E$. Finally, F_{WW} is given by F_{22} in Figure 6.3d, where $r_2 = r_W$ and $r_1 = r_E$.

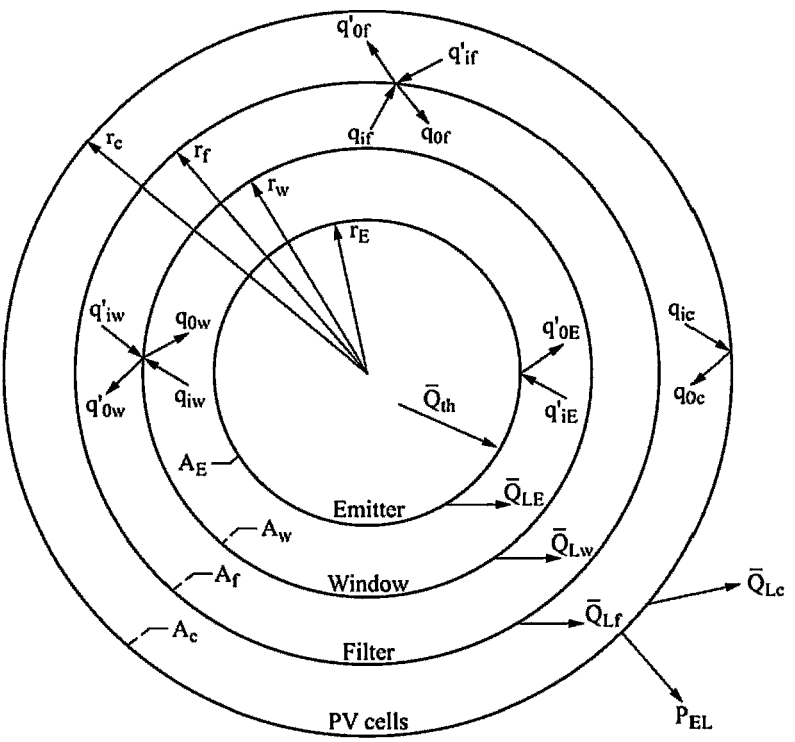

P_{EL} = Total electrical power output, W
$\bar{Q}_{th}$ = Total power input, W
$\bar{Q}_{Lm}$ = Total power loss for component m, W
A_m = Surface area of component m, cm^2

q_{im} = Radiative flux incident on concave (negative) side of component m
q_{0m} = Radiative flux originating from concave (negative) side of component m
q'_{im} = Radiative flux incident on convex (positive) side of component m
q'_{0m} = Radiative flux originating from convex (positive) side of component m

Figure 6.8.—Schematic representation of general cylindrical TPV system.

Applying equations (6.7) and (6.30) to (6.61) yields the following equation for q_{oW}.

$$q_{oW}\left(1-\rho_W F_{WW}\right)=\rho_W\left(q'_{oE}F_{WE'}+\tau_W q_{of}F^{W}_{Wf}+\tau_f\tau_W q_{oC}F^{fW}_{WC}\right)+q_W \tag{6.62}$$

Similarly, for the concave sides of the filter and PV cells, the following equations are obtained.

$$\begin{gathered} q_{of}\left[1-\rho_f\left(F_{ff}+\tau_W^2F^{W}_{ff}\right)\right]= \\ \rho_f\left[q'_{oW}F_{fW'}+\tau_W q'_{oE}F_{fE'}+\tau_W q_{oW}F^{W}_{fW}+\tau_f q_{oC}\left(F^{f}_{fC}+\tau_W^2F^{fW}_{fC}\right)\right]+q_f \end{gathered} \tag{6.63}$$

$$\begin{gathered} q_{oC}\left[1-\rho_C\left(F_{CC}+\tau_f^2F^{f}_{CC}+\tau_f^2\tau_W^2F^{fW}_{CC}\right)\right]= \\ \rho_C\left[\tau_W\tau_f q'_{oE}F_{CE'}+\tau_f q'_{oW}F_{CW'}+q'_{of}F_{Cf'}+\tau_W\tau_f q_{oW}F^{fW}_{CW}+\tau_f q_{of}\left(F^{f}_{Cf}+\tau_W^2F^{fW}_{Cf}\right)\right]+q_C \end{gathered} \tag{6.64}$$

Now consider the convex sides of the filter, window, and emitter. Applying equations (6.5) and (6.31) yields the following results.

$$q'_{of}=\rho'_f q_{oC}F_{f'C}+q'_f \tag{6.65}$$

$$q'_{oW}=\rho'_W\left(q_{of}F_{W'f}+\tau_f q_{oC}F_{W'C}\right)+q'_W \tag{6.66}$$

$$q'_{oE}=\rho'_E\left(q_{oW}F_{E'W}+\tau_W q_{of}F_{E'f}+\tau_W\tau_f F_{E'C}q_{oC}\right)+q'_E \tag{6.67}$$

Equations (6.62) and (6.67) form a set of six linear algebraic equations for the radiation fluxes q_{oW}, q_{of}, q_{oC}, q'_{of}, q'_{oW}, and q'_{oE}. The system of six equations can be reduced to two equations for the radiation flux leaving the emitter, q'_{oE}, and the radiation flux leaving the PV cells, q_{oC}. The first step in this long and tedious process is to eliminate q_{oW}, q'_{oW}, and q'_{of} from the system of equations by substituting equations (6.62) for q_{oW} and (6.66) for q'_{oW} in (6.63) to obtain the following equation for q_{of} as a function of q_{oC} and q'_{oE}.

$$\begin{gathered} q_{of}\left[1-d_f-\rho'_W\rho_f F_{fW'}F_{W'f}\right]=\rho_f\left[\tau_W\left(F_{fE'}+\frac{\rho_W}{D_W}F_{WE'}F^{W}_{fW}\right)q'_{oE}+\right. \\ \left.\tau_f\left(\rho'_W F_{W'f}F_{fW'}+c_W\right)q_{oC}+F_{fW'}q'_W+\frac{\tau_W}{D_W}F^{W}_{fW}q_W\right]+q_f \end{gathered} \tag{6.68}$$

$$c_W = F_{fC}^{f} + \tau_W^2 \left(F_{fC}^{fW} + \frac{\rho_W}{D_W} F_{fW}^{W} F_{WC}^{fW} \right) \tag{6.69}$$

$$d_f = \rho_f \left[F_{ff} + \tau_W^2 \left(F_{ff}^{W} + \frac{\rho_W}{D_W} F_{fW}^{W} F_{Wf}^{W} \right) \right] \tag{6.70}$$

$$D_W = 1 - \rho_W F_{WW} \tag{6.71}$$

Now substitute equation (6.62) for q_{oW}, (6.65) for q'_{of}, (6.66) for q'_{oW}, and (6.68) for q_{of} in equation (6.64) to obtain one equation for q'_{oE} and q_{oC}. A second equation for q'_{oE} and q_{oC} is obtained by substituting equation (6.62) for q_{oW} and (6.68) for q_{of} in equation (6.67). Therefore, the following two simultaneous equations for q_{oC} and q'_{oE} are obtained,

$$a_E q'_{oE} - a_C q_{oC} = S_E \tag{6.72}$$

$$-b_E q'_{oE} + b_C q_{oC} = S_C \tag{6.73}$$

where

$$\begin{aligned} a_E = &\left[1 - \frac{\rho'_E \rho_W}{D_W} F_{E'W} F_{WE'} \right] \left[1 - \rho'_W \rho_f F_{fW'} F_{W'f} - d_f \right] - \\ &\rho'_E \rho_f \tau_W^2 \left[F_{E'f} F_{fE'} + \frac{\rho_W}{D_W} F_{E'W} F_{Wf}^{W} \right] \left[F_{fE'} + \frac{\rho_W}{D_W} F_{WE'} F_{fW}^{W} \right] \end{aligned} \tag{6.74}$$

$$\begin{aligned} a_C = \rho'_E \tau_W \tau_f \Big\{ &\left[F_{E'C} \left(1 - d_f \right) + \rho'_W \rho_f F_{fW'} \left(F_{E'f} F_{W'C} - F_{E'C} F_{W'f} \right) \right] + \\ &\frac{\rho_W}{D_W} \left[1 - \rho'_W \rho_f F_{fW'} F_{W'f} - d_f \right] F_{E'W} F_{WC}^{fW} + \\ &\rho_f \left[c_W \left(F_{E'f} + \frac{\rho_W}{D_W} F_{E'W} F_{Wf}^{W} \right) + \frac{\rho_W \rho'_W}{D_W} F_{E'W} F_{fW'} F_{W'C} F_{Wf}^{W} \right] \Big\} \end{aligned} \tag{6.75}$$

$$b_C = \left(1-\rho'_W\rho_f F_{fW'}F_{W'f} - d_f\right)\left(1-\rho_C\rho'_f F_{Cf'}F_{f'C}\right) - \rho_C\left\{\rho'_W\,\tau_f^2\left[F_{CW'}F_{W'C}\left(1-d_f\right)+\rho_f\left(F_{CW'}F_{W'f}c_W + F_{W'C}F_{fW'}c_f\right)\right]+ c_C\left[1-\rho'_W\rho_f F_{fW'}F_{W'f} - d_f\right]+\rho_f\tau_f^2 c_f c_W\right\} \tag{6.76}$$

$$b_E = \rho_C\tau_W\tau_f\left[F_{CE'}\left(1-d_f\right)+\rho'_W\rho_f F_{W'f}\left(F_{CW'}F_{fE'} - F_{fW'}F_{CE'}\right)+\rho_f F_{fE'}c_f + \frac{\rho_W}{D_W}F_{WE'}d_W\right] \tag{6.77}$$

$$S_E = \left[1-\rho'_W\rho_f F_{fW'}F_{W'f} - d_f\right]\left[q'_E + \frac{\rho'_E}{D_W}F_{E'W}q_W\right]+ \rho'_E\tau_W\left[F_{E'f}+\frac{\rho_W}{D_W}F_{E'W}F^W_{Wf}\right]\left[q_f+\rho_f\left(F_{fW'}q'_W+\frac{\tau_W}{D_W}F^W_{fW}q_W\right)\right] \tag{6.78}$$

$$S_C = \left[1-\rho'_W\rho_f F_{fW'}F_{W'f} - d_f\right]\left[q_C+\rho_C\left(F_{Cf'}q'_f+\frac{\tau_W\tau_f}{D_W}F^{fW}_{CW}q_W\right)\right]+ \rho_C\tau_f\left\{\left[F_{CW'}\left(1-d_f\right)+\rho_f F_{fW'}c_f\right]q'_W+\left[c_f+\rho'_W F_{CW'}F_{W'f}\right]\left[q_f+\frac{\rho_f\tau_W}{D_W}F^W_{fW}q_W\right]\right\} \tag{6.79}$$

$$c_C = F_{CC}+\tau_f^2\left[F^f_{CC}+\tau_W^2\left(F^{fW}_{CC}+\frac{\rho_W}{D_W}F^{fW}_{CW}F^{fW}_{WC}\right)\right] \tag{6.80}$$

$$c_f = F^f_{Cf}+\tau_W^2\left(F^{fW}_{Cf}+\frac{\rho_W}{D_W}F^{fW}_{CW}F^W_{Wf}\right) \tag{6.81}$$

$$d_W = F^{fW}_{CW}\left(1-\rho'_W\rho_f F_{fW'}F_{W'f} - d_f\right)+\rho_f F^W_{fW}\left(\rho'_W F_{CW'}F_{W'f}+c_f\right) \tag{6.82}$$

The system of equations (6.72) and (6.73) for the cylindrical geometry reduces to the planar geometry [equations (6.53) and (6.54)], using the condition that view-factors between concave surfaces vanish (problem 6.9).

Just as in the case of the planar geometry, when the optical properties are functions of wavelength, the radiation fluxes will also be functions of wavelength. Therefore, in order to calculate the $\bar{Q}_m$ quantities required for the determination of the efficiency [equation (6.35)], the equations for q'_{oE} and q_{oC} must be solved at each wavelength. As mentioned at the end of Section 6.3, such a large calculation requires a computer solution.

6.5 Efficiency of TPV Systems

6.5.1 Overall Efficiency

At the beginning of Section 6.3 [equation (6.35)], the TPV system efficiency, η_T, is defined. To evaluate the effect upon η_T of the various parts of the system, split the efficiency into three parts as follows,

$$\eta_T = \eta_{th}\eta_c\eta_{PV} \tag{6.83}$$

where η_{th} is the thermal efficiency, η_c is the cavity efficiency, and η_{PV} is the photovoltaic efficiency.

6.5.2 Thermal Efficiency

The thermal efficiency, η_{th}, accounts for conductive, convective, and radiative heat loss from the emitter, plus any heat loss that occurs between the thermal source, $\bar{Q}_{th}$, and the emitter

$$\eta_{th} = \frac{\bar{Q}_{th} - \bar{Q}_{LE}}{\bar{Q}_{th}} = \frac{\bar{Q}_E}{\bar{Q}_{th}} \tag{6.84}$$

The net power leaving the emitter is $\bar{Q}_E$ and is obtained from equation (6.34c) by including only the positive terms (primed quantities). Any negative going radiation (unprimed quantities) is included in the loss term, $\bar{Q}_{LE}$. Also, $\tau_E = 0$, since the emitter is opaque.

$$\bar{Q}_E = A_E \int_0^\infty \frac{\varepsilon'_E}{1-\varepsilon'_E}\left[\varepsilon_b(\lambda, T) - q'_{oE}\right] d\lambda \tag{6.85}$$

6.5.3 Cavity Efficiency

The cavity efficiency, η_{cf}, gives the fraction of useful radiation delivered to the PV cells by the *optical cavity*, which consists of the emitter, window, and filter,

$$\eta_c = \frac{\bar{Q}_C}{\bar{Q}_E} \tag{6.86}$$

where $\bar{Q}_C$ is the useful power delivered to the PV array. It includes only photons with sufficient energy to produce current in the PV array $\left(\lambda \le \lambda_g = \frac{hc_o}{E_g}\right)$.

$$\bar{Q}_C = A_a \int_o^{\lambda_g} q_{iC} d\lambda = A_a \int_o^{\lambda_g} \frac{1}{\rho_C}\left[q_{oC} - \varepsilon_C e_b\left(\lambda, T_C\right)\right] d\lambda \tag{6.87}$$

Here A_a is the PV array area.

6.5.4 Photovoltaic Efficiency

Finally, the photovoltaic efficiency is the following,

$$\eta_{PV} = \frac{P_{EL}}{\bar{Q}_C} \tag{6.88}$$

where the electrical power output P_{EL} is computed in Chapter 5. The output power density can be expressed in several ways, one of which is equation (5.239),

$$P_{EL} = FFV_{oc}I_{sc} \tag{5.239}$$

where the fill factor, FF, and open circuit potential, V_{oc}, are slowly varying functions of the short circuit current, I_{sc}, (see Chapter 5).

Once $q_{oC}(\lambda)$ and $q_{oE}(\lambda)$ are obtained by solving either equations (653) and (6.54) for a planar system, or equations (6.72) and (6.73) for a cylindrical system, the efficiencies, η_C and η_{PV} can be calculated.

6.6 Summary

Chapter 6 develops the radiation transfer theory necessary to calculate the power output and efficiency of a TPV energy converter. The major assumptions of the theory are that the components of the TPV system behave in a diffuse manner and that the radiation intensity is uniform over the surface of a component. With these assumptions, the necessary quantities in the analysis are introduced:

1) View-factor or configuration factor, F_{ij} [equation (6.6)].
2) Radiation flux leaving the surface of a component, q_o [equations (6.30) and (6.31)].
3) Energy supplied to a component, $\bar{Q}$ [equation (6.34)].
4) Radiation flux per wavelength incident on a component, Q [equation (6.5)].

Using these quantities, equations for the radiation fluxes leaving the emitter, q'_{oE}, and the PV array, q_{oC}, are derived for both a planar geometry [equations (6.53) and (6.54)] and a cylindrical geometry [equations (6.72) and (6.73)]. Finally, the following efficiencies are introduced:

1) TPV system efficiency, $\eta_T = \eta_{th}\eta_C\eta_{PV}$ [equation (6.35)].
2) Thermal efficiency, η_{th} [equation (6.84)].
3) Cavity efficiency, η_C [equation (6.86)].
4) Photovoltaic efficiency, η_{PV} [equation (6.88)].

References

[1] R. Siegel, and J. R. Howell, Thermal Radiation Heat Transfer, 2nd ed., Hemisphere Publishing Corp., New York, 1981.
[2] D. E. Bornside, and R. A. Brown, J. Thermophysics, 4, 414-416 (1990).
[3] B. S. Good, D. L. Chubb, and R. A. Lowe, Proceedings of the Second NRL Conference on Thermophotovoltaic Generation of Electricity, AIP Conference Proceedings, 358 (1996).
[4] M. Crawford, ASME publication 72-WA/HT-16, ASME Winter Annual Meeting, Aug. 4, 1972.

Problems

6.1 In calculating a view-factor, it is useful to split the double integration in equation (6.6) into two parts. If A_i is an infinitesimal area, then equation (6.6) becomes the following,

$$F_{dij} = \frac{1}{\pi}\int_{A_j}\frac{\cos\theta_i \cos\theta_j}{S^2}\,dA_j$$

where the subscript di denotes that i is an elemental area. Once F_{dij} is calculated, then F_{ij} can be determined from the following equation.

$$F_{ij} = \frac{1}{A_i}\int_{A_i} F_{dij}\,dA_i$$

For a plane elemental area dA_1 parallel to a circular disk of radius r_2 and area A_2 as shown, calculate F_{d12}. Using F_{d12}, calculate the view-factor for two parallel circular disks as shown in Figure 6.3a.

6.2 For two parallel circular disks of the same radius, R, separated a distance, h, and with centers along the same normal, show that for large $z = \frac{R}{h}$ the view-factor can be approximated as follows.

$$F_{21} = F_{12} \approx 1 - \frac{1}{z} + \frac{1}{2z^2} - O\left(\frac{1}{z^3}\right) \qquad \text{for } z \gg 1$$

Similarly, for two directly opposed square disks with sides of length, a, and separated by a distance, h, show that for large $x = \frac{a}{h}$, the view-factor can be approximated as follows.

$$F_{21} = F_{12} \approx 1 - \frac{2}{x} + \frac{2}{\pi}\left[2 + \frac{\pi}{4} + \ln\left(\frac{x}{\sqrt{2}}\right)\right]\frac{1}{x^2} - O\left(\frac{1}{x^4}\right) \qquad \text{for } x \gg 1$$

Compare the view-factors calculated using the approximate expressions with the exact results (Figure 6.3) for x = 4 and 6 for the square disks. Also, make the same calculation for circular disks with areas equal to the square disks areas $\left(z = \frac{x}{\sqrt{\pi}}\right)$. Based upon these results, which configuration is more advantageous for a TPV system?

6.3 For two concentric cylinders of radii, r_1 and r_2 ($r_2 > r_1$), and length, ℓ, show that for $L = \frac{\ell}{r_1} \gg z = \frac{r_2}{r_1}$ the view-factor F_{21} can be approximated by the following expression.

$$F_{21} \approx \frac{1}{z} - \frac{1}{\pi z L}\left\{\frac{\pi}{2}\left(z^2 - 1\right) - \left[z^2 - \left(\frac{z^2 - 1}{2L}\right)^2 + O\left(\frac{1}{L^4}\right)\right]\cos^{-1}\frac{1}{z}\right\}$$

$$\text{for } L \gg z$$

6.4 Compare the view-factors, F_{12} and F_{21}, for parallel circular disks of the same radius, R_d, with centers along the same normal and with the same distance between them, $h = R_2 - R_1$, as concentric cylinders with radii, R_1, R_2, ($R_2 > R_1$) and length, ℓ, where the disk surface area, πR_d^2, and inner cylinder area, $2\pi R_1 \ell$ are equal. Make the comparison for $z = \dfrac{R_2}{R_1} = 2$ and $L = \dfrac{\ell}{R_1} = 8$. Use the results from problems 6.2 and 6.3 for F_{12} to show that to first order in $\dfrac{h}{R_d}$,

$$\frac{F_{12}\big|_{disk}}{F_{12}\big|_{cy}} \approx \frac{1 - h_r}{1 - h_r\sqrt{\dfrac{2}{L}}} \qquad \text{where} \qquad h_r = \frac{h}{R_d},\ L = \frac{\ell}{R_1}$$

6.5 Make the same comparison as in problem 6.3; however, assume $\pi R_d^2 = 2\pi R_2 \ell$, rather than $\pi R_d^2 = 2\pi R_1 \ell$.

6.6 With the aid of Figure 6.5, set up the six equations for the six unknown quantities, q_{o1}, q_{o2}, q_{o3}, q_{o4}, q_{i2}, and q_{i3}. Then solve for the reflectance, ρ_{12}, transmittance, τ, and absorptance, α_{12}, defined as follows.

$$\rho_{12} = \frac{q_{o1}}{q_{i1}} \qquad \tau = \frac{q_{o4}}{q_{i1}} \qquad \alpha_{12} = \frac{q_{i1} - q_{o1} - q_{o4}}{q_{i1}}$$

6.7 Solve equations (6.22) through (6.24) for t and R for the case when $R_1 = R_2 = R$ to obtain the results given by equations (6.27) through (6.28).

6.8 Making use of Figure 6.7 and equations (6.5), (6.30), and (6.31) derive equations (6.64) and (6.67) for q_{oc} and $q_{oE'}$ in a cylindrical geometry TPV system.

6.9 Show that the equations for a planar TPV system [equations (6.53) and (6.54)] can be obtained from the cylindrical geometry equations (6.72) and (6.73) using the condition that view-factors between concave surfaces vanish.

6.10 Derive an equation for the window loss, $\overline{Q}_{WL}$, from equation (6.34c) in terms of $q_{oE'}$ and q_{oC} using equations (6.62), (6.66), and (6.68).

Chapter 7
Radiation Losses in Optical Cavity

At this point it is appropriate to consider the factors that determine the efficient utilization of the radiation that leaves the emitter. In other words, how much of the emitted radiation that reaches PV cells can be converted to electrical energy? Radiation leaving the emitter is lost in two ways. First, radiation can escape from the system by "leaking" out between the components. This loss is controlled by the view-factors, which depend upon the system geometry (planar or cylindrical). The second radiation loss process is absorption. There are absorption losses for the window, filter, and any other component lying between the emitter and PV cells. Radiation leakage is the main topic of this chapter.

It is the cavity efficiency, η_c, defined by equation (6.86) that accounts for the leakage and absorption losses. Also, the power, $\overline{Q}_C$, in the definition of η_c only includes the radiation that can be converted to electrical energy by the PV cells. Therefore, the cavity efficiency accounts for the effectiveness of the emitter-filter combination in shaping the radiation spectrum to match the PV cell spectral response, as well as, radiation leakage losses.

This chapter presents derivations of the cavity efficiency of both planar and cylindrical geometry TPV system. End reflectors to prevent leakage of radiation from the system are also included. Based on the derived cavity efficiencies the importance of view-factors in preventing leakage of radiation is discussed.

7.1 Symbols

A	area
$e_b(\lambda,T)$	emissive power of blackbody [equation (1.120)]
F	view-factor
$F_{o\text{-}\lambda T}$	fraction of blackbody intensity or emissive power lying in region 0-λT [equation (1.137)]
q	radiant energy per unit time per unit wavelength per unit area, W/cm^{2}nm
$\overline{Q}$	radiant energy per unit time, W
ε	spectral emittance
λ	wavelength, μm
ρ	spectral reflectance

τ spectral transmitance
η_c cavity efficiency [equation (6.86)]

Subscripts or Superscripts

b end reflector
C PV array
E emitter
f filter
W window

7.2 Cavity Efficiency for Planar Filter and Selective Emitter TPV Systems without a Window

Consider the cavity efficiency, η_c, for a planar TPV system. To calculate $\bar{Q}_C$ and $\bar{Q}_E$, the solution to the radiation flux equations for q'_{oE} and q_{oC} [equations (6.53) and (6.54)] must first be obtained. To simplify the problem, several approximations can be made. First, since the window, filter, and PV cells are at much lower temperatures than the emitter, it is reasonable to neglect the emissive powers of the window (q_W and q'_W), filter (q_f and q'_f), and PV cells (q_C). Also, assume the window reflectances and absorption are small ($\rho_W = \rho_{W'} = \alpha_W \approx 0$) so that $\tau_W = 1$ and there is no window loss ($\bar{Q}_{LW} = 0$). Neglecting the emissive power of the window, filter, and PV cells and assuming $\tau_W = 1$ ($\rho_W = \rho_{W'} = \alpha_W = 0$) yields the following result for equations (6.53) and (6.54).

$$\left(1-\rho'_E\rho_f F_{E'f}F_{fE'}\right)q'_{oE} - \rho'_E\tau_f F_{E'C}q_{oC} = \varepsilon'_E e_\lambda\left(\lambda, T_E\right) \tag{7.1}$$

$$-\rho_C\tau_f F_{CE'}q'_{oE} + \left(1-\rho'_f\rho_C F_{f'C}F_{Cf'}\right)q_{oC} = 0 \tag{7.2}$$

Solving for q'_{oE} and q_{oC} yields for following,

$$q'_{oE} = \frac{1-\rho'_f\rho_C F_{f'C}F_{Cf'}}{DEN_p}\varepsilon'_E e_b\left(\lambda, T_E\right) \tag{7.3}$$

$$q_{oC} = \frac{\rho_C\tau_f F_{CE}}{DEN_p}\varepsilon'_E e_b\left(\lambda, T_E\right) \tag{7.4}$$

where

$$\mathrm{DEN_p} = \left(1-\rho'_E\rho_f F_{E'f} F_{fE'}\right)\left(1-\rho'_f\rho_C F_{f'C} F_{Cf'}\right) - \rho'_E\rho_C\tau_f^2 F_{CE'} F_{E'C} \tag{7.5}$$

Now assume that the filter and PV cells are together so that $F_{f'C} = F_{Cf'} = 1$, and thus $F_{E'f} = F_{E'C}$ and $F_{fE'} = F_{CE'}$. This is a logical arrangement for a practical system since the filter and PV cells, which must be cooled, can be handled by a single cooling system in this arrangement. In addition, $F_{f'C} = F_{Cf'} = 1$ eliminates the radiation "leakage" between the filter and PV cells. Therefore, if the filter and PV cells are together, then equations (7.3) and (7.4) become the following.

$$q'_{oE} = \frac{1-\rho'_f\rho_C}{\mathrm{DEN_p}}\varepsilon'_E e_b\left(\lambda, T_E\right) \tag{7.6}$$

$$q_{oC} = \frac{\rho_C\tau_f}{\mathrm{DEN_p}}\varepsilon'_E e_b\left(\lambda, T_E\right) \tag{7.7}$$

$$\mathrm{DEN_p} = 1-\rho'_f\rho_C - \rho'_E\left[\rho_C\left(\tau_f^2 - \rho_f\rho'_f\right) + \rho_f\right] F_{E'C} F_{CE'} \tag{7.8}$$

Now using equation (7.6) in equation (6.85), and equation (7.7) in equation (6.87) the following results are obtained.

$$\bar{Q}_E = A_E \int_o^\infty \left\{\frac{1-\left[\rho_f + \rho_C\left(\tau_f^2 - \rho_f\rho'_f\right)\right] F_{E'C} F_{CE'}\rho_C\rho'_f}{\mathrm{DEN_p}}\right\}\varepsilon'_E e_b\left(\lambda, T_E\right)\mathrm{d}\lambda \tag{7.9}$$

$$\bar{Q}_C = A_C F_{CE'} \int_o^{\lambda_g} \frac{\tau_f}{\mathrm{DEN_p}}\varepsilon'_E e_b\left(\lambda, T_E\right)\mathrm{d}\lambda \tag{7.10}$$

As expected, the radiation leaving the emitter, $\bar{Q}_E$, is directly proportional to the emitter emissive power, $\varepsilon'_E e_b$. And the useful radiation reaching the PV cells, $\bar{Q}_C$, is directly proportional to the product of the emitter emissive power, the filter transmission, τ_f, and the view-factor the PV array has of the emitter, $F_{CE'}$.

Using equations (7.9) and (7.10), the cavity efficiency, η_c, becomes the following.

$$\eta_c = F_{E'C}\frac{\displaystyle\int_o^{\lambda_g}\frac{\tau_f}{DEN_p}\varepsilon'_E e_b(\lambda,T_E)\,d\lambda}{\displaystyle\int_o^{\infty}\left\{\frac{1-\left[\rho_f+\rho_C\left(\tau_f^2-\rho_f\rho'_f\right)\right]F_{E'C}F_{CE'}-\rho_C\rho'_f}{DEN_p}\right\}\varepsilon'_E e_b(\lambda,T_E)\,d\lambda} \tag{7.11}$$

In obtaining equation (7.11) the relation $A_E F_{E'C} = A_C F_{CE'}$ is used. Also, it should be remembered that equation (7.11) applies to a planar system with no window, negligible filter and PV cell emissive powers, and with the filter and PV cells together ($F_{f'C} = F_{Cf'} = 1$). As equation (7.11) shows, the cavity efficiency is directly proportional to the view-factor the emitter has of the PV cells, $F_{E'C}$.

For a selective emitter system without a filter ($\tau_f = 1$, $\rho_f = \rho'_f = 0$), equation (7.11) becomes the following.

$$\eta_c = F_{E'C}\frac{\displaystyle\int_o^{\lambda_g}\frac{\varepsilon'_E e_b(\lambda,T_E)}{1-\rho_C\rho'_E F_{E'C}F_{CE'}}\,d\lambda}{\displaystyle\int_o^{\infty}\left[\frac{1-\rho_C F_{E'C}F_{CE'}}{1-\rho_C\rho'_E F_{E'C}F_{CE'}}\right]\varepsilon'_E e_b(\lambda,T_E)\,d\lambda} \qquad \text{Selective Emitter System} \tag{7.12}$$

Similarly, for a filter system with a blackbody emitter ($\varepsilon'_E = 1$, $\rho'_E = 0$) equation (7.11) becomes the following.

$$\eta_c = F_{E'C}\frac{\displaystyle\int_o^{\lambda_g}\left[\frac{\tau_f}{1-\rho'_f\rho_C}\right]e_b(\lambda,T_E)\,d\lambda}{\displaystyle\int_o^{\infty}\left\{\frac{1-\left[\rho_f+\rho_C\left(\tau_f^2-\rho_f\rho'_f\right)\right]F_{E'C}F_{CE'}-\rho_C\rho'_f}{1-\rho'_f\rho_C}\right\}e_b(\lambda,T_E)\,d\lambda} \qquad \text{Filter System} \tag{7.13}$$

For $0 \le \lambda \le \lambda_g$, it is necessary that $\rho_C \approx 0$ in order to obtain large PV efficiency. As already mentioned in Chapter 5, anti-reflection coatings are used to obtain $\rho_C \approx 0$ for $0 \le \lambda \le \lambda_g$. As a result, equation (7.12) becomes the following.

$$\eta_c = F_{E'C}\left[1+\frac{\displaystyle\int_{\lambda_g}^{\infty}\left[\frac{1-\rho_C F_{E'C}F_{CE'}}{1-\rho_C\rho'_E F_{E'C}F_{CE'}}\right]\varepsilon'_E e_b(\lambda,T_E)\,d\lambda}{\displaystyle\int_0^{\lambda_g}\varepsilon'_E e_b(\lambda,T_E)\,d\lambda}\right]^{-1} \quad \text{Selective Emitter System} \quad \rho_C = 0 \text{ for } 0\le\lambda\le\lambda_g \tag{7.14}$$

For a selective emitter system, equation (7.14) shows, if $\varepsilon'_E = 0$ for $\lambda_g < \lambda < \infty$, then the cavity efficiency is $\eta_c = F_{E'C}$. This is the maximum possible cavity efficiency for either a selective emitter or filter TPV system. The term in equation (7.14),

$$\frac{1-\rho_C F_{E'C}F_{CE'}}{1-\rho_C\rho'_E F_{E'C}F_{CE'}} \le 1 \tag{7.15}$$

presents another way to attain maximum η_c. Obviously, if $\rho_C F_{E'C}F_{CE'} \approx 1$ for $\lambda_g < \lambda < \infty$, then $\eta_c \to F_{E'C}$. Thus, if the PV cells can be made highly reflective ($\rho_C \approx 1$) for $\lambda_g < \lambda < \infty$, then the term given by equation (7.15) is minimized. The back surface reflector (BSR) on the PV array discussed in Chapter 4 is one possible method to achieve large ρ_C. For now, neglect the advantage of reflecting PV cells. Because of the inequality given by equation (7.15), the following result for η_c applies.

$$\eta_c \approx F_{E'C}\left[\frac{1}{1+\dfrac{\varepsilon'_{E\ell}}{\varepsilon'_{Eb}}f(u_g)}\right] \quad \text{Selective Emitter System} \tag{7.16}$$

In equation (7.16), ε'_{Eb} is the total emitter emittance for $0 \le \lambda \le \lambda_g$, and $\varepsilon'_{E\ell}$ is the total emitter emittance for $\lambda_g < \lambda < \infty$. The function $f(u_g)$, (problem 7.1) is the integrated blackbody emissive power that lies in the range $\lambda_g < \lambda < \infty$ divided by the integrated blackbody emissive power in the range $0 \le \lambda \le \lambda_g$ and is given in terms of the $F_{o\text{-}\lambda T}$ function of equation (1.137). The parameter, $u_g = \dfrac{E_g}{kT_E}$, is the dimensionless PV cell bandgap energy, which is a key parameter in determining the system efficiency.

$$\varepsilon'_{Eb} = \frac{\int_0^{\lambda_g} \varepsilon'_E e_b(\lambda, T_E)\, d\lambda}{\int_0^{\lambda_g} e_b(\lambda, T_E)\, d\lambda} \tag{7.17}$$

$$\varepsilon'_{E\ell} = \frac{\int_{\lambda_g}^{\infty} \varepsilon'_E e_b(\lambda, T_E)\, d\lambda}{\int_{\lambda_g}^{\infty} e_b(\lambda, T_E)\, d\lambda} \tag{7.18}$$

$$f(u_g) = \frac{\int_{\lambda_g}^{\infty} e_b(\lambda, T_E)\, d\lambda}{\int_0^{\lambda_g} e_b(\lambda, T_E)\, d\lambda} = \frac{1 - F_{o-\lambda_g T_E}}{F_{o-\lambda_g T_E}} \qquad u_g = \frac{E_g}{kT_E} = \frac{hc_o}{k\lambda_g T_E} \tag{7.19}$$

The emittances ε'_{Eb} and $\varepsilon'_{E\ell}$ are functions of T_E and λ_g. However, they are slowly varying functions of T_E so that the major temperature dependence of η_c is through the function $f(u_g)$. As shown in problem 7.1 for $u_g > 1$, which is the case for TPV systems, the function, $f(u_g)$, is the following.

$$f(u_g) = \frac{\pi^4}{15}\left[\sum_{m=1}^{\infty} \frac{e^{-mu_g}}{m}\left(u_g^3 + \frac{3}{m}u_g^2 + \frac{6}{m^2}u_g + \frac{6}{m^3}\right)\right]^{-1} - 1 \tag{7.20}$$

This is a monotonically increasing function of u_g.

For a filter system to attain large η_c, the filter must have large transmittance, τ_f, and therefore, low reflectance, $\rho_f = \rho'_f = 0$, for $0 \le \lambda \le \lambda_g$. For $\lambda_g \le \lambda \le \infty$ where the PV cells cannot produce useful power, the filter reflectance, ρ_f, must be large; therefore, $\tau_f \approx 0$ in order to have large η_c. Therefore, for the filter system, make the following approximations. For $0 \le \lambda \le \lambda_g$, $\rho_C \approx 0$, and $\rho_f F_{E'C} F_{CE'} \ll 1$, and for $\lambda_g < \lambda < \infty$, $\tau_f^2 \ll \rho_f \rho'_f$. With these approximations, equation (7.13) becomes the following,

$$\eta_c \approx F_{E'C}\frac{\tau_{fb}}{1+f\left(u_g\right)\left[1-\rho_{f\ell}F_{E'C}F_{CE'}\right]} \quad \text{Filter System} \tag{7.21}$$

where τ_{fb} is the total transmittance of the filter for $0 \le \lambda \le \lambda_g$, $\rho_{f\ell}$ is the total reflectance of the left side (Figure 6.7) of the filter for $\lambda_g < \lambda < \infty$. The function $f(u_g)$, which also appears in η_c for the selective emitter system [equation (7.16)] is given by equation (7.19). Just as in the case of $\varepsilon'_{E\ell}$ and ε'_{Eb}, τ_{fb} and $\rho_{f\ell}$ will be slowly varying functions of T_E and λ_g.

$$\tau_{fb} = \frac{\int_o^{\lambda_g}\tau_f e_b\left(\lambda, T_E\right)d\lambda}{\int_o^{\lambda_g} e_b\left(\lambda, T_E\right)d\lambda} \tag{7.22}$$

$$\rho_{f\ell} = \frac{\int_{\lambda_g}^{\infty}\rho_f e_b\left(\lambda, T_E\right)d\lambda}{\int_{\lambda_g}^{\infty} e_b\left(\lambda, T_E\right)d\lambda} \tag{7.23}$$

Compare η_c for the selective emitter [equation (7.16)] and filter systems [equation (7.21)]. First, as already mentioned the maximum possible value for η_c is $F_{E'C}$ for both systems. Second, for the filter system, η_c is directly proportional to the transmittance, τ_{fb}. The selective emitter system does not suffer this transmittance loss. Third, although ε'_{Eb}, $\varepsilon'_{E\ell}$, τ_{fb}, and $\rho_{f\ell}$ depend upon λ_g and T_E, the function $f(u_g)$, where $u_g = \frac{hc_o}{\lambda_g kT_E} = \frac{E_g}{kT_E}$, determines the main dependence of η_c for both systems on the PV cell bandgap energy, E_g, and the emitter temperature, T_E. Since $f(u_g)$ is a monotonically increasing function of u_g, η_c is a monotonically decreasing function of u_g. Therefore, it would appear that it is desirable to use the lowest bandgap energy PV cell. However, as shown in Chapter 5, the PV efficiency, η_{PV}, decreases with decreasing E_g. Therefore, the overall efficiency, η_T, will be a maximum for some optimum value of $u_g = \frac{E_g}{kT_E}$. This feature has been demonstrated in Chapter 2 for an ideal TPV system. Finally, to

attain large η_c for the filter system requires that $\rho_{f\ell} F_{E'C} F_{CE'} \to 1$. Thus, not only must the filter reflectance, $\rho_{f\ell} \to 1$, but also the product of the view-factors, $F_{E'C} F_{CE'} \to 1$, to attain large η_c. In the case of a selective emitter system, this dependence upon the view-factor product does not exist. To attain large η_c for the selective emitter system requires only that $\frac{\varepsilon'_{E\ell}}{\varepsilon'_{Eb}} \to 0$. The view-factor product dependence for the filter system results because the long wavelength ($\lambda > \lambda_g$) photons leaving the emitter that cannot be converted to electrical energy must be reflected back to the emitter to attain large η_c. In the emission and reflection process, photons "leak" out of the system because $F_{E'C} F_{CE'} < 1$. The selective emitter system η_c does not have the view-factor product dependence since the long wavelength photons are controlled only by the emittance ratio $\frac{\varepsilon'_{E\ell}}{\varepsilon'_{Eb}}$.

To illustrate the strong dependence of η_c on $F_{E'C}$ consider the case of a "perfect" selective emitter system and a "perfect" filter system. The perfect selective emitter system means that $\frac{\varepsilon'_{E\ell}}{\varepsilon'_{Eb}} = 0$ in equation (7.16) so that

$$\eta_c = F_{E'C} \qquad \text{Perfect Selective Emitter System} \qquad (7.24)$$

The perfect filter system means that $\rho_{fl} = \tau_{fb} = 1$ in equation (7.21) so that

$$\eta_c = \frac{F_{E'C}}{1 + f\left(u_g\right)\left[1 - F_{E'C} F_{CE'}\right]} \qquad \text{Perfect Filter System} \qquad (7.25)$$

Comparing equations (7.24) and (7.25) notice that η_c for the perfect selective emitter system will always be greater than η_c for the perfect filter system.

In Figure 7.1 η_c for the perfect selective emitter and perfect filter systems are compared for a planar geometry consisting of two parallel circular disks. In this case, $F_{E'C} = F_{CE'}$ and using the results given in Figure 6.3a

$$F_{E'C} = F_{CE'} = 1 - \left(\frac{h}{R}\right)\left[\sqrt{1 + \left(\frac{h}{2R}\right)^2} - \frac{h}{2R}\right] \qquad (7.26)$$

where h is the distance between the circular emitter and PV cells, and R is the radius of the emitter and PV cells.

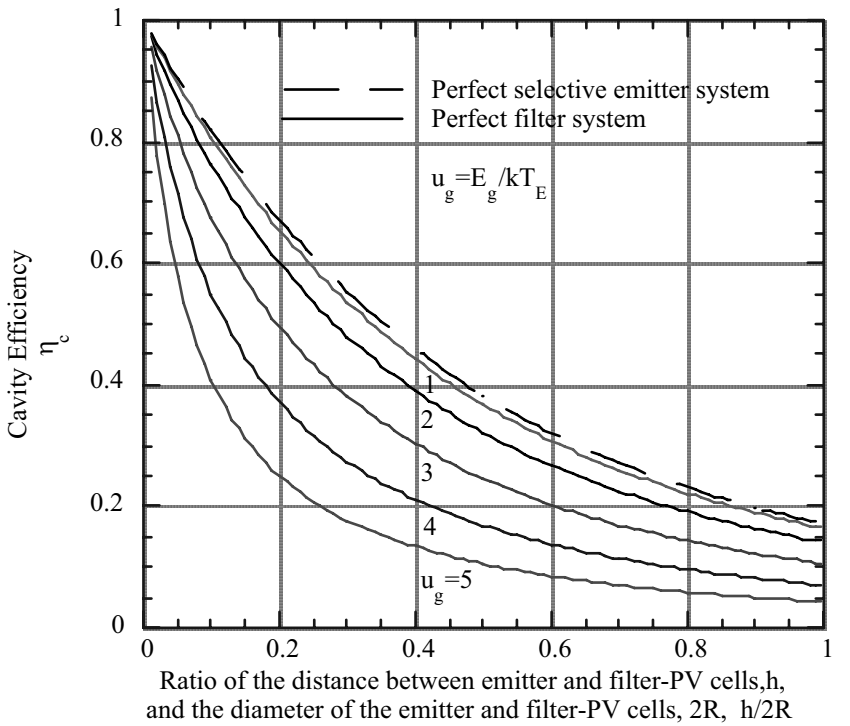

Figure 7.1 - Comparison of cavity efficiency, η_c, for perfect selective emitter and perfect filter TPV systems of planar circular disk geometry.

As Figure 7.1 shows, η_c is very sensitive to $\frac{h}{2R}$. This is especially so for the perfect filter system when $u_g > 2$. For a representative TPV system, $4 < u_g < 6$ (for $E_g = 0.7$eV and $T_E = 1700$K, $u_g = 4.8$.). It appears $\frac{h}{2R} < 0.1$ is required to attain large η_c for a perfect filter system of planar circular disk geometry. In the case of the perfect selective emitter system, the $\frac{h}{2R}$ dependence is not as severe. However, even for the perfect selective emitter system, it appears $\frac{h}{2R} \leq 0.2$ is required to attain large η_c.

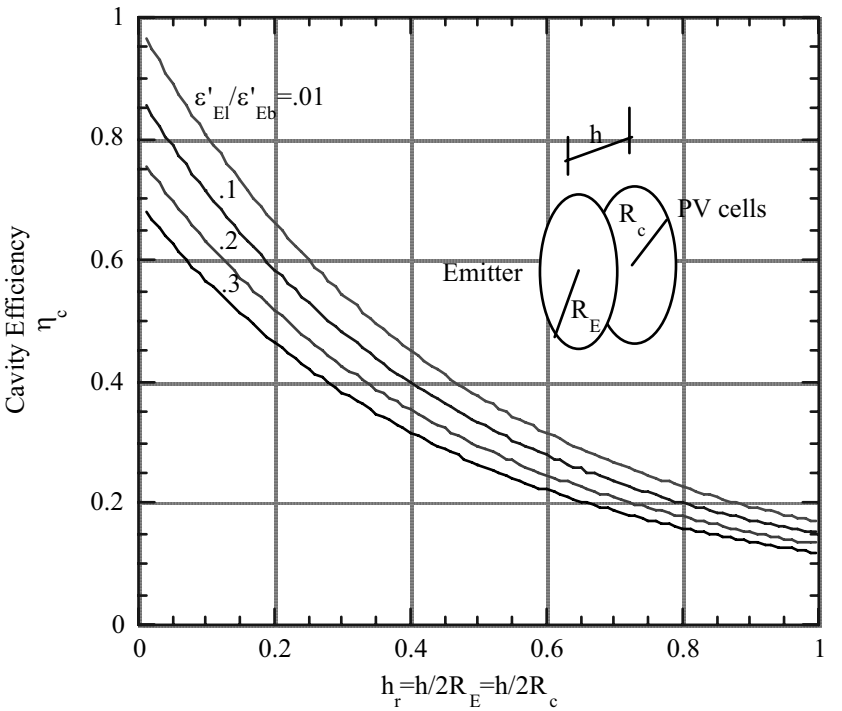

Figure 7.2a) - Dependence of cavity efficiency, η_c, on dimensionless emitter to PV cell spacing, h_r, for various values of the emitter emittance ratio, $\varepsilon'_{El}/\varepsilon'_{Eb}$, for a dimensionless PV cell bandgap energy, u_g=4.

Now consider the same comparison for a selective emitter system with $\frac{\varepsilon'_{E\ell}}{\varepsilon'_{Eb}} > 0$ [equation (7.16)] and a filter system with $\tau_{fb} < 1$ and $\rho_{f\ell} < 1$ [equation (7.21)]. Figure 7.2a shows η_c as a function of $\frac{h}{2R}$ for several values of the emittance ratio, $\frac{\varepsilon'_{E\ell}}{\varepsilon'_{Eb}}$, and the dimensionless PV cell bandgap energy, $u_g = 4$, for the planar circular disk, selective emitter system.

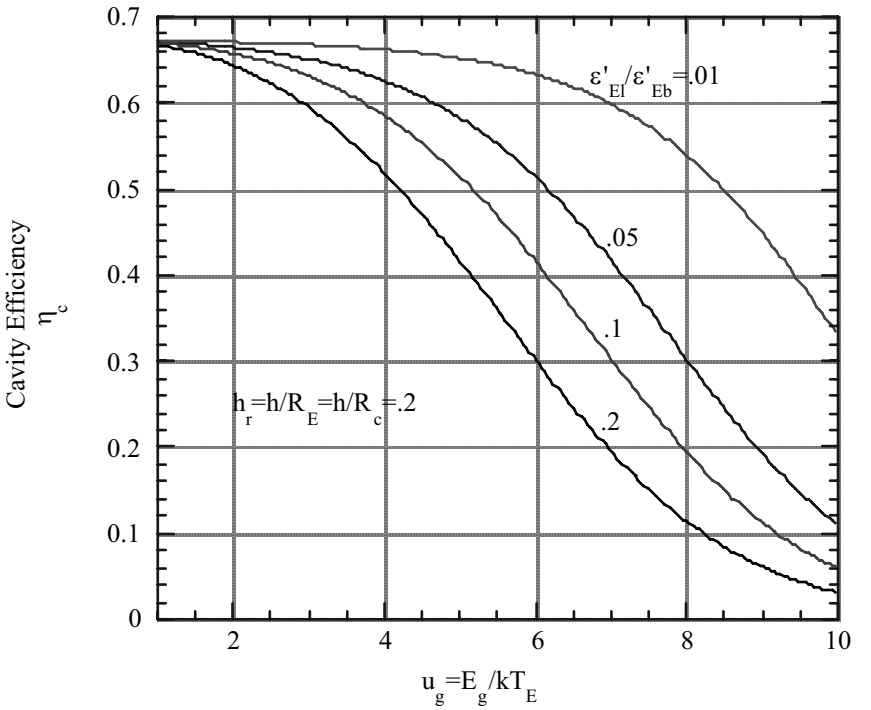

Figure7.2b) - Dependence of cavity efficiency, η_c, for circular disk selective emitter TPV system on dimensionless PV cell bandgap energy, u_g, for various values of the emitter emittance ratio, $\varepsilon'_{El}/\varepsilon'_{Eb}$ for a dimensionless emitter to PV cell spacing, h_r=.2

Similarly, Figure 7.3a shows $\frac{\eta}{\tau_{fb}}$ as a function of $\frac{h}{2R}$ for several values of the long wavelength reflectance, $\rho_{f\ell}$, and u_g = 4 for the planar circular disk, filter system. It should be noted that $\frac{\varepsilon'_{E\ell}}{\varepsilon'_{Eb}}$ and $\rho_{f\ell}$ dependence upon λ_g and T_E is being neglected in Figure 7.2 and 7.3.

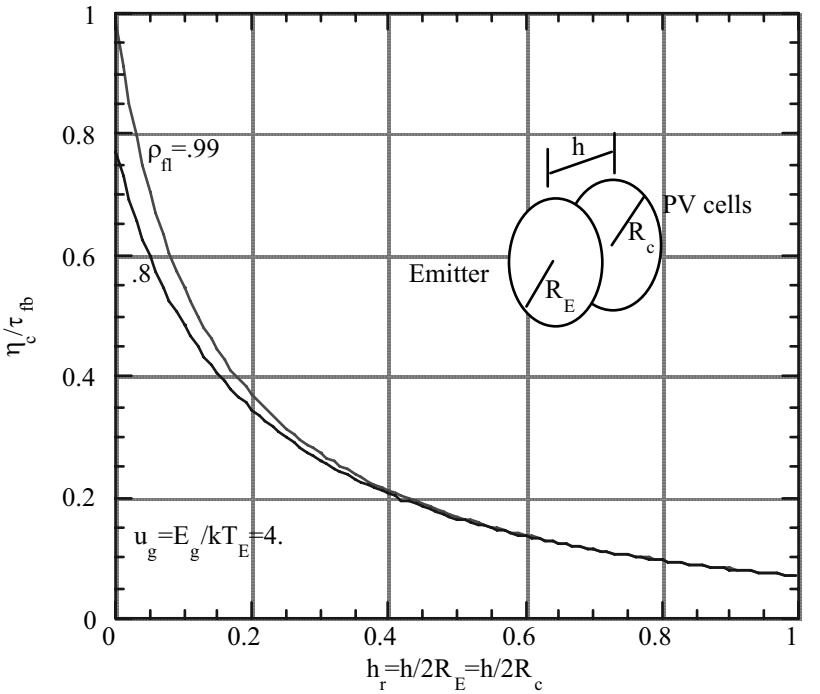

Figure 7.3a) - Dependence of the ratio of the cavity efficiency,η_c, to the filter transmittance for photon energies greater than the PV cell bandgap energy, τ_{fb}, for a circular disk filter TPV system on dimensionless emitter to PV cell spacing, h_r, for various values of the filter reflectance for photon energies below the PV cell bandgap energy,ρ_{fl}, for a dimensionless PV cell bandgap energy,u_g=4.

Figures 7.2a and 7.3a illustrate several important results. For the filter system, $\frac{\eta_c}{\tau_{fb}}$ becomes independent of ρ_{fl} as $\frac{h}{2R}$ becomes greater than approximately 0.4. For $\frac{h}{2R} > 0.4$, the view-factor product $F_{E'C}F_{CE'} \to 0$ in equation (7.21). Therefore, the term $\rho_{fl}F_{E'C}F_{CE'}$ becomes negligible. Thus, no matter how large the filter reflectance, ρ_{fl}, the filter is completely ineffective unless $\frac{h}{2R} < 0.4$.

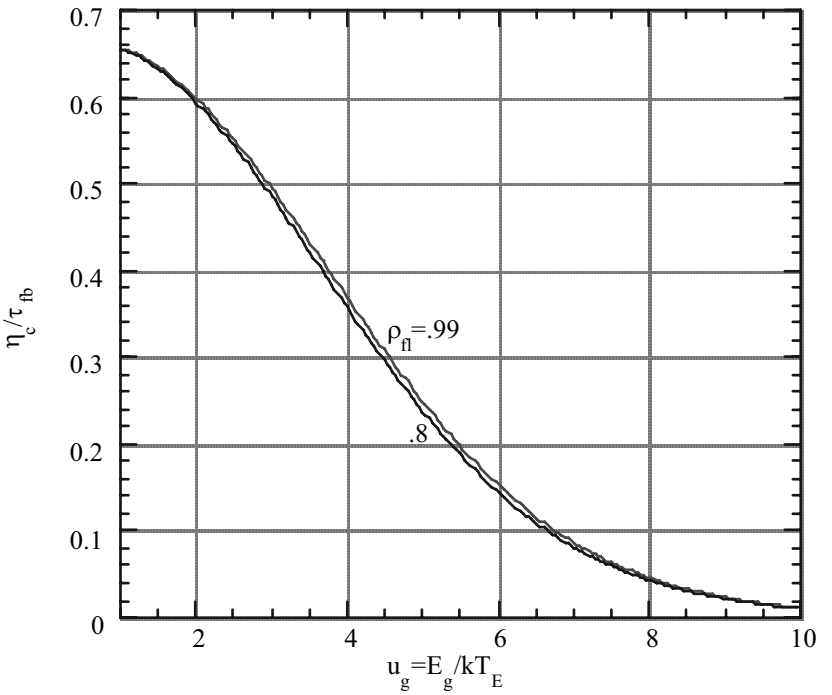

Figure 7.3b) - Dependence of the ratio of the cavity efficiency,η_c, to the filter transmittance for photon energies greater than the PV cell bandgap energy, τ_{fb}, for circular disk filter TPV system on dimensionless PV cell bandgap energy, u_g, for various values of the filter reflectance for photon energies below the PV cell bandgap energy,ρ_{fl}, for a dimensionless emitter to PV cell spacing, h_r=.2.

The selective emitter system has a similar result, however, at a much larger value of $\frac{h}{2R}$. For large $\frac{h}{2R}$, the view-factor $F_{E'C} \to 0$ so that η_c [equation (7.16)] becomes independent of $\frac{\varepsilon'_{E\ell}}{\varepsilon'_{Eb}}$ and u_g. Also, comparing Figures 7.2b and 7.3b, note that for a selective emitter system with $\frac{\varepsilon'_{E\ell}}{\varepsilon'_{Eb}} < 0.1$, the efficiency is much less sensitive to u_g than for the filter system, regardless of how large $\rho_{f\ell}$ becomes. Thus, a selective emitter

system is more effective in attaining large η_c for low emitter temperatures ($u_g \gg 1$) than a filter system.

From the preceding emitter-filter efficiency discussion it is obvious that view-factors, which account for leakage of radiation from the system, have a major impact upon the performance of a TPV system. The next section discusses how a cylindrical geometry can improve the cavity efficiency.

7.3 Cavity Efficiency for Cylindrical Filter and Selective Emitter TPV Systems without a Window

For a cylindrical geometry, equations (6.72) and (6.73) must be solved before the cavity efficiency, η_c, can be determined. Similar to the planar geometry system (section 7.2), neglect the window loss ($\tau_W = 1$, $\rho_W = \rho'_W = q_W = q'_W = 0$) the filter and PV cell emissive powers ($q_f = q'_f = q_C = 0$) and assume the filter and PV cells are together so that $F_{E'f} = F_{E'C}$, $F_{fE'} = F_{CE'}$, and $F_{f'C} = F_{Cf'} = 1$. In addition, the following view-factor conditions apply if the filter and cells are together; $F_{ff} + F_{ff}^{W} = F_{fC}^{f} + F_{fC}^{fW} = F_{Cf}^{f} + F_{Cf}^{fW} = F_{CC}^{f} + F_{CC}^{fW} = F_{22}$, $F_{CC} = 0$. Where, F_{22} is given in Figure 6.3d with $R_1 = R_E$ (emitter radius), $R_2 = R_C$ (PV cell radius), and ℓ is the length of the cylinder (emitter, filter, and PV cells all the same length). Using the conditions just described, equations (6.72) and (6.73) become the following,

$$\left[1-\rho_f\left(F_{22}+\rho'_E F_{E'C}F_{CE'}\right)\right]q'_{oE} - \rho'_E\tau_f F_{E'C}q_{oC} = q'_E\left(1-\rho_f F_{22}\right) \tag{7.27}$$

$$-\rho_C\tau_f F_{CE'}q'_{oE} + \left(1-\rho_C\rho'_f-\gamma_C F_{22}\right)q_{oC} = 0 \tag{7.28}$$

Where,

$$\gamma_C = \rho_C\left(\tau_f^2 - \rho_f\rho'_f\right) + \rho_f \tag{7.29}$$

Solving equations (7.27) and (7.28) yields the following.

$$q'_{oE} = \frac{1-\rho_C\rho'_f-\gamma_C F_{22}}{DEN_C}\varepsilon'_E e_b\left(\lambda, T_E\right) \tag{7.30}$$

$$q_{oC} = \frac{\rho_C\tau_f F_{CE'}}{DEN_C}\varepsilon'_E e_b\left(\lambda, T_E\right) \tag{7.31}$$

$$\mathrm{DEN_C} = 1 - \rho_C \rho'_f - \gamma_C \left(F_{22} + \rho'_E F_{E'C} F_{CE'} \right) \tag{7.32}$$

Comparing the planar results [equations (7.6) and (7.7)] to the cylindrical results [equations (7.30) and (7.31)] note that an additional term, $\gamma_C F_{22}$, appears for the cylindrical case. This additional term results from the self view-factor, F_{22}, of the filter and PV cells in a cylindrical geometry.

Now consider the efficiency using equations (6.85), (6.86), (and (6.87).

$$\eta_c = \frac{\bar{Q}_C}{\bar{Q}_E} = F_{E'C} \frac{\displaystyle\int_0^{\lambda_g} \frac{\tau_f}{\mathrm{DEN_C}} \varepsilon'_E e_b(\lambda, T_e)\, d\lambda}{\displaystyle\int_0^{\infty} \frac{1 - \rho_C \rho'_f - \gamma_C \left(F_{22} + F_{E'C} F_{CE'} \right)}{\mathrm{DEN_C}} \varepsilon'_E e_b(\lambda, T_e)\, d\lambda} \tag{7.33}$$

The condition $A_C F_{CE'} = A_E F_{E'C}$ has been used in obtaining equation (7.33). Just as in the case of a planar geometry system, η_c is directly proportional to the view-factor the emitter has of the PV cells, $F_{E'C}$.

Similar to Section 7.2, consider the two possible systems: selective emitter without a filter ($\tau_f = 1$, $\rho_f = \rho'_f = 0$, $\gamma_C = \rho_C$) and filter with a blackbody emitter ($\varepsilon'_E = 1$, $\rho'_E = 0$). Also, assume $\rho_C \approx 0$ for $0 \le \lambda < \lambda_g$, which, as pointed out in 7.2, is a requirement in order to attain high PV efficiency. For the cylindrical selective emitter system, the efficiency is the same result as that for the planar system.

$$\eta_c \approx \left[\frac{F_{E'C}}{1 + \dfrac{\varepsilon'_{E\ell}}{\varepsilon'_{Eb}} f(u_g)} \right] \qquad \text{Selective Emitter} \tag{7.16}$$

Here $\varepsilon'_{E\ell}$ [equation (7.18)] is the emittance of the selective emitter for $\lambda_g \le \lambda < \infty$, and ε'_{Eb} [equation (7.17)] is the emitter emittance for $0 \le \lambda \le \lambda_g$, and $f(u_g)$ is given by equation 7.19). As stated in section 7.2, $\varepsilon'_{E\ell}$, ε'_{Eb}, and u_g are functions of λ_g and T_E. However, the major contribution of T_E and λ_g dependence for η_c occurs through $f(u_g)$.

Consider the cylindrical filter system with a blackbody emitter ($\varepsilon'_E = 1, \rho'_E = 0$). Also, assume $\rho_C \approx 0$ and $\rho_f \left[F_{E'C} F_{CE'} + F_{22} \right] \ll 1$ for $0 \le \lambda \le \lambda_g$ and $\tau_f^2 \ll \rho_f \rho'_f$ for $\lambda_g \le \lambda < \infty$. Thus, following result is obtained for η_c (problem 7.3).

$$\eta_c \approx F_{E'C}\,\frac{\displaystyle\int_0^{\lambda_g}\tau_f e_b\left(\lambda,T_E\right)d\lambda}{\displaystyle\int_0^{\lambda_g} e_b\left(\lambda,T_E\right)d\lambda+\int_0^{\infty}\frac{1-\rho_f\left(F_{22}+F_{E'C}F_{CE'}\right)}{1-\rho_f F_{22}}e_b\left(\lambda,T_E\right)d\lambda}$$

Cylindrical Filter System (7.34)

If $\rho_f F_{22} \ll 1$, equation (7.34) reduces to the planar geometry result, equation (7.21) (problem 7.3). To attain large efficiency $F_{E'C} \to 1$, which means the emitter and PV cells must be close together ($R_E \to R_C$). In that case, $F_{22} \to 0$ so that $\rho_f F_{22} \ll 1$ for an efficient system.

The cavity efficiency expression for a cylindrical selective emitter system is identical to the planar system expression. Also, the cavity efficiency expression for a cylindrical filter TPV system is approximately identical to the planar system expression. Therefore, for T_E, E_g and the optical properties being the same, the major difference in efficiency between planar and cylindrical geometries results from the difference in view-factor, $F_{E'C}$, for the two geometries.

$$\frac{\eta_c\big|_C}{\eta_c\big|_p} \approx \frac{F_{E'C}\big|_C}{F_{E'C}\big|_p} \tag{7.35}$$

Here subscript C denotes a cylindrical system and subscript p a planar system. For the selective emitter system, equation (7.35) is exact. It is only an approximation for the filter system. In Figure 7.4, $F_{E'C}\big|_C$ and $F_{E'C}\big|_p$ are plotted for a planar system consisting of a circular emitter and circular filter-PV cell combination of equal radius, R_p, and a cylindrical system for length, ℓ, with inner cylindrical emitter of radius R_E, and outer concentric filter-PV cell combination of radius R_C. It was assumed that the spacing, h, between the emitter and filter-PV cell combination is the same for both geometries and that the emitter areas are the same in both geometries. As a result, the following condition holds for Figure 7.4.

$$\frac{R_C}{R_E} = 1 + 2\left(\frac{h}{R_p}\right)\left(\frac{\ell}{R_p}\right) \tag{7.36}$$

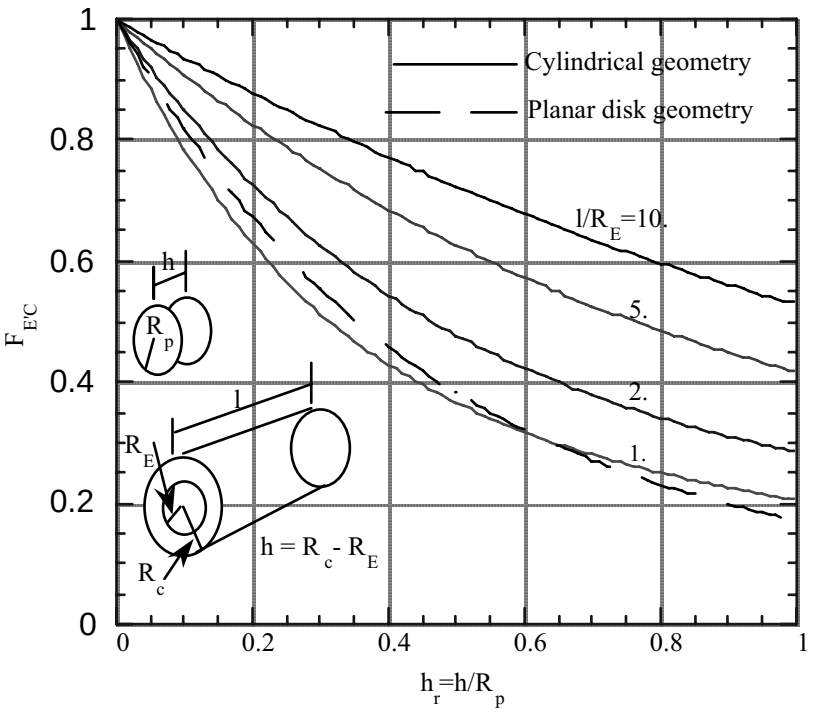

Figure 7.4 Comparison of planar disk and cylindrical geometry view factors, F_{EC}, for equal spacing,h, and equal emitter areas, $\pi R_p^2 = 2\pi R_E \ell$.

Results in Figure 7.4 are shown as a function of $\frac{h}{R_p}$ for several values of $\frac{\ell}{R_p}$. The view-factor for the planar system, $F_{E'C}\big|_p$ is given by equation (7.26). For the cylindrical system, using equation (6.7), $F_{E'C}\big|_C$ is given by,

$$F_{E'C}\big|_C = \frac{A_C}{A_E} F_{CE'}\big|_C = \left(\frac{R_C}{R_E}\right) F_{CE'}\big|_C \tag{7.37}$$

where $F_{CE'}\big|_C$ is given by F_{21} in Figure 6.3d, with $z = \frac{R_C}{R_E}$ and $L = \frac{\ell}{R_E}$.

As Figure 7.4 shows, $F_{E'C}\big|_C > F_{E'C}\big|_p$, except for $\frac{h}{R_p} < 0.6$ when $\frac{\ell}{R_E} = 1$. Therefore, a cylindrical geometry yields a larger η_c than a planar geometry if $\frac{\ell}{R_E} \geq 2$. Also note that the cylindrical geometry advantage increases with increasing $\frac{\ell}{R_E}$.

In the case of a perfect selective emitter ($\frac{\varepsilon'_{E\ell}}{\varepsilon'_{Eb}} \approx 0$), $\eta_c = F_{E'C}$. Therefore, the results in Figure 7.4 give the maximum possible cavity efficiency for either a planar or cylindrical selective emitter system. Now consider a perfect cylindrical filter system so that $\tau_f = 1$ ($\rho_f = \rho'_f = 0$) for $0 \leq \lambda \leq \lambda_g$, and $\rho_f = 1$ for $\lambda_g < \lambda < \infty$. Therefore, equation (7.34) becomes the following.

$$\eta_c = \frac{F_{E'C}}{1 + f\left(u_g\right)\left[1 - \frac{F_{E'C}F_{CE'}}{1 - F_{22}}\right]} \qquad \text{Perfect Cylindrical Filter System} \qquad (7.38)$$

Comparing this result with the planar geometry result [equation (7.25)] the additional term, $1\text{-}F_{22}$, appears for the cylindrical geometry. In a practical cylindrical TPV system, the length of the cylinder, ℓ, will be large compared to the radius, R_E. As a result, the view-factor the outer cylinder has of the bases of the cylinder is small, and $1 - F_{22} \approx F_{CE'}$. In that case the view-factor term in the denominator of equation (7.38) reduces to $(1 - F_{E'C})$.

In Figure 7.5, the cavity efficiency, η_c, for the perfect filter system [equation (7.38)] is plotted as a function of $\frac{R_C}{R_E}$ for $\frac{\ell}{R_E} = 5$ and several values of $u_g = \frac{E_g}{kT_E}$. Similar to a planar perfect filter system (Figure 7.1), the cylindrical perfect filter system is very sensitive to u_g. For representative values of u_g ($4 \leq u_g \leq 6$), Figure 7.5 indicates that $\frac{R_C}{R_E} < 1.3$ is required to achieve large η_c. Comparing Figure 7.1 and 7.5 note that

η_c does not decrease as rapidly with increasing $\frac{R_C}{R_E}$ for the cylindrical geometry as it does with increasing $\frac{h}{2R}$ for the planar geometry.

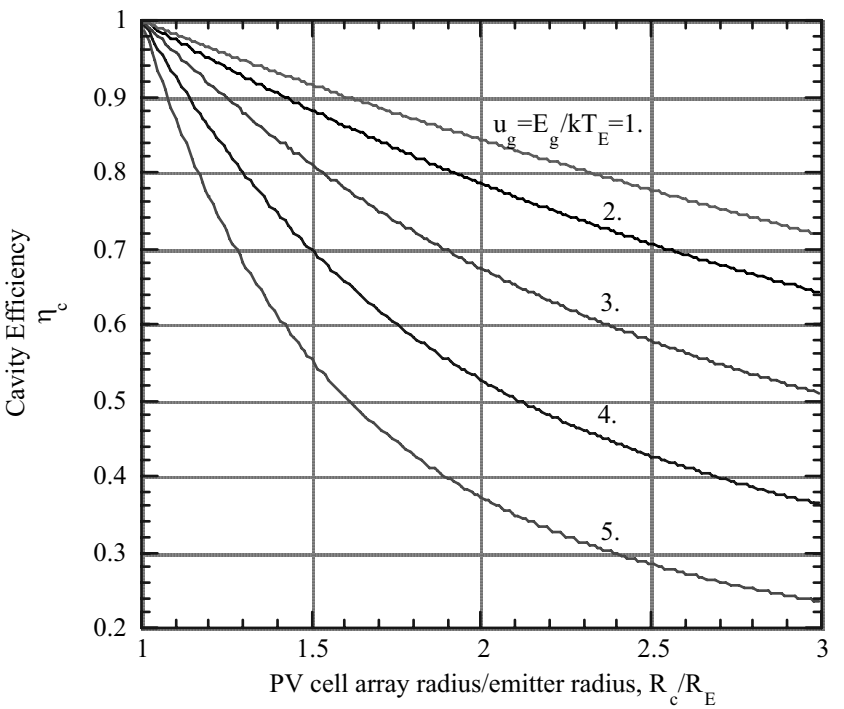

Figure 7.5 - Cavity efficiency, η_c, for perfect cylindrical geometry filter TPV system as a function of the ratio of the inner emitter radius, R_E, to the outer PV cell array radius, R_c for several values of the PV cell dimensionless bandgap energy, $u_g=E_g/kT_E$. Dimensionless length of cylinder, $\ell/R_E = 5$.

For both selective emitter and filter TPV systems, the cavity efficiency can be improved by using a cylindrical geometry rather than a planar geometry. This occurs because the view-factor, $F_{E'C}$, for the cylindrical geometry is larger than $F_{E'C}$ for a

planar geometry when both systems have the same area emitters and equal spacing between emitter and PV cells. With larger $F_{E'C}$, the radiation "leakage" is reduced in the cylindrical system. Another method for reducing the radiation leakage is to place highly reflecting surfaces in locations where the leakage occurs. Thus, for the cylindrical geometry, the leakage can be reduced if highly reflecting bases are added to the cylinders. Similarly, for the planar geometry, the leakage can be reduced if an outer highly reflecting tube surrounds the system. The next section analyses systems that utilize end reflectors.

7.4 Cavity Efficiency for TPV Systems with Reflectivity End Caps

7.4.1 Development of Radiation Transfer Equations

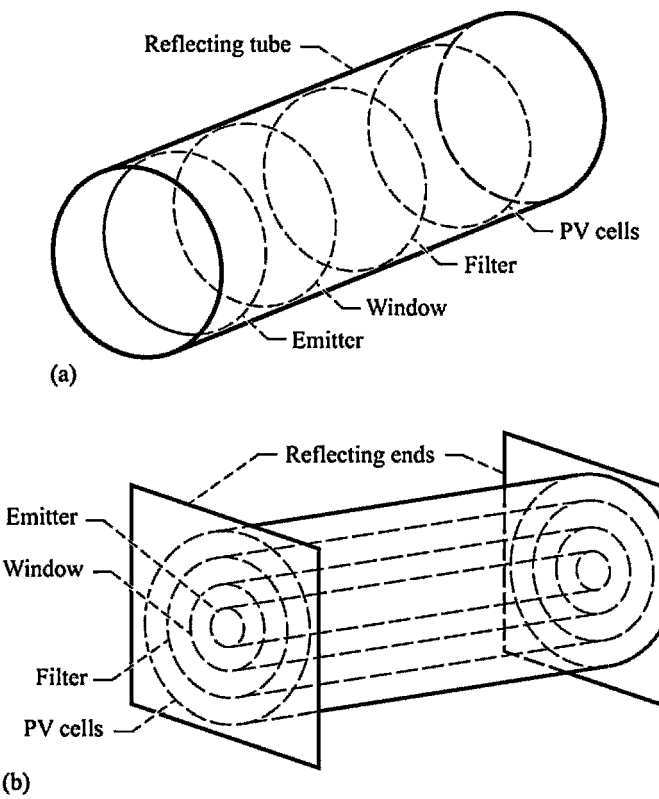

Figure 7.6.—Schematic drawings of TPV systems using reflecting end caps to reduce radiation losses. (a) Planar disk TPV system with reflecting end cap. (b) Cylindrical TPV system with reflecting end caps.

Figure 7.6 is a schematic of planar and cylindrical TPV systems that have reflecting ends to reduce radiation losses. To determine the cavity efficiency for these systems the radiation transfer equations must now include the radiation fluxes that leave and are incident on the reflecting ends. Consider the cylindrical system shown schematically in Figure 7.7. The end reflectors are bases for the concentric emitter, window, filter, and PV cells that make up the system. The area of the end reflectors is split into three regions: A_a, A_b, and A_d, as shown in Figure 7.7. This splitting is necessary since the radiation fluxes incident and leaving the end reflectors is not uniform over the entire reflector area, ($A_s = A_a + A_b + A_d$). Non-uniformity of the radiation fluxes occurs because part of the radiation reaching the end reflectors from each of the system components passes through the window or filter while the remaining part that passes through the window or filter suffers a transmission loss. Splitting the end reflector into three regions makes the uniform flux assumption for each of the three regions a reasonable approximation. As pointed out in Chapter 6, the uniform flux approximation together with diffuse surfaces are the basic assumptions that allow the development of the radiation transfer equations.

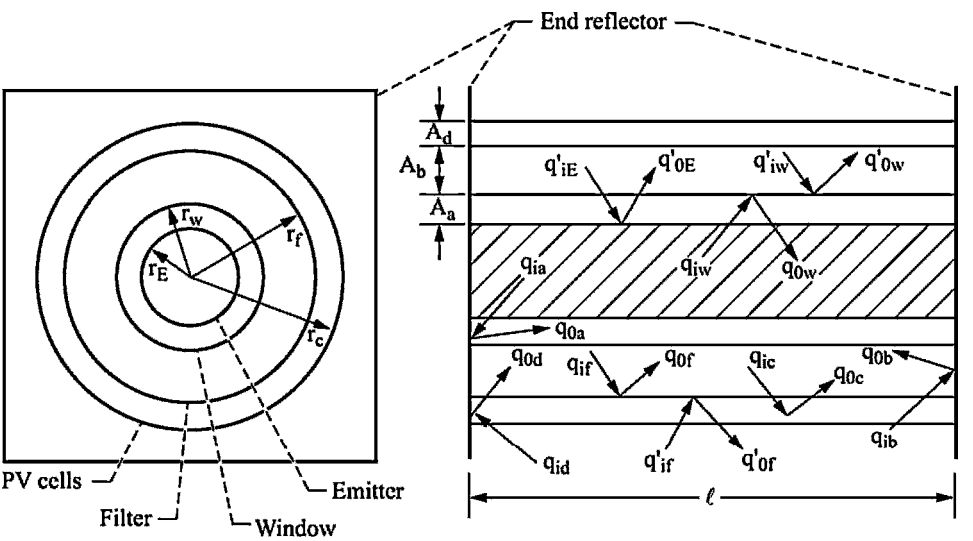

A_a = End reflector area between emitter and window
A_b = End reflector area between window and filter
A_d = End reflector area between filter and PV cells

Figure 7.7.—Schematic drawing of cylindrical TPV system with reflecting end caps.

The radiation transfer equations will now be developed for the cylindrical system. Previously in section 6.4 (problem 6.9) it was shown that the transfer equations for the planar system can be obtained from the cylindrical system equations by using the condition that view-factors between concave surfaces vanish. When end reflectors are added view-factors between the end reflectors and concave surfaces for radiation that passes through the window or filter must also vanish to obtain the planar equations. Begin by considering the total radiation incident on A_a from each of the other parts of the system. Using equation (6.5) and Figure 7.7 to identify the various q's the following result is obtained for q_{ia}, the flux incident on A_a.

$$\begin{aligned} A_a q_{ia} = {} & q'_{oE} F_{E'A} A_E + q_{oW} F_{Wa} A_W + \tau_W q_{of} F_{fa}^W A_f + \tau_f \tau_W q_{oC} F_{Ca}^{fW} A_C \\ & + \tau_f \tau_W q_{od} F_{da}^{fW} A_d + \tau_W q_{ob} F_{ba}^W A_b + q_{oa} F_{aa} A_a \end{aligned} \tag{7.39}$$

Now use equations (6.7) and (6.30) for q_{ia} to obtain the following result.

$$q_{oa}\left(1-\rho_a F_a\right) = \rho_a \left\{ q'_{oE} F_{aE'} + q_{oW} F_{aW} + \tau_W \left[q_{of} F_{af}^W + \tau_f \left(F_{aC}^{fW} q_C + F_{ad}^{fW} q_{od} \right) + q_{ob} F_{ab}^W \right] \right\} + q_a \tag{7.40}$$

The view-factor notation is explained in section 6.2.2. For example, F_{aC}^{fW} is the view-factor of end reflector area, A_a, as seen by the PV cells for radiation that passes through the filter and window. The superscripts refer to the components through which the radiation passes and the subscripts to the components which are the source and receiver of the radiation. The radiation flux, q_a, is the emissive power of area A_a, and is defined by equation (6.41).

Similar to equation (7.40) for q_{oa}, equations for radiation flux q_{ob} leaving end reflector area A_b and radiation flux q_{od} leaving end reflector area A_d can be derived.

$$\begin{aligned} q_{ob}\left(1-\rho_b F_{bb}\right) = {} & \rho_b \left\{ q'_W F_{bW'} + q_{of} \left[F_{bf} + \tau_W^2 F_{bf}^W \right] + \tau_W \left[q'_{oE} F_{bE'}^W + q_{oW} F_{bW}^W + q_{oa} F_{ba}^W \right] \right. \\ & \left. \tau_f \left[q_C \left(F_{bC}^f + \tau_W^2 F_{bC}^{fW} \right) + q_{oa} F_{ba}^W + q_{od} F_{bd}^f \right] \right\} + q_b \end{aligned} \tag{7.41}$$

$$\begin{aligned} q_{od}\left(1-\rho_d F_{dd}\right) = {} & \rho_d \left\{ q'_{of} F_{df''} + q_{oC} \left[F_{dC} + \tau_f^2 \left(F_{dC}^f + \tau_W^2 F_{dC}^{fW} \right) \right] \right. \\ & + \tau_f \left[q_{of} \left(F_{df}^f + \tau_W^2 F_{df}^{fW} \right) + q'_{oW} F_{dW'}^f + q_{ob} F_{db}^f \right] \\ & \left. + \tau_f \tau_W \left[q'_{oE} F_{dE'}^{fW} + q_{oW} F_{dW}^{fW} + q_{oa} F_{da}^{fW} \right] \right\} + q_d \end{aligned} \tag{7.42}$$

Similar to q_a for end reflector area A_a, q_b, and q_d are the emissive power of end reflector areas Ab and A_d, and are defined by equation (6.41).

Equations (7.40) through (7.42) give q_{oa}, q_{ob}, and q_{od} in terms of the radiation fluxes leaving all the components of the system. To complete the system of equations the results derived in section 6.4 [equations (6.62) through (6.67)] must be modifies to include q_{oa}, q_{ob}, and q_{od} (problem 7.4). When terms that account for radiation leaving the end reflectors are added to equations (6.62) through (6.67), the following equations are obtained.

$$\begin{aligned} q_{oW}\left[1-\rho_W F_{WW}\right] = \rho_W \Big\{ & q'_{oE} F_{WE'} + \tau_W q_{of} F^W_{Wf} + \tau_W \tau_f q_{oC} F^{fW}_{WC} + q_{oa} F_{Wa} \\ & + \tau_W q_{ob} F^W_{Wb} + \tau_W \tau_f q_{od} F^{fW}_{Wd} \Big\} + q_W \end{aligned} \tag{7.43}$$

$$\begin{aligned} q_{of}\left[1-\rho_f\left(F_{ff}+\tau_W^2 F^W_{ff}\right)\right] = \rho_f \Big\{ & \tau_W q'_E F_{fE'} + q'_{oW} F_{fW'} + \tau_W q_{oW} F^W_{fW} + \tau_f q_{oC}\left(F^f_{fC} + \tau_W^2 F^{WC}_{fC}\right) \\ & + \tau_W q_{oa} F^W_{fa} + q_{ob}\left[F_{fb} + \tau_W^2 F^W_{fb}\right] + \tau_f q_{od}\left[F^f_{fd} + \tau_W^2 F^{fW}_{fd}\right] \Big\} + q_f \end{aligned} \tag{7.44}$$

$$\begin{aligned} q_{oC}\left[1-\rho_C\left(F_{CC}+\tau_f^2 F^f_{CC} + \tau_f^2\tau_W^2 F^{fW}_{CC}\right)\right] = \rho_C \Big\{ & \tau_W \tau_f q'_{oE} F_{CE'} + \tau_f q'_{oW} F_{CW'} + q'_{of} F_{Cf'} \\ & \tau_W \tau_f q_{oW} F^{fW}_{CW} + \tau_f q_{of}\left[F^f_{Cf} + \tau_W^2 F^{fW}_{Cf}\right] + \tau_W \tau_f q_{oa} F^{fW}_{Ca} + \tau_f q_{ob}\left[F^f_{Cb} + \tau_W^2 F^{fW}_{Cb}\right] \\ & + q_{od}\left[F_{Cd} + \tau_f^2\left(F^f_{Cd} + \tau_W^2 F^{fW}_{Cd}\right)\right] \Big\} + q_C \end{aligned} \tag{7.45}$$

$$q'_{of} = \rho'_f\left[q_{oC} F_{f'C} + q_{od} F_{f'd}\right] + q'_f \tag{7.46}$$

$$q'_{oW} = \rho'_W\left[q_{of} F_{W'f} + \tau_f q_{oC} F_{W'C} + q_{ob} F_{W'b} + \tau_f F^f_{W'd} q_{od}\right] + q'_W \tag{7.47}$$

$$\begin{aligned} q'_{oE} = \rho'_E\Big[& q_{oW} F_{E'W} + \tau_W q_{of} F_{E'f} + \tau_W \tau_f q_{oC} F_{E'C} + q_{oa} F_{E'a} + \tau_W q_{ob} F^W_{E'b} \\ & + \tau_W \tau_f F^{fW}_{E'd} q_{od}\Big] + q'_E \end{aligned} \tag{7.48}$$

Equations (7.40) through (7.48) make up a system of nine algebraic equations for the radiation fluxes leaving the emitter, window, filter, and PV cells, as well as, the three sections of the end reflectors. The solutions will be functions of the view-factors and component optical properties, which are functions of the wavelength. In addition, the emissive powers are functions of the component temperatures. As stated earlier the planar geometry equations can easily be obtained from equations (7.40) through (7.48). This is accomplished by setting all view-factors between concave surfaces of the window, filter, and PV cells (view-factors with two unprimed subscripts of W, f, or C). Also, view-factors between the end reflectors and concave surfaces of the window,

filter, or PV cells for radiation that passes through the window or filter [view-factors with one end reflector subscript (a, b, or d) and superscript of f, W, or fW].

In the remainder of the chapter we will consider a simplified TPV system to show how end reflectors can improve cavity efficiency.

7.4.2 Radiation Transfer Equations for TPV Systems with Close Coupled Emitter-Window and Filter-PV Cells

In a practical TPV system it is likely that the emitter and window will be close together in order to minimize the conductive and convective heat loss from the emitter. Also, it is likely that the filter will be physically connected to the PV cells in order that the same cooling system can be used for the filter and PV cells. Therefore, consider a TPV system with the emitter and window, and the filter and PV cells very close together. In that case the following view-factor approximations can be made.

$$F_{E'W} = F_{WE'} = F_{f'C} = F_{Cf'} = 1 \tag{7.49a}$$

$$F_{E'f} = F_{W'f} = F_{W'C} = F_{E'C} \tag{7.49b}$$

$$F_{fE'} = F_{fW'} = F_{CW'} = F_{CE'} \tag{7.49c}$$

$$F^{f}_{fC} = F^{f}_{Cf} = F^{f}_{CC} = F_{ff} \equiv F_{22} \tag{7.49d}$$

$$F^{fW}_{CC} = F^{fW}_{fC} = F^{fW}_{Cf} = F^{fW}_{CW} = F^{fW}_{WC} = F^{W}_{fW} = F^{W}_{Wf} = F^{W}_{ff} = F_{WW} = F_{CC} = 0 \tag{7.49e}$$

Since end reflector areas A_a and A_d vanish (use Figure 7.7) the following results apply.

$$\begin{aligned} &F_{E'a} = F_{aE'} = F^{fW}_{E'd} = F^{fW}_{dE'} = F_{Wa} = F_{aW} = F_{f'd} = F_{df'} = F^{W}_{fa} = F^{W}_{af} = F_{Cd} = F_{dC} = F^{W}_{bW} = \\ &F^{W}_{Wb} = F^{W}_{fb} = F^{w}_{bf} = F^{fW}_{Cb} = F^{fW}_{bC} = F^{fW}_{Ca} = F^{fW}_{aC} = F_{aa} = F^{W}_{ab} = F^{W}_{ba} = F_{dd} = F^{f}_{db} = F^{f}_{bd} = 0 \end{aligned} \tag{7.49f}$$

$$F^{W}_{E'b} = F_{W'b}\ , \qquad F^{W}_{bE'} = F_{bW'} \tag{7.49g}$$

$$F^{f}_{Cb} = F_{fb}\ , \qquad F^{f}_{bC} = F_{bf} \tag{7.49h}$$

Note that a new view-factor, F22, has been introduced in equation (7.49d). This is the self view-factor for the filter-PV cell combination and is given in Figure 6.3 where $z = \dfrac{R_C}{R_E}$, $L = \dfrac{\ell}{R_E}$.

Since $A_a = A_d = 0$, $q_{oa} = q_{od} = q_a = q_d = 0$, and equations (7.40) and (7.42) vanish and using equation (7.49a) through (7.49h) the remaining transfer equations become the following.

$$q_{ob}\left(1-\rho_b F_{22}\right) = \rho_b\left\{\tau_W q'_{oE} F_{bW'} + q'_{oW} F_{bW'} + q_{of} F_{bf} + \tau_f q_{oC} F_{bf}\right\} + q_b \tag{7.50}$$

$$q_{oW} = \rho_W q'_{oE} + q_W \tag{7.51}$$

$$q_{of}\left(1-\rho_f F_{22}\right) = \rho_f\left\{\tau_W q'_{oE} F_{CE'} + q'_{oW} F_{CE'} + \tau_f q_{oC} F_{22} + q_{ob} F_{fb}\right\} + q_f \tag{7.52}$$

$$q_{oC}\left(1-\rho_C \tau_f^2 F_{22}\right) = \rho_C\left\{\tau_W \tau_f q'_{oE} F_{CE'} + \tau_f q'_{oW} F_{CE'} + \tau_f q_{of} F_{22} + q'_{of} + \tau_f q_{ob} F_{fb}\right\} + q_C \tag{7.53}$$

$$q'_{of} = \rho'_f q_{oC} + q'_f \tag{7.54}$$

$$q'_{oW} = \rho'_W\left\{q_{of} F_{E'C} + \tau_f q_{oC} F_{E'C} + q_{ob} F_{W'b}\right\} + q'_W \tag{7.55}$$

$$q'_{oE} = \rho'_E\left\{q_{oW} + \tau_W q_{of} F_{E'C} + \tau_W \tau_f q_{oC} F_{E'C} + \tau_W q_{ob} F_{W'b}\right\} + q'_E \tag{7.56}$$

Equations (7.50) through (7.56) are a system of seven equations for the seven radiation fluxes; q'_{oE}, q_{oW}, q'_{oW}, q_{of}, q'_{of}, q_{oC}, and q_{ob}. The system can be simplified in the following manner. First, substitute equation (7.51) for q_{oW} in equation (7.56), and multiply the resulting equation by ρ'_W. From this result subtract equation (7.55) multiplied by $\rho'_E \tau_W$. This yields the following relation between q'_{oW} and q'_{oE}.

$$\rho'_E \tau_W q'_{oW} = \rho'_W\left(1-\rho'_E \rho_W\right) q'_{oE} + \rho'_E \tau_W q'_W - \rho'_W \rho'_E q_W - \rho'_W \rho'_E \tag{7.57}$$

Now substitute (7.54) for q'_{of} in (7.53) and multiply the resulting equation by ρ_f, then subtract this result from equation (7.52) after multiplying (7.52) by $\rho_C \tau_f$. As a result, the following relation between q_{of} and q_{oC} is obtained.

$$\rho_C \tau_f q_{of} = \rho_f\left(1-\rho_C \rho'_f\right) q_{oC} + \rho_C \tau_f q_f - \rho_f \rho_C q'_f - \rho_f q_C \tag{7.58}$$

Substituting (7.57) and (7.58) for q'_{oW} and q_{of} in (7.50) yields the following equation for q_{ob} in terms of q'_{oE} and q_{oC}.

$$q_{ob}\left(1-\rho_b F_{bb}\right)=\rho_b\left\{\left[\tau_W+\frac{\rho'_W\left(1-\rho'_E\rho_W\right)}{\rho'_E\tau_W}\right]F_{bW'}q'_{oE}+\left[\tau_f+\frac{\rho_f\left(1-\rho_C\rho'_f\right)}{\rho_C\tau_f}\right]F_{bC}q_{oC}\right\}$$
$$+\rho_b\left[F_{bW'}\left(q'_W-\frac{\rho'_W}{\tau_W}q_W-\frac{\rho'_W}{\rho'_E\tau_W}q'_E\right)+F_{bf}\left(q_f-\frac{\rho_f}{\tau_f}q'_f-\frac{\rho_f}{\rho_C\tau_f}q_C\right)\right]+q_b \tag{7.59}$$

The final steps in this simplification process are to obtain two equations for q'_{oE} and q_{oC}. To do this first substitute (7.51) for q_{oW}, then substitute (7.57) for q'_{oW}, (7.58) for q_{of}, and (7.59) for q_{ob} in (7.56). Similarly, replace q'_{oW}, q_{of}, and q_{ob} using (7.57), (7.58), and (7.59) in equation (7.53). As a result the following two equations for q'_{oE} and q_{oC} result.

$$a_E q'_{oE}-a_C q_{oC}=S_E \tag{7.60}$$

$$-b_E q'_{oE}+b_C q_{oC}=S_C \tag{7.61}$$

Terms appearing in equations (7.60) and (7.61) are defined as follows.

$$a_E=1-\rho'_E\rho_W-\frac{\rho_b}{D_b}\gamma_E F_{W'b}F_{bW'} \tag{7.62}$$

$$a_C=\frac{\rho'_E\tau_W}{\rho_C\tau_f}\gamma_C f_{E'C} \tag{7.63}$$

$$b_E=\frac{\rho_C\tau_f}{\rho'_E\tau_W}\gamma_E f_{CE'} \tag{7.64}$$

$$b_C=1-\rho_C\rho'_f-\gamma_C f_{CC} \tag{7.65}$$

$$S_E=\left(1-\frac{\rho'_W\rho_b}{D_b}F_{W'b}F_{bW'}\right)\left(q'_E+\rho'_E q_W\right)+\tau_W\rho'_E\left[\frac{F_{W'b}}{D_b}\left(q_b+\rho_b F_{bW'}q'_W\right)\right.$$
$$\left.+f_{E'C}\left(q_f-\frac{\rho_f}{\tau_f}q'_f-\frac{\rho_f}{\rho_C\tau_f}q_C\right)\right] \tag{7.66}$$

$$S_C = \left[1-\rho_f f_{CC}\right]\left[q_C + \rho_C q'_f\right] + \tau_f \rho_C \left[\frac{F_{fb}}{D_b} q_b + f_{CC} q_f + f_{CE'}\left(q'_W - \frac{\rho'_W}{\tau_W} - \frac{\rho'_W}{\rho'_E \tau_W} q'_E\right)\right] \tag{7.67}$$

$$\gamma_E = \rho'_E\left(\tau_W^2 - \rho_W \rho'_W\right) + \rho'_W \tag{7.68}$$

$$\gamma_C = \rho_C\left(\tau_f^2 - \rho_f \rho'_f\right) + \rho_f \tag{7.69}$$

$$D_b = 1 - \rho_b F_{bb} \tag{7.70}$$

$$f_{E'C} = F_{E'C} + \frac{\rho_b}{D_b} F_{W'b} F_{bf} \tag{7.71}$$

$$f_{CE'} = F_{CE'} + \frac{\rho_b}{D_b} F_{fb} F_{bW'} \tag{7.72}$$

$$f_{CC} = F_{22} + \frac{\rho_b}{D_b} F_{fb} F_{bf} \tag{7.73}$$

Equations (7.62) through (7.73) apply for a cylindrical geometry. To obtain the radiation flux equations that apply for a planar system merely set $F_{22} = 0$ in equation (7.73) so that $f_{CC} = \frac{\rho_b}{D_b} F_{fb} F_{bf}$.

Equations (7.60) and (7.61) can be solved for q'_{oE} and q_{oC} to obtain the following results.

$$q'_{oE} = \frac{\left(1-\rho_C \rho'_f - \gamma_C f_{CC}\right) S_E + \frac{\rho'_E \tau_W}{\rho_C \tau_f} \gamma_C f_{E'C} S_C}{DEN_b} \tag{7.74}$$

$$q_{oC} = \frac{\left(1 - \rho'_E \rho_W - \frac{\rho_b}{D_b} \gamma_E F_{W'b} F_{bW'}\right) S_C + \frac{\rho_C \tau_f}{\rho'_E \tau_W} \gamma_E f_{CE'} S_E}{DEN_b} \tag{7.75}$$

$$DEN_b = \left(1 - \rho'_E \rho_W - \frac{\rho_b}{D_b} \gamma_E F_{W'b} F_{bW'}\right)\left(1 - \rho_C \rho'_f - \gamma_C f_{CC}\right) - \gamma_C \gamma_E f_{E'C} f_{CE'} \qquad (7.76)$$

7.4.3 Cavity Efficiency

The cavity efficiency, η_c, is defined by equation (6.86). In order to determine η_c the solutions for q'_{oE} and q_{oC} given by equations (7.74) and (7.75) must be substituted into equations (6.85) and (6.87) to obtain $\bar{Q}_E$ and $\bar{Q}_C$. To simplify the analysis assume that the emissive power of the emitter, $q'_E = \varepsilon'_E e_b(\lambda, T_E)$, is much greater than all the other emissive powers. As pointed out earlier in section 7.2 this is a reasonable approximation because the emitter has the highest temperature in the system. Also, the emitter will have the largest emittance, ε'_E, except in the case of a selective emitter where ε'_E will be small for part of the spectrum. If only the emitter emissive power terms are retained in the source terms, S_E and S_C of equations (7.74) and (7.75) then the following results are obtained for q'_{oE} and q_{oC} (problem 7.5).

$$q'_{oE} = \left[\frac{\left(1 - \rho_C \rho'_f - \gamma_C f_{CC}\right)\left(1 - \rho'_W \frac{\rho_b}{D_b} F_{W'b} F_{bW'}\right) - \rho'_W \gamma_C f_{E'C} f_{CE'}}{DEN_b}\right] q'_E \qquad (7.77)$$

$$q_{oC} = \frac{\rho_C \tau_f \tau_W}{DEN_b} f_{CE'} q'_E \qquad (7.78)$$

Where DEN_b is given by equation (7.76). Using equations (7.77) and (7.78) in (6.85) and (6.87) yields the following result for the cavity efficiency (problem 7.6).

$$\eta_c \equiv \frac{\bar{Q}_C}{\bar{Q}_E}$$

$$= \frac{A_C}{A_E} \frac{\displaystyle\int_0^{\lambda_g} \frac{\varepsilon'_E \tau_W \tau_f}{DEN_b} f_{CE'} e_b(\lambda, T_E)\, d\lambda}{\displaystyle\int_0^{\infty} \frac{\varepsilon'_E}{DEN_b} \left\{ \begin{array}{c} \left[1-\rho_C\rho'_f-\gamma_C f_{CC}\right]\left[1-\rho_W-\left(\tau_W^2+\rho'_W(1-\rho_W)\right)\frac{\rho_b}{D_b}F_{W'b}F_{bW'}\right] \\ -\gamma_C\left[\tau_W^2+\rho'_W(1-\rho_W)\right]f_{E'C}f_{CE'} \end{array} \right\} e_b(\lambda, T_E)\, d\lambda} \tag{7.79}$$

The approximation made in deriving equation (7.79) are:

1) emitter and window together ($F_{E'W} = F_{WE'} = 1$)
2) filter and PV cells together ($F_{f'C} = F_{Cf'} = 1$)
3) emissive powers of window (q_W, q'_W), filter (q_f, q'_f), PV cells (q_C), and end caps (q_b), small compared to emissive power of emitter (q'_E).

It should be remembered that equation (7.79) applies for a cylindrical geometry. However, as stated earlier, by setting $F_{22} = 0$ in the definition of f_{CC} [equation (7.73)] the planar geometry cavity efficiency is also given by equation (7.79). In sections 7.2 and 7.3 the cavity efficiency for planar [equation (7.11)] and cylindrical [equation (7.33)] geometry systems was derived for the case of no window and no end reflectors. These results can be obtained from equation (7.79) by setting $\rho_b = 0$, $\rho_W = \rho'_W = 0$, and $\tau_W = 1$, for both planar and cylindrical geometries, and additionally $F_{22} = 0$ for the planar system.

The view-factor term, $f_{CE'}$, in the numerator of equation (7.79) must remain within the integral because it contains the wavelength dependent end cap reflectance, ρ_b. However, it is a reasonable approximation to assume ρ_b is a constant. In that case $f_{CE'}$ can be removed from the integral so that the following result is obtained (problem 7.7).

$$\eta_c \sim \frac{A_C}{A_E} f_{CE'} = f_{E'C} \tag{7.80}$$

Whereas without reflecting end caps $\eta_c \sim F_{E'C}$, the addition of end caps results in an "effective" view-factor.

$$f_{E'C} = F_{E'C} + \frac{\rho_b}{(1-\rho_b F_{bb})} F_{W'b} F_{bf} \tag{7.81}$$

The end caps enter in other terms of equation (7.79), however the major contribution to η_c of the end caps enters through $f_{E'C}$. Equation (7.81) can be simplified as follows. Since the end caps view either the emitter-window combination, the filter-PV cell combination, or themselves the following relation must be satisfied.

$$F_{bW'} + F_{bf} + F_{bb} = 1 \tag{7.82}$$

Similarly, since the emitter and window are together.

$$F_{E'C} + F_{W'b} = 1 \tag{7.83}$$

Now use equations (7.82) and (7.83) in (7.81).

$$f_{E'C} = F_{E'C} \left[\frac{1-\rho_b \left(1 - F_{bW'} - \dfrac{F_{bf}}{F_{E'C}} \right)}{1-\rho_b (1 - F_{bW'} - F_{bf})} \right] \tag{7.84}$$

As equation (7.84) shows, if the emitter-window combination is very close to the filter-PV array combination so that $\dfrac{F_{bf}}{F_{E'C}} \approx F_{bf}$, then $F_{EC} \approx F_{E'C}$. Thus the end reflectors do not contribute.

Now consider the case $\rho_b \approx 1$, which yields the largest value of $f_{E'C}$. In that case $f_{E'C}$ becomes the following.

$$f_{E'C} = F_{E'C} \left[\frac{F_{bW'} + \dfrac{F_{bf}}{F_{E'C}}}{F_{bW'} + F_{bf}} \right] \qquad \rho_b = 1 \tag{7.85}$$

This result applies to both planar and cylindrical geometries. First consider a planar geometry. If all the components have the same area then $F_{bW'} = F_{bf}$ and $f_{E'C}$ is the following.

$$\eta_c \sim f_{E'C} = \frac{1}{2}\left(1 + F_{E'C}\right) \qquad \rho_b = 1, \text{ planar geometry with equal area components} \qquad (7.86)$$

Thus the addition of a reflecting tube (Figure 7.6a) for the case where $\rho_b = 1$ yields a minimum effective view-factor of 0.5 even if $F_{E'C} \approx 0$. For a perfect selective emitter system (section 7.2) $\eta_c = f_{E'C}$ so that $\eta_c \geq 0.5$ if a reflecting tube with $\rho_b = 1$ is used regardless of the distance between the emitter and the PV cells. Note that if the reflecting tube is tapered from the emitter to the PV cells ($A_E = A_W > A_f = A_C$) then $F_{bW'} > F_{bf}$ and for $\rho_b = 1$.

$$\eta_c \sim f_{E'C} < \frac{1}{2}\left(1 + F_{E'C}\right) \qquad \rho_b = 1, \text{ planar geometry with } A_E > A_C \qquad (7.87)$$

Thus although it may seem that tapering down in area ($A_E > A_C$) should focus the radiation at the PV cells and thus improve the cavity efficiency the opposite is true. With increasing taper ($A_C > A_E$) $F_{bW'} < F_{bf}$ and the following applies.

$$\eta_c \sim f_{E'C} > \frac{1}{2}\left(1 + F_{E'C}\right) \qquad \rho_b = 1, \text{ planar geometry with } A_C > A_E \qquad (7.88)$$

Thus increasing taper produces a larger η_c than decreasing taper. Now consider a cylindrical geometry. Since the filter area is larger than the window area, $F_{bf} > F_{bW'}$. As a result,

$$\eta_c \sim f_{E'C} > \frac{1}{2}\left(1 + F_{E'C}\right) \qquad \rho_b = 1, \text{ cylindrical geometry} \qquad (7.89)$$

Comparing this result with the planar geometry [equation (7.86)] we see that the end reflectors are more beneficial for the cylindrical geometry.

7.5 Summary

This chapter considers radiation leakage losses from TPV systems. It is the cavity efficiency, η_c, defined by equation (6.86) that determines the leakage losses. Therefore, the major part of the chapter is the derivation of the cavity efficiencies for planar and cylindrical geometry TPV systems. End reflectors to prevent leakage losses were included in the derivations. Some of the important conclusions that resulted are the following.

1) The view-factor between the emitter and PV array is the major factor in determining radiation leakage losses. The cavity efficiency is directly proportional to this view-factor.
2) Cylindrical geometry is more advantageous than a planar geometry for limiting leakage losses (Figure 7.4).
3) Filter TPV system is more sensitive to emitter to PV array view-factor than selective emitter system (Figures 7.2, 7.3, and 7.5).
4) Addition of end reflectors results in an effective emitter to PV array view-factor, $f_{E'C}$ [equation (7.81)], that is greater than the emitter-PV view-factor, $F_{E'C}$.
5) For a perfect end reflectors (reflectance = $\rho_b = 1$) the following occurs.
   a) $\eta_c \sim f_{E'C} = \frac{1}{2}\left(1 + F_{E'C}\right)$ for a planar geometry with equal area components.
   b) $\eta_c \sim f_{E'C} > \frac{1}{2}\left(1 + F_{E'C}\right)$ for a cylindrical geometry.

Problems

7.1 Using the black emissive power [equation (1.120) show that $f(u_g)$ given by equation (2.19) can be written as follows.

$$f\left(u_g\right) = \frac{1 - F_{o-\lambda_g T_E}}{F_{o-\lambda_g T_E}}$$

Where $F_{o-\lambda_g T_E}$ is given by equation (1.137) and $u_g = \frac{E_g}{kT_E} = \frac{hc_o}{k\lambda_g T_E}$. Then for $u_g > 1$ show that $f(u_g)$ is given by the following expression.

$$f\left(u_g\right) = \frac{\pi^4}{15\sum_{m=1}^{\infty}\left[\frac{e^{-mu_g}}{m}\left(u_g^3 + \frac{3u_g^2}{m} + \frac{6u_g}{m^2}\frac{6}{m^3}\right)\right]} - 1 \qquad \text{for } u_g > 1$$

Hint: $$\int x^3 e^{ax} dx = \frac{e^{ax}}{a}\left[x^3 - \frac{3x^2}{a} + \frac{6x}{a^2} - \frac{6}{a^3}\right]$$

7.2 Derive equation (7.21) for a planar filter TPV system from equation (7.13) using the following approximations.

1) for $0 \le \lambda \le \lambda_g$, $\rho_C \approx 0$ and $\rho_f F_{E'C} F_{CE'} \ll 1$
2) for $\lambda_g < \lambda < \infty$, $\tau_f^2 \ll \rho_f \rho_f'$

7.3 Derive equation (7.34) for a cylindrical filter TPV system with a blackbody emitter from equation (7.33) using the following approximations.

1) for $0 \le \lambda \le \lambda_g$, $\rho_C \approx 0$ and $\rho_f \left[F_{22} + F_{E'C} F_{CE'} \right] \ll 1$
2) for $\lambda_g \le \lambda < \infty$, $\tau_f^2 \ll \rho_f \rho_f'$

Show that equation (7.33) reduces to the planar filter TPV system result [equation (7.21)] if $\rho_f F_{22} \ll 1$.

7.4 Derive equation (7.45) using the radiation transfer theory results of section 6.2 [equations (6.5), (6.7), (6.30), (6.31)].

7.5 Derive equation (7.78) for the radiation flux leaving the PV cells, q_{oC}, when only the emitter emissive power terms are retained in the source terms S_E and S_C in equation (7.75).

7.6 Use equation (7.77) in (6.85) to obtain $\bar{Q}_E$ [denominator of equation (7.79)].

7.7 Using the view-factor result $A_i F_{ij} = A_j F_{ji}$, show that $A_E f_{E'C} = A_C f_{CE'}$ where $f_{E'C}$ and $f_{CE'}$ are given by equations (7.71) and (7.72) and $A_E = A_W$, $A_C = A_f$.

7.8 For a planar TPV system with perfect end reflectors ($\rho_b = 1$) where the emitter and window are together and the filter and PV array are together the cavity efficiency, η_c, is directly proportional to the effective view-factor, $f_{E'C} = \frac{1}{2}\left(1 + F_{E'C}\right)$. Where $F_{E'C}$ is the view-factor for the emitter to the PV array. For a system without end reflectors $\eta_c \sim F_{E'C}$. Calculate the ratio $\frac{f_{E'C}}{F_{E'C}}$ for a planar system with circular emitter and PV array of radii 5cm ($R_E = R_C = 5$cm) when the distance between the emitter and PV array is h = 0.5cm and h = 1cm. What can be said about the benefit of perfect end reflectors for the two cases?

This page intentionally left blank

Chapter 8
TPV System Performance

Preceding chapters have concentrated on two objectives. The earliest chapters explained and quantified the performance of the major components of a TPV system. Later chapters developed the analysis to calculate the performance of a TPV system. Therefore, the major objective of this chapter is to describe the radiation transfer method for determining the performance of a TPV system.

The performance is a function of the thermal power input, the geometry of the optical cavity, and the optical properties of the various components. In Chapter 6 radiation transfer theory was applied to obtain the radiation fluxes leaving the surfaces of the optical cavity. These results are used to calculate TPV system performance. The two major assumptions of the radiation transfer analysis are the following. First, the surfaces behave in a diffuse manner so that the radiation intensity is the same in all directions. Second, it is assumed that the fluxes incident and leaving a surface are constant over the area of that surface.

8.1 Symbols

A	surface area, cm^2
A_o	ideality factor
c_o	vacuum speed of light, 2.9979×10^{10} cm/sec
e	electron charge, 1.602×10^{-19}, Coul
e_b	blackbody emissive power, watts/cm^2 nm
E_g	bandgap energy, eV
F_{ab}	view-factor for radiation leaving area a and impinging on area b
FF	fill factor
h	Planck's constant, 6.62×10^{-34}, J-sec
I	current, Amps
J	current density, Amps/cm^2
k	Boltzmann constant, 1.38×10^{-23} J/K
P_{EL}	electrical power output, watts
q	radiative energy flux, watts/cm^2 nm
Q	radiative power at wavelength, λ, watts/nm
$\overline{Q}$	total radiative power, watts
R	resistance, ohms or reflectivity

T	temperature, K
u_g	E_g/kT_E, dimensionless bandgap energy
V	voltage, volts
ε	emittance
λ	wavelength, nm
ρ	reflectance
τ	transmittance
η	efficiency

Subscripts

b	denotes reflector of optical cavity
C	denotes PV array in optical cavity
E	denotes emitter in optical cavity

8.2 TPV System Model

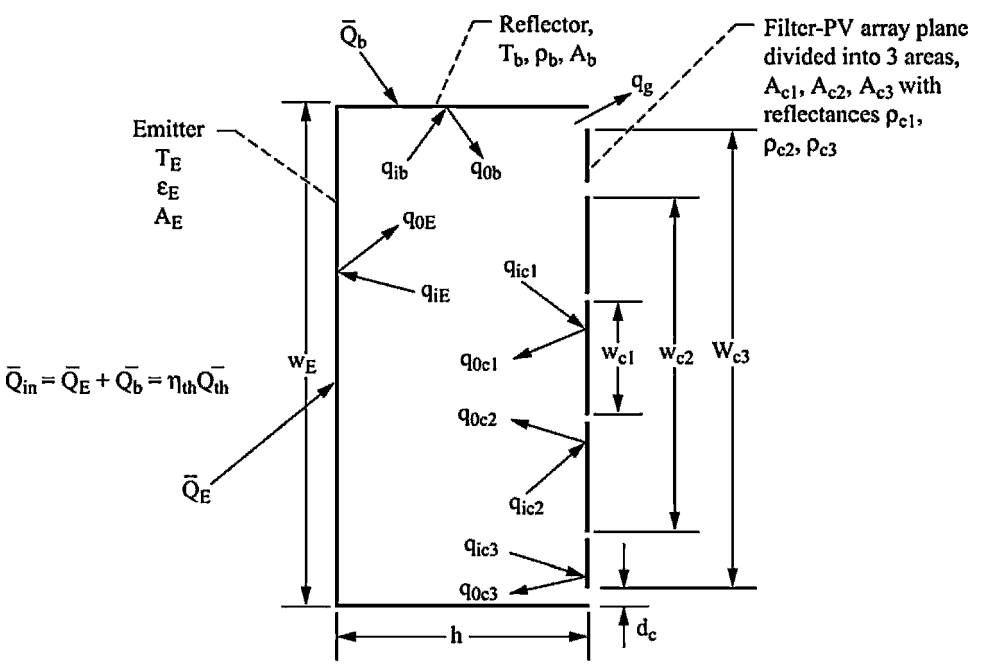

Figure 8.1.—Schematic drawing of TPV system model showing radiation power densities incident and leaving each component.

Illustrated in Figure 8.1 is the planar geometry optical cavity model that is to be considered. A planar emitter that can be either circular or rectangular in shape is separated a distance, h, from a plane that is divided into three areas: A_{C1}, A_{C2}, and A_{C3}. At this plane are located the PV arrays and filters. If a filter is used, it is assumed that the filter and PV array are together so that the view-factor between the filter and PV array is 1. It is assumed that a vacuum exists between the emitter and PV array so that no convective heat transfer occurs between the emitter and PV array. The vacuum condition would occur naturally in a TPV system for a space application.

The reflector surface, b, is attached to the emitter so that $T_b = T_E$. Attaching the reflector to the emitter eliminates the leakage of radiation from the cavity that would exist if a gap existed between the emitter and reflector.

Dividing the filter-PV array plane into three areas gives flexibility to the analysis. For example, A_{C1} and A_{C2} can be filter-PV arrays, and A_{C3} can be a reflecting surface such as gold. Or for another example, all three areas can be filter-PV arrays.

The total efficiency of the system is the following [equation (6.83)],

$$\eta_T = \eta_{th}\eta_c\eta_{PV} = \frac{\overline{Q}_{in}}{\overline{Q}_{th}}\frac{\overline{Q}_C}{\overline{Q}_{in}}\frac{P_{EL}}{\overline{Q}_C} = \frac{P_{EL}}{\overline{Q}_{th}} \tag{8.1}$$

where η_{th} is the thermal efficiency [equation (6.84)], η_c is the cavity efficiency [equation (6.86)], and η_{PV} is the photovoltaic efficiency [equation (6.88)]. Note that $\overline{Q}_{in} = \overline{Q}_E + \overline{Q}_b$ has replaced $\overline{Q}_E$ in the definition of η_c, since thermal energy is being supplied to the reflector, as well as, to the emitter. Only η_c and η_{PV} are calculated for the system in Figure 8.1. The thermal efficiency, η_{th}, depends on the heat source, which is not being considered. In the next section, the radiation transfer equations are developed and solutions for the radiation power densities are given.

8.3 Radiation Transfer Equations

The basic radiation transfer equation is given by equation (6.5),

$$Q_{ab} = \tau_{ab} q_{oa} F_{ab} A_a \qquad \text{W/nm} \tag{8.2}$$

where Q_{ab} is the radiation power incident on area A_b that originates at area A_a. Also, τ_{ab} is the transmittance of the media between A_a and A_b, q_{oa} is radiation power per unit area per wavelength leaving A_a and F_{ab} is the view-factor from area A_a to area A_b. Equation (8.2) assumes q_{oa} is uniform across A_a. In addition, assume the radiation fluxes arriving at an area, q_i, are also uniform across the area. In that case, $Q_{ia} = q_{ia}A_a$, where q_{ia} is the total incident flux on area A_a. Also, the view-factor relation given by equation (6.7)

applies. Thus, applying equation (8.2) and equation (6.7) to the radiation leaving all areas that view area A_b the following is obtained.

$$q_{ib} = \sum_a \tau_{ab} q_{oa} F_{ba} \tag{8.3}$$

Also, the flux leaving a surface is the sum of the emitted and reflected fluxes [equation (6.30)]. Therefore, equation (8.3) becomes the following,

$$q_{ob} = \rho_b q_{ib} + \varepsilon_b e_b\left(\lambda, T_b\right) = \rho_b \sum_a \tau_b q_{oa} F_{ba} + \varepsilon_b e_b\left(\lambda, T_b\right) \tag{8.4}$$

where ε_b is the spectral emittance of A_a and $e_b(\lambda,T_b)$ is the blackbody emissive power at the temperature of A_b, which is given by equation (1.120).

Now apply equation (8.4) to each of the surfaces in Figure 8.1, noting that $\tau_{ab} = 1$ since a vacuum exists in the optical cavity.

$$q_{oE} - \rho_E\left[F_{EC1} q_{oC1} + F_{EC2} q_{oC2} + F_{EC3} q_{oC3} + F_{Eb} q_{ob}\right] = \varepsilon_b e_b\left(\lambda, T_E\right) \tag{8.5}$$

$$q_{ob}\left(1 - \rho_b F_{bb}\right) - \rho_b\left[F_{bE} q_{oE} + F_{bC1} q_{oC1} + F_{bC2} q_{oC2} + F_{bC3} q_{oC3}\right] = \varepsilon_b e_b\left(\lambda, T_b\right) \tag{8.6}$$

$$q_{oC1} - \rho_{C1}\left[F_{C1E} q_{oE} + F_{C1b} q_{ob}\right] = \varepsilon_{C1} e_b\left(\lambda, T_{C1}\right) \tag{8.7}$$

$$q_{oC2} - \rho_{C2}\left[F_{C2E} q_{oE} + F_{C2b} q_{ob}\right] = \varepsilon_{C2} e_b\left(\lambda, T_{C2}\right) \tag{8.8}$$

$$q_{o3} - \rho_{C3}\left[F_{C3E} q_{oE} + F_{C3b} q_{ob}\right] = \varepsilon_{C3} e_b\left(\lambda, T_{C3}\right) \tag{8.9}$$

Notice the $\rho_b F_{bb}$ term in equation (8.6). It occurs because the reflector has a view of itself.

Equations (8.5) through (8.9) form a set of five linear algebraic equations for the five unknown q_o's. The following solutions for q_{oE} and q_{ob} are obtained after a tedious amount of algebraic manipulation,

$$q_{oE}\left(\lambda\right) = \frac{\left(aB_2 + bE_2\right)}{DEN} \tag{8.10}$$

$$q_{ob}(\lambda) = \frac{(aB_1 + bE_1)}{DEN} \tag{8.11}$$

where,

$$a = \varepsilon_E e_b(\lambda, T_E) + \rho_E \left[F_{EC1}\varepsilon_{C1} e_b(\lambda, T_{C1}) + F_{EC2}\varepsilon_{C2} e_b(\lambda, T_{C2}) + F_{EC3}\varepsilon_{C3}(\lambda, T_{C3}) \right] \tag{8.12}$$

$$b = \varepsilon_b e_b(\lambda, T_b) + \rho_b \left[F_{bC1}\varepsilon_{C1} e_b(\lambda, T_{C1}) + F_{bC2}\varepsilon_{C2} e_b(\lambda, T_{C2}) + F_{bC3} e_b(\lambda, T_{C3}) \right] \tag{8.13}$$

$$B_1 = \rho_b \left[F_{bE} + \rho_{C1} F_{C1E} F_{bC1} + \rho_{C2} F_{C2E} F_{bC2} + \rho_{C3} F_{C3E} F_{bC3} \right] \tag{8.14}$$

$$B_2 = 1 - \rho_b \left[F_{bb} + \rho_{C1} F_{C1b} F_{bC1} + \rho_{C2} F_{C2b} F_{bC2} + \rho_{C3} F_{C3b} F_{bC3} \right] \tag{8.15}$$

$$E_1 = 1 - \rho_E \left[\rho_{C1} F_{C1E} F_{EC1} + \rho_{C2} F_{C2E} F_{EC2} + \rho_{C3} F_{C3E} F_{EC3} \right] \tag{8.16}$$

$$E_2 = \rho_E \left[F_{Eb} + \rho_{C1} F_{C1b} F_{EC1} + \rho_{C2} F_{C2b} F_{EC2} + \rho_{C3} F_{C3b} F_{EC3} \right] \tag{8.17}$$

$$DEN = E_1 B_2 - E_2 B_1 \tag{8.18}$$

Equations (8.10) and (8.11) are solutions for $q_{oE}(\lambda)$ and $q_{ob}(\lambda)$ in terms of the view-factors, optical properties, and temperatures of each of the five areas. Knowing q_{oE} and q_{ob}, solutions for q_{oC1}, q_{oC2}, and q_{oC3} are obtained using equations (8.7) through (8.9).

The view-factors depend upon the geometry of the optical cavity. For the model shown in Figure 8.1, the areas A_E, A_{C1}, A_{C2}, and A_{C3} can be either circular or square with a corresponding cylindrical or square prism shaped reflector. View-factor expressions for parallel circular disks, identical, parallel opposed rectangles, and unequal, parallel, coaxial squares are given in Figure 6.3. These three view-factors are all that are required to calculate the necessary view-factors for either the circular or square geometry as shown in Figure 8.1. Consider F_{EC1}; this view-factor is given in Figure 6.3a for a circular geometry and Figure 6.3c for a square geometry. Thus, using the reciprocity relation [equation (6.7)] the view-factor F_{C1E} can be calculated.

$$F_{C1E} = \frac{A_E}{A_{C1}} F_{EC1} \tag{8.19}$$

From view-factor algebra,

$$F_{EC2} = F_{E(C1+C2)} - F_{EC1} \tag{8.20}$$

where $F_{E(C1 + C2)}$ is the view-factor for the area A_E to the area $A_{C1} + A_{C2}$ and is given in Figure 6.3a for circular geometry and Figure 6.3c for square geometry. Using the reciprocity relation,

$$F_{C2E} = \frac{A_E}{A_{C2}} F_{EC2} \tag{8.21}$$

Similarly,

$$F_{EC3} = F_{E(C1+C2+C3)} - F_{E(C1+C2)} \tag{8.22}$$

where $F_{E(C1+C2+C3)}$ is the view-factor from A_E to $A_{C1} + A_{C2} + A_{C3}$ and is given in Figure 6.3. And from the reciprocity relation,

$$F_{C3E} = \frac{A_E}{A_{C3}} F_{EC3} \tag{8.23}$$

Again using view-factor algebra,

$$F_{Eb} = 1 - F_{E(C1+C2+C3+g)} \tag{8.24}$$

where $F_{E(C1+C2+C3+g)}$ is the view-factor from area A_E to area $A_{C1} + A_{C2} + A_{C3} + A_g$ and is given in Figure 6.3. Using reciprocity the following is obtained.

$$F_{bE} = \frac{A_E}{A_b} F_{Eb} \tag{8.25}$$

Also,

$$F_{C1b} = 1 - F_{C1E} \tag{8.26}$$

$$F_{bC1} = \frac{A_{C1}}{A_b} F_{C1b} \tag{8.27}$$

where F_{C1E} is given by equation (8.19).

Obtaining F_{C2b} and F_{C3b} requires the following view-factor algebra.

$$F_{C2b} = 1 - F_{C2E} \tag{8.28}$$

$$F_{C3b} = 1 - F_{C3E} \tag{8.29}$$

F_{C2E} and F_{C3E} are given by equations (8.21) and (8.22). From reciprocity.

$$F_{bC2} = \frac{A_{C2}}{A_b} F_{C2b} \tag{8.30}$$

$$F_{bC3} = \frac{A_{C3}}{A_b} F_{C3b} \tag{8.31}$$

From symmetry and using view-factor algebra it can be shown that F_{bb} is the following (problem 8.1),

$$F_{bb} = 1 - 2F_{bE} \tag{8.32}$$

where F_{bE} is given by equation (8.25). All the necessary view-factors that appear in equations (8.5) through (8.9) are given by equations (8.19) through (8.32). To calculate the radiation flux that escapes through the gap the following equation applies,

$$q_g = F_{gE} q_{oE} + F_{gb} q_{ob} \tag{8.33}$$

where (problem 8.2),

$$F_{gE} = \frac{A_E}{A_g}\left[1 - F_{Eb} - F_{EC1} - F_{EC2} - F_{EC3}\right] \tag{8.34}$$

$$F_{gb} = \frac{A_b}{A_g}\left[F_{bE} - F_{bC1} - F_{bC2} - F_{bC3}\right] \tag{8.35}$$

and all the view-factors appearing in equations (8.34) and (8.35) have already been defined.

The view-factors, given by equations (8.19) through (8.32) and the spectral emittances and reflectances of each of the surfaces in the optical cavity are all the

parameters required to obtain the solutions for q_{oE}, q_{ob}, q_{oC1}, q_{oC2}, and q_{oC3}. Knowing the fluxes allows the calculation of the cavity and photovoltaic efficiencies.

8.4 Solution Method for TPV System Model

The cavity efficiency is the following,

$$\eta_c = \frac{\overline{Q}_C}{\overline{Q}_{in}} \tag{8.36}$$

where $\overline{Q}_{in} = \overline{Q}_E + \overline{Q}_b$ is the power input to the emitter and reflector. $\overline{Q}_E$ is given by equation (6.85).

$$\overline{Q}_E = A_E \int_o^\infty \frac{\varepsilon_E}{1-\varepsilon_E}\left[e_b(\lambda, T_E) - q_{oE}\right] d\lambda \tag{8.37}$$

Similarly,

$$\overline{Q}_b = A_b \int_o^\infty \frac{1-\rho_b}{\rho_b}\left[e_b(\lambda, T_E) - q_{ob}\right] d\lambda \tag{8.38}$$

In obtaining equations (8.37) and (8.38), the relation $\varepsilon = 1 - \rho$ is used since the emitter and reflector are opaque, $\tau = 0$ [see equation (1.229)]. If areas A_{C1}, A_{C2}, and A_{C3} contain PV arrays, then the incident, useful power, $\overline{Q}_C$ is the following,

$$\overline{Q}_C = A_{C1} \int_o^{\lambda_g} \tau_{C1} q_{iC1} d\lambda + A_{C2} \int_o^{\lambda_g} \tau_{C2} q_{iC2} d\lambda + \tau_{C3} A_{C3} \int_o^{\lambda_g} \tau_{C3} q_{iC3} d\lambda \tag{8.39}$$

where τ_{C1}, τ_{C2}, and τ_{C3} are the filter transmittances and λ_g is the wavelength corresponding to the PV array bandgap energy, E_g.

$$\lambda_g = \frac{1.24 \times 10^3}{E_g} \text{ nm} \qquad E_g \text{ in eV} \tag{8.40}$$

If there is no filter, then $\tau_{C1} = \tau_{C2} = \tau_{C3} = 1$ in equation (8.39). Since $\rho q_i = q_o - \varepsilon e_b(\lambda, T)$, equations (8.7)-(8.9) can be used to replace q_{ic2} and q_{ic3} in equation (8.39).

$$\overline{Q}_C = A_{C1}\int_o^{\lambda_g}\tau_{C1}\left[F_{C1E}q_{oE} + F_{C1b}q_{ob}\right]d\lambda + A_{C2}\int_o^{\lambda_g}\tau_{C2}\left[F_{C2E}q_{oE} + F_{C2b}q_{ob}\right]d\lambda + A_{C3}\int_o^{\lambda_g}\tau_{C3}\left[F_{C3E}q_{oE} + F_{C3b}q_{ob}\right]d\lambda \tag{8.41a}$$

Using the view-factor reciprocity relation, this can be written as follows.

$$\overline{Q}_C = A_E\int_o^{\lambda_g}\left[\tau_{C1}F_{EC1} + \tau_{C2}F_{EC2} + \tau_{C3}F_{EC3}\right]q_{oE}d\lambda + A_b\int_o^{\lambda_g}\left[\tau_{C1}F_{bC1} + \tau_{C2}F_{bC2} + \tau_{C3}F_{bC3}\right]q_{ob}d\lambda \tag{8.41b}$$

If only A_{C1} contains a PV array, then the $\tau_{C2}F_{EC2}$, $\tau_{C3}F_{EC3}$, $\tau_{C2}F_{bC2}$, and $\tau_{C3}F_{bC3}$ terms must be removed from equation (8.41b). As can be seen from equations (8.37), (8.38), and (8.41b), once $q_{oE}(\lambda)$ and $q_{ob}(\lambda)$ are known, the cavity efficiency can be calculated.

The PV efficiency is the following [equation (6.88)],

$$\eta_{PV} = \frac{P_{EL}}{\overline{Q}_C} \tag{6.88}$$

where the electrical power output, P_{EL}, depends upon which of the three areas, A_{C1}, A_{C2}, and A_{C3} have PV arrays. If all three areas have PV arrays, then P_{EL} is the following,

$$P_{EL} = P_{ELC1} + P_{ELC2} + P_{ELC3} \tag{6.89}$$

where the electrical power from each array is given by equation (5.228).

$$P_{EL} = N_J\left(V_M - R_s I_{LM}\right)I_{LM} \tag{5.228}$$

Here N_J is the number of series connected junctions in the PV array, V_M is the junction voltage for maximum P_{EL}, and is the root of equation (5.223). In addition, R_s is the series resistance of each junction, and I_{LM} is the load current for maximum P_{EL} and is given as a function of V_M by equation (5.229).

The electrical power output of an array can also be given in terms of the fill factor, FF, short circuit current, I_{sc}, and open circuit voltage, V_{oc} [equation (5.239)].

$$P_{EL} = FFV_{oc}I_{sc} \tag{5.239}$$

Where I_{sc} is the root of equation (5.217a), V_{oc} is the root of equation (5.218a), and FF is given by equation (5.240).

All the quantities that appear in equations (5.228) and (5.239) for P_{EL} are functions of the PV array series resistance, R_s, and shunt resistance, R_{sh}, the photon generated current, I_{ph}, and the dark saturation current, I_s. The resistance and dark saturation current can be determined experimentally for each PV array. And the photon generated current is given as a function of the internal quantum efficiency, η_Q, by equation (5.249),

$$I_{ph} = A_{Ja}\frac{e}{hc_o}\int_o^{\lambda_g}(1-R_C)\lambda\eta_Q\tau_C q_{iC}d\lambda \tag{5.249}$$

where A_{Ja} is the active area of a single junction in the PV array, R_C is the spectral reflectivity at the filter-PV array interface or the vacuum-PV interface if no filter is used, and q_{iC} is the incident radiation flux. For the no filter case, $\tau_C = 1$. The incident flux, q_{iC}, for each of the three areas, A_{C1}, A_{C2}, and A_{C3}, are obtained using equations (8.7) through (8.9) and the result $\rho q_i = q_o - \varepsilon e_b(\lambda,T)$. For example, if area A_{C1} contains a PV array, then I_{phC1} is the following.

$$I_{phC1} = A_{C1a}\frac{e}{hc_o}\int_o^{\lambda_{gC1}}\tau_{C1}(1-R_{C1})\lambda\eta_{QC1}\left[F_{C1E}q_{oE} + F_{C1b}q_{ob}\right]d\lambda \tag{8.42}$$

If PV arrays exist on A_{C2} and A_{C3}, then I_{phC2} and I_{phC3} are obtained from equation (8.42) by replacing the C1 subscripts by C2 and C3.

The spectral reflectivity, $R_C(\lambda)$, and transmittance, $\tau_C(\lambda)$, and the emitter spectral emittance, $\varepsilon_E(\lambda)$, are the important spectral control parameters. Obviously, the ideal situation would have $\varepsilon_E \to 1$ and $\tau_C \to 1$ ($\rho_C = 0$) for $\lambda < \lambda_g$ and $\varepsilon_E \to 0$ and $\rho_C \to 1$ ($\tau_C = 0$) for $\lambda > \lambda_g$. In that case, $\eta_c \to 1$. The use of a selective emitter, such as the rare earths, discussed in Chapter 3, will produce large ε_E for $\lambda > \lambda_g$ but has the disadvantage of large ε_E for $\lambda > 5\mu m$. Tandem plasma-interference and the resonant array filters discussed in Chapter 4 can be fabricated that have $\rho_C \to 1$ for $\lambda > \lambda_g$. Therefore, a combination of a selective emitter and a filter may be a viable solution for effective spectral control. However, absorptance in the filter is a problem, as is shown in Section 8.4.2. An alternative to a filter is the backside reflector (BSR) on the PV array as

discussed in Chapter 4. In that case, by using an anti-reflective coating on the PV array, $\tau_C \rightarrow 1$ and $\rho_C \rightarrow 0$ for $\lambda < \lambda_g$. Also, there is no filter absorptance loss.

All the quantities necessary to calculate η_c and η_{PV} have been written as functions of q_{oE} and q_{ob}, which are obtained from equations (8.10) and (8.11). However, before q_{oE} and q_{ob} can be determined, the emitter and reflector temperatures, T_E and T_b, as well as the, temperatures T_{C1}, T_{C2}, and T_{C3} of A_{C1}, A_{C2}, and A_{C3} must be known. In a TPV system, the temperatures, T_{C1}, T_{C2}, and T_{C3} are fixed by the waste heat radiator. If A_{C1}, A_{C2}, and A_{C3} all contain PV arrays, then that temperature is much lower than T_E and T_b so that the $e_b(\lambda,T_{C1})$, $e_b(\lambda,T_{C2})$, and $e_b(x,T_{C3})$ terms in equations (8.10) and (8.11) can be neglected.

To determine T_E and T_b as functions of the input power, $\overline{Q}_{in}$, an energy balance must be applied to the optical cavity. Conservation of energy requires the following relation be satisfied,

$$\overline{Q}_{in} = \overline{Q}_E\left(T_E\right) + \overline{Q}_b\left(T_b\right) \tag{8.43}$$

where $\overline{Q}_E$ and $\overline{Q}_b$ are given by equations (8.37) and (8.38) and depend upon q_{oE} and q_{ob}. Therefore, an iterative process is required to satisfy equation (8.43). Since the emitter and reflector are connected, assume $T_E = T_b$. Also, assume $T_{C1} = T_{C2} = T_{C3}$ is given or that the T_{C1}, T_{C2}, and T_{C3} emittance terms can be neglected. As a result, equation (8.43) is a function of only a single temperature, T_E. To begin the iterative process, a value for T_E is assumed and q_{oE} and q_{ob} are then determined as functions of λ by equations (8.10) and (8.11). Using these results for q_{oE} and q_{ob}, values for $\overline{Q}_E$ and $\overline{Q}_b$ are calculated using equations (8.37) and (8.38). If the correct value of T_E is assumed then the sum of $\overline{Q}_E$ plus $\overline{Q}_b$ will equal $\overline{Q}_{in}$. If too large a value of T_E is assumed, then $\overline{Q}_E + \overline{Q}_b > \overline{Q}_{in}$. If too small a value of T_E is assumed, then $\overline{Q}_E + \overline{Q}_b < \overline{Q}_{in}$. Therefore, an iteration expression for T_E that converges to the proper solution is the following,

$$T_E^{i+1} = T_E^i - C_I\left[\overline{Q}_{in} - \left(\overline{Q}_E^i + \overline{Q}_b^i\right)\right] \tag{8.44}$$

where T_E^{i+1} is the i + 1 approximation for T_E and T_E^i is the ith approximation for T_E, and C_I is an iteration constant with the units K/W that must be given. $\overline{Q}_E^i$ and $\overline{Q}_b^i$ are calculated using T_E^i. Once T_E has converged to the value that satisfies equation (8.43) the cavity and PV efficiencies can be calculated.

A Mathematic program that calculates all the radiation fluxes and the efficiencies η_c and η_{PV} for a square optical cavity like that shown in Figure 8.1 is described in Appendix F. The enclosed CD-ROM contains the program. In the program, PV arrays exist on all three areas A_{C1}, A_{C2}, and A_{C3}. Also, $C_I = 0.5$ K/W has been chosen for the iteration constant. In addition, the program allows for a gap to exist between the emitter and the reflector. However, if a gap exists between the emitter and the reflector, then $T_b \neq T_E$. In that case, a separate energy balance on the reflector must be used to determine T_b for a given T_E. Then the overall energy balance, $\overline{Q}_{in} = \overline{Q}_E\left(T_E\right)$, must be applied to determine T_E.

8.5 Results of TPV System Model for Hypothetical System

Consider a hypothetical TPV system with the following components.

Emitter-	gray body emitter with $\varepsilon_E = 0.6$, $\rho_E = 1 - \varepsilon_E = 0.4$
Reflector-	constant reflectance, $\rho_b = 0.7$, $\varepsilon_b = 1 - \rho_b = 0.3$
PV arrays-	bandgap energy, $E_g = 0.6$eV ($\lambda_g = 2070$nm), constant quantum efficiency, $\eta_Q = 0.9$, dark saturation current density at 300K, $J_s = 8 \times 10^{-7}$ A/cm^2, ideality factor, $A_o = 1$, series resistance, $R_s = 0.06\Omega$, shunt resistance, $R_{sh} = 2000\Omega$, percent active area = 0.9
Filter-	back surface reflector (BSR), $\rho_C = 0.1$ for $0 \le \lambda \le \lambda_g$, $\rho_C = 0.9$ for $\lambda_g < \lambda < \infty$

InGaAs is a possible material for making a 0.6eV bandgap energy PV array with characteristics like those presented above.

Assume each of the three areas, A_{C1}, A_{C2}, and A_{C3} are covered by PV arrays. Referring to Figure 8.1, the dimensions of the square optical cavity are the following: $w_{C1} = 6$cm, $w_{C2} = 9$cm, $w_{C3} = 10$cm, $h = 0.2$cm, and $d_C = 0.05$cm. Each PV array is assumed to consist of 25 junctions. Area A_{C1} is covered with four arrays, area A_{C2} is covered with five arrays, and A_{C3} is covered with two arrays. Thus, the area of each array on A_{C1} is $\frac{A_{C1}}{4}$ and the area of each junction is $\frac{A_{C1}}{(4\times 25)}$. Similarly, $\frac{A_{C2}}{5}$ is the area of each array and $\frac{A_{C2}}{(5\times 25)}$ is the area of each junction on A_{C2}, and $\frac{A_{C3}}{2}$ is the area of each array and $\frac{A_{C3}}{(2\times 25)}$ is the area of each junction on A_{C3}.

With this input data, the Mathematica program in Appendix F produces the results shown in Figure 8.2. Shown are the radiation fluxes incident on and leaving the various

surfaces plus the electrical power generated by each of the PV arrays. The emitter and reflector temperatures are $T_E = T_b = 1232K$, the cavity efficiency is $\eta_c = 0.57$ while the PV efficiency of each of the PV arrays is $\eta_{PV} = 0.31$. As a result, the TPV efficiency is $\eta_{TPV} = \eta_c\eta_{PV} = 0.18$ and the electrical power out is $P_{EL} = 44W$.

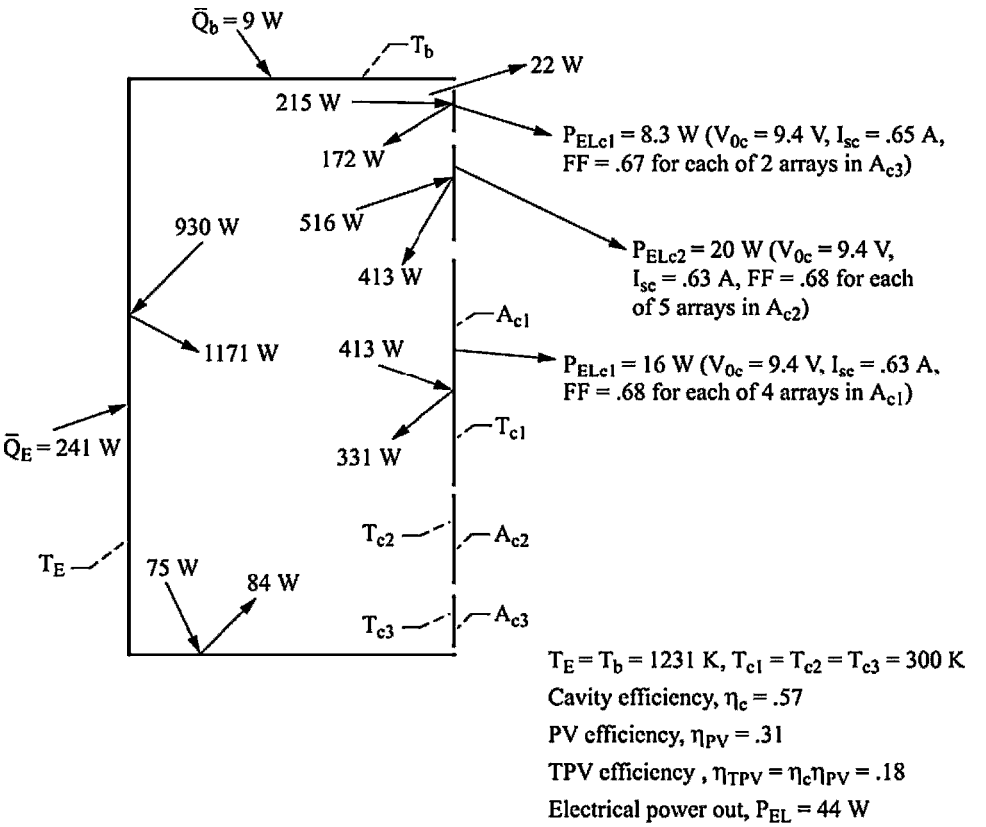

Figure 8.2.—Performance of planar, square geometry TPV system with the following properties; gray body emitter with emittance, $\varepsilon_E = .6$ ($\rho_E = 1 - \varepsilon_E = .4$), constant reflectance reflector, $\rho_b = .7$ ($\varepsilon_b = 1 - \rho_b = .3$), $E_g = .6e$ V ($\lambda_g = 2070$ mm) PV arrays with constant quantum efficiency, $\eta_Q = .9$, dark saturation current density at 300 K, $J_s = 8{\times}10^{-7}$ A/cm^2 ideality factor, $A_0 = 1.0$, series resistance, $R_s = .06\ \Omega$, shunt resistance, $R_{sh} = 2000\ \Omega$, percent active area = .9 and a back surface reflector (BSR) with reflectance, $\rho_c = .1$ for $0 \le \lambda \le \lambda_g$ and $\rho_c = .9$ for $\lambda_g < \lambda < \infty$.

Note that 22W of radiation leak out the 0.05cm gap between the reflector and the PV array. This is a significant fraction of the total 250W thermal energy input. Also

notice the large radiation fluxes that are circulating within the optical cavity. The emitter is emitting 1171W and receiving 930W. Most of the 1171W is incident on the PV arrays. Thus, if a filter with even a small absorptance were present, the absorptance loss would be significant.

8.5.1 Importance of Radiation Leakage

The leakage of radiation from the optical cavity through the 0.05cm gap between the PV arrays and the reflector can be prevented by connecting the reflector to the PV arrays. Obviously, this will result in thermal conduction from the hot reflector to the cold PV arrays. However, this conduction loss can be minimized by using a very thin material to connect the reflector and the PV arrays. Consider an optical cavity with no gaps between the reflector and the emitter, and the emitter and the reflector and the PV arrays. Thus, the emitter width, $w_E = w_{C3} = 10$cm in Figure 8.1. Using the same properties as used for Figure 8.2, the program in Appendix F was used to calculate the performance. With the gap eliminated, the temperature increases from $T_E = T_b = 1231$K to $T_E = T_b = 1251$K and the cavity efficiency increases from $\eta_c = 0.57$ to $\eta_c = 0.64$. While the PV efficiency remains the same, the TPV efficiency increases from $\eta_{TPV} = 0.18$ to $\eta_{TPV} = 0.20$, and the electrical power output increases from $P_{EL} = 44$W to $P_{EL} = 49$W.

Thus, eliminating the gap results in a significant increase in the cavity efficiency and TPV efficiency. Remember, however, the heat conduction loss between the reflector and PV arrays has been neglected. Inclusion of the conduction loss will reduce the gain in efficiency. However, as stated earlier, the conduction loss can be minimized by using a very thin material to connect the reflector and PV arrays.

8.5.2 Importance of Filter Absorptance

As already mentioned, the large value of the radiation flux incident on the filter-PV array means that a significant absorptance loss will occur even for small values of the filter spectral absorptance. Consider the interference-plasma filter presented in Chapter 4 (Figure 4.22). That filter has very low absorptance (≈ 0.01) at all wavelengths except in the band-pass region around $\lambda = 1500$nm where it reaches a maximum of 0.15. Using the optical properties of this filter and the emitter and PV array properties used for Figure 8.2, the system performance has been calculated using the Mathematica program. These results are shown in Figure 8.3.

As a result of the filter absorptance, 70W of power is lost from the system. The large reflectance (> 0.96) for $\lambda > 2000$nm results in bettrer cavity efficiency, $\eta_c = 0.63$, compared to $\eta_c = 0.57$ for the BSR case of Figure 8.2. However, a lower PV efficiency, $\eta_{PV} = 0.27$, compared to $\eta_{PV} = 0.31$ for Figure 8.2, results in a lower TPV efficiency, $\eta_{TPV} = 0.17$, compared to $\eta_{TPV} = 0.18$ for Figure 8.2. The PV efficiency is lower even

though the temperature is considerably higher, $T_E = T_b = 1505K$, compared to $T_E = T_b = 1231K$. The higher temperature and cavity efficiency means there is more convertible radiation incident on the PV arrays. However, for the case in Figure 8.3 most of the 70W absorbed by the filter occurs in the range $1200 \leq \lambda \leq 2000nm$ where the PV spectral response is highest. As a result, the short circuit current is lower than for the case in Figure 8.2 and as a result the PV efficiency is lower.

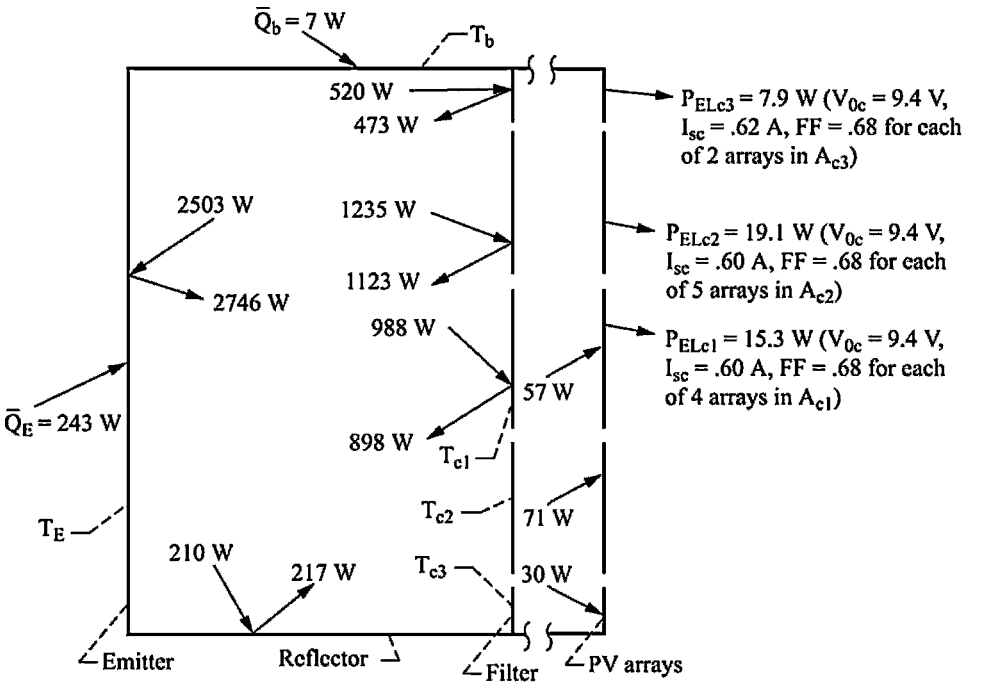

$T_E = T_b = 1505$ K, $T_{c1} = T_{c2} = T_{c3} = 300$ K
Cavity efficiency, $\eta_c = .63$
PV efficiency, $\eta_{PV} = .27$
TPV efficiency , $\eta_{TPV} = \eta_c \eta_{PV} = .17$
Electrical power out, $P_{EL} = 42$ W
Power absorbed by filter = 70 W

Figure 8.3.—Performance of planar, square geometry TPV system with the same properties as used in Figure 8.2 except the back surface reflector (BSR) has been replaced by the interference-plasma filter with the optical properties shown in Figure 4.22. Note that the incident PV array radiation fluxes shown are the useful fluxes, not the total fluxes.

If a front surface filter is used for spectral control in a TPV system, it must have negligible absorptance, especially in the wavelength range where the PV arrays have the largest spectral response. If a filter can be fabricated using only dielectric (non-conducting) materials, then a non-absorbing filter is possible.

8.6 TPV System with Selective Emitter and Back Surface Reflector (BSR)

Combining a selective emitter with a back surface reflector (BSR) on the PV arrays is a method of spectral control that makes possible large cavity efficiency. A rare earth selective emitter provides large emittance for the range of wavelengths that are convertible by the PV arrays. Also, in the range $\lambda_g < \lambda < 5\mu m$, where $\lambda_g = \frac{hc_o}{E_g}$ is the wavelength corresponding to the PV bandgap energy, the emittance is small. For $\lambda > 5\mu m$ the emittance becomes large again. However, a BSR has large reflectance for $\lambda > 5\mu m$. As a result, the majority of these photons are not lost but are reflected back to the emitter where they are absorbed.

Consider the planar geometry system of Figure 8.1 that uses an erbium aluminum garnet, $Er_3Al_5O_{12}$, emitter with the optical properties given in Figure 3.6. Assume the temperature gradient across the emitter and scattering can be neglected. As a result, the spectral emittance for the case where the substrate is deposited on the emitter is the following (see problem 3.7),

$$\varepsilon_E(\lambda) = \frac{\left(1-\bar{R}_{fo}\right)\left[1-4\bar{R}_{fs}E_3^2(\kappa_d)\right]}{1-4\bar{R}_{fs}E_3(\kappa_d)\left[\bar{R}_{fo}E_3(\kappa_d)+\mu_M^2\left(1-\bar{R}_{fo}\right)E_3\left(\frac{\kappa_d}{\mu_M}\right)\right]} \tag{8.45}$$

where $\kappa_d = K(\lambda)d$ is the optical depth, K is the extinction coefficient, and d is the emitter thickness. Also $\bar{R}_{fo}$ is the normal reflectivity at the emitter-vacuum interference and $\bar{R}_{fs}$ is the normal reflectivity at the emitter-substrate interface.

$$\mu_M^2 = 1-\left(\frac{1}{n_f}\right)^2 \tag{8.46}$$

$$\bar{R}_{fo} = \left(\frac{n_f-1}{n_f+1}\right)^2 \tag{8.47}$$

$$\bar{R}_{fs} = \frac{\left(n_{sR} - n_f\right)^2 + n_{sI}^2}{\left(n_{sR} + n_f\right)^2 + n_{sI}^2} \tag{8.48}$$

Here n_f is the index of refraction of $Er_3Al_5O_{12}$, and n_{sR} is the real part of the substrate index of refraction, and n_{sI} is the imaginary part of the substrate index of refraction. For this example assume, $\bar{R}_{fs} = 0.8$, which is representative of a low spectral emittance material such as platinum on $Er_3Al_5O_{12}$. Using the optical properties of $Er_3Al_5O_{12}$ given in Figure 3.6 and an emitter thickness, d = 0.01cm, in equation (8.45) yields the spectral emittance shown in Figure 8.4.

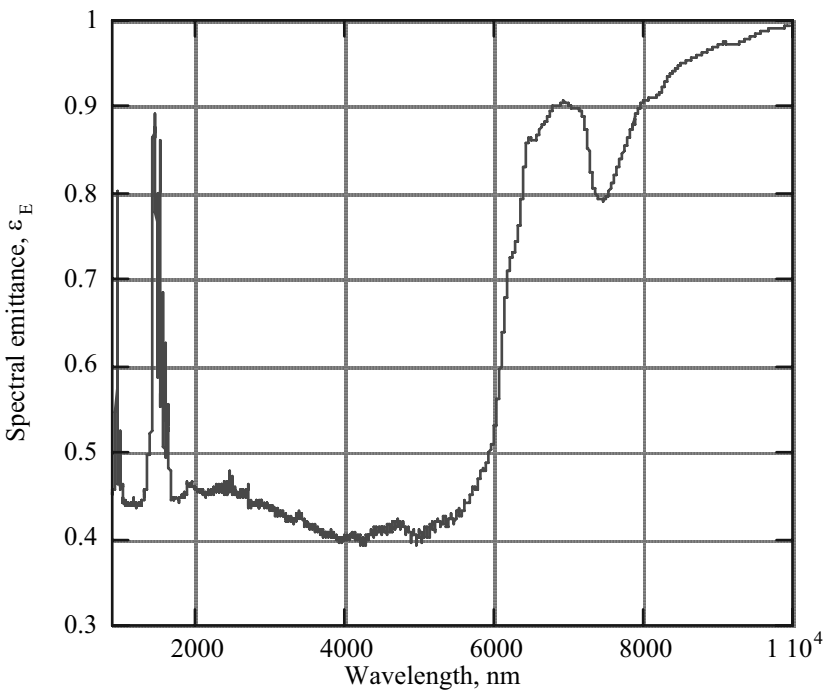

Figure 8.4 -Spectral emittance of erbium aluminum garnet, $Er_3Al_5O_{12}$, of thickness d=.01cm with deposited substrate using optical properties shown in Figure 3.6 and neglecting temperature gradient across emitter. Reflectivity at substrate-garnet interface, R_{fs}=.8.

The spectral emittance shown in Figure 8.4 and the same optical cavity conditions that were used in Figure 8.2 produce the results shown in Figure 8.5. These results have been obtained using the Mathematica program described in Appendix F. In order to include the large changes in $Er_3Al_5O_{12}$ emittance with wavelength, the step size was set at $\Delta\lambda$ = deltalyS = 1nm. With a gray body emitter of emittance, $\varepsilon_E = 0.6$, and no gap between the reflector and PV arrays the efficiencies were $\eta_c = 0.64$, $\eta_{PV} = 0.31$, and $\eta_{TPV} = 0.20$ at a temperature, $T_E = T_b = 1251K$. These results are nearly the same as those for the $Er_3Al_5O_{12}$ selective emitter. Thus, using the selective emitter results in no improvement in performance. The most significant improvement occurs when the gap between the reflector and PV arrays is eliminated. In that case for the gray body emitter, η_c increases from 0.57 to 0.64 and η_{TPV} increases from 0.18 to 0.20.

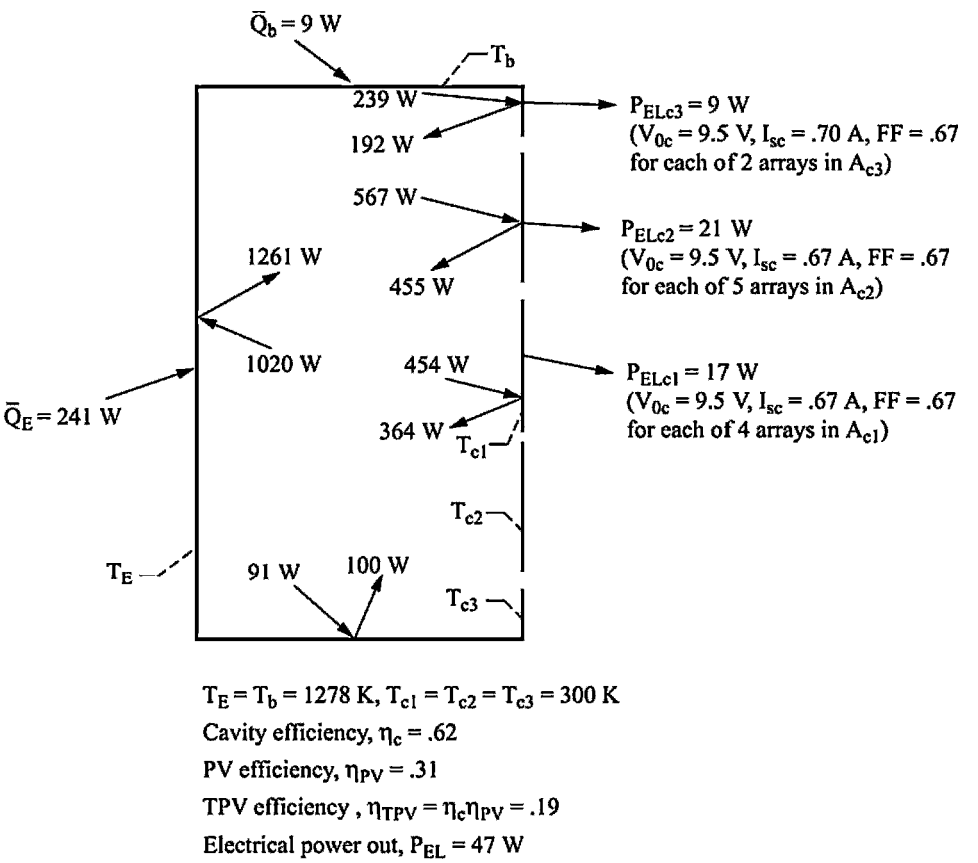

Figure 8.5.—Performance of planar, square geometry TPV system with the same properties as used in Figure 8.2 except that the gray body emitter has been replaced by an erbium aluminum garnet selective emitter with optical properties given in Figure 3.6.

8.6.1 Dependence of TPV Performance upon Input Power

Consider the system shown in Figure 8.1 with the gap between the reflector and the PV arrays removed so that $w_E = w_{C3} = 10$cm, $w_{C1} = 6$cm, $w_{C2} = 9$cm, and h = 0.2cm. Also, assume the same properties as used in Figure 8.2. Using the Mathematica program in Appendix F the efficiencies, temperature, and electrical power output have been calculated as a function of the thermal input power, $\bar{Q}_E + \bar{Q}_b$. These results are shown in Figure 8.6.

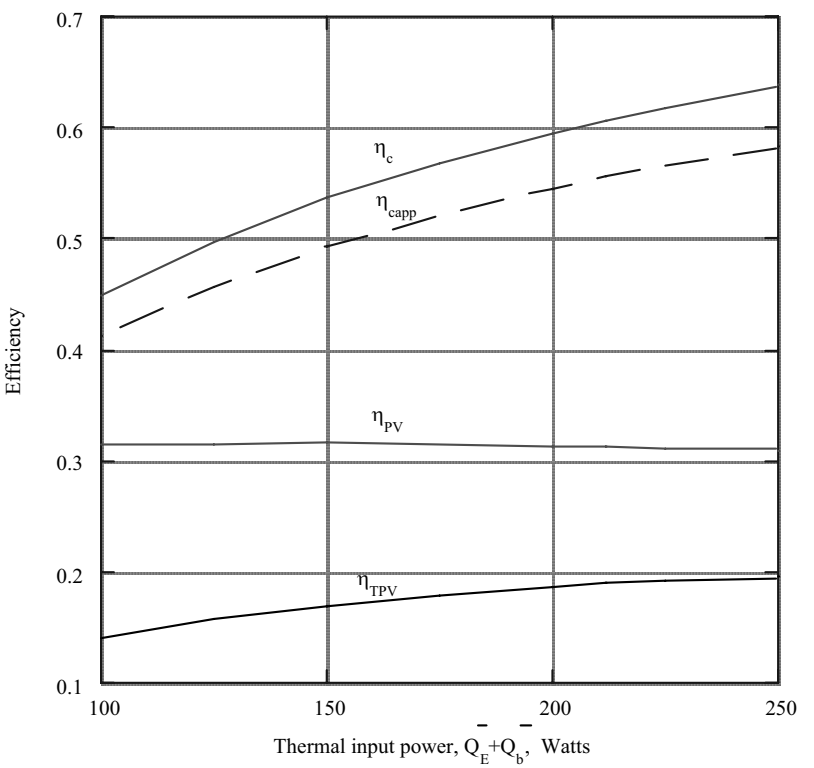

Figure 8.6a) - Effect of thermal input power on cavity efficiency, η_c, approximate cavity efficiency, η_{capp} (eq. 8.55), PV efficiency, η_{PV}, and TPV efficiency, η_{TPV}, of a planar, square geometry TPV system with the same conditions as in Figure 8.2 with the gap removed between the reflector and PV arrays so that $w_E = w_c = 10$ cm.

The photovoltaic efficiency, η_{PV}, remains nearly constant while the cavity efficiency, η_c, increases with increasing input power. As a result, the TPV efficiency, η_{TPV}, also increases. For constant optical properties for $0 \le \lambda \le \lambda_g = \frac{hc_o}{E_g}$, as is the case being considered, and if $R_s = 0$ and $R_{sh} \to \infty$ then η_{PV} is given by equation (5.252). The two integral terms in that equation are functions of $u_g = \frac{E_g}{kT_E}$. For the results in Figure 8.6, $u_g > 5.5$. Therefore, the integrals can be evaluated using the approximation, $u_g \gg 1$ (problem 8.4).

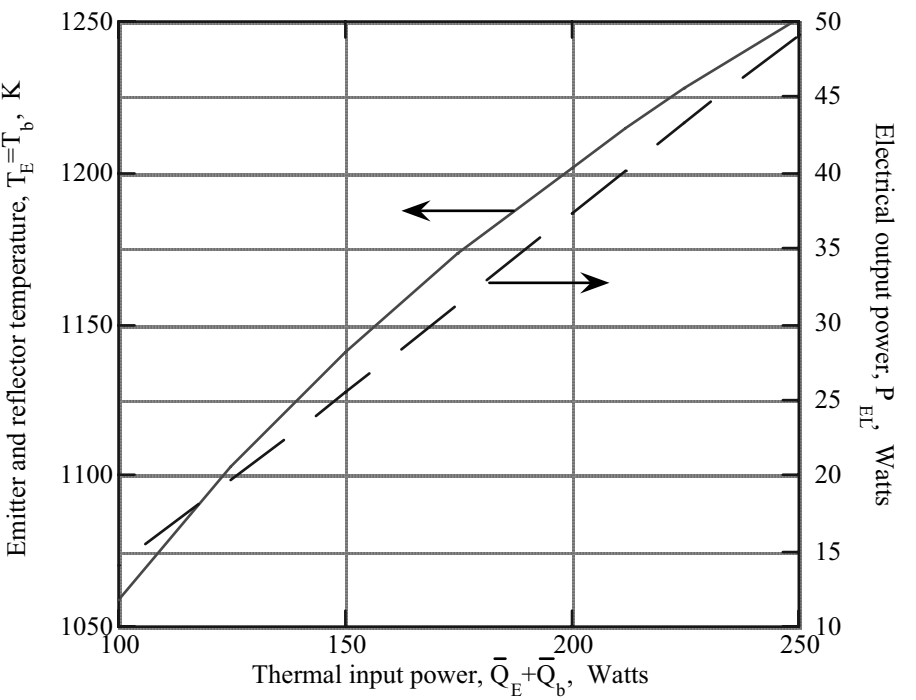

Figure 8.6b) - Effect of thermal input power on the emitter and reflector temperatures, $T_E=T_b$, and electrical power output, P_{EL} of a planar, square geometry TPV system with the same conditions as in Figure 8.2 with the gap removed between the reflector and PV arrays so that $w_E=w_c=10$ cm.

In that case, equation (5.252) becomes the following.

$$\eta_{PV} \approx \frac{A_{Ca}}{A_C}\left(1-R_C\right)\eta_Q FF\left(\frac{V_{oc}}{E_g}\right) \qquad \begin{array}{l}\varepsilon_E = \text{ constant}\\ \rho_C = \text{ constant}\\ \eta_Q = \text{ constant}\\ u_g \gg 1\end{array} \tag{8.49}$$

The open circuit voltage, $V_{oc} \sim \ln I_{sc}$ and the fill factor, FF, is a slowly varying function of V_{oc}. Thus, both V_{oc} and FF will be slowly varying functions of I_{sc}, which depends upon T_E [equation (5.251)]. Thus, η_{PV} is nearly independent of T_E and therefore, also of the input thermal energy, as Figure 8.6 indicates. Now use equation (8.49) to calculate η_{PV} for the PV arrays in area A_{C1} in Figure 8.2. In that case, $\frac{A_{C1a}}{A_{C1}} = \frac{0.9}{N_J}$, where $N_J = 25$ is the number of junctions in each of the four arrays that fill area A_{C1}. Therefore,

$$\eta_{PV} \approx \frac{0.9}{25}\left(1-0.1\right)0.9\left(0.68\right)\left(\frac{9.4}{0.6}\right) = 0.31 \tag{8.50a}$$

which agrees with the result in Figure 8.2.

For the results in Figure 8.6, the optical properties are constant in the regions $0 \le \lambda \le \lambda_g$ and $\lambda_g < \lambda < \infty$. As a result, a simplified result for the cavity efficiency, η_c, can be derived. Since the area of the reflector, A_b, is much less than the area of the emitter, A_E, the contribution to $\bar{Q}_C$ of the reflector can be neglected. As a result, since ε_E is a constant, the cavity efficiency is given approximately by the following expression,

$$\eta_c \approx \frac{1-\varepsilon_E}{\varepsilon_E} F_{EC} \frac{\int_o^{\lambda_g} q_{oE}\, d\lambda}{\int_o^{\infty}\left[e_b\left(\lambda, T_E\right) - q_{oE}\right] d\lambda} \tag{8.50b}$$

where $F_{EC} = F_{EC1} + F_{EC2} + F_{EC3}$. The flux leaving the emitter, q_{oE}, is given by equation (8.10), where the terms are functions of the optical properties and view-factors. For the results in Figure 8.6, the optical properties are constants except the PV cell reflectance, where $\rho_{Cg} = \rho_{C1} = \rho_{C2} = \rho_{C3} = 0.1$ for $0 \le \lambda \le \lambda_g$, and $\rho_{C\ell} = \rho_{C1} = \rho_{C2} = \rho_{C3} = 0.9$ for

$\lambda_g \le \lambda < \infty$. And since $T_{C1} = T_{C2} = T_{C3} \ll T_E$ the parameter, a, in equation (8.10) can be approximated as $a \approx \varepsilon_E\, e_b(\lambda, T_E)$. Also, $B_2 \approx 1$, $aB_2 \gg bE_2$, $E_1B_2 \gg E_2B_1$, and $E_1 = 1 - \rho_E\rho_{Cg}(F_{C1E}F_{EC1} + F_{C2E}F_{EC2} + F_{C3E}F_{EC3})$ for $0 \le \lambda \le \lambda_g$, and $E_1 = 1 - \rho_E\rho_{C\ell}(F_{C1E}F_{EC1} + F_{C2E}F_{EC2} + F_{C3E}F_{EC3})$ for $\lambda_g < \lambda < \infty$. When the emitter and PV arrays are very close together, as they are for the results in Figure 8.6, where h = 0.2cm, then the sum of the view-factor products in the expression for E_1 is nearly 1. Therefore, $E_1 \approx 1 - \rho_E\rho_{Cg}$ for $0 \le \lambda \le \lambda_g$, and $E_1 \approx 1$ for $\lambda_g < \lambda < \infty$, since $\rho_E\rho_{Cg} = 0.4(0.1) = 0.04 \ll 1$. Using these results in equation (8.10) to calculate q_{oE}, results in the following expression for q_{oE}.

$$q_{oE} \approx \varepsilon_E e_b\left(\lambda, T_E\right) \qquad 0 \le \lambda \le \lambda_g \tag{8.51}$$

$$q_{oE} \approx \frac{\varepsilon_E e_b\left(\lambda, T_E\right)}{1-\rho_E\rho_{C\ell}} = \frac{\varepsilon_E e_b\left(\lambda, T_E\right)}{1-\rho_{C\ell}\left(1-\varepsilon_E\right)} \qquad \lambda_g < \lambda < \infty \tag{8.52}$$

Using equations (8.51) and (8.52) in (8.50b) and $\varepsilon_E = 1 - \rho_E$ yields the following result.

$$\eta_c \approx F_{EC}\left[1 + \frac{\left(1-\rho_{C\ell}\right)}{\left[1-\rho_{C\ell}\left(1-\varepsilon_E\right)\right]} \frac{\int_{\lambda_g}^{\infty} e_b\left(\lambda, T_E\right) d\lambda}{\int_{o}^{\lambda_g} e_b\left(\lambda, T_E\right) d\lambda}\right]^{-1} \tag{8.53}$$

Now use the approximation $e^{u_g} \gg 1$ where $u_g = \dfrac{E_g}{kT_E}$. As a result the integral term becomes the following (problem 8.5).

$$H\left(u_g\right) \equiv \frac{\int_{\lambda_g}^{\infty} e_b\left(\lambda, T_E\right) d\lambda}{\int_{o}^{\lambda_g} e_b\left(\lambda, T_E\right) d\lambda} \approx \frac{\pi^4 e^{u_g}}{15\left(u_g^3 + 3u_g^2 + 6u_g + 6\right)} - 1 \qquad u_g = \frac{E_g}{kT_E} \tag{8.54}$$

Therefore,

$$\eta_c \approx \frac{F_{EC}}{1+\dfrac{1-\rho_{C\ell}}{1-\rho_{C\ell}\left(1-\varepsilon_E\right)}H\left(u_g\right)} \qquad \begin{array}{l}\varepsilon_E = \text{ constant} \\ \rho_{C\ell} = \text{ constant for } \lambda_g < \lambda < \infty \\ e^{u_g} \gg 1\end{array} \qquad (8.55)$$

For the conditions in Figure 8.6, $F_{EC} \approx 1$. Using equation (8.55) with $F_{EC} = 1$ yields the result for η_{capp} shown in Figure 8.6. The shape of the η_{capp} curve follows closely the shape of the actual η_c curve but underestimates the value of η_c. Thus, equation (8.55) is a conservative approximation for η_c.

8.7 Importance of PV Array Temperature on TPV Performance

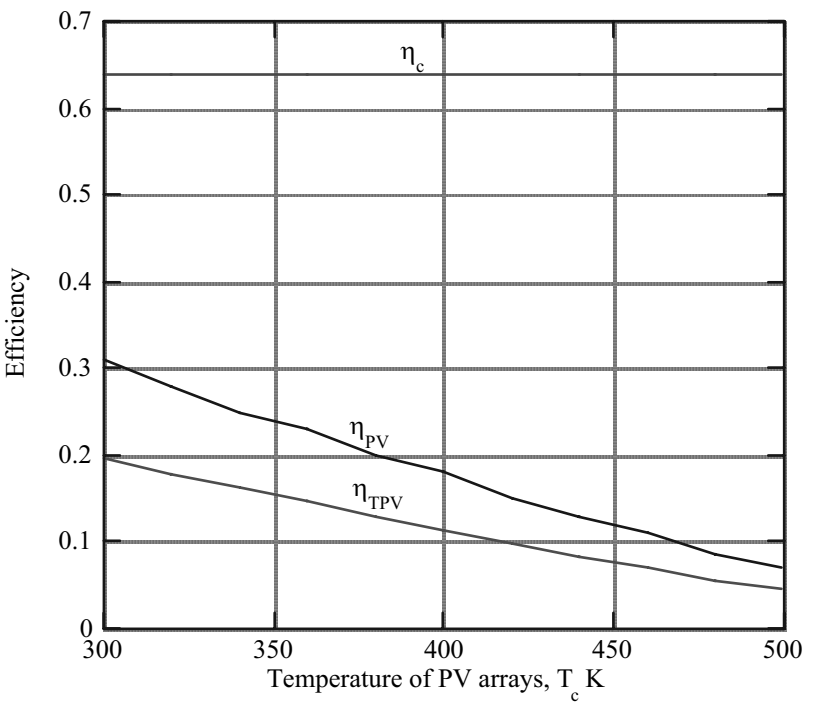

Figure 8.7 Effect of PV array temperature on efficiencies for the same conditions as in Figure 8.2 with the gap removed between the reflector and PV arrays so that $w_E = w_{c1} = 10.$ cm.

The dark saturation current increases rapidly with increasing PV array temperature [see equation (5.132)]. As a result the PV efficiency will decrease with increasing PV array temperature.

Figure 8.7 shows the effect of PV array temperature on η_c, η_{PV}, and η_{TPV} for the same conditions as in Figure 8.2 with the gap removed between the reflector and PV arrays. At $T_{C1} = T_{C2} = T_{C3} = 300K$ the dark saturation current density was $J_s = 8 \times 10^{-7}$ A/cm^2. At other temperatures, J_s was calculated using equation (5.132).

The cavity efficiency experiences a very small increase as the PV array temperature increases. This results from useful above bandgap energy emitted by the PV arrays that is added to the optical cavity radiation. However, the PV efficiency shows more than a factor of four decrease in going from $\eta_{PV} \approx 0.3$ at $T_C = 300K$ to $\eta_{PV} \approx 0.07$ at $T_C = 500K$. As a result the TPV efficiency also shows a similar decrease.

In a space application PV array temperature is a critical parameter. Since the waste heat must be rejected by radiation, the size of the waste heat radiator is proportional to T_C^4. Therefore, to minimize the size of the waste heat radiator T_C should be large. However, T_C means low efficiency, which in turn results in increased mass of the thermal energy source. Thus, there will be some optimum efficiency and PV array temperature that will yield the lowest mass system (problem 8.6).

For terrestrial applications the waste heat can be rejected by thermal conduction and convection. As a result, the waste heat radiator size is not as strongly dependent on T_C as for a space application.

8.8 Review of Radiation Transfer Method

As stated at the beginning of the chapter, the radiation transfer method assumes isotropic radiation and uniform fluxes incident and leaving a surface. The isotropic assumption is necessary in order to remove the intensity, i, from the double integral that determines the radiation flux leaving a surface [equation (6.4)]. This results in the double integral becoming merely a geometrical factor, the view-factor. Without the isotropic assumption, the method would be very cumbersome since not only would the double integral depend upon the intensity, but the radiation transfer equation [equation (1.139)], which determines the intensity, would depend upon direction, θ, as well as distance, s. For a TPV system with a non-isotropic emitting emitter, the radiation transfer method is not appropriate.

Although the radiation transfer method assumes uniform fluxes incident and leaving a surface, non-uniform fluxes over a surface area can be included by splitting the area into several parts. Each part will have different incident and leaving fluxes. This was done in the earlier examples by splitting the filter-PV area into three parts. Each surface area that is included results in a linear algebraic equation for the leaving flux, q_o, [equation (8.4)]. Thus, the number of algebraic equations to be solved will

equal the number of surface areas. This set of equations will be a function of the reflectances and emittances of each of the surfaces, which are in turn functions of the wavelength. Therefore, the radiation transfer method easily accounts for any rapid changes with wavelength, such as those in the spectral emittance of a selective emitter or the reflectance of an interference filter. Whereas a method that split the spectrum into several wavelengths regions with constant optical properties in each region cannot account for rapid changes.

8.9 Summary

The objective of this chapter has been to apply the radiation transfer method to calculate the performance of a TPV system. This method assumes that the radiation incident and leaving the various surfaces in the optical cavity is isotropic and uniform over the various surfaces. The method is applied to a hypothetical planar, square geometry, optical cavity. Significant results from that example are the following.

1) Leakage of radiation from the optical cavity, even from very small openings, is a significant loss.
2) Large radiation power fluxes circulate about the optical cavity. As a result, if a front surface filter is used for spectral control, its absorptance must be negligible in order to avoid a large absorptance loss.
3) To obtain high efficiency, the method for spectral control may be less important than avoiding radiation leakage from the optical cavity.
4) In a system with constant properties for $0 \le \lambda \le \lambda_g$, the PV efficiency is nearly independent of the emitter temperature and thus the input thermal power. Whereas the cavity efficiency increases with emitter temperature and thermal input power resulting in a similar increase in the TPV efficiency.
5) Since PV efficiency is a sensitive function of the PV array temperature, the PV efficiency decreases rapidly with increasing PV array temperature. The cavity efficiency is nearly independent of the PV array temperature. As a result, TPV efficiency decreases with increasing PV array temperature.

Problems

8.1 Obtain the expression given by equation (8.32) for the view-factor, F_{bb}, for the optical cavity shown in Figure 8.1. Hint: Make use of symmetry.

8.2 Using view-factor algebra and the view-factor reciprocity relation [equation (6.7)] show that the view-factors F_{gE} and F_{gb} for Figure 8.1 are given by equations (8.25) and (8.26).

8.3 Leakage of radiation from the optical cavity through gaps that may exist between the emitter and the reflector and between the PV arrays and the reflector is a significant loss in a TPV system. One way of estimating this loss is as follows. With small gaps the optical cavity behaves much like a blackbody. Thus, the upper limit on the radiation that escapes through a small gap can be approximated as follows,

$$\bar{Q}_{gap} \approx A_{gap}\sigma_{sb}T_E^4$$

where A_{gap} is the gap area, σ_{sb} is the Stefan-Boltzmann constant, and T_E is the emitter temperature. Using the above expression estimate the radiation loss through the gap between the PV arrays and the reflector for the system in Figure 8.2.

8.4 Evaluate the integral quotient term,

$$\frac{\int_{u_g}^{\infty}\frac{u^2}{e^u-1}du}{\int_{u_g}^{\infty}\frac{u^3}{e^u-1}du}$$

in equation (5.252) for $u_g \gg 1$.

8.5 Evaluate the integral quotient term,

$$H(\lambda)=\frac{\int_{o}^{\lambda_g} e_b(\lambda,T_E)\,d\lambda}{\int_{o}^{\infty} e_b(\lambda,T_E)\,d\lambda}$$

where $e_b(\lambda,T_E)$ is the blackbody emissive power [equation (1.127)], using the approximation $e^{u_g} \gg 1$. Where $u_g = \frac{hc_o}{\lambda_g T_E}$.

8.6 The mass of a TPV system for a space application is made up of three parts.

$$M_s = M_{th} + M_{TPV} + M_{RAD}$$

Where M_s is the total system mass, M_{th} is the mass of the thermal energy source, M_{TPV} is the mass of the TPV system, and M_{RAD} is the mass of the waste heat radiator. Assume each of the component masses are given by the following functions,

$$M_{th} = m_{th}\bar{Q}_{in} \qquad m_{th} - \frac{kg}{W}$$

$$M_{TPV} = m_{TPV}P_{EL} \qquad m_{TPV} - \frac{kg}{W}$$

$$M_{RAD} = m_{RAD}A_{RAD} \qquad m_{RAD} - \frac{kg}{m^2}$$

where m_{th}, m_{TPV}, and m_{RAD} are constants, $\bar{Q}_{in}$ is the thermal input power, P_{EL} is electrical output power, and A_{RAD} is the radiator area. Assume the power radiated by the waste heat radiator is the following,

$$P_{RAD} = \sigma_{sb}\varepsilon_{RAD}T_C^4A_{RAD}$$

where σ_{sb} is the Stefan-Boltzmann constant, ε_{RAD} is the total emittance of the radiator, and T_C is the PV array temperature. Derive an equation for the system specific mass, $m_s = \frac{M_s}{P_{EL}}$ in terms of the efficiency, η_{TPV}, T_C, m_{th}, m_{TPV}, m_{RAD}, and $\sigma_{sb}\varepsilon_{RAD}$. Using that result, obtain the following expression for the PV array temperature, T_{CMIN}, that yields the minimum value of M_s.

$$\alpha_m\bar{T}_{CMIN}^5 + \bar{T}_{CMIN} + \gamma_m = 0$$

Where $\bar{T}_{CMIN} = \frac{T_{CMIN}}{T_o}$, $\alpha_m = \sigma_{sb}\varepsilon_{RAD}\left(\frac{m_{th}}{m_{RAD}}\right)T_o^4$, and $\gamma_m = 4\left(1-\eta_{TPV}\right)\frac{\eta_{TPV}}{\frac{d\eta_{TPV}}{d\bar{T}_C}}$,

and T_o is the value of T_C when $\eta_{TPV} = 0$, so that $\bar{T}_C \le 1$. Now assume η_{TPV} is a linear function of T_C.

$$\eta_{TPV} = a\left(T_o - T_C\right) = aT_o\left(1-\bar{T}_C\right)$$

Obtain the equation for $\bar{T}_{CMIN}$ in this case and solve it for $\frac{\alpha_m}{aT_o} \ll 1$ and $\frac{\alpha_m}{aT_o} \gg 1$. $\frac{\alpha_m}{aT_o} \ll 1$ implies that the radiator specific mass, m_{RAD} is much larger than the thermal source specific mass, m_{th}. What is significant about the result for T_{CMIN} when $\frac{\alpha_m}{aT_o} \gg 1$?

This page intentionally left blank

This page intentionally left blank

Appendix A – Exponential Integrals

Given below are several useful exponential integral relations. A complete list of exponential integral relations is given in reference [1].

For real positive x, the nth exponential integral is defined as follows for n, a real positive integer.

$$E_n(x) = \int_o^1 u^{n-2} \exp\left(-\frac{x}{u}\right) du \tag{A-1}$$

or

$$E_n(x) = \int_1^\infty \frac{1}{t^n} \exp(-xt)\, dt \tag{A-2}$$

Differentiating equation (A-1) yields the following.

$$\frac{d}{dx} E_n(x) = -E_{n-1}(x) \qquad n \geq 2 \tag{A-3}$$

$$\frac{d}{dx} E_1(x) = -\frac{e^{-x}}{x} \tag{A-4}$$

Integrating equation (A-1) yields,

$$\int E_n(x)\, dx = -E_{n+1}(x) \tag{A-5}$$

Integration of equation (A-1) by parts yields the following recurrence relation.

$$nE_{n+1}(x) = e^{-x} - xE_n(x) = e^{-x} + x\frac{d}{dx} E_{n+1}(x) \tag{A-6}$$

Using equation (A-6) $E_n(x)$ can be determined in terms of $E_1(x)$.

For x = 0,

$$E_1(0) = +\infty \tag{A-7}$$

$$E_n(0) = \frac{1}{n-1} \qquad n \geq 2 \tag{A-8}$$

For large values of x, the following approximation applies.

$$E_n(x) \approx \frac{e^{-x}}{x} \tag{A-9}$$

The general series expansion for $E_n(x)$ is given in reference [1].

$$E_n(x) = \frac{(-x)^{n-1}}{(n-1)!}\left[-\ln x + \psi(n)\right] - \sum_{\substack{m=0 \\ m \neq n-1}}^{\infty} \frac{(-x)^m}{(m-n+1)m!} \tag{A-10}$$

where,

$$\psi(1) = -\gamma \tag{A-11}$$

$$\psi(n) = -\gamma + \sum_{m=1}^{n-1} \frac{1}{m} \tag{A-12}$$

and $\gamma = 0.577216$ is the Euler constant.

The following approximations [2] have been used for $E_2(x)$ and $E_3(x)$.

$$E_2(x) \approx 0.9e^{-1.8x} \tag{A-13}$$

$$E_2(x) \approx \frac{3}{4} e^{-\frac{3}{2}x} \tag{A-14}$$

$$E_3(x) \approx \frac{1}{2} e^{-\frac{3}{2}x} \tag{A-15}$$

$$E_3(x) \approx \frac{1}{2} e^{-1.8x} \tag{A-16}$$

References

[1] M. Abramowitz, and I. Stegun, Handbook of Mathematical Functions with Formulas, Graphs, and Mathermatical Tables, Appl. Math. Ser. 55, National Bureau of Standards, 1964.

[2] R. Siegel, and J. R. Howell, Thermal Radiation Heat Transfer, second edition, Hemisphere Publishing, 1981, pg 842.

This page intentionally left blank

Appendix B – Coupled Energy and Radiation Transfer Equations

When radiation energy transfer is comparable to conduction energy transfer for a solid material, the energy equation and radiation transfer equations must be solved simultaneously. This appendix presents the numerical procedure for obtaining this solution under the following assumptions.

1) One dimensional planar geometry (x only spatial variable)
2) Isotropic scattering of radiation (source function independent of θ)
3) Extinction coefficient, $K(\lambda)$, independent of x
4) Index of refraction, n_f, independent of x
5) Snell's law satisfied t boundaries, x = 0 and x = d
6) Reflectivity at boundaries approximated by reflectivity for normal incidence, $\overline{R}$
7) No external source of radiation
8) Temperature at x = 0 same as substrate temperature, T_s

Figure 3.8 shows the two planar geometries to be considered with no external radiation ($i_r = 0$). The equations that must be solved simultaneously to determine T(x) and $\overline{q}(x,\lambda)$ are the one dimensional energy equation [equation (1.160)] and the source function equation [equation (3.74) or equation (3.77)].

$$-k_{th}\frac{dT}{dx}+\overline{q}(x)=\text{constant}=-k_{th}\left.\frac{dT}{dx}\right|_{x=0}+\overline{q}(0)=-k_{th}\left.\frac{dT}{dx}\right|_{x=d}+\overline{q}(d) \qquad \text{(B-1)}$$

$$S(\kappa,\lambda) = n_f^2(1-\Omega)\frac{e_b(\lambda,T)}{\pi} +$$

$$\frac{\Omega}{2D}\left\{G(\kappa)\left[\overline{\tau}_{fs}\varepsilon_{son}n_o^2\frac{e_b(\lambda,T_s)}{\pi} + 2\int_o^{\kappa_d} S(\kappa^*) + \left(\overline{\rho}_{fs}E_2(\kappa^*)\mu_M(1-\overline{\rho}_{fs})E_2\left(\frac{\kappa^*}{u_M}\right)\right)d\kappa^*\right]\right.$$

$$\left. +2H(\kappa)\int_o^{\kappa_d} S(\kappa^*)\left[\overline{R}_{fo}E_2(\kappa_d-\kappa^*) + \mu_M(1-\overline{R}_{fo})E_2\left(\frac{\kappa_d-\kappa^*}{\mu_M}\right)\right]d\kappa^*\right\} \qquad \text{(B-2)}$$

$$+\frac{\Omega}{2}\int_o^{\kappa_d} S(\kappa^*)E_1(|\kappa^*-\kappa|)d\kappa^* \qquad \text{with gap}$$

$$S(\kappa) = n_f^2(1-\Omega)\frac{e_b(\lambda,T)}{\pi}$$

$$+\frac{\Omega}{2D'}\left\{G(\kappa)\left[n_f^2\varepsilon_{fsn}\frac{e_b(\lambda,T_s)}{\pi} + 2\overline{R}_{fs}\int_o^{\kappa_d} S(\kappa^*)E_2(\kappa^*)d\kappa^*\right]\right.$$

$$\left. +2H'(\kappa)\int_o^{\kappa_d} S(\kappa^*)\left[\overline{R}_{fo}E_2(\kappa_d-\kappa^*) + \mu_M(1-\overline{R}_{fo})E_2\left(\frac{\kappa_d-\kappa^*}{\mu_M}\right)d\kappa^*\right]\right\} \qquad \text{(B-3)}$$

$$+\frac{\Omega}{2}\int_o^{\kappa_d} S(\kappa^*)E_1(|\kappa^*-\kappa|)d\kappa^* \qquad \text{no gap}$$

From assumption 3) the following expression applies for the optical depth.

$$\kappa(x,\lambda) = K(\lambda)x \qquad \text{(B-4)}$$

The total radiation flux, $\overline{q}(x)$, is the following,

$$\overline{q}(x) = \int_o^{\infty} q(Kx,\lambda)d\lambda = \int_o^{\infty} q(\kappa,\lambda)d\lambda \qquad \text{(B-5)}$$

where $q(\kappa,\lambda)$ is given by equation (3.63) for the case of a dielectric gap between the film and substrate, and equation (3.69) for no dielectric gap. The functions D, D', $G(\kappa)$, $H(\kappa)$, and $H'(\kappa)$ in equations (B-2) and (B-3) are given by equations (3.66), (3.71), (3.75), (3.76), and (3.78).

Equation (B-1) is a first order differential equation for T(x) while (B-2) or (B-3) are integral equations for S(κ). To obtain solutions for T(x) and S(κ), boundary conditions must be applied. The boundary conditions on S(κ) are already included in the G(κ), H(κ), and $H'(\kappa)$ terms appearing in equations (B-2) and (B-3). For T(x) there are two possible boundary conditions.

1) Temperature at x = 0 and x = d specified, $T(0) = T_s$ and $T(d) = T_f$.
2) Temperature at x = 0 specified, $T(0) = T_s$, and a vacuum at x = d so that $\left.\frac{dT}{dx}\right|_{x=d} = 0$.

The numerical procedure for solving for T(x) and S(κ,λ) for the two boundary conditions is outlined below.

1) For either boundary condition, T_s is given and a linear temperature variation, $T(x) = T_s - (T_s - T_f)\left(\frac{x}{d}\right)$, is assumed. For boundary condition 1), T_f is given and for boundary condition 2), the value for T_f is an initial guess.
2) Using the assumed temperature variation, either equation (B-2) or (B-3) is solved for $S_i(\kappa,\lambda)$, (subscript i denotes the i^{th} approximation) at each wavelength for a given extinction coefficient, K(λ), and scattering albedo, Ω(λ). The method of solution is described later in this appendix.
3) $S_i(\kappa,\lambda)$ is then used to calculate $q_i(\kappa,\lambda)$, given by either equation (3.63) or (3.69).
4) $\overline{q}_i(x)$ is calculated using equation (B-5).
5) Equation (B-1) is solved for $T_i(x)$ using $\overline{q}_i(x)$ from step 4). For boundary condition 1), the constant in equation (B-1) is now $\overline{q}(0) - k_{th}\left.\frac{dT}{dx}\right|_{x=0}$, where $\left.\frac{dT}{dx}\right|_{x=0}$ is computed for $T_i(x)$. For boundary condition 2), the constant in equation (B-1) is $\overline{q}_i(d)$. The integration of equation (B-1) can be performed using such methods as the trapezoidal rule, Simpson's rule, or Runge-Kutta.
6) Using the new $T_i(x)$, steps 2) through 5) are repeated. The process is continued until T(d) converges to T_f for boundary condition 1) or until $\overline{q}_{i+1}(d)$ converges to $\overline{q}_i(d)$ for boundary condition 2).

Once a solution for T(x) and S(κ,λ) is obtained, the emitter performance can be calculated. The spectral emittance, ε(λ) is given as follows.

$$\varepsilon(\lambda) = \frac{q(d,\lambda)}{n_o^2 e_b(\lambda, T_s)} \tag{B-6}$$

The useful radiated power, $\bar{q}_b$, is given by equation (3.170), and the total radiated power is given by equation (3.171).

The solution of equation (B-2) or (B-3) for $S(\kappa,\lambda)$ is obtained by an iterative process. If scattering is neglected ($\Omega = 0$), then $S(\kappa,\lambda) = n_f^2 \frac{e_b(\lambda, T)}{\pi}$. Therefore, this becomes the first approximation, $S_1(\kappa,\lambda)$, for the source function. The $S_1(\kappa,\lambda)$ solution is used to evaluate the integrals on the right hand side of equations (B-2) or (B-3 to obtain the second approximation, $S_2(\kappa,\lambda)$. This process is continued until $S(\kappa,\lambda)$ converges.

There is a singularity at $\kappa^* = \kappa$ in the last integral of equation (B-2) or (B-3), since $E_1(0) \rightarrow \infty$. However, it is an integrable singularity.

Application of the numerical procedure outlined above was applied to an EAG selective emitter with a Pt substrate in reference [1]. Results of that study show that the temperature varies nearly linearly across the emitter, as was assumed in section 3.8.2. The deviation from linearity is greatest at the highest temperatures. At the highest temperatures the parameter, γ [equation (3.95)], which is the ratio of radiation to the thermal conduction, becomes significant.

References

[1] B. S. Good, D. L. Chubb, and A. Pal, Proceedings of 4th NREL Conference on Thermophotovoltaic Generation of Electricity, AIP Conference Proceedings, 460, (1999), 214.

Appendix C – 2 × 2 Matrix Algebra

The product of two 2 × 2 matrices is the following,

$$\left[a_{ij}\right]\left[b_{ij}\right]=\begin{bmatrix}a_{11} & a_{12}\\ a_{21} & a_{22}\end{bmatrix}\begin{bmatrix}b_{11} & b_{12}\\ b_{21} & b_{22}\end{bmatrix}=\begin{bmatrix}\left(a_{11}b_{11}+a_{12}b_{21}\right) & \left(a_{11}b_{12}+a_{12}b_{22}\right)\\ \left(a_{21}b_{11}+a_{22}b_{21}\right) & \left(a_{21}b_{12}+a_{22}b_{22}\right)\end{bmatrix}=\left[\sum_{m=1}^{2}a_{im}b_{mj}\right] \tag{C-1}$$

with the product also a 2 × 2 matrix. Matrix multiplication is associative, i.e.,

$$\left\{\left[a_{ij}\right]\left[b_{ij}\right]\right\}\left[c_{ij}\right]=\left[a_{ij}\right]\left\{\left[b_{ij}\right]\left[c_{ij}\right]\right\} \tag{C-2}$$

but in general not communicative.

$$\left[a_{ij}\right]\left[b_{ij}\right]\neq\left[b_{ij}\right]\left[a_{ij}\right] \tag{C-3}$$

The inverse of a matrix $\left[a_{ij}\right]^{-1}$, is a matrix such that its product with the given matrix is the unit matrix.

$$\left[a_{ij}\right]\left[a_{ij}\right]^{-1}=\left[a_{ij}\right]^{-1}\left[a_{ij}\right]=\begin{bmatrix}1 & 0\\ 0 & 1\end{bmatrix} \tag{C-4}$$

The inverse of a 2 × 2 matrix is the following.

$$\left[a_{ij}\right]^{-1}=\begin{bmatrix}\frac{a_{22}}{\Delta} & -\frac{a_{12}}{\Delta}\\ -\frac{a_{21}}{\Delta} & \frac{a_{11}}{\Delta}\end{bmatrix} \tag{C-5}$$

Where Δ is the determinant of A_{ij}.

$$\Delta = \begin{vmatrix} a_{11} & a_{12} \\ a_{21} & a_{22} \end{vmatrix} = a_{11}a_{22} - a_{12}a_{21} \tag{C-6}$$

Appendix D – Mathematica Program for Multi-layer Interference Filter

The Mathematica (version 5.1) program, which is included on the CD-R disk, calculates the reflectance (rhop), transmittance (taup), and absroptance (alphop) of a multi-layer interference filter as a function of wavelength (ly) for a given angle of incidence (thetao). The total number of layers (num) are split into five groups (a, b, c, d, e). Input quantities are the design wavelengths of each group (lydesigna, lydesignb, lydesignc, lydesignd, lydesigne), the number of layers in each group (numa, numb, numc, numd, nume), the number of times each group is repeated (alpha, beta, gamma, epsilon, psi), the number of wavelength points (numpoints), the initial wavelength (lyo), the interval between wavelength points (deltaly), the index of refraction of the surrounding dielectric medium (n_o), the index of refraction of the dielectric substrate (nend), real (nr) and imaginary (ni) parts of indices of refraction of each layer, and the relative magnetic permeability (mu) of each layer. The values for nr, ni, and mu are given as a Table of values beginning with the layer next to the substrate (ni[[1]], nr[[1]], and mu[[1]]).

The logic statement, polar, is used to determine the polarization of the incident radiation. For polar = True, the polarization is p (electric field in the plane of incidence); if polar = False, the polarization is s (electric field perpendicular to the plane of incidence).

There are two options for the thicknesses of the layers in a group. One satisfies ¼ lydesign,

$$d = \frac{\text{lydesign}}{4.\ \text{nmag costhmag}} \tag{D-1}$$

and the other satisfies ½ lydesign,

$$d = \frac{\text{lydesign}}{2.\ \text{nmag costhmag}} \tag{D-2}$$

where $\text{nmag} = \sqrt{nr^2 + ni^2}$ and $\text{costhmag} = \sqrt{\left(\text{Re}[\theta]\right)^2 + \left(\text{Im}[\theta]\right)^2}$. The logic statement, design determines which d option is to be used. If design = True, then ¼ lydesign is used and if design = False, then ½ lydesign is used.

Also included is a program to calculate the filter efficiency [equation (4.4)], total transmittance [equation (4.5)], total reflectance [equation (4.6)], and total absorptance [equation (4.7)] as a function of emitter temperature, T_E. A constant emitter emittance is assumed for this calculation.

Appendix E – Quantum Mechanics

In Chapter 1 it is shown that the classical Maxwell's equations for electromagnetic radiation lead to a wave equation [equation (1.29)]. The solution [equation (1.10)] for the electric and magnetic fields that constitute electromagnetic radiation is a propagating plane wave. Electromagnetic radiation has both wave properties, such as interference, and particle properties, such as the momentum of a photon. Quantum mechanics extends the duality of the wave and particle description to all matter. It is the Schrödinger equation that describes the behavior of a particle or system of particles.

$$\left[-\frac{\hbar^2}{2m}\nabla^2 + V\right]\psi = j\hbar\frac{2\psi}{2t} \tag{E-1}$$

Where m is the particle mass, $\hbar = \frac{h}{2\pi}$ where h is the Plank constant (6.624×10^{-34} joule-sec), V is the potential energy of the particle, $\nabla^2 = \nabla\bullet\nabla = \frac{\partial^2}{\partial x^2} + \frac{\partial^2}{\partial y^2} + \frac{\partial^2}{\partial z^2}$, $j = \sqrt{-1}$, t is the time, and ψ is the wave function that describes the particle motion.

The solution to equation (E-1) is separable into spatial and time dependent parts if the potential energy is independent of time.

$$\psi(x,y,z,t) = u(x,y,z)v(t) \tag{E-2}$$

Substituting (E-2) in (E-1) yields

$$\frac{1}{u}\left[-\frac{\hbar^2}{2m}\nabla^2 + V(x,y,z)\right]u = \frac{j\hbar}{v}\frac{\partial v}{\partial t} \equiv E \tag{E-3}$$

Therefore,

$$v(t) = \exp\left(-\frac{J}{\hbar}Et\right) \tag{E-4}$$

where the constant E is the energy of the particle. The spatial part of (E-3) can thus be written as follows.

$$\mathrm{H}u(\mathrm{x},\mathrm{y},\mathrm{z}) = \mathrm{E}u(\mathrm{x},\mathrm{y},\mathrm{z}) \tag{E-5}$$

Equation (E-5) is a so-called *eigenvalue equation*, with the constant E being the eigenvalue, and H is the *Hamiltonian operator* defined as follows.

$$\mathrm{H} = -\frac{\hbar^2}{2\mathrm{m}}\nabla^2 + \mathrm{V}(\mathrm{x},\mathrm{y},\mathrm{z}) \tag{E-6}$$

It is equation (E-5) that must be solved to determine the wave function $\psi(\mathrm{x},\mathrm{y},\mathrm{z},\mathrm{t})$ that corresponds to the energy E.

Consider a free particle (V = 0) moving only in the x direction ($\nabla^2 = \frac{\mathrm{d}^2}{\mathrm{dx}^2}$). In that case (E-5) is the following.

$$-\frac{\hbar^2}{2\mathrm{m}}\frac{\mathrm{d}^2u}{\mathrm{dx}^2} = \mathrm{E}u \tag{E-7}$$

This is a second order linear differential equation with the following plane wave solution.

$$u(\mathrm{x}) = \mathrm{A}e^{\mathrm{jkx}} + \mathrm{B}e^{-\mathrm{jkx}} \tag{E-8}$$

Where A and B are constants. Substituting (E-8) in (E-7) yields the following.

$$\mathrm{k} = \sqrt{\frac{2\mathrm{mE}}{\hbar^2}} \tag{E-9}$$

Thus, combining equation (E-4) and (E-5), the wave function for a free particle moving only in the ±x direction is the following.

$$\begin{aligned}\psi(\mathrm{x},\mathrm{t}) &= \left[\mathrm{A}e^{\mathrm{jkx}} + \mathrm{B}e^{-\mathrm{jkx}}\right]e^{-\frac{\mathrm{jE}}{\hbar}\mathrm{t}} \\ \psi(\mathrm{x},\mathrm{t}) &= \mathrm{A}e^{\mathrm{jkx}} + \mathrm{B}e^{-\mathrm{j}\left(\mathrm{kx}+\frac{\mathrm{E}}{\hbar}\mathrm{t}\right)}\end{aligned} \tag{E-10}$$

This is like the plane wave solution that satisfies Maxwell's equation discussed in Chapter 1. The wave number, k, is related to the particle energy, E, by equation (E-9). It is also related to the particle momentum p = mv for a free particle as follows,

$$k = \frac{2\pi}{\lambda} = \frac{p}{\hbar} \tag{E-11}$$

where λ is the deBroglie wave length. For a particle moving in three dimensions, the wave function is the following,

$$\psi(x,y,z,t) = Ae^{j\left(\vec{k}\cdot\vec{x}-\frac{E}{\hbar}t\right)} + Be^{-j\left(\vec{k}\cdot\vec{x}-\frac{E}{\hbar}t\right)} \tag{E-12}$$

where

$$\vec{k} = \frac{\vec{p}}{\hbar} \tag{E-13}$$

For a many particle system, equation (E-1) is difficult to solve since the ∇^2 and potential energy V terms include the coordinates of all the particles. An excellent introduction to quantum mechanics is presented in reference [1]. Reference [2] is an excellent reference for the application of quantum mechanics to semiconductors.

An important quantity necessary to calculate the density of charge carriers in a material is the *density of states function*, D(E). It determines the number of energy states that are available to a charge carrier per unit of volume. In a conduction band of a conductor or a semiconductor, the electrons are essentially free. They are confined only by the boundaries of the material. In that case, the wave function for an electron moving in the x direction is given by equation (E-8), which can be written as follows.

$$u(x) = A'\cos k_x x + B'\sin k_x x \tag{E-14}$$

At the boundaries of the material, the wave function must vanish. If the x direction boundaries are at x = 0 and x = L, then equation (E-14) yields the following.

$$A' = 0 \tag{E-15a}$$

$$A'\cos k_x L + B'\sin k_x L = 0 \tag{E-15b}$$

Thus,

$$B' \sin k_x L = 0 \tag{E-16}$$

and disregarding the trivial solution ($B' = 0$) for (E-16) to be satisfied, the following must apply.

$$k_x = \frac{n_x \pi}{L} = \frac{p_x}{\hbar} \qquad n_x = 0, 1, 2, ... \tag{E-17}$$

Similarly, for the y and z motion

$$k_y = \frac{n_y \pi}{L} = \frac{p_y}{\hbar} \qquad n_y = 0, 1, 2, 3, ... \tag{E-18}$$

$$k_z = \frac{n_z \pi}{L} = \frac{p_y}{\hbar} \qquad n_z = 0, 1, 2, 3, ... \tag{E-19}$$

Thus, the momentum of the electron, $\vec{p} = \hbar \vec{k}$, is limited to integral multiples of $\frac{\pi}{L}$ in each direction.

Now determine the number of momentum or energy states per unit of volume. One unit of change in n_x, n_y, and n_z will result in an infinitesimal change in p_x, p_y, and p_z. Thus, from equations (E-17) through (E-19), each available momentum state occupies the volume

$$dp_x dp_y dp_z = \left(\frac{h}{2L} \right)^3 \tag{E-20}$$

in momentum space. Assuming $\vec{k}$ is isotropic, an infinitesimal volume in momentum space for positive values of momentum is $\frac{1}{8}\left(4\pi p^2 dp\right)$. The $\frac{1}{8}$ factor accounts for the fact that only the positive quadrant of momentum space is possible. Therefore, the number of available states in this volume is

$$2\left[\frac{4\pi p^2 dp}{8\left(\frac{h}{2L}\right)^3}\right] = \frac{8\pi L^3}{h^3} p^2 dp \qquad \text{(E-21)}$$

The factor of 2 occurs because 2 electrons, one with spin +½ and one with spin –½, are allowed. Thus, the density of states function is the following.

$$D(p)dp = \frac{8\pi L^3 p^2 dp}{h^3 L^3} = \frac{8\pi}{h^3} p^2 dp \qquad \text{(E-22)}$$

In terms of the energy, $E = \frac{\hbar^2 k^2}{2m_e} = \frac{p^2}{2m_e}$, equation (E-22) becomes

$$D(E)dE = 4\pi\left(\frac{2m_n^*}{h^2}\right)^{3/2}\sqrt{E}\,dE \qquad \text{(E-23)}$$

Where the effective mass, m_n^*, has been substituted for the electron mass to account for the effect of the ion cores on the free electron motion. Effective mass is discussed in section 5.2.

References

[1] R. H. Dicke, and J. P. Wittke, Introduction to Quantum Mechanics, Addison-Wesley Publishing Co., 1960.

[2] K. F. Brennan, The Physics of Semiconductors with Application to Optoelectronic Devices, Cambridge University Press, 1999.

This page intentionally left blank

Appendix F – Mathematica Program for Planar Geometry TPV Model

The Mathematica (version 5.1) program, included on the CD-R disk, solves the set of radiation transfer equations given by equations (8.10) and (8.11) for q_{oE} and q_{ob}, and equations (8.7) through (8.9) for q_{oC1} and q_{oC3}. These equations apply to the planar TPV system illustrated in Figure 8.1 where the emitter and filter-PV array are square. Also, the program allows for gaps between the reflector and the emitter and PV array. The filter-PV array is divided into three concentric areas, A_{C1}, A_{C2}, and A_{C3}, where A_{C1} is the inner most area and is surrounded by A_{C2}, and A_{C3} is the outer most area. As the program is written, all three areas are covered by PV arrays. However, the program can be easily modified to allow other types of surfaces to exist on A_{C1}, A_{C2}, and A_{C3}. Only the optical properties of those surfaces are required as input.

The optical properties must be given within the wavelength range lybegin ≤ ly ≤ lylong. Where lybegin is the wavelength of the first data point and lylong is the wavelength of the last data point. The wavelength spacing between data points is deltalyS and numse is the total number of data points. As a result, lylong = numse*deltalyS + lybegin. To compute the contribution to the radiation fluxes for wavelengths beyond lylong, it is assumed the optical properties have constant values given by their value at ly = lylong. It is assumed that the reflector reflectance, rhob, is a constant.

In the first segment of the program, all the view-factors are calculated. At the end of that segment, the view-factors are printed. A check is made on the view-factor calculations as well. If the quantities Fecheck and F_{bcheck} equal one, then the view-factors are correct. Following the view-factor segment, various input quantities such as the PV array temperatures, T_{C1}, T_{C2}, and T_{C3}, as well as, the beginning wavelength, lybegin, for the emitter emittance, filter-PV array reflectance and transmittance, and the PV array spectral response data must be supplied.

In the third segment, the emitter spectral emittance must be supplied. This can be done either in a tabular or functional form. At the end of that segment, the spectral emittance is plotted as a function of wavelength.

In the fourth segment, the filter or PV array reflectance (and transmittance if filter used) data must be supplied. Again, this can be in the form of tabular or functional data. At the end of that segment, the spectral reflectance, transmittance, and

absorptance are plotted as functions of wavelength. The reflectance of the reflector, ρ_b, is assumed to be constant.

Segment five contains the input data for the PV arrays quantum efficiency. This data can also be in tabular or functional form. The end of that segment shows the spectral response as a function of wavelength.

In the sixth segment, the input data, other than quantum efficiency, for the PV arrays must be supplied. This includes the number of arrays, Na, in each of the three areas, A_{C1}, A_{C2}, A_{C3}, and the number of junctions, Nj, in each array. Additional input quantities are the ideality factor, Ao, series resistance, rs, shunt resistance, rsh, and the dark saturation current density, jsc, at 300K. The dark saturation current density for any other temperature is calculated using equation (5.132). At the end of that section, the spectral response is plotted as a function of wavelength.

In the last segment, the radiation transfer equations are solved. An iteration process described in Section 8.3 is used to obtain the emitter temperature, T_E, and reflector temperature, T_b (T_b is assumed equal to T_E). After the temperature and radiation fluxes have been calculated, the cavity and PV efficiencies are calculated. The PV electrical output, Pel, for each array is calculated using the method described in Section 5.12. At the end of the last section all the radiation fluxes and PV parameters are printed out along with efficiencies. Also, the radiation fluxes leaving the emitter, q_{oE}, and reflector, q_{ob}, plus the radiation flux absorbed by area A_{c1}, qinc11, and the photon generated current densities produced by each PV array are plotted as functions of wavelength.

This page intentionally left blank

This page intentionally left blank

Index

This page intentionally left blank